komunikácie

COMMUNICATIONS

SCIENTIFIC LETTERS OF THE UNIVERSITY OF ŽILINA

Volume 25

UNIVERSITY
OF ŽILINA

ISSN 1335-4205

1953 70 2023

3/2023

UNIVERSITY OF ŽILINA
EDIS-Publishing House
UNIZA

1953 70 2023

EDIS-Publishing House of the University of Žilina (UZ) is one of the University of Žilina's consituents. The beginning of its existence dates back to 1990. In the course of its work, the publishing house has published more than 4 900 titles of book publications, especially university textbooks, scientific monographs, scripts, prose, but also enriched the book market with titles of regional, children's and popular literature.
Students and professional public have the opportunity to purchase published titles in the „Selling Study Literature" directly on the premises of the University of Žilina, in the EDIS shop or upon order on a „cash on delivery" basis. All published titles are available at: www.edis.uniza.sk.

EDIS-Publishing House of the University of Žilina offers book titles in English

Lenka Černá, Jozef Daniš
APPLICATION OF COST ALCULATIONS IN THE TARIFF POLICY FORMATION IN RAILWAY TRANSPORT
ISBN 978-80-554-1391-4 Price 7.61 €

Jozef Gašparík et al.
RAILWAY TRAFFIC OPERATION
ISBN 978-80-554-1281-8 Price 15.80 €

Eva Nedeliaková, Jana Sekulová
EVALUATION OF QUALITY IN RAILWAY TRANSPORT
ISBN 978-554-1272-6 Price 8.00 €

Anna Tomová
ECONOMICS OF AIR NAVIGATION SERVICES
ISBN 978-80-554-0905-4 Price 14.30 €

Jozef Melcer
Dynamics of structures
ISBN 978-80-554-1698-4 Price 19.00 €

Felix Fedorovič Rybakov, Alexander Nikolaevič Lyakin, Štefan Cisko et.al.
GLOBALIZATION AND DEVELOPMENT OF INFRASTRUCTURE
ISBN 978-80-554-0719-7 Price 19.80 €

Marica Mazurek
MODELS OF BRANDING AND THEIR APPLICATION
ISBN 978-80-554-1705-9 Price 9.00 €

Michal Kvet, Karol Matiaško, Marek Kvet
USB - BECOME EXPERT IN MYSQL PRACTICES FOR DATABASE SYSTEMS IN MYSQL
ISBN 978-80-554-1786-8 Price 13.50 €

Ján Bujňák, Ružica Nikolić, Jelena Djoković
STEEL STRUCTURES COLLECTION OF SOLVED PROBLEMS WITH EXCERPTS FROM THEORY
ISBN 978-80554-0404-2 Price 9.34 €

Martin Bugaj
Aeromechanics 1
ISBN 978-80-554-1675-5 Price 14.50 €

Tetiana Hovorushchenko et.al.
CD - INTELLIGENT INFORMATION-ANALYTICAL TECHNOLOGIES...
ISBN 978-80-554-1729-5 Price 3.50 €

Karol Matiaško, Michal Kvet, Marek Kvet
CD - Practices for database systems
ISBN 978-80-554-1397-6 Price 2.20 €

Michal Kvet, Karol Matiaško, Štefan Toth
USB - Practical SQL for Oracle Cloud
ISBN 978-80-554-1880-3 Price: 11,30 €

Veronika Valašková, Daniela Kucharová
USB - Statics of structures 3
ISBN 978-80-554-1826-1 Price: 8,90 €

EDIS-Publishing House UNIZA

Univerzitná 8215/1,
010 26 Žilina,
Slovakia

e-mail: edis_objednavky@uniza.sk, edis@uniza.sk
www.edis.uniza.sk

KOMUNIKÁCIE
COMMUNICATIONS

A - OPERATION AND ECONOMICS

TRANSFORMATION OF STRATEGIC MANAGEMENT PRINCIPLES OF AIR TRANSPORT AND LOGISTICS ENTERPRISES IN CONDITIONS OF INSTABILITY A111
S. Lytvynenko, O. Petrenko, T. Luchnikova, O. Vysochylo, M. Kutsenko

APPROACH TO DETERMINE TRANSPORT DELAYS AT UNSIGNALIZED INTERSECTIONS A124
O. Bieletska, Y. Liubyi, S. Ocheretenko, D. Muzylyov, V. Ivanov, I. Pavlenko

ECONOMIC ASSESSMENT OF TRANSPORT MOVEMENTS OF THE URBAN POPULATION IN AGGLOMERATIONS A137
D. KAPSKI, V. KUZMENKO, L. KHMELNITSKAYA

B - MECHANICAL ENGINEERING

TECHNICAL MAINTENANCE OF VEHICLES: IMPROVEMENT OF RELIABILITY OF THE MAJOR COMPONENTS AND UNITS B165
D. R. Tortbayeva, S. S. Pernebekov, U. A. Ussipbayev, B. Z. Shoibekov, A. O. Kazenova

OPTIMIZATION OF THE INJECTION MOLD RUNNER SYSTEM OF THE TRANSPORT MEANS PLASTIC PARTS B176
D. Čechmánek, R. Kohár, F. Brumerčík, M. Lukáč, J. Fiačan

STRENGTH ASSESSMENT OF AN IMPROVED DESIGN OF A TANK CONTAINER UNDER OPERATING CONDITIONS B186
S. Panchenko, J. Gerlici, G. Vatulia, A. Lovska, A. Rybin, O. Kravchenko

ANALYSIS OF THE TEST BENCH DESIGN INFLUENCE ON THE COOLING PERFORMANCE OF A RAIL VEHICLE BRAKE DISC B194
V. Pavelčík, J. Dižo, M. Blatnický, V. Ishchuk, D. Molnár

DETERMINING BASIC GEOMETRIC PARAMETERS OF THE APRON CONVEYOR DRIVE B201
B. G. Moldabayev, A. V. Rozhkov, O. T. Balabayev

DESIGN OF POWER TRANSFORMER WITH FREQUENCY 1 KHz B209
M. Franko, R Kučera, Z. Biel, R. Holček, M. Frivaldský

COMPARATIVE ANALYSIS OF HYBRID COMPOSITES BASED ON A356 AND ZA-27 ALLOYS REGARDING THEIR TRIBOLOGICAL BEHAVIOR B215
B. Stojanović, S. Gajević, N. Miloradović, R. Nikolić, S. Miladinović, P. Svoboda, A. Vencl

SHAPE OPTIMIZATION OF A COLUMN MODELLING THE BRIDGE SPAN UNDER A SPECIFIC LOAD - NUMERICAL AND EXPERIMENTAL STUDIES B228
J. Szmidla, A. Jurczyńska

DEVELOPING AND STUDYING THE METHOD OF ULTRASONIC PURIFICATION AND UTILIZATION OF INTERNAL COMBUSTION ENGINE EXHAUST GASES B245
I. Pak, A. Kadyrov, B. Askarov, B. D. Suleev, A. Karsakova

DESIGN OF A BICYCLE'S STRUCTURAL COMPONENTS AND A COMPARISON OF THEIR CHARACTERISTICS IN STEEL, ALUMINUM AND CARBON B259
L. Pompáš, F. Brumerčík, Ľ. Kučera, L. Smetanka

C - ELECTRICAL ENGINEERING IN TRANSPORT

NODE RINGING REDUCTION OF SYNCHRONOUS BUCK CONVERTER C48
M. Frivaldský, M. Pčola, Z. Biel, R. Kučera, M. Franko, R. Holček

EFFICIENCY COMPARISON OF Si IGBT AND SiC MOSFET BASED THREE-PHASE INVERTERS C56
Z. Biel, M. Pčola, J. Ondrejička, M. Franko, M. Frivaldský

D - CIVIL ENGINEERING IN TRANSPORT

STRENGTH CHARACTERISTICS OF Fe-SMA REINFORCEMENT IN RC BEAM WITH EXPERIMENTATION AND FINITE ELEMENT MODELING D54
P. Jadhav, A. Gite, R. L. Wankhade

MECHANICAL PROPERTIES INVESTIGATION AND OPTIMIZATION OF AMBIENTLY CURED ALKALI-ACTIVATED CONCRETE D71
K. Saibaba, B. Kondraivendhan

E - MANAGEMENT SCIENCE AND INFORMATICS IN TRANSPORT

HIGHLY SECURE AND ACCURATE DEEP SLICING FOR 5G WIRELESS NETWORKS FOR EFFICIENT RESOURCE UTILIZATION E15
A. Naveena

F - SAFETY AND SECURITY ENGINEERING IN TRANSPORT

IMPACT OF ROUGHNESS AND FRICTION PROPERTIES OF ROAD SURFACE OF URBAN STREETS ON THE TRAFFIC SAFETY F51
A. Beketov, S. Khalimova

THE DANGEROUS FACTORS IDENTIFICATION FEATURES OF OCCUPATIONAL HAZARDS IN THE TRANSPORTATION CARGO PROCESS F64
V. Tsopa, S. Cheberyachko, Y. Litvinova, M. Vesela, O. Deryugin, I. Bas

This is an open access article distributed under the terms of the Creative Commons Attribution 4.0 International License (CC BY 4.0), which permits use, distribution, and reproduction in any medium, provided the original publication is properly cited. No use, distribution or reproduction is permitted which does not comply with these terms.

TRANSFORMATION OF STRATEGIC MANAGEMENT PRINCIPLES OF AIR TRANSPORT AND LOGISTICS ENTERPRISES IN CONDITIONS OF INSTABILITY

Sergiy Lytvynenko[1], Olha Petrenko[2], Tatyana Luchnikova[3], Oksana Vysochylo[4], Maksym Kutsenko[5]

[1]Logistics Department, National Aviation University, Kyiv, Ukraine
[2]Department of Business Logistics and Transport Technologies, State University of Infrastructure and Technologies, Kyiv, Ukraine
[3]Department of Trade Business and Logistics, State University of Trade and Economics, Kyiv, Ukraine
[4]Department of Management, National Transport University, Kyiv, Ukraine
[5]Department "Railway Stations and Junctions", Ukrainian State University of Railway Transport, Kharkiv, Ukraine

*E-mail of corresponding author: sergiy.lytvynenko@edu-nau.com.ua

Sergiy Lytvynenko 0000-0001-7185-1193,
Tatyana Luchnikova 0000-0003-0624-5829,
Maksym Kutsenko 0000-0001-6020-7749
Olha Petrenko 0000-0002-1869-7999,
Oksana Vysochylo 0000-0002-6187-2801,

Resume

The significance of this study is derived from instability situations faced by various markets, particularly in the transport and logistics sectors, and the necessity to ascertain methods for their future advancement. The aim of this paper is to determine transformative modifications in the fundamental principles of strategic management for companies engaged in transport and logistics markets. In the course of the research, various methods were employed, including generalization, system analysis, abstract-logical method, systemic approach, analysis and synthesis method, graphical method, induction, deduction, comparison and systematization method, expert analysis, and selective observations. As a result, the authors identified the prerequisites for the transformation of unique and oversized air carriers into 3PL (Third-Party Logistics) operators, which are divided into the following blocks: needs, threats and risks, and product uniqueness.

Article info

Received 27 November 2022
Accepted 15 May 2023
Online 5 June 2023

Keywords:

strategic management
instability
crisis
transport and logistics sector
logistics operator

Available online: https://doi.org/10.26552/com.C.2023.049

ISSN 1335-4205 (print version)
ISSN 2585-7878 (online version)

1 Introduction

Initially, the history of the strategic management evolution should be analyzed. According to David [1], the strategic management can be defined as the art and science of formulating, implementing and evaluating cross-functional solutions allowing the company to achieve its goals. Thus, the strategic management focuses on the integrated interaction of management, marketing, finance, production, research, and information systems to achieve organizational success. We disagree with the F. David's opinion who emphasizes that the term "strategic management" is sometimes used as a synonym for the term "strategic planning", which is completely incorrect. The strategic planning is a preliminary stage of the evolution and it concerns only the formulation of strategy, while the term strategic management should be used to describe the complex process of strategy formation, implementation and evaluation.

The strategic management of enterprises is inextricably linked to the green economy. Currently, management pays increased attention to this problem both at the macro and micro levels. Environmental priorities are identified as key factors in the economic development in the world's leading countries.

In the early 2000s, the transition to the principles of sustainable development was outlined by the UN and other global organizations as the most appropriate for countries. Their reports still emphasize the importance of sustainable development [2].

A large number of researchers believe that

sustainable development remains dominant, while developed countries consider the greening of the economy a breakthrough opportunity for their development. The importance of sustainable development is emphasized to end poverty, ensure prosperity, and create better conditions for health, education, and social needs [3-4]. Sustainability at the organizational level is also crucial [5-7]. At the same time, there are researchers who criticize the central role of sustainable development as a dominant worldview [8].

Understanding the sources of sustainable competitive advantage has become the main focus of studying the strategic management. The strategic management is the process and approach to defining the goals of the organization, developing policies, programs, paradigms and plans to achieve these goals, as well as the allocation of resources. The strategic management can be considered the management of the combined components of the strategy process: strategy development, implementation and evaluation [9].

The problems of enterprises' strategic management have been investigated by many authors and a number of important scientific tasks have been successfully solved. However, enterprises in various sectors of the economy are undergoing dynamic development, the external environment is changing rapidly, and new challenges are emerging. These shifts have particularly affected companies in the transportation and logistics sector. It is logistics operators, air carriers, global freight forwarders and other participants in the transport and logistics market that have begun to actively engage in global supply chains, which are created to ensure organizational, trade, production and investment activities in the context of globalization and transformational changes in the global economy.

2 Literature review

Within the classical management theory, M. Porter [10] studies the progress of the development of dynamic theory of strategic management. The reasons for higher efficiency in a certain period of time (a cross-sectional problem) and the dynamic process of creating competitive positions (a longitudinal problem) are highlighted. Ainuddin et al. [11] studied the influence of key attributes of the resource, such as value, rarity, imitability and organization, on the productivity of the enterprise. Ainuddin et al. believe that international joint ventures as an object of the study are especially valuable for the world practice.. However, if the cost, rarity and indispensability are important factors in the efficiency, then the value, rarity and imitability are critical attributes for organizational capabilities.

Aspects related to the creation of various associations and alliances are also important since it is necessary to reorganize business processes while creating new structural associations. The period of the scientific development of strategic management on its own basis falls on the late 1980s - 1990s, when the resource concept was actively developing and became dominant. There was a division of strategic goals and resources, along with almost complete compliance of the content, process and context of the successful enterprise development [12]. The resource concept is still popular, although its existence is possible only as an integral part of the basis of the new theory of the company. The development of enterprises in the context of globalization has led to the importance of valuable advantages over competitor, the share of intangible assets, the innovation implementation, the effective use of organizational culture as a tool for enterprise management, and the high dynamics of change in the world markets. They formed the basis of the concept of dynamic capabilities.

This concept is characterized by the joint development of both external and internal competitive advantages, full compliance with the content, process, and context of the management strategies, the effective management of resource groups' flows and the effective combinations of them, as well as creating new forms of the enterprise management [12]. The study of Shuen [13] should be considered an interesting continuation of the concept of dynamic capabilities. In particular, Shuen proposed a new paradigm of Web 2.0 strategies for business based on the reconfiguration of outsourcing competencies using the synergy effect. The critical analysis of the paper makes it possible to state that the author has made a significant contribution to the implementation of dynamic capabilities.

In continuation of Shuen's scientific research, it is worth considering a scientific work by Alojairi [14], where the authors proposed a model of the network business innovation cycle, which proves that network capabilities are an important internal factor, positively affecting innovations in business models of Internet sellers and benefits consumers. In accordance with the analysis of the recent researches, the fifth stage in development of the theory of strategic management of enterprises was identified. It is based on further implementation of fundamentally new strategies, providing competitive advantages based on new paradigms of Web 2.0 strategy, implementation of the network business innovation cycle models, bioadaptive management, etc.

At the same time, the updated concept of dynamic abilities based on foresight competencies and other derivatives becomes dominant. Competitive advantages are formed as a result of the symbiotic complex development of internal and external advantages, ensuring absolute consistency of the content, process, and context. This stage was fully formed in the early 2020s although some of its components were successfully implemented in the previous decade. The further development of the theory

of strategic management of enterprises will continue to be based on the concept of dynamic capabilities. The process of strategic management of the enterprise is based on the belief that organizations must constantly monitor events and trends, while the speed and scale of changes affecting organizations is growing sharply. The strategic management process is dynamic and continuous. Changing any of the main components of the model may require changing all its components [1].

The conclusions [15] should be fully supported regarding the fact that differences between firms will deepen, with strategic resources and coordination playing a key role. The tasks of enterprises now include creating strategically valuable resources in current markets and using them effectively in adjacent markets, as well as implementing hybrid strategies [16]. All of these aspects are most fully manifested in the transportation and logistics market. And for logistics operators, the transition to the concept of a SMART provider-integrator of comprehensive logistics solutions in supply chains means a shift from a resource-based to a strategic outlook.

Within the framework of the study [17], the paradoxical aspects of strategic resources were analyzed through a critical analysis of evolutionary trajectories. In particular, they identified conditions when an abundance of resources can make a firm vulnerable, making it potentially weak. It should be noted that this opinion of the authors is fully consistent with the principles of the SMART model of a provider-integrator of comprehensive logistics solutions, in which the desired asset structure is defined as light.

A critical analysis of the scientific literature has revealed that despite the significant contribution of scholars to the development of theoretical and practical aspects of enterprises' strategic management, the problem of creating the foundations for strategic management of transport and logistics enterprises in the context of instability, transformational changes, globalization and intensification of their involvement in global supply chains remains unresolved.

3 Methodological framework

Recent studies outline that commercial enterprises consist of portfolios of idiosyncratic and difficult to trade assets and competencies, that is, resources. Under these conditions, at some point in time, competitive advantages may arise from the possession of scarce but relevant and difficult-to-imitate assets, especially the know-how. However, in the fast-paced business environment, which is open to a global competition and characterized by the geographical and organizational distribution of innovation and production sources, a sustainable advantage requires something more than ownership of assets that are difficult to reproduce (knowledge). It also requires unique and difficult to reproduce dynamic capabilities [18]. One of the components of the concept of dynamic capabilities is foresight competences. The scientific works of Salunke, Weerawardena and McCall-Kennedy [19], D. T Teece [20], Wang and Ahmed [21], Wilden, Gudergan, Nielsen and Lings [22] and others are dedicated to the study of these competencies.

The special feature of such an activity is to anticipate certain events on the basis of specific patterns that are recognized as characteristic of companies, their groups or even entire markets. In modern researches, much attention is paid to the interrelationship between business and society. The classics of modern management Porter and Kramer [23] noted the growing interest in corporate social responsibility. They also stated that business decisions and social policy must adhere to the principle of common value. In accordance with the concept of global innovation networks, which was studied by Kim and Park [24], the company's innovativeness is largely determined by a research and development network outside the country. In general, an effective combination of external and internal factors of knowledge management can be a key factor in the enterprise's success [25]. According to Teece [26], it is possible to fully implement innovations only with a well-developed and consistent business model.

As revealed in the study [27], the impact of governance mechanisms on the relationship between decision-making practices for sustainable strategic investment, industry 4.0 technologies, circular economy methods, and financial performance of companies is becoming a key factor in sustainable value creation and sustainable performance for it.

A number of methods are used to solve the problems of strategic management of enterprises. According to the results of the analysis of recent scientific studies, it is worth noting the active use of expert evaluation and interviewing methods [28], comparative and economic-statistical analysis, ranking [29], and methods necessary for developing a management tool for the company [30].

Ensuring the flexibility and scalability of business models is also extremely important in the strategic management of enterprises [31]. Researches confirmed that the implementation of innovations in several divisions of one enterprise is much more effective in terms of mastering innovations [32]. The concept of open innovations should be considered comprehensive for the general innovation theory [33]. The paper of Arefieva et al. [34] is dedicated to the management of sustainable development of human capital reproduction. It should be recognized that the mechanism of sustainable development management through the human capital reproduction proposed by the authors deserves further development. Conceptual model of economic stability monitoring business processes of the company in the period of sustainable development proposed Arefieva et al. [35].

The model and the method of assessment of the effectiveness of financial processes management in

logistic systems of industrial enterprises were substantiated in work by Bondarenko, Palyvoda and Kyrylenko [36]. Problems of organizing the production activity of network air carriers as one of the most difficult formations in transport and logistics markets are investigated in other works [37-38]. Undoubtedly, these scientific works have made a significant contribution to determining the prerequisites for the transformation of strategic management of these companies.

Thus, all of the above proves the need to make changes to the strategic management of companies in the transport and logistics sector, which is the focus of the study.

In implementing the research, the authors used the following methods: generalization and system analysis, abstract and logical method - in creating a scheme for implementing a new paradigm for the development of enterprise strategic management theory; systematic approach, analysis and synthesis, graphical - in systematizing the principles of effective strategic management of an enterprise; induction, deduction, comparison and systematization - in determining the prerequisites for transforming carriers of unique and oversized cargoes into 3 PL operators; expert analysis, sample observations - when determining innovative principles of strategic logistics management of 4 PL (Fourth Party Logistics) operator.

4 Results

It should be highlighted that, in line with current trends and as noted earlier, companies are actively integrating into Industry 4.0, which focuses on ensuring the creation of new business models and information transformation. Whereas, in the case of Industry 5.0, which has been actively implemented in developed countries, including the EU, the key transformation should be full integration with the green course, leading to better sustainability and circular economy, as well as improving the resilience of value chains and ecosystems to new challenges [39].

In view of this, it can be argued that the main reasons for the importance of changes in the strategic management of transport and logistics companies, including in the methodology, should be the need to

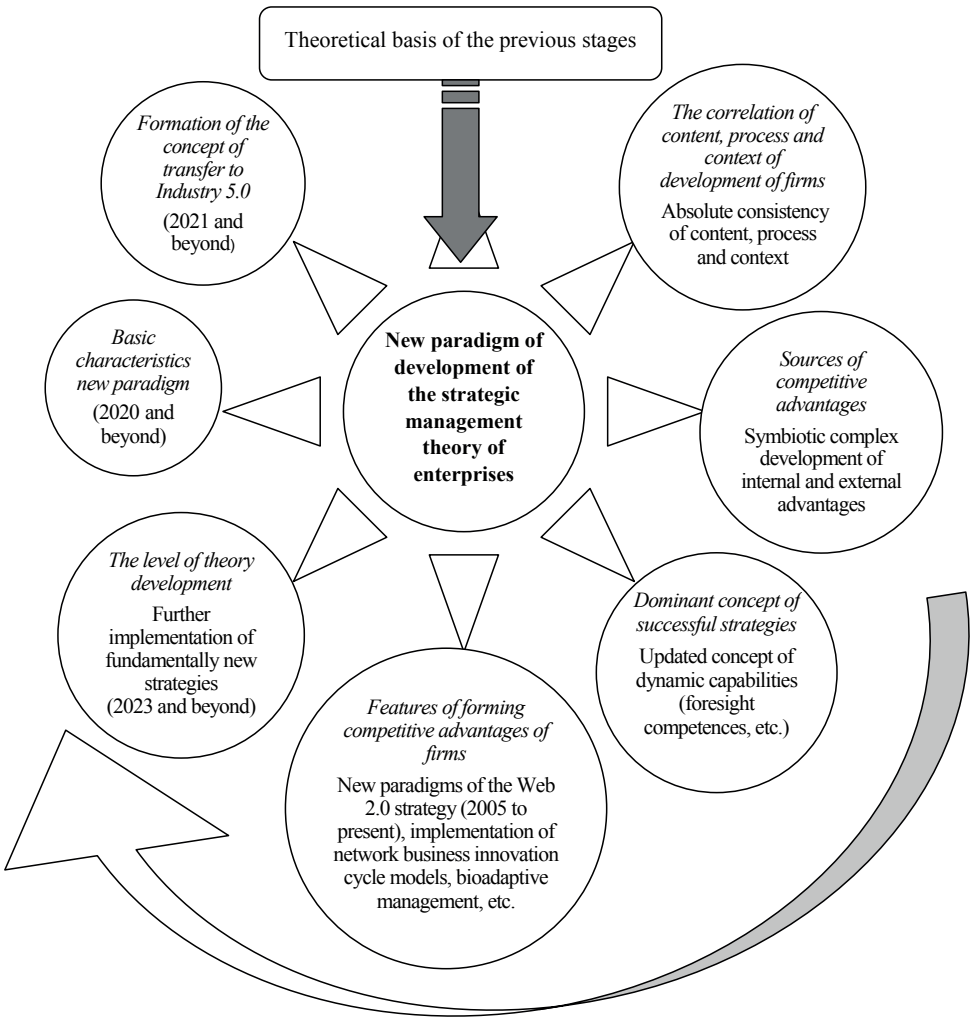

Figure 1 *Scheme for the implementation of a new paradigm of development of the strategic management theory of enterprises*

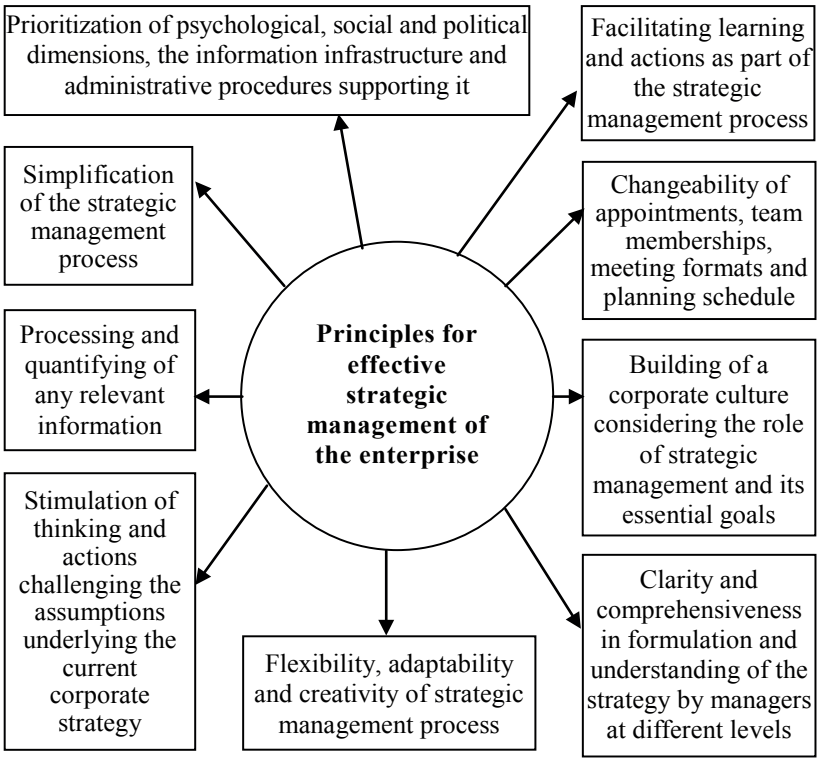

Figure 2 *Principles of effective strategic management of the enterprise*

meet the growing demands of customers, increased competition, energy and resource efficiency, and ultimately the vital need to integrate as full participants in global supply chains.

Thus, according to the recent trends described above, the following scheme for the implementation of a new paradigm of development of the strategic management theory of enterprises can be designed, Figure 1.

The principles of effective strategic management of the enterprise, proposed by Lenz [40], were systematized and graphically represented in Figure 2. The success of transport and logistics enterprises largely depends on the stable development of the national economy and international relations. The service industry around the world is more susceptible to the negative effects of crises than, for example, manufacturing. These schemes complement the theoretical foundations of strategic management of enterprises and can be useful for scholars, postgraduates, and doctoral students.

It should be noted that the formation of a new paradigm for the development of enterprise strategic management theory became possible with the direct implementation of generalization processes and the use of system analysis tools, as well as the application of the abstract and logical method.

To systematize the principles of effective strategic management of an enterprise, the authors used a system approach, the method of analysis and synthesis, and the graphical method for visual presentation of the results.

Participants in the transport and logistics market can be divided into three major groups as follows: suppliers of logistics services, subcontractors and consumers of the services. When creating innovative business models with the help of the relevant concepts of strategic management, systemic and situational approaches has become the norm for Western companies.

Therefore, the use of these principles when building systems of domestic transport and logistics market participants will significantly improve the quality and adequacy of these systems. For instance, Ukrainian leading companies are still only on the way to the full implementation of innovative strategic management principles. Leading foreign logistics operators, such as Kuehne+Nagel, ECOL, DB Schenker, GEFCO and others becomes the engine of innovative changes in the transport and logistics markets excluding OECD countries.

The active digitalization of the world economy has been one of the key trends of recent decades. The trend has come to developing countries, including transport and logistics companies. A cross-cutting information system becomes an integral part of a successful business. The abandonment of fragmentary information solutions is a key requirement of the market in modern conditions. It was noted that conceptually the information system of participants in transport and logistics markets should consist of two components, namely the external component, including tools that provide the information system settings, and the internal component, including object and subject of management, tools for resource management, planning, optimization of company's

activities and management of logistics processes. It was also found that the external component has lower productivity and lower quality than the internal one.

The development of informatization of participants in transport and logistics markets should be aimed at creating the information environment including not only a set of information systems and applications, but also mechanisms, models, factors, processes, resources, etc. The concept of informatization should be focused on solving problems related to the organization of cargo delivery, ensuring interaction between the participants in the delivery process and the full satisfaction of cargo clientele. It should also be kept in mind that carriers usually perform only part of the transportation, while the delivery process itself is provided by logistics companies or freight forwarders. So, the task of such an information system is the cross-cutting digitization of delivery processes of different participants to ensure the reliability and timeliness of delivery with a high level of coordination.

The concept of informatization of participants in transport and logistics markets should provide for constant updating of information systems both through the introduction of new information systems and the creation of new mechanisms, tools and instruments to implement information solutions. In accordance with the theoretical foundations of information systems and environment for enterprises of different economic sectors, the information environment of participants in transport and logistics markets should provide high-quality horizontal and vertical integration of all components, information security, compliance with certain criteria and standards. In addition, there is a need to develop a number of highly specialized techniques, guidelines and recommendations that would ensure the effective operation of this environment and its painless change if needed.

A unified information system is the main component of the information environment of participants in transport and logistics markets, as mentioned above. However, it cannot exist without meeting certain requirements and the availability of tools for its implementation. This toolkit should consist of the methodology, the mechanism and the system of effective implementation of the information system of participants in transport and logistics markets. The methodology should reflect the suitability of the chosen concept of informatization with the choice of the appropriate set of methods and approaches to solving the problem, while the mechanism should include a number of tools and instruments to resolve the problem.

A set of schemes should be used to control the management and the organization of relationships between the centers of responsibility and business processes of participants in transport and logistics markets that are involved in the implementation and improvement of the information system. It should be noted that the requirements for the environmental component of the logistics business are growing constantly. Based on the classification of logistics operators, it can be argued that after the currently classified five levels of PL operators, the next one will be a level related to the environmental aspect of the logistics service. However, the currently classified 5 level PL "virtual logistics operator" can be considered quite environmentally oriented compared to previous levels.

5 Discussion

In most countries of the world, port and warehouse logistics operators are in a winning position. Due to the increase in the cost of the entire supply chain and as a result of attracting more expensive cargoes, port and warehouse logistics operators were able to increase tariffs. Moreover, these companies did not face the need to change the strategic management principles of their activities, involving radical restructuring of their business models in view of the COVID-19 crisis, which affected other participants in the transport and logistics markets. However, domestic port operators continue to address the challenges they faced earlier. It is now clear that they need to improve their financial stability through increased competitiveness and to ensure customer-oriented principles in operation. In Ukraine, the warehouse logistics market is developing in a wave-like manner, while the demand for smart warehouses, fulfilment services, solutions for separate storage of perishable goods, etc. are increasing.

As for the transport companies, the specifics of transforming their strategic management principles should be analyzed in detail. There is a large number of them and the principles of their management are completely different. Some of cargo carriers should be classified as companies with a high level of profitability, while others develop their business models based on the benefits of high business turnover. These circumstances are determined, primarily, by the markets in which these companies operate. It is worth noting that at present the vast majority of traditional air cargo carriers perform only the functions of transporting goods from airport to airport, without performing any additional functions, which is quite justified. Usually, when structuring the air transportation market, traditional and low-cost airlines are distinguished as two poles of development, which is not entirely true. In addition, such a gradation is carried out on the principle of forming a route network, which is also not entirely correct. There is a need for a comprehensive analysis of business models of air carriers as part of the strategic management.

A quantitative assessment of the global air network is an extremely complex and non-trivial task. The qualitative analysis, which involves clustering and scenario modeling of the global air transport system, allows to identify its vulnerable elements under different operating conditions, to determine peripherals up to

95% of air transport network nodes, to form a simulation model to study the air network redevelopment using a multilayer structure paradigm, and to understand the effectiveness of the perspective air traffic networks. The structure of the airline network is formed on the basis of a multifactor model. It means the analysis of factors influencing the existence and configuration of the structure of large network airlines' systems in hub airports. There are four basic business models of air carriers, which are formed in accordance with existing trends in world air transport markets. Analyzing the conditions of air carriers' operation for these four models, there is a number of characteristics that are inherent in each of them.

The classic network model, in which cargo is transported by reloading cargo to a passenger's aircraft, is the most common. Thus, all large passenger carriers operate in this segment. On its basis we have proposed most of the theoretical and methodological developments. These tools can also be applied to other business models of air carriers, but they must be significantly redesigned, depending on the characteristics and conditions of their usage. In most research, classic business models are analyzed, focusing on the passenger component. The situation with the spread of COVID-19 dramatically changed the balance in the air transport markets. It was the network airlines among cargo carriers that suffered the most, especially those that organized the delivery of goods in the cargo compartments of passenger aircrafts. With the cancellation of passenger flights in the spring of 2020, these carriers were put on the brink of disaster. They could not fully fulfill cargo contracts, the demand for which even increased during that period, as the delivery of goods on passenger planes was financially unprofitable. The strategic management principles of these airlines began to change sufficiently. They actively abandoned the purely network model and began to operate on a point-to-point basis, which was considered an outdated model of doing business in early 2020. The transformation of the strategic management principles of such airlines continues.

By mid-2021, one can note the systemic nature of changes and the fact that the situation is gradually improving. However, adaptive quarantine measures around the world, mass vaccination have not become a panacea and failed to restore passenger flows to pre-crisis levels. Consequently, network air carriers are forced to hybridize their business models and use both network business principles and point-to-point flights. The performance of purely cargo flights has also dramatically increased for such carriers. This is due to a number of factors. The main one is the presence of unsatisfactory effective demand in most markets, which has led to an increase in tariffs by 200-400%. The lack of transportation capacity has changed the model of doing business, making network carriers less customer-oriented.

The hybridization of an airline's business model refers to the process of combining individual aspects of activity from a variety of existing carrier types within a specific company, while maintaining an optimal level of efficiency to ensure effective production and economic performance.

The business model of express freight transportation has gained popularity in recent decades and is developing extremely rapidly. A typical business model of the express transportation market are companies that have an air carrier in their structure, while other structural units perform functions of supplying chain management, handling, ground delivery of special cargoes with temperature restrictions, etc. Such companies as Federal Express, UPS and TNT are recognized leaders among express carriers. FedEx Corporation includes FedEx Office, FedEx Express, FedEx Ground, FedEx Freight, FedEx Custom Critical, FedEx Supply Chain, FedEx Trade Networks and FedEx Services. The role and tasks of each FedEx division are limited to its area of responsibility within the global business. Therefore, no transformational change in the production and logistics activities of FedEx Express can take place. The same can be noted about other market participants.

The combined business model can be regarded as independent cargo divisions of large corporations of carriers. The most striking examples are Lufthansa Cargo and Emirates Cargo, which are part of the most diversified airlines Lufthansa Group and Emirates Group respectively. The effectiveness of aviation business diversification can vary, but a well-organized diversification strategy can ensure reliable cross-functional benefits and provide significant value for both the parent organization and the subsidiary. Charter transportation of goods can be carried out according to different schemes and principles. This component of the world cargo market, in turn, is divided into a number of segments, each of them being characterized by its own specific features. Charter air carriers operate in specific markets where they are forced to expand the range of provided services. The market for the delivery of oversized and heavy cargo by air is also one of the specific ones. In this case, the carrier should create a product that is radically different from the product of traditional air cargo carriers.

First of all, the specific characteristic of the product created on this market by air carriers is the need to take into account the compliance of infrastructure and unique parameters of cargoes with the parameters of service devices at different stages of delivery and processing. This should involve at least one other mode of transport (for instance, road), the use of unique loading and unloading equipment, special customs clearance of goods and obtaining all permits for transportation. In addition, the carrier of oversized and heavy cargo very often solves a complex problem, that is, to develop projects for the delivery of these goods on one of the key principles of logistics - "door to door". Considering the air transport markets of unique and oversized cargo, they are largely

evolving into a kind of global markets for the delivery of such cargo on a door-to-door basis, i.e. the air carrier becomes a logistics operator and organizes delivery. Consequently, it does not perform exclusively functions of the carrier.

When transporting monocargoes, one of the main conditions for successful transportation is to ensure complete safety of the cargo, the condition of absolute preservation of the cargo properties and the speed of delivery. Integrated logistics systems and cargo movement control systems based on global satellite systems are very relevant information tools for optimizing the delivery of cargo units. Such systems are now being actively implemented in the international and domestic freight markets. The use of these systems allows to determine the coordinates of geographical objects anywhere and anytime. They are also actively used on road vehicles and ships to solve the problem of navigation dispatching. It is possible to use these systems to optimize the route of transportation, organize work and ensure the safety of vehicles.

At the same time, the delivery of oversized and heavy cargoes requires carriers to develop their own techniques of transportation. The delivery of heavy and oversized cargo requires consideration of a number of risks, ranging from delayed delivery to non-compliance or incomplete compliance with customs and legal formalities. The analysis of air carriers' operation in this market is also complicated due to the performance of transportation in a mixed way with the use of air transport by airlines-operators. This type of services is no longer something unique, and airlines are actively developing it to ensure the delivery of heavy and oversized cargoes on the "door to door" logistics principles. The aircraft in the air transport market of unique and oversized cargoes has unique characteristics and is able to carry specialized heavy monocargoes. Initially, the entry into the world commercial aviation market of the military transport aircraft An-124 was perceived skeptically by Western experts at that time. However, the successful certification of transport modification of the An-124-100 plane allowed to testify to the beginning of a new era in air transportation.

Until the early 1990s, the transportation of turbines, rockets and generators was the prerogative of almost exclusively maritime transport, while the use of aviation to transport such cargoes, even on a permanent basis, seemed a real utopia. However, from the very beginning the airlines-operators of An-124-100 aircraft (and its subsequent modifications) were able to impose competition on maritime carriers and to prove that the transportation of unique and oversized cargoes by air has a number of serious advantages to a solid cargo clientele. The main ones are the speed of delivery, the provision of a high level of cargo safety and the absence of the need to divide it into separate parts, in the case of monocargoes. The strategic management of such companies has changed significantly. In times of crisis, on the contrary, the need for transportation of special categories of cargoes is growing.

It should be noted that despite such a variety of companies engaged in the organization of delivery of oversized cargo, ensuring its multimodal delivery with the involvement of air transport remains unresolved. There are several air carriers engaged in the delivery of oversized cargo on the world market, including Volga-Dnepr and Antonov Airlines. These carriers often faced the problem of the disruption of the aviation part of the multimodal delivery of oversized cargo due to the fault of the delivery organizer or companies responsible for delivery by other transport modes. For the air carrier, this immediately resulted in significant financial costs (the standstill of the An-124-100 aircraft and its subsequent modifications costs up to $150 thousand per 24 hours). It could rarely be reimbursed in full as the cargo owner pays only the delivery cost. Of course, such risks can be pre-insured but this is not a panacea. Apart from that, airlines were forced to face inflated prices for the oversized cargo delivery initially by air, which made them consider the possibility of developing such projects on their own. At present, Volga-Dnepr and Antonov Airlines already have significant successful experience in planning projects for the delivery of oversized cargo by air. The next step was the development and successful implementation of similar projects in multimodal connections by airlines.

In view of the above-mentioned circumstances, air carriers have gradually begun to take over some of the functions that are related not only to the aviation component of the oversized cargo delivery. Undoubtedly, the performance of additional functions that are not typical to carriers only, i.e. 2 PL (Second Party Logistics) operators, makes such carriers higher-level operators. Since in this case the carrier of oversized cargo assumes a number of functions that are inherent in 3 PL operators, namely designing and applying special information solutions, vehicle management, consolidation of shipments, repackaging and labeling, providing a set of loading and unloading works, it can be considered so-called "basic 3 PL operator" (Third Party Logistic) or the Integrated Logistics Service Provider. The prerequisites for the transformation of unique and oversized cargo carriers into 3 PL operators are presented in Figure 3.

These aspects of strategic management include the development of methodical tools and practical recommendations on strategic management of enterprises and can be useful for employees of transport and logistics companies, airlines, government officials and employees of local governments. The best practices of companies were actively used in their development.

The transformation of the strategic management principles of unique and oversized cargo carriers in the crisis period was insignificant and determined by the general redistribution of cargo flows. The scientific literature identifies main types of risks including the

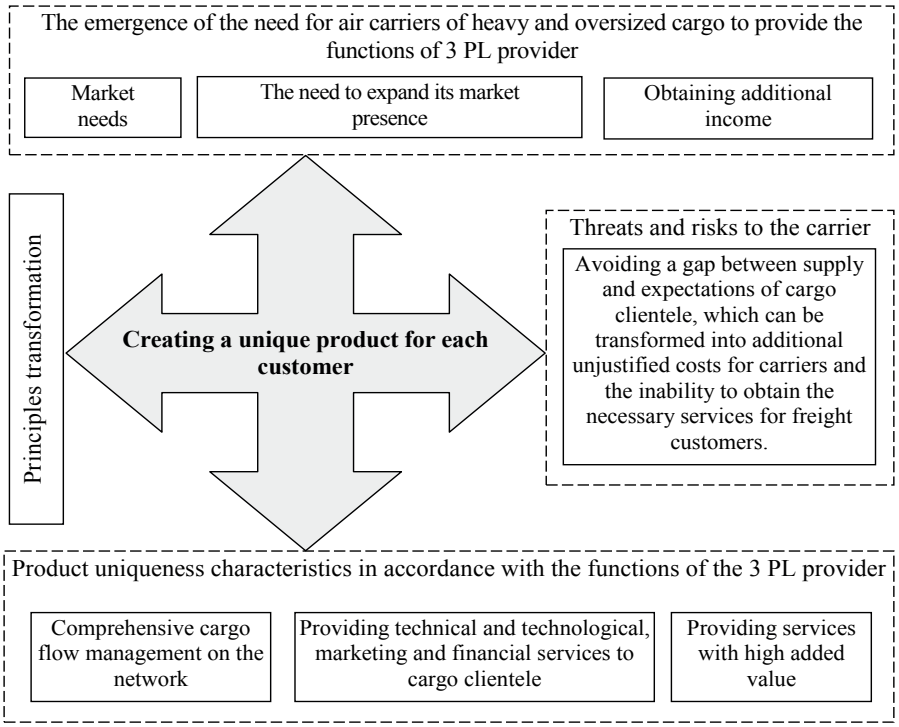

Figure 3 *Prerequisites for the transformation of unique and oversized cargo carriers into 3 PL operators*

risks associated with the transportation of cargoes. Regarding the delivery of special categories of cargoes, transport risks also increase significantly. The delivery of dangerous, perishable goods and live animals requires a number of precautions to reduce risk levels. These risks are more related to the physicochemical properties of such goods than to the transport process. Procedural aspects in the delivery of these categories of special goods by air are clearly regulated by international documents such as International Air Transport Association (IATA) Dangerous Goods Regulations, Live Animals Regulations, Perishable Cargo Regulations.

Determining the prerequisites for the transformation of carriers of unique and oversized cargo into 3 PL operators was based on the use of induction, deduction, comparison and systematization methods, with the obligatory incorporation of practical experience.

Other organizational and legal forms of air carriers are less popular for domestic air carriers. Federal Express, UPS, TNT and others are engaged in cargo transportation on specialized cargo planes. The combined type of cargo transportation in both luggage compartments on passenger aircrafts and on specialized cargo aircrafts is carried out by cargo air carriers established as subsidiaries and in addition to the passenger air transport business (Emirates Cargo, Lufthansa Cargo, etc.). The transfer of a specialized cargo aircraft as a complete package of cargo services (including team and maintenance) under the wet leasing scheme (e.g. Aircraft, Crew, Maintenance and Insurance - ACMIs) is also actively practiced in world markets. This model was actively implemented in the market of heavy and oversized air cargo transportation 10-15 years ago. Currently, the concept of "green airport" as an environmentally safe participant in the urban transport cluster is being actively promoted. Although the concept of "green airport" is relevant not only for business models of urban airports, it is the environmental factor in the city that becomes indisputably essential and should be addressed in the first place.

Relevant decisions have already been made at the level of the International Civil Aviation Organization (ICAO) requiring appropriate changes in the national legislation of the participating countries, including Ukraine. The intensification of a competition in the logistics market is caused by the strategic principles of the development of a number of leading logistics operators. These are usually the previously mentioned divisions of leading foreign logistics companies, such as Kuehne+Nagel, ECOL, DB Schenker, GEFCO and others. The transition to the principles of integrated logistics and complexity of logistics solutions is also expressed in the strategy of leadership by the product, a full customer orientation, the availability of a value proposition and the network principle of forming logistics operator's business model. In general, the innovative principles of strategic management of the logistics 4 PL operator are presented in Figure 4.

The definition of innovative principles of strategic logistics management for 4 PL operator was based on the use of expert analysis and a number of sample observations.

A competence approach as dominant in such conditions is provided by an integrated quality

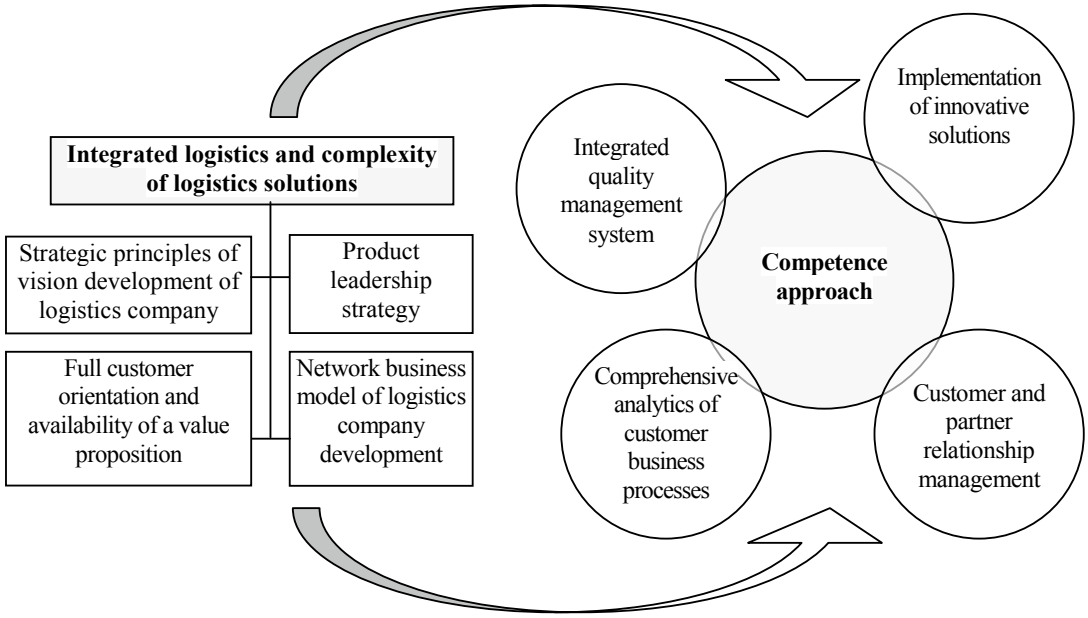

Figure 4 *Innovative principles of strategic management of logistics 4 PL operator*

management system, the comprehensive analytics of customer business processes, the implementation of innovative solutions and customer relationship management.

6 Conclusions

A critical analysis of the evolution of scientific views on the strategic management of enterprises allows to claim that the term "strategic management" should not be equated with the term "strategic planning", as the latter was a preliminary stage in the evolution of scientific opinions. Having studied the stages of the development of the strategic management, the fifth stage of development of the strategic management theory was formed on the basis of further implementation of fundamentally new strategies, providing the development of competitive advantages on new paradigms of Web 2.0 strategy, the implementation of the network business innovation cycle, bioadaptive management, etc. The weak implementation of innovative principles of strategic management of domestic participants in transport and logistics markets was noted, while foreign logistics operators are likely to become the leaders.

The key trend of recent decades is digitalization which is also actively implemented in the transport and logistics market. The concept of informatization of participants in transport and logistics markets should be implemented in the integrated information environment with the mandatory use of adaptation mechanisms and models. The greening of the logistics business is facilitated by the decisions of relevant international institutions and the desire of companies for business recycling. The transformation of the strategic management principles of transport and logistics companies in the context of the crisis has been successful. While port and warehouse operators have not felt these negative effects of the crisis, network airlines are ones of the most affected. This is primarily due to the intersection of cargo and passenger flows in these types of carriers and the organization of joint business for the delivery of passengers and goods, which has had serious consequences for the freight segment caused by a catastrophic drop in demand and a ban on passenger traffic.

Other airlines suffered much less which can be explained by the separation of cargo flows. The strategic management principles of unique and oversized air cargo carriers such as 3 PL operators have been changed. This is slightly related to the COVID-19 crisis and has much deeper consequences for the evolutionary transformation of the business model of these types of carriers. Similarly, the change in the strategic management principles of the logistics 4 PL operator cannot be considered a consequence of the companies' response to the crisis. The preconditions for such a transformation are long overdue and have reached the market in full only now.

Grants and funding

The authors received no financial support for the research, authorship and/or publication of this article.

Conflicts of interest

The authors declare that they have no known competing financial interests or personal relationships that could have appeared to influence the work reported in this paper.

References

[1] DAVID, F.R. *Strategic management: concepts and cases*. London: Pearson Higher Education, 2013. ISBN 978-0-13-612098-8.

[2] The sustainable development goals report 2022. New York: United Nations Publications, 2022.

[3] MEGYESIOVA, S., LIESKOVSKA, V. Analysis of the sustainable development indicators in the OECD countries. *Sustainability* [online]. 2018, **10**(12), 4554. eISSN 2071-1050. Available from: https://doi.org/10.3390/su10124554

[4] BAIN, P. G., KROONENBERG, P. M., JOHANSSON, L.-O., MILFONT, T. L., CRIMSTON, C., KURZ, T., BUSHINA, E., CALLIGARO, C., DEMARQUE, CH., GUAN, Y., PARK, J. Public views of the sustainable development goals across countries. *Nature Sustainability* [online]. 2019, **2**(9), p. 819-825. eISSN 2398-9629. Available from: https://doi.org/10.1038/s41893-019-0365-4

[5] VAN ZANTEN, J. A., VAN TULDER, R. Improving companies' impacts on sustainable development: a nexus approach to the SDGS. *Business Strategy and the Environment* [online]. 2021, **30**(8), p. 3703-3720. eISSN 1099-0836. Available from: https://doi.org/10.1002/bse.2835

[6] KHARAZISHVILI, YU., BUGAYKO, D., LYASHENKO, V., SOKOLOVSKIY, V., BARANOV, V. Strategizing for sustainable development of transport systems in the safety dimension. *IOP Conference Series: Earth and Environmental Science* [online]. 2021, **915**, 012025. ISSN 1755-1307, eISSN 1755-1315. Available from: https://doi.org/10.1088/1755-1315/915/1/012025

[7] LOZANO, R., BARREIRO-GEN, M. Organisations' contributions to sustainability. An analysis of impacts on the sustainable development goals. *Business Strategy and the Environment* [online]. 2022, early view, p. 1-12. eISSN 1099-0836. Available from: https://doi.org/10.1002/bse.3305

[8] KOTZE, L. J., ADELMAN, S. Environmental law and the unsustainability of sustainable development: a tale of disenchantment and of hope. *Law Critique* [online]. 2022, p. 1-22. ISSN 0957-8536, eISSN 1572-8617. Available from: https://doi.org/10.1007/s10978-022-09323-4

[9] OMALAJA, M. A., ERUOLA, O. A. Strategic management theory: concepts, analysis in relation to corporate competitive advantage from the resource based. *Philosophy. Economic Analysis* [online]. 2011, **44**(1-2), p. 59-77. ISSN 1821-2573, eISSN 2560-3949. Available from: https://www.library.ien.bg.ac.rs/index.php/ea/article/view/194/190

[10] PORTER, M. E. Towards a dynamic theory of strategy. *Strategic Management Journal* [online]. 1991, **12**(S2), p. 95-117. eISSN 1097-0266. Available from: https://doi.org/10.1002/smj.4250121008

[11] AINUDDIN, R. A., BEAMISH, P. W., HULLAND, J. S., ROUSE, M. J. Resource attributes and firm performance in international joint ventures. *Journal of World Business* [online]. 2007, **42**(1), p. 47-60. ISSN 1090-9516, eISSN 1878-5573. Available from: https://doi.org/10.1016/j.jwb.2006.11.001

[12] KATKALO, V. S. Evolution of the theory of strategic management. *Question of the Economy / Voprosy Ekonomiki* [online]. 2007, **12**, p. 143-145. ISSN 0042-8736. Available from: https://doi.org/10.32609/0042-8736-2007-12-143-145

[13] SHUEN, A. *Web 2.0: a strategy guide: business thinking and strategies behind successful Web 2.0 implementations*. California: O'Reilly Media, 2018. ISBN 9781492049722.

[14] ALOJAIRI, A., AKHTAR, N., MUHAMAD, ALI H., BASIOUNI, A. F. Assessing Canadian business IT capabilities for online selling adoption: a net-enabled business innovation cycle (NEBIC) perspective. *Sustainability* [online]. 2019, **11**(13), 3662. eISSN 2071-1050. Available from: https://doi.org/10.3390/su11133662

[15] D'ORIA, L., CROOK, T. R., KETCHEN JR, D. J., SIRMON, D. G., WRIGHT, M. The evolution of resource-based inquiry: a review and meta-analytic integration of the strategic resources-actions-performance pathway. *Journal of Management* [online]. 2021, **47**(6), p. 1383-1429. ISSN 0149-2063, eISSN 1557-1211. Available from: https://doi.org/10.1177/0149206321994

[16] FURR, N. R., EISENHARDT, K. M. Strategy and uncertainty: resource-based view, strategy-creation view, and the hybrid between them. *Journal of Management* [online]. 2021, **47**(7), p. 1915-1935. ISSN 0149-2063, eISSN 1557-1211. Available from: https://doi.org/10.1177/01492063211011

[17] MILLER, D., LE BRETON-MILLER, I. Paradoxical resource trajectories: when strength leads to weakness and weakness leads to strength. *Journal of Management* [online]. 2021, **47**(7), p. 1899-1914. ISSN 0149-2063, eISSN 1557-1211. Available from: https://doi.org/10.1177/014920632097

[18] TEECE, D.J. *Dynamic capabilities and strategic management: organizing for innovation and growth*. Oxford: Oxford University Press, 2011. ISBN 978-0199691906.

[19] SALUNKE, S., WEERAWARDENA, J., MCCOLL-KENNEDY, J. R. Towards a model of dynamic capabilities in innovation-based competitive strategy. *Industrial Marketing Management* [online]. 2011, **40**(8), p. 1251-1263. ISSN 0019-8501, eISSN 1873-2062. Available from: https://doi.org/10.1016/j.indmarman.2011.10.009

[20] TEECE, D. J. A dynamic capabilities-based entrepreneurial theory of the multinational enterprise. *Journal of International Business Studies* [online]. 2014, **45**(1), p. 8-37. ISSN 0047-2506, eISSN 1478-6990. Available from: https://doi.org/10.1057/jibs.2013.54

[21] WANG, C. L., AHMED, P. K. Dynamic capabilities: a review and research agenda. *International Journal of Management Reviews* [online]. 2007, **9**(1), p. 31-51. ISSN 0149-2063, eISSN 1557-1211. Available from: https://doi.org/10.1111/j.1468-2370.2007.00201.x

[22] WILDEN, R., GUDERGAN, S. P., NIELSEN, B. B., LINGS, I. Dynamic capabilities and performance. *Long Range Planning* [online]. 2013, **46**(1-2), p. 72-96. ISSN 0024-6301, eISSN 1873-1872. Available from: https://doi.org/10.1016/j.lrp.2012.12.001

[23] PORTER, M. E., KRAMER, M. R. Strategy and society: the link between competitive advantage and corporate social responsibility. *Harvard Business Review*. 2006, **84**(12), p. 78-92. ISSN 0017-8012.

[24] KIM, C., PARK, J-H. The global research-and-development network and its effect on innovation. *Journal of International Marketing* [online]. 2010, **18**(4), p. 43-57. ISSN 1069-031X, eISSN 1547-7215. Available from: https://doi.org/10.1509/jimk.18.4.43

[25] CASSIMAN, B., VEUGELERS, R. In search of complementarity in innovation strategy: internal R&D and external knowledge acquisition. *Management Science* [online]. 2006, **52**(1), p. 68-82. ISSN 0025-1909, eISSN 1526-5501. Available from: https://doi.org/10.1287/mnsc.1050.0470

[26] TEECE, D. J Business models, business strategy and innovation. *Long Range Planning* [online]. 2010, **43**(2/3), p. 172-194. ISSN 0024-6301, eISSN 1873-1872. Available from: https://doi.org/10.1016/j.lrp.2009.07.003

[27] ALKARAAN, F., ELMARZOUKY, M., HUSSAINEY, K., VENKATESH, V. G. Sustainable strategic investment decision-making practices in UK companies: the influence of governance mechanisms on synergy between Industry 4.0 and circular economy. *Technological Forecasting and Social Change* [online]. 2023, **187**, 122187. ISSN 0040-1625, eISSN 1873-5509. Available from: https://doi.org/10.1016/j.techfore.2022.122187

[28] TAKACS, F., BRUNNER, D., FRANKENBERGER, K. Barriers to a circular economy in small- and medium-sized enterprises and their integration in a sustainable strategic management framework. *Journal of Cleaner Production* [online]. 2022, **362**, 132227. ISSN 0959-6526, eISSN 1879-1786. Available from: https://doi.org/10.1016/j.jclepro.2022.132227

[29] BILICHENKO, O., TOLMACHEV, M., POLOZOVA, T., ANISKEVYCH, D., MOHAMMAD, A. L. A. K. Managing strategic changes in personnel resistance to open innovation in companies. Journal of Open Innovation: Technology, Market, and Complexity [online]. 2022, **8**, 151. eISSN 2199-8531. Available from: https://doi.org/10.3390/joitmc8030151

[30] BARBOSA, M., CASTANEDA-AYARZA, J. A., FERREIRA, D. H. L. Sustainable strategic management (GES): sustainability in small business. *Journal of Cleaner Production* [online]. 2020, **258**, 120880. ISSN 0959-6526, eISSN 1879-1786. Available from: https://doi.org/10.1016/j.jclepro.2020.120880

[31] BOCK, A. J., OPSAHL, T., GEORGE, G. Business model innovation and strategic flexibility: a study of the effects of informal and formal organization. In: 2010 Academy of Management Annual Meeting, Montreal, Canada: proceedings. 2010.

[32] HORTINHA, P., LAGES, C., FELIPE, L. The trade-off between customer and technology orientations: impact on innovation capabilities and export performance. *Journal of International Marketing* [online]. 2011, **19**(3), p. 36-58. ISSN 1069-031X, eISSN 1547-7215. Available from: https://doi.org/10.1509/jimk.19.3.36

[33] TROTT, P., HARTMANN, D. A. Why open innovation is old wine in new bottles. *International Journal of Innovation Management* [online]. 2009, **13**(4), p. 715-736. ISSN 1363-9196, eISSN 1757-5877. Available from: https://doi.org/10.1142/S1363919609002509

[34] AREFIEVA, O., POLOUS, O., AREFIEV, S., TYTYKALO, V., KWILINSKI A. Managing sustainable development by human capital reproduction in the system of company's organizational behavior. *IOP Conference Series: Earth and Environmental Science* [online]. 2021, **628**, 012039. ISSN 1755-1307, eISSN 1755-1315. Available from: https://doi.org/10.1088/1755-1315/628/1/012039

[35] AREFIEVA, O., PILETSKA S., KHAUSTOVA, V., POBEREZHNA, Z., ZYZ, D. Monitoring the economic stability of the company's business processes as a prerequisite for sustainable development: investment and security aspects. *IOP Conference Series: Earth and Environmental Science* [online]. 2021, **628**, 012042. ISSN 1755-1307, eISSN 1755-1315. Available from: https://doi.org/10.1088/1755-1315/628/1/012042

[36] BONDARENKO, O., PALYVODA, O., KYRYLENKO, O. Development of a model for the estimation of financial processes in logistic systems at industrial enterprises. *Eastern-European Journal of Enterprise Technologies* [online]. 2018, **5**(1(95)), p. 6-16. ISSN 1729-3774, eISSN 1729-4061. Available from: https://doi.org/10.15587/1729-4061.2018.142628

[37] BO, W., GRYGORAK, M., VOITSEHOVSKIY, V., LYTVYNENKO, S., GABRIELOVA, T., LYTVYNENKO, L., IVANOV, Y. Assessment of the implementation of a cargo traffic management system. *Proceedings of the*

Bulgarian Academy of Sciences / *Comptes Rendus de l'Acade'mie Bulgare des Sciences* [online]. 2019, **72**(4), p. 503-509. ISSN 1310-1331, eISSN 2367-5535. Available from: https://doi.org/10.7546/CRABS.2019.04.10

[38] SEN, Y., VOITSEHOVSKIY, V., LYTVYNENKO, S., BORETS, I., RUSANOVA, S., LYTVYNENKO, L. Realization of a nonlinear multiproduct model of cargo traffic management of the network air carrier. *Comptes Rendus de l'Acade'mie Bulgare des Sciences.* 2021, **74**(4), p. 561-567. ISSN 1310-1331, eISSN 2367-5535.

[39] DIXSON-DECLEVE, S., BALLAND, P.-A., BRIA, F. Industry 5.0: a transformative vision for Europe. ESIR Policy Brief No. 3. Luxembourg: Publications Office of the European Union, 2022.

[40] LENZ, R. T. Managing the evolution of the strategic planning process. *Business Horizons* [online]. 1987, **30**(1), p. 34-39. ISSN 0007-6813, eISSN 1873-6068. Available from: https://doi.org/10.1016/0007-6813(87)90020-6

This is an open access article distributed under the terms of the Creative Commons Attribution 4.0 International License (CC BY 4.0), which permits use, distribution, and reproduction in any medium, provided the original publication is properly cited. No use, distribution or reproduction is permitted which does not comply with these terms.

APPROACH TO DETERMINE TRANSPORT DELAYS AT UNSIGNALIZED INTERSECTIONS

Olha Bieletska[1], Yevhen Liubyi[1], Serhii Ocheretenko[1], Dmitriy Muzylyov[2], Vitalii Ivanov[3,*], Ivan Pavlenko[4]

[1]Department of Transport Systems and Logistics, Kharkiv National Automobile and Highway University, Kharkiv, Ukraine
[2]Department of Transport Technologies and Logistics Department, State Biotechnological University, Kharkiv, Ukraine
[3]Department of Manufacturing Engineering, Machines and Tools, Sumy State University, Sumy, Ukraine
[4]Department of Computational Mechanics named after Volodymyr Martsynkovskyy, Sumy State University, Sumy, Ukraine

*E-mail of the corresponding author: ivanov@tmvi.sumdu.edu.ua

Olha Bieletska 0000-0002-6256-8705,
Serhii Ocheretenko 0000-0001-5132-5647,
Vitalii Ivanov 0000-0003-0595-2660,
Yevhen Liubyi 0000-0003-0681-0920,
Dmitriy Muzylyov 0000-0002-8540-6987,
Ivan Pavlenko 0000-0002-6136-1040

Resume

This study proposes an approach to determine transport delays at unsignalized intersections, according to the theory of stationary Poisson flow and considering the priority of vehicle traffic in competing directions. The accuracy of the proposed approach was estimated by comparing the average values of delays of vehicles performing a left turn from a minor road and their actual values obtained as a result of processing data from field studies. The results of the accuracy evaluation at unsignalized intersections of non-equivalent roads indicate the obtained results' reliability, because the calculation error does not exceed 10 %, as well as the possibility of using the developed approach in the process of transport planning and unsignalized intersections modelling.

Article info

Received 26 February 2023
Accepted 24 May 2023
Online 19 June 2023

Keywords:

transport systems
sustainable transportation
traffic control
traffic flow
sustainable cities
queuing system
field studies

Available online: https://doi.org/10.26552/com.C.2023.052

ISSN 1335-4205 (print version)
ISSN 2585-7878 (online version)

1 Introduction

In recent years, a constantly rising level of motorization has caused vehicle congestion in Ukrainian cities' road networks, especially their centers. The central parts of cities are characterized by a high density of the road network, which provides a convenient approach to various places of attraction, disperses traffic and pedestrian flows in space and creates an extensive network of urban passenger traffic routes. However, the higher the density of the road network, the more often traffic and pedestrian flows cross and the non-optimal regulation negatively affects the economy. Negative effects in the last decades include a significant increase in road accidents, increased environmental pollution and more frequent traffic congestion. To reduce the impact of a rising level of motorization, it is necessary to develop the effective measures to improve the road safety in cities [1-4] avoiding risks [5-6].

The impact of transport on the environment is primarily determined by the downtime and delays. If the transport speed is high enough, the environmental impact is slight, particularly noise pollution. If the matter concerns the more frequent impact of traffic flows, we get more serious consequences, up to socio-economic issues - especially for cities. A delay indicates excess time consumed by a vehicle, compared to the control value. It is one of the most widely used criteria for assessing the quality of traffic management at intersections and is used in analyzing road investment [1].

It should also be understood that in most cases, transport delays are local and private problems that can be observed and investigated not only in terms of planning the development of an overall master plan of the territory but in the small areas, as well. Therefore, to reduce the vehicle delays on the road network, it is necessary to determine a rational traffic light cycle at

regulated intersections and pay special attention to reducing vehicle delays at unsignalized intersections. There are controversial issues at such intersections that cause accidents with actual damages. Thus, the problem under consideration is technical and socio-economic, as mentioned above. However, considering the situations where a delay is temporary and, at the same time, the geometry and peculiarities of functioning transport delay areas are diversified, it is necessary to identify the possibilities of the technique for eliminating delays. This issue requires development of mathematical models for determining the transport delays at unsignalized intersections under different conditions.

2 Literature review

Determining the transport delays at intersections aims to estimate and develop effective measures to increase the road traffic efficiency. Methods for estimating the transport delays at unsignalized intersections can be divided into two groups: based on empirical studies and various analytical models. The methods of the first group allow to solve problems for selected local objects, but they are specified by sufficiently high accuracy. The advantages of the second group methods are operational versatility and flexibility, while the disadvantage is lower estimation accuracy. The analysis results of the most widely used approaches to determine delays at unsignalized intersections are presented below.

The basis for calculating the transport delays at unsignalized intersections in the post-Soviet space (e.g., Ukraine, Moldova, Georgia, etc.) are the results of Kremenets's studies, [7-8]. He considered that when crossing an unsignalized intersection with indicated main and minor roads, time losses occurred in the secondary direction with the lack of driver priority in traffic. The study [7] noted that the components of time losses, even with constant intensities at intersections, vary over wide ranges and differ for each vehicle. Considering the impact of many random factors, time losses are estimated by the average delay of one vehicle and are calculated with some assumptions. In general, the expression for determining the average delay can be written as follows [7]:

$$t_{\Delta H} = t_{\Delta H1} + t_{\Delta H2} + t_{\Delta H3}, \tag{1}$$

where:
$t_{\Delta H1}$ is the average waiting time for an acceptable interval, s,
$t_{\Delta H2}$ is the average delay associated with staying in a line of vehicles formed on the minor road, s,
$t_{\Delta H3}$ is the average delay related to braking the vehicle before the intersection, s

The following $t_{\Delta H1}$ is taken as equal to the ratio of the total duration of unacceptable intervals to the number of acceptable ones, [8]. It depends on the number of vehicles in a line before the main road. It can be determined using the fundamentals of the queuing theory, provided that the secondary direction of the traffic can be represented as a service line with an exponential distribution of arrival time requirements and service time. In turn, $t_{\Delta H3}$ is defined as the difference between the time required for braking before the intersection and the further vehicle acceleration and its passing time under free conditions.

With constant deceleration and acceleration while changing the speed and with an exponential distribution of the probability of time intervals occurrence between cars on the main road, the average delay of a vehicle in this direction of the minor road can be defined as [8]:

$$t_{\Delta H} = \frac{e^{N_{mn}t_{bd}} - N_{mn}t_{bd} - 1}{N_{mn} - N_{mr}(e^{\lambda t_{bd}} - N_{mn}t_{bd} - 1)} + \\ + \frac{V_v}{7.2}\left(\frac{1}{a_d} + \frac{1}{a_a}\right), \tag{2}$$

where:
N_{nm} is the main road intensity in both directions, veh./s,
N_{mr} is the average intensity per one lane of the minor road in the relevant direction, veh./s, t_{bd} is a boundary interval, s,
a_d, a_a is deceleration and acceleration of the vehicle, m/s^2,
V_v is the vehicle speed under free conditions, m/s

The average vehicle delay at an unsignalized intersection is defined as the average value of delays for all directions of the minor road [8]:

$$t_{\Delta Hn} = \frac{\sum_1^n t_{\Delta H} N_j}{\sum_1^n N_j}, \tag{3}$$

where:
N_j is the traffic intensity on the j-th direction of the minor road, veh./s,
n is the number of directions on the minor road.

By analogy with the Kremenets' model, the authors of [9] have developed a model of the total transport delay for all possible directions at an X-shaped unsignalized intersection that can be calculated as:

$$T = \sum_{i=1}^{n} t_{wi} + n(t_{ul}d_l + t_{ur}d_r + t_{us}d_s) + nC, \tag{4}$$

where:
t_{wi} is the time spent for the i-th vehicle waiting in a line, s,
n is the vehicles number per time unit, veh.,
t_{ul}, t_{ur}, t_{us} is the average time for performing a left turn, right turn, moving straight, respectively, s,
d_l, d_r, d_s is the share of vehicles moving left, right and straight, respectively,
C is the time for braking and acceleration, s

It should be noted that the presented model for calculating the total transport delays is more applicable for the economic assessment of traffic management efficiency than the average delay, which mainly specifies the service quality of a particular vehicle [9].

The authors of [10] proposed determining the vehicle delays at an unsignalized intersection based on the traffic flow field studies. The authors have developed a software package that allows to calculate the total delay time, average delay time, the length of a vehicle line and the number of vehicles that arrived. It should be noted that the article's content does not clarify the models, methods and algorithms incorporated in the software shell for calculating transport delays at unsignalized intersections.

The foreign theory (primarily the United States, Australia, and Eastern European countries) of transport regulation focuses on estimating delays and lengths of queues. Transport delays and the vehicle queue length are the main indicators introducing the concept of level of service (LOS) and used in assessing the adequacy of road lane length before the intersection, fuel consumption and exhaust emissions. Today's delay models used for intersections are generally described from deterministic and stochastic points of view to reflect both the constancy and randomness of traffic flow properties [11].

Tanner's approach is one of the first attempts to calculate delays at unsignalized intersections for vehicles moving in a secondary direction [12]. His approach is based on the following issues: vehicles arrive at the intersection randomly; the main traffic flow creates an alternating updating process with the time spent on crossing the intersection by a group (bunch) of vehicles, while the time intervals between the groups (bunches) of vehicles are distributed exponentially; the vehicles of secondary direction cross the main road at regular intervals during the presented interval, which is limited by the arrival time of the next group (bunch) of vehicles.

In turn, Kimber et al. [13-14] proposed an approach to estimate delays at an unsignalized intersection and predicted the length. Authors have analyzed the correlation between the delay and traffic flow intensity for minor roads.

In the paper [15], Troutbeck proposed to consider the following parameters in the model for determining vehicle delays at unsignalized intersections: an average delay with a little secondary flow; a degree of the secondary flow saturation; an indicator that quantifies the effect of minor flow queuing.

For intersections with the traffic priority, Heidemann [16] presented a formula for calculating transport delays on a secondary road as a saturation function.

For example, in the two-way stop-controlled intersections, the authors of [17] divided the total transport delay into queuing and service delays. In this case, the queue delay is determined by the time from the arrival of the vehicle at the end of the queue to its approach to the stop line. In turn, a service delay is a time between the vehicle's arrival at the stop line and its departure.

Considering the results of driver behavior observations, Horowitz [18] improved the queue-waiting model for all-way stop-controlled intersections. The authors of [19] developed a probabilistic model of delays representing the driver's behavior when deciding on manoeuvring that applies to describing a right turn at a T-junction.

In the study [20], three existing models of delays at unsignalized intersections were compared: the HCM 94 model, the Akcelik-Troutbeck model and the SIDRA 5 model. The differences in the calculation results are presented in the paper and these models are improved based on the simulation results. The total delay at unsignalized junction with relative priority under [21] has four components: delay to deceleration (braking); queue delay; delay in waiting for the possibility to turn (waiting time for a break in the main flow); acceleration delay (running-away).

The authors of [22] propose models for estimating queuing delays and service delays at the two-way stop-controlled intersections, where the service delay is calculated as a function of the degree of competing flows. In turn, the average value of the service delay and its variance are used as input parameters for the delay estimation.

Kaysi and Alam [23] used a simple simulation model to study the traffic service quality at unsignalized intersections with priorities. The developed simulation model reflected drivers' behavior and the traffic flow interaction process. The authors concluded that the basic models considering the peculiarities of driver's behavior (driver learning and impatience, aggressive driver attitudes) and the interaction of traffic flows differ from the simple perception of critical gaps at unsignalized intersections.

In most cases, to clarify drivers' behavior characteristics on highways, it is necessary to conduct time-consuming real-field investigations (video surveillance, survey) with subsequent processing, verification and calibration of obtained results. The question of studying drivers' behavior at both signalized and unsignalized intersections has been given numerous research papers. The main issues that are considered in these scientific publications are the following: studies of an acceptable critical interval for various maneuvers implementation at intersections [24-25]; cross-roads capacity studies [26]; studying reasons for making false decisions when crossing intersections [27], etc. It should be understood that there are many examples when drivers of conflicting flows at unsignalized intersections cooperate. An example of such cooperation is the provision by main road drivers of ways right for the secondary road drivers in various congestion (critical) situations. Such cooperation is a positive from the viewpoint of secondary flows since delays at intersections are reduced for them. On the other hand, even a slight speed decrease in driving in main directions reduces intersection throughput. The best way to define truth in

this matter may be using software complexes of traffic modelling.

Based on the simulation modelling results by AWSIM, the authors of [28] developed empirical models for estimating delays and queue lengths at all-way-stop-controlled intersections. A better correlation than exponential form models characterizes the proposed generalized form of the delay model. In the paper [29], Luttinen studied the relationship between the delay and a traffic on minor roads.

Cvitanic et al. [30] developed a new model for estimating the total delay at unsignalized intersections using the queuing theory. Brilon in [31] tried to test methods for calculating delays based on the queuing theory. The author developed a technique using Markov chains to obtain numerically accurate results. Stochastic modelling and empirically obtained data were used to assess the accuracy of obtained approximating models. The author has developed equations that can be used to calculate the value of delays at unsignalized intersections under the free traffic conditions.

Chandra et al. [32] developed a service delay model and conducted a microscopic analysis of delay in mixed traffic. The study revealed a significant impact of the share of heavy vehicles in the conflicting flow on the value of service delay.

The Transportation Research Board presented a procedure for estimating transport delays at unsignalized intersections in HCM [33]. In this case, delays are estimated separately for each secondary direction flow and left-turning flows of the main direction. According to this study, a delay is the time from when a vehicle stops at the end of the queue to when the vehicle leaves the stop line. A similar approach is used in the Malaysian HCM [33].

$$D = \frac{3600}{C_{m,x}} + 900T\left[\frac{V_x}{C_{m,x}} - 1 + \sqrt{\left(\frac{V_x}{C_{m,x}} - 1\right)^2 + \frac{\left(\frac{3600}{C_{m,x}}\right)\left(\frac{V_x}{C_{m,x}}\right)}{450T}}\right] + 5, \quad (5)$$

where: D total delay, s/veh.,
V_x - flow speed for traffic direction x, veh./h,
$C_{m,x}$ - throughput of direction x, veh./h,
T - period of analysis, h (T = 0.25 for a 15-min period).

In turn, the average delay for the secondary direction is estimated as a traffic capacity function and a saturation degree, where the capacity is expressed as a function of the degree of the conflicting flow.

The author of [34] proposed a new approach to determine delays at unsignalized intersections that allows one to estimate the change in the average delay depending on the previous queue and variable throughput. The advantage of this approach is the possibility of obtaining sufficiently accurate results for an extended period, for example, a day.

Another group includes approaches to determine delays at unsignalized intersections based on applying micro-modelling and regression dependencies. Particular attention should be paid to Caliendo's work [35]; the presented models of the delay time, downtime and peak queue were developed using AIMSUN and can be used for decision-making by transport infrastructure designers and road operators.

One of the recent studies should be emphasized [36], where modelling the transport delays at unsignalized intersections, using an artificial neural network was carried out using Malaysia as an example. Obtained results showed that the neural network, could predict the delay at unsignalized intersections more accurately than the approaches presented in the Malaysian HCM and HCM 2010. The accuracy of the developed models was estimated based on the field study results at three intersections with different configurations.

In addition to traffic flows, the transport delays amount within a coverage area of unsignalized intersections is impacted by pedestrian crossing presence. Pedestrian flows create additional obstacles to traffic and can be accident reasons since it is extremely difficult consider the pedestrians' behavior by drivers driving through the unsignalized intersections. The study of accounting challenges for pedestrians and drivers' behavior within unsignalized intersections is described in many scientific publications. Turner et al. [37] evaluated various engineering measures that could be used to improve pedestrian safety within unsignalized intersections and formulated recommendations on the feasibility of using them at various kinds of unsignalized intersections. In the investigation [38], a large volume of real-field observations of transport and pedestrian flow interaction, within unsignalized intersections, were carried out. The obtained results are more aimed at accounting for pedestrian behavior for delays in mixed traffic conditions. Moreno et al. [39] designed a model predicting the pedestrian behavior at an unsignalized intersection at different locations around it. The results show that the model can provide crossing intentions within a 3-second time window. In addition to the above, a separate component of traffic participants can be considered categories of persons with special needs, which include blind, elderly, children and people with limited mobility, which significantly affect the traffic conditions and efficiency at unsignalized intersections. For such person categories, engineering structures are developed and information tools are introduced based on smart technologies that increase the driving safety on street and road networks. Information to these persons about the current traffic functioning can be obtained through the corresponding applications in smartphones, as well as smart bracelets [40-41].

It should be noted that most of the analyzed studies were performed in countries where the traffic management at unsignalized intersections, their geometric parameters, drivers' behavior and traffic rules' abidance are significantly different from Ukrainian

realities. Almost all the considered approaches for determining the transport delays refer to unsignalized intersections of two types: two-way stop-controlled and all-way stop-controlled, that indicates development of models for determining delays at unsignalized intersections, with an organization that differs from the worldwide traffic, for example, unsignalized intersections of equivalent roads are often found on the territory of Ukraine. The priority in developing a new approach should be given to analytical modelling, allowing one to obtain universal models, which will be possible at unsignalized intersections of any type. The developed approach will be based on the principles of the simplest flow, which will allow for taking into account the priority of vehicles passing in conflicting directions.

3 Purpose and objectives of the study

A general scientific challenge addressed in this study is improving the road traffic efficiency in urban areas. Herewith, the study object is traffic flows through unsignalized intersections. This problem cannot be considered as well-studied, confirmed by numerous research and design works analyzed in this field. In such cases, various approaches are used to determine the transport delays - from analytical models to applying specialized software, for example, VISSIM or others [42-43]. It should be understood that the software tools for modelling the transport flows allow specialists to obtain an important data set for analyzing and predicting traffic, including the transport delays. However, information completeness received ensures applying only the commercial versions of such a software, which is not always accessible to Ukrainian transportation planning and modelling experts because their costs are high. The main focus of the paper is on designing analytical models for determining transport delays at unsignalized intersections.The main focus of the paper is on designing analytical models for determining transport delays at unsignalized intersections The main model advantage is the possibility to accurately assess received calculations based on empirical results of traffic observations at these road infrastructure objects.

That is why the main focus of the paper is to create the main paper aims to create mathematical models for calculating transport delays at various types of unsignalized intersections: with equivalent and unequal traffic directions. Therefore, the priority study objectives are the following:

- Theoretical aspects are designing analytical models of average transport delays at unsignalized intersections with different priorities;
- Experimental studies conduct and process the traffic flow video surveillance results at unsignalized intersections. The proposed approach assesses the accuracy of results of calculating the transport delays according to developed analytical models based on data obtained during the empirical observations.

It should also be noted that the proposed models are being created for the first time.

4 Study materials on vehicle delays at unsignalized intersections development of analytical models of vehicle delays at unsignalized intersections

4.1 Unsignalized intersection with equivalent directions

Suppose that λ_1, λ_2 are the intensities of vehicles approaching an unsignalized intersection from competing directions, s^{-1}, Δ_1, Δ_2 - time to pass the intersection by vehicles moving in competing directions time to pass the intersection by vehicles moving in competing directions, s Then congestion of the directions will be determined as:

- for direction 1

$$\rho_1 = \lambda_1 \Delta_1, \tag{6}$$

- for direction 2

$$\rho_2 = \lambda_2 \Delta_2. \tag{7}$$

In turn, the average duration of the loaded period for each direction is determined as follows:

- for direction 1

$$P_1 = \frac{\Delta_1}{1 - \rho_1}, \tag{8}$$

- for direction 2

$$P_2 = \frac{\Delta_2}{1 - \rho_2}. \tag{9}$$

In this case, the total congestion of both directions of the equivalent unsignalized intersection will be determined as the sum of Equations (6) and (7)

$$\rho = \rho_1 + \rho_2 \tag{10}$$

and the total intensity of vehicles approaching to an unsignalized intersection of equivalent directions is:

$$\lambda = \lambda_1 + \lambda_2. \tag{11}$$

Using Equations (10) and (11), will make it possible to determine the average passing time of the dynamic dimensions of a vehicle across an equivalent unsignalized intersection in Equation (12) and the average duration of the loaded period when vehicles cross a two-way intersection in Equation (13):

$$\Delta = \frac{\rho}{\lambda}, \tag{12}$$

$$P = \frac{\Delta}{1-\rho}. \tag{13}$$

If the total intensity of vehicles approaching to an unsignalized intersection of equivalent directions is known, it becomes possible to determine the average free time If the total intensity of vehicles approaching to an unsignalized intersection of equivalent directions is known, it becomes possible to determine the average free time:

$$T_0 = \frac{1}{\lambda}. \tag{14}$$

The average passing time of vehicles from each of the equivalent directions of an unsignalized intersection is determined based on the values of the average duration of the loaded period for vehicles crossing the intersection:

- for direction 1

$$T_1 = \frac{P_1}{P_1 + P_2} P, \tag{15}$$

- for direction 2

$$T_2 = \frac{P2}{P_1 + P_2} P. \tag{16}$$

Here is used an assumption of the stationary flow of vehicles approaching to an unsignalized intersection. It follows that a vehicle arriving at an unsignalized intersection can get into three probable states:
{0} - free intersection;
{1} - the intersection is loaded with vehicles moving from the first direction;
{2} - the intersection is loaded with vehicles moving from the second direction.

Taking into account this fact, the stationary probability of an arriving vehicle getting into the corresponding state will be determined as:

$$p_i = \frac{T_i}{T_0 + T_1 + T_2}. \tag{17}$$

Given the assumption stated in the work, as well as taking into account the equation for calculating the average waiting time of Zilbertal [44], the conditional average delay time of vehicles of the *i*-th direction got into the delay state can be defined from Equation (18):

$$T_i^O = \frac{B_i}{2T_i}, i = 1.2, \tag{18}$$

where:
B_i is the second moment of the loaded period of passing the *i*-th direction of an unsignalized intersection (the mathematical expectation of a squared random variable).

Within the limits of this work, the second moment of the loaded period of passing in each direction is calculated as:

- for direction 1

$$B_1 = \frac{\Delta_1^2}{(1-\rho_1)^3}, \tag{19}$$

- for direction 2

$$B_2 = \frac{\Delta_2^2}{(1-\rho_2)^3}. \tag{20}$$

The average vehicle delay for each equivalent direction of an unsignalized intersection is calculated based on Equations (17) and (18):

- for direction 1
-

$$W_1 = p_2 T_2^O = p_2 \frac{B_2}{2T_2} = \frac{B_2}{2(T_0 + T_1 + T_2)} = \\ = \frac{\frac{\Delta_2^2}{(1-\rho_2)^3}}{2(T_0 + T_1 + T_2)}, \tag{21}$$

- for direction 2

$$W_2 = p_1 T_1^O = p_1 \frac{B_1}{2T_1} = \frac{B_1}{2(T_0 + T_1 + T_2)} = \\ = \frac{\frac{\Delta_1^2}{(1-\rho_1)^3}}{2(T_0 + T_1 + T_2)}. \tag{22}$$

In turn, the average vehicle delay at an unsignalized intersection of equivalent directions can be calculated as:

$$W = \frac{\lambda_1 W_1 + \lambda_2 W_2}{\lambda_1 + \lambda_2}. \tag{23}$$

4.2 Unsignalized intersection with non-equivalent directions (relative priority)

The first direction has a relative priority compared to the second direction (allowing them to complete the movement of a vehicle arriving at the intersection from the second direction).

The approach to determining the vehicle delays at an unsignalized intersection with non-equivalent directions and the assumption that the flow of vehicles approaching the intersection is stationary is identical as for the case 4.1. The main difference is the consideration of vehicles manoeuvring at unsignalized intersections with relative priority. So, the average delay for vehicles of the main (first) direction is calculated as follows:

$$W_1 = \frac{\lambda_1 \Delta_1^2}{2(1-\rho_1)}. \tag{24}$$

The average delay of the secondary (second) direction vehicles is calculated as a matter of necessity for the mandatory passing of vehicles moving along the main (first) direction:

$$W_2 = \frac{\lambda_1 \Delta_1^2 + \lambda_2 \Delta_2^2}{2(1-\rho_1)(1-\rho_1-\rho_2)}. \tag{25}$$

Additionally, the average vehicle delay at an unsignalized intersection with non-equivalent directions is calculated similarly to Equation (23).

5 The field study results of transport delays at unsignalized intersections

The developed approach for determining delays at unsignalized intersections was tested on the example of two T-junctions with a relative priority (unsignalized intersection with non-equivalent directions), where the delay was determined for vehicles performing a left turn from a minor road. To obtain the initial data (traffic intensity in directions, passing the time of the dynamic dimensions, the actual time of vehicle delay) for calculating vehicle delays, video monitoring of traffic flows was carried out at unsignalized intersections in Kharkiv: Les Serdyuk St. -Novo-Solonetskaya St. and Saltovskoye Shosse St. - 7th Gvardeyska Army St.

Video monitoring was organized in such a way as to have the possibility to record vehicle movement in all directions. Current traffic monitoring was carried out in the morning peak period (7.30 - 8.30 a.m.) on weekdays (from Monday up to and including Friday). As a result of processing the field study materials of traffic at selected intersections, the average values of traffic intensity for the morning peak period on weekdays have been defined. The results are shown in Figure 1.

Based on the results of traffic studies at selected intersections, the average values of the actual vehicle delay, when performing the left turn from a minor road, are determined: it is 37.9 s for the intersection of Les Serdyuk St. -Novo-Solonetskaya St., it is 27.3 s for the intersection of Saltovskoye Shosse St. - 7th Gvardeyska Army St.

Based on the obtained values of the traffic flow intensity and passing time of vehicle dynamic dimensions, the delay values for vehicles performing the left turn from a minor road are calculated using Equations (6) - (20), (24), (25) (direction 2-3, Figure 1). Thus, the estimated delay values for vehicles performing a left turn from a minor road are 34.2 s for the intersection of Les Serdyuk St. -Novo-Solonetskaya St. and 24.8 s for the intersection of Saltovskoye Shosse St. - 7th Gvardeyska Army St.

Estimating accuracy of calculation for average values of transport delays, defined with designed analytical models is carried out by their comparison to empirical delay values of vehicles performing a maneuver to turn left from the secondary road. For both unsignalized intersections selected as objects of experimental studies,

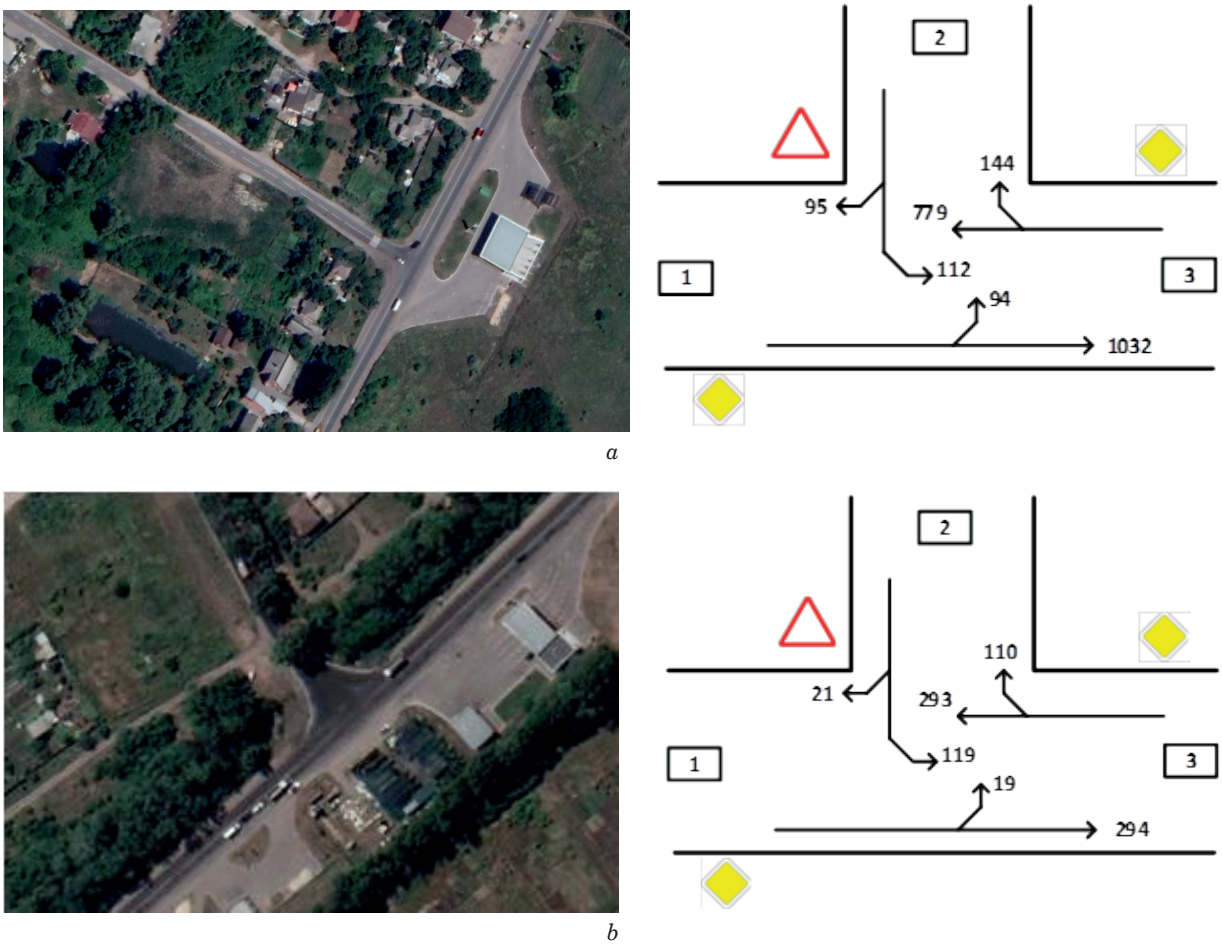

Figure 1 *The cartogram of vehicle traffic intensity: a - the intersection of Les Serdyuk St. -Novo-Solonetskaya St. b - the intersection of Saltovskoye Shosse St. - 7th Gvardeyska Army St.*

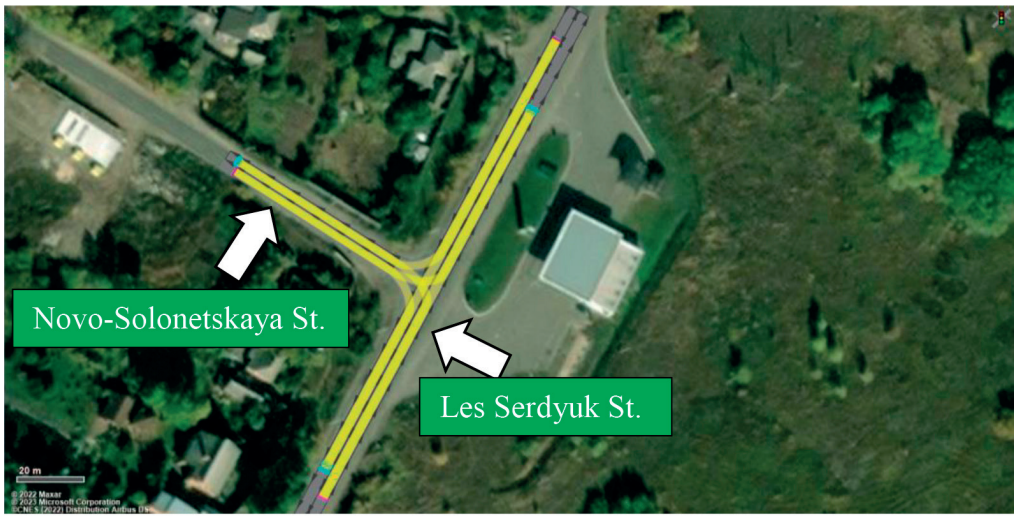

Figure 2 *Visualization of Vehicle Routes at Les Serdyuk St. Intersection - Novo-Solonetskaya St. using VISSIM*

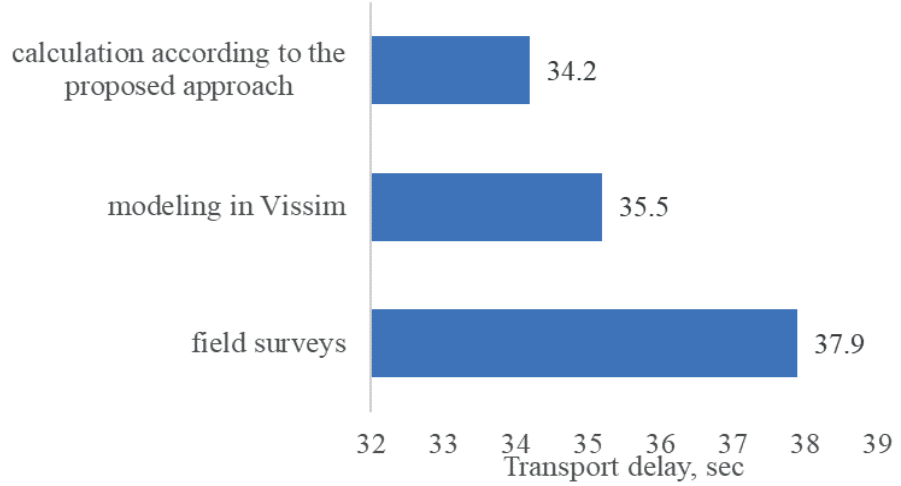

Figure 3 *Results comparison of calculating vehicle delays turning left from the minor road to the main traffic direction at unsignalized intersections Les Serdyuk St. - Novo-Solonetskaya St.*

the average relative deviation does not exceed 10 %: for the intersection Les Serdyuk St. -Novo-Solonetskaya St. - 9.8 %; for the intersection Saltovskoye Shosse St. - 7th Gvardeyska Army St. - 9.2 %. The obtained results indicate a relatively high accuracy of modelling the transport delays at unsignalized intersections using designed analytical models and the possibilities of their application in practice.

6 Discussing the study results of transport delays at unsignalized intersections

Currently, the main way to represent the traffic flow is through traffic simulation on streets and highways. In this study, VISSIM was used to evaluate the proposed analytical models for determining delays at unsignalized intersections and to assess the effect of increasing the traffic intensity on main and minor roads on its value. For the unsignalized intersection Les Serdyuk St. - Novo-Solonetskaya St., a simulated traffic model was designed according to the following data (Figure 2):

- traffic flow intensity - average weekdays peak values are considered (Figure 1);
- traffic composition: on the main road (Les Serdyuk St.) - cars 94 %, trucks (lorries) 5 %, buses 1 %; by minor road (Novo-Solonetskaya St.) - cars 98 %, trucks (lorries) 2 %;
- permitted speed - up to 50 km/h;
- overall vehicle dimensions - cars: length up to 5 m; width up to 2.1 m; trucks: length up to 11 m; width up to 2.5 m; buses: length up to 12 m, width up to 2.5 m.

According to the simulation results, the average delay values of vehicles turning left from the minor road to the main road and general delays at the intersection were set. The results confirm the preliminary conclusion on a sufficiently high accuracy of delay calculation based on the proposed analytical models (Figure 3). It should also be noted that the deviation of the results

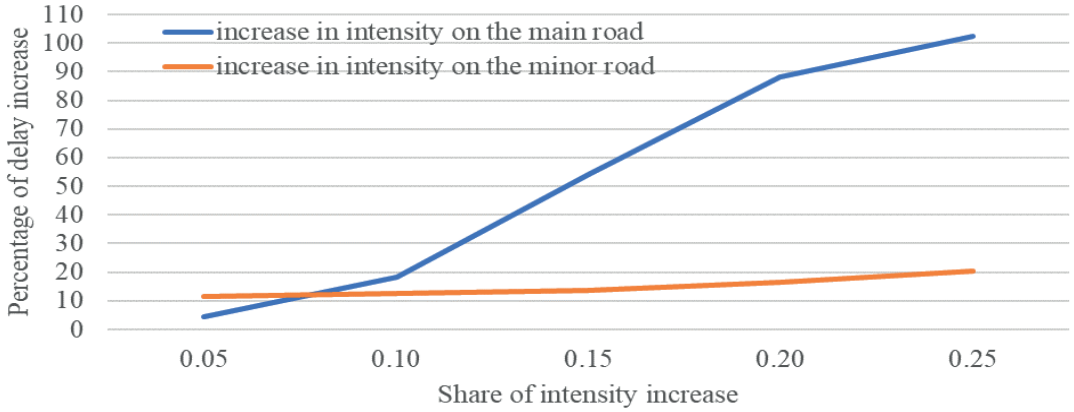

Figure 4 *Effect characterization of traffic intensity change on average vehicle delays turning left from Novo-Solonetskaya St. to Les Serdyuk St.*

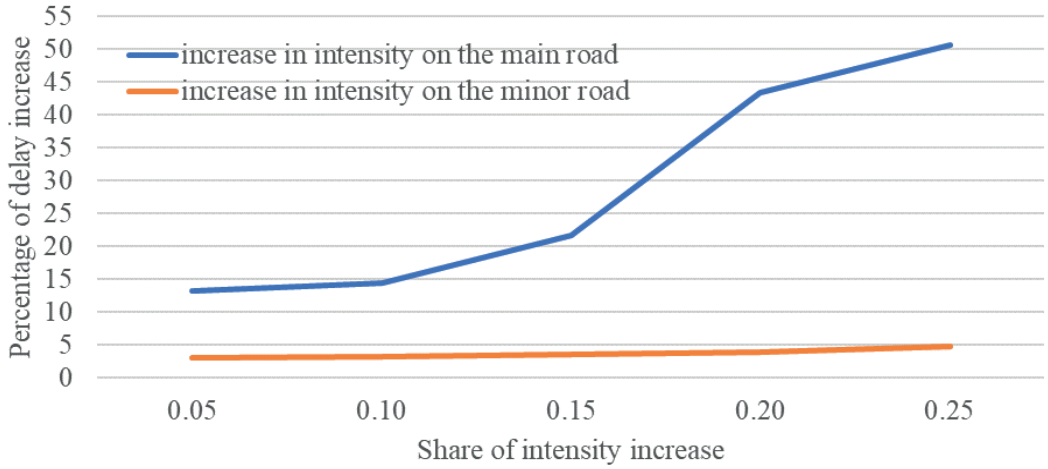

Figure 5 *Effect characterization of traffic intensity change on values of total vehicle delays at unsignalized intersections Les Serdyuk St. - Novo-Solonetskaya St.*

in calculating delay average values of vehicles turning left from the minor road to the main traffic direction obtained using Vissim (35.2 s) from their empirical value (37.9 s) is about 7 %. This percentage characterizes the obtained transport model as suitable for the initial assessment of traffic terms at unsignalized intersections and for providing a simulation experiment.

A good opportunity is having a simulation model at one's disposal. It helps to study the nature of impact of the amount traffic intensity changing in different directions on delay values at selected unsignalized intersections. This study analyzed the effect in traffic volumes changes (increase in intensity from 5 % to 25 %) separately on the main and secondary roads on vehicle delays turning left from the minor road to the main one (Figure 4) and total delays (Figure 5).

The obtained data indicate a significant impact on delay values in traffic intensity in the main direction (main road). This influence is especially noticeable with an increase in intensity on the main road by more than 10-15 %. With a further increase in intensity, the appearance of congestion is observed.

It should be noted that factors affecting the transport delay value quantity at unsignalized intersections and which researchers are actively using are the next: intersection geometry, traffic intensity, dynamic vehicle characteristics, traffic composition (most often represented through freight transport share), pedestrian traffic intensity (if pedestrian crossings are within the intersection), as well as drivers' behavior. Analytical models, based on the proposed approach for determining delays at unsignalized intersections, consider most of the above factors. They can be used to preliminary assess the traffic conditions at unsignalized intersections.

It should be added that when calculating delays from designed analytical models, empirical data on passage time of intersection vehicles were used (averages: the main road is 2 s; the minor road is 8 s), characterizing the specific intersections and specific time periods during which it was recorded, which may affect calculation accuracy of the transport delays under other conditions and other unsignalized intersections. To improve the calculation accuracy of transport delays according to designed analytical models, it is necessary to consider the stochastic characteristics of parameters for process variables during appropriate maneuvers implementation (mergers, crossing) at unsignalized intersections. With this parameter, a critical time

interval can be chosen between cars (critical gap), which can be determined by several approaches [24, 45-49].

Given the traffic management similarity at unsignalized intersections and exits from adjacent areas to city highways, it is advisable to consider the possibility of adapting designed analytical models for determining the transport delays at entrances (exits) from such urban road network elements.

7 Conclusions

The analysis results of current methods for estimating transport delays at unsignalized intersections indicate the limited capabilities of models based on empirical data and a relatively low accuracy of calculations using analytical models.

The developed approach to determine delays at unsignalized intersections is based on the principles of a queuing system, considering the priority of traffic in competing directions.

The findings of evaluating the accuracy of calculating the delays of vehicles performing a left turn from a minor road using developed analytical models, at selected unsignalized intersections, indicate their reliability and objectivity (divergence is not higher than 10 %), as well as the possibility of their use for preliminary assessment of traffic conditions at unsignalized intersections. The traffic simulation results in Vissim confirm the high accuracy of the delay calculation using the proposed approach.

Improvement of the proposed analytical models is possible by considering probabilistic components in them, when drivers perform appropriate maneuvers on main and minor roads at acceptable limit intervals (critical gap).

It is necessary to conduct additional real-field traffic observations to obtain a complete and accurate assessment of actual vehicle delays at selected intersections. It allows for obtaining a larger data array, determining the trip times of dynamic vehicle dimensions of different types while fulfilling various maneuvers in all the possible traffic directions.

Acknowledgment

The research was partially carried out within the project "Digital twin framework for cellular manufacturing systems: design and simulation" of The NAWA Ulam Programme (grant number BPN/ULM/2022/1/00045). The research was partially supported by the International Association for Technological Development and Innovations.

Conflict of Interest

The authors declare that they have no known competing financial interests or personal relationships that could have appeared to influence the work reported in this paper.

References

[1] TAPIO LUTTINEN, R. *Capacity and level of service at Finnish unsignalized intersections*. Finnra Reports 1/2004, Helsinki: Finnish Road Administration, Traffic Engineering, 2004. ISBN 951-803-180-0, ISSN 1457-9871.

[2] AHMED, A., SADULLAH, A. F. M., YAHYA, A. S. Analysis of the effect of directional traffic volume and mix on road traffic crashes at three-legged unsignalized intersections. *Transportation Engineering* [online]. 2021, **3**, 100052. ISSN 2666-691X. Available from: https://doi.org/10.1016/j.treng.2021.100052

[3] ZHANG, X., YAN, X. Predicting collision cases at unsignalized intersections using EEG metrics and driving simulator platform. *Accident Analysis and Prevention* [online]. 2023, **180**, 106910. ISSN 0001-4575. Available from: https://doi.org/10.1016/j.aap.2022.106910

[4] JENA, S., PATRO, S., DUTTA, M., BHUYAN, P. K. Assessment of service quality at unsignalized intersections using traffic simulation and computational intelligence. *Transportation Letters. The International Journal of Transportation Research* [online]. 2022, **14**(4), p. 365-377. ISSN 1942-7867, eISSN 1942-7875. Available from: https://doi.org/10.1080/19427867.2020.1868179

[5] POHUDINA, O., MORIKOVA, A., HAIDABRUS, B., KIYKO, S., DRUZHININ, E. Comparison of metoheuristic search methods for the task of choosing a rational set of measures to risks' respond. In: *Integrated computer technologies in mechanical engineering - 2020. ICTM 2020* [online]. NECHYPORUK, M., PAVLIKOV, V., KRITSKIY, D. (eds.). Lecture Notes in Networks and Systems. Vol. 188. Cham: Springer, 2021. ISBN 978-3-030-66716-0, eISBN 978-3-030-66717-7, p. 657-666. Available from: https://doi.org/10.1007/978-3-030-66717-7_56

[6] KIYKO, S. G., DRUZHININ, E. A., KOBA, S. A., HAIDABRUS, B. V. A mathematical background for information technology of project's processes integration taking into account risk factors. *Metallurgical and Mining Industry*. 2014, **6**(3), p. 66-70. ISSN 2076-0507.

[7] KREMENETS, Y., PECHERSKIY, M. *Technical means of road traffic control / Tekhnicheskie sredstva regulirovaniya dorozhnogo dvizheniya* (in Russian). Moskow: Transport, 1981.

[8] KREMENETS, Y., PECHERSKIY, M., AFANASEV, M. *Technical means of road traffic management / Tekhnicheskie sredstva organizatsii dorozhnogo dvizheniya* (in Russian). Moskow: Akademkniga, 2005. ISBN 5-94628-111-9.

[9] KUNITSYA, O., ZAKABLUK, O. Determination of the real traffic delay at unsignalized intersections in one level/ Viznachennya diysnoi transportnoi zatrimki na neregulovanikh perekhrestyakh v odnomu rivni (in Ukrainian). *Bulletin of Kharkov National Automobile and Highway University / Visti Avtomobilno-Dorozhnogo Universitetu*. 2009, **2**(9), p. 46-51. ISNN 1990-7796.

[10] UDZHUKHU, A., LABUTIN, A. Application of methods for calculation of traffic delays in practice/Primenenie metodik rascheta transportnykh zaderzhek na praktike (in Ukrainian). *Bulletin of the Donetsk Academy of Automobile Transport / Vestnik Donetskoy Akademii Avtomobilnogo Transporta*. 2018, **3**, p. 34-40. ISSN 2219-8180, eISSN 2518-7899.

[11] LEVASHEV, A., MIKHAYLOV, A., GOLOVNYKH, I. *Designing regulated intersections / Proektirovanie reguliruemykh peresecheniy* (in Russian). Irkutsk: IrGTU, 2007. ISBN 978-5-8038-0458-1.

[12] TANNER, J. A Theoretical analysis of delays at an uncontrolled intersection. *Biometrika* [online]. 1962, **49**(1/2), p. 163-170. eISSN 1464-3510. Available from: https://doi:10.1093/biomet/49.1-2.163

[13] KIMBER, R., HOLLIS, E., MARLOW, M. Flow/delay relationships for major/minor priority junctions. *Traffic Engineering and Control*. 1977, **18**(11), p. 516-519. ISSN 0041-0683.

[14] KIMBER, R., HOLLIS, E. *Traffic queues and delays at road junctions*. Wokingham, Berkshire United Kingdom; Transport and Road Research Laboratory, 1979. ISSN 0266-7045.

[15] TROUTBECK, R. J. Average delay at an unsignalized intersection with two major streams each having a dichotomized headway distribution. *Transportation Science* [online]. 1986, **20**(4), p. 272-286. ISSN 0041-1655, eISSN 1526-5447. Available from: https://doi: 10.1287/trsc.20.4.272. 1986

[16] HEIDEMANN, D. Queue length and waiting-time distributions at priority intersections. *Transportation Research Part B: Methodological* [online]. 1991, **25**(4), p. 163-174. ISSN 0191-2615, eISSN 1879-2367. Available from: https://doi.org/10.1016/0191-2615(91)90001-Y

[17] KYTE, M., CLEMON, C., MAHFOOD, N., LALL, B. K., KHIST, C. J. Capacity and delay characteristics of two-way stop-controlled intersections. *Transportation Research Record* [online]. 1991, **1320**, p. 160-167. ISSN 0361-1981. Available from: https://onlinepubs.trb.org/Onlinepubs/trr/1991/1320/1320-020.pdf

[18] HOROWITZ, A. J. Revised queueing model of delay at all-way stop-controlled intersections. *Transportation Research Record* [online]. 1993, **1398**, p. 49-53. ISSN 0361-1981. Available from: https://onlinepubs.trb.org/Onlinepubs/trr/1993/1398/1398-007.pdf

[19] MADANAT, S. M., CASSIDY, M. J., WANG, M. H. Probabilistic delay model at stop-controlled intersection. *Journal of Transportation Engineering* [online]. 1994, **120**(1), p. 21-36. ISSN 0733-947X, eISSN 1943-5436. Available from: https://doi.org/10.1061/(ASCE)0733-947X(1994)120:1(21)

[20] AKCELIK, R., CHRISTENSEN, B., CHUNG, E. A comparison of three delay models for sign-controlled intersections. In: 3rd International Symposium on Highway Capacity: proceedings. Vol. 1. 1998. ISBN 8774919059, p. 35-56.

[21] NIELSEN, O. A., FREDERIKSEN, R. D., SIMONSEN, N. Stochastic user equilibrium traffic assignment with turn-delays in intersections. *International Transactions in Operational Research* [online]. 1998, **5**(6), p. 555-568. eISSN 1475-3995. Available from: https://doi.org/10.1111/j.1475-3995.1998.tb00137.x

[22] AL-OMARI, B., BENEKOHAL, R. F. Hybrid delay models for unsaturated two-way stop-controlled intersections. *Journal of Transportation Engineering* [online]. 1999, **125**(4), p. 291-296. ISSN 0733-947X, eISSN 1943-5436. Available from: https://doi.org/10.1061/(ASCE)0733-947X(1999)125:4(291)

[23] KAYSI, I., ALAM, G. Driver behavior and traffic stream interactions at unsignalized intersections. *Journal of Transportation Engineering* [online]. 2000, **126**(6), p. 498-505. ISSN 0733-947X, eISSN 1943-5436. Available from: https://doi.org/10.1061/(ASCE)0733-947X(2000)126:6(498)

[24] LIUBYI, Y., BIELETSKA, O. Experimental research of traffic delays at the adjacent territory exit. *Advances in Mechanical Engineering and Transport* [online]. 2021, **1**(16), p. 106-116. ISSN 2313-5425. Available from: https://doi.org/10.36910/automash.v1i16.513

[25] MUSTAFAYEV H., GETSOVICH, E. Experimental investigation of the driver's behavior at uncontrolled intersections in cross traffic flows. *Automobile Transport* [online]. 2018, **48**, p. 98-102. ISSN 2219-8342, eISSN 2309-981X. Available from: https://doi.org/10.30977/AT.2219-8342.2018.42.0.98

[26] ADVANI, M., GUPTA, N. J., VELMURUGAN, S., MADHU, E., CHANDRA, S. Defining and analyzing forceful gap behavior at unsignalized intersections. *Transportation Research Record: Journal of the Transportation Research Board* [online]. 2020, **2674**(8), p. 420-428. ISSN 0361-1981, eISSN 2169-4052. Available from: https://doi.org/10.1177/0361198120925258

[27] ARAMITA, B. A., MAIMUNAH, S., PURWANTO, E., TOHOM, F. Evaluation of driver behavior when crossing unsignalized intersection from minor road to major road. *RSF Conference Series: Engineering and Technology*

[online]. 2022, **2**(2), p. 109-118. ISSN 2809-6878, eISSN 2809-6843. Available from: https://doi.org/10.31098/cset.v2i2.564

[28] TIAN, Z. Z., KYTE, M., VANDEHEY, M., KITTELSON, W., ROBINSON, B. Simulation-based study of traffic operation characteristics at all-way-stop-controlled intersections. *Transportation Research Record: Journal of the Transportation Research Board* [online]. 2001, **1776**(1), p. 75-81. ISSN 0361-1981, eISSN 2169-4052. Available from: https://doi.org/10.3141/1776-10

[29] LUTTINEN, R. T. Movement capacity at two-way stop-controlled intersections. *Transportation Research Record: Journal of the Transportation Research Board* [online]. 2004, **1883**(1), p. 198-202. ISSN 0361-1981, eISSN 2169-4052. Available from: https://doi.org/10.3141/1883-23

[30] CVITANIC, D., BRESKI, D., VIDJAK, B. Review, testing and validation of capacity and delay models at unsignalized intersections. *Promet - Traffic and Transportation* [online]. 2007, **19**(2), p. 71-82. ISSN 0353-5320, eISSN 1848-4069. Available from: https://traffic.fpz.hr/index.php/PROMTT/article/view/937

[31] BRILON, W. Delay at unsignalized intersections. *Transportation Research Record: Journal of the Transportation Research Board* [online]. 2008, **2071**(1), p. 98-108. ISSN 0361-1981, eISSN 2169-4052. Available from: https://doi.org/10.3141/2071-12

[32] CHANDRA, S., AGRAWAL, A., RAJAMMA, A. Microscopic analysis of service delay at uncontrolled intersections in mixed traffic conditions. *Journal of Transportation Engineering* [online]. 2009, **135**(6), p. 323-329. ISSN 0733-947X, eISSN 1943-5436. Available from: https://doi.org/10.1061/(ASCE)0733-947X(2009)135:6(323)

[33] TRB Transportation Research Board of the National Academies. *HCM2010 - Highway Capacity Manual*. *Vol. 3: Interrupted flow*. USA: National Academy of Sciences, 2010. ISBN 0-309-06681-6.

[34] BRILON, W. Average delay at unsignalized intersections for periods with variable traffic demand. *Transportation Research Record: Journal of the Transportation Research Board* [online]. 2015, **2483**(1), p. 57-65. ISSN 0361-1981, eISSN 2169-4052. Available from: https://doi.org/10.3141/2483-07

[35] CALIENDO, C. Delay time model at unsignalized intersections. *Journal of Transportation Engineering* [online]. 2014, **140**(9), p. 1-13. ISSN 0733-947X, eISSN 1943-5436. Available from: https://doi.org/10.1061/(ASCE)TE.1943-5436.0000696

[36] MOHAMMAD, M. A., PUAN, O. B. Traffic delay estimation using artificial neural network (ANN) at unsignalized intersections. In: 3rd International Conference on Civil, Structural and Transportation Engineering ICCSTE'18: proceedings [online]. 2018. Paper 106. Available from: https://doi.org/10.11159/iccste18.106

[37] TURNER, S., FITZPATRICK, K., BREWER, M., PARK, E. S. Motorist yielding to pedestrians at unsignalized intersections: findings from a national study on improving pedestrian safety. *Transportation Research Record* [online]. 2006, **1982**(1), p. 1-12. ISSN 0361-1981, eISSN 2169-4052. Available from: https://doi.org/10.1177/0361198106198200102

[38] TOWHIDUL, I., SHISHIR KUMAR, S. A., S M RAHAT, R., SUDIPTA, B. Road crossing behavior of pedestrians at unsignalized intersection under mixed traffic condition. In: 2nd International Conference on Research and Innovation in Civil Engineering ICRICE-2020: proceedings. 2020. Paper ID 123. Available from: http://surl.li/gracy

[39] MORENO, E., DENNY, P., WARD, E., HORGAN, J., EISING, C., JONES, E., GLAVIN, M., PARSI, A., MULLINS, D., DEEGAN, B. Pedestrian crossing intention forecasting at unsignalized intersections using naturalistic trajectories. *Sensors* [online]. 2023, **23**(5):2773. eISSN 1424-8220. Available from: https://doi.org/10.3390/s23052773

[40] PERISA, M., CVITIC, I., PERAKOVIC, D., HUSNJAK, S. Beacon technology for real-time informing the traffic network users about the environment. *Transport* [online]. 2019, **34**(3), p. 373-382. ISSN 1648-4142, eISSN 1648-3480. Available from: https://doi.org/10.3846/transport.2019.10402

[41] PERAKOVIC, D., PERISA, M., SENTE, R. E., ZORIC, P., BUCAK, B., IGNJATIC, A., MISIC, V., VULETIC, M., BIJELICA, N., BRLETIC, L., PAPAC, A. Smart wristband system for improving quality of life for users in traffic environment. smart technology trends in industrial and business management. In: *Smart Technology Trends in Industrial and Business Management. EAI/Springer Innovations in Communication and Computing* [online]. CAGANOVA, D., BALOG, M., KNAPCIKOVA, L., SOVIAR, J., MEZARCIOZ, S. (eds.). Cham: Springer, 2019. ISBN 978-3-319-76997-4, eISBN 978-3-319-76998-1, p. 429-450. Available from: https://doi.org/10.1007/978-3-319-76998-1_32

[42] BARI, C. S., GUNJAL, T. V., DHAMANIYA, A. A simulation approach for evaluating congestion and its mitigation measures on urban arterials operating with mixed traffic conditions. *Communications - Scientific letters of the University of Zilina* [online]. 2022, **24**(3), p. D126-D140. ISSN 1335-4205, eISSN 2585-7878. Available from: https://doi.org/10.26552/com.C.2022.3.D126-D140

[43] KALASOVA, A., CERNICKY, L., KUBIKOVA, S. Microscopic Simulation of coordinated route in the city of Zilina. *Communications - Scientific letters of the University of Zilina* [online]. 2014, **16**(2), p. 46-50. ISSN 1335-4205, eISSN 2585-7878. Available from: https://doi.org/10.26552/com.C.2014.2.46-50

[44] ZILBERTAL, A. *Tram economy / Tramvaynoe khozyaystvo* (in Russian). Moscow: Gostransizdat, 1932.
[45] KOCIANOVA, A. The capacity limits of roundabouts. *Communications - Scientific letters of the University of Zilina* [online]. 2014, **16**(4), p. 81-86. ISSN 1335-4205, eISSN 2585-7878. Available from: https://doi.org/10.26552/com.C.2014.4.81-86
[46] KOCIANOVA, A., PITLOVA, E. Critical gaps at unsignalized intersections with bending right-of-way. *Communications - Scientific letters of the University of Zilina* [online]. 2018, **20**(4), p. 69-75. ISSN 1335-4205, eISSN 2585-7878. Available from: https://doi.org/10.26552/com.C.2018.4.69-75
[47] CELKO, J., KOVAC, M., HUSZAROVA, K. Influence of selected vehicle manoeuvres on reduction of the urban roads capacity. *Communications - Scientific letters of the University of Zilina* [online]. 2019, **21**(4), p. 81-89. ISSN 1335-4205, eISSN 2585-7878. Available from: https://doi.org/10.26552/com.C.2019.4.81-89
[48] BHATT, K., SHAH, J. Reckoning level of risk and severity (LORS) based on the gap acceptance at a three-legged uncontrolled intersection of a rural highway. *Communications - Scientific letters of the University of Zilina* [online]. 2023, **25**(1), p. F1-14. ISSN 1335-4205, eISSN 2585-7878. Available from: https://doi.org/10.26552/com.C.2023.013
[49] BAGHERI, M., BARTIN, B., OZBAY, K. Simulation of vehicles' gap acceptance decision at unsignalized intersections using SUMO. *Procedia Computer Science* [online]. 2022, **201**, p. 321-329. ISSN 1877-0509. Available from: https://doi.org/10.1016/j.procs.2022.03.043

This is an open access article distributed under the terms of the Creative Commons Attribution 4.0 International License (CC BY 4.0), which permits use, distribution, and reproduction in any medium, provided the original publication is properly cited. No use, distribution or reproduction is permitted which does not comply with these terms.

ECONOMIC ASSESSMENT OF TRANSPORT MOVEMENTS OF THE URBAN POPULATION IN AGGLOMERATIONS

Denis Kapski, Vasili Kuzmenko, Liudmila Khmelnitskaya*

Automotive and Tractor Faculty, Belarusian National Technical University, Minsk, Republic of Belarus

*E-mail of corresponding author: millakhmelnitskaya@gmail.com

Denis Kapski 0000-0001-9300-3857, Vasili Kuzmenko 0000-0002-4248-415X,
Liudmila Khmelnitskaya 0000-0002-0400-5453

Resume

The article deals with the problem of estimating criteria of the road traffic quality used in domestic (Belarus) and foreign research works. Each separate property of the road traffic, as well as their entire set - the so-called "quality", can be assessed by means of losses - the smaller the loss is, the better the property and the higher the quality are. Evaluation using losses, which are expressed in money, is very convenient and clear, since it allows comparing contradictory properties of road traffic not only the each other, but the costs' expenses involved in their improving, as well. The value of the costs estimate of the time spent by a user in the process of travelling has not been officially established and is the subject of research. The proposed methodology makes it possible to assess, not only the quality of the road traffic in general, but its main components, as well, for example, traffic management or road conditions. It has been proved by methodology implementation findings on the streets in Minsk.

Article info

Received 26 January 2023
Accepted 22 May 2023
Online 26 June 2023

Keywords:

road traffic
transport system
time of travelling

Available online: https://doi.org/10.26552/com.C.2023.053

ISSN 1335-4205 (print version)
ISSN 2585-7878 (online version)

1 Introduction

The problems of motorization are relevant for many countries, including Belarus, where, according to expert data, the road transport currently provides more than 70 % of the volume of passenger traffic and more than 74.5 % of the volume of freight traffic and the high social importance of passenger road transport is due to the fact that it provides 85 % of work trips in cities. In the urban passenger transport system, the key participant is the resident facing the need to commute [1]. Human activity is determined by the presence of many alternatives of travelling (the ability to choose the method and route of transport), as well as the target function (minimization of costs associated with travelling, quality of transportation/trip). The choice of people is determined not only by the costs and time of travel, it also depends on reliability of transportation provided.

It should be noted that the use of individual means of mobility changes the structure of road traffic, redistributes passenger traffic in favour of a new type of traffic. It allows reducing the intensity of using car traffic and public transport, unclog the road network and increase the speed of traffic flow, improve the qualitative characteristics of public transport, reduce the so-called haulage time and to increase the efficiency of its use, to improve the overall road safety. The variability of the duration of a trip is peculiar to all the types of transport, although it is most clearly manifested in the urban road transport. It often results in significant additional time spending for the population. At the same time, there are still no methods allowing conducting a comprehensive economic assessment of the costs associated with the time of travelling by urban public transport. It is obvious that implementation of measures and projects to improve the work of urban public transport and to develop the transport infrastructure and traffic conditions in cities causes changes in the conditions of the land transport movement and directly affects the time spent by users of the urban public transport for travelling. Accordingly, the reduction in total travel time leads to the possibility of using the resulting savings in a more efficient way. Thus, one can say that the travel time is for the most part an overhead time in a person's life. Hence, there is an interest in minimizing the time spent on transport movements in cities.

Currently, it is necessary to develop a methodology for assessing the costs associated with the time of travel

by urban passenger transport and the reliability of the urban transport system. This will provide an adequate assessment of the effectiveness of investments in the implementation of projects to organize the road traffic and improve the work of urban transport systems.

Losses can be used to evaluate both the individual characteristics of road traffic as well as the overall collection of those characteristics, or so-called "quality"; the smaller the loss, the better the characteristic and the higher the quality are [1-2]. Evaluation using losses that are expressed in money is very practical and straightforward since it enables comparison of opposing characteristics of road traffic not only to one another but also to the costs associated with their improvement. [3]. Obviously, when assessing the quality of the road traffic, those costs must be compared that cover all the aspects of the urban transport system.

The value of the loss costs estimates of the time unit by the user in the process of travelling has not been officially established and is the subject of research. The proposed methodology makes it possible to assess not only the quality of the road traffic in general, but its main components, as well, for example, the traffic management or road conditions.

2 Literature review

The system of the road transport fulfils 2/3 of the total volume of transport services. 8-10 % of the working population is involved in the road traffic services. Each person deals with the road transport system for about one hour per day on average, it means they spend up to 7% of their active time. Consequently, the road transport together with the road traffic serve as one of the most important life-sustaining environmental systems in modern society [1-2].

Due to the gigantic scale and other peculiarities of the road traffic, even minor drawbacks in its work cause enormous losses in economic, environmental, safety and social spheres. As far as the shortfall in work of Belarusian road traffic is quite significant today, the losses are so great that they affect the development of the state and the population wellbeing.

According to the UNO report on studying urbanization prospects, about 66% of the planet population (6.5 B people) will live in cities by 2050. At the same time, according to the World Bank, 80% of gross domestic product is generated by cities, they are the heart of economic and social interaction [2, 4]. Transport systems play a crucial role in the development of urban areas, as they are an important component of Public Economics: transport systems ensure the mobility of the population, expand trade and business opportunities. Transport increases the competitive ability of cities, improves the economic environment of regions and living standards.

People's choice of transport is conditioned not only by financial and time losses, but by the comfort and safety of travelling, as well. The use of personal mobility devices changes the structure of travel, redistributes a passenger traffic flow in favour of a new means of travelling, enables to unload the road net and to increase the travelling speed of a traffic stream, to improve the qualitative indicators of public transport functioning. Personal mobility devices also makes possibility for reducing the so-called "transportation time" out of the common time budget and to advance the efficiency of their use, to improve the overall road traffic safety.

Increase in the number of personal cars causes traffic jams and boosts the number of car accidents. It brings on emissions of harmful substances and greenhouse gases into the atmosphere, increase in noise level. All of these deteriorates the road traffic quality as a whole.

Problems of motorizations are of great current interest for many countries, including Belarus. In the system of urban public transport, a city resident is a crucial participant who faces the necessity to commute. Person's activities are conditioned by many alternatives of travel (an opportunity to choose the means and routes of travel, type of vehicle), as well as by the target function (costs minimization connected with travelling, the quality of travelling) [5-7]. People's choice of transport is conditioned not only by financial and time losses, the comfort of travelling, but it depends on the safety of transportation. The variety in trip duration is unique to all modes of transportation, although it is most visible in urban road transportation. It frequently leads in significant extra time spent by the populace. At the same time, no tools exist for undertaking a full economic assessment of the expenditures connected with the time spent traveling by urban public transportation.

It is obvious that the implementation of measures and projects to improve the work of urban public transport and to develop the transport infrastructure affects the time spent by the users of urban public transport on travelling. The reduction in total travel time leads to the possibility of using the resulting savings in a more efficient way.

One must distinguish economic losses in road transport from those in the road traffic, though they are closely connected. Losses in the road transport system - are the total losses in all the subsystems, including the road traffic system. It is common knowledge that the road transport system includes such subsystems as roads, means of transport, automobile transportation, protection of rights, motorway service, personnel training, etc. In all of these subsystems great economic losses can be found, which are connected with the following:

- production prime costs (including service) - practically everywhere in Belarus due to the outdated equipment, faulty technologies, the quality of the labour force, transportation process expenses etc., the production prime costs are much higher

than in the mature developed economies;
- not the best possible decisions are made - there are not the best road locations, wrong location of fuel stations, prolonged time periods of construction, reconstruction or repair work, etc.;
- the second-rate reliability and short exploitation time period of the products used in the road transport infrastructure - technological machines and equipment, tools, training systems, etc.
- An important role is played by the quality of final products and services, which are produced in the road transport infrastructure, but they are revealed already in the process of travelling: the quality of roadway paving, of vehicles, of management systems, personnel training, etc. One can easily notice that the quality discussed, together with the faulty traffic process control, is one of the main causes of economic losses in the road traffic. Those losses are associated with optional expenses of the traffic process that are mostly of economic value. They are the following:
- delay (time loss) of transport through reducing the speed of movement or through an unwanted standstill in a street and road network;
- coming to a full standstill, which consists of such stages as putting on the brake, the standstill itself, starting the movement and accelerating;
- excess mileage in all of its forms;
- excess fuel consumption through an unfavourable brake-release mode;
- accelerated vehicle and road surface wear through an unfavourable brake-release mode;
- pedestrians' delay (time loss);
- pedestrians' excess mileage;
- delay of passengers (they are taken into account as a part of the delay and excess mileage of transport).

The list above discusses the so-called immediate expenses. However, there are also the mediate (direct) expenses such as, for example: loss of profit by traffic participants due to unplanned traffic delays, losses of profit in related sectors due to failure to deliver duties, loss of expected gain due to partial use of opportunities, etc. All of the above results in enormous economic losses.

All the processes in the road transport system can be roughly divided into two stages - preparation for travelling and the travelling process itself. During the first stage, all the necessary infrastructure is created: road construction and maintenance, production (or acquiring) and maintenance of vehicles, creation of management systems, personnel training, etc. At the second stage, passengers and cargo are relocated in the created conditions. Obviously, very significant expenses are required at the first stage - the so-called expenses in the infrastructure. Of no less importance are the expenses of the second stage - travel (relocation) expenses: time losses, fuel consumption, road and vehicle wear, emissions, car accidents, etc. And one more thing. Road traffic caters for all the spheres of our life, all the country's population takes part in it, our roads, streets and facilities are public ownership. For these reasons, transport maintenance costs are considered as public, whole-of-government, nationwide. That is why any loss in the transport system, regardless of the reason, consequences or casualties, is a national loss. As a result, any losses in the road transport or road traffic systems, regardless of the fact whether we know about them or not, turn out to be our own losses. Consequently, all of us are extremely interested in the decrease in these losses.

The notion "transport maintenance costs" has several meanings. In its first meaning, when we speak about the huge regional or national road transport systems, it usually denotes an overall costs taking into account all the components of the system. A noteworthy detail is that while choosing means of travelling, people assume not the physical time losses, but base on a psychological assessment of the travel duration. Therewith, the psychological assessment of travel duration is inadequate. For this reason, a notion of overhead (total) costs of time is usually used, which is obtained in view of weighing coefficients of a psychological assessment of travel duration. Such approach to calculations suggests that the coefficient value does not depend on the time period and travel conditions. Apart from the time period, the psychological assessment of travel duration is also influenced by individual psychological peculiarities of a person, his physical well-being and conditions of travelling [5, 8]. People can estimate actual time losses in an adequate way or not, over- or underestimate the value. It means that while choosing the technical and technological maintenance of transportation processes to get adequate results, one should take into account the combination of factors, which determine the time spent by the users of urban public transport on travel and influence the psychological assessment of its duration. The value of monetary estimate of a time unit loss while travelling is not discovered in Belarus yet. It is a subject for research. To sum it up, the travel time is mostly overhead time of a person's life. Therefore, it is of great interest to minimize the time losses while travelling around a city [5].

Value of Travel Time Savings (VTTS) is the most important factor in assessing the profitability of investments in transport infrastructure [9-11]. Becker [12] and DeSepra [13] were the first to find a solution in the field of economic theory of time assessment, drawing the dependence of time allocation on a consumer choice, based on utility maximization and taking into account the restrictions on income and the minimum time required to perform any actions. They used a variety of methods to assess people's preferences to pay for time savings. Where it was possible to observe behavioural patterns, for example, the choice of a mode of transport or route, as well as to track other random factors, ratings were derived based on the revealed preferences. The most commonly used methods are those of

Table 1 *Determination of VTTS valuation by different experts*

Source/Researcher	Value of Travel Time Savings (VTTS)		Remark
	For business and work trips	For educational/cultural/ personal (for recreation) trips	
Venables [18]	61% of the gross costs of hiring or 85% of the employee's gross salary		Applied to the French accounting system
Boiteux and Baumstark [19]	61% of the hourly costs of employment or 85% of the employee's gross wages	Recommends increasing VTTS by 50% with high occupancy of the interior of urban passenger transport and 100% when walking to the stopping point and waiting	Do approaches vary across groups defined by mode of transport, driver or passenger, or type of employment
Gwilliam [10]	133% of wages per hour (employer estimate)	33% - for adults, 15% - for children from household income per hour	Waiting/walking - 150% of the costs of the trip by urban passenger transport (for the transport organizations the costs consist of the hourly costs of operating the vehicle, the driver's wages per hour and the costs of using the infrastructure)
Mackie and Worsley [14]		90% of the value for commuting and back	For time spent "forced" commuting to and from work – 25% of the average for Labour and business travel

stated preferences, which use questionnaires to identify a hypothetical choice of a travel option that varies in several dimensions. This approach enables a researcher to take into account a number of behavioural alternatives and independent variables.

Most studies use discrete choice technologies (choice from a finite set of alternatives), for example, logistic analysis to assess parameters that affect the choice of a particular mode of transport or route. As the number of published studies was growing, some researchers also began using the meta-analysis to assess the reasons for the variation in results of individual studies [1, 5]. Value of Travel Time studies conducted in the United States have found that the value of business travel time is often set equal to the gross hourly costs of working hours, including payroll taxes and fringe benefits. Some studies have found that the time value for car users is lower than for drivers and the time value for shopping travel or recreation trips is lower than that for commuting.

In the UK, as seen from the work by Mackie et al. and from the UK Transport Analysis Guidance (TAG) [14], it is customary to distinguish between modes of transport by the average income of the population and not by the distance. The Value of Travel Time Savings (VTTS) value for commuting to and from work is set at less than 25% of the business trips average and VTTS for other purposes is 90% of the value for commuting. Gwilliam assumes that the World Bank uses 33% of hourly household income for adults and 15% for children to estimate the VTTS [10].

The studies by Concas and Kolpakov recommend a rate of 50% of the average salary in a country both for commuting and for other personal trips [15]. They assign the VTTS to only 35% of travel time reduction in urban public transport while sitting and 100% - when travelling while standing and up to 175% of earnings - to the waiting in uncomfortable conditions. The TAG [14] and Zhang et al. [16] recommend that the VTTS should be doubled in comparison with the normal value for walking and cycling and 2.5 times when waiting, although cycling can be considered as a beneficial use of time. The Value of Travel Time Savings is of practical use for assessing the social benefits resulting in transport projects implementation, but they are difficult to use for predicting the number of people who will choose a particular mode of transport or route. These aspects determine the differences in travel time reduction estimates. At the same time, such assessments should take into account the possibility of using the travel time for remote work, taking into account development of modern information and telecommunication technologies and robotics, for physical exercise (cycling) and so on. Variations in the duration of the trip over a certain period of time would be different for different pairs of points of the beginning and end of the trip, depending on both the reliability of each segment of the trip and the correlation of delays between the segments. Value of Travel Time Savings (VTTS) Studies are conducted not only to understand the motivations of users' travel decisions, but to assess the impact of measured factors

on other groups of people, as well, often separated in time and space. Each assessment depends on the demographic characteristics of the travelling population, mode of transport, time, location and purpose of travel and the choice of alternatives available, so the chosen explanatory variables should be important while making these decisions.

The VTTS is not the same for different types of trips (labour, cultural, domestic, business) [17]. Value of Travel Time Savings studies are often based on factors influencing the choice of mode of transport, including comfort, private space and prestige, duration and costs of travel. If different modes of transport are relatively close substitutes for each other, concerning a place, purpose and distance of travel, it is advisable to assume that the incomes and preferences of transport network users are distributed identically between and within modes of transport, which gives an overall value of travel time savings. As can be seen from Table 1, the results of studies are heterogeneous enough to eliminate some arbitrariness in the estimates.

3 Results

Vrubel [3] proposed a new universal assessment criterion - "road traffic losses", which is understood as the socio-economic costs of the unforced expenses of the traffic process. This criterion is applicable to assess the quality of both road traffic in general and its individual properties. Since the quality is assessed in monetary terms, it is possible to compare not only the quality of individual properties of road traffic, but the costs of achieving this quality, as well. This makes the comparison evident and allows optimizing easily and quickly (according to the criterion of losses minimization) the decisions made on the traffic organization. [1, 4]. The proposed criterion is gradually being introduced into the practice of traffic management. Methods for calculating the economic and environmental losses for the most typical facilities, as well as the basic (preliminary) methods for calculating car accident losses for individual typical facilities have been developed. In the Policy of ensuring the road traffic safety in the Republic of Belarus, losses are recognized as the main assessment criterion of the road traffic quality and it is required to improve the methods for calculating losses.

In recent years, views on the goals and methods of designing the urban transport systems have changed. The main problems in Belarusian road traffic, among others, are: the excessive dependence of population of some regions on individual cars, congestion with motor transport in cities, especially their centres [4]. Road traffic in the country is characterized by the increasing integration of the road traffic management with other types of transport and urban planning. An obligatory element of transport projects is the assessment of their impact on the urban environment in terms of accidents, as well as environmental and social friendliness [4, 12].

Belarusian National Technical University has developed a methodology and is modifying a procedure for assessing the quality of road traffic on a given section of the street and road network (SRN), which takes into account economic, environmental and car accident losses (social losses, unfortunately, due to the lack of reliable methods and validated formulae, are not yet taken into account) [3]. This methodology is based on calculating, summing up and comparing the losses at a given section of the SRN for any option of traffic management. It enables to quantify (in monetary terms) and therefore optimize any traffic management decisions.

Obviously, when assessing the quality, one must compare the costs that cover all the aspects of the urban transport system. In the simplest cases, when assessing the quality of the control options at an individual facility, it is sufficient to compare the losses from traffic expenses only. In general cases, one must consider the costs of losses of road traffic expenses and the costs of changes in road traffic conditions.

Those costs and expenses are very diverse and manifest themselves in a variety of forms, for example, in the form of the costs of land given for the road, emissions into the atmosphere, the support of a huge mass of people serving road traffic and road transport, car accidents, disobedience of road users, wasted time, etc. Therefore, comparing them is very difficult and rather conditional. However, there is always a certain normalized sum of costs and expenses that characterizes the cost of transport maintenance or transport service. These costs are made up of two main components - infrastructure costs and traffic expenses:

$$C = Z + E, \tag{1}$$

where:
C - the costs of transport maintenance or transport service;
Z - infrastructure costs;
E - traffic expenses.

All these are estimated in monetary units, for example, in rubles or conditional currency units, or, as it is often accepted, in rubles/year or USD/year.

If the investigated costs are close to the minimal possible one, then it is considered that the system works in the optimal way, without losses. If these costs are not minimal, then there are losses, which are understood as the excess of the investigated costs over the minimal possible one:

$$L = C + Cmin, \tag{2}$$

where:
L - losses in the investigated system;
C - investigated costs of transport maintenance or transport service;
$Cmin$ - the minimal possible costs.

The concept of the "minimal possible costs" is rather relative and has an extended interpretation. Firstly, all the unnecessary costs, such as car accidents, are considered to be expenses, although it is known that accident-free traffic does not exist. Secondly, the standard permitted speed, for example, in settlements (60 km/h) is taken as a basis for comparison to the speed of commuting. To gain such a speed any-place is impossible. Thirdly, to achieve the lowest possible costs, it is necessary to bring together all the best world achievements in the location or a system under investigation, which is also almost impossible. Therefore, the minimal possible costs today actually act not as a standard, but rather as a kind of cue that one must aim for. As a result, the concept of "a loss" implies not only what we have lost, but also what we have missed, have not used, taken, etc.

Comparison of losses is carried out according to the so-called "unital/single/normalized" losses, including both economic and social components:

$$L = L_e + L_s, \tag{3}$$

where:
L - normalized losses of a given type rubles/year;
L_e - economic component of a given type of losses, rubles/year;
L_s - social component of a given type of losses, rubles/year.

The definition of the social component is carried out using the so-called "social coefficient", K_s, showing how many rubles a society agrees to pay (or has already paid) to avoid the socio- economic losses of a given type, per 1 ruble at a given time:

$$K_s = \frac{L_e + L_s}{L_e} = 1 + \frac{L_s}{L_e}. \tag{4}$$

Normalized losses of a given type can be defined as the product of the economic component times the social coefficient:

$$L = L_e \times K_s, \; rub/year. \tag{5}$$

The total normalized losses in the investigated location or in the investigated system are determined from the formula:

$$L_\Sigma = L_{ekon} \times K_{sekon} + L_{ecol} \times K_{ecol} + \\ + L_a \times K_{sa} + L_s \times K_{ss}, \text{ rub/year}, \tag{6}$$

where:
L_{ekon} and K_{sekon} - the economic component and the social coefficient of economic losses resp;
Le_{col} and K_{secol} - the same for ecological losses;
L_a and K_{sa} - the same for accident losses;
L_s and K_{ss} - the same for social losses.

Since losses are, by definition, derivative of value, they can be characterized in the same way as costs - global, of travel expenses and in the infrastructure.

Costs losses, as well as the costs themselves, can be divided into four types - economic, environmental, accident and social. All of these types are quite closely related and it is sometimes difficult to draw a clear line between them. Therefore, this division, as well as the given names should be considered conditional or operating names. However, more than 20 years of using this classification have shown that it is clear and quite user-friendly, especially when analyzing the loss structure of an individual site or system.

Obviously, in assessing the quality of large systems, global costs covering all the aspects of the road transport system must be compared. In the simplest cases, it is sufficient to compare only the travel costs losses when assessing the quality of control options at a single facility. In general, the so-called comparative costs, including travel costs losses and costs of (limited) changes in traffic conditions, etc. should be considered:

$$C = L_\Sigma + Z \text{ rub/year}, \tag{7}$$

where:
C - comparative costs;
L_Σ - total normalized losses;
Z - annual normalized costs of changes in travel conditions.

The object to be studied is divided into elementary areas, which are either conflicting objects or similar sections of a road. At each conflict point (or zone) or at a given section of a road, all the losses' types are defined and the results are summed. The resulting value of the total loss is added to the annual normalized costs in the infrastructure and the comparative value is set at which the quality is assessed. The absolute estimate is characterized by the comparative value of road traffic at the site under study, θ = C, rub/year. Three types of estimates are considered: absolute - θ, relative - θ_r and comparative - θ_c. The relative estimate is the ratio of the absolute estimate to the normalizes (current) volume of traffic:

$$\theta_r = \frac{\theta}{F_{(Q_1, Q_2, L)}} \times x, \text{ rub/year}, \tag{8}$$

where:
$F_{(Q_1, Q_2, L)}$ - some function, which characterizes the normalizes volume of traffic;
x - the dimension of the function that describes the volume of traffic, such as cars, automobile kilometres, etc.

Obviously, only the characteristics of the conflicting flows are relevant to the conflict objects

For the road sections (Q_1, Q_2) are the characteristics of the flows and the road section's length, respectively. There are several approaches to definition of the normalized volume of traffic. For example, for the conflict objects the following formula is used:

$$F_{(Q_1,Q_2,L)} = \sqrt{Q_1 \times Q_2} \ , \tag{9}$$

for the road sections:

$$F_{(Q_1,Q_2,L)} = Q \times L \, . \tag{10}$$

A comparative estimate is a quotient of the relative estimate of the object being investigated by the relative estimate of the prototype object, normalized to the usual, for example, a ten-point rating system:

$$\theta_s = \frac{\theta_{ri}}{\theta_{rprot}} \times \delta_{10} \ , \tag{11}$$

where:
θ_{ri} - relative estimate of the object being investigated;
θ_{rprot} - relative estimate of the prototype object;
δ_{10} - some constant (in this case 10).

Obviously, it is possible to select such elementary objects, which by agreement can be accepted as prototype objects. By comparing the relative estimates of the surveyed object and the prototype object, it is easy to make a comparative assessment of any object or section of the road network.

The proposed methodology makes it possible to evaluate not only the quality of road the traffic in general, but of its main components, as well, such as traffic management or road conditions. To evaluate the quality of the management, it is necessary to find the best way to manage under the given road conditions and traffic-pedestrian load and compare it to the existing ones.

Thus, the main features of the methodology being developed for evaluation of the quality of the road traffic were briefly considered. As it can be seen, the valuation principle and valuation criteria are extremely simple - the less the losses (comparative value), the better. The assessment itself is somewhat more complex and includes three types of estimates for at least three subsystems. As for the determination of the total losses, without which no assessment can be made, this is the most difficult task. It requires automated data collection, its processing and storage, prediction of characteristics and losses, optimization of management, etc. All these requires considerable intellectual capacity and appropriate infrastructure. This is no longer a technical task, but a social and national one.

Figure 1 shows a fragment of a linear graph of the traffic losses on a city street, where accident, environmental, economic and total annual losses are shown for each elementary section.

Such information will make it possible to systematically distribute the available opportunities for scientific and practical activities to improve the quality of the road traffic. In addition, it will demonstrate the true importance of traffic, especially its urban component, where, on busy streets, millions of dollars are lost annually. This should contribute to a positive change in the attitude of managers to the organization of traffic in cities. Figure 2 shows a comparison of various sets of measures to improve the quality of traffic on the main street of the largest city of Minsk. It can be seen that the two options are comparable in terms of payback periods, but have different “survivability” and relevance, which makes one of the options more attractive for saving capital investments for a longer period, despite its costs.

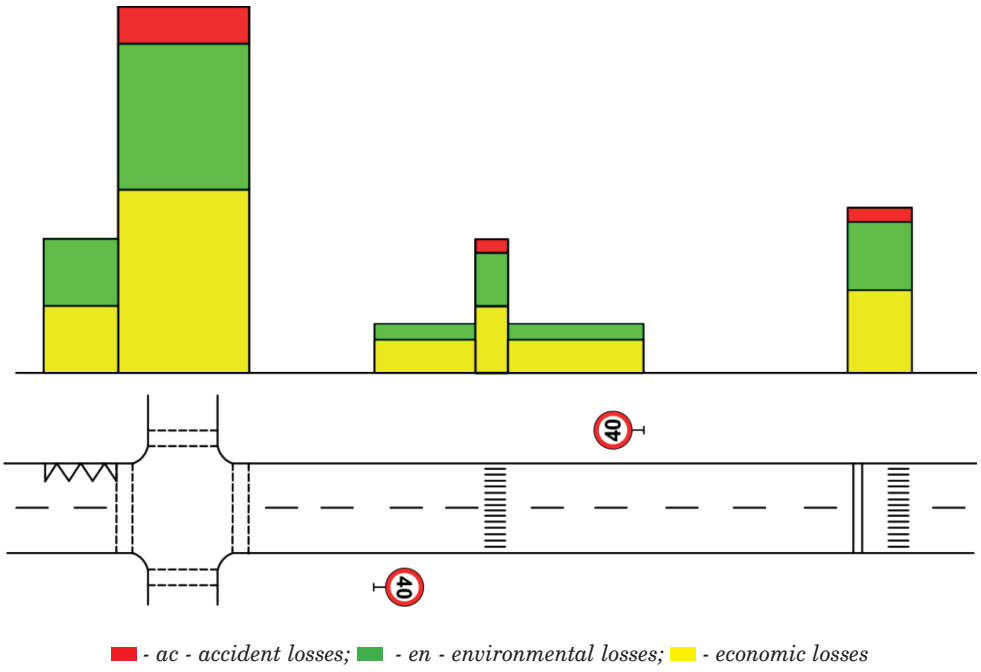

Figure 1 *Linear graph of losses on a city street*

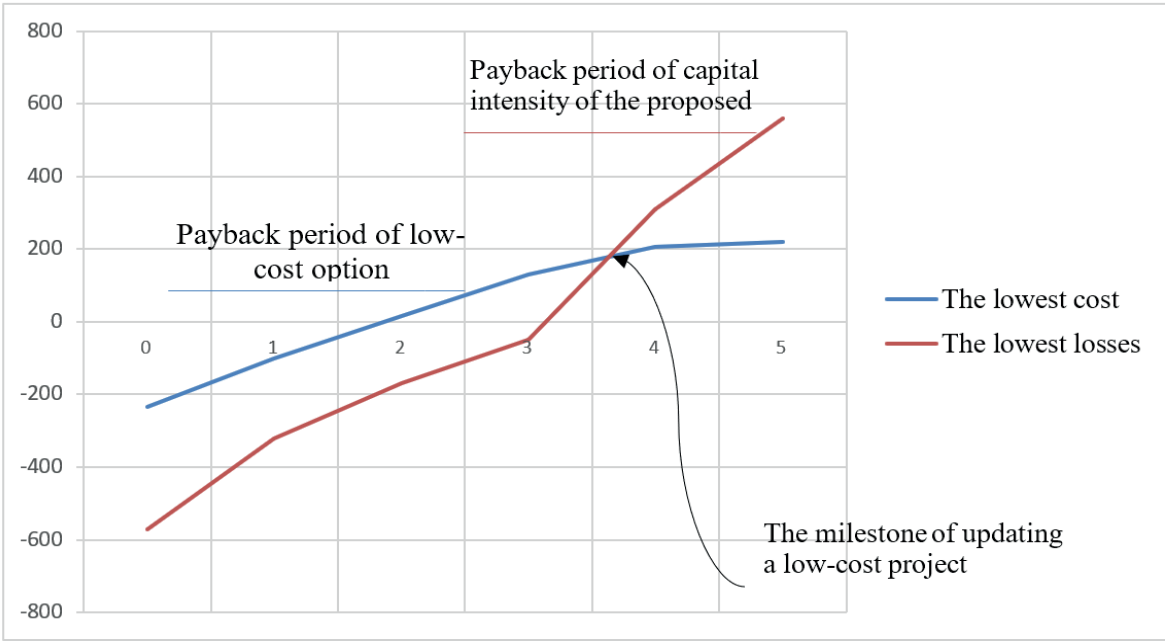

Figure 2 *Application of the developed methodology (Street K. Cetkin)*

4 Discussion

It is clear that the management of traffic and of the entire road transport system cannot be based on erroneous criteria and be carried out in a rudimentary manner, resulting in huge and increasing losses. While it is costly to build sophisticated management systems, it is not only necessary but also very beneficial, as the road traffic losses exceed those costs by several orders. Assessing the quality of decision-making is the foundation of any management system. Nowadays, the first steps to establish an objecting reliable methodology for assessing the quality of the road traffic and transport systems are being taken in the Republic of Belarus. The popularization, implementation and improvement of the methodology lead to hope that huge losses in the road traffic would be noticed by the society and the problem of their reduction would move things forward. The valuation of urban transport efficiency is the subject of further research.

Undoubtedly, it is desirable to take into account the final economic consequences of expanding production, wages and employment when assessing losses [3]. Under these assumptions, it is supposed to allow more accurately exploring the area called "standard scope of cost-benefit analysis". However, with the standard application of transport cost-benefit analysis, there are problems that can be described as follows.:

- the scope of benefits covered in the standard cost-benefit analysis that is limited by the practical possibilities of forecasting and estimating;
- improvements in urban transport systems and traffic conditions can stimulate fundamental changes in the number or location of institutions, households and employers that are not included in the standard cost-benefit analysis [20]. Therefore, there is a possibility to extend this conducted research taking into account such conditions.

For some USA states, cost-benefit analysis has not been mandatory and has not been considered at all in the transport investment decisions [21], while in Northern Europe and Australia such analysis has been dominating in the decision-making [22-23].

This research supports the idea of the obligatory projects' revision, based on the careful strategy planning under national, regional and local missions and aims of the country [24].

The economic impact analysis of the project is also supposed to be used in the pre-project assessment for a direct forecast of the resulting final economic effects [25-26].

5 Conclusions

A sharp increase in car flows in urban transport systems in recent years is caused by:

- the constant intensive growth in the level of population motorization;
- the increase in the number of business trips;
- the use of passenger cars with small volumes of cargo transportation;
- the emergence of "commercial" routes.

This has resulted in significant overloads of transport networks, especially in the central parts of cities. It also has led to an increased level of accidents and environmental impact on urban ecosystems and a decrease in traffic speeds. In this regard, the whole range of tasks arises, related to improving the comfort

of movement and the quality of citizens' life in general, which is possible by optimizing the operation of route passenger transport and increasing its attractiveness for users of all the levels. The proposed methodology is applicable to assess the effectiveness of measures aimed at reducing delays in route passenger transport, as well as to compare the technical and economic indicators of the proposed options, including when using the international CBA methodology (Cost Benefit Analysis). The methodology, in fact, is a business model for assessing the implementation of standard measures aimed at improving the quality of the entire transport system of cities and the efficiency of the route passenger transport, in particular.

The analysis of the studies carried out showed that there is no universal methodological approach to the economic valuation of the expenses associated with the travel time of the urban population and the efficiency of the urban transport system. The results of the studies confirm the point of view that the effectiveness of the implemented transport projects aimed at improving the quality of road traffic and the efficiency of the transport system is directly linked to the reduction of the travel time total costs. The developed methodological approach to the economic estimation of unanticipated (unenforced) road traffic losses in each specific transport system related to the time of travel, would ensure the selection of the best priority for urban traffic management and is an effective tool for investment priority guidelines in transport infrastructure and urban traffic management. The developed method for the economic evaluation of the efficiency of transport solutions, based on the total travel time losses of road users and the efficiency of the transport system, allows evaluating and justifying investments in transport projects of any level, i.e. to select and justify rational (optimal) decisions on the road traffic management (organization) and to plan the work of urban public transport.

Grants and funding

The authors received no financial support for the research, authorship and/or publication of this article.

Conflicts of interest

The authors declare that they have no known competing financial interests or personal relationships that could have appeared to influence the work reported in this paper.

References

[1] Road transport facts and figures. How healthy and environmentally friendly is our transport today? [online] [accessed 2022-08-21]. Available from: https://thepep.unece.org/sites/default/files/2021- 05/eMagazine%20Road%20transport%20facts%20%20figures_updated%2017%20May%202021_1.pdf

[2] KAPSKIJ, D., SAMOILOVICH, T. Theoretical basis for an economic evaluation of road accident losses. *Transport* [online]. 2009, **24**(3) p. 200-204 [accessed 2022-9-03]. ISSN 1648-4142, eISSN: 1648-3480. Available from: https://doi.org/10.3846/1648-4142.2009.24.200-204

[3] VRUBEL, Y., KAPSKI, D., KOT, E. *Determination of losses in road traffic* (in Russian). Minsk: BNTU, 2006. ISBN 985-479-493-8.

[4] World development indicators - World Bank Group [online] [accessed 2022-9-03]. 2004. Available from: https://doi.org/10.3846/1648-4142.2009.24.200-204http://documents.worldbank.org/curated/en/517231468762935046/World-development-indicators-2004

[5] KAPSKI, D. *Methodology for improving the quality of road traffic*. Minsk, BNTU, 2018. ISBN 978-985-583-184-7.

[6] BINSUWADAN, J., DE JONG, G., BATLEY, R., WEAT, P. The value of travel time savings in freight transport: a meta-analysis. *Transportation* [online]. 2022, **49**, p. 1183-1209. ISSN 0049-4488, eISSN 1572-9435. Available from: https://doi.org/10.1007/s11116-021-10207-2

[7] WARDMAN, M., CHINTAKAYALA, V. P. K., DE JONG, G. Values of travel time in Europe: review and metaanalysis. *Transportation Research Part A: Policy and Practice* [online]. 2016, **94**, p. 93-111. ISSN 0965-8564, eISSN 1879-2375. Available from: https://dx.doi.org/10.1016/j.tra.2016.08.019

[8] ESSEN, H., FIORELLO, D., EL BEYROUTY, K., BIELER, C., VAN WIJNGAARDEN, L., SCHROTEN, A., PAROLIN, R., BRAMBILLA, M., SUTTER, D., MAFFII, S., FERMI, F. *Handbook on the external costs of transport. Version 2019-1.1* [online] [accessed 2022-9-03]. Brussels: Publications Office European Commission, Directorate-General for Mobility and Transport, 2020. ISBN 978-92-76-18184-2. Available from: https://doi.org/10.2832/51388

[9] TEVENSON, M., THOMPSON J., HERICK DE SA, T., EWING, R., MOHAN, D., MCCLURE, R., TIWARI, G., GILES-CORTI, B., SUN, X., WALLACE, M., WOODCOCK, J. Land use, transport and population health: estimating the health benefits of compact cities. *The Lancet* [online]. 2016, **388**, p. 2925-2935. ISSN 0140-6736. Available from: https://doi.org/10.1016/S0140-6736(16)30067-8

[10] GWILLIAM, K. M. The value of time in economic evaluation of transport projects: lessons from recent research - The World Bank [online] [accessed 2022-11-13]. 1997. Available from: https://documents1.worldbank.org/curated/en/759371468153286766/pdf/816020BRI0Infr 00Box379840B00PUBLIC0.pdf
[11] JONES, H., MOURA, F., DOMINGOS, T. Transport infrastructure project evaluation using cost-benefit analysis. *Procedia - Social and Behavioral Sciences* [online]. 2014, **111**, p. 400-409 [accessed 2022-11-13]. ISSN 1877-0428. Available from: https://doi.org/10.1016/j.sbspro.2014.01.073
[12] BECKER, G. A theory of the allocation of time. *The Economic Journal* [online]. 1965, **75**(299), p. 493-517 [accessed 2022-11-13]. ISSN 0013-0133, eISSN 1468-0297. Available from: https://doi.org/10.2307/2228949
[13] DE SERPA, A. A theory of the economics of time. *The Economic Journal* [online]. 1971, **81**(324), p. 828-846. ISSN 0013-0133, eISSN 1468-0297. Available from: https://doi.org/10.2307/2230320
[14] MACKIE, P., WORSLEY, T. International comparisons of transport. Appraisal practice: overview report [online] [accessed 2022-11-13]. University of Leeds: Institute for Transport Studies, 2013. Available from: https://assets.publishing.service.gov.uk/government/uploads/system/uploads/attachment_data/file/209530/final-overview-report.pdf
[15] CONCAS, S., KOLPAKOV, A. Synthesis of research on value of time and value of reliability. Final report contract no. BD549 46 [online]. Florida: Center for Urban Transportation Research, University of South Florida, 2009. Available from: https://www.nctr.usf.edu/pdf/77806.pdf
[16] ZHANG, A., BOARDMAN, A., GILLEN, D., WATERS, W. Towards estimating the social and environmental costs of transportation in Canada [online] [accessed 2022-09-08]. Vancouver BC: Centre for Transportation Studies, University of British Columbia, 2005. Available from: http://www.bv.transports.gouv.qc.ca/mono/0965490.pdf
[17] FOSGERAU, M. Automation and the value of time in passenger transport. International Transport Forum Discussion Papers. No. 2019/10 [online] [accessed 2022-09-08]. Paris: OECD Publishing, 2019. Available from: https://www.itf-oecd.org/sites/default/files/docs/automation-vot-passenger-transport.pdf
[18] VENABLES, A. J. Incorporating wider economic impacts within cost-benefit appraisal. International Transport Forum Discussion Papers. 2016-05 [online] [accessed 2022-09-08]. Paris: OECD Publishing, 2016. Available from: https://www.itf-oecd.org/sites/default/files/docs/incorporating-wider-economic-impacts-cba.pdf
[19] BOITEUX, M., BAUMSTARK, L. General Commissariat of the transport plan: choice of investments and cost of nuisances/Commissariat general du plan transports: choix des investissements et cout des nuisances (in French) [online] [accessed 2022-09-08]. 2001. Available from: https://www.vie-publique.fr/sites/default/files/rapport/pdf/014000434.pdf
[20] LITMAN, T. A. Value of travel time reliability and cost-benefit analysis. In: Transportation cost and benefit analysis II - travel time costs [online] [accessed 2022-07-27]. Victoria Transport Policy Institute, 2009. Available from: http://www.vtpi.org/tca/tca0502.pdf
[21] FOSGERAU, MThe valuation of travel time variability International Transport Forum Discussion Papers. No. 2016/04 [online]. Paris: OECD Publishing, 2016. Available from: https://doi.org/10.1787/49bc1165-en
[22] WEISBROD, G, MULLEY, C., HENSHER, D. Recognising the complementary contributions of cost benefit analysis and economic impact analysis to an understanding of the worth of public transport investment: a case study of bus rapid transit in Sydney, Australia. *Research in Transportation Economics* [online]. 2016, **59**, p. 450-461. ISSN 0739-8859, eISSN 1875-7979. Available from: https://doi.org/10.1016/j.retrec.2016.06.007
[23] GUHNEMANN, A., KELLY, C., MACKIE, P., WORSLEY, T. International comparison of transport appraisal practice - annex 1 England country report. Research report [online] [accessed 2023-01-27]. UK: Institute for Transport Studies, 2013. Available from: https://eprints.whiterose.ac.uk/76698/1/annex-1-england.pdf
[24] BECKER, G. S. A Theory of the allocation of time. *The Economic Journal* [online]. 1965, **75**(299), p. 493-517. ISSN 0013-0133, eISSN 1468-0297. Available from: https://doi.org/10.2307/2228949
[25] BAUMOL, W. J. Income and substitution effects in the Linder theorem. *The Quarterly Journal of Economics* [online]. 1973, **87**(4), p. 629-633. ISSN 0033-5533, e ISSN 1531-4650. Available from: https://doi.org/10.2307/1882030
[26] JONES, H., MOURA F., DOMINGOS, T. Transport infrastructure project evaluation using cost-benefit analysis. *Procedia - Social and Behavioral Sciences* [online]. 2014, **111**, p. 400-409. ISSN 1877-0428. Available from: https://doi.org/10.1016/j.sbspro.2014.01.073

This is an open access article distributed under the terms of the Creative Commons Attribution 4.0 International License (CC BY 4.0), which permits use, distribution, and reproduction in any medium, provided the original publication is properly cited. No use, distribution or reproduction is permitted which does not comply with these terms.

TECHNICAL MAINTENANCE OF VEHICLES: IMPROVEMENT OF RELIABILITY OF THE MAJOR COMPONENTS AND UNITS

Dinara R. Tortbayeva*, Saken S. Pernebekov, Ussen A. Ussipbayev, Baurzhan Z. Shoibekov, Aikerim O. Kazenova

M. Auezov South Kazakhstan University, Shymkent, Republic of Kazakhstan

*E-mail of corresponding author: tortbayevadinarar@gmail.com

Dinara R. Tortbayeva 0000-0003-1648-2991,
Ussen A. Ussipbayev 0000-0002-0206-7757,
Aikerim O. Kazenova 0000-0001-9341-1922
Saken S. Pernebekov 0000-0001-7775-5370,
Baurzhan Z. Shoibekov 0000-0001-8117-910X

Resume

The purpose is to determine the impact of operating conditions on the reliability of vehicles, to identify the main causes of failure of truck units and assemblies and to find ways to improve their reliability. The main methods are a systematic approach to analysis of complex technological systems, the fault tree analysis to identify the most common causes of failure of trucks in the climatic conditions of Central Asia. It has been revealed that one of the frequent causes of failure of units and assemblies is fatigue failure, the finite element modelling of which allowed the study to obtain a diagram of limit deviations for various cycle asymmetries and as a result, the ability to predict the process of fatigue failure under the influence of external factors. The study results are aimed at the possibility of predicting the failure of components and assemblies of trucks conditioned by fatigue failure.

Article info

Received 18 January 2023
Accepted 14 April 2023
Online 15 May 2023

Keywords:

cyclic loading
fatigue failure
cycle stress
endurance limit
truck

Available online: https://doi.org/10.26552/com.C.2023.045

ISSN 1335-4205 (print version)
ISSN 2585-7878 (online version)

1 Introduction

A modern vehicle is a complex system, a set of joint elements - components that ensure the performance of its functions, made of various materials, with high precision machining of the surfaces of parts and, in turn, is part of the "vehicle-driver-road-environment" system and its properties are manifested in interaction with the elements of this system. The operation of vehicles is carried out in various road and climatic conditions, which is conditioned by the influence of various mechanical, physical and chemical factors on it, causing a change in its technical condition. Therefore, the significance of the criteria for the vehicle operation depends on the conditions in which this criterion is manifested, on the operating conditions and natural and climatic environment [1-3]. The study by Mozharova [4] defines operational conditions as conditions that were formed as a result of the organisation of production with the participation of an automobile fleet and the performance of technical and technological maintenance of vehicles. The natural and climatic conditions include the terrain, the amount of precipitation per year, the average temperature and the type (connectivity) of soil. The performance of systems and assemblies, that is, the intensity of their wear is affected by the quality of the road surface, which, in turn, depends on the terrain [5-6].

In the Republic of Kazakhstan and in the Central Asian region, a sharply continental and dry climate prevails with a hydrothermal coefficient of no more than 0.8, which corresponds to an arid zone. The annual temperature difference is significant, since in winter the temperature can drop to -50 °C and in summer it can rise to + 70 °C in some areas. Daily temperature drops reach 20-30 °C. With the exception of the northern regions, soils in Kazakhstan are represented by chestnut, brown semi-desert soil, dry-type playa and desert sands. Considering the type (connectivity) of soils and low precipitation, the air dustiness reaches 0.1-0.3 g of dust per 1 m^3 of air [7]. The technical conditions of a vehicle are determined by the changing properties of its components, affecting serviceability and operability. The theoretical state parameter curves change smoothly over time but are influenced by external factors resulting in broken curves. The main causes of technical changes

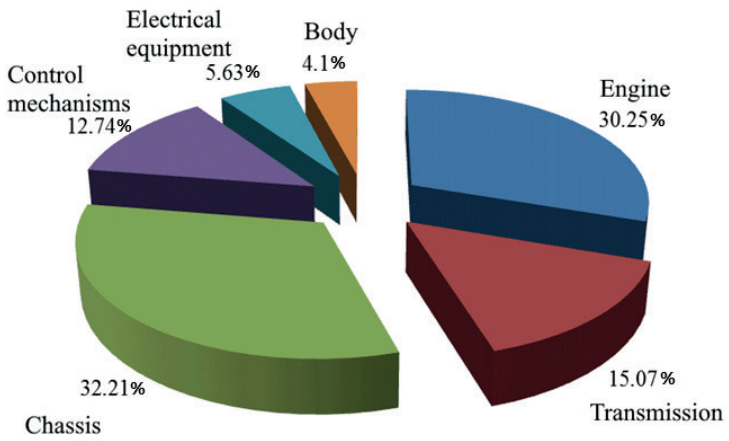

Figure 1 *Percentage of malfunctions in the major units of trucks, source: compiled by the authors*

Table 1 *Parameters of reliability indicators*

Characterized reliability property	Indicators	Basic equation
Reliability	Probability of no-failure	$P(t) = \frac{N - n(t)}{N}$
	Failure rate	$\lambda(t) = \frac{n(t)}{N_{cp} \cdot \Delta t}$
	Failure intensity	$\mu(t) = \frac{n(t_2) - n(t_1)}{t_2 - t_1}$
	Time to failure	$T = \frac{1}{\mu(t)}$

in vehicles, units, and mechanisms are wear, plastic deformation, fatigue damage, corrosion, and physico-chemical and temperature changes. Figure 1 shows the percentage of malfunctions for major truck units.

Analysis of research papers byTurdikulov and Kushakov [8], V. G. Kozlovet al. [9] showed that natural and climatic conditions (temperature differences, air dustiness) have a negative impact on the fatigue strength of vehicle components. Fatigue failure occurs on surfaces of the cams and gear teeth, in the rolling bearings of the transmission, in the antifriction layer of the engine crankshaft bearing shells. Fatigue failure is also observed in extreme operating conditions (prolonged overloads, low or high temperatures) in springs, semi-axles, frames. In the reference literature and technical characteristics of materials, σ_{-1} is used as a criterion of the fatigue endurance limit. However, to investigate fatigue strength in difficult operating conditions, this criterion is low informative, therefore, in the presented studies, a more informative criterion will be used that characterizes the resistance of metal to cyclic loads - a diagram of limit deviations for various cycle asymmetries. The fault-tolerance of products is determined by their reliability, durability, maintainability and preservation. Reliability of components and assemblies of trucks is a key property for studying fault-tolerance, the calculations of which would allow predicting the operating time of a vehicle. Reliability, durability, maintainability and survivability are characterized by the quantitative single and complex indicators [10-11]. The currently available parameters of reliability indicators in accordance with the assessed properties are shown in Table 1.

Research in the field of predicting failures of complex engineering systems is conducted in various countries and in various areas: information systems, production equipment, vehicles as complex systems [12-15]. Despite a large number of research papers on the reliability of vehicles, the problem of reduced reliability in difficult climatic conditions has been rather understudied, which leads to high repair costs, downtime. This paper considers reliability in relation to engineering systems and their elements from the position of adapting them to difficult conditions, which would allow comprehensively considering the causes of vehicle failure and suggesting ways to improve reliability.

The purpose of the study is to determine the impact of operating conditions on the reliability of vehicles, to identify the main causes of failure of truck units and assemblies and to find ways to improve their reliability.

2 Materials and methods

The study focused on a KrAZ-65053 motor vehicle chassis from Kremenchuk Automobile Plant, equipped with PAP-60/80 lifting units for major repairs of oil and gas wells and used in heavy machinery plant production in Kazakhstan. The reliability analysis

Table 2 *Mechanical properties of 40CN2MA steel*

Yield strength σ_t (MPa)	Tensile strength σ_V (MPa)	Elongation 5 %	Reduction ψ (%)	Impact strength (J/mm)	Brinell hardness HB
780	980	15	50	6	230-285

showed a significant number of failures in wheels and axles during technological operation. Statistical methods identified the main causes of failures, which were analyzed and formed the basis for building a fault tree. The semi-axle of the front-drive axle was selected as the investigated part, during its operation, fatigue failures were most often observed. The half-axle of the front-drive axle is included in the assembly unit of the differential of the front axle of the KrAZ truck, designed to rotate the half-axles at different speeds when turning the vehicle and prevent twisting of the shafts and the distribution of torque between the wheels. The semi-axle, in turn, is designed to transfer torque from the differential to the wheels. The part in the assembly unit operates at high rotational speeds as well as in a reverse loading cycle. The working environment of the part is the front axle casing. The maximum dimensions of the part are Ø 66 mm and length 1.108 mm.

The part is made of 40CN2MA steel, the mechanical properties of the material are shown in Table 2 [16]. The presented mechanical properties are necessary for further finite element modelling.

Fatigue (cyclic) loading is the most common type of loading that parts and components of mechanisms experience during operation. It is accepted that the assessment of the strength of the product, from the action of cyclic loading, is reduced to comparing the values of the calculated stresses obtained and the values of the endurance limit of the material from which the product is made. M_{-1} is used as a criterion of the fatigue endurance limit. Its values are obtained as a result of fatigue tests. The tests are carried out on laboratory samples of small diameter (7-10 mm) made of a rod. The surface of the samples is carefully polished. Next, a series of tests of samples is carried out during bending by a symmetrical loading cycle. In the first test, a load value is applied that creates maximum cycle stresses close to the yield strength. The number of loading cycles that the sample has sustained before destruction is measured. Next, the load is reduced and the next test is carried out to measure the number of loading cycles that the sample withstands before destruction. Thus, the load is gradually reduced until the sample can withstand the base number of loading cycles (107 cycles) without destruction. According to the test results, a "Stress-cycle" graph is built.

Due to the fact that three main types of loading cycles are considered in mechanical engineering (symmetrical cycle, pulsating (zero) cycle, asymmetric cycle) and fatigue tests consider only symmetrical cycle, to obtain a more informative criterion characterizing the resistance of metal to cyclic loads, a diagram of limit deviations for various cycle asymmetries is constructed in the coordinates of the average cycle stress (X-axis) and maximum cycle stress (Y-axis) and allows evaluating the fatigue resistance of the future product at the design stage. The necessary characteristics of the cycle: the mean cycle stress σ_m and the highest cycle stress σ_{max} [17]. The ANSYS Workbench software suite was used to obtain the values necessary for constructing the diagram.

3 Results and discussion

Reliability indicators like failure-free operation, failure rate, and mean time to failure are important for assessing components and predicting system failures. A failure tree is an effective top-down method for analyzing product reliability and identifying causes of failure. It models the complex interactions of system parts and considers specific and general causes of failure, their interaction, and influence on each other [18]. The failure tree analysis uses Boolean abbreviations and clipping set analysis to assess system reliability and operability based on failure rate, fault mode probability, and recovery rate. The method has advantages and disadvantages depending on its scope. In mechanical engineering, the failure tree is useful for visually identifying potential failure points, analyzing system reliability quantitatively and qualitatively, and gaining detailed insight into system behavior. The method's main advantage is the ability to eliminate irrelevant system elements and events and focus on the most significant causes of malfunctions leading to system failure or accidents.

Limitations of the method: allows presenting events that depend on the time or the order of their occurrence; if the operation of the system depends on its state, then the method ceases to be flexible when rebuilding the system. These shortcomings can be eliminated by using Markov models to study the main events of the fault tree. Thus, combining the principles of failure tree analysis with Markov models provides the best results in relation to engineering systems. [19]. In the studies [18-20], the method of analyzing the failure tree for various engineering systems was used; the use of this method allowed reducing the time for diagnosing the cause of failures and increasing the efficiency of the systems. The presented method is included in national standards, for example, as the standard of the United States of America MIL-HDBK-217 "Reliability prediction of electronic equipment" [21] or the Russian RD 03-418-01 "Guidelines for risk analysis of hazardous

Table 3 *Fault statistics - part I*

Indicator	Number of faults	Percentage ratio	Fault tree index
Chassis			
Frame	635	100	
deflections, distortions of breakage			F.1
A) overloading of the vehicle	336	53	F.1.A
B) strong tremors when moving	209	33	F.1.B
C) unfavourable climatic conditions	89	14	F.1.C
Axles	4.125	100	
Swivel axle assembly	1.238	100	A.S.
1) mounting hole thread failure	738	100	A.S.1
A) natural wear and tear	502	68	A.S.1.A
B) plastic deformation	236	32	A.S.1.B
2) hub bearing wear	271	100	A.S.2
A) lack of oil	154	57	A.S.2.A
B) natural wear and tear	117	43	A.S.2.B
3) crack formation	223	100	A.S.3
A) fatigue wear	167	75	A.S.3.A
B) natural ageing	56	25	A.S.3.B
Semi-axles	2.310	100	A.S-A.
1) breakage (twisting)	1.063	100	A.S-A.1
A) fatigue wear	510	48	A.S-A.1.A
B) severe operating conditions	213	20	A.S-A.1.B
C) unfavourable climatic conditions	213	20	A.S-A.1.C
D) hidden defects (shells, microcracks)	127	12	A.S-A.1.D
2) wear of the half-axle splined joint	647	100	A.S-A.2
A) insufficient anchoring	453	70	A.S-A.2.A
B) fatigue wear	194	30	A.S-A.2.B
3) wear or destruction of the half-axle bearing	600	100	A.S-A.3
A) deformation of the half-axle	360	60	A.S-A.3.A
B) natural wear and tear	120	20	A.S-A.3.B
C) lack of oil	120	20	A.S-A.3.C
U-joint	990	100	A.U.
1) wear of crosspins	526	100	A.U.1
A) lack of lubrication	274	52	A.U.1.A
B) natural wear and tear	252	48	A.U.1.B
2) wear of needle bearings	464	100	A.U.2
A) lack of lubrication	316	68	A.U.2.A
B) natural wear and tear	148	32	A.U.2.B

production facilities" [22]. Based on the statistics of truck malfunctions in the period from 2014 to 2017, which are listed in Tables 3 and 4, 13, 380 malfunctions account for the chassis [23]. To simplify the construction of the failure tree and for the convenience of its analysis, fault indices for the failure tree have been introduced.

Based on the analysis of statistical data, a failure tree was constructed (Figure 3). The principle of causal relationships for constructing a logical-probabilistic model of the failure tree, it can also be called tree of malfunctions, undesirable events, accidents, incidents, which is described in [24] and implemented in the constructions presented in Figure 3. To find possible causes of system failures and failures of its elements, a multilevel model is constructed that has a graphological structure of the effects of violations and malfunctions on the functioning of the system under study. Various approaches can be used to model the analysis of the failure tree, but the most common methods of construction can be summarised in several steps. First, it is necessary to identify an undesirable event. An undesirable event acts as the root for building a failure tree, one event for one tree. In this case, that is a failure (breakdown) of the truck's chassis.

Secondly, all the reasons that affect an undesirable event will be highlighted and analyzed if the probability of the influence of these reasons on the event is 0 or more, it is included in the failure tree, for trucks these data are summarised in Tables 3 and 4. To identify the causes of failures, it is recommended to use a systematic approach that can help limit the study to only those malfunctions that directly affect the failure of the system in question, but at the same time would allow avoiding skipping malfunctions affecting an undesirable event. Then, for the selected event, all the causes are numbered, then in accordance with the selected system

Table 4 *Fault statistics - part II*

Indicator	Number of faults	Percentage ratio	Fault tree index
Suspensions	5.420	100	
Hydraulic absorbers	2.331	100	S.H.
1) break of airtightness of the rod seal	1.119	100	S.H.1
A) ageing	358	32	S.H.1.A
B) natural wear and tear	425	38	S.H.1.B
C) poor build quality	190	17	S.H.1.C
D) severe operating conditions	146	13	S.H.1.D
2) violation of the integrity of the rod coating	723	100	S.H.2
A) abrasive wear	549	76	S.H.2.A
B) poor build quality	174	24	S.H.2.B
3) damage to internal valves	489	100	S.H.3
A) severe operating conditions	298	61	S.H.3.A
B) unfavourable climatic conditions	191	39	S.H.3.B
Semi-elliptical springs	3.089	100	S.S-E.
1) sagging or breakage of sheets	1.236	100	S.S-E.1
A) lack of lubrication	408	33	S.S-E.1.A
B) fatigue wear	445	36	S.S-E.1.B
C) violation of the correct fixing	272	22	S.S-E.1.C
D) severe operating conditions	111	8	S.S-E.1.D
2) loss of elasticity	1.112	100	S.S-E.2
severe operating conditions			
3) wear or breakage of pins and bushings in the spring eyes	741	100	S.S-E.3
A) corrosion	482	65	S.S-E.3.A
B) lack of lubrication	259	35	S.S-E.3.B
Wheels	3.200	100	
Disks	1.115	100	W.D.
bearing backlash or jamming			W.D.1
A) lack of lubrication	814	73	W.D.1.A
B) natural wear and tear	301	27	W.D.1.B
Tires	2.085	100	W.T.
tire wear			W.T.1
A) non-compliance with pressure standards	1.001	48	W.T.1.A
B) violation of wheel mounting angles	542	26	W.T.1.B
C) severe operating conditions	438	21	W.T.1.C
D) unfavourable climatic conditions	104	5	W.T.1.D

and used for graphical implementation of building a failure tree (Figure 2). The main characteristics of the fault tree are determined by the symbols “AND” and “OR”, which allow building a failure tree based on the previously conducted selection of an undesirable event, substantiation and analysis of the reasons causing the system failure [25]. The “AND” gate represents a combination of events that must occur simultaneously for the top event to occur and the “OR” gate represents a combination of events where only one event needs to occur for the top event to occur.

The truck’s chassis failure tree analysis, based on malfunctions in Kazakhstan’s climate, shows severe operating conditions and unfavorable weather as the main causes of failure. Although these reasons for failure appear much more frequently in Kazakhstan, they should be considered during truck design and manufacturing and during operation and maintenance. Fatigue wear significantly impacts the chassis’ trouble-free operation, especially under severe operating and adverse climatic conditions. Predicting failure due to fatigue wear is a difficult task and requires a detailed consideration of the mechanisms of fatigue failure of metals and methods of their study, since fatigue failures begin with appearance of the hard-to-detect microscopic cracks and the maximum dynamic loads that cause them are less than with static destruction [26]. Fatigue failures occur during the cyclic application of loads exceeding the endurance limit of the metal part. At a certain number of loading cycles, fatigue failure of parts occurs, associated with the gradual accumulation and growth of fatigue cracks. Improvement of calculation methods and manufacturing technology of vehicles (improvement of metal quality and manufacturing accuracy, exclusion of stress concentrators) will lead to a significant reduction in cases of fatigue failure of parts. As a rule, it is observed in extreme operating conditions (prolonged overloads, low or high temperatures) in springs, semi-axles, frames.

The analysis shows common causes of chassis failures

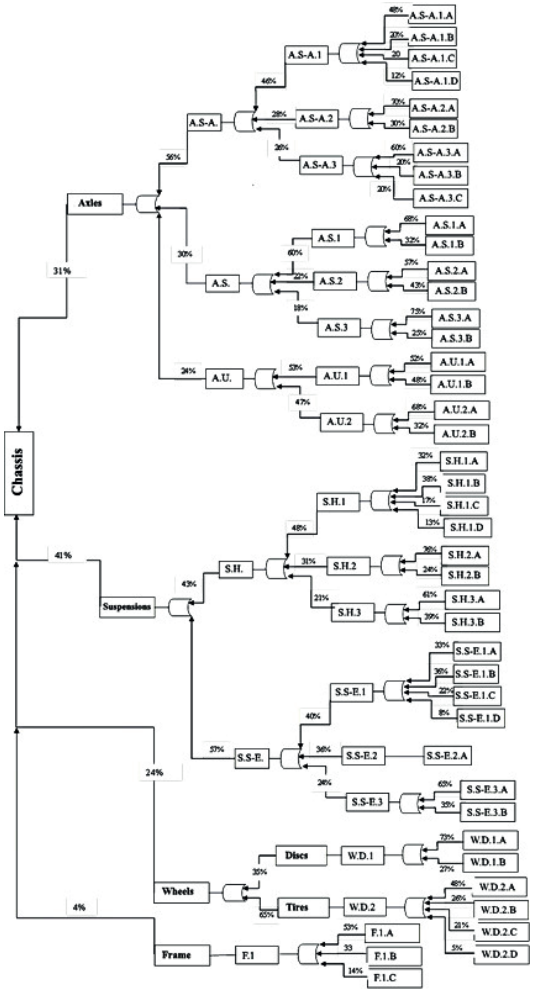

Figure 2 *Failure tree by chassis, note is presented in Table 5*

as related to suspension, axles, semi-elliptical springs, and wheels. Semi-axles and swivel axle assembly have the highest percentage of failures among axles. Wear of crosspins is the primary cause of U-joint failures. Hydraulic absorbers have the highest percentage of failures among suspensions. Sagging or breakage of sheets is the most common failure among semi-elliptical springs. Tire wear is the most common failure among wheels. Regular maintenance and inspection of all components is important to prevent system failures. The study proposes a method for constructing a diagram of limit deviations for various asymmetries of the half-axle operation cycle. Below are the steps required to obtain this diagram. At the first stage of the research, fatigue tests of a semi-axle made of 40CN2MA steel were carried out, the results of which are presented in a graph. The main criteria for failure in determining the strength limits and constructing fatigue curves are complete destruction or the appearance of macro cracks of a given size. At least 15 identical samples were tested to construct the fatigue curve and determine the endurance limits corresponding to the possibility of destruction of 50%. Three samples were tested in the stress range of 0.95-1.05 from the endurance limit corresponding to the possibility of destruction of 50%. The test base for determining the endurance limits is accepted: 10 to 10^6 cycles. The constructed fatigue strength curve is shown in Figure 3. As can be seen from Figure 3, the curve asymptotically approaches the horizontal line. The ordinate of this asymptote is the endurance limit, the greatest stress of the cycle, at which the destruction of the material will never occur. The results correlate with the results obtained in [27].

Thus, the entry σ_{-1} = 519 MPa for 40CN2MA steel means that this is the highest normal stress at which a small diameter rod with a polished surface will not collapse under the action of bending stress in a symmetrical cycle. Consequently, in products of a different design, size and in other cases of cyclic loading, when using the value σ-1, there is not enough information about the fatigue failure process. Based on the above, it is fair to assume that the endurance limit is not a sufficient criterion for assessing the resistance of a metal. At the second stage, a computational 3D model of the lever was created in the computer-aided design (CAD) system, which is transmitted in the ANSYS Workbench software suite via a plug-in built into the menu [28]. A material with the necessary properties was created in the ANSYS Workbench software suite. To specify the material, it is necessary to specify the

Table 5 *Note for Figure 2*

Fault tree index	Possible Issues
A.S-A.	Semi-axles
A.S-A.1	breakage
A.S-A.1.A	fatigue wear
A.S-A.1.B	severe operating conditions
A.S-A.1.C	unfavourable climatic conditions
A.S-A.1.D	hidden defects (shells, microcracks)
A.S-A.2	wear of the half-axle splined joint
A.S-A.2.A	insufficient anchoring
A.S-A.2.B	fatigue wear
A.S-A.3	wear or destruction of the half-axle bearing
A.S-A.3.A	deformation of the half-axle
A.S-A.3.B	natural wear and tear
A.S-A.3.C	lack of oil
A.S. Swivel axle assembly	mounting hole thread failure
A.S.1	natural wear and tear
A.S.1.A	plastic deformation
A.S.2	hub bearing wear
A.S.2.A	lack of oil
A.S.2.B	natural wear and tear
A.S.3	crack formation
A.S.3.A	fatigue wear
A.S.3.B	natural ageing
A.U. U-joint	wear of crosspins
A.U.1.A	lack of lubrication
A.U.1.B	natural wear and tear
A.U.2	wear of needle bearings
A.U.2.A	lack of lubrication
A.U.2.B	natural wear and tear
S.H. Hydraulic absorbers	break of airtightness of the rod seal
S.H.1	ageing
S.H.1.A	natural wear and tear
S.H.1.B	poor build quality
S.H.1.C	severe operating conditions
S.H.1.D	severe operating conditions
S.H.2	violation of the integrity of the rod coating
S.H.2.A	abrasive wear
S.H.2.B	poor build quality
S.H.3	damage to internal valves
S.H.3.A	severe operating conditions
S.H.3.B	unfavourable climatic conditions
S.S-E. Semi-elliptical springs	sagging or breakage of sheets
S.S-E.1	lack of lubrication
S.S-E.1.A	fatigue wear
S.S-E.1.B	violation of the correct fixing
S.S-E.1.C	severe operating conditions
S.S-E.1.D	severe operating conditions
S.S-E.2	loss of elasticity
S.S-E.3	wear or breakage of pins and bushings in the spring eyes
S.S-E.3.A	corrosion
S.S-E.3.B	lack of lubrication
W.D.1	bearing backlash or jamming
W.D.1.A	lack of lubrication
W.D.1.B	natural wear and tear
W.D.2	tire wear
W.D.2.A	non-compliance with pressure standards
W.D.2.B	violation of wheel mounting angles
W.D.2.C	severe operating conditions
W.D.2.D	unfavourable climatic conditions
F.1	deflections, distortions of breakage
F.1.A	overloading of the vehicle
F.1.B	strong tremors when moving
F.1.C	unfavourable climatic conditions

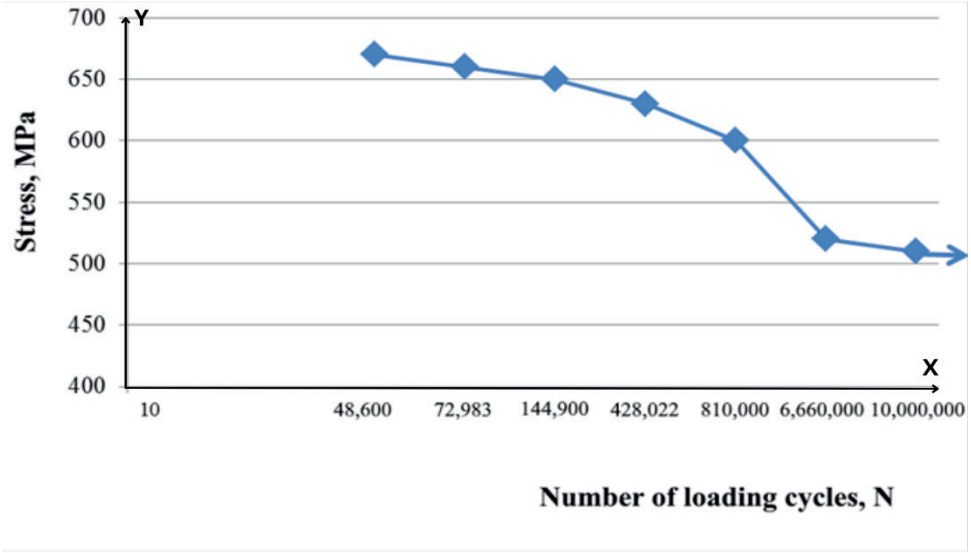

Figure 3 *The resulting fatigue curve in coordinates σ-N*

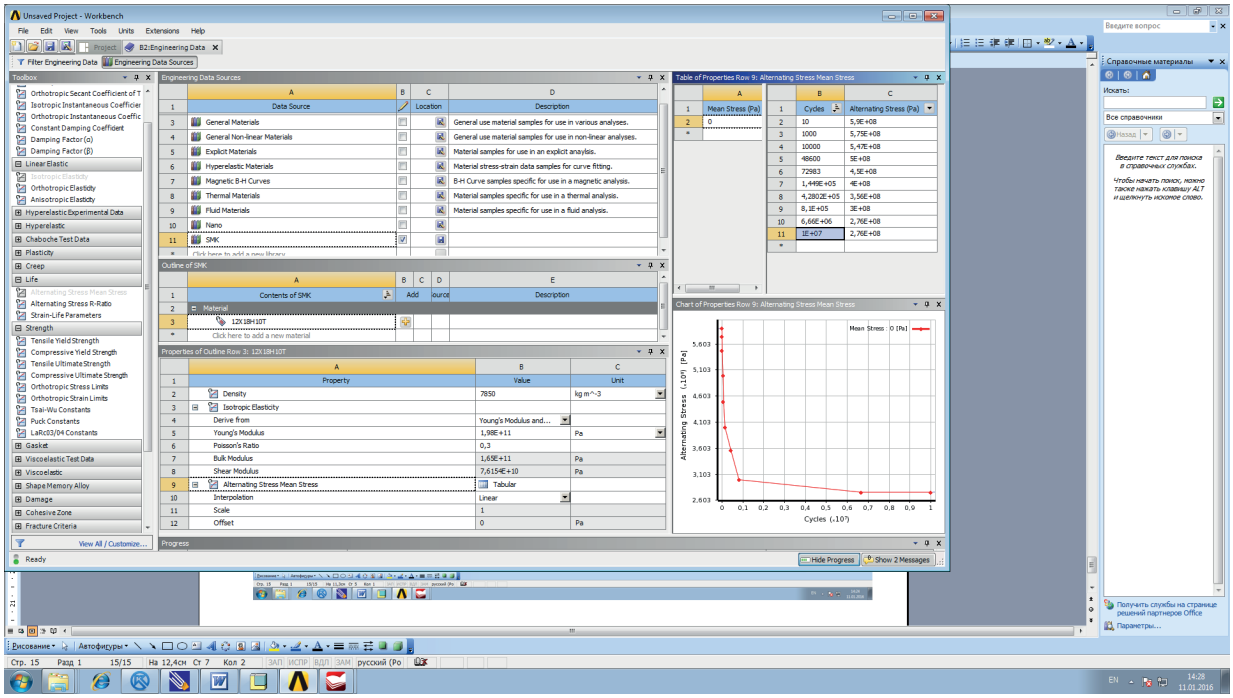

Figure 4 *Setting the fatigue curve*

density, modulus of elasticity and Poisson's ratio. The value of density and other parameters is taken from the reference literature [29], the temperature to which this density corresponds is optional.

For fatigue calculations, the Alternating Stress Mean Stress option from the Life option set is required. At this stage, the fatigue curve is set. The values shown in Figure 4 are entered in the Table of Properties Row 9: Alternating Stress Mean Stress window. In column B - cycles, in column C - stresses corresponding to them. Column A indicates the average cycle stress for the experimentally obtained fatigue curve (Figure 4). As already indicated earlier, the fatigue curve was obtained for a symmetric loading cycle, $\sigma_m = 0$. Calculations in the ANSYS Workbench software suite are carried out by the finite element method. Next, it is necessary to generate a grid of finite elements on the model and apply anchors and loads. The vertical load is set as - 8900 N along the Z axis. It should provide a stress level close to the endurance limit. After the calculation is completed, the type of result should be selected. The general stresses that arise in the structure are of interest. The resulting stresses are close to the endurance limit of this steel (515 MPa).

The stress limit diagram will be constructed from a series of points. The first point is the limit of endurance of steel with a symmetrical loading cycle, therefore, it will have coordinates $(0; \sigma_{-1})$ on the graph. The last point of the diagram is the tensile strength, it will have coordinates $(\sigma_B; \sigma_B)$. It is necessary to get the points

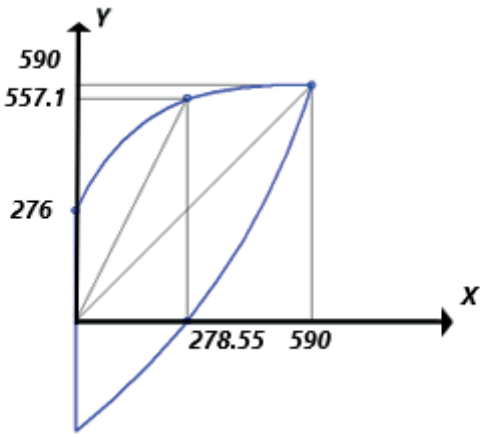

Figure 5 *Boundary stress diagram*

between coordinates. These will be endurance limits for the load cycles with asymmetry coefficients from -1 to 1. It is necessary to repeat the calculation with different load values to obtain endurance limits. As a result of the calculations, a number of points are obtained on which the boundary stress diagram is constructed (Figure 5). The result is the following. The endurance limit was 557.1 MPa. The average cycle stress was 278.55 MPa. The point has coordinates (278.55; 557.1). The boundary stress diagram is constructed in the coordinates of the average cycle stress (X-axis) and the maximum cycle stress (Y-axis).

This diagram allows evaluating the fatigue resistance of a future product at the design stage. It is enough to know the following cycle characteristics: the average cycle stress σ_m and the highest cycle stress σ_{max}. Fatigue resistance is estimated as follows: a point is plotted on the diagram, the coordinates of which are the average and maximum cycle stress; if the point is in the area that is bounded by the curves σ_{max} and σ_{min}, then the fatigue failure of the future product will not happen during the established service term. The experimental results obtained and the simulation data will serve as the basis for calculating the reliability of the front drive axle. The operability of parts can be determined by various criteria. The main criteria used in mechanical engineering are the criteria of strength, rigidity, wear resistance, heat resistance and vibration resistance.

When calculating reliability, the values obtained as a result of calculations are used and compared to the boundary values characterising strength (endurance limit, strength and fluidity), maximum load, resource, maximum displacement, heat resistance of oil and materials, dynamic stability and, according to data obtained empirically, as a result of experiments or observations during operation [30-31]. The study by Ostrejkovskii [32] presents a calculation of performance according to the strength criterion, where the limit of endurance acts as the boundary value characterizing strength. For calculations, the equivalence coefficient of the regime is used, the main criterion of which is the coefficient k, depending on the exponent of the degree m of the fatigue curve. The coefficient k is selected depending on the stresses and the number of cycles for different samples and materials, but the proposed coefficient does not consider the asymmetry of the cycle. To expand the possibility of calculation equations for predicting trouble-free operation in various operating conditions and to improve the accuracy of the results obtained, it is proposed to use the values obtained for the boundary stress diagram instead of the values from the fatigue curve.

4 Conclusions

A review of methods for analyzing the reliability of engineering systems is carried out, while the truck is considered as a complex system. The calculation of statistical data to identify the most frequent failures showed that for trucks operating under constant load conditions, 32% of breakdowns occur on the chassis. The paper discusses the existing methods of predicting failures. The process of compiling a failure tree has been investigated and based on those data, the failure trees for the chassis of a truck have been developed. A scheme for constructing a failure tree is proposed, which allows analyzing the nature, causes and consequences of failures of the chassis elements, which allows solving complex issues to improve the reliability of the system.

It is revealed that the main causes of failure are natural wear, fatigue failure, severe operating conditions. Unfavourable conditions are the complex causes of malfunctions of the chassis of trucks operating in the Republic of Kazakhstan. The data obtained would allow reducing the time for troubleshooting vehicles during the technical operation and maintenance. It is determined that when the vehicle components work at different loading cycles, the value of the endurance limit used is not always sufficiently informative. Thus, the study proposes a method for constructing a boundary stress diagram using the example of the front axle

half-axle, which allows evaluating and predicting the behaviour of the part material depending on its design and with different cycle asymmetries. The values of the cycle stresses, obtained as a result of modelling, can be used to calculate the reliability of the semi-axle according to the criterion of endurance chapel, which would improve the accuracy of calculations.

In terms of future research, it may be useful to expand the study to include other types of vehicles or machinery and to consider additional factors that may contribute to failures. It may also be beneficial to conduct more detailed analyses of specific components or subsystems within the vehicle to gain a better understanding of the root causes of failures. Additionally, the study highlights the importance of considering the effects of severe operating conditions and unfavorable climate on reliability of the chassis. Therefore, it may be worthwhile to conduct further research on the effects of these factors on other vehicle components and systems.

Grants and funding

The authors received no financial support for the research, authorship and/or publication of this article.

Conflicts of interest

The authors declare that they have no known competing financial interests or personal relationships that could have appeared to influence the work reported in this paper.

References

[1] THULE, C., LAUSDAHL, K., GOMES, C., MEISL G., LARSEN, P. G. Maestro: the INTO-CPS co-simulation framework. *Simulation Modelling Practice and Theory* [online]. 2019, **92**, p. 45-61. ISSN 1569-190X. Available from: https://doi.org/10.1016/j.jmsy.2019.04.008

[2] DOLZHENKO, N., MAILYANOVA, E., ASSILBEKOVA, I., KONAKBAY, Z. Analysis of meteorological conditions significant for small aviation and training flights at the airfield "balkhash" for planning and flight safety purposes. *News of the National Academy of Sciences of the Republic of Kazakhstan, Series of Geology and Technical Sciences* [online]. 2021, **2**(446), p. 62-67. ISSN 2224-5278. Available from: https://doi.org/10.32014/2021.2518-170X.35

[3] IMASHEVA, G. M., DOLZHENKO, N. A., ANAYATOVA, R. K., DORONINA, Y. V. Commercial use of aircraft based on safety risk. *Journal of Advanced Research in Law and Economics* [online]. 2018, **9**(8), p. 2615-2621. ISSN 2068-696X. Available from: https://doi.org/10.14505/jarle.v9.8(38).10

[4] MOZHAROVA, V. Transport in Kazakhstan: modern situation, problems and development prospects. Almaty: Kazakhstan Institute for Strategic Studies under the President of the Republic of Kazakhstan, 2011.

[5] PRENTKOVSKIS, O., TRETJAKOVAS, J., SVEDAS, A., BIELIATYNSKYI, A., DANIŪNAS, A., KRAYUSHKINA, K. The analysis of the deformation state of the double-wave guardrail mounted on bridges and viaducts of the motor roads in Lithuania and Ukraine. *Journal of Civil Engineering and Management* [online]. 2012, **18**(5), p. 761-771. ISSN 1392-3730. Available from: https://doi.org/10.3846/13923730.2012.731252

[6] OLEKSANDRA, S., KRAYUSHKINA, K., KHYMERIK, T., ANDRII, B. Method of increasing the roughness of the existing road. *Procedia Engineering* [online]. 2016, **165**, p. 1766-1770. ISSN 1877-7058. Available from: https://doi.org/10.1016/j.proeng.2016.11.920

[7] Competitiveness of logistics and transport in the Republic of Kazakhstan [online]. 2019. Available from: https://www.un-ilibrary.org/content/books/9789210042208/read

[8] TURDIKULOV, M., KUSHAKOV, S. Testing vehicles in mountainous conditions and dry and hot climate. In: *Wheeled vehicle safety in operating conditions*. FEDOTOV, A. I. (ed.). Irkutsk: National Research Irkutsk State Technical University, 2017. p. 169-173.

[9] KOZLOV, V. G., SKRYPNIKOV, A. V., SAMTSOV, V. V., NIKITIN, V. V., BOLTNEV, D. E., BOROVLEV, A. O. Influence of natural and technogenic factors on the complexity of construction of timber highways [online]. 2021. Available from: https://iopscience.iop.org/article/10.1088/1755-1315/659/1/012137/pdf

[10] GOST 27.002-2015 "Dependability in technics. Terms and definitions" [online]. 2017. Available from: https://docs.cntd.ru/document/1200136419.

[11] KURMANOV, A. K., ERMAGANBET, A. C., AHANOV, S. M., RAHATOV, S. Z., RYSPAYEV, K. S. Improvement of rotary disperser efficiency. *Life Science Journal*. 2014, **11**(10 spec. issue), p. 407-411. ISSN 1097-8135.

[12] KAUR, K., KAUR, K. Failure prediction and health status assessment of storage systems with decision trees. In: *Advanced informatics for computing research* [online]. LUHACH, A., SINGH, D., HSIUNG, P. A., HAWARI, K., LINGRAS, P., SINGH, P. (eds.). Cham: Springer, 2019, ISBN 978-981-15-0110-4, eISBN 978-981-15-0111-1, p. 366-376. Available from: https://doi.org/10.1007/978-981-15-0111-1

[13] MARTINEZ-LUCAS, G., PEREZ-DIAZ, J. I., CHAZARRA, M., SARASUA, J. I., CAVAZZINI, G., PAVESI, G., ARDIZZON, G. Risk of penstock fatigue in pumped-storage power plants operating with variable speed

in pumping mode, *Renewable Energy* [online]. 2019, **133**, p. 636-646. ISSN 0960-1481. Available from: https://doi.org/10.1016/j.renene.2018.10.060

[14] HELMER, T., KUHBECK, T., GRUBER, CH., KATES, R. Development of an integrated test bed and virtual laboratory for safety performance prediction in active safety systems. In: FISITA 2012 World Automotive Congress: proceedings [online]. Lecture Notes in Electrical Engineering, vol 197. Springer, Berlin, Heidelberg, 2013. ISBN 978-3-642-33804-5, eISBN 978-3-642-33805-2, p. 417-431. Available from: https://doi.org/10.1007/978-3-642-33805-2_34

[15] TULTAYEV, B., BALBAYEV, G., ZHAUYT, A. A Kinematic analysis of flat leverage mechanism of the fourth class for manipulators. *IOP Conference Series: Materials Science and Engineering* [online]. 2017, **230**(1), 012047. ISSN 1757-8981 Available from: https://doi.org/10.1088/1757-899X/230/1/012047

[16] GOST 4543-71 "Structural alloy steel bars. Specifications" [online]. 1973. Available from: https://docs.cntd.ru/document/1200005485

[17] SERENSEN, S. V., KOGAEV, V. P., SHNEIDEROVICH, R. M. *Bearing capacity and strength calculation of machine parts*. Moscow, Mashinostroyeniye, 1985.

[18] WANG, F., ZHENG, P., DAI, J., WANG, H., WANG, R. Fault tree analysis of the causes of urban smog events associated with vehicle exhaust emissions: a case study in Jinan, China, *Science of the Total Environment* [online] 2019, **668**, p. 245-253. ISNN 1569-1705 Available from: http://dx.doi.org/10.1016/j.scitotenv.2019.02.348

[19] MA, D., ZHOU, ZH., JIANG, Y., DING, W. Constructing bayesian network by integrating FMEA with FTA. In: International Conference on Instrumentation, Measurement, Computer, Communication and Control: proceedings [online]. IEEE. 2014, ISBN 978-1-4799-6575-5, p. 696-700. Available from: https://doi.org/10.1109/IMCCC.2014.148

[20] TANG, T., LU, Y., ZHOU, T., JING, H., SUN, H. FTA and FMEA of braking system based on relex 2009. In: International Conference on Information Systems for Crisis Response and Management: proceedings [online]. IEEE. 2012. ISBN 978-1-4577-0369-0, eISBN 978-1-4577-0368-3, p. 106-112. Available from: https://doi.org/10.1109/ISCRAM.2011.6184087

[21] MIL-HDBK-217 "Reliability prediction of electronic equipment" [online]. 1991. Available from: https://www.quanterion.com/wp-content/uploads/2014/09/MIL-HDBK-217F.pdf

[22] RD 03-418-01 "Guidelines for risk analysis of hazardous production facilities" [online]. 2001. Available from: https://docs.cntd.ru/document/1200012878

[23] Agency for strategic planning and reforms of the Republic of Kazakhstan Bureau of National statistics [online]. 2021. Available from: https://stat.gov.kz/

[24] MAKAROVA, I., SHUBENKOVA, K., MUKHAMETDINOV, E., MAVRIN, V., ANTOV, D., PASHKEVICH, A. ITS safety ensuring through situational management methods. In: *Intelligent transport systems - from research and development to the market uptake* [online]. T. KOVACIKOVA, L. BUZNA, G. POURHASHEM, G. LUGANO, Y. CORNET, N. LUGANO (eds.). Cham, Springer, 2018. ISBN 978-3-319-93709-0, eISBN 978-3-319-93710-6, p. 133-143. Available from: https://doi.org/10.1007/978-3-319-93710-6

[25] XIN, S., ZHANG, L., JIN, X., ZHANG, Q. Reconstruction of the fault tree based on accident evolution. *Process Safety and Environmental Protection* [online]. 2019, **121**, p. 307-311. ISSN 0957-5820. Available from: http://dx.doi.org/10.1016/j.psep.2018.11.003

[26] WANG, Z., WEI, S., BAO, K., LIU, Y., PENG, S., ZHANG, Q. Analysis of multiple failure behaviors of steering knuckle ball hinge of multi-axle heavy vehicle. 2021, **13**(10), p. 1-8. ISSN 1687-8132. Available from: https://doi.org/10.1177/16878140211052287

[27] TORYIAMA, T., MURAKAMI, Y. The √area parameter model for evaluation of effects of various artificial defects and mutual interaction of small defects at the fatigue limit. *Journal of the Society of Materials Science* [online]. 1993, **42**, p. 1160-1166. ISSN 1880-7488. Available from: https://doi.org/10.2472/jsms.42.1160

[28] BASOV, K. A., KRASKOVSKIJ, D. G. *ANSYS in examples and tasks*. Moscow, KompyuterPress, 2002. ISBN 5-89959-092-0.

[29] SURJADI, J. U., GAO, L., DU, H., LI, X., XIONG, X., FANG, N.X., LU, Y. Mechanical metamaterials and their engineering applications. *Advanced Engineering Materials* [online]. 2019, **21**(3), 1800864. ISSN 1438-1656. Available from: https://doi.org/10.1002/adem.201800864

[30] WU, P., MENG, X., SONG, L., ZUO, W. Crash risk evaluation and crash severity pattern analysis for different types of urban junctions: fault tree analysis and association rules approaches. *Transportation Research Record: Journal of the Transportation Research Board* [online]. 2019, **2673**(1), p. 403-416. ISSN 0361-1981, eISSN 2169-4052. Available from: https://doi.org/10.1177/0361198118822

[31] PERNEBEKOV, S. S., USSIPBAYEV, U., SADYKOV, Z., AZHIBEKOV, K., URALOV, B. Selection of methods of optimization of indicators of reliability of cars. *PONTE Journal* [online]. 2018, **74**(10), p. 32-36. ISSN 2694-4839. Available from: http://dx.doi.org/10.21506/j.ponte.2018.10.3

[32] OSTREJKOVSKIJ, V.A. *Reliability theory*. Moscow, Vysshaya shkola, 2003. ISBN 5-06-004053-4

This is an open access article distributed under the terms of the Creative Commons Attribution 4.0 International License (CC BY 4.0), which permits use, distribution, and reproduction in any medium, provided the original publication is properly cited. No use, distribution or reproduction is permitted which does not comply with these terms.

OPTIMIZATION OF THE INJECTION MOLD RUNNER SYSTEM OF THE TRANSPORT MEANS PLASTIC PARTS

Damián Čechmánek*, Róbert Kohár, František Brumerčík, Michal Lukáč, Jakub Fiačan

Department of Design and Mechanical Elements, Faculty of Mechanical Engineering, University of Zilina, Zilina, Slovakia

*E-mail of corresponding author: damian.cechmanek@fstroj.uniza.sk

Damián Čechmánek 0000-0003-2143-6009,
František Brumerčík 0000-0001-7475-3724,
Jakub Fiačan 0000-0001-5171-8467
Róbert Kohár 0000-0001-7872-2829,
Michal Lukáč 0000-0003-3390-5319,

Resume

This paper describes the optimization of dimensions of the individual injection mold runner system of the plastic part used as the frame for various devices in transport means. Nowadays, the great emphasis is placed on the production time and finances associated with design and production. As a result, simulations are being employed increasingly. This paper aims to describe the design the optimum size and shape of the sprues and runners required for proper filling and to simulate the injection molding process to avoid problems and defects that tend to be caused by an incorrectly sized runner system. As a result, some adjustments were made to the size of the runner system to eliminate problems with underfilling, overfilling, air traps and weld lines. The difficulties with the original design were fixed by the optimized solution, which improved the monitored parameters. Additionally, the technological parameters of the injection process were modified, resulting in lower stress on the injection mold in the injection process.

Article info

Received 24 March 2023
Accepted 2 May 2023
Online 16 May 2023

Keywords:

runner system
injection molding
injection mold
constructional design
analysis

Available online: https://doi.org/10.26552/com.C.2023.046

ISSN 1335-4205 (print version)
ISSN 2585-7878 (online version)

1 Introduction

The plastic injection molding is a highly efficient way of producing a wide range of thermoplastic products and offers many advantages. Injection molding ensures the production of complex and intricate shapes of plastic products in short production cycles with excellent surface quality, good dimensional and shape accuracy and high reproducibility of mechanical and physical properties [1]. Injection molding can be used to manufacture plastic products by injecting molten polymer under high pressure into a designed mold [2]. The injection mold must be well designed and manufactured before any products can be molded [3].

In addition to the proper design of the mold cavity, the proper design of the runner system is very important, as well. The runner system ensures the passage of molten plastic from the injection molding machine nozzle to the mold cavity [4]. The cold runner system consists of the sprue, the main runner, the runner branch, the cold slug and the gates [5]. An important factor is the location of the gates, which can affect the direction of flow and solidification of the melt during and after the filling. The design of the runner system, especially the gate system, is critical to eliminate underfill, overfill and weld lines [6].

In recent years, many programs for computer simulation of injection molding processes have been developed and among the most widely used programs is Autodesk Inventor [7]. This software is often used to optimize the injection molding process. The development of computer simulation techniques that mimic the injection molding process, such as CAE, has the potential to replace the costly trial-and-error experiments that have been associated with the process [8]. These experiments were used at a time when the mentioned CAE software did not yet exist. They consisted in designing a distribution system of a certain shape and dimensions according to general design rules and procedures and then modifying it to achieve an optimal solution.

In this paper, the dimensions of the runner system

are optimized using the Autodesk Inventor software. The parameters monitored were the injection process parameters, simulation of filling time, plastic flow, confidence of filling, quality prediction, air traps and weld lines. Finally, the results of the analysis were compared between the two variations of the runner system's size.

The proper design of the mold runner system is based on the use of various progressive systems, such as design CAD systems [9-11] or calculation FEM systems [12-15], which support the design process of the molded part significantly.

2 Analysis of mold filling

The mold-filling analysis was created using the Autodesk Inventor Mold Design. The basis of the analysis is the design of the injection mold. The first step of the design is to insert a 3D model of the plastic part and adjust its orientation, concerning the opening direction of the injection mold. This is followed by selection of a suitable type of material. For this analysis, SCHULAMID 6 GF 30 plastic from manufacturer A. Schulman GMBH was chosen. Next, the mold design proceeds with creation of the cavity and the core. It consists of defining the position of the gate location and workpiece setting, creating the patch surfaces and creating the runoff surface. Subsequently, the main parts of the injection mold are created using the "Generate core and cavity" command. The design then continues by sketching the runner and selecting its shape and dimensions. According to Fattori [16] the runner should not be too big or too small. It requires much more force to fill the cavities if it is too small and there is a danger that they will freeze off before

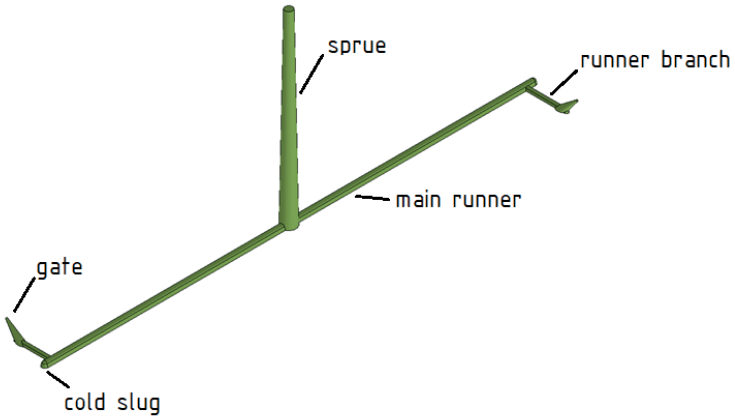

Figure 1 *Runner system of the original design*

a) *b)*

Figure 2 *Elements of the runner system of the original design*
a) Main runner b) Runner branch

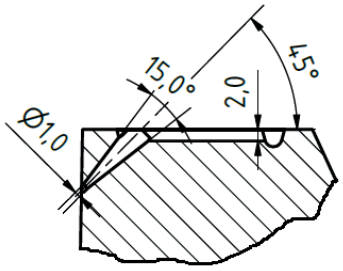

Figure 3 *Submarine-type gate of the original design*

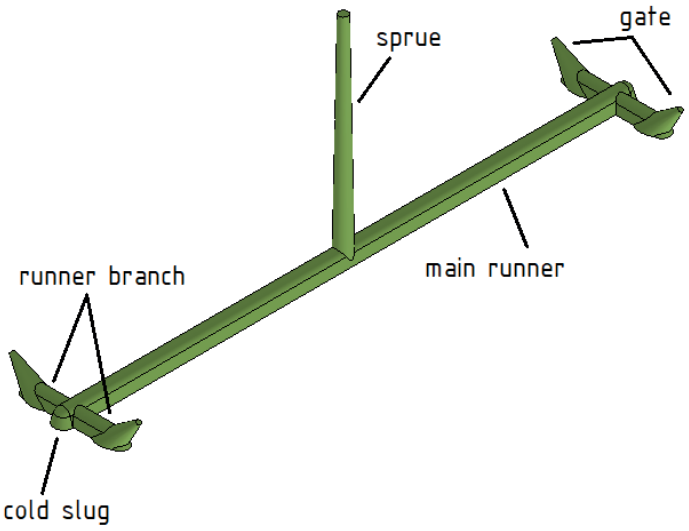

Figure 4 *Runner system of the optimized design*

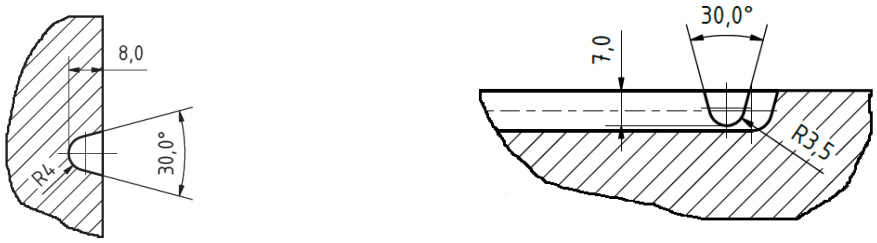

a) *b)*

Figure 5 *Elements of the runner system of the optimized design*
a) Main runner b) Runner branch

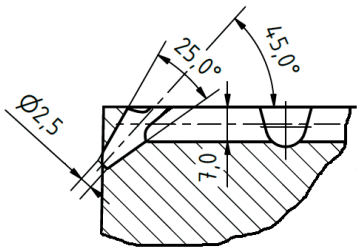

Figure 6 *Submarine-type gate of the optimized design*

the part is completely packed out. Even if reground material is allowed, a large runner should still be avoided because it can increase cycle time. Determining the size of a runner, just like a gate, is a balancing act. To properly size a runner, one has to start at the gate end and work the way back toward the sprue. The shape and corresponding dimensions of the gate are defined using the command "Gate". For the ejection system to function correctly, the injection molded product must remain on the side of the cavity after the mold has been opened. This is ensured using the cold wells, which were defined in the next design step. The next step was to create the inserts for the holes that contain the product. The last step is creation of the mold base. The type of the mold base, its manufacturer and dimensions are selected; next, the position and type of ejectors, sprue bushing and locating ring. Once the mold has been successfully designed, it is still necessary to define the mold processing setup input parameters, such as mold temperature, melt temperature, the maximum injection pressure of the machine and the opening time of the machine fixture. In both variants of the runner system design, the input parameters were the same. The change of parameters does not depend on the shape and dimensions of the system, but are based on the product data sheet that is supplied with the plastic. Then, the analysis can be started using the "Mould filling analysis" command.

Original design

The original design of the runner system, Figure 1, consists of a sprue, which is formed by the sprue bushing and a main runner, which is U-shaped of a depth of 3 mm, Figure 2a. It is further formed by a runner branch, which has the same shape and a depth of 2 mm, Figure 2b. The termination of the runner branch is formed by the gates. A submarine-type gate with a diameter of 1 mm was chosen, Figure 3.

Optimized design

The optimized design of the runner system, Figure 4, consists of a sprue, which is formed by the sprue bushing and a main runner, which is U-shaped of a depth of 8 mm, Figure 5a. It is further formed by a runner branch having the same shape and a depth of 7 mm, Figure 5b. The termination of the runner branches is formed by the gates. A submarine-type gate with a diameter of 2.5 mm was chosen, Figure 6.

2.1 Parameters of the injection molding process

The resulting values of the technological parameters of the analysis for the original design can be seen in Table 1 and for the optimized design in Table 2. The actual filling time represents the filling time of the injection mold cavities. The simulation of the filling time for both designs can be seen in Figures 7 and 8. The main role of injection pressure, in conjunction with injection velocity, is to ensure the volumetric filling of

Table 1 *Parameters of the injection molding process of the original design*

Parameter	Value
Actual filling time	1.50 (s)
Actual injection pressure	180.0 (MPa)
Clamped force area	21397.15 (mm^2)
Max. clamp force during filling	59.38 (t)
Velocity/pressure switch-over at % volume	99.1 (%)
Velocity/pressure switch-over at time	1.48 (s)
Estimated cycle time	15.49 (s)

Table 2 *Parameters of the injection molding process of the optimized design*

Parameter	Value
Actual filling time	1.71 (s)
Actual injection pressure	94.202 (MPa)
Clamped force area	23973.13 (mm^2)
Max. clamp force during filling	54.527 (t)
Velocity/pressure switch-over at % volume	99.02 (%)
Velocity/pressure switch-over at time	1.69 (s)
Estimated cycle time	15.15 (s)

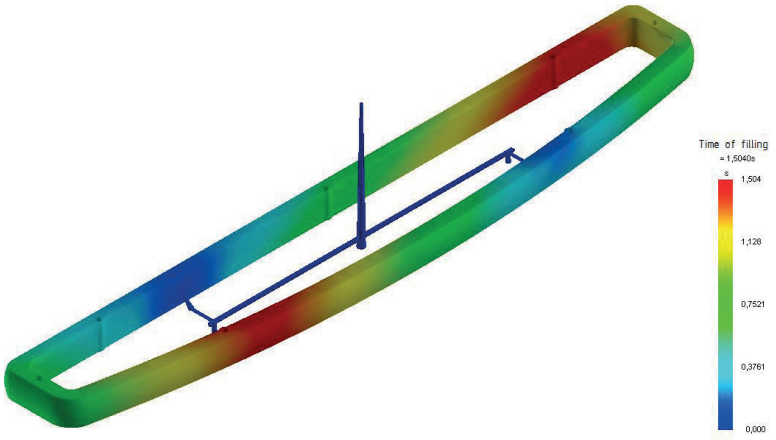

Figure 7 *Actual filling time of the original design*

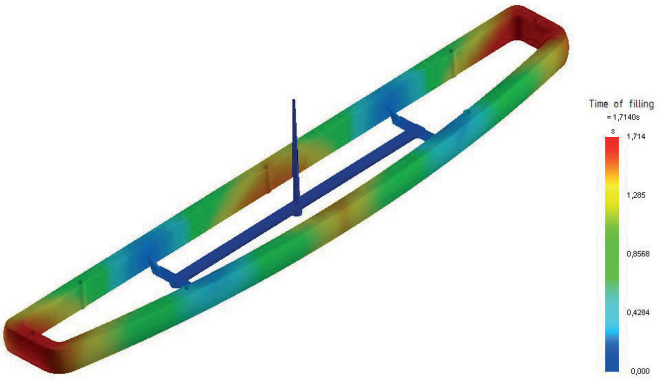

Figure 8 *Actual filling time of the optimized design*

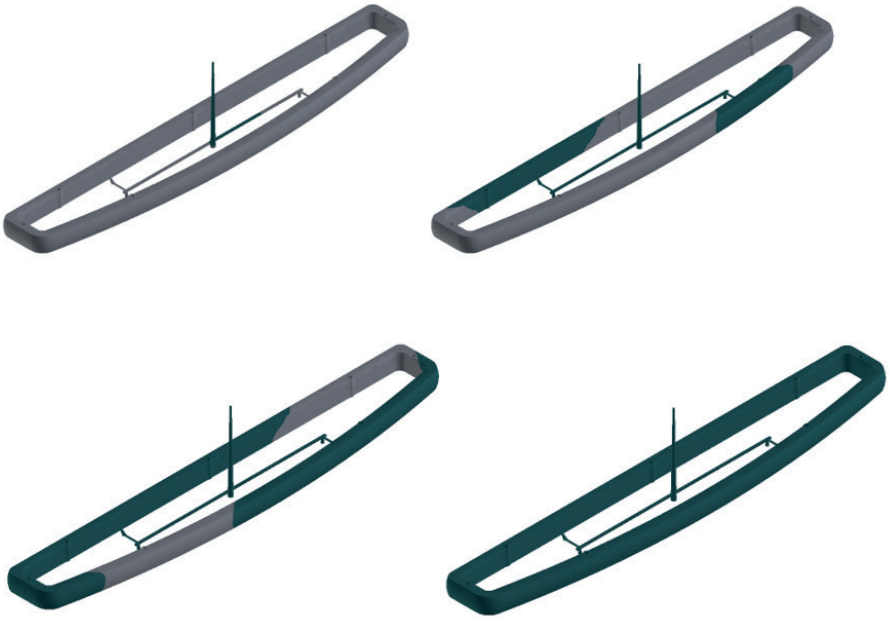

Figure 9 *Simulation of the plastic flow of the original design*

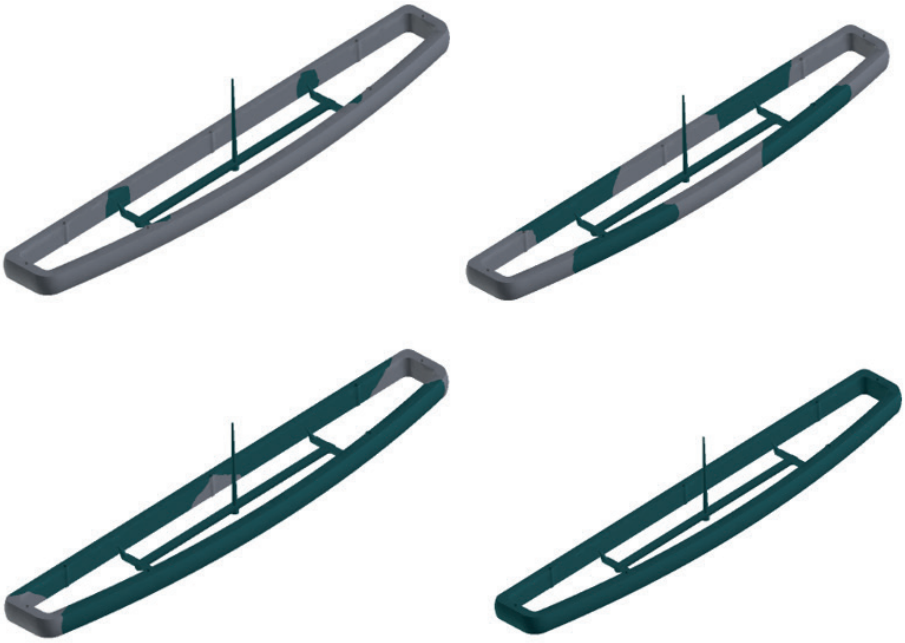

Figure 10 *Simulation of the plastic flow of the optimized design*

the mold cavity with the least possible melt shear stress, which is also related to a reduction in the strength stress of the injection mold. The clamping force is a reaction against the injection pressure and its magnitude must ensure the production of an injection molded product without burrs and overshoots. When switching from the injection pressure to the overpressure phase, there is a change in the control of the injection process. In the injection phase, the flow rate and injection velocity are regulated and in the overpressure phase, the pressure is regulated [4]. The last parameter of the analysis is the estimated filling time. This is composed of five main periods, namely the clamping time, injection time, dwelling time, cooling time, mold opening time and ejection time.

2.2 Simulation of the plastic flow

Figure 9 shows a simulation of the plastic flow in the mold cavity of the original design, Figure 10 represents the flow in the optimized design. The melt advances from the injection unit through the nozzle tip into the sprue and then into the main runner. Next, it passes through the runner branch and flows into the forming cavity through the gate. Simulation of the flow shows that there are no problems and thus the entire cavity space is filled with the melt at the end of the cycle.

2.3 Confidence of fill

Another output of the simulation is the confidence of fill, which shows the probability of filling the cavity area with plastic under the normal injection molding conditions. The simulation result is derived from the pressure and temperature results. If the filling process does not fill the molding cavity and results in a short shot, the design must be modified, the gate location changed, the plastic type reconsidered and the process conditions modified. Appropriate adjustments must also be made if the quality of the injected product is not satisfactory. Figure 11, shows confidence in filling in the original design, Figure 12, shows confidence in filling in the optimized design [17].

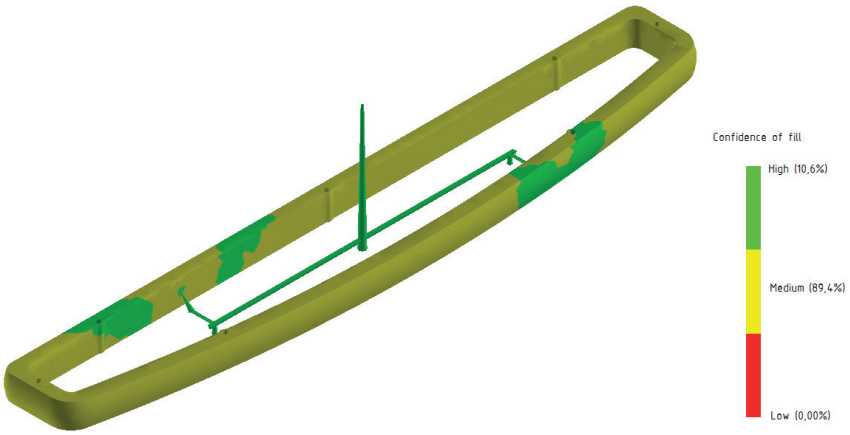

Figure 11 *Confidence of fill of the original design*

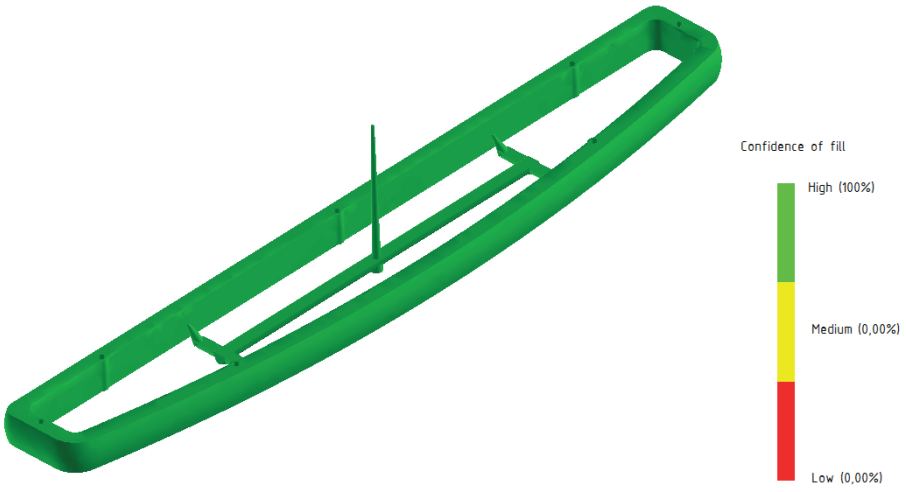

Figure 12 *Confidence of fill of the optimized design*

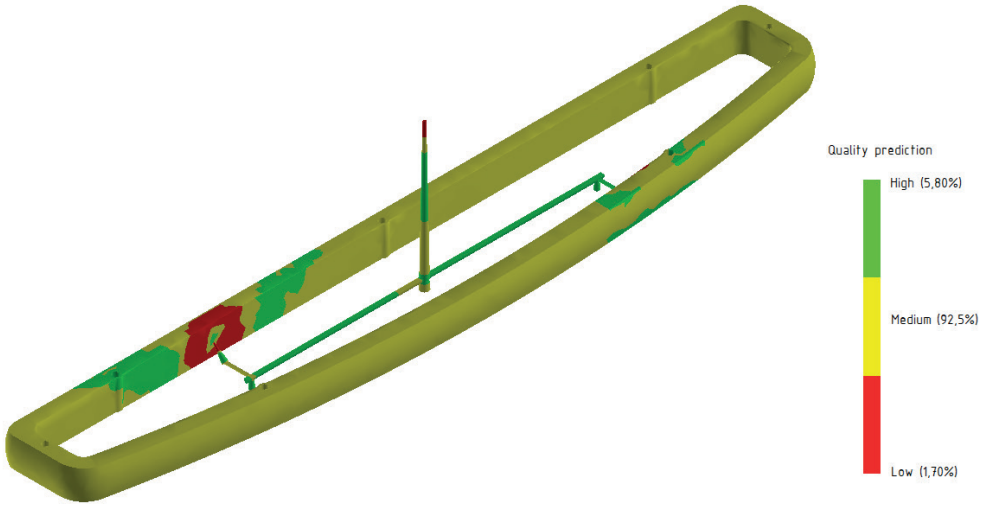

Figure 13 *Quality prediction of the original design*

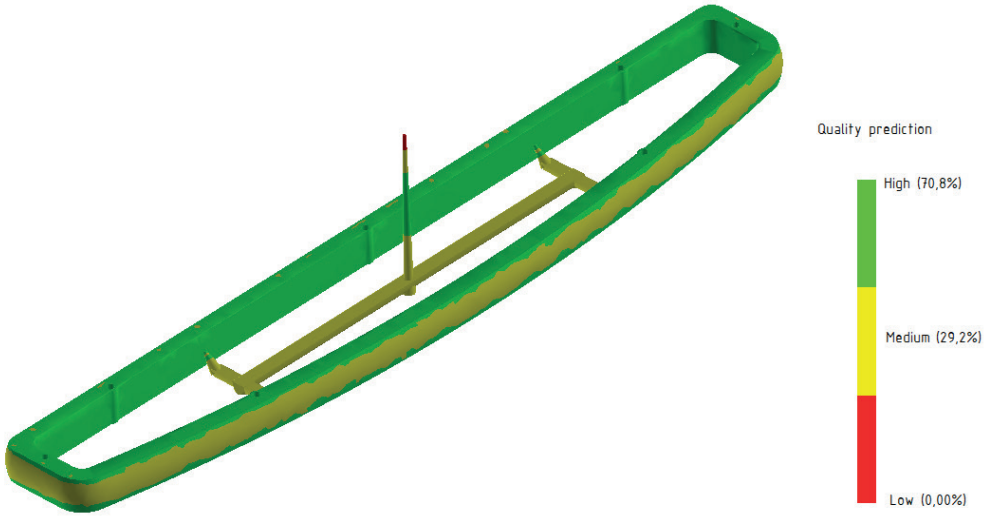

Figure 14 *Quality prediction of the optimized design*

2.4 Quality prediction

The task of the quality prediction simulation is to estimate the quality of the mechanical properties and appearance of the injected product. The basis for this analysis is the functional filling of the mold cavity. The simulation result is derived from pressure, temperature and other results. Figure 13 represents the quality of the injected product of the original design and Figure 14 represents the quality of the injected product of the optimized design. The quality of the parts of the injected product shown in green should be high, the yellow color represents the parts with limited quality and the red color represents the quality problems [18].

2.5 Air traps

When the mold is closed in the injection molding process, the air in the mold cavity is sealed. After a batch of melt is injected, the enclosed air is pushed in front of the melting face, enclosed by it, compressed and excessively heated, which can lead to its expansion. The inability of the air to escape leads to several problems. Expansion is responsible for the local degradation of the melt and as it burns it turns black and its surface contains residues from combustion. Another problem can be insufficient melt flow, resulting in an untouched spot at the edge or in the middle of the shot area or shape. This leads to apparent defects and technical problems such as:

- Insufficient melt flowability - solidification of the melting face,
- Air sealing - appearance of bubbles in the walls of the injected product,
- Increased probability of weld lines leading to reduced local strength,
- Internal stresses,
- Increase in anisotropy of product properties and The greater probability of mold corrosion due to

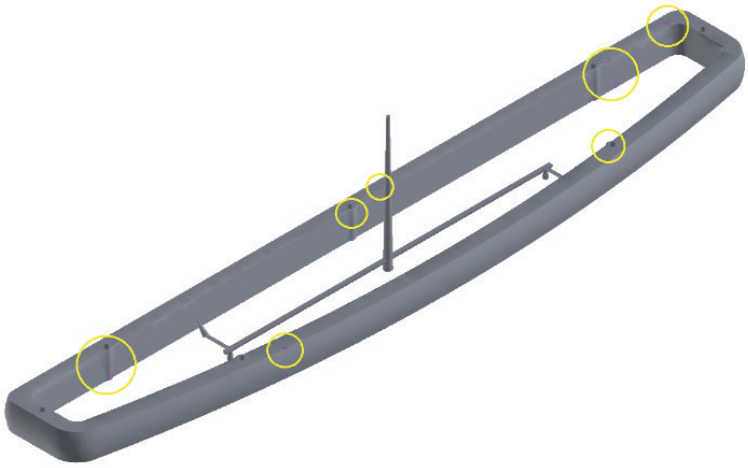

Figure 15 *Air traps of the original design*

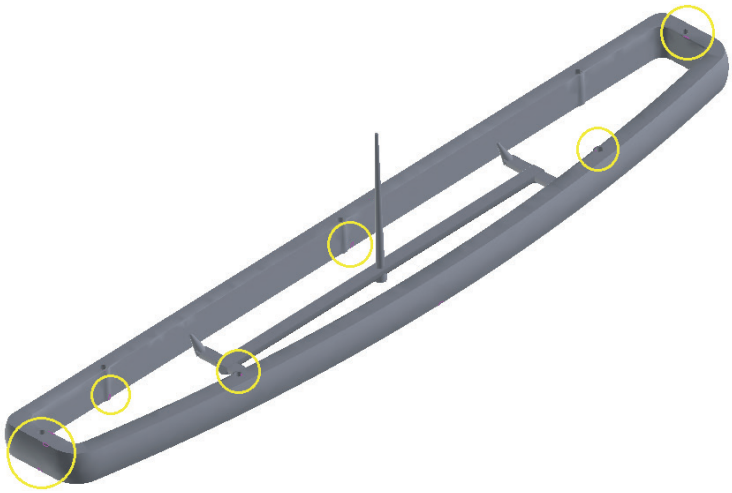

Figure 16 *Air traps of the optimized design*

an increase in temperature and pressure, leading to the release of gases from the injected material that can chemically react with the mold material.

There are several methods to prevent the air trap problems. The first method uses simulation programs output of which is a prediction of the occurrence of air traps. The second method uses the knowledge and experience of the designer, who already considers the method of venting in the mold design process. The last way is to address venting after the mold has been tested, if necessary [4].

In this mold design, the venting of the molding cavity was already considered during the design process. The venting is implemented through the following design modifications. The core is designed as a divided part and consists of a core plate and a core insert. There is a gap between the two to ensure the air leakage. A further modification are the gaps between the ejector holes and the ejectors themselves and the gaps for false cores, which provide sufficient space for air leakage. Figure 15 shows the predicted locations of the air traps for the original design, Figure 16 for the optimized design. The air traps are located close to the holes for the ejectors and false cores, which was also required for the proper function of the injection mold.

2.6 Weld lines

Occurrence of the weld lines is directly related to filling of the molded cavity. A weld line occurs when the main melt stream is split into two or more streams by the mold elements in the mold cavity, or when the melt streams from multiple gates meet. Weld lines virtually always occur on the opposite side of the bypassed shape from the gate. The melt faces of the split flow cold and then join frontally, laterally, or tangentially. The weld lines adversely affect the properties of the product, specifically strength and appearance. Simulation programs can be used to predict the occurrence of weld lines, which would reveal potential problems before the actual mold production [4]. As can be seen in Figure 17 (original design) and Figure 18 (optimized design), the occurrence of weld lines is minimal and they are located at the meeting points of the melt faces.

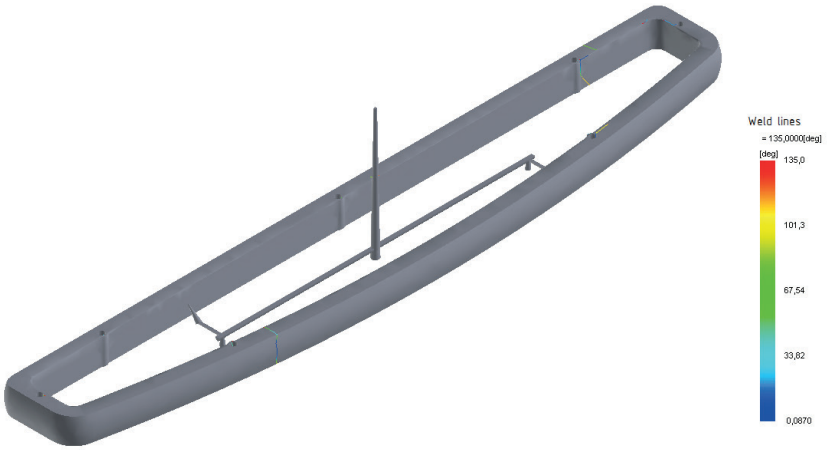

Figure 17 *Weld lines of the original design*

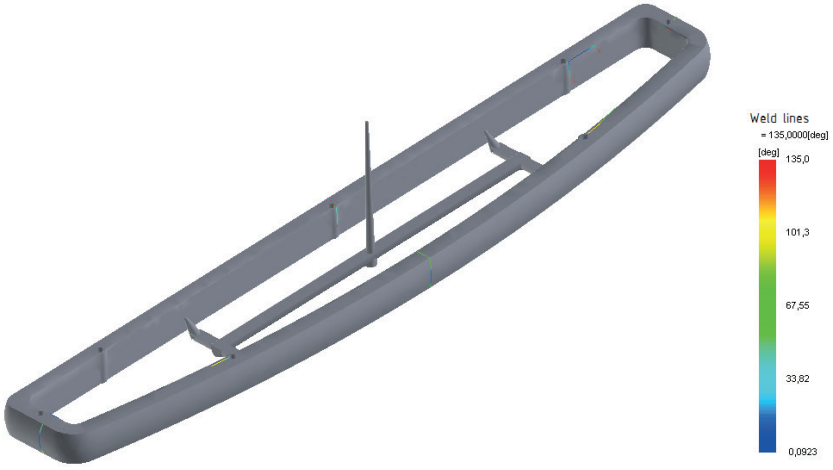

Figure 18 *Weld lines of the optimized design*

3 Conclusions

When designing an injection mold, it is necessary to follow a set of rules and recommendations that are generally known. The mold design process is very complex and consists of several areas. The selection of the type and proper design of the runner system is an essential part of this process. The runner system ensures the transfer of the melt from the injection molding machine to the injection mold. Its function is very important and the overall functionality of the injection process and product characteristics depend on it.

In the field of injection mold design, simulation programs are of great help. They have the advantage of providing the design results before the actual production of the injection mold. This results in a reduction in design and production time, as well as in cost savings associated with the production of prototypes. Autodesk Inventor software program was used for this optimization.

The original design of the runner system was a simple shape with certain dimensions. Based on the analysis carried out, it was found that the dimensions of the runner system do not provide the melt with sufficient space for the proper filling and may be responsible for development of defects. By evaluating the results of this analysis and its technological parameters, it was concluded that the dimensions of the runner system of the original design needed to be optimized. The optimization of the runner system design consisted in modifying the dimensions of the runner system and increasing the number of gates. This solution improved the melt flow into the mold cavity, ensured higher filling confidence and better product quality and eliminated the problems of the original design. In addition, the technological parameters of the injection process were changed, resulting in lower stress on the injection mold in the injection process. The advantage of lower stress is to ensure a longer lifetime of the injection mold.

The result of the runner system optimization process is a solution that meets the requirements for its function. This is proven by the results of the analysis, which are an excellent basis for the subsequent production of the injection mold.

Acknowledgement

The research was supported by the Cultural and Educational Grant Agency of the Ministry of Education, Science, Research and Sport of the Slovak Republic under the project No. 045ZU- 4/2021.

Conflicts of interest

The authors declare that they have no known competing financial interests or personal relationships that could have appeared to influence the work reported in this paper.

References

[1] LENFELD, P. Technologie II. [online] [accessed 2023-02-06]. 2009. Available from: http://www.ksp.tul.cz/cz/kpt/obsah/vyuka/skripta_tkp/sekce_plasty/04.htm

[2] BOBCIK, L. *Moulds for plastics processing: injection molding of thermoplastics. Part 1/Formy pro zpracovani plastu: vstrikovani termoplastu. Cast 1* (in Czech). 2. ed. Brno: Uniplast, 1999.

[3] GRESKOVIC, F., SPISAK, E., DULEBOVA, L., VARGA, J., FABIAN, M. *Plastic processing tools - injection moulds/Nastroje na spracovanie plastov - vstrekovacie formy* (in Slovak). 1. ed. Kosice: Technical University of Kosice, Faculty of Mechanical Engineering, 2010. ISBN 978-80-553-0350-5.

[4] ZEMAN, L. *Injection molding of plastics/Vstrikovani plastu* (in Czech). 1. ed. Prague: Grada Publishing, a.s., 2018. ISBN 978-80-271-0614-1.

[5] Gates and runners - Xcentric Mold [online] [accessed 2023-02-14]. Available from: https://www.xcentricmold.com/gates-and-runners/

[6] ZEMAN, L. *Injection molding of plastics 2/Vstrikovani plastu 2* (in Czech). 1. ed. Prague: Grada Publishing, a.s., 2021. ISBN 978-80-271-1294-4.

[7] Choosing a 3D CAD program for molding design - protolabs [online] [accessed 2023-02-13]. Available from: https://www.protolabs.com/en-gb/resources/design-tips/3d-cad-programs/

[8] IVORY, R. Advantages of CAE/CAM for plastic injection molding [online] [accessed 2023-02-06]. 2014. Available from: https://info.crescentind.com/blog/bid/69398/advantages-of-cae-cam-for-plastic-injection-molding

[9] SKYBA, R., HRCEK, S., SMETANKA, L., MAJCHRAK, M. Creation of calculation 3D model of slewing bearing. In: *Current methods of construction design. Lecture notes in mechanical engineering* [online].

[10] MEDVECKY, S., HRCEK, S., KOHAR, R., BRUMERCIK, F., KONSTANTOVA, V. (eds.). Cham: Springer, 2019. ISBN 978-3-030-33145-0, eISBN 978-3-030-33146-7, p. 149-157. Available from: https://doi.org/10.1007/978-3-030-33146-7_18

[11] STEININGER, J., HRCEK, S., SMETANKA, L., SKYBA, R. Optimisation procedure of inner geometry in spherical roller bearings with regard to their durability. *Scientific Journal of Silesian University of Technology - Series Transport* [online]. 2020, **106**, p. 173-181. ISSN 0209-3324, eISSN 2450-1549. Available from: https://doi.org/10.20858/sjsutst.2020.106.15

[12] HRCEK, S., BRUMERCIK, F., SMETANKA, L., LUKAC, M., PATIN, B., GLOWACZ, A. Global sensitivity analysis of chosen harmonic drive parameters affecting its lost motion. *Materials* [online]. 2021, **14**(17), 5057. eISSN 1996-1944. Available from: https://doi.org/10.3390/ma14175057

[13] HRCEK, S., SMETANKA, L., STEININGER, J., PATIN, B. Increase of durability in the area of line contact with curved body geometry. *Mechanism and Machine Theory* [online]. 2022, **176**, 105010. Available from: https://doi.org/10.1016/j.mechmachtheory.2022.105010

[14] SKYBA, R., HRCEK, S., SMETANKA, L., MAJCHRAK, M. Strength analysis of slewing bearings. *Transportation Research Procedia* [online]. 2019, **40**, p. 891-897. ISSN 2352-1457, eISSN 2352-1465. Available from: https://doi.org/10.1016/j.trpro.2019.07.125

[15] WEIS, P., KUCERA, L., PECHAC, P., MOCILAN, M. Modal analysis of gearbox housing with applied load. *Procedia Engineering* [online]. 2017, **192**, p. 953-958. ISSN 1877-7058. Available from: https://doi.org/10.1016/j.proeng.2017.06.164

[16] FATTORI, J. Tooling: how to properly size, gates, runners and sprues. Part 3. [online]. [accessed 2023-02-17] 2020. Available from: https://www.ptonline.com/blog/post/tooling-how-to-properly-size-gates-runners-and-sprues-part-3

[17] Confidence of fill result - Autodesk [online] [accessed 2023-02-08]. Available from: https://knowledge.autodesk.com/support/inventor/learn-explore/caas/CloudHelp/cloudhelp/2021/ENU/Inventor-Help/files/GUID-ABE48DE8-B01A-4A24-8AB4-E84A674AF3AA-htm.html

[18] Quality prediction result - Autodesk Moldflow Adviser [online] [accessed 2023-02-10]. Available from: https://help.autodesk.com/view/MFAA/2016/ENU/?guid=GUID-4F115A68-4469-4414-BB62-80B341FAC3AF

This is an open access article distributed under the terms of the Creative Commons Attribution 4.0 International License (CC BY 4.0), which permits use, distribution, and reproduction in any medium, provided the original publication is properly cited. No use, distribution or reproduction is permitted which does not comply with these terms.

STRENGTH ASSESSMENT OF AN IMPROVED DESIGN OF A TANK CONTAINER UNDER OPERATING CONDITIONS

Sergii Panchenko[1], Juraj Gerlici[2], Glib Vatulia[3], Alyona Lovska[2,*], Andrij Rybin[1], Oleksandr Kravchenko[2]

[1]Ukrainian State University of Railway Transport, Kharkiv, Ukraine
[2]University of Zilina, Zilina, Slovak Republic
[3]O. M. Beketov National University of Urban Economy in Kharkiv, Kharkiv, Ukraine

*E-mail of corresponding author: alyonaLovskaya.vagons@gmail.com

Sergii Panchenko 0000-0002-7626-9933,
Glib Vatulia 0000-0002-3823-7201,
Andrij Rybin 0000-0001-7546-0077,
Juraj Gerlici 0000-0003-3928-0567,
Alyona Lovska 0000-0002-8604-1764,
Oleksandr Kravchenko 0000-0003-4677-2535

Resume

The publication presents the results of research into the strength of an improved tank container. The tare of a tank container can be reduced through application of composite material for the tank. In this case its mass can be 46% lower than that of a metal tank. The strength of the tank was calculated by computer simulation. The maximum stress occurs in its lower part and is about 295 MPa.

The dynamic loading of a tank can be reduced by application of elastic elements in the fittings of a tank container. The reduction in dynamic load is achieved by the elastic friction forces generated in the fittings. The results of mathematical modelling of the tank container dynamics proved the effectiveness of this solution.

Article info

Received 7 February 2023
Accepted 2 May 2023
Online 23 May 2023

Keywords:

tank container
improvement construction
dynamic load
construction strength
container transportation

Available online: https://doi.org/10.26552/com.C.2023.047

ISSN 1335-4205 (print version)
ISSN 2585-7878 (online version)

1 Introduction

One of the most mobile transport facilities widely used for combined transportation is containers. This is by a reason, that they can be transported by almost all types of transport: rail, road, air and sea. In case of railway transport, containers are the most often transported on a flat car (Figure 1 [1]).

At present the use of tank containers is increasing due to higher volume of liquid freight transported along international transport corridors (Figure 2 [2-3]).

The demand for inter-modal tank containers is increasingly growing. There is a need for development and introduction of innovative tank containers with improved characteristics. The designing of such structures for tank containers requires the introduction of measures for their better strength during operational modes which will provide ecological compatibility [4-7] of combined transportation and lower maintenance costs.

2 Analysis of recent research and publications

The issue of the dynamic loading and the strength of tank containers was studied by many researchers. Study [8] presents the study of the loading to a tank container on the flat car during a shunting impact. The calculation of the accelerations to a tank container included a technological gap between fixed fittings and container fittings. The longitudinal forces on the flat wagon were approximately 2.2 - 2.8 MN according to the tank container load.

However, the maximum longitudinal force on the flatcar during shunting is 3.5 MN [9]. Therefore, improved values of accelerations to a tank container in operation can be obtained by means of additional research.

Studies [10-11] have presented the results of optimization of the tank car structures and substantiated development and introduction of tank containers as transport means into operation. They designed improved

a) b)

Figure 1 *Placement of containers on a flat car*
a) dry bulk containers; b) tank containers

a) b)

Figure 2 *Tank container*
a) model T11-254 / T11-254.2; b) model T14-254

tank container structures. The strength model of a tank container included the normative loading values given in [9]. The study into the strength of tank container with improved operational loading values (compliance of freight, displacements of container fittings relative to fixed fitting, etc.) was not included.

The strength calculation for a tank car in operational loading are described in article [12]. The authors used the ABAQUS calculation tool. The case of static loading on the tank container structure according to ISO 1496-3 [13] was included in the calculation.

Study [14] presents the calculation of the dynamic of a tank container transported by road or rail transport. This study was used for the research into an advanced tank container structure. Besides, these studies do not give the engineering solutions to reduction of the loading on the tank container structure.

The issue of how the structural solution for tank containers impacts their loading in operation is studied in [15]. The work caclulated the stress strain state of a tank container. The authors substantiated the structural solution for a hatch in the tank.

However this tank container structure does not include elements intended for reduction of the loading at operational loading modes.

Study [16] presents the research into the strength of a tank container. The authors analyzed how the finite element mesh influences the stresses of a tank container. However, the authors did not provide solutions for improvements in the bearing structure of a tank container for improved strength in operational modes.

The analysis of literature [8-16] shows that there is a possibility for further developments and improvements of the tank containers in order to provide their strength and higher operational efficiency.

3 The aim and main objectives of the article

The objective of the publication is research into the loading of the tank container with the tank of composite material and improved container fittings. The given objective can be achieved by means of the following tasks:

- determine the strength of the tank of a container of composite material; and
- study the longitudinal loading on the structure of a tank container on the flat car during a shunting impact.

4 Presentation of the main content of the article

In their previous studies the researchers developed the method to reduce the material capacity of tank container by improving its frame through replacing the rectangular cross-section, used in the standard structure, for the circular pipes which provide both strength conditions and operational reliability (Figure 3).

The new structure of a frame of container is calculated for loading mentioned in [9]. It was found that the improved structure of the frame is 354 kg lighter than that of its existing analogue, which together with their massive state produces a considerable economic effect.

The tank container tare can also be decreased if the tank is made of composite material. The mass can be reduced by 46 % in comparison with a metal tank. The substantiation of this solution was made with the computer modelling of the strength of the tank. The graphic work for the tank container have been made in SolidWorks (Figure 4).

The model included several pads mounted in the

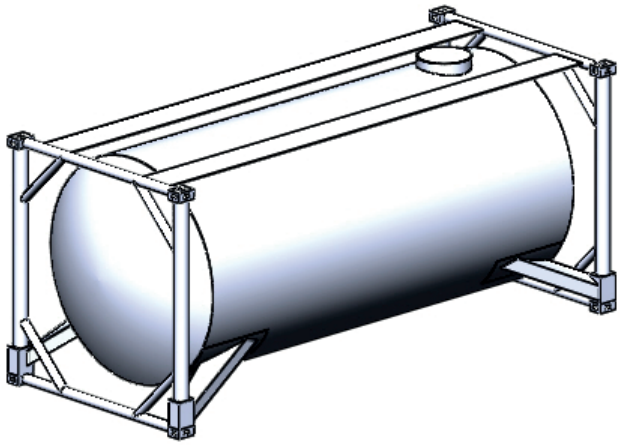

Figure 3 *Spatial model of an improved tank container*

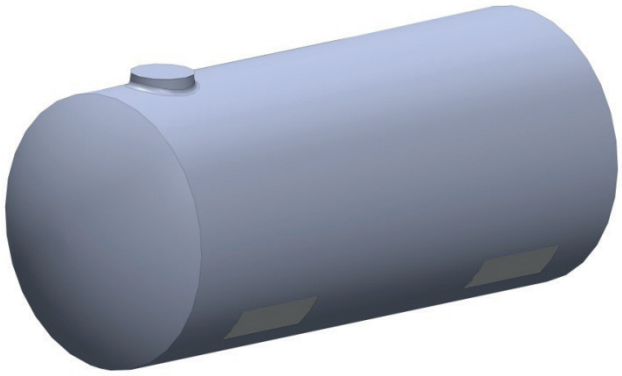

Figure 4 *Model of the tank*

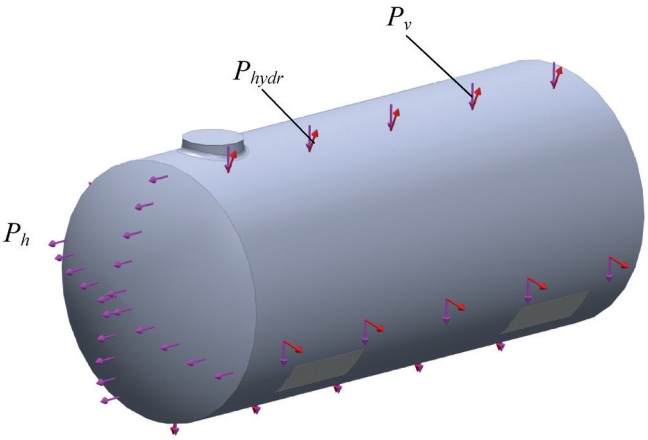

Figure 5 *Design diagram of the tank*

area where the tank rested on the frame with the geometry identical to the padding sheets.

The strength calculation was made with the FEM in SolidWorks Simulation [17-20].

It was taken into account that the tank was made of a composite with linear elastic orthotropic characteristics [21-22]. The limit strength along the fiber was 1100-1300 MPa and across the fiber - 650 MPa. The number of layers in the material was taken equal to 2. The strength calculation for the tank was made as if for a thin shell. The model was secured in the areas of support of the tank on the padding sheets. The model was rigidly fixed.

The FEM was built with tetrahedrons [23-24], the optimum of which was calculated with FAM [25-27].

The elements in the mesh was 13065, and nodes - 38714. The calculation diagram is given in Figure 5.

The pressure to the tank P_h was determined to the formula [9]:

$$P_h = N \cdot \frac{m_v}{m_{br}} \cdot \frac{1}{F}, \quad (1)$$

where:

N - impact force to a coupler, MN; m_v - mass of freight in the tank, kg; m_{br} - gross mass of a container, kg; F - area of the internal cross section of the tank, m^2.

Petrol was taken as liquid freight.

The hydrostatic pressure was determined by formula:

$$P_{hydr} = \rho \cdot g \cdot h, \quad (2)$$

where:

ρ - density of liquid freight, kg/m^3; h - height of the freight distribution in the tank, m; g - acceleration of gravity, m/s^2.

The maximum stresses in the tank of a tank container occur in its bottom part and amount to about 295 MPa (Figure 6), which is 8% lower than in the standard structure.

Distribution of the stresses by the length of the cylindrical (bottom) part of the tank is given in Figure 7.

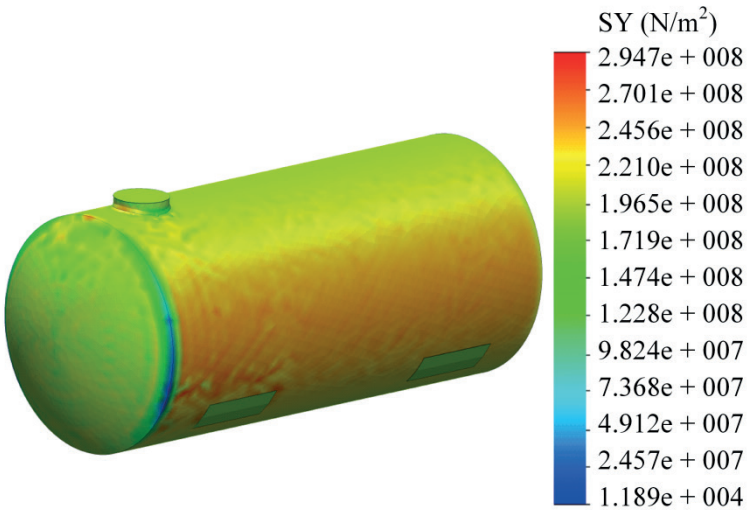

Figure 6 *Stress state of the tank*

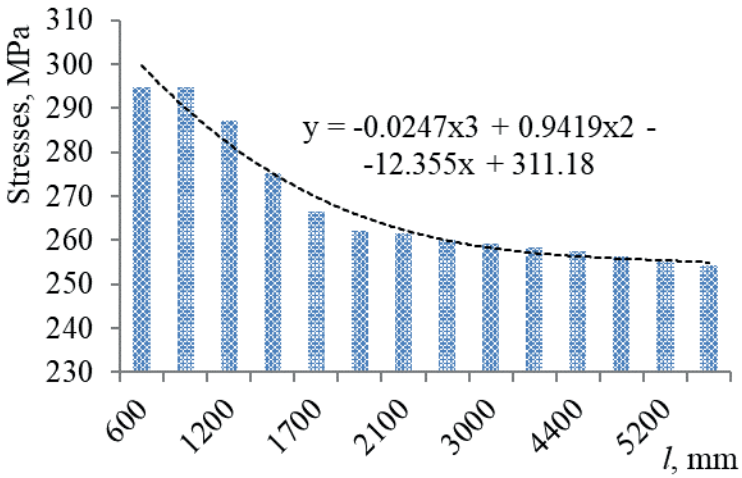

Figure 7 *Distribution of the stresses by the length of the cylindrical (bottom) part of the tank*

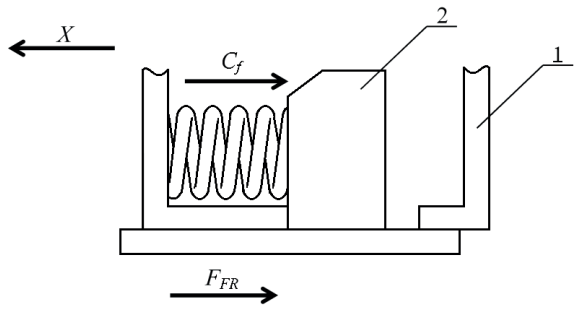

Figure 8 *Diagram of interaction container and flat car*
1 - container; 2 - flat car;
C_f - stiffness of the fitting spring, kN/m; F_{FR} - friction force, kN

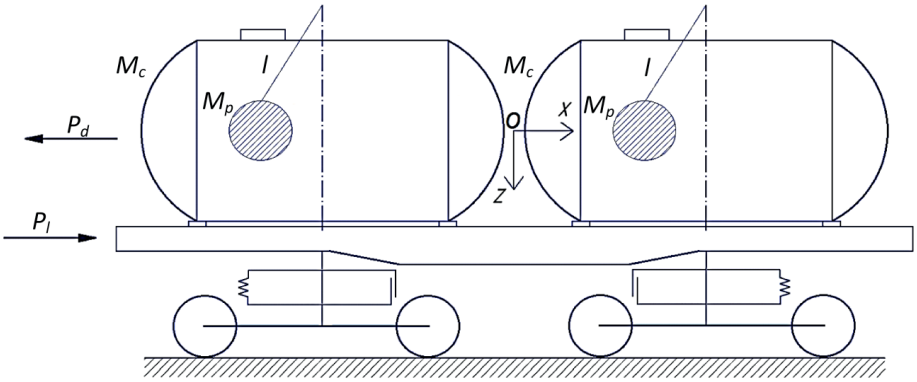

Figure 9 *Action of the longitudinal force to a flat car*

The maximum stresses occur on the side of the hatch and decrease along the tank length.

The loading of the tank can also be reduced by application of elastic elements in the tank container fittings (Figure 8).

The solution was substantiated through the mathematic modelling of the dynamic of a tank container. The calculation included the shunting impact of a flat car (Figure 9).

The accelerations of a tank container were studies through the mathematical model:

$$\begin{cases} M_{FC}^{gr} \cdot \ddot{q}_1 = P - \sum\limits_{i=1}^{n} \begin{pmatrix} F_{FR} \cdot sign(\dot{q}_1 - \dot{q}_2) + \\ + C_f(q_1 - q_2) \end{pmatrix}, \\ M_c \cdot \ddot{q}_2 = \sum\limits_{i=1}^{n} \begin{pmatrix} F_{FR} \cdot sign(\dot{q}_1 - \dot{q}_2) + \\ + C_f(q_1 - q_2) + M_P \cdot l \cdot q_3 \end{pmatrix}, \\ I_P \cdot \ddot{q}_3 = M_P \cdot l \cdot \ddot{q}_2 - g \cdot M_P \cdot l \cdot q_3, \end{cases} \quad (3)$$

where:
M_{FC}^{gr} - gross mass of a flat car, t; P_l - longitudinal force, kN; F_{FR} - friction force, kN; M_c - mass of a tank container, t; l_f - stiffness of elastic elements, kN/m; M_P - mass of a pendulum simulating the displacements of liquid freight in a tank container, t; l - length of a pendulum rod, m; I_P - inertia moment of a pendulum, t · m^2; q_1, q_2, q_3 - coordinates corresponding to displacements of flat car, tank container and freight relative to the longitudinal axle.

The movement of the liquid bulk cargo was described by a set of mathematical pendulums [8]. The value of the longitudinal impact force acting on the flat car was assumed to be 3.5 MN [9].

The hydrodynamic characteristics of the liquid bulk cargo were determined according to the method given in [28]. Petrol was taken into account as a liquid cargo. The hydrodynamic characteristics of the liquid cargo were made with the maximum admissible load of the tank container according to [29]. Based on the calculations performed in accordance with [28], the value of I_p = 250 t · m^2 was obtained.

Equation (3) was solved in MathCad [30-34]. To do this, it was reduced to the Cauchy form and then integrated using the Runge-Kutta method. In this case, one can write:

$$F(t,y) = \begin{bmatrix} y_2 \\ y_4 \\ y_6 \\ \dfrac{P_l - \sum\limits_{i=1}^{n} \begin{pmatrix} F_{FR} \cdot sign(y_2 - y_4) + \\ + C_f(y_1 - y_3) \end{pmatrix}}{M_{FC}^{gr}} \\ \dfrac{\sum\limits_{i=1}^{n} \begin{pmatrix} F_{FR} \cdot sign(y_2 - y_4) + \\ + C_f(y_1 - y_3) + M_P \cdot l \cdot y_5 \end{pmatrix}}{M_c} \\ \dfrac{M_P \cdot l \cdot \dot{y}_4 - g \cdot M_P \cdot l \cdot y_5}{I_P} \end{bmatrix}, \quad (4)$$

$$Z = rkfixed(Y0, tn, tk, n, F).$$

where:
Y0 - the vector with initial conditions, *tn, tk* - initial and final integration variables, *n'* - number of steps, *F* - the symbolic vector.

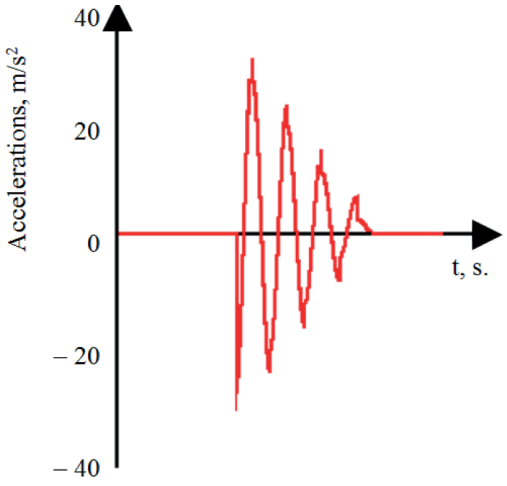

Figure 10 *Accelerations to the tank container*

The generalised accelerations acting on the components of the mechanical system were calculated in the array $ddq_{j,i}$:

$$ddq_{j,1} = \frac{P_l - \sum_{i=1}^{n}\begin{pmatrix} F_{FR} \cdot sign(y_2 - y_4) + \\ + C_f(y_1 - y_3) \end{pmatrix}}{M_{FC}^{gr}}, \tag{5}$$

$$ddq_{j,2} = \frac{\sum_{i=1}^{n}\begin{pmatrix} F_{FR} \cdot sign(y_2 - y_4) + \\ + C_f(y_1 - y_3) + M_p \cdot l \cdot y_5 \end{pmatrix}}{M_c}, \tag{6}$$

$$ddq_{j,3} = \frac{M_P \cdot l \cdot \dot{y}_4 - g \cdot M_P \cdot l \cdot y_5}{I_P}. \tag{7}$$

On the basis of the calculation the authors obtained the accelerations of an improved tank container structure (Figure 10).

This value of acceleration was about 40 m/s² (≈ 4g), thus it was within the allowable values.

5 Conclusions

The study deals with calculation of the strength of a tank container made of composite material and fittings with elastic-friction bonding. The use of composite materials will reduce the weight of the boiler by 46% compared with metal. The use of elastic-friction bonds in the fittings will reduce the dynamic load of the tank container during the operational regimes.

To investigate the strength of the tank container boiler, calculations were made using the finite element method. The stresses in the tank occur in its bottom part and amount to about 295 MPa, which is 8 % lower than that of the standard structure.

The longitudinal loading on the improved container located on the car during a shunting impact was studied. It was found that the accelerations to a container were about 40 m/s² (4g); the calculation included the elastic-frictional connections in the fittings; they do not exceed the allowable values. The total rigidity of the elastic elements for one tank container must be within a range of 426 - 535 kN/m.

This study will contribute to the development of tank containers with better technical and operational characteristics, higher operational efficiency and improved environmental friendliness of container transport.

Acknowledgements

This contribution was elaborated within execution of the project " Scholarships for Excellent Researchers Threatened by the Military Conflict in Ukraine ", code 09I03-03-V01.

Conflicts of interest

The authors declare that they have no known competing financial interests or personal relationships that could have appeared to influence the work reported in this paper.

References

[1] Carpathian wagons at Rail Expo 2019 - new grain trucks, containers, railway platform [online]. Available from: https://railexpoua.com/novyny/karpatski-vahony-na-rail-expo-2019-novi-zernovozy-konteinery-zaliznychna-platforma/

[2] Industry publication for rail transport specialists [online]. Available from: https://www.railway.supply/uk/kontejner-czisterna-t50-225-t50-225-1/
[3] Industry publication for rail transport specialists [online]. Available from: https://www.railway.supply/uk/kontejner-czisterna-t14-254/
[4] SOLOVIOVA, L., STRELKO, O., ISAIENKO, S. Container transport system as a means of saving resources. *IOP Conference Series: Earth and Environmental Science* [online]. 2020, **459**, 05200. ISSN 1755-1307, eISSN 1755-1315. Available from: https://doi:10.1088/1755-1315/459/5/052070
[5] STEISUNAS, S., DIZO, J., BUREIKA, G., ZURAULIS, V. Examination of vertical dynamics of passenger car with wheel flat considering suspension parameters. *Procedia Engineering* [online]. 2017, **187**, p. 235-241. ISSN 1877-7058. Available from: https://doi.org/10.1016/j.proeng.2017.04.370
[6] DIZO, J., BLATNICKY, M., STEISUNAS, S. Assessment of a rail vehicle running with the damaged wheel on a ride comfort for passengers. *MATEC Web of Conferences* [online]. 2017, **157**, 03004. eISSN 2261-236X. Available from: https://doi.org/10.1051/matecconf/201815703004
[7] SOUKUP, J., SKOCILAS, J., SKOCILASOVA, B., DIZO, J. Vertical vibration of two axle railway vehicle. *Procedia Engineering* [online]. 2017, **177**, p. 25-32. ISSN 1877-7058. Available from: https://doi.org/10.1016/j.proeng.2017.02.178
[8] BOGOMAZ, G. I., MEKHOV, D. D., PILIPCHENKO, O. P., CHERNOMASHENTSEVA, Y. G. Loading of tank-containers, proceeding from the railway platform, when hitting the coupler. Collection of scientific works "Dynamics and rotation of mechanical systems". 1992. p. 87-95.
[9] DSTU 7598:2014. Freight wagons. General requirements for calculations and design of new and modernized wagons of 1520 mm track (non-self-propelled). Kiev, Ukraine: UkrNDNTS, 2015.
[10] MYAMLIN, S. V., KEBAL, Y. V., KONDRATYUK, S. M. Perspective designs of tank containers for transportation of light oil products, ammonia and hydrocarbon gases. *Railway Transport of Ukraine*. 2012, **2**, p. 44-46. ISSN 2311-4061.
[11] LISOWSKI, E., CZYZYCKI, W. Transport and storage of LNG in container tanks. *Journal of KONES Powertrain and Transport*. 2011, **18**(3), p. 193-201. ISSN 1231-4005, e-ISSN 2354-0133.
[12] BHATTACHARYYA, R., HAZRA, A. A study on stress analysis of ISO tank container. In: 58th Congress of The Indian Society of Theoretical and Applied Mechanics: proceedings. 2013.
[13] ISO 1496-3:2019. Series 1 freight containers. Specification and testing. Part 3: Tank containers for liquids, gases and pressurized dry bulk. Switzerland: International Organization for Standardization, 2019.
[14] TIERNAN, S., FAHY, M. Dynamic FEA modelling of ISO tank containers. *Journal of Materials Processing Technology* [online]. 2002, **124**(1-2), p. 126-132. ISSN 0924-0136, eISSN 1873-4774. Available from: https://doi:10.1016/S0924-0136(02)00196-6
[15] TSYGANSKAYA, L. V. Influence of design solutions of tank containers on their loading during transportation by rail. Dissertation 05.22.07. St. Petersburg, 2006.
[16] MAKEEV, S. V., BUILENKOV, P. M. Features of the calculation of the stress-strain state of the tank-container, taking into account the actual loading in operation. In: 14th International Scientific and Technical Conference dedicated to the memory of Doctor of Technical Sciences, Professor E. G. Zudov: proceedings. Vol. T1: Mining and metallurgical production. Mechanical engineering and metalworking. 2018. p. 174-184.
[17] FOMIN, O., GERLICI, J., GORBUNOV, M., VATULIA, G., LOVSKA, A., KRAVCHENKO, K. Research into the strength of an openwagon with double sidewalls filled with aluminium foam. *Materials* [online]. 2021, **14**(12), 3420. eISSN 1996-1944. Available from: https://doi.org/10.3390/ma14123420
[18] FOMIN, O., GORBUNOV, M., GERLICI, J., LOVSKA, A., KRAVCHENKO, K. Dynamics and strength of circular tube open wagons with aluminum foam filled center sills. *Materials* [online]. 2021, **14**(8), 1915. eISSN 1996-1944. Available from: https://doi.org/10.3390/ma14081915
[19] FOMIN O., LOVSKA, A. Determination of dynamic loading of bearing structures of freight wagons with actual dimensions. *Eastern-European Journal of Enterprise Technologies* [online]. 2021, **2/7**(110), p. 6-15. ISSN 1729-3774, eISSN 1729-4061. Available from: https://doi.org/10.15587/1729-4061.2021.220534
[20] PANCHENKO, S., GERLICI, J., VATULIA, G., LOVSKA, A., PAVLIUCHENKOV, M., KRAVCHENKO, K. The analysis of the loading and the strength of the flat rack removable module with viscoelastic bonds in the fittings. *Applied Sciences* [online]. 2023, **13**(1), 79. eISSN 2076-3417. Available from: https://doi.org/10.3390/app13010079
[21] KONDRATIEV, A. V., GAIDACHUK, V. E. Mathematical analysis of technological parameters for producing superfine prepregs by flattening carbon fibers. *Mechanics of Composite Materials* [online]. 2021, **57**, p. 91-100. ISSN 0191-5665, eISSN 1573-8922. Available from: https://doi.org/10.1007/s11029-021-09936-3
[22] VAMBOL, O., KONDRATIEV, A., PURHINA, S., SHEVTSOVA, M. Determining the parameters for a 3D-printing process using the fused deposition modeling in order to manufacture an article with the required

structural parameters. *Eastern-European Journal of Enterprise Technologies* [online]. 2021, **2/1**(110), p. 70-80. ISSN 1729-3774, eISSN 1729-4061. Available from:https://doi.org/10.15587/1729-4061.2021.227075

[23] PANCHENKO, S., VATULIA, G., LOVSKA, A., RAVLYUK, V., ELYAZOV, I., HUSEYNOV, I. Influence of structural solutions of an improved brake cylinder of a freight car of railway transport on its load in operation. *EUREKA: Physics and Engineering* [online]. 2022, **6**, p. 45-55. ISSN 2461-4254, eISSN 2461-4262. Available from: https://doi.org/10.21303/2461-4262.2022.002638

[24] LOVSKA, A., STANOVSKA, I., NERUBATSKYI, V., HORDIIENKO, D., ZINCHENKO, O., KARPENKO, N., SEMENENKO, Y. Determining features of the stressed state of a passenger car frame with an energy-absorbing material in the girder beam. *Eastern-European Journal of Enterprise Technologies* [online]. 2022, **5/7**(119), p. 44-53. ISSN 1729-3774, eISSN 1729-4061. Available from: https://doi.org/10.15587/1729-4061.2022.265043

[25] VATULIA, G., LOVSKA, A., PAVLIUCHENKOV, M., NERUBATSKYI, V., OKOROKOV, A., HORDIIENKO, D., VERNIGORA, R., ZHURAVEL, I. Determining patterns of vertical load on the prototype of a removable module for long-size cargoes. *Eastern-European Journal of Enterprise Technologies* [online]. 2022, **6/7**(120), p. 21-29. ISSN 1729-3774, eISSN 1729-4061. Available from: https://doi.org/10.15587/1729-4061.2022.266855

[26] FOMIN, O., LOVSKA, A., SKURIKHIN, D., NERUBATSKYI, V., SUSHKO. D. Special features of the vertical loading on a flat car transporting containers with elastic-viscous links in their interaction units. In: 26th International Scientific Conference Transport Means 2022: proceedings. Part I. 2022. p. 629-633.

[27] LOVSKAYA, A. Assessment of dynamic efforts to bodies of wagons at transportation with railway ferries. *Eastern-European Journal of Enterprise Technologies* [online]. 2014, **3/4**(69), p. 36-41. ISSN 1729-3774, eISSN 1729-4061. Available from: https://doi.org/10.15587/1729-4061.2014.24997

[28] KRIVOVYAZYUK, Y. P. Estimation of the equivalent loading of four-axle railway tanks with liquid cargoes of different density at longitudinal impacts. Dissertation 05.22.07. Dnepropetrovsk, 1986.

[29] Rules for the transport of dangerous goods. To the agreement on international railway freight traffic. Volume 3. Organization of Commonwealths of Railways, 2011.

[30] KOSHLAN, A., SALNIKOVA, O., CHEKHOVSKA, M., ZHYVOTOVSKYI, R., PROKOPENKO, Y., HURSKYI, T., YEFYMENKO, A., KALASHNIKOV, Y., PETRUK, S., SHYSHATSKYI, A. Development of an algorithm for complex processing of geospatial data in the special-purpose geoinformation system in conditions of diversity and uncertainty of data. *Eastern-European Journal of Enterprise Technologies* [online]. 2019, **5/9**(101), p. 16-27. ISSN 1729-3774, eISSN 1729-4061. Available from: https://doi.org/10.15587/1729-4061.2019.180197

[31] STASTNIAK, P., KURCIK P., PAVLIK, A. Design of a new railway wagon for intermodal transport with the adaptable loading platform. *MATEC Web of Conferences* [online], 2018, **235**, 00030. eISSN 2261-236X. Available from: https://doi.org/10.1051/matecconf/201823500030

[32] STASTNIAK, P., MORAVCIK, M., BARAN, P., SMETANKA, L. Computer aided structural analysis of newly developed railway bogie frame. *MATEC Web of Conferences* [online], 2018, **157**, 02051. eISSN 2261-236X. Available from: https://doi.org/10.1051/matecconf/201815702051

[33] LOVSKA, A, FOMIN, O., PISTEK, V., KUCERA, P. Dynamic load and strength determination of carrying structure of wagons transported by ferries. *Journal of Marine Science and Engineering* [online], 2020, **8**(11), 902. eISSN 2077-1312. Available from: https://doi.org/10.3390/jmse8110902

[34] STASTNIAK, P. Freight long wagon dynamic analysis in S-curve by means of computer simulation. *Manufacturing Technology* [online], 2015, **15**(5), p. 930-935. ISSN 1213-2489, eISSN 2787-9402. Available from: https://doi.org/10.21062/ujep/x.2015/a/1213-2489/MT/15/5/930

This is an open access article distributed under the terms of the Creative Commons Attribution 4.0 International License (CC BY 4.0), which permits use, distribution, and reproduction in any medium, provided the original publication is properly cited. No use, distribution or reproduction is permitted which does not comply with these terms.

ANALYSIS OF THE TEST BENCH DESIGN INFLUENCE ON THE COOLING PERFORMANCE OF A RAIL VEHICLE BRAKE DISC

Vladimír Pavelčík, Ján Dižo*, Miroslav Blatnický, Vadym Ishchuk, Denis Molnár

Faculty of Mechanical Engineering, University of Zilina, Zilina, Slovak Republic

*E-mail of corresponding author: jan.dizo@fstroj.uniza.sk

Vladimír Pavelčík 0000-0003-3470-7883,
Miroslav Blatnický 0000-0003-3936-7507,
Denis Molnár 0000-0002-9540-8636
Ján Dižo 0000-0001-9433-392X,
Vadym Ishchuk 0000-0003-2024-382X,

Resume

The presented article aims at assessment of the influence of test bench design on the cooling performance of a rail vehicle brake disc. The test bench is designed for experimental analyses of rail vehicles' brake components. The work includes an introduction to the solved problem, as well as a description of importance of airflow simulations in virtual environment. Creation of a geometrical model and its most important features are described. The research is performed by means of the computational fluid dynamics. For this method, it is important to set-up the boundary conditions, which are presented in the next part of the article. The results of the computational fluid dynamics simulations are presented for the solid disc and for the ventilated disc. The simulations of the solid disc showed the better convergence of calculations for various time-steps in comparison to the ventilated disc.

Article info

Received 4 February 2023
Accepted 20 April 2023
Online 22 May 2023

Keywords:

a rail vehicle disc brake
computational fluid dynamics
simulation of cooling
a solid disc
a ventilated disc

Available online: https://doi.org/10.26552/com.C.2023.048

ISSN 1335-4205 (print version)
ISSN 2585-7878 (online version)

1 Introduction

Safety is an extremely important point of view during design, development or any other lifecycle stage of all the types of vehicles. Concerning safety, braking plays vital role. This is even more important for rail vehicles, as these can operate at higher velocities and with higher masses than cars. Even though the rail vehicles can be equipped with brakes of multiple types, a frictional brake should always be present. One type of frictional brakes is the disc brake, now widely used for all the high-speed trains, as well as for passenger wagons of casual trains.

To ensure proper functionality during operation, certification procedure is standardized in UIC (International railway union) leaflets [1-2]. These certification procedures aim to provide set of simulations of certain conditions for different types of brakes. Another leaflet [3] regulates certification requirements for the test benches themselves. Requirements for performance is present in that leaflet, however, no exact design is required by it. As a consequence, various design solutions for various test benches might satisfy the same performance requirements [4-5]. An integral part of the test bench is its ventilation subsystem that provides air from environment with satisfying parameters. This article discusses a particular solution of a ventilation subsystem installed on the test bench. Each design might influence the experiments differently, so in the leaflet, there is a standardized way to check that the cooling performance of the ventilation system is similar enough throughout all the test benches and results are comparable [6-8].

There are several ways of how the design of the ventilation system can affect the cooling performance of the brake disc. First, with the total mass flow around the brake disc (or pads), the velocity of the air changes and so do the parameters of forced convection. Moreover, the parameters of the flow (e.g. temperature) have serious impact, as well. However, these influences are subject to the test described in the leaflet, so after successful certification, there is no need to discuss them further [9-10].

One of the ways the airflow can affect the cooling

of the brake disc, is that the flow direction on the local scale (turbulences, eddies) can have some impact on results of the experiment by the means of providing slightly different airflow on opposite friction surfaces of the disc. To assess this influence, the computational fluid dynamics (CFD) can help to isolate this effect from others on the disc (for example inevitable geometry imperfections in production, material imperfections, test bench geometry imperfections etc.). As a numerical method, a CFD simulation is suitable for observation and evaluation of concomitant effects, as suggested by many authors, for example [11-14]. The best metric to compare the results of the simulations seems to be the same as is used for experiments - averaging temperature on the friction surfaces of the disc [15-17].

From the above mentioned, the following two objectives arose. The first and main objective is to assess the influence of a test bench geometry, namely the inlet pipe's shape, on the cooling performance on the brake disc via the CFD simulation. The secondary objective is a side objective to roughly assess the maximum time step size for such simulations, so that the solution can converge and provide acceptable results.

2 Model creation, geometry

The room of the test bench consists of four main parts. An inlet pipe serves as the source of cooling air driven from outside the building to the brake mechanism. In the beginning of the pipe is a primary fan, which is regulated to maintain the proper velocity at the outlet of the inlet pipe. However, this fan is incapable of providing enough mass-flow for the highest velocities, and so in the final part of the inlet pipe, the secondary fan is installed, which is not regulated and is active only at simulated train speed of 160 $km \cdot h^{-1}$ and above.

The second and the most important part is the test bench itself. It consists of the frame of the brake, the braking mechanism, bearings etc. The airflow is directed towards the brake disc and further direction is influenced by the disc and the braking conditions. The third part is the outlet pipe located behind the frame (flow-wise) and provides suction power to remove products of braking (heat and solid dust particles). The remaining part is a moveable covering. From airflow point of view, this covering separates the test bench

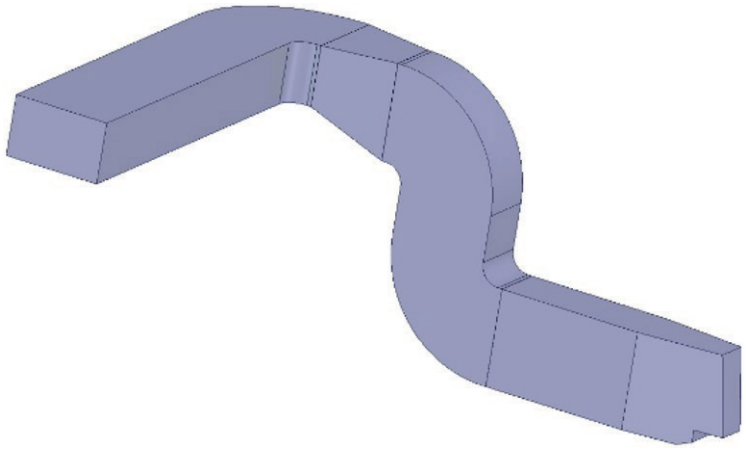

Figure 1 *A geometry for the CFD simulations - an inlet pipe*

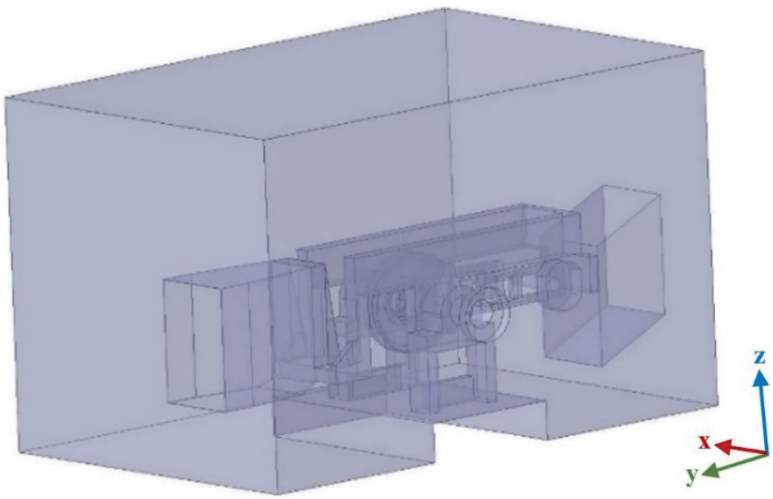

Figure 2 *A geometry for the CFD simulations - a test bench*

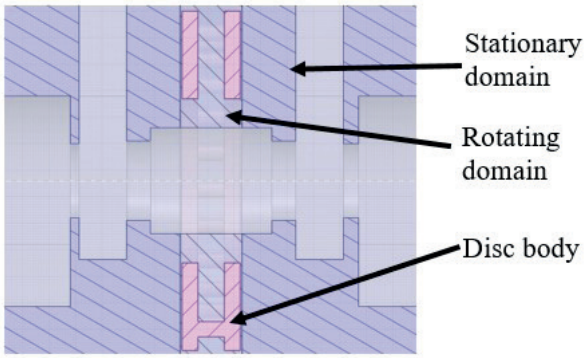

Figure 3 *Bodies in a model for the "sliding meshes" simulation*

Table 1 *Boundary conditions for simulation of airflow in the inlet pipe*

Boundary condition / setting	Value
Material in the domain	Air, constant density 1.225 kg·m^{-3}
Mass flow inlet - primary fan	2 kg·s^{-1}
Pressure outlet	0 Pa

Table 2 *Boundary conditions for simulation of airflow around the test bench*

Boundary condition	Value
Material - stationary + rotating domain	Air, constant density 1.225 kg·m^{-3}
Angular velocity of rotating domain	357 rpm (equivalent to simulated train speed 60 km·h^{-1})
Velocity inlet	Velocity profile obtained by previous simulation
Suction - mass flow outlet	3.87 kg·s^{-1}
Pressure outlet - floor	0 Pa
All walls	No roughness, stationary relative to adjacent cell zone
Time step size	0.00047 s (cca. 1° of rotation)

environment from the rest of the room and thus making the space out of the covering aerodynamically irrelevant for test bench.

The exact CAD model was created from the first three parts and this model was heavily simplified for the purpose of CFD simulations [18-20]. However, even after these simplifications, the computational costs of this problematics remained relatively high. The CAD model was then converted into a CFD model - enclosure of the bodies, while keeping the size of the enclosure same as the size of the real covering.

Various discs are mounted in the brake test bench, so two different simplified discs have been examined in simulations. The simplest disc is solid with a groove and the second is simplified brake disc with radial vanes. These two discs represent the edge cases for effectivity of cooling from ventilation point of view.

For the selected method of simulating the disc rotation - "sliding meshes" - another body had to be created inside the domain. This body needs to cylindrically enclose the disc.

The basic components of an analysed CFD simulation model are shown in Figures 1 to 3. Figure 1 depicts a geometry of an inlet pipe. A geometry of the test bench, which is used for the simulation computation, is shown in Figure 2. Figure 3 depicts a cross-section view of the solid disc model with individual components.

3 Simulation settings, boundary conditions and mesh

The airflow analysis was split between the simulation of airflow around the test bench and the simulation of airflow in the inlet pipe. For the latter one, the domain consisted only of the first part of the geometry (inlet pipe). The goal of this sub-simulation is only to find the velocity profile at the outlet of the inlet pipe. Settings and boundary conditions for this sub-simulation are presented in Table 1.

Due to the complexity of the problem, both brake discs were simulated in a single constant regime. Rotation was simulated using the principle of sliding meshes with angular velocity of rotating domain simulating particular train velocity. Settings and boundary conditions of this regime are summarized in Table 2 and the thermal properties for cooling are summarized in Table 3.

The mesh used in all bodies was made using the Mosaic meshing in Ansys Fluent Meshing, the

Table 3 *Thermal properties and time-dependent simulation settings*

Property	Body	Value
Density	Air	1.225 kg·m^{-3}
	Disc	8030 kg·m^{-3}
Thermal conductivity	Air	0.0242 W·m^{-1}·K^{-1}
	Disc	40 W·m^{-1}·K^{-1}
Specific heat	Air	1006.43 J·kg^{-1}·K^{-1}
	Disc	502.48 J·kg^{-1}·K^{-1}
Initial temperature (homogenous throughout the body)	Air	288 K
	Disc	600 K

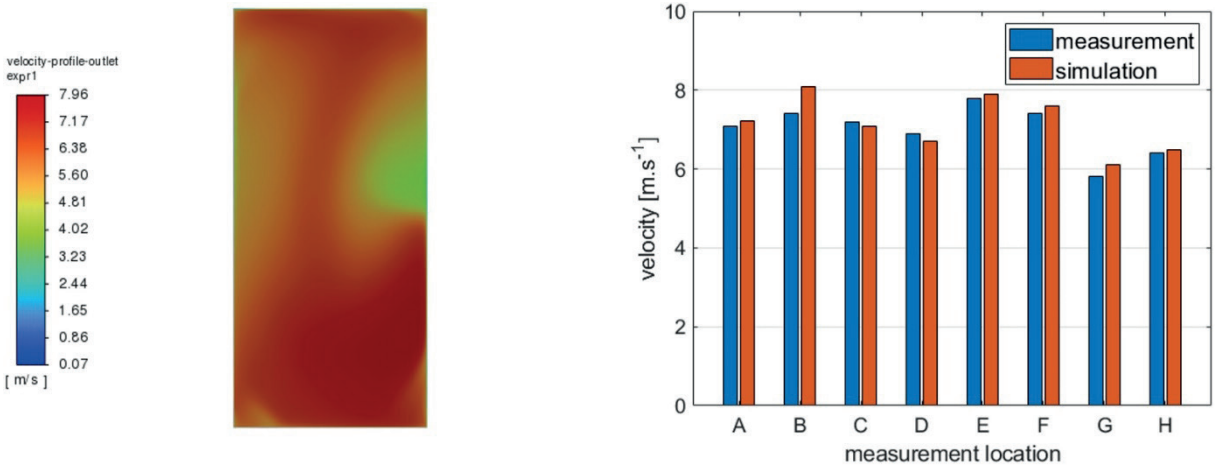

Figure 4 *A velocity profile on the outlet of the inlet pipe (left), the comparison of the measured vs. simulated values (right)*

final mesh contained polyhedral prisms near the wall and hexahedral elements farther from the wall with polyhedral buffer layers.

4 Results and discussion

From the simulation of airflow in the inlet pipe, the velocity profile is obtained at the interface between the inlet pipe and the main stationary domain. This velocity profile is presented in Figure 4.

A measurement was performed to prove the results of this simulation. A total of eight points were selected (and spaced almost equally) near the inner perimeter of the profile and velocity of flowing air has been measured using simple handheld anemometer. A comparison of measured and simulated values can be found in Figure 4. Generally, the correlation between them is good and the velocity profile is accepted as an input to the main simulation.

During the real measurements, the temperature is measured 1 mm under the frictional surfaces, in three locations on both sides of the disc and the temperature is averaged between those three sensors. In these simulations, temperature is averaged on the whole surface of friction.

As for the minor objective - the minimum applicable time step size - for solid disc, the disc temperature contours after one minute of cooling are presented in Figure 5. The gradient in the tangential direction in the middle of the friction surface is clearly visible in the contours created with time step size 1 s and 0.5 s but are not present when the time step size is 0.05 s. Therefore, the time step 0.05 s can be considered as the maximum time step size for model with solid disc. Figure 5 shows an example of the simulation computations results of a solid disc. It includes three various temperature distributions in the solid disc after the 1st minute. Figure 6 depicts the results of simulation computation for the ventilated brake disc. As the numerical simulation was successful only for the time step of 0.005 s, it includes only one illustration of temperature distribution in the disc body.

On the other hand, the model with ventilated disc has the only single time step size successfully simulated - 0.005 s. All the other (bigger) time steps showed poor convergence or no convergence at all. No significant tangential gradients are present in this case, as can be seen in Figure 6. For ventilated disc, its aerodynamic drag was used as an additional criterion of convergence and was in good proximity with values presented by [17]. In addition, the results were in good accordance with the rig tests described by [10].

To compare the influence of turbulent and swirling

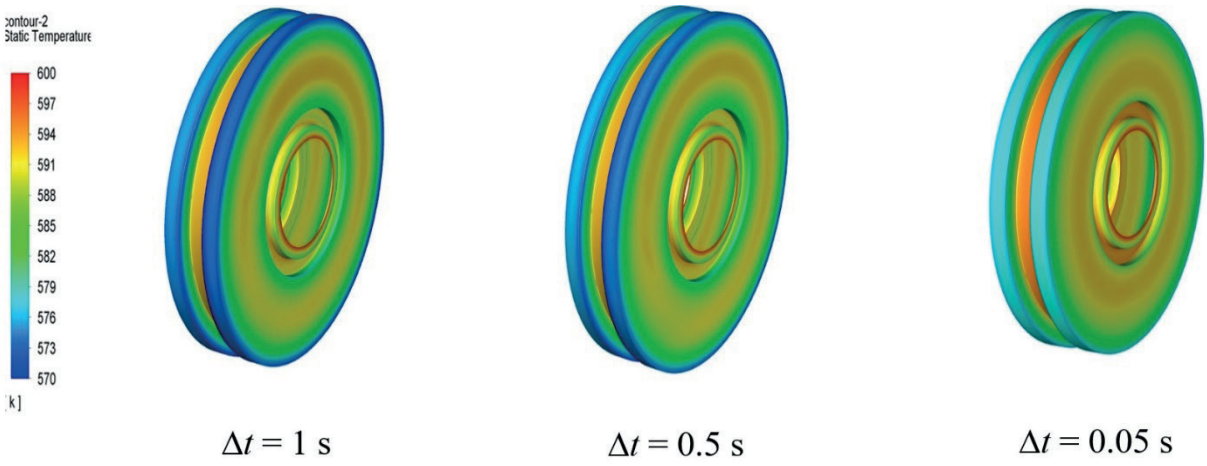

Figure 5 *Temperature contours on the surface of a solid disc at different time steps after the 1st minute*

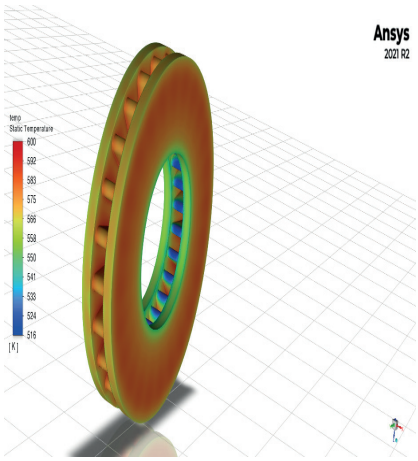

Figure 6 *Temperature contours on the surface of a ventilated disc for the time steps 0.005 s after the 1st minute*

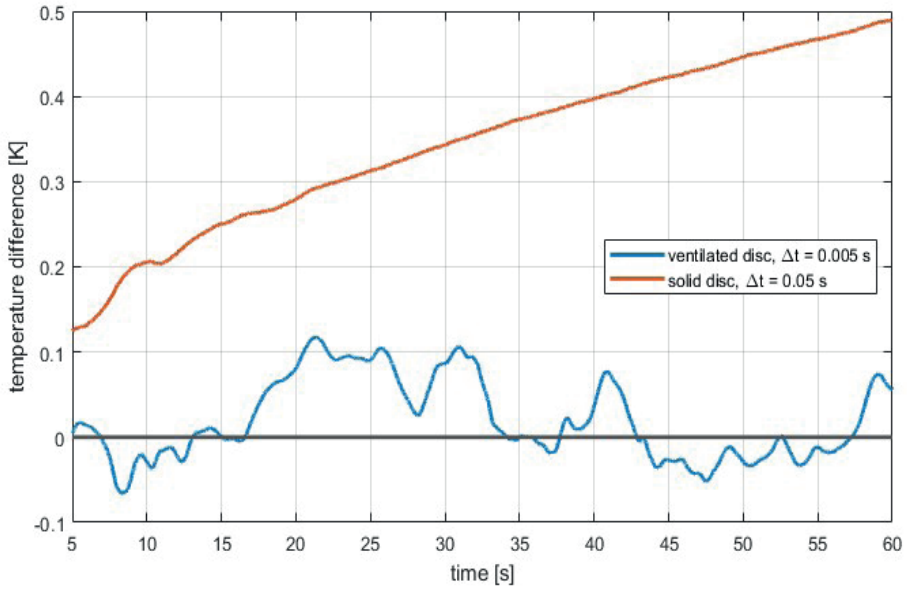

Figure 7 *Evolution of temperature differences between the friction surfaces of the brake discs in terms of time*

flow from the inlet pipe on the cooling performance of the either of the brake discs, curves for both successful cases are presented in Figure 7. The two curves are depicted - for the solid disc (a red curve) and for the ventilated disc (a blue curve). For the non-ventilated disc, the trend is clearly visible, as the difference of temperatures on frictional surfaces increases in time. Contrary to the solid disc, the curve for ventilated disc shows neither increasing nor any other trend in time.

5 Conclusions

From the results, for the goals stated at the end of the introductory part, following statements can be concluded:

- For the non-ventilated disc, the maximum allowable time step is (in simulated case) 0.05 s (cca 10 degree of revolution), whereas for ventilated disc, this value is 0.005 s (cca 1 degree of revolution). Bigger time steps caused the simulation either to diverge or to provide unrealistic results.
- The airflow provided by the inlet pipe causes different sides of the solid disc to be cooled at different pace, while the ventilated disc makes these differences diminish and no trend was observed over time.
- Combining the previous statements, simulations with ventilated disc can be heavily simplified by removing most of the test bench geometry, as it shows little to no influence on its cooling performance.

Acknowledgement

This publication has been partially supported by the project KEGA 031ZU-4/2023: "Development of the key competencies of the graduate of the study program Vehicles and Engines" and by support of Operational Program Integrated Infrastructure 2014-2020 of the project "Innovative Solutions for Propulsion, Power and Safety Components of Transport Vehicles, code ITMS 313011V334, co-financed by the European Regional Development Fund".

Conflicts of interest

The authors declare that they have no known competing financial interests or personal relationships that could have appeared to influence the work reported in this paper.

References

[1] UIC 541-3 Brakes - disc brakes and their applications - general conditions for the certification of brake pads.
[2] UIC 541-4 Composite brake blocks - general conditions for certification and use.
[3] UIC 548 Brakes - requirements of friction test benches for the international certification of brake pads and brake blocs.
[4] GERLICI, J., LACK, T., HARUSINEC, J. Development of test stand protoype for rail vehicles brake components. *Communications - Scientific Letters of the University of Zilina* [online]. 2014, **16**(3A), p. 27-32. ISSN 1335-4205, eISSN 2585-7878. Available from: https://doi.org/10.26552/com.C.2014.3A.27-32
[5] GERLICI, J., GORGUNOV, M., KRAVCHENKO, K., KOSTYUKEVICH, A., NOZHENKO, O., LACK, T. Experimental rigs for wheel/rail contact research. *Manufacturing Technology: Journal for Science, Research and Production* [online]. 2016, **16**(5), p. 909-916. ISSN 1213-2489. Available from: https://doi.org/10.21062/ujep/x.2016/a/1213-2489/MT/16/5/909
[6] GERLICI, J., LACK., T., HARUSINEC, J. Rail vehicles brake components test stand railbcot constructional solution. In: 22nd International Conference on Current Problems in Rail Vehicles: proceedings. Part I. 2019. p. 159-170.
[7] KOCH, S., KOPPEN, E., GRABNER, N., VON WAGNER, U. On the influcence of multiple equilibrium positions on brake noise. *Facta Universitatis, Series: Mechanical Engieering* [online]. 2021, **19**, p. 613-632. ISSN 0354-2025, eISSN 2335-0164. Available from: https://doi.org/10.22190/FUME210106020K
[8] MOTLAGH, V. G., AHMADZADEHTALATAPEH, M. Optimization of air distributionn patterns by arrangements of air inlets and outlets: Case study of an operating room. *Journal of Applied and Computational Mechnaics* [online]. 2022, **8**, p. 809-830. eISSN 2383-4536. Available from: https://doi.org/10.22055/JACM.2020.32443.2015
[9] INCROPERA, F.P., DEWITT, D. P., BERGMAN, T. L., LAVINE, A. S. *Fundamentals of heat and mass transfer*. USA: John Wiley and Sons, 2007. ISBN 987-0471457282.
[10] KRAVCHENKO, K., HAUSER, V., GORBUNOV, M. Estimating the brake disc air resistance by scaled test rig and by computer simulation. *Transportation Research Procedia* [online]. 2019, **40**, p. 737-744. ISSN 2352-1457, eISSN 2352-1465. Available from: https://doi.org/10.1016/j.trpro.2019.07.104

[11] ZHUOJUN, L., JIANYONG, Z. Conjugate heat transfer study on a ventilated disc of highspeed trains during braking. *Journal of Mechanical Science and Technology* [online]. 2013, **28**(5), p. 1887-1897. ISSN 1738-494X, eISSN 1976-3824. Available from: https://doi.org/10.1007/s12206-014-0336-7

[12] ZHANG, S., ZHANG, J. Modeling and analysis on fluid-solid-thermal physical field coupling of ventilated disc brake. *Jixie Gongcheng Xuebao / Journal of Mechanical Engineering* [online]. 2019, **55**(8), p. 154-164. ISSN 0577-6686. Available from: https://doi.org/10.3901/JME.2019.08.154

[13] STASTNIAK, P., MORAVCIK, M., BARAN, P., SMETANKA, L. Computer aided structural analysis of newly developed railway bogie frame. *MATEC Web of Conferences* [online]. 2017, **157**, 02051. eISSN 2261-236X. Available from: https://doi.org/10.1051/matecconf/201815702051

[14] DURAND, A., MEHEL, A., MURZYN, F., PUECH, S., LARRARTE, F. Numerical study of particle dispersion emitted from train brakes in underground station. In: 23rd Transport and Air Pollution Conference: proceedings. 2019.

[15] MASTRONE, M. N., CONCLI, F. Numerical modeling of fluid's aeration: analysis of the power losses and lubricant distribution in gearboxes. *Journal of Applied and Computational Mechanics* [online]. 2023, **9**, p. 83-94. eISSN 2383-4536. Available from: https://doi.org/10.22055/JACM.2022.40666.3625

[16] VOLOV, V. T., BONDARENKO, A. A., OVCHINNIKOV, D. V., ATAPIN, V. V., KOU, L. Optimization of lubricant concumtion in the wheel/rail friction system. *Acta Polytechnica Hungarica* [online]. 2022, **19**(3), p. 21-36. ISSN 1785-8860, eISSN 2064-2687. Available from: https://doi.org/10.12700/APH.19.3.2022.3.3

[17] GERLICI, J., FOMINA, Y., KRAVCHENKO, K. The dependence of the aerodynamic drag on the rolling stock motion speed. *Transportation Research Procedia* [online]. 2021, **55**, p. 723-730. ISSN 2352-1465, eISSN 2352-1457. Available from: https://doi.org/10.1016/j.trpro.2021.07.174

[18] YEVTUSHENKO, A., KUCIEJ, M., TOPCZEWSKA, K. Effect of the temporal profile of the friction power on temperature of a pad-disc brake system. *Journal of Theoretical and Applied Mechanics* [online]. 2019, **57**(2), p. 461-473. ISSN 1429-2955, eISSN 2543-6309. Available from: https://doi.org/10.15632/jtam-pl/105465

[19] TOPCZEWSKA, K., SCHLATTMANN, J., ABDULLAH, O. I. Temperature and thermal stresses distributions in a dry friction clutch. *Journal of Theoretical and Applied Mechanics* [online]. 2020, **58**(2), p. 351-360. ISSN 1429-2955, eISSN 2543-6309. Available from: https://doi.org/10.15632/jtam-pl/116593

[20] YEVTUSHENKO, A., TOPCZEWSKA, T., KUCIEJ, M. Analytical determination of the brake temperature mode during repetitive short-term braking. *Materials* [online]. 2021, **14**(8), 1912. eISSN 1996-1944. Available from: https://doi.org/10.3390/ma14081912

This is an open access article distributed under the terms of the Creative Commons Attribution 4.0 International License (CC BY 4.0), which permits use, distribution, and reproduction in any medium, provided the original publication is properly cited. No use, distribution or reproduction is permitted which does not comply with these terms.

DETERMINING BASIC GEOMETRIC PARAMETERS OF THE APRON CONVEYOR DRIVE

Baurzhan G. Moldabayev, Alexander V. Rozhkov*, Oyum T. Balabayev

Abylkas Saginov Karaganda Technical University, Karaganda, Kazakhstan

*E-mail of corresponding author: alexktpm@mail.ru

Baurzhan G. Moldabayev 0000-0002-2102-1834, Alexander V. Rozhkov 0000-0001-9408-9461, Oyum T. Balabayev 0000-0001-6212-9350

Resume

The article provides an analysis of the classical design of the apron conveyor, which revealed the significant disadvantages. The study is devoted to the improvement of the plate conveyor design, which would provide an increase in the speed and performance of the conveyor, and allow to create conveyors of any required length and installation angle.

As a result of the research work, the following are determined: dependencies of the value of the specific traction force of the drive on the power of the engine and the value of its relative pole division; dependence of the active area of the linear asynchronous motors [LAM] on its power and conveyor speed; dependence of the distance between the intermediate drives on the power of the drive and the angle of installation of the conveyor.

Article info

Received 22 December 2022
Accepted 17 May 2023
Online 29 May 2023

Keywords:

apron conveyor
linear asynchronous motor
relative pole pitch
active element
geometric parameters
conveyor speed
angle of setting
specific traction force

Available online: https://doi.org/10.26552/com.C.2023.050

ISSN 1335-4205 (print version)
ISSN 2585-7878 (online version)

1 Introduction

Increasing the efficiency of the process of open-source mining is the use of conveyor transport. One of the types of conveyors used is a plate conveyor [1].

Figure 1 shows the general appearance of the plate conveyor.

The diagram of the classical plate conveyor is shown in Figure 2.

The carrier belt of the conveyor consists of separate plates connected to chains that are driven by drive sprockets.

In open-pit mining conveyor applications, the maximum possible conveyor angle and the possibility of transporting a lump rock mass are important.

Conveyor transport is the best positioned at the angle of natural derailment of the quarry, which is 30-40 °. The classical design of the plate conveyor allows its installation at a maximum angle of 25 °. At large installation angles, the load is sliding over the carrier surface under the action of its own weight. The use of partitions makes it possible to hold the load on the load-bearing sheet.

Load sliding dividers are welded to the conveyor carrier plate, allowing the conveyor to be installed at 35-40 ° inclinations. The plate conveyor makes it possible to transport large chunks of mountain mass, as the load moves together with the carrier cloth, so there is no impact of the load on stationary rollers, as in belt conveyors.

At the same time, the classical design of the plate conveyor has certain disadvantages - significant dynamic loads in the traction unit and the maximum length of the conveyor.

Significant dynamic loads that limit the speed of the traction and load-bearing organ of the plate conveyor are caused by the physical processes that occur when the traction chain of the drive sprocket is curved.

The drive sprocket circumference with the traction chain is shown in Figure 3.

Since the sprocket rotates at an angular speed ω, the start and end of the link of the traction chain move at a speed:

$$v_e = \omega R_e, \tag{1}$$

where: ω - the speed at which the asterisk rotates;
R_e - start and end radius of the chain link.

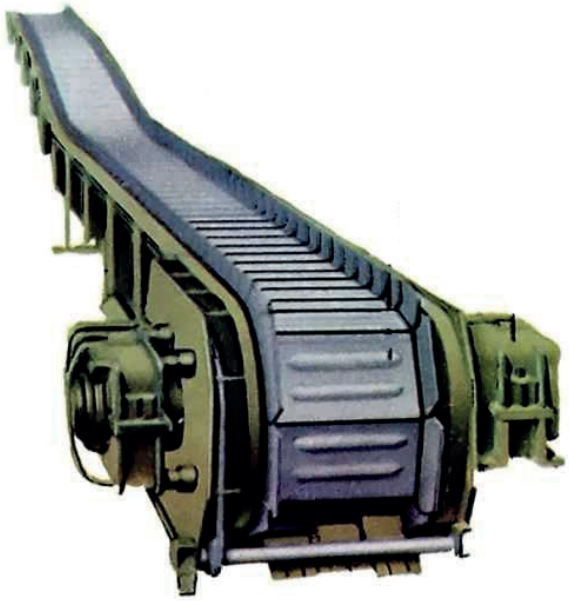

Figure 1 *Apron conveyor*

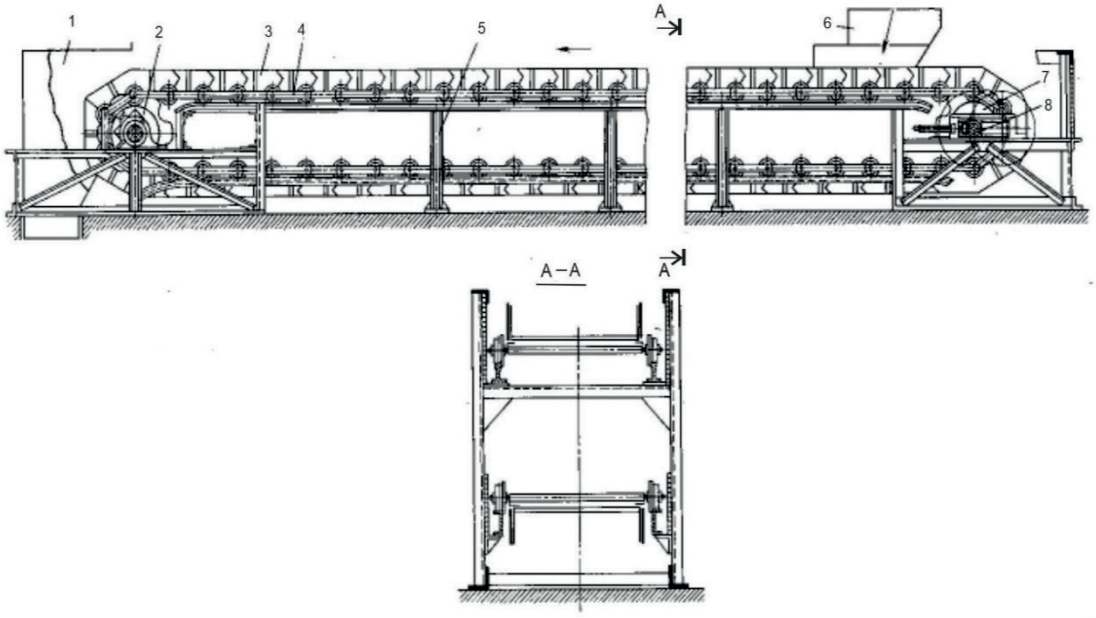

1- unloading funnel; 2 - drive sprocket; 3 - load-carrying belt; 4 - traction chains; 5 - bed; 6 - loading funnel; 7 - sprocket; 8 - tension device

Figure 2 *Structural design of a traditional apron conveyor*

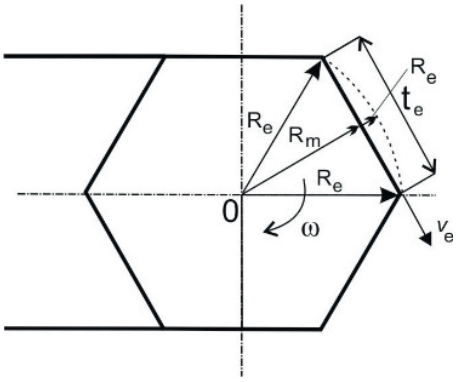

Figure 3 *The drive sprocket chain bending diagram*

If the drive sprocket is at rest, the middle of the link of the traction chain t_e is at a distance $R_m < R_e$ from the drive sprocket axis (Figure 3).

When the drive sprocket is rotated, the link of the traction chain is subjected to elastic deformation, leading the center of the link of the traction chain to a distance from the axis of the drive sprocket R_e.

This process causes additional loads on the traction unit, depending on the speed of rotation of the drive sprocket and the speed of the conveyor. Numerous experimental studies have shown that the maximum speed of these conveyors is 1.2 m/s. The tension at any point of the traction body of the plate conveyor can be determined by:

$$S_e = S_S + LA, \tag{2}$$

where: S_e, S_s - are the tension at the beginning and end of traction organ section, respectively; A - a coefficient depending on the linear load on the traction organ, the drag of the traction unit and the installation angle of the conveyor; L -length of the plot. At the same time, the force in the traction organ is limited by its strength ratio:

$$S_e < [S], \tag{3}$$

where: [S]- permissible traction tension.

From Equation (3) and Equation (4) follows:

$$L = \frac{[S] - S_e}{A}. \tag{4}$$

The single-drive conveyor is thus limited in length.

Research of the possibility of using the conveyor transport in difficult conditions of deep quarries shows a fairly high efficiency of these solutions [2]. The continuous technology of the conveyor process can be improved by using inclined conveyors [3].

Conveyor lifts can be placed both on the side of the quarry and in inclined shafts [4].

Scientific research has been carried out on many issues of improving the technology of mining, dedicated to improving the safety and intensity of mining operations, which is ensured by the use of the conveyor transport [5-8]. Cyclic-flow technology, along with the conveyor transport, involves the use of vehicles to deliver rock mass to the transfer point to the conveyor [9-10].

Various design solutions for conveyor lifts are being offered. For example, it is proposed to use a conveyor lift made of composite elastomer and diaphragm plates of the carrier body, which allows implementing a large angle of inclination and a significant lifting height of the transported material. An increase in the possible angle of installation of the conveyor, in some cases, is achieved by using the method of backing up the transported cargo, by using transverse dividing plates in the design of the carrier body of the conveyor [11]. In addition, there are known cases of using of linear induction motors in the conveyor transport drives, which makes it possible to provide a significant length of the conveyor line and lifting height [12].

The development of a special design of an apron conveyor that allows transporting cargo of a necessary height at the shortest length, while ensuring minimal costs, is a task of current interest.

Disadvantages of the plate conveyors can be eliminated by using intermediate drives with LAM.

In this way, the research is needed to determine the design parameters of intermediate conveyor drives with the LAM.

2 Problem statement

The aim of the study is to establish the basic geometric parameters of intermediate drives of plate conveyor with LAM. To achieve this objective, it is necessary to:

1. Set the value of the specific traction force of the drive the dependence on the power of the engine and the value of its relative pole pitch.
2. Set the area of the active part of a linear asynchronous motor the dependence on its power and conveyor speed.
3. Sett the distance between the intermediate drives the dependence on the drive power and the angle of setting of the conveyor.

3 An apron conveyor with linear drives

The structural design of an apron conveyor with a system of several drives with linear asynchronous motors is shown in Figure 4.

The apron conveyor operates as follows:

- plates *2* are interconnected through the swivel assembly of plates 3;
- interconnection of plates *2* allows performing the functions of a traction-bearing body of the apron conveyor;
- the traction force is transmitted to the traction-bearing plates *2* through the developed rotors of 8 linear motors, which are set in motion from interaction with the stators *9* of linear motors;
- rotors *8* of linear motors have a developed (linear) view and are fixed to axis *4* of travel rollers with flange *6*;
- stators *9* of linear motors also have a developed (linear) view and are fixed to frame *1* of the conveyor;
- the number and the distribution step of linear motors (rotors *8* and stators *9*) are determined by calculation depending on the operating conditions.

The developed apron conveyor with linear motors allows significant reducing dynamic loads and increasing the length of one conveyor, due to the absence of traction chain sprockets.

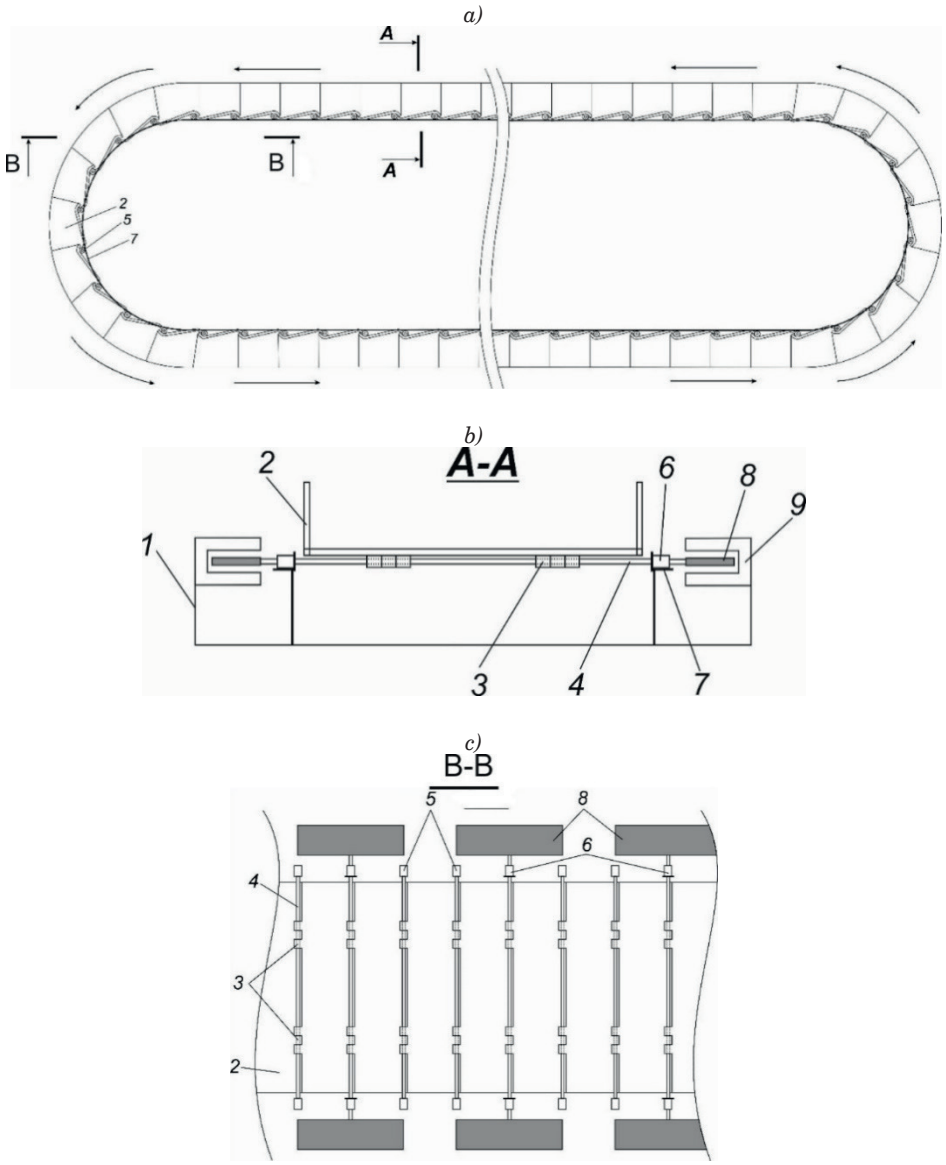

Figure 4 *Structural design of an apron conveyor with a system of several drives with linear asynchronous motors: a) The side view of the conveyor; b) A-A conveyor section; c) B-B conveyor section;1-frame, 2 - base, 3 - plate swivel assembly, 4 - axle, 5 - travel rollers, 6 - travel flanged rollers, 7 - travel roller guides, 8 - linear motor rotors, 9 - linear motor stators*

4 Determining the specific traction forces of the apron conveyor intermediate drive

A specific traction force can be determined according to the following dependence [13-14]:

$$f_{sp,force} = \frac{4\mu_0 A^2 \varepsilon \tau_\delta}{\pi\left[(1+\beta_x)^2 + \varepsilon^2\right]}, [Nm^{-2}], \quad (5)$$

where: μ_0 - is magnetic permeability in vacuum [H/m];
A - is the linear current load [A];
β_x - is the dimensionless coefficient accounting for the magnetic conductor steel saturation;
ε - is the electromagnetic slip;
τ_δ - is the relative pole pitch of the linear asynchronous motor (LAM).

The relative pole pitch is determined by the expression:

$$\tau_\delta = \frac{\tau}{\delta}, \quad (6)$$

where: δ -is the gap between inductor and secondary element LAM,
τ -is the pole pitch LAM calculated according to the dependence [m]:

$$\tau = \frac{v_1}{2(1-s)f}, m, \quad (7)$$

where: v_1 - is the secondary element speed (conveyor speed) [m/s];
s - is the slip amount;
f - is the alternate current frequency [1/s];
δ - is engine air gap [m].

Values of the specific traction force for various engine powers and the relative value of the pole pitch calculated by Equation (5), are shown in Figure 5.

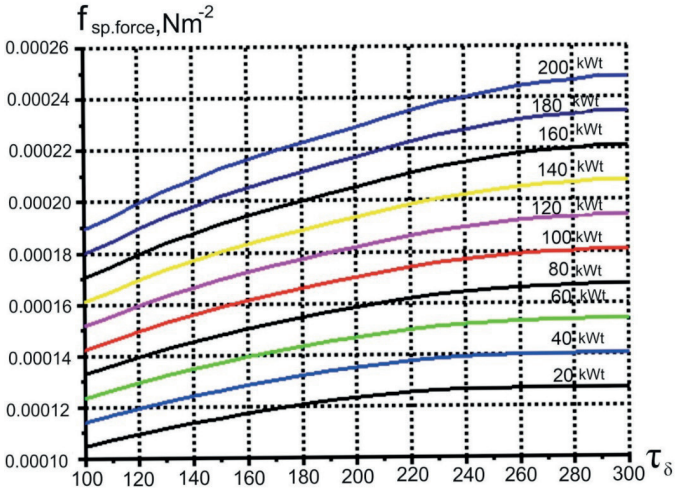

Figure 5 *Specific traction forces of a linear intermediate drive*

5 Determining the basic geometric parameters of the apron conveyor intermedicate linear drive

Using the dependences of the specific traction force, one next determines the geometric dimensions of a linear asynchronous motor for a steeply inclined apron conveyor.

Resistance to the cargo branch of the apron conveyor movement is determined by the formula:

$$W_w = [(q_w + q_{conv})w\cos\beta + (q_w + q_{conv})\sin\beta]gL, \quad [N], \tag{8}$$

where q_w, q_{conv} - are the load per unit length and the mass per unit length of the tension-skidding body, respectively, [kg/m];

w - is specific resistance to the tension-skidding body movement of the apron conveyor, w = 0.0025;

β - is the angle of the conveyor mounting [rad];

L - is the conveyor section length [m].

Taking the values of the relative pole pitch equal to τ_δ = 200, with the power values of the traction motors N = 50, 100, 200 kW, one obtains, according to the graphs (Figure 5), the values of specific traction forces that are respectively equal to 0.00014, 0.00017 and 0.00020 Nm^{-2}.

The drive pull force is determined by the ratio:

$$T_{i,j} = \frac{N_i}{v_j}, [N], \tag{9}$$

where: N_i - is the i- th value of the drive power LAM [kW];

v_j - is the j-th value of the conveyor speed [m/s].

The required area of the secondary element active part is determined by the expression:

$$S_{i,j} = \frac{T_{i,j}}{f_{sp.force}}, [m^2], \tag{10}$$

where $f_{sp.force}$ - is the specific traction force of LAM, [Nm^{-2}].

The areas of the secondary element active part dependences on the conveyor speed, with the drive power of 50, 100 and 200 kW, are presented in Figure 6.

The distance between the drives of the conveyor is determined from the ratio of the equality of the drive traction force to resistance of the traction-carrying body movement:

$$F = W_w, \text{ [N]}. \tag{11}$$

Substituting Equation (8) and Equation (9) into Equation (11), one obtains the expression for calculating the distance between the drives:

$$L_{k,j} = \frac{N}{v_j\begin{bmatrix}(q_w + q_{conv})w\cos\beta_k + \\ +(q_w + q_{conv})\sin\beta_k\end{bmatrix}}g, [m]. \tag{12}$$

The dependences of the distance between the drives on the speed and the angle of setting the conveyor, calculated by Equation (12) for different performance and power, are shown in Figures 7-9.

A specific example of determining the geometric parameters of the LAM and the distance between the drives is considered next.

According to the dependences shown in Figures 3 and 4, at the speed v = 4 m/s, the load per unit length q_w = 200 kg/m, the conveyor performance will be:

$$Q = 3.6 * q_w * v = 2880 \text{ t/h} \tag{13}$$

With the angle of setting β = 35 degrees and the drive power N = 200 kW, the LAM active part area will be S = 2.5 m^2, the distance between the drives L= 20 m.

The obtained geometric parameters with a sufficient conveyor performance can well be implemented in the actual design of the conveyor.

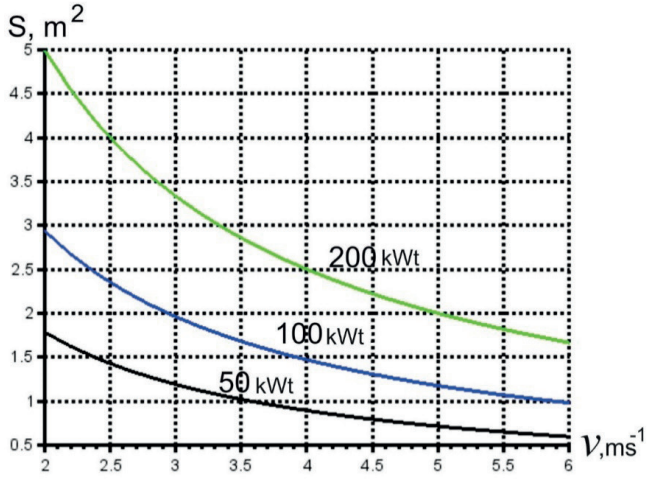

Figure 6 *Intermediate drive active part areas*

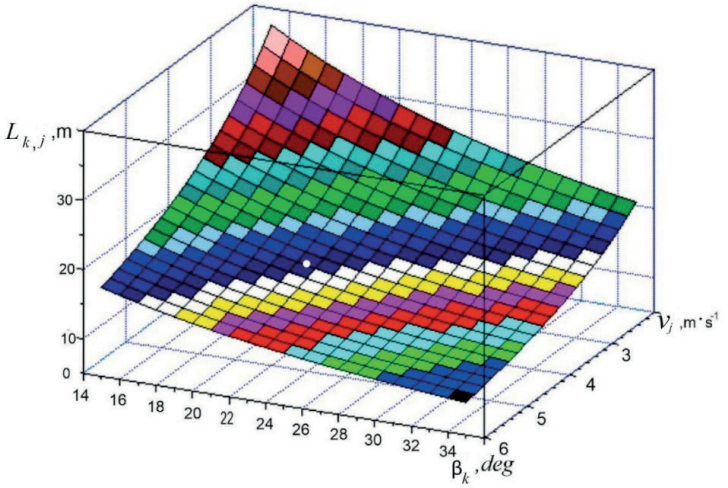

Figure 7 *The distance between the intermediate drives dependence on the conveyor speed and the angle of setting for Q = 1000 t/h, N = 50 kW*

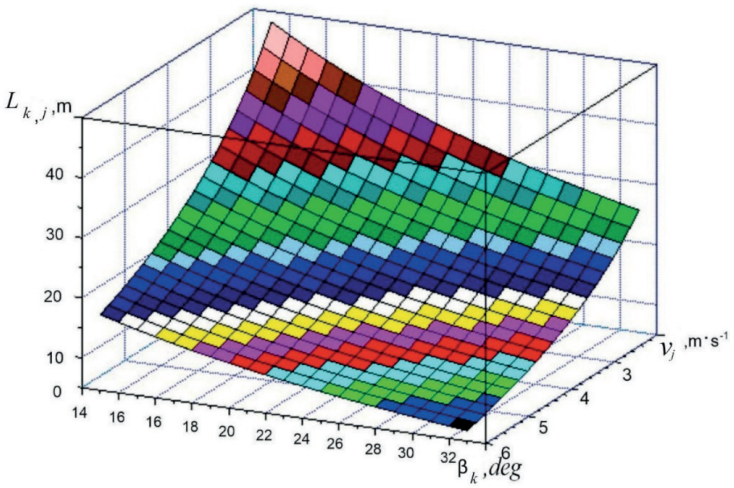

Figure 8 *The distance between the intermediate drives dependence on the conveyor speed and the angle of setting for Q = 1500 t/h, N = 100 kW*

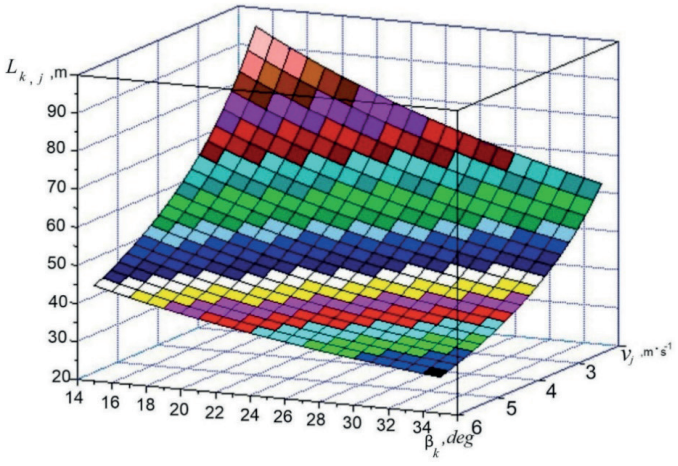

Figure 9 *The distance between the intermediate drives dependence on the conveyor speed and the angle of setting for Q = 2000 t/h, N = 200 kW*

Thus, the use of the LAM in intermediate drives of steeply inclined apron conveyors is quite achievable.

6 Conclusions

As a result of the study:

- The dependence of the value of the specific traction force of the intermediate drive of the plate conveyor with the LAM on the power of the engine and the value of the relative pole division thereof have been determined.
- At the value of the relative pole division τ = 200 and the change in engine power from 20 to 200 kW, the specific traction forces of the intermediate drive have values from 13*10-5 N m^{-2} to 25*10 N m^{-2}, which is acceptable for the geometrical parameters of the secondary LAM element.
- The area of the active part of the LAM is determined by its power and the speed of a conveyor. Within the range of changing the conveyor speed from 3 to 5 m/s and the drive power from 10 to 200 kW required by the operating conditions of conveyor transport in open mining, the area of the active part of the LAM has values from 2 to 3.2 m^2, which shows that it is possible to design the LAM with these parameters.
- The dependence of the distance between the intermediate drives of a plate conveyor with the LAM from the power of the drive and the angle of installation of the conveyor is determined.
- Within the range of change in conveyor performance from 1000 to 2000 t/h, average conveyor speed 4 m/s and drive power from 100 to 200 kW, the drive distance is between 15 and 50 m, which is quite feasible when designing a plate conveyor with intermediate drives based on the LAM, for specific operating conditions.
- Studies have shown that the use of intermediate-drive plate conveyors based on the LAM is very promising for increasing the efficiency of transport processes in open-pit mining.

Grants and funding

The authors received no financial support for the research, authorship and/or publication of this article.

Conflicts of interest

The authors declare that they have no known competing financial interests or personal relationships that could have appeared to influence the work reported in this paper.

References

[1] SPIVAKOVSKY, A. O., DYACHKOV, V. K. *Transporting machines. Textbook for engineering universities*. 3. revised. ed. Moscow: Mashinostroenie: 1983.

[2] BURMISTROV, K. V., GOLOVEI, S. I., KRUTIKOVA, A. V., DAUTBAEV, Z. R. Study of the possibility of using conveyor transport in complex mining and geological conditions of deep high-performance quarries. *Modern Problems of the Transport Complex of Russia*. 2016, **6**(2), p. 32-38. ISSN 2222-9396.

[3] GAVRISHEV, S. E., BURMISTROV, K. V., TOMILINA, N. G. Classification of technological schemes for opening deep horizons using steeply inclined lifts in a combined method of field development. *Izvestiya vuzov / Mining Journal*. 2013, **7**, p. 9-15. ISSN 2227-2917.

[4] GAVRISHEV, S. E., KALMYKOV, V. N., BURMISTROV, K. V., TOMILINA, N. G., ZALYADNOV, V. Y. Performance evaluation of opening supplies schemes with the use of quarry lifts. *Vestnik of the Magnitogorsk State Technical Universityn*. 2014, **1**, p. 8-12. ISSN 1995-2732, eISSN 2412-9003.
[5] OSINTSEV, N. A. *Safety of transport and technological processes of open pit mining: monograph*. Magnitogorsk: Magnitogorsk Publishing House, 2010.
[6] BURMISTROV, K. V., GAVRISHEV, S. E. Improving the efficiency of the development of ore deposits based on the intensification of mining operations in open pit areas. Magnitogorsk: Magnitogorsk Publishing House, 2005.
[7] GAVRISHEV, S. E., BURMISTROV, K. V., KOLONYUK, A. A. *The intensity of the formation of the working zone of deep quarries*. Magnitogorsk: Magnitogorsk Publishing House, 2012.
[8] VAN DER BORG, L. S. M. Y. Patent NL 0002533776 Belt conveyor. MPC B65G 23/23. Application 2011104086/11. 2014.
[9] KOLGA, A. D., MOSKOVKA, E. V. Improving the environmental friendliness of the use of dump trucks as part of road trains in open-pit mining. *Modern Problems of the Transport Complex of Russia*. 2016, **6**(1), p. 55-57. ISSN 2222-9396.
[10] KOLGA, A. D., RAKHMANGULOV, A. N., OSINTSEV, N. A., SLADKOWSKI, A. V., STOLPOVSKIKH, I. N. Robotic transport complex of automotive vehicles for handling of rock mass at the process of open cast. *Transport Problems / Problemy Transportu*. 2015, **10**(2), p. 109-116. ISSN 1896-0596, eISSN 2300-861X.
[11] HUAXIA, Q. Patent CH 103395614. Delivery device and delivery method for open mining. MPC B65G37/00. Application 201310358028.8. 2013.
[12] LIN, L. Patent CH 109051538. Built-in belt conveyor with wavelike blocking edge and transverse separating plate. MPC B65G 21/06. Application 201810947963.0. 2018.
[13] SVECHARNIK, D. V. *Linear electric drive*. Moscow: Energy, 1979.
[14] OGARKOV, M. E., SKOROBOGATOV, A. V. Practical recommendations for determining the main dimensions of linear induction motors. *PNRPU Mechanics Bulletin*. 2013, **7**, p. 115-122. ISSN 2224-9893, eISSN 2226-1869.

This is an open access article distributed under the terms of the Creative Commons Attribution 4.0 International License (CC BY 4.0), which permits use, distribution, and reproduction in any medium, provided the original publication is properly cited. No use, distribution or reproduction is permitted which does not comply with these terms.

DESIGN OF POWER TRANSFORMER WITH FREQUENCY 1 kHz

Marek Franko[1,*], Roman Kučera[1], Zdeno Biel[1], Roman Holček[1], Michal Frivaldský[2]

[1]EVPU a.s., Nova Dubnica, Slovakia
[2]Faculty of Electrical Engineering and Information Technologies, University of Zilina, Zilina, Slovakia

*E-mail of corresponding author: franko@evpu.sk

Marek Franko 0000-0003-1829-6455, Michal Frivaldský 0000-0001-6138-3103

Resume

This paper deals with the noise level of power transformers operating at a middle frequency from 800 Hz to 2000 Hz. The factors that influence the noise produced by power transformers are size, design and operating conditions. The research shows that the noise level of power transformers can vary widely depending on these factors. The paper discusses an overview of different types of power transformers core and their impact on the transformer's noise performance. This paper describes the design of a middle-frequency power transformer, its material composition and the design of the magnetic circuit and windings, operating in the frequency range 800 to 2000 Hz, with a capacity of 200 kVA, air-cooled, to be fed from a suitable frequency converter, characterized by reduced noise. The proposed solution allows implementation of galvanically isolated DC-DC converters for auxiliary traction drives and other DC-DC converters.

Article info

Received 12 May 2023
Accepted 9 June 2023
Online 28 June 2023

Keywords:

power transformer
transformer-based noise
soft magnetic materials
nanocrystalline materials

Available online: https://doi.org/10.26552/com.C.2023.055

ISSN 1335-4205 (print version)
ISSN 2585-7878 (online version)

1 Introduction

Power transformers can produce several types of noise, including magnetostriction noise, stray magnetic field noise and electrical noise. The level of noise produced by a transformer depends on several factors, such as the design of the transformer, the quality of the materials used and the operating conditions.

At a frequency of 1 kHz, the noise level of a power transformer can vary widely, depending on its size and design. In general, larger transformers tend to produce more noise than smaller ones, due to their greater physical size and the larger magnetic fields they generate.

The noise level of a power transformer is typically expressed in decibels (dB) or in terms of sound pressure level (SPL), measured in decibels relative to a reference sound pressure level. The noise level of a typical power transformer ranges from around 20 dB SPL to 70 dB SPL, depending on the transformer's size, design and operating conditions.

The immediate component of galvanically isolated DC-DC converters of higher voltage and power are isolation transformers. Due to the required size and weight of the converters, these are switched at higher frequencies, while the isolation transformer in question must also operate at a higher frequency than the middle-frequency power transformer (MfT). If for most converters of smaller power ratings, the switching frequencies are from 5 to 20 kHz, but in the case of converters with a power rating of hundreds of kVA the switching frequencies with regard to losses in the semiconductor switches are up to about 1 kHz. For these switching frequencies the magnetic circuit material, the winding and its insulation system must be designed.

Among the available materials, magnetically soft amorphous metal materials (AMMs), nanocrystalline materials (NCMs) or ferrites can be used for the MfTs in question. The use of ferrite cores for this power class of MfTs is not relevant due to, among other things, the size and weight of such MfTs. Depending on what is commercially available on the market, depending on the shape of the cores, toroidal or split (cut, "2U" shaped and glued on the side edges) cores of both AMM and NCM can be used. Toroidal cores of AMM or NCM are available in a much wider range, but their use is technologically almost impossible for MfTs of hundreds of kVA, due to the manufacturability of the windings. Only the split cores can be considered, of which the

NCM ones are preferable, but they are only available in a narrower range, of limited dimensions and their main drawback is their considerably high price, which predisposes them only for higher frequencies. The AMM cores are already available in larger sizes and weights, at an acceptable price, but their main drawback is the splitting section, which is a source of excessive noise resulting from electromagnetic forces generated in the core and manifested by mechanical vibrations with consequent significant noise. The source of the noise is the magnetostrictive forces originating in the large magnetostriction coefficient, which is characteristic for the AMM tapes. In specific tests, it has been shown that the use of these cores in MfTs has resulted in noise levels such that their use has proved to be unacceptable, despite the fact that the manufacturer declares their use also in the middle frequency transformers.

EVPU a.s. has been developing and manufacturing static semiconductor traction converters for more than a decade and part of the equipment of traction vehicles is also the need to design and develop smoothing chokes for traction motors or traction intermediate circuit. Several types of middle frequency power transformer and chokes been designed for traction converters [1-5].

In the design of a power isolating traction converter for supplying vehicle's auxiliary drives with a power 200 kVA, the care must be taken on several design issues. Considering the high power, application, losses of power semiconductor elements, a switching frequency of 900 Hz was selected for this purpose, it was necessary to design a power middle-frequency isolation transformer. During the tests of the prototype isolation transformer, a high level of noise was observed at this operating frequency. Therefore, the source of noise and possible solution was investigated, which is described in this paper.

2 Design of power transformer with frequency 900 Hz

The objective was to design a transformer with a target power of up to 200 kVA, with an operating frequency of 900 (1000 Hz), with a voltage ratio of 2000 V/890 V, with forced air cooling. According to the design and the elaborated design documentation, a prototype transformer type T1O-200-2000/893 was manufactured with the following parameters:

- Rated power 200 kVA
- Primary voltage (rms value) 2000 V (4000 V_{max})
- Secondary voltage (rms value) 893 V
- Frequency 900 Hz
- Test voltage (N1 ↔ N2) 9.5kV; 50 Hz; 60 s

The basis of the prototype transformer was a core

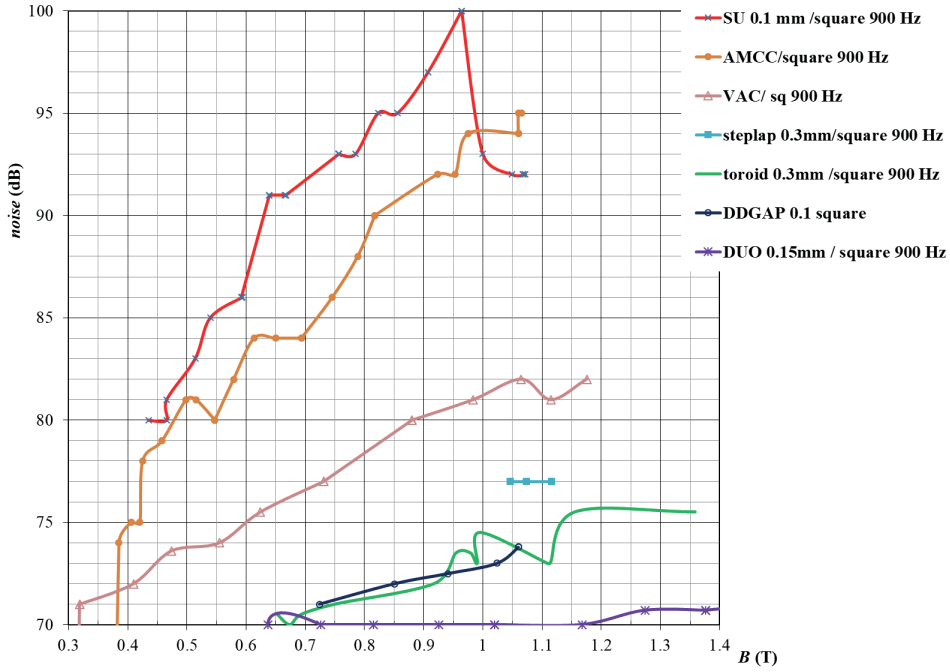

Key: ***SU*** *standardized split tape core, sheet thickness 0.1 mm (material: C5 korno)*
AMCC *AMM cut core (material: Metglas Alloy 2605SA1)*
VAC *NCM cut core (material: Vitroperm 500)*
Steplap *stacked core, transformer sheet thickness 0.3 mm*
Toroid *toroid core, transformer sheet thickness 0.3 mm*
DDGAP *bent core, transformer sheet thickness 0.1 mm*
DUO *bent core, transformer sheet thickness 0.15 mm*

Figure 1 *Comparison of measured noise vs. flux density for different types of magnetic circuit at an operating frequency of 900 Hz*

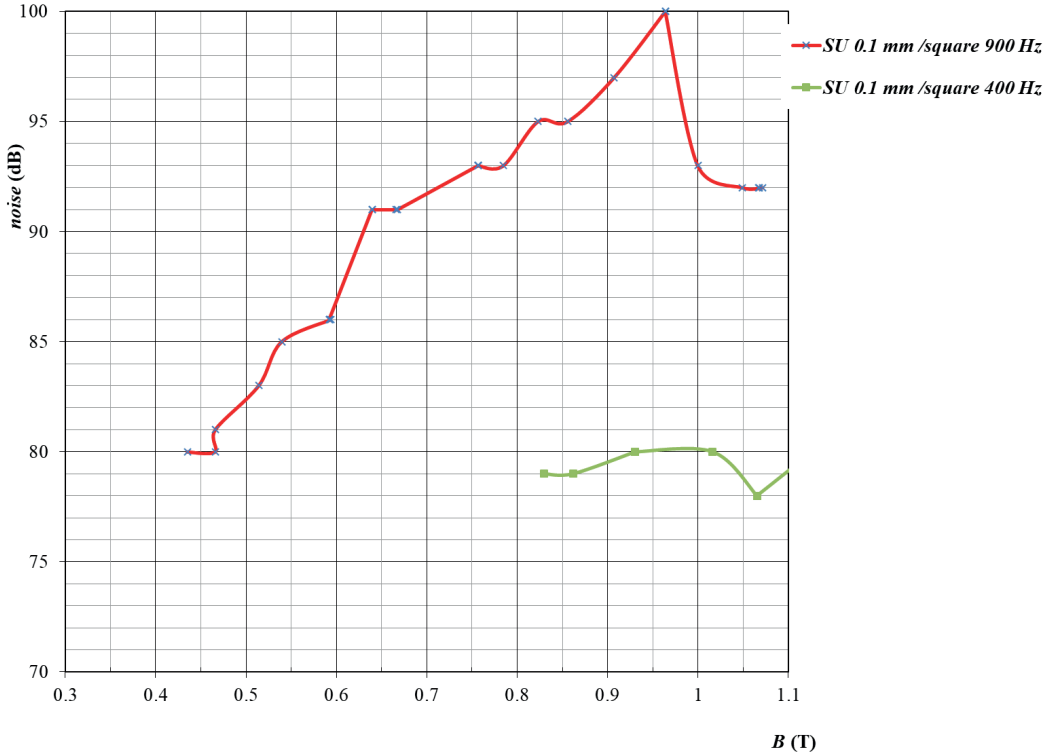

Figure 2 *Comparison of measured noise for standard split core at frequencies 400 and 900 Hz*

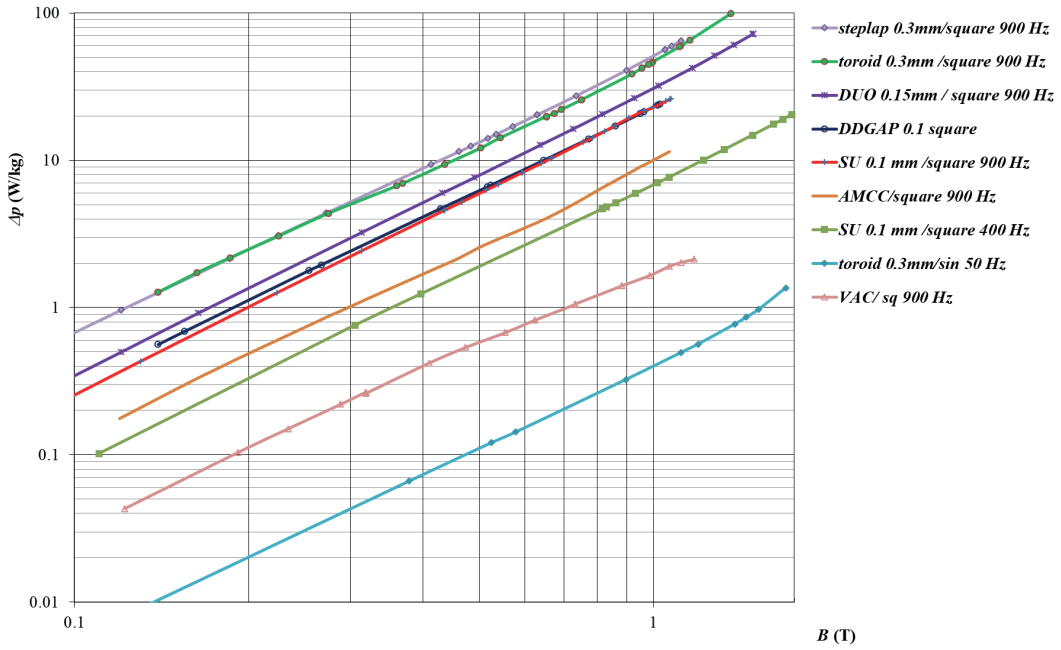

Figure 3 *Comparison of measured specific iron losses from flux density for different types of cores (core design and material)*

made from the amorphous metal materials type UMCCC-2553. The transformer design is a shell type with 6 pieces (2xC) of core. During measurements on the prototype transformer, a very negative phenomenon was found - noise, the level of which exceeded the limit of 80 dB (limit value of traction equipment) already at an induction of approx. 0.45 T, at the nominal operating point it was approx. 100÷104 dB.

A number of measurements and experiments have been devoted to identifying the reasons for existence and elimination of noise [6-8]. In Figure 1, a comparison of the noise of the selected magnetic circuits can be seen as a function of the flux density at a frequency of 900 Hz and when supplied with a voltage with a square-shaped waveform. It should be noted here that this was not an exact noise measurement in a noiseless chamber, but in

a) b)

Figure 4 *Photography of isolation transformer T1O-200-2000/893: a) a prototype of the transformer with a built core made from AMM; b) a new design with a bent core made of 0.1 mm thick transformer sheet*

laboratory conditions with possible noise overlap from the external environment. The measured characteristics is further complemented by a remark, the conclusion that the measured noise was about 3÷5 dB lower when supplied with a sinusoidal voltage waveform. For full information, Figure 2 shows the measured noise for a cut core composed of 0.1 mm thick transformer sheet at 900 and 400 Hz, for a frequency of 5 Hz the noise was unmeasurable under the given conditions with respect to the background i.e. less than 60 dB.

From these measurements it was concluded that the main cause of the noise is the operating frequency of 900 Hz, which is not only clearly audible to the human ear, but the oscillation, the banging of the sheet metal in the air gap, is of such a magnitude that it results in a significant noise.

In addition to noise measurements, these measurements also identified specific core losses in the magnetic circuits, see Figure 3, where it can be seen why an AMM (type UMCCC) was chosen for the prototype implementation (Figure 4), which at this frequency of 900 Hz is the second best after the NCM cores (VAC), but the VAC cores are not produced in the required size.

As mentioned above, different variants were analysed, either in shape, core design (2xC core, toroid, DDGAP) or material used (amorphous AMCC, UMCCC, nanocrystalline VITROPERM 500, VITROPERM 500F, 0.3; 0.15; 0.1 mm sheet metal). Considering the noise, the chosen application, the losses, the manufacturing possibilities, etc., the folded core "step lap" design became the basis for the final design of the transformer and the material chosen was GT 100, i.e. sheet metal with a thickness of 0.1 mm.

The above shortcomings were eliminated by a new way of designing the magnetic circuit and windings of the MfT based on the requirement to suppress magnetostriction in the core sheet metal bundle of the magnetic circuit and thus minimize the noise caused by this phenomenon, as much as possible. The essence of the solution is that for the cores of the MfT magnetic circuit, an electrical sheet of 0.1 thickness, or thinner, with a smaller coefficient of magnetostriction, is used. This sheet is cut in the longitudinal direction and bent by AEMcore technology into an "O" shape, with the individual sheets in contact to form a distributed air gap, with the individual sheets in the bundle having the ability to dilate and thus compensate for the effect of the magnetostriction phenomenon. The actual joining of the plates may be in the coupling or in the column, whichever is more convenient from the point of view of assembly. The number of individual cores of the magnetic circuit also depends on the power of the transformer. The method and design of the individual cores and their assembly into a complete magnetic circuit and the requirement to design at least one winding as a high-voltage winding make it necessary to design the transformer as a core transformer, with two concentric coils of individual windings. Losses arising in the individual cores of the magnetic circuit are dissipated by forced air cooling, the cooling channels being formed by insulating spacers between the individual cores. Likewise, losses arising in the windings are dissipated from the surfaces of the individual windings, by means of channels formed therein by insulating wedges, also

Table 1 *Parameters of the designed transformer*

Parameter	Value
Rated power	200 kVA
Primary voltage (rms value)	2000 V (4000 V_{max})
Secondary voltage (rms value)	893 V
Frequency	900 Hz
Test voltage (N1 ↔ N2)	9.5kV; 50 Hz; 60 s
Insulation temperature class	F
Cooling AF	forced air, >5 m/s
Cooling AF	forced air, >5 m/s
Load type	S1 (permanent)
Operating ambient temperature	-40 °C ÷ +60 °C
Vibration and shock according to	EN 60373
primary winding resistance	0.01945 Ω
secondary winding resistance	0.00232 Ω
short-circuit voltage	9 %
The weight of the transformer	118 kg

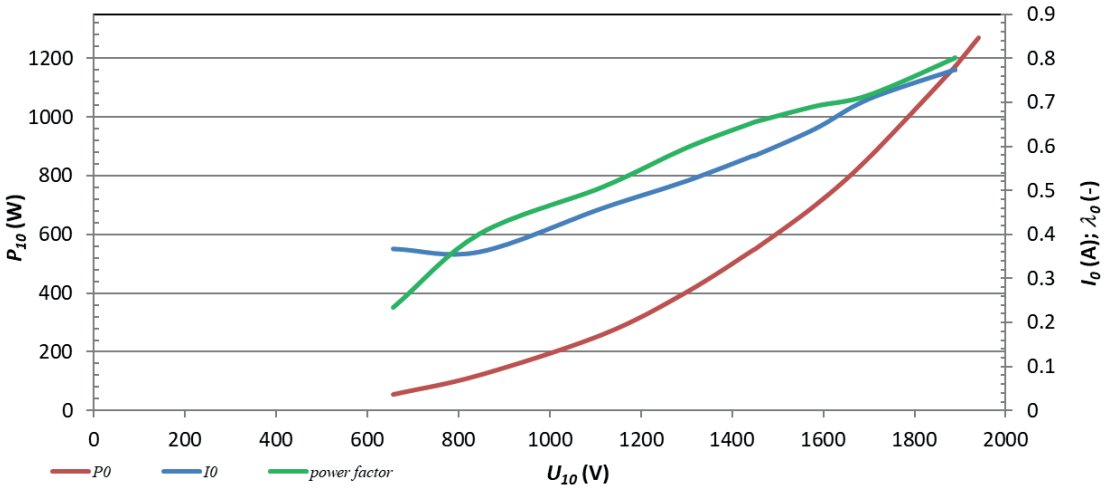

Figure 5 *Measured no load characteristics*

filling the insulating barrier between the windings by means of cooling air. The nominal parameters of designed transformer are listed in Table 1, while the initial experimental verification of the operational properties is shown in Figure 5.

The title of the article states a frequency of 1 kHz, whereas the actual operating frequency of the tuned power circuit was 900 Hz in the final. The conclusions stated are also valid for a frequency of 1000 Hz. The design of the transformer was done analytically based on the experience of the author's team in the development of the Mf transformer series.

3 Conclusion

This paper deals with the noise level of power transformers operating at 900 Hz, the source of which is the transformer core. The study examines the factors that influence the noise produced by the core of a power transformer and consequently the selection of a suitable core type and manufacturing technology. The design of a middle-frequency power transformer, its material composition and the design of the magnetic circuit and winding, operating in the frequency 900 Hz, with a power 200 kVA, cooled by air, to be fed from a suitable frequency converter characterised by reduced noise, are described. Considering the noise, the chosen application, the losses, the manufacturing possibilities, etc., the folded core "step lap" design, became the basis for the final design of the transformer and the material chosen was GT 100, i.e. sheet metal with a thickness of 0.1 mm. The proposed solution allows implementation of the galvanically isolated DC-DC converters for auxiliary traction drives and other DC-DC converters. The findings of this paper can be used in the design and operation of

power transformers and help mitigate the impact of transformer's noise on the surrounding environment.

Acknowledgment

This publication was realized with support of Operational Program Integrated Infrastructure 2014 - 2020 of the project: Innovative Solutions for Propulsion, Power and Safety Components of Transport Vehicles, code ITMS 313011V334, co-financed by the European Regional Development Fund".

Conflicts of interest

The authors declare that they have no known competing financial interests or personal relationships that could have appeared to influence the work reported in this paper.

References

[1] KUCHTA, J., FRANKO, M. The concept of the traction circuits for modernizing electric locomotives on two traction feed systems. In: 18th International Conference Current Problems in Rail Vehicles PRORAIL 2007: proceedings (in Slovak). 2007. ISBN 978-80-89276-06-6, p. 377-385.

[2] KUCHTA, J., KUCERA, R., FRANKO, M., FULIER, M. Modernization of locomotive r.361 from the perspective of development of new components of traction equipment. In: 20th International Conference Contemporary Issues in Rolling Stock PRORAIL 2011: proceedings (in Slovak). Vol. II. 2011. ISBN 978-80-89276-31-8, p. 193-202.

[3] KUCHTA, J., FRANKO, M., ILONCIAK, J. Concept of traction and auxiliary converters for diesel-electric locomotives. In: 22nd International Conference Contemporary Problems in Rolling Stock PRORAIL 2015: proceedings (in Slovak). 2015. ISBN 978-80-89276-48-6.

[4] FRANKO, M., KUCERA, R., BUDAY, J. Modernization of locomotive s.365 with regard of new components of traction equipment. In: 24th International Conference Contemporary Issues in Rolling Stock PRORAIL 2019: proceedings (in Slovak). 2019. ISBN 978-80-89276-58-5, p. 127-134.

[5] KUCERA, R., FRANKO, M., BUDAY, J., KOVAC, M. Assessment of interoperability subsystems "railway vehicle" of series 365 related to the required parameters and tests of traction converter and auxiliary converter. In: 24th International Conference Contemporary Issues in Rolling Stock PRORAIL 2019: proceedings (in Slovak). 2019. ISBN 978-80-89276-58-5, p. 381-387.

[6] RAJNAK, M., TIMKO, M., KOPCANSKY, P., PAULOVICOVA, K., KUCHTA, J., FRANKO, M., KURIMSKY, J., DOLNIK, B., CIMBALA, R. Transformer oil-based magnetic nanofluid with high dielectric losses tested for cooling of a model transformer. *IEEE Transactions on Dielectrics and Electrical Insulation* [online]. 2019, **26**(4), p. 1343-1349. ISSN 1070-9878, eISSN 1558-4135. Available from: https://doi.org/10.1109/TDEI.2019.008047

[7] KANG, M., ENJETI, P. N., PITEL, I. J. Analysis and design of electronic transformers for electric power distribution system. *IEEE Transactions on Power Electronics* [online]. 1999, **14**(6), p. 1133-1141. ISSN 0885-8993, eISSN 1941-0107. Available from: https://doi.org/10.1109/63.803407

[8] HUANG, P., MAO, CH., WANG, D., WANG, L., DUAN, Y., QIU, J., XU, G., CAI, H. Optimal design and implementation of high-voltage high-power silicon steel core medium-frequency transformer. IEEE Transactions on Industrial Electronics [online]. 2017, **64**(6), p. 4391-4401. ISSN 0278-0046, eISSN 1557-9948. Available from: https://doi.org/10.1109/TIE.2017.2674591

This is an open access article distributed under the terms of the Creative Commons Attribution 4.0 International License (CC BY 4.0), which permits use, distribution, and reproduction in any medium, provided the original publication is properly cited. No use, distribution or reproduction is permitted which does not comply with these terms.

COMPARATIVE ANALYSIS OF HYBRID COMPOSITES BASED ON A356 AND ZA-27 ALLOYS REGARDING THEIR TRIBOLOGICAL BEHAVIOUR

Blaža Stojanović[1], Sandra Gajević[1,*], Nenad Miloradović[1], Ružica Nikolić[2], Slavica Miladinović[1], Petr Svoboda[3], Aleksandar Vencl[4]

[1]University of Kragujevac, Faculty of Engineering, Kragujevac, Serbia
[2]Research Centre, University of Zilina, Zilina, Slovakia
[3]Faculty of Mechanical Engineering, Brno University of Technology, Brno, Czechia
[4]University of Belgrade, Faculty of Mechanical Engineering, Belgrade, Serbia

*E-mail of corresponding author: sandrav@kg.ac.rs

Blaža Stojanović 0000-0003-4790-2856,
Nenad Miloradović 0000-0001-6846-6091,
Slavica Miladinović 0000-0002-4408-0634,
Aleksandar Vencl 0000-0002-2208-4255
Sandra Gajević 0000-0002-7169-8907,
Ružica Nikolić 0000-0003-3042-8916,
Petr Svoboda 000-0003-3091-4025,

Resume

The comparative analysis of the two hybrid composites, obtained by the compocasting process, based on A356 and ZA-27 alloys and reinforced with 10 wt. % SiC and 0, 1 and 3 wt. % graphite (Gr) is presented. Optimisation of their tribological behaviour was performed by the Taguchi method and the artificial neural network (ANN). Tribological tests were performed on a block-on-disk tribometer, at three sliding speeds, three normal loads and a sliding distance of 600 m, without lubrication. Results obtained by the ANOVA showed that the hybrid composites based on A356 alloy have the better wear resistance and that the composite reinforced with 10 wt. % SiC and 1 wt. % Gr has the lowest wear rate. The lowest coefficient of friction was obtained for a composite based on ZA-27 alloy reinforced with 10 wt. % SiC, at a normal load of 10 N and sliding speed of 1 m/s.

Article info

Received 25 April 2023
Accepted 19 June 2023
Online 27 June 2023

Keywords:

wear
hybrid composites
A356
ZA-27
Taguchi design
artificial neural network

Available online: https://doi.org/10.26552/com.C.2023.056

ISSN 1335-4205 (print version)
ISSN 2585-7878 (online version)

1 Introduction

Requirements of the modern society, from the aspect of the service life increase and reduction of mass and thus the construction prices, initiated development of the new composites based on light metals. Composite materials could be made with metal, ceramic or polymer matrix and contain two or more physically distinct and mechanically separable materials [1]. Out of all the metal matrix composites (MMCs), the largest share in the world production belongs to composite materials based on aluminium alloys – over 30 % of the total production of composite materials. This market share is primarily due to the large use of MMCs with an aluminium matrix in aerospace, automotive, electronics and military industries. With an annual growth rate of 6 – 7 %, composite materials with a metal matrix are very interesting and promising materials. Hybrid composites are composites with two or more types or shapes of reinforcements.

Sardar et al. [2] have modelled the tribological characteristics of Al-Zn-Mg-Cu matrix composites with help of artificial neural network (ANN) and genetic algorithm (GA) methodology. They varied the amount of the Al_2O_3 particles (0 - 20 wt. %), load (20 - 80 N), abrasive size (9 - 105 μm) and sliding speed (0.125 - 1.50 m/s). The ANN and GA were used to reduce the wear rate, coefficient of friction and roughness of the abraded surface. The lowest wear rate and coefficient of friction were for 15 ± 2 wt. % of particles amount in the composite, while roughness was lower for particle amount in the range from 10 to 20 wt. %. At confirmation of experiments, the error results were lower than, or equal to, 12 %, which indicates the good

applicability of the developed model. It has been shown that the simultaneous use of ANN and GA leads to reliable results, which can be obtained in a relatively short period.

Nwobi-Okoye et al. [3] performed modelling and multi-objective optimisation of age hardening process parameters of composites based on A356 alloy, using the ANN and adaptive neuro-fuzzy inference system (ANFIS). By data analysis, it was concluded that the ANN with coarse experimental data points for learning is more effective than the ANFIS in predicting the process outputs. Ekka et al. [4] applied the regression analysis and the ANN method to predict the wear rate and coefficient of friction of hybrid composites. They came to a similar conclusion by analysing the experimental data – it was found that the ANN is more efficient in predicting the wear rate than the regression analysis.

Güler et al. [5, 6], considered the effect of content of the nano graphite particles on the wear behaviour of ZA27 based hybrid composites and nano composite bearing materials with enhanced corrosion properties. The lowest wear loss was obtained for the hybrid nanocomposites with content of 4 vol. % of graphite and 4 vol. % of alumina. The abrasion was the dominant wear mechanism in all the hybrid nanocomposites except for the mentioned one, where the adhesion was the dominant wear mechanism. For the nanocomposites obtained by mechanical milling, followed by hot pressing, authors reported that an increase of the milling duration improved the corrosion resistance of the nanocomposite bearing materials.

Celebi et al. [7], studied the effect of the nanoparticle content on the microstructure and mechanical properties of the ZA27 based hybrid composites produced by the powder metallurgy. Due to the lubricating properties of Gr, the negative effect of the mechanical-milling process caused the composite powder size to increase with cold-welding and to take a flaky shape. As the n-Gr ratio increased, cold-welding and agglomeration of additives during the mechanical milling increased the amount of porosity, while the tensile strength and hardness values of (hybrid nano composite materials) HNMs decreased as the n-Gr ratio increased, an increase was achieved with the increase in the n-Al_2O_3 ratio.

Feng, Wang and Wang [8], analysed the influence of graphite morphology on hyperthermal friction and wear behaviours of aluminium alloys with high silicon content. The volumetric wear loss results denote that (Al-27Si)-5FG (fake graphite) composites possess the superior wear resistance with respect to the Al-27Si and (Al-27Si)-5PG (particle graphite) composites for all the test temperatures. Due to the weak bonding of graphite particles, (Al-27Si)-5PG has the biggest volume wear. When the temperature rises to 400 °C, coefficient of friction of all the samples had a big fluctuations because of aluminium matrix softening and vibrations.

Ashebir et al. [9], reviewed the mechanical and metallurgical behaviour of hybrid reinforced aluminium metal matrix composites, various production methods, as well as the effect of various reinforcement ceramic particles and graphite (Gr) on the mechanical and metallurgical properties of MMCs. They pointed that the graphite, used as a solid lubricant between the composite material and the counter-body significantly lowered the composite wear, without the requirement of lubrication.

The microstructural, mechanical and tribological behaviour of aluminium-silicon A356 alloy and zinc-aluminium ZA-27 alloy hybrid metal matrix composites, is presented in [10-14]. Many authors have found that optimisation methods, such as Taguchi, GA, particle swarm optimisation (PSO) and others, can be successfully used when optimising the production parameters [15-16], processing or composition of composites [17-20], but that the better results are obtained by training or using the ANN. In this paper, the tribological behaviour of composites with the addition of graphite as a second reinforcement is optimised with the use of the Taguchi method and ANN. The matrices used for production of hybrid composites were A356 and ZA-27 alloys.

2 Experimental procedures

2.1 Materials and manufacturing

Two different matrices were used in production of the composites: the A356 alloy and ZA-27 alloy, reinforced with 10 wt. % SiC, the average size of 40 μm. Graphite (Gr) was also added to the composites. The average Gr particles size was 35 μm, while the amount of Gr particles varied and was 1 and 3 wt. %. Hybrid composites were obtained by applying the compocasting process. A detailed description of the process of obtaining the hybrid composites with the A356 base can be found in [21] and for the composites with the ZA-27 base in [18]. Structures of investigated composites (A356+10SiC and ZA-27+10SiC) and hybrid composites (A356+10SiC+1Gr, A356+10SiC+3Gr, ZA-27+10SiC+1Gr, ZA-27+10SiC+3Gr) are shown in Figure 1. It can be noticed that the SiC particles distribution is favourable and that the area of the matrix without particles is reduced. The soft Gr particles did not retain their average size during the composite production process. They were eroded and crushed in the process of preparation, so their final size was much smaller than the starting one.

Before examining the tribological characteristics, the hardness of the obtained composites was measured. The hardness of the tested materials was measured according to Vickers method (load of 10 kg) and the measurements were repeated 3 times and the mean values are presented in Table 1.

It was observed that the addition of a larger amount

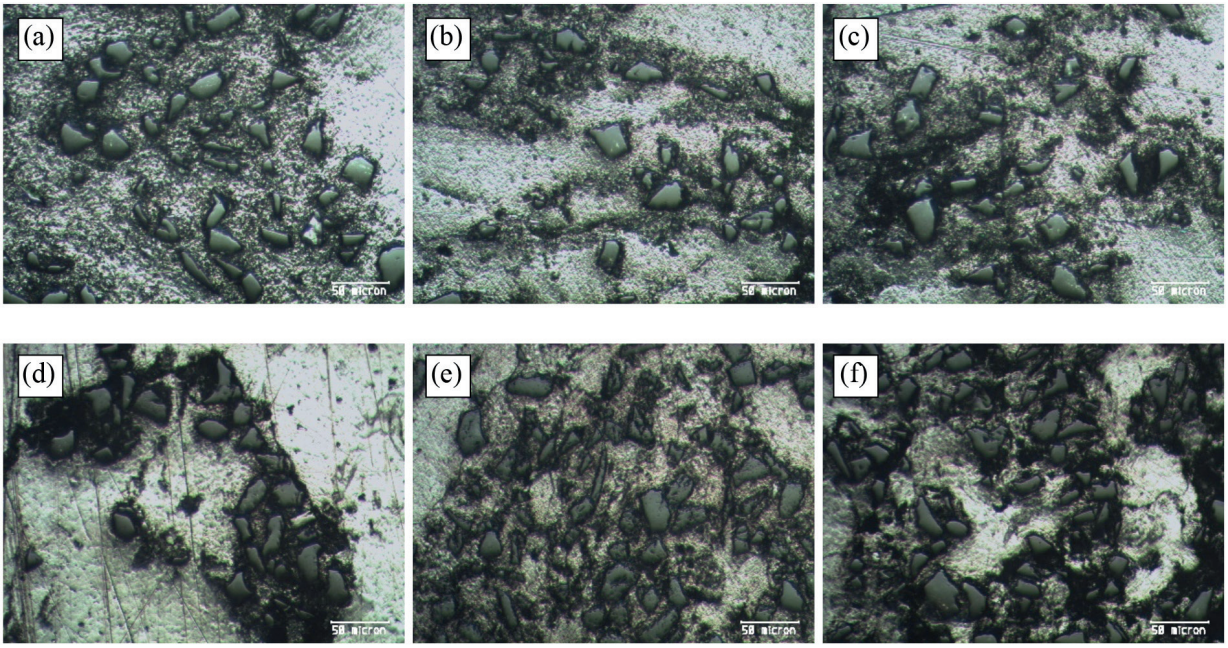

Figure 1 *Structures of the tested composites: (a) A356+10SiC, (b) A356+10SiC+1Gr, (c) A356+10SiC+3Gr, (d) ZA-27+10SiC, (e) ZA-27+10SiC+1Gr and (f) ZA-27+10SiC+3Gr*

Table 1. *Hardness of the tested composites*

Test no.	Material	HV
1	A356+10 wt.%SiC	68
2	A356+10 wt.% SiC+1 wt.% Gr	60
3	A356+10 wt.% SiC+3 wt.% Gr	46
4	ZA-27+10 wt.% SiC	125
5	ZA-27+10 wt.% SiC+1 wt.% Gr	127
6	ZA-27+10 wt.% SiC + 3 wt.% Gr	114

of graphite (3 wt.%) leads to a decrease in hardness for both hybrid composites. It is evident that the measured hardness values are correlated with the wear of the composite.

2.2 Wear and friction tests

The wear and friction tests of hybrid composites with different matrices were performed in dry sliding conditions, on a tribometer with the block-on-disc contact geometry. The material of the disc was a MANCOVA steel of hardness of 62-64 HMRC and a diameter of 35 mm and thickness of 6.35 mm, while the block materials were made of tested hybrid composites. The geometry of the contact pairs was in accordance with the standard ASTM G77. Values of the coefficient of friction (COF) were monitored during the test and through the data acquisition system stored in the PC. The wear rate used in the further analysis was obtained by calculations based on the wear scar width, which was measured on a universal measuring microscope, after 600 m of sliding distance. All the tribological tests were repeated 3 times and mean values are shown in the wear rate results.

2.3 Experimental design

The modern approach to experiments is closely connected with the use of the experiments' design. Experimental planning is a powerful tool for experimental statistical research of complex systems. Its application provides a practical and efficient way of varying the influential or input factors at different levels, contributing to an objective understanding of the researched system/process with help of statistics. The experimental design methodology is a systematic way to plan, perform and interpret the results of experiments, to obtain as much information as possible, while performing as few experiments as possible [22].

Realisation of the experimental test in this research was performed according to the defined plan, which consisted of selected factors and their levels given in Table 2. The sliding distance for all the tests was kept

Table 2 *Levels for various control factors*

Control factor	Units	Level I	Level II	Level III
(A) Material	-	A356+10SiC	ZA-27+SiC	-
(B) Gr amount	wt.%	0	1	3
(C) Normal load	N	10	20	30
(D) Sliding speed	m/s	0.25	0.50	1.0

Table 3 *Experimental design using L54 orthogonal array and wear and friction test results*

Test no.	A	B	C	D	Wear rate $\times 10^{-3}$, mm^3/m	S/N ratio for wear rate	COF	S/N ratio for COF
1	A356+10SiC	0	10	0.25	0.367	8.7067	0.703	3.06089
2	A356+10SiC	0	20	0.25	1.548	-3.7954	0.690	3.22302
3	A356+10SiC	0	30	0.25	1.846	-5.3246	0.650	3.74173
4	A356+10SiC	0	10	0.50	0.687	3.2609	0.689	3.23562
5	A356+10SiC	0	20	0.50	1.768	-4.9496	0.655	3.67517
6	A356+10SiC	0	30	0.50	2.119	-6.5226	0.621	4.13817
7	A356+10SiC	0	10	1.00	0.869	1.2196	0.640	3.87640
8	A356+10SiC	0	20	1.00	2.144	-6.6245	0.623	4.11024
9	A356+10SiC	0	30	1.00	2.310	-7.2722	0.579	4.74643
10	A356+10SiC	1	10	0.25	0.135	17.3933	0.724	2.80523
11	A356+10SiC	1	20	0.25	0.696	3.1478	0.710	2.97483
12	A356+10SiC	1	30	0.25	1.687	-4.5423	0.680	3.34982
13	A356+10SiC	1	10	0.50	0.197	14.1107	0.694	3.17281
14	A356+10SiC	1	20	0.50	0.909	0.8287	0.677	3.38823
15	A356+10SiC	1	30	0.50	1.833	-5.2632	0.660	3.60912
16	A356+10SiC	1	10	1.00	0.282	10.9950	0.657	3.64869
17	A356+10SiC	1	20	1.00	1.253	-1.9590	0.652	3.71505
18	A356+10SiC	1	30	1.00	2.085	-6.3821	0.646	3.79535
19	A356+10SiC	3	10	0.25	0.173	15.2391	0.733	2.69792
20	A356+10SiC	3	20	0.25	1.372	-2.7471	0.743	2.58022
21	A356+10SiC	3	30	0.25	2.306	-7.2572	0.824	1.68146
22	A356+10SiC	3	10	0.50	0.244	12.2522	0.712	2.95040
23	A356+10SiC	3	20	0.50	1.580	-3.9731	0.717	2.88962
24	A356+10SiC	3	30	0.50	2.532	-8.0693	0.771	2.25891

constant at 600 m. The varied factors were different composite matrices, amount of composite reinforcements, normal load and sliding speed.

Based on the defined factors and the adopted levels, the Taguchi orthogonal array L54 was obtained with Minitab 16. The experimental results are shown in Table 3, as well as the values of the S/N (signal-to-noise) ratios obtained by the data analysis. In the Taguchi method, the transformation of experimental results into the S/N relationships is mandatory. There are three categories of the S/N relationships: "smaller-is-better", "larger-is-better" and "nominal-is-best". In this case, the quality characteristic S/N ratio "smaller-is-better" was selected for the analysis of the composite wear rate [14]. Statistical analysis of variance is used to consider statistically worthy parameters so that the optimal combination of parameters can be predicted.

3 Results and discussion

3.1 Wear rate and coefficient of friction

Depending on the purpose of the output, the appropriate characteristics was chosen. However, regardless of the selected output category, the higher S/N ratio corresponds to the better-quality characteristics and, more precisely, to the smaller variance of the output characteristics (response) around the desired (target) value. The arithmetic mean of the S/N ratio was calculated for each level of the considered factors in comparison to the wear rate (Table 4).

Based on the results of the S/N ratios (Table 4 and Figures 2 and 3), it can be determined which of the considered factors has the greatest influence on the wear rate. In addition, an optimal combination of

Table 3 *(continued) Experimental design using L54 orthogonal array and wear and friction test results*

Test no.	A	B	C	D	Wear rate $\times 10^{-3}$, mm³/m	S/N ratio for wear rate	COF	S/N ratio for COF
25	A356+10SiC	3	10	1.00	0.346	9.2185	0.690	3.22302
26	A356+10SiC	3	20	1.00	1.894	-5.5476	0.708	2.99933
27	A356+10SiC	3	30	1.00	2.952	-9.4023	0.750	2.49877
28	ZA-27+10SiC	0	10	0.25	0.512	5.8146	0.486	6.26549
29	ZA-27+10SiC	0	20	0.25	2.237	-6.9933	0.513	5.79088
30	ZA-27+10SiC	0	30	0.25	2.441	-7.7514	0.538	5.38758
31	ZA-27+10SiC	0	10	0.50	0.531	5.4981	0.513	5.80104
32	ZA-27+10SiC	0	20	0.50	2.288	-7.1891	0.532	5.47524
33	ZA-27+10SiC	0	30	0.50	2.606	-8.3195	0.553	5.13765
34	ZA-27+10SiC	0	10	1.00	0.592	4.5536	0.527	5.56214
35	ZA-27+10SiC	0	20	1.00	2.402	-7.6115	0.552	5.16279
36	ZA-27+10SiC	0	30	1.00	2.703	-8.6369	0.583	4.68514
37	ZA-27+10SiC	1	10	0.25	0.365	8.7541	0.483	6.31926
38	ZA-27+10SiC	1	20	0.25	2.002	-6.0293	0.497	6.07462
39	ZA-27+10SiC	1	30	0.25	2.258	-7.0745	0.517	5.73187
40	ZA-27+10SiC	1	10	0.50	0.422	7.4938	0.497	6.07112
41	ZA-27+10SiC	1	20	0.50	2.206	-6.8721	0.505	5.94106
42	ZA-27+10SiC	1	30	0.50	2.339	-7.3806	0.530	5.51940
43	ZA-27+10SiC	1	10	1.00	0.512	5.8146	0.511	5.83328
44	ZA-27+10SiC	1	20	1.00	2.245	-7.0243	0.535	5.43942
45	ZA-27+10SiC	1	30	1.00	2.401	-7.6078	0.540	5.34891
46	ZA-27+10SiC	3	10	0.25	0.252	11.9720	0.500	6.01713
47	ZA-27+10SiC	3	20	0.25	2.033	-6.1627	0.516	5.74869
48	ZA-27+10SiC	3	30	0.25	2.231	-6.9700	0.532	5.48013
49	ZA-27+10SiC	3	10	0.50	0.384	8.3134	0.516	5.75206
50	ZA-27+10SiC	3	20	0.50	2.051	-6.2393	0.532	5.48013
51	ZA-27+10SiC	3	30	0.50	2.288	-7.1891	0.547	5.24184
52	ZA-27+10SiC	3	10	1.00	0.451	6.9165	0.539	5.36500
53	ZA-27+10SiC	3	20	1.00	2.091	-6.4071	0.556	5.09694
54	ZA-27+10SiC	3	30	1.00	2.358	-7.4509	0.568	4.91762

Table 4 *Response table for signal-to-noise ratios for wear rate and COF*

Level	Wear rate				COF			
	Material	Gr amount, %	Normal load, N	Sliding speed, m/s	Material	Gr amount, %	Normal load, N	Sliding speed, m/s
1	0.2496	-2.8854	8.7515	0.3544	3.261	4.615	4.537	4.385
2	-2.3622	0.4668	-4.7860	-1.1228	5.579	4.597	4.431	4.430
3		-0.7502	-7.1343	-2.4005		4.049	4.293	4.446
Delta	2.6118	3.3522	15.8857	2.7549	2.319	0.566	0.244	0.061
Rank	4	2	1	3	1	2	3	4

factors can be determined to achieve the minimal wear of hybrid composites. Based on Table 4 and according to the ranking of factors, it was determined that the greatest influence has the normal load, followed by other factors in this order: Gr amount, sliding speed and material. Main effects plots (Figures 2a and 3a) show that composites based on A356 alloy had lower wear and higher friction than the composites based on ZA-27 alloy. This is most probably because the SiC reinforcements protruded more to the surface of the A356 alloy thus protecting the matrix and inducing the higher friction [10]. As expected, the higher load and speed induced higher wear rates, while load and speed had a low impact on the COF values.

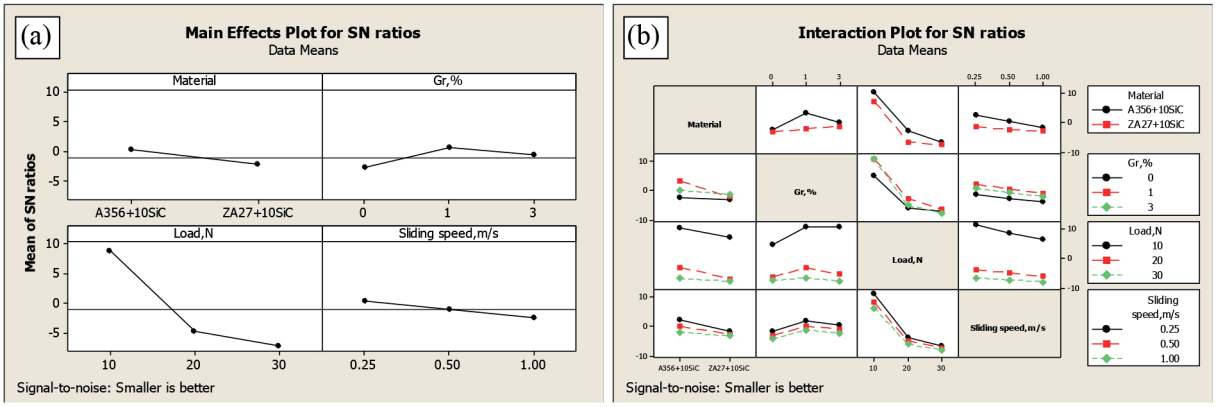

Figure 2 *The S/N ratio for the wear rate: (a) main effects plot and (b) interaction plot*

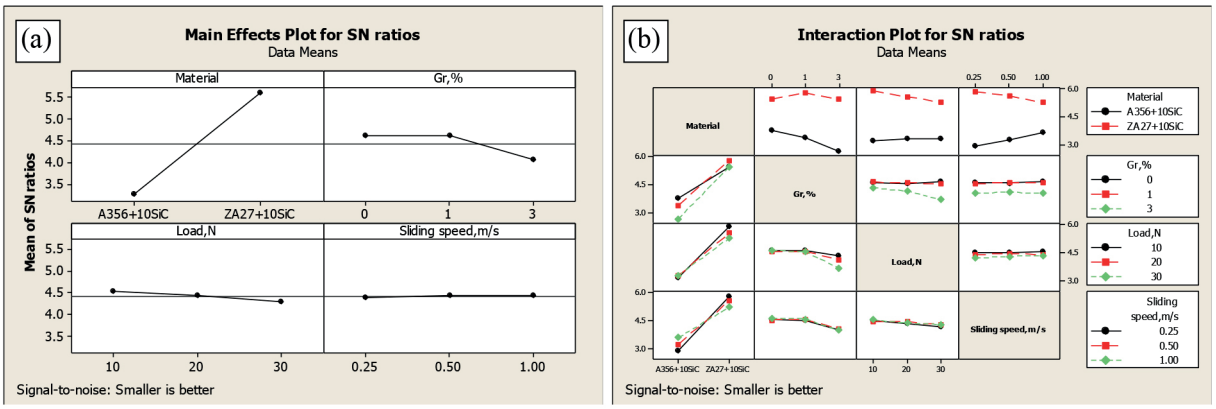

Figure 3 *The S/N ratio for the coefficient of friction: (a) main effects plot and (b) interaction plot*

The optimal combination of factors for achieving the minimum wear rate is A1-B2-C1-D1, i.e. using the composites based on aluminium alloy, A356/10 wt. % SiC with reinforcement content of 1 wt. % Gr, at a normal load of 10 N and sliding speed of 0.25 m/s. For the minimum COF, the optimal combination of factors is A2-B1-C1-D3, i.e. using the composites based on zinc alloy, ZA-27/10 wt. % SiC, with reinforcement content of 0 wt. % Gr, at a normal load of 10 N and sliding speed of 1 m/s. Figures 2b and 3b show graphs of factor interactions, according to which the existence of influence of interactions between individual factors on the wear rate is observed.

A more precise determination of the influence of factors and their interactions on the wear rate and COF of composites was performed using analysis of variance (ANOVA). With help of the ANOVA analysis, the values of members, which define the statistically significant members that represent input variables (factors), whose change affects the change of the output variable (wear rate), are obtained. The ANOVA analysis was applied at the significance level of 5 % (i.e. 95 % confidence level). The level of significance was defined by the p-value, which indicates the member's influence on the wear rate. If the calculated p-value is less than 0.05 that member affects wear, while members with a p-value greater than 0.10 should be omitted from further analysis because that indicates that they do not affect the output.

Following the results obtained by the ANOVA analysis, a large influence of normal load on the wear rate of hybrid composites of 84.53 % was observed in the last column of Table 5. It was followed by the influence of the graphite amount (3.31 %), the influence of the matrix material of the composite (2.94 %) and the influence of the sliding speed (2.19 %), while the influence of interactions was less than 3 %. Observing the results of ANOVA analysis for the COF (Table 6), a large influence of the composite matrix of 82.89 % is observed, followed by the influence of the Gr amount of 4.26 %, while the influence of the normal load and sliding speed is less than 1 %. Influence of factor interactions on the COF of 3.17 % and 4.50 % corresponds to material × Gr amount and material × sliding speed, respectively.

Figure 4 shows the contour plots of the influencing factors on the wear rate (wear maps). Based on the diagram, minimal wear was achieved by tracking the lighter colours. By adjusting the factors to certain values, it is possible to achieve the target value of the wear rate.

The wear rate increases with the load increase, while the addition of Gr particles up to 1.5 wt. % decreases the wear. Further adding of the Gr particles, above 1.5 wt. %, starts to increase the wear rate. The effect of the reinforcement in the composite is prominent at the higher applied load of around 25 N. It was noticed that the small amount of Gr particles, up to around 0.5 wt. %, at the lowest load, does not affect improving

Table 5 *Analysis of variance for the S/N ratios for wear rate*

Source	DF	Seq SS	Adj SS	Adj MS	F-value	p-value	Pr, %
Material	1	92.09	92.09	92.09	66.74	0.000	2.94
Gr amount	2	103.67	103.67	51.83	37.56	0.000	3.31
Normal load	2	2646.81	2646.81	1323.40	959.05	0.000	84.53
Sliding speed	2	68.43	68.43	34.21	24.79	0.000	2.19
Material × Gr amount	2	51.40	51.40	25.70	18.62	0.000	1.64
Material × normal load	2	20.78	20.78	10.39	7.53	0.002	0.66
Material × sliding speed	2	15.42	15.42	7.71	5.59	0.009	0.49
Gr amount × normal load	4	71.91	71.91	17.98	13.03	0.000	2.30
Gr amount × sliding speed	4	0.46	0.46	0.12	0.08	0.987	0.01
Normal load × sliding speed	4	21.42	21.42	5.36	3.88	0.012	0.68
Residual error	28	38.64	38.64	1.38			1.23
Total	53	3131.03					100.00

S = 1.175, R^2 = 98.8 %, R^2 (adj) = 97.7 %

Table 6 *Analysis of variance for the S/N ratios for COF*

Source	DF	Seq SS	Adj SS	Adj MS	F-value	p-value	Pr, %
Material	1	72.5696	72.5696	72.5696	1151.29	0.000	82.89
Gr amount	2	3.7274	3.7274	1.8637	29.57	0.000	4.26
Normal load	2	0.5381	0.5381	0.2691	4.27	0.024	0.61
Sliding speed	2	0.0357	0.0357	0.0179	0.28	0.755	0.04
Material × Gr amount	2	2.7760	2.7760	1.3880	22.02	0.000	3.17
Material × normal load	2	1.2452	1.2452	0.6226	9.88	0.001	1.42
Material × sliding speed	2	3.9399	3.9399	1.9700	31.25	0.000	4.50
Gr amount × normal load	4	0.8471	0.8471	0.2118	3.36	0.023	0.97
Gr amount × sliding speed	4	0.0624	0.0624	0.0156	0.25	0.909	0.07
Normal load × sliding speed	4	0.0440	0.0440	0.0110	0.17	0.950	0.05
Residual error	28	1.7649	1.7649	0.0630			2.02
Total	53	87.5504					100.00

S = 0.2511, R^2 = 98.0 %, R^2 (adj) = 96.2 %

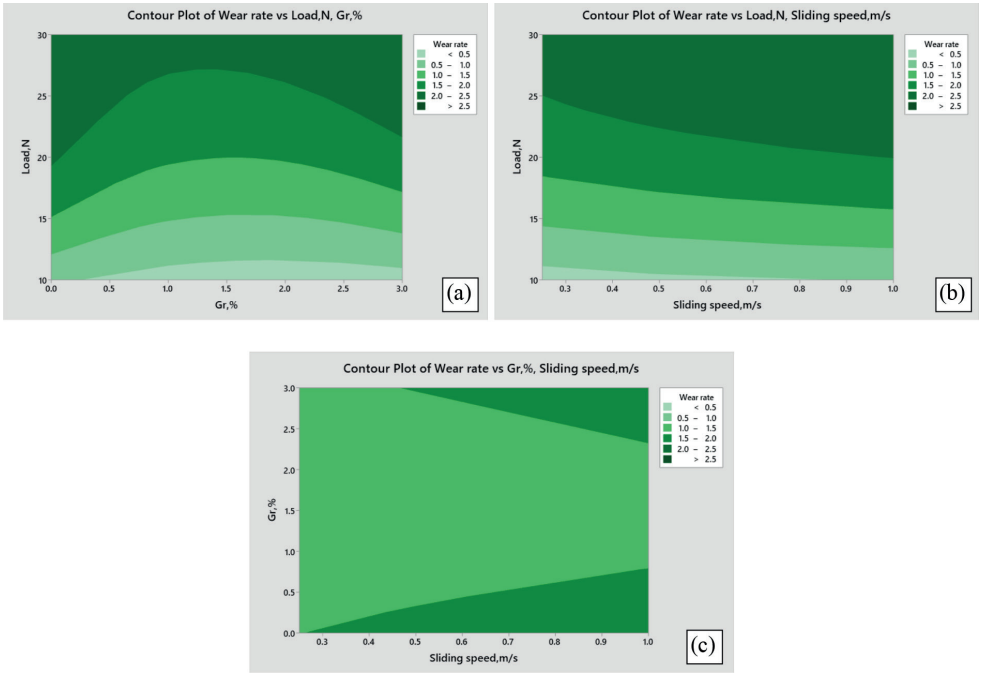

Figure 4 *Diagram of the wear rate dependence on: (a) normal load and reinforcement content, (b) normal load and sliding speed and (c) reinforcement content and sliding speed*

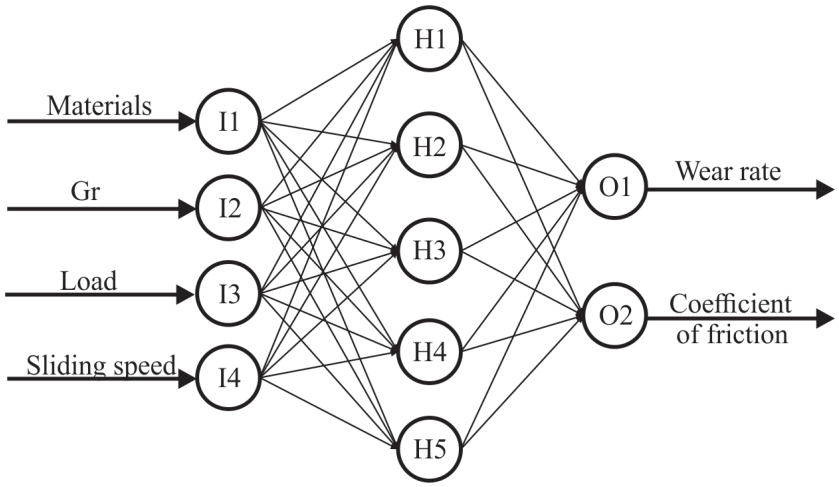

Figure 5 *The ANN architecture*

the wear resistance. The influence of the Gr particles amount on the composite wear, regarding the sliding speed, is manifested at higher sliding speeds.

3.2 The ANN prediction

The principle of solving problems using neural networks is similar to that of the human brain. Like the human brain, neural networks are made up of simple interconnected units called nodes or neurons. Neural networks are not programmed, but they learn from experience through the recognition of patterns and the interrelationship between data, so it is not important for them to know the theory behind the phenomenon. The data, based on which the network is trained, come to the input layer, then they are transferred to the hidden layer and, finally, the predicted data is obtained via the output layer [2,19]. The number of input parameters means the number of neurons in the input layer, the number of output parameters means how many neurons there are in the output layer, while the number of neurons in the hidden layer is not precisely defined and depends on the experience of a person who is modelling the network.

In the used ANN, the signals were transmitted from the input to the output, with feed-forward back propagation neural network. The Levenberg-Marquardt network training function was used in the formation and training of the network because it is recommended due to its accuracy and speed. In the hidden layer, the neurons work based on the Log-Sigmoid transfer function (logsig) and in the output layer - based on the Linear Transfer Function (purelin). In the input layer, some parameters are varied. In this case, there are four parameters: material, amount of graphite, normal load and sliding speed. Results of the experiment, i.e. the wear rate and COF are in the output layer. Several networks, with different numbers of neurons in the hidden layer (5, 10 and 15), were trained, but the network with 5 neurons in the hidden layer proved to be the best. The used network scheme was with the 4-5-2 architecture (Figure 5).

After the network training, in addition to the predicted data, the regression diagrams for training, validation, testing and the total regression coefficient were obtained (Figure 6). When developing each network, the total regression coefficient tends to be as close to 1 as possible. After training the network with the 4-5-2 architecture, the regression coefficient of 0.99456 was obtained, which shows a very good correlation with the experimental data. From Figure 6, it can be observed that the majority of the input data to the neural network were used for training (as much as 60 %), while 20 % was used for validation and 20 % for testing the developed neural network.

3.3 Wear mechanisms

The worn surfaces of the blocks were imaged on an SEM microscope and representative wear scars are shown in Figure 7. The EDS analysis of the chemical composition of individual samples was performed, as well. Before analysing the samples, they were cleaned and degreased with petrol in the ultrasonic bath. Such a sample preparation was performed to prevent contamination of the microscope, as well as to obtain a realistic picture of the condition of the worn surfaces. Appearances of all the composite samples worn surfaces were similar, regardless of the normal load and sliding speed. From Figure 7 one can see that the main wear mechanism was the adhesive wear [12]. Adhesive wear pits of irregular shape and uneven depth are visible on the worn surface of the blocks, together with the protruded SiC particles and transferred disc (counter-body) material. Regarding the counter-body sliding direction, it can be noticed that the transfer of the material occurs mainly in the first half of the wear scar and the adhesive wear pits appear mainly in the second half of the wear scar.

The SEM images and EDS analysis of the composites' samples show the presence of iron (Fe), oxygen (O), silicon (Si) and carbon (C), Figure 8. The

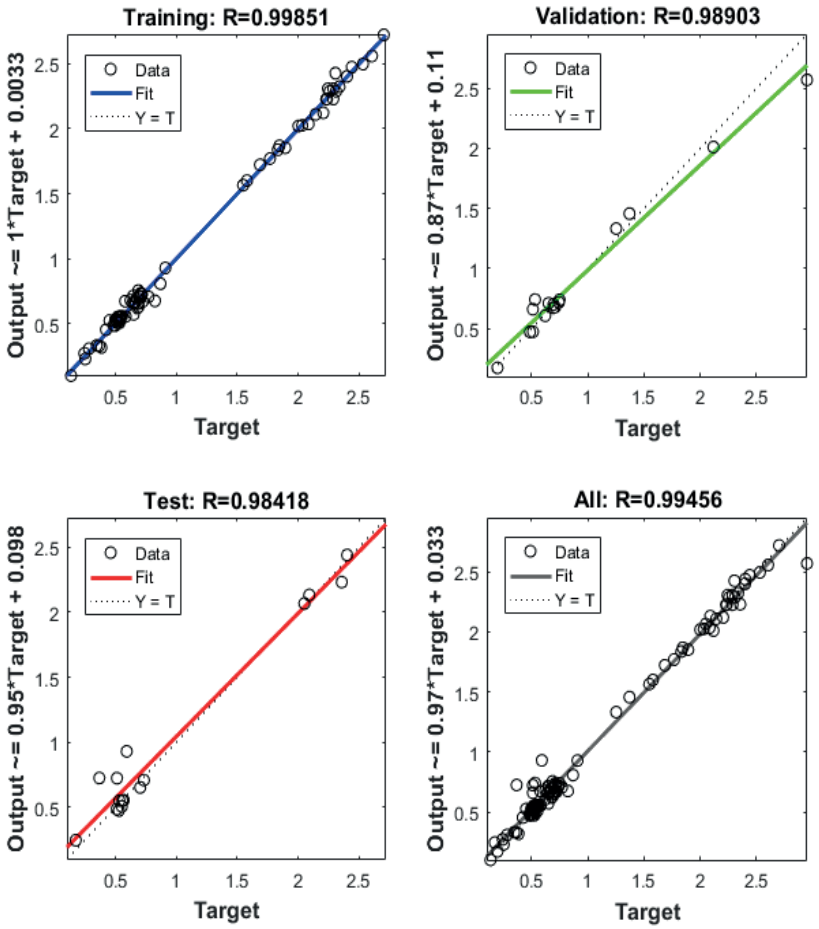

Figure 6 *Regression coefficients of the trained network*

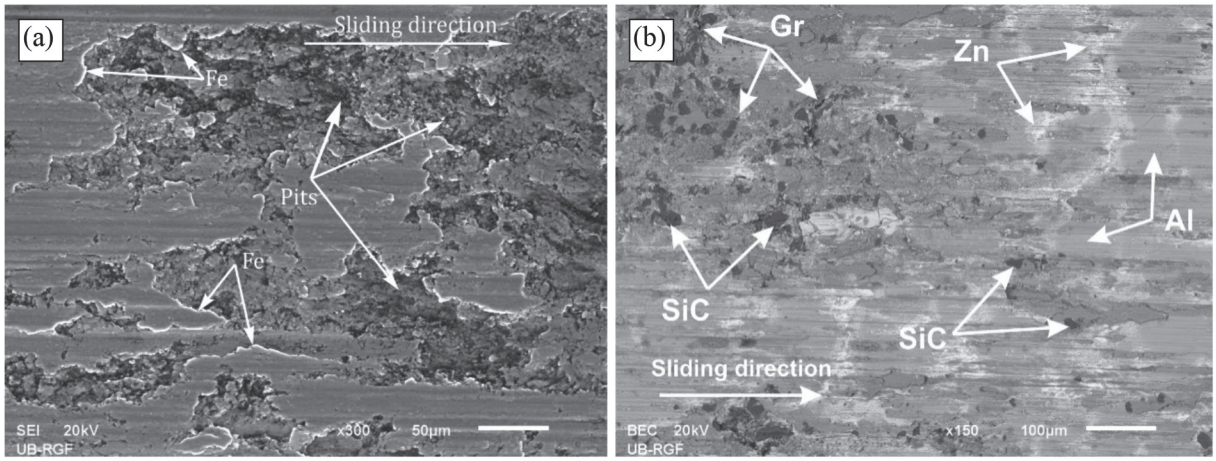

Figure 7 *The SEM image of the worn surfaces for a normal load of 10 N and sliding speed of 0.25 m/s: (a) A356+10SiC+1Gr and (b) ZA-27+10SiC+1Gr*

presence of Fe (Spectrum 2) indicates that the surface layer of the steel disc was also worn and that transfer of counter-body material occurred. The wear of the steel disc is mainly caused by the presence of the protruded SiC hard particles (Spectrum 3). The oxidized worn iron particles and matrix material formed a mechanically mixed layer (MML) [23-24], which was confirmed by the EDS analysis (Spectrum 1).

4 Conclusions

The Taguchi design and ANN can be successfully used to analyse the parameters influencing the wear rate and coefficient of friction of the tested hybrid composites. Application of the Taguchi method reduces the number of conducted experiments and the time of their realisation, as well as the costs. The ANOVA

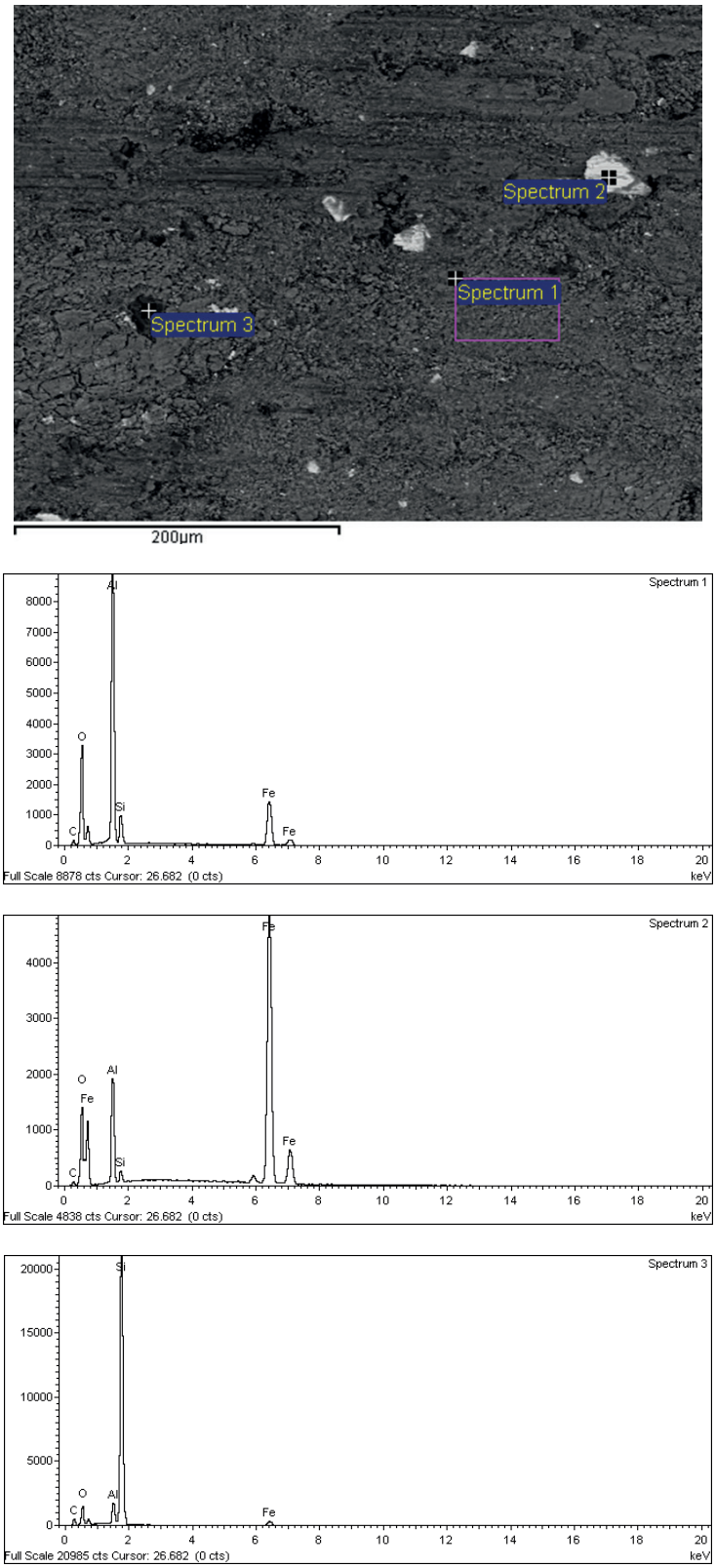

Figure 8 *The EDS analysis of hybrid composite A356+10SiC+1Gr at the normal load of 10 N and the sliding speed of 0.25 m/s*

analysis of influential parameters very precisely shows the influence of individual parameters. Based on the obtained results, it is possible to predict the wear rate and coefficient of friction, as well as to determine the values of the influential parameters that give the minimum values. An artificial neural network is used to verify the obtained results. Matching the results, using the Taguchi method and the ANN, confirmed the

justification of the application of these methods.

Based on the obtained results, it can be concluded that both hybrid composites have better characteristics than the corresponding matrix alloys. For the given test conditions, the wear of hybrid composites based on A356 alloy is lower than the wear of hybrid composites based on ZA-27 alloy, while for the coefficient of friction, it is the opposite. The dominant mechanism is adhesive wear, which is manifested through delamination and transfer of materials between the contact surfaces. Formation of the MML layers was observed in both types of composites (with aluminium alloy matrix and zinc alloy matrix).

The normal load has the highest influence on wear, followed by the amount of graphite, the matrix material and the sliding speed, while the matrix material is the most influential factor on friction. The lowest wear rate was obtained for the composite based on A356 alloy, reinforced with 10 wt. % SiC and 1 wt. % Gr, at a normal load of 10 N and a sliding speed of 0.25 m/s. The lowest coefficient of friction was obtained for the composite based on ZA-27 alloy, reinforced only with 10 wt. % SiC, at a normal load of 10 N and a sliding speed of 1 m/s.

By examining the hardness of the produced composites for tribological tests, uniform results were obtained, which unequivocally confirms the good distribution of particles, as well as justification of application of this process for obtaining the composite materials. By adding the graphite, the coefficient of friction of the tested materials increased. The main reasons for that increase are the type of contact geometry, as well as a large drop in hardness of the tested material. A large decrease in hardness is evident in the composite with 3 wt.% Gr, where the coefficient of friction has the highest values.

Acknowledgements

This paper presents the research results obtained within realisation of the project TR 35021, supported by the Ministry of Science, Technological Development and Innovation of the Republic of Serbia. Aleksandar Vencl acknowledges the project financially supported by the Republic of Serbia, Ministry of Science, Technological Development and Innovation (Contract No. 451-03-47/2023-01/200105). Ruzica Nikolic acknowledges the project "Innovative Solutions for Propulsion, Power and Safety Components of Transport Vehicles", code ITMS 313011V334 of the Operational Program Integrated Infrastructure 2014-2020 co-financed by the European Regional Development Fund. Petr Svoboda acknowledges the project FSI-S-23-8245, funded by the Ministry of Education, Youth and Sports of the Czech Republic. Collaboration through the CEEPUS network CIII-BG-0703 and bilateral Project 337-00-577/2021-09/16 between Republic of Serbia and Republic of Austria is also acknowledged.

Conflicts of interest

The authors declare that they have no known competing financial interests or personal relationships that could have appeared to influence the work reported in this paper.

References

[1] OGUNDIJI, O. E., OYATOGUN G. M. Tensile and flexural properties of polyester composites reinforced by iron filings. *Tribology and Materials* [online]. 2022, **1**(4), p. 157-162. ISSN 2812-9717. Available from: https://doi.org/10.46793/tribomat.2022.020

[2] SARDAR, S., DEY, S., DAS, D. Modelling of tribological responses of composites using integrated ANN-GA technique. *Journal of Composite Materials* [online]. 2021, **55**(7), p. 873-896. ISSN 0021-9983. Available from: https://doi.org/10.1177/0021998320960520

[3] NWOBI-OKOYE, C. C., OCHIEZE, B. Q., OKIY, S. Multi-objective optimization and modelling of age hardening process using ANN, ANFIS and genetic algorithm: results from aluminum alloy A356/cow horn particulate composite. *Journal of Materials Research and Technology* [online]. 2019, **8**(3), p. 3054-3075. ISSN 2238-7854. Available from: https://doi.org/10.1016/j.jmrt.2019.01.031

[4] EKKA, K. K., CHAUHAN, S. R., GOEL, V. Study on the sliding wear behavior of hybrid aluminum matrix composites using Taguchi design and neural network. *Proceedings of the Institution of Mechanical Engineers, Part L: Journal of Materials: Design and Applications* [online]. 2016, **230**(2), p. 537-549. ISSN 1464-4207. Available from: https://doi.org/10.1177/1464420715581393

[5] GULER, O., CUVALCI, H., CANAKCI, A., CELEBI, M. The effect of nano graphite particle content on the wear behavior of ZA27 based hybrid composites. *Advanced Composites Letters* [online]. 2017, **26**(2), p. 30-36. ISSN 0963-6935, EISSN 2633-366X. Available from: https://doi.org/10.1177/096369351702600201

[6] CELEBI, M., GULER, O., CANAKCI, A., CUVALCI, H. The effect of nanoparticle content on the microstructure and mechanical properties of ZA27-Al2O3-Gr hybrid nanocomposites produced by powder metallurgy. *Journal of Composite Materials* [online]. 2021, **55**(24), p. 3395-3408. ISSN 0021-9983, eISSN 1530-793X. Available from: https//doi.org/z0.1177/00219983211015719

[7] GULER, O., CELEBI, M., DALMIS, R., CANAKCI, A., CUVALCI, H. Novel ZA27/B 4 C/graphite hybrid nanocomposite-bearing materials with enhanced wear and corrosion resistance. *Metallurgical and Materials Transactions A* [online]. 2020, **51**, p. 4632-4646. ISSN 1073-5615. Available from: https://doi.org/10.1007/s11661-020-05863-5

[8] FENG, C., WANG, Y., WANG, Z. Influence of graphite morphology on hyperthermal friction and wear behaviors of aluminum-high silicon alloys. *Silicon* [online]. 2022, **14**, p. 9153-9161. ISSN 1876-990X, eISSN 1876-9918. Available from: https://doi.org/10.1007/s12633-021-01524-3

[9] ASHEBIR, D. A., MENGESHA, G. A., SINHA, D. K., An insight into mechanical and metallurgical behavior of hybrid reinforced aluminum metal matrix composite. *Advances in Materials Science and Engineering* [online]. 2022, 7843981. ISSN 1687-8434, eISSN 1687-8442. Available from: https://doi.org/10.1155/2022/7843981

[10] BOBIC, I., RUZIC, J., BOBIC, B., BABIC, M., VENCL, A., MITROVIC, S. Microstructural characterization and artificial aging of compo-casted hybrid A356/SiC_p/Gr_p composites with graphite macroparticles. *Materials Science and Engineering A* [online]. 2014, **612**, p. 7-15. ISSN 0921-5093. Available from: https://doi.org/10.1016/j.msea.2014.06.028

[11] AJAY KUMAR, K., MALLIKARJUNA, C., Microstructure and mechanical properties of A356/Al_2O_3/MoS_2 hybrid nanocomposites. *Materials Today: Proceedings* [online]. 2022, **54**(2), p. 415-420. ISSN 2214-7853. Available from: https://doi.org/10.1016/j.matpr.2021.09.472

[12] VENCL, A., VUCETIC, F., BOBIC, B., PITEL, J., BOBIC, I. Tribological characterization in dry sliding conditions of compocasted hybrid A356/SiC_p/Gr_p composites with graphite macroparticles. *The International Journal of Advanced Manufacturing Technology* [online]. 2019, **100**(9-12), p. 2135-2146. ISSN 0268-3768. Available from: https://doi.org/10.46793/tribomat.2022.014

[13] GURUNAGENDRA, G. R., RAJU, B. R., PUJAR, V., AMITH, D. G., POORNACHANDRA, SIDDESHA, H. S., Mechanical, wear and corrosion properties of micro particulates reinforced ZA-27 hybrid MMC by stir casting: a review. *Materials Today: Proceedings* [online]. 2021, **46**(17), p. 7602-7607. ISSN 2214-7853. Available from: https://doi.org/10.1016/j.matpr.2021.01.892

[14] VENCL, A., STOJANOVIC, B., GOJKOVIC, R., KLANCNIK, S., CZIFRA, A., JAKIMOVSKA, K., HARNICAROVA, M. Enhancing of ZA-27 alloy wear characteristics by addition of small amount of SiC nanoparticles and its optimisation applying Taguchi method. *Tribology and Materials* [online]. 2022, **1**(3), p. 96-105. ISSN 2812-9717. Available from: https://doi.org/10.46793/tribomat.2022.014

[15] HAGHDADI, N., ZAREI-HANZAKI, A., KHALESIAN, A. R., ABEDI, A. R. Artificial neural network modelling to predict the hot deformation behavior of an A356 aluminum alloy. *Materials and Design* [online]. 2013, **49**, p. 386-391. ISSN 0261-3069. Available from: https://doi.org/10.1016/j.matdes.2012.12.082

[16] STALIN, B., KUMAR, P. R., RAVICHANDRAN, M., KUMAR, M. S., MEIGNANAMOORTHY, M. Optimization of wear parameters using Taguchi grey relational analysis and ANN-TLBO algorithm for silicon nitride filled AA6063 matrix composites. *Materials Research Express* [online]. 2019, **6**(10), 106590. eISSN 2053-1591. Available from: https://doi.org/10.1088/2053-1591/ab3d90

[17] DANIEL, S. A. A., PUGAZHENTHI, R., KUMAR, R., VIJAYANANTH, S. Multi objective prediction and optimization of control parameters in the milling of aluminum hybrid metal matrix composites using ANN and Taguchi-Grey relational analysis. *Defence Technology* [online]. 2019, **15**(4), p. 545-556. ISSN 2096-3459. Available from: https://doi.org/10.1016/j.dt.2019.01.001

[18] MILORADOVIC, N., VUJANAC, R., STOJANOVIC, B., PAVLOVIC, A. Dry sliding wear behavior of ZA27/SiC/Gr hybrid composites with Taguchi optimization. *Composite Structures* [online]. 2021, **264**, 113658. ISSN 1879-1085. Available from: https://doi.org/10.1016/j.compstruct.2021.113658

[19] STOJANOVIC, B., GAJEVIC, S., KOSTIC, N., MILADINOVIC, S., VENCL, A. Optimization of parameters that affect wear of A356/Al2O3 nanocomposites using RSM, ANN, GA and PSO methods. *Industrial Lubrication and Tribology* [online]. 2022, **74**(3), p. 350-359. ISSN 0036-8792 Available from: https://doi.org/10.1108/ILT-07-2021-0262

[20] STOJANOVIC, B., TOMOVIC, B., GAJEVIC, S., PETROVIC, J., MILADINOVIC, S. Tribological behavior of aluminum composites using Taguchi design and ANN. *Advanced Engineering Letters* [online]. 2022, **1**(1), p. 28-34. eISSN 2812-9709. Available from: https://doi.org/10.46793/adeletters.2022.1.1.5

[21] STOJANOVIC, B., BABIC, M., VELICKOVIC, S., BLAGOJEVIC, J. Tribological behavior of aluminum hybrid composites studied by application of factorial techniques. *Tribology Transactions* [online]. 2016, **59**(3), p. 522-529. eISSN 1547-397X. Available from: https://doi.org/10.1080/10402004.2015.1091535

[22] VORKAPIC, M., MLADENOVIC, I., PERGAL, M., IVANOV, T., BALTIC, M. Optimisation of tensile stress of poly(lactic acid) 3D printed materials using response surface methodology. *Tribology and Materials* [online]. 2022, **1**(2), p. 70-80. ISSN 2812-9717. Available from: https://doi.org/10.46793/tribomat.2022.009

[23] RAJESH, A. M., KALEEMULLA, K. M., SALEEMSAB D., BHARATH K. N. Generation of mechanically mixed layer during wear in hybrid aluminum MMC under as-cast and age hardened conditions. *SN Applied Sciences* [online]. 2019, **1**(8), 860. ISSN 2523-3971. Available from: https://doi.org/10.1007/s42452-019-0906-5

[24] SHETTY, R. J., HINDI, J., GURUMURTHY, B. M., HEGDE, A., SHIVAPRAKASH, Y. M., SHARMA, S., MURTHY, A., MURALISHWARA, K. Effect of metallic reinforcement and mechanically mixed layer on the tribological characteristics of Al-Zn-Mg alloy matrix composites under T6 treatment. *Cogent Engineering* [online]. 2023, **10**(1), 22009001. ISSN 2331-1916. Available from: https://doi.org/10.1080/23311916.2023.2200900

This is an open access article distributed under the terms of the Creative Commons Attribution 4.0 International License (CC BY 4.0), which permits use, distribution, and reproduction in any medium, provided the original publication is properly cited. No use, distribution or reproduction is permitted which does not comply with these terms.

SHAPE OPTIMIZATION OF A COLUMN MODELLING THE BRIDGE SPAN UNDER A SPECIFIC LOAD - NUMERICAL AND EXPERIMENTAL STUDIES

Janusz Szmidla, Anna Jurczyńska*

Czestochowa University of Technology, Czestochowa, Poland

*E-mail of corresponding author: anna.jurczynska@pcz.pl

Janusz Szmidla 0000-0002-7475-7925, Anna Jurczyńska 0000-0002-8505-3157

Resume

This work is dedicated to the problem of optimizing the shape of columns modelling bridge span subjected to the selected specific load case. Based on Hamilton's principle, motion equations and boundary conditions were defined. Taking into account the static criterion of loss of stability and the condition of constant volume of systems, the values of geometric parameters of the analyzed column were determined at which the maximum critical load value was obtained. The simulated annealing algorithm was used to find the maximum critical force being a function of many variables. Within the kinetic criterion of loss of stability, the range of changes in the natural frequency of optimized columns as a function of external load was determined. Based on the obtained results it was concluded that it is possible to control the dynamic properties while improving the stability of the system.

Article info

Received 1 March 2023
Accepted 18 June 2023
Online 10 July 2023

Keywords:

bridge span
shape optimization
nonprismatic rod
free vibrations
stability

Available online: https://doi.org/10.26552/com.C.2023.059

ISSN 1335-4205 (print version)
ISSN 2585-7878 (online version)

1 Introduction

The issue of stability and free vibrations plays a significant role in the design and exploitation of mechanical devices and civil engineering structures. With proper system operation, correctly conducted static and dynamic analyzes guarantee that the machine or structure will not be damaged at stresses much lower than the allowable one. Currently, scientists' research is focused on increasing the strength of structures and the possibility of controlling their dynamic properties. Among the factors that are analyzed in the context of improving the properties of slender systems - devices or their parts are, among others:

- the possibility of using elastic or piezoceramic elements, supporting the systems with elastic foundations with different characteristics [1-6] or using oscillators [7];
- analysis of nonlinearities in the system: geometric [7-11], material (physical) [8, 12-14], resulting from friction [8];
- optimization of the shape of the system [15-17].

The last two factors are of a particular importance. Changing the shape of the structural elements can affect not only the strength, but it can also reduce the weight of the structure and thus lower the costs. Including nonlinearities in the models increases the quality of mapping the actual behaviour of the system - it enables a more accurate study of the behaviour of the system during operation. The role of stability and vibrations of slender systems has received increased attention in recent years, across a number of disciplines. Physical models, similar to those analyzed in this paper, are commonly found in constructions (bridge spans) [18-23] or in the mining industry (support structures).

A new approach to the stability studies of non-prismatic Bernoulli-Euler columns loaded axially was proposed in [16]. The described method of rigid elements consists of dividing a column into n segments, then each of them is additionally divided into k members. Each of the segments from the first division can be replaced with a rigid, multi-segment joint element (two rigid segments connected by a joint and springs: translational and rotating). The research considered double symmetrical columns with a cross-section that change continuously and stepwise (multi-segment system).

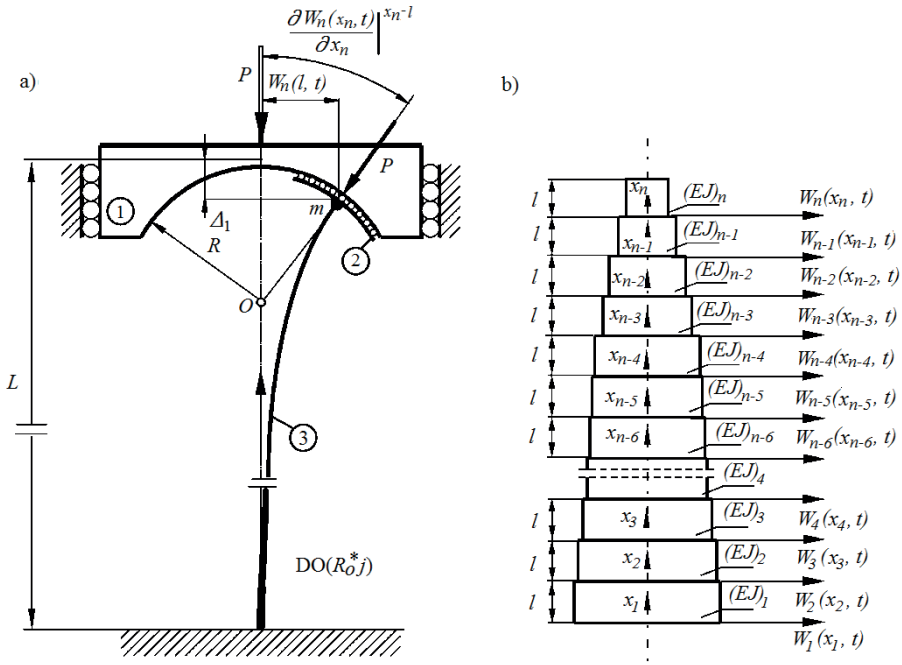

Figure 1 *Physical model of the column a) under follower force directed towards positive pole, b) division into segments*

The problem of stability was also dealt with by Li [24-25]. In his works, he analyzed columns with a stepped and continuous change of the cross-section along the axis. The research covered the impact of various load cases (conservative or tracking), system geometry and mounting methods, including support by rotational and translational springs, on the value of the critical load. The transfer matrix method and the finite element method were used to solve the boundary problems presented in the works.

An explicit equation for the buckling load value of the non-prismatic columns with non-uniform distribution of longitudinal forces was developed in [26]. Taking into account the Euler dependence on the critical load, the authors presented a series of graphs specifying the value of the correction factor taking into account the type of convergence, the size of the cross-section and the method of loading the structure. The maximum recorded error, resulting from the comparison of the proposed method and analytical calculations, did not exceed 7 %.

This article deals with the issue of stability and free vibrations of a geometrically nonlinear column with a nonprismatic element, modelling the bridge support structure. The analysis covered the change of the bifurcation load (only the loss of the rectilinear form of the static equilibrium was examined) and the change of the natural frequency. The shape of the bar with a variable cross-section was optimized using a modified simulated annealing algorithm. The theoretical and numerical studies were experimentally verified.

2 Physical model of the system

Figure 1 presents a physical model of the considered column in the construction variant of loading heads 1 and load taking heads 2 with a circular outline (constant curvature). Under the follower load, with the force directed towards the positive pole (case of specific load), the direction of the loading force goes through the fixed point O - the centre of the loading and load taking head. The parts of the load taking heads are infinitely rigid. The columns 3 are rigidly fixed on one side ($x_1 = 0$) and they are connected at the free end ($x_n = l$) with the load taking head 2. Reduced mass of elements, being a part of the load taking head was taken into account in the field with the point mass m.

The method of issue description adopted in this paper consists in the division of a column (Figure 1b) into smaller segments (with indexes $I = 1..n$) with a circular cross-section, mass per unit length (ρA_i) and flexural rigidity (EJ_i), described by length l and diameter d, as well as the transverse displacement $W_i(x_i,t)$. The optimization of the shape is limited to selection of diameters of particular segments of the systems at which the maximum critical load value is obtained. This assumption causes that the maximum value of critical force, which is a function of many variables (diameters and lengths of particular column segments) is searched for:

$$P_{\max} = f\left(d_1, d_2, \ldots, d_n, \frac{L}{n}\right). \tag{1}$$

The value of the critical force P_{kr} of the optimized columns was related to the constant along the length L of the flexural rigidity $(EJ)_{pr}$ of comparison columns:

$$\lambda_{oc} = \frac{P_{kr} L^2}{(EJ)_{pr}}. \tag{2}$$

In the solution of the subject issue, the constant total length L, the constant total volume V, constant value of the longitudinal elasticity E, as well as optimized and relevant comparison (prismatic) columns, are assumed.

In this section, exemplary designations of the considered columns have been implemented:

- DO(R^*) - optimized column subjected to the follower force load, directed towards the positive pole with a stepwise variable flexural rigidity, with the parameter of the loading and load taking head R^*;
- DP(R^*) - the column with a constant at the length of the flexural rigidity system $(EJ)_{pr}$ (comparative) subjected to load with tracking force directed towards the positive pole, with the parameter of the loading head R^*.

3 Equations of the boundary problem

Determination of motion equations and boundary conditions of the considered systems was conducted under the Hamilton's principle (the principle of least action):

$$\delta \int_{t_1}^{t_2} \left(T - \sum_{\xi=1}^{3} V_\xi \right) dt = 0, \tag{3}$$

Where T means kinetic energy, V - potential energy, t - time, δ - operator of variations.

The kinetic energy T of the considered columns is the sum of the kinetic energy of the column and kinectic energy of the body of mass m (transverse inertia):

$$T = \sum_{i=1}^{n} \frac{(\rho A_i)}{2} \int_0^l \left[\frac{\partial W_i(x_i,t)}{\partial t} \right]^2 dx_i + \\ + \frac{m}{2} \left[\frac{\partial W_n(l,t)}{\partial t} \right]^2, \tag{4}$$

where A_i - is the cross-sectional area of the i-th segment of the optimized column.

The components of the potential energy were defined as follows:

- flexural elastic energy:

$$V_1 = \sum_{i=1}^{n} \frac{(EJ_i)}{2} \int_0^l \left[\frac{\partial^2 W_i(x_i,t)}{\partial x_i^2} \right]^2 dx_i, \tag{5}$$

- energy of the force P vertical component:

$$V_2 = -\frac{P}{2} \sum_{i=1}^{n} \int_0^l \left[\frac{\partial W_i(x_i,t)}{\partial x_i} \right]^2 dx_i, \tag{6}$$

- energy of the force P horizontal component:

$$V_3 = \frac{P}{2} R \left[\frac{\partial W_n(x_n,t)}{\partial x_n} \Big|^{x_n = 1} \right]^2, \tag{7}$$

where:

$$\varphi = \frac{W_0}{R-r} = \frac{R \frac{\delta W_n(x_n,t)}{\delta x_n} \Big|^{x_n = l} - W_n(l,t)}{R-r}, \\ \beta_0 = \frac{W_n(l,t) - r \frac{\delta W_n(x_n,t)}{\delta x_n} \Big|^{x_n = l}}{R-r}. \tag{8}$$

Known a priori, the geometrical boundary conditions of the considered problem, are:

- at the attachment point ($x_1 = 0$):

$$W_1(0,t) = \frac{\partial W_1(x_1,t)}{\partial x_1} \Big|_{x1=0} = 0, \tag{9}$$

- continuity conditions

$$W_\zeta(l,t) = W_{\zeta+1}(0,t), \frac{\partial W_\zeta(x_{\zeta,t})}{\partial x_\zeta} \Big|^{x\zeta=1} = \\ \frac{\partial W_{\zeta+1}(x_{\zeta+1,t})}{\partial x_{\zeta+1}} \Big|_{x\zeta+1=0}, \text{where } \zeta = 1 \ldots (n-1). \tag{10}$$

After application of geometrical dependencies between the elements of the head taking the load, with the follower force directed towards the pole, the following was obtained:

$$W_n(l,t) - R \frac{\partial W_n(x_n,t)}{\partial x_n} \Big|^{x_n = l} = 0. \tag{11}$$

Considering the Hamilton's principle in Equation (3), after a priori application of the relevant boundary conditions in Equations (9)-(11) and after algebraic transformations, it was obtained:

- differential equations of motion of the considered system:

$$(EJ_i) \frac{\partial^4 W_i(x_i,t)}{\partial x_i^4} + P \frac{\partial^2 W_i(x_i,t)}{\partial x_i^2} + \\ + (\rho A_i) \frac{\partial^2 W_i(x_i,t)}{\partial t^2} = 0, i = 1 \ldots n, \tag{12}$$

- natural continuity conditions:

$$\frac{\partial^2 W_\zeta(x_\zeta,t)}{\partial x_\zeta^3} \Big|^{x\zeta=1} = \\ \chi_{\zeta+1} \frac{\partial^2 W_{\zeta+1}(x_{\zeta+1},t)}{\partial x_{x\zeta+1}^2} \Big|_{x\zeta+1=0}, \tag{13}$$

$$\frac{\partial^3 W_\zeta(x_\zeta,t)}{\partial x_\zeta^2}\bigg|^{x_\zeta=1} = \chi_{\zeta+1}\frac{\partial^3 W_{\zeta+1}(x_{\zeta+1},t)}{\partial x_{x_{\zeta+1}}^3}\bigg|_{x_{\zeta+1}=0}, \tag{14}$$

- natural boundary conditions at the free end of the systems ($x_n = l$):
-

$$\frac{\partial^2 W_n(x_n,t)}{\partial x_n^3}\bigg|^{x_n=1} - \frac{1}{R}\frac{\partial^2 W_n(x_n,t)}{\partial x_n^2}\bigg|^{x_n=1} - \frac{m}{(EJ_n)}\frac{\partial^2 W_n(x_n,t)}{\partial t^2} = 0, \tag{15}$$

where: $k_n^2 = P/(EJ_n)$, $\chi_{\zeta+1} = (EJ_{\zeta+1})/(EJ_\zeta)$.

4 Solution of the boundary problem - energetic method

Conducting research on optimization requires knowledge of the critical load values of the considered columns, with the adopted criterion of constant volume. To determine the critical load parameter, it is sufficient to apply the static stability criterion (energetic method). Condition for the existence of a minimum total potential energy was recorded in the following form:

$$\partial \sum_{\xi=1}^{3} V_\xi = 0. \tag{16}$$

Potential energy of the system (see Equations (5)-(7)), after previous separation of variables of the function $W_i(x_i,t)$, in relation to spatial x_i and time t coordinates:

$$W_i(x_i,t) = y_i(x_i)\cos(\omega t), \tag{17}$$

has the following form:

$$\sum_{\xi=1}^{3} V_\xi = \sum_{i=1}^{n}\frac{(EJ_i)}{2}\int_0^l [y_i^{II}(x_i)]^2 dx_i - \frac{P}{2}\sum_{i=1}^{n}\int_0^l [y_i^I(x_i)]^2 dx_i + \frac{PR}{2}[y_i^I(l)]^2. \tag{18}$$

The boundary conditions in Equations (9)-(11), (13)-(15) after applying Equation (17) are as follows:

$$y_1(0) = y_1^I(0) = 0, \tag{19}$$

$$y_n(l) = Ry_n^I(l), \tag{20}$$

$$y_n^{III}(l) - \frac{1}{R}y_n^{II}(l) = 0, \tag{21}$$

$$y_\zeta(l) = y_{\zeta+1}(0), \tag{22}$$

$$y_\zeta^I(l) = y_{\zeta+1}^I(0), \tag{23}$$

$$y_\zeta^{II}(l) = \chi_{\zeta+1}y_{\zeta+1}^{II}(0), \tag{24}$$

$$y_\zeta^{III}(l) = \chi_{\zeta+1}y_{\zeta+1}^{III}(0). \tag{25}$$

Taking into account the Equations (18), (19) and (22) - (24) in Equation (16), the following displacement equations were obtained:

$$y_i^{IV}(x_i) + k_i^2 y_i^{II}(x_i) = 0,\ i = 1...n. \tag{26}$$

The general solutions of Equation (26) were described by the function:

$$y_i(x_i) = D_{i1}\sin(k_i x_i) + D_{i2}\cos(k_i x_i) + D_{i3}x_i + D_{i4}, \tag{27}$$

where D_{ik} are integration constants (κ =1, ..., 4).

Based on the solutions of Equation (27) of displacement equations and relevant boundary conditions in Equations (19)-(25), a system of equations was obtained, which in the matrix form, was recorded as follows:

$$G_s\Lambda = 0 \tag{28}$$

where: $\Lambda = [D_{11}\ D_{11}\ D_{11}\ D_{11}\ \ldots\ D_{n1}\ D_{n2}\ D_{n3}\ D_{n4}]^{\mathrm{T}}$ and G_s means the square matrix of a degree dependent on the number of n segments of considered columns.

Thus, the following is obtained:

$$G_s = \left[\begin{array}{ccc|ccc} F_0 & 0 & 0 & 0 & 0 & 0 \\ H_1^l & H_2^0 & 0 & 0 & 0 & 0 \\ 0 & H_2^l & H_3^0 & 0 & 0 & 0 \\ \hline 0 & 0 & 0 & H_{n-2}^l & H_{n-1}^0 & 0 \\ 0 & 0 & 0 & 0 & H_{n-1}^l & H_n^0 \\ 0 & 0 & 0 & 0 & 0 & F_n \end{array}\right], \tag{29}$$

$$F_0 = \begin{bmatrix} 0 & 1 & 0 & 1 \\ k_1 & 0 & 1 & 0 \end{bmatrix},$$

$$H_{\zeta+1}^0 = \begin{bmatrix} 0 & -1 & 0 & -1 \\ -k_{\zeta+1} & 0 & -1 & 0 \\ 0 & \chi_{\zeta+1}k_{\zeta+1}^2 & 0 & 0 \\ \chi_{\zeta+1}k_{\zeta+1}^3 & 0 & 0 & 0 \end{bmatrix},$$

$$H_\zeta^1 = \begin{bmatrix} \sin(k_\zeta l) & \cos(k_\zeta l) & l & 1 \\ k_\zeta\cos(k_\zeta l) & -k_\zeta\sin(k_\zeta l) & 1 & 0 \\ -k_\zeta^2\sin(k_\zeta l) & -k_\zeta^2\cos(k_\zeta l) & 0 & 0 \\ -k_\zeta^3\cos(k_\zeta l) & k_\zeta^3\sin(k_\zeta l) & 0 & 0 \end{bmatrix}, \tag{30}$$

$$F_n = \begin{bmatrix} f_{11} & f_{12} & f_{12} & f_{14} \\ f_{21} & f_{22} & f_{23} & f_{24} \end{bmatrix}.$$

The matrix coefficient $\boldsymbol{F}_n$ was recorded as:

$$f_{11} = -k_n^3\cos(k_n l) + \frac{k_n^2\sin(k_n l)}{R},$$

$$f_{12} = k_n^3\sin(k_n l) + \frac{k_n^2\cos(k_n l)}{R}, f_{13} = 0, f_{14} = 0, \tag{31}$$

$$f_{21} = \sin(k_n l) - Rk_n\cos(k_n l),$$

$$f_{22} = \cos(k_n l) + Rk_n\sin(k_n l), f_{23} = l - R, f_{24} = 1.$$

The transcendental equation for the critical load value is as follows:

$$\det G_s = 0. \tag{32}$$

5 Solution of the boundary issue - vibration method

Based on the solution of the boundary issue with the kinetic criterion of stability, the range of changes in natural vibrations frequency ω as a function of the external load P of the considered columns was determined. For this purpose, Equations of motion (12) are taken into account, which, after separating the variables with respect to spatial coordinates x_i and time t (see the Equation (17)), are in the following form:

$$y_i^{IV}(x_i) + k_i^2 y_i^{II}(x_i) - \Omega_i^2 y_i(x_i) = 0,\ i = 1...n. \tag{33}$$

The results of Equations (33) are:

$$y_i(x_i) = C_{1i}\cosh(\alpha_i x_i) + C_{2i}\cos(\beta_i x_i) + \\ + C_{3i}\sinh(\alpha_i x_i) + C_{4i}\sin(\beta_i x_i), \tag{34}$$

where $C\kappa_i$ are integration constants (κ =1,...,4) and:

$$\alpha_i^2 = \sqrt{-0.5k_i^2 + (0.25k_i^4 + \Omega_i^2)}, \\ \beta_i^2 = \sqrt{-0.5k_i^2 + (0.25k_i^4 + \Omega_i^2)}, \\ \Omega_i^2 = \frac{(\rho A_i)\omega^2}{(EJ_i)},\ k_i = \sqrt{\frac{P}{(EJ_i)}}. \tag{35}$$

After applying Equation (34) to relevant boundary conditions, the following system of equations was obtained:

$$G_D\, col\{C_{11}\ C_{21}\ C_{31}\ C_{41}\ \ldots\ C_{1n}\ C_{2n}\ C_{3n}\ C_{4n}\} = 0. \tag{36}$$

The determinant of the matrix of coefficients $\boldsymbol{G_D}$ equalized to zero is a transcendental equation on the neutral vibrations frequency ω (within the range of loss of the rectilinear form of the static equilibrium) of the considered systems, that is:

$$G_D\, col\{C_{11}\ C_{21}\ C_{31}\ C_{41}\ \ldots\ C_{1n}\ C_{2n}\ C_{3n}\ C_{4n}\} = 0. \tag{37}$$

6 Simulated annealing

The method of simulated annealing consists in a heuristic algorithm belonging to the class of non-

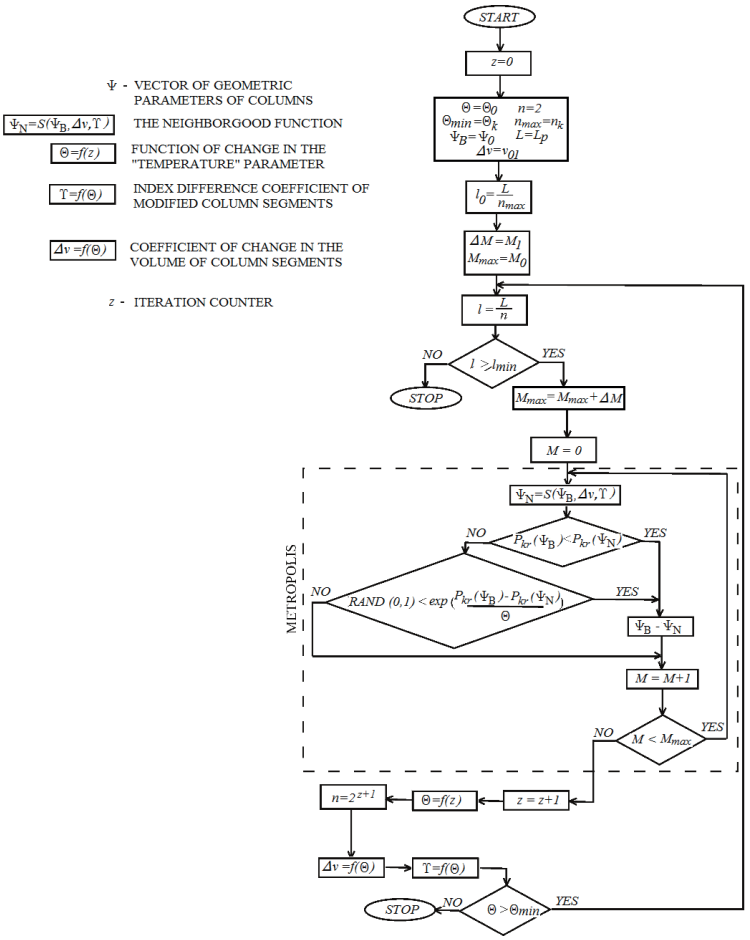

Figure 2 *A block diagram of the modified method of simulated annealing*

deterministic algorithms. This method is a modification of the "hill climbing algorithm". The performance of the algorithm requires defining four parameters: the initial representation of the result, the generator of random changes in the results (neighbourhood function), the evaluation function (cost) and the annealing schedule. The additional parameter Θ called "temperature" is not directly related to variables subjected to optimization, but it only controls the performance of the algorithm. The value of the parameter Θ affects only the probability of passing from one point in the search space to another and is selected in a manner depending on a given optimization issue.

Figure 2 presents a block diagram of the applied method of simulated annealing. In the considered method, a new solution Ψ_N selected by modifying the current result Ψ_B, is always accepted when an increase is obtained in the value of the function of the result evaluation defined by Equation (1). Otherwise, the acceptance occurs with a certain probability equal to:

$$p_a = \exp\left(-\frac{\Delta f}{\Theta}\right), \tag{38}$$

where: Δf is the difference of the value of the evaluation function defined by the Equation (1) and:

$$\Psi = \left[d_1 \;\; d_2 \;\; \ldots \;\; d_{n-2} \;\; d_{n-1} \;\; d_n \;\; \frac{L}{n}\right]. \tag{39}$$

The core of the algorithm is the procedure called Metropolis, which was used for simulation of the annealing process under a given "temperature"Θ. In the Metropolis procedure, a number of iterations defined by the parameter M was performed at the same value of the parameter Θ. Then, the "temperature" was reduced according to the adopted "annealing schedule", which was described by the dependency $\Theta = f(z)$ (see Figure 3a). The number of M_{max} iterations in subsequent initiation of the Metropolis procedure was increased by a certain value ΔM.

7 Modified method of simulated annealing

In the method of simulated annealing, apart from the change of the value of parameters Θ and M, an additional modification of the performance of the function $S(\Psi_B)$ was assumed, which generates a neighbourhood result (neighbourhood function). In the considered case, the performance of the neighbourhood function was changed along with the change of the "temperature" parameter (Figure 3).

The applied method of selection of a new shape consists in the "transfer" of a certain part of volume, described by the coefficient Δv, from a randomly selected segment (with the index i) to another segment of the column (with the index j), selected also in a random manner (Figure 3b). This is done by changing the diameters of selected segments (d_i, d_j) into new diameters (d_i', d_j'). The lengths of segments l remain unchanged. Thanks to application of such a solution, the fixed column volume criterion, adopted in this paper, has been met. New diameters of segments are calculated from the equations:

$$d_i' = \sqrt{(1 - \Delta v)d_i}, \; d_j' = \sqrt{d_j + \Delta v d_i}, \tag{40}$$

where: $i, j \in (0..n)$ - indices of the segments subjected to modifications, $\Delta v \in (0..1)$ - volume change coefficient.

The maximum allowable difference between indices of segments $|i - j|$, the diameters of which (d_i, d_j) are changed and the volume change factor Δv ($\Delta v = f(\Theta)$), defining what part of the volume of a given segment (with the index i) will be transferred to another segment (with the index j), are also changed. The segment whose volume is increased (diameter d_j') is any segment of the column selected in a random manner. The segment described by the parameter of the diameter d_i', the volume of which is reduced, is also selected in a random manner, however, in this case some restrictions are imposed on the selection.

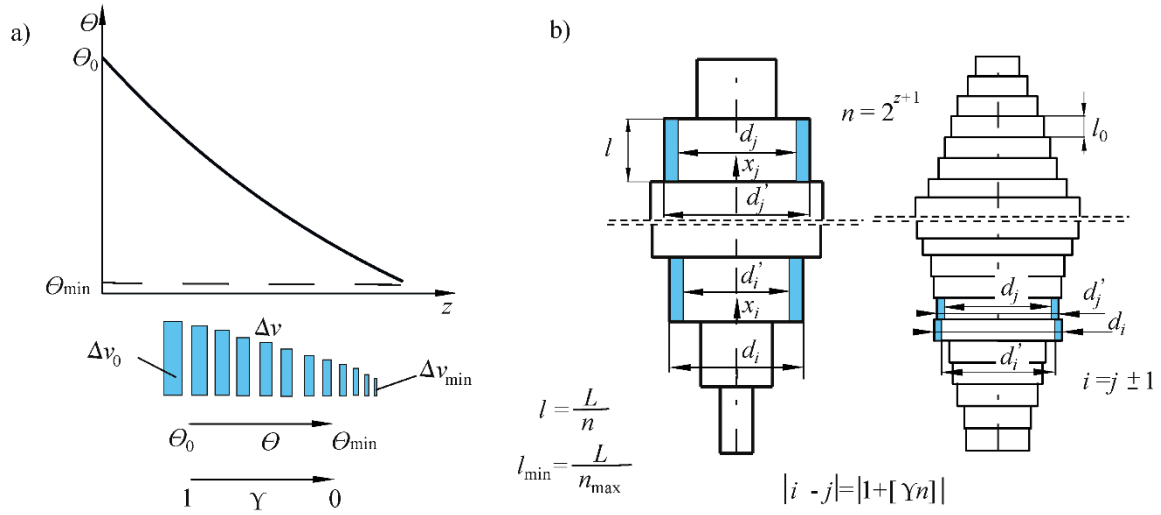

Figure 3 *a) change of the "temperature" parameter, b) modification of the neighbourhood function*

At the initial stage of optimization, selection of this segment can be completely random. However, at the final stage, it is possible to select only one of the two segments adjacent to the element whose volume is increased ($i = j \pm 1$). The maximum difference of indices of modified segments, defined as the product of the number of segments n and the coefficient Y (Y = $f(\Theta)$), where Y=1...0. Taking into account the second variable parameter, the volume change coefficient Δv, a certain set value of Δv_0 was assumed at the beginning of the calculation. Those values were decreased together with the decrease of the parameter, until the minimum value $\Delta v_{\min}$, defined at the beginning, was reached at $\Theta_{\min}$ (Figure 3). The application of such a solution significantly accelerated the optimization process, especially at the beginning of the calculation. The parameters Δv, Y, similar to Θ and M were modified after each time the Metropolis procedure was carried out. As a result of the described modification, the neighbourhood function was recorded as:

$$\Psi_N = S(\Psi_B, \Delta v, Y). \tag{41}$$

Another implemented modification of the algorithm of simulated annealing is a change of the number of segments n constituting a part of a slender system, made together with the change in the value of the mentioned parameters, that is:

$$n = 2^{z+1}. \tag{42}$$

Each segment of the column is divided into two segments with lengths equal to half of the length of the divided segment. The diameters of both segments are equal to the diameter of the divided segment. In the considered cases of column loads, the system was originally divided into two segments (z = 0). The number of segments n into which the slender system was divided, was changed in geometrical progression with a quotient equal to 2 to $n_{\max}$ value (maximum number of segments). The division was carried out after each Metropolis step loop until the length of the segment l was greater or equal to the minimum length $l_{\min}$:

$$l_{\min} = \frac{L}{n_{\max}}. \tag{43}$$

Implementation of the above-mentioned modifications to the algorithm of simulated annealing results in a significant acceleration of the shape optimization process. Thanks to the initial division into a small number of segments, it is possible to quickly determine the "coarse" shape of the columns. At the final stage of calculations, when the length of segments is short, small changes in shape result in smoothing the shape of the systems.

7.1 Function of changing the "temperature" parameter

A significant problem in the simulated annealing is the appropriate selection of the method of lowering the parameter Θ. Too rapid lowering of the "temperature" has a negative effect on the accuracy of the algorithm, too slow - increases the calculation time. The parameter Θ is used in determining the probability of acceptance (see Equation (34)) of the worse solution. This probability depends on the difference in the evaluation function Δf, as well. The application of variable parameters of neighbourhood generation and the change in the number of segments n of the system causes that the mean value Δf decreases with each implementation of Metropolis. In the analyzed cases, the mean value Δf had almost exactly double in each successive Metropolis. The described change should be taken into account in the "annealing schedule". For the statement ($-\Delta f / \Theta$) in Equation (34) to behave as expected, the value of the parameter Θ should be reduced accordingly in each iteration z.

8 The results of numerical calculations and experimental research

This section presents the results of numerical calculations with the use of a static and kinetic stability criterion. In the considered case of a specific load, appropriate results of theoretical research were presented, with selected geometrical parameter of the load taking heads, that is R_o^*.

Based on the energy method, the scope of critical load changes of optimized columns and their shape was determined, with the assumed criteria of the fixed volume of the systems. The scope of changes in the natural vibrations in the external load function and the form of vibrations were obtained by solving the boundary conditions, using the vibration method. Additional experimental research was carried out with regard to the value of natural vibrations frequency.

8.1 Results of numerical calculations - static stability criterion

Taking into consideration the transcendental equation for the value of critical value (see the Equation (32)), numerical calculations were carried out to determine the maximum value of the critical force P_{kr} of columns, in the considered cases of natural load. Numerical calculations were carried dividing the column into n = 128 segments. The introduction of the division of columns into a larger amount of segments did not significantly affect the obtained result and

it extended the time of numerical calculations. The obtained increase in the critical load with division into 128 and 256 segments differed by at most 0.18%. The value of critical load of optimized system DO(R_o^* j) and the parameters of load taking heads were related to the total constant length L of the system and the constant flexural rigidity $(EJ)_p$ of prismatic (comparative) column DP(R_o^* j).

Figure 4 shows the scope of changes in the critical parameters of the column load as a function of changes in the parameters of load taking heads. The results of numerical calculations were presented in the case of the systems with an optimized shape DO(R_o^* j) (solid lines) and corresponding columns DP(R_o^* j) (dashed lines) with a constant along the length of the flexural rigidity system.

At the considered values of the radius R of the loading head, each of the critical load change curves was characterized by occurrence of the maximum value of the critical load parameter λ_{oc}. In the case of comparative columns with fixed flexural rigidity $(EJ)_p$ the extreme value is determined at parameters R_o^* = 0.5. The range of the value of radius R of the loading head, changing from zero to the length of the column $L(R_o^* \in \langle 0,1 \rangle)$ was taken into account in the calculation. If R_o^* = 0, then the Euler's load case is obtained.

The percentage increase in the critical load δ_o of the optimized column with the changed flexural rigidity is presented in Figure 5, where:

$$\delta_O = \frac{\lambda_{ocDO(R_o^* j)} - \lambda_{ocDP(R_o^* j)}}{\lambda_{ocDP(R_o^* j)}} 100\% \tag{44}$$

Considering the division of columns into n - 128 segments, the critical load increase by at most 40.64% was obtained.

Figure 6 shows the shapes of models of optimized columns (optimum diameter distribution), with selected geometrical parameters of loading and load taking heads. The physical models of considered columns (see Figure 1) were built from segments which have been described by a fixed diameter d_i and fixed length l.

As a result of numerical calculations of the optimization issue, "stepped" shapes of the systems were obtained. Due to a significant number of segments, in relation to the total length L of columns, the actual shapes were approximated by polynominals of a relevant degree (with the highest possible correlation coefficient and the lowest standard deviation, in relation to the actual shapes) and they were drawn as smooth. Taking into account the assumed criterion for the constant volume of systems, the outline of prismatic (comparative) columns are marked with the dashed lines. For each of the presented shapes, values of the critical force, the

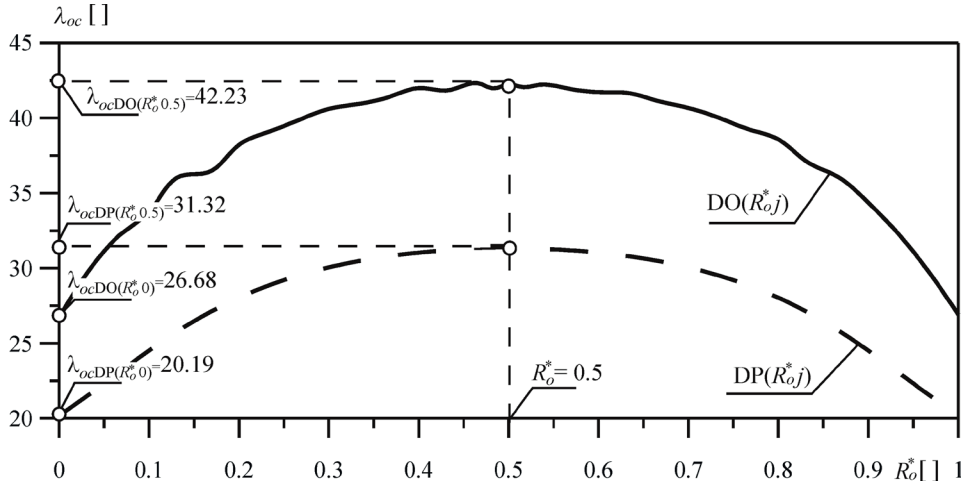

Figure 4 *Change of the critical load parameter λ_{oc} as a function of the parameter value R_o^* of columns DO(R_o^* j), DP(R_o^* j)*

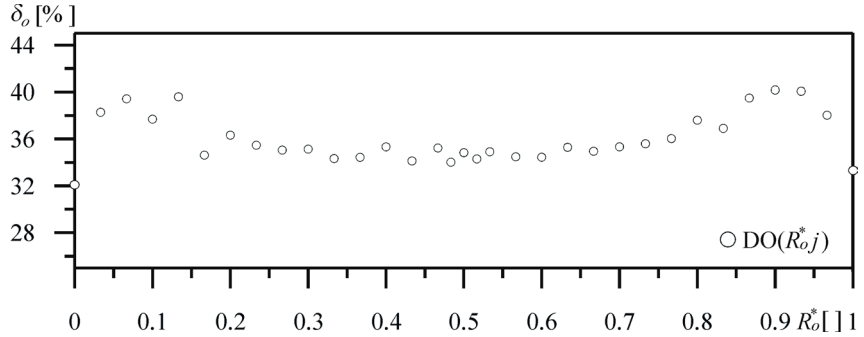

Figure 5 *The percentage increase in the critical load δ_o as a function of the parameter value R_o^* of columns DO(R_o^* j)*

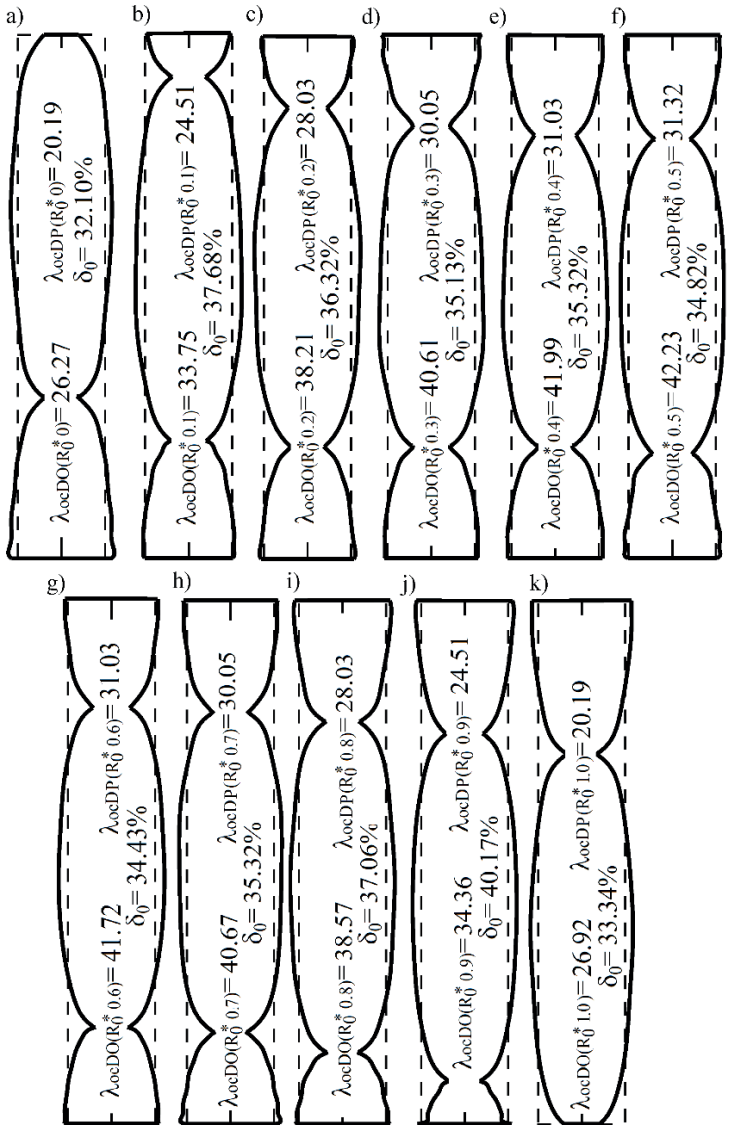

Figure 6 *The shape of the optimized column DO(R_o^* j) with the variable parameter value R_o^* j of the loading and load taking head: a) $R_o^* = 0$, b) $R_o^* = 0.1$, c) $R_o^* = 0.2$, d) $R_o^* = 0.3$, e) $R_o^* = 0.4$, f) $R_o^* = 0.5$, g) $R_o^* = 0.6$, h) $R_o^* = 0.7$, i) $R_o^* = 0.8$, j) $R_o^* = 0.9$, k) $R_o^* = 1.0$*

corresponding optimized and prismatic column, as well as the percentage increase of the critical load parameter, were given. It has been limited to the selected values of the parameter R_o^* of the loading and load taking head. In a specific case $R_o^* = 0$ (Figure 6a), a characteristic feature for all the presented shapes is the presence of narrowings in the cross-section along the length of the columns. The location of the points described by the minimum value of the diameter depends on the value of geometric parameters of heads that are involved in the specific load case discussed.

8.2 Results of numerical calculations - free vibrations

Taking into account the solution of the boundary issue, which has been obtained based on the kinetic stability criterion, numerical calculations were carried out with regard to the value of natural vibrations frequency ω of a column DO(R_o^* *j*). Taking into account the variable flexural rigidity of optimized columns, it has been limited to determination of the nature of changes in the first two basic natural vibrations frequencies in a dimensionless form $(\Omega_{o1}, \Omega_{o2})$, as a function of a dimensionless load parameter λ_o, with selected values R_o^*, Δr of heads performing the specific load cases, which are discussed. The following is assumed:

$$\lambda_o = \frac{PL^2}{(EJ)_p}, \tag{45}$$

$$\Omega_o = \frac{(\rho A)_p \omega^2 L^4}{(EJ)_p}, \tag{46}$$

where: A - cross-section area of the comparative column
$(\rho A)_p$ - specific mass per unit length of the comparative column.

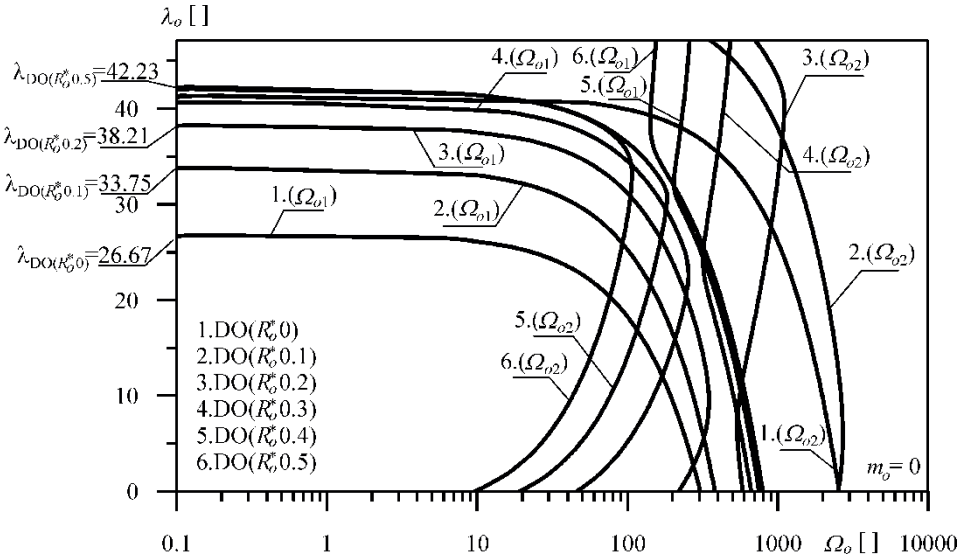

Figure 7 *Curves on the plane load parameter λ_o - parameter of natural vibrations frequency λ_o (system DO(R_o^* j))*

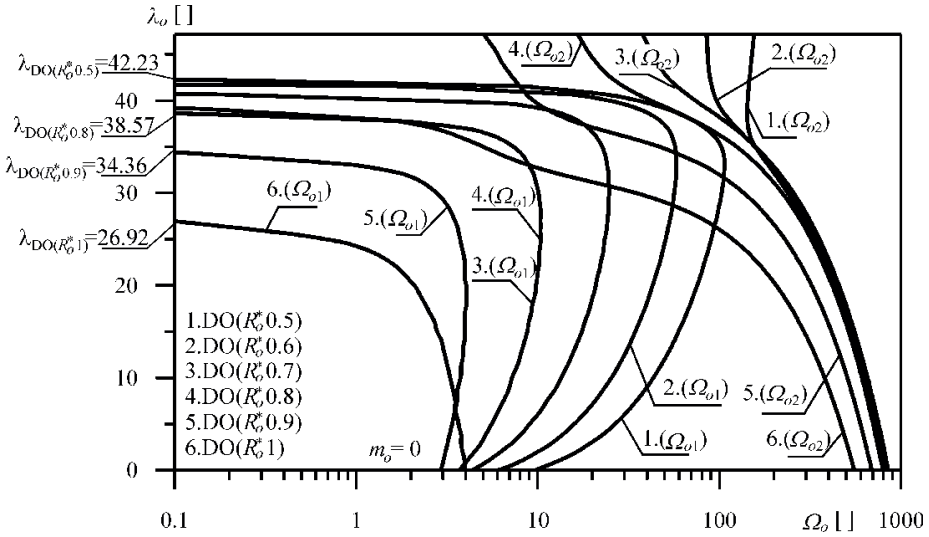

Figure 8 *Curves on the plane load parameter λ_o - parameter of natural vibrations frequency λ_o (system DO(R_o^* j))*

The results of numerical calculations of changes in eigenvalues of the column DO(R_o^* *j*) are presented in Figures 7 and 8. In case of $R_o^* = 0$ (the curves 1 - Figure 7), the scope of changes in the natural vibrations frequency corresponds to the model of the column in which the Euler load case was implemented.

The scope of changes of the basic natural vibrations frequency of columns DO(R_o^* *j*) and DP(R_o^* *j*), with selected parameters of heads R_o^* is shown in Figure 9. In the calculations, the zero value of the point mass *m* at the free end of the column was assumed, where:

$$m_o = \frac{m}{(\rho A)_p L}, \tag{47}$$

The value of the critical load of the discussed columns, in case of certain geometrical parameters of loading heads, were achieved with the parameter Ω_{o1}= 0. The values of the critical load parameter, which were obtained based on the kinetic stability criterion, are identical as in the case of application of the static criterion. Depending on the value of geometric parameters of the loading and load taking head, the presented courses of the basic frequency of natural vibrations Ω_{o1}, in the plane λ_o - Ω_o (Figure 9) have a negative, positive or zero inclination.

Figure 10 shows the forms of vibrations (M1, M2, M3) corresponding to the first three natural vibrations frequencies (parameters: Ω_{o1}, Ω_{o2}, Ω_{o3}) of the considered column. The forms of vibrations were determined with the normalization condition, assuming the value of the integrated constant of the motion equation result - normalization as to the constant, that is:

$$C_{\ln} = 1 \tag{48}$$

Taking into account Equation (48) in the dependence in Equation (36), after the prior rejecting of one of the geometric boundary conditions, a heterogenous system

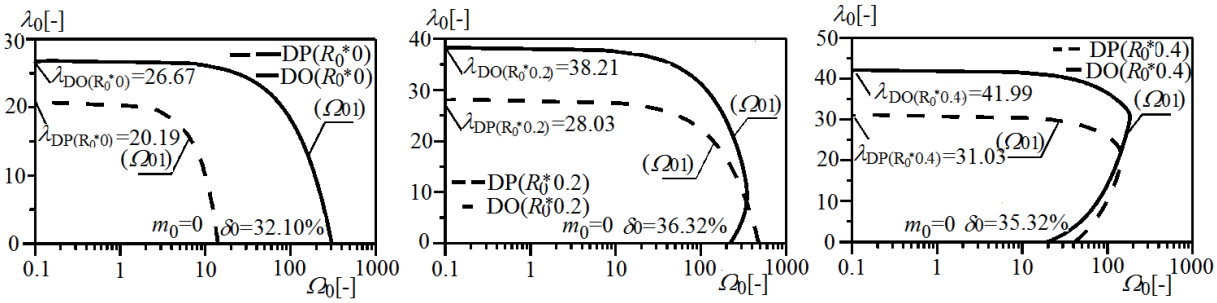

Figure 9 *Curves on the plane load parameter λ_o - basic frequency of natural vibrations parameter λ_{o1} of the optimized column DO(R_o^* j) and the comparative column DP(R_o^* j))*

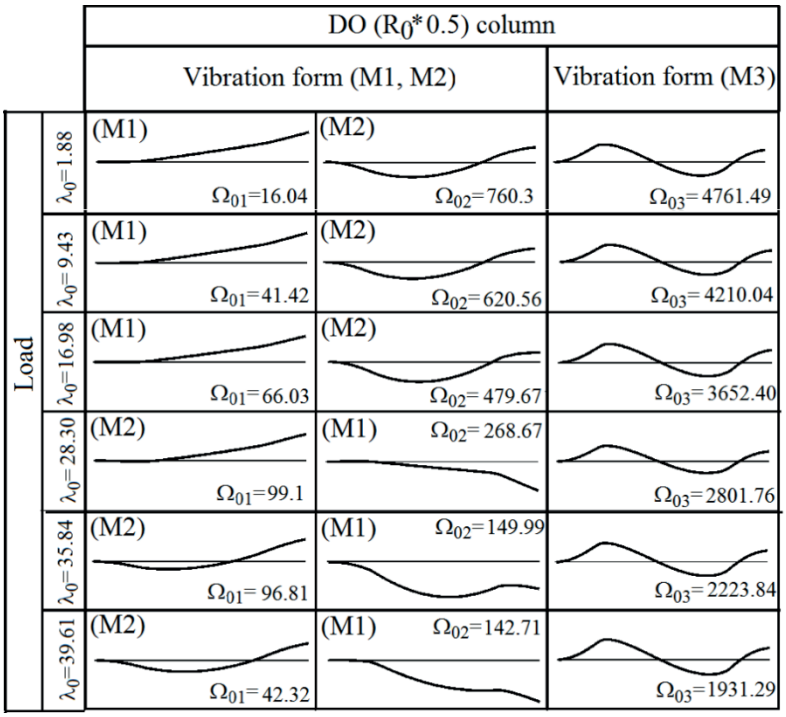

Figure 10 *The forms of vibrations of the column DO(R_o^*0.5)*

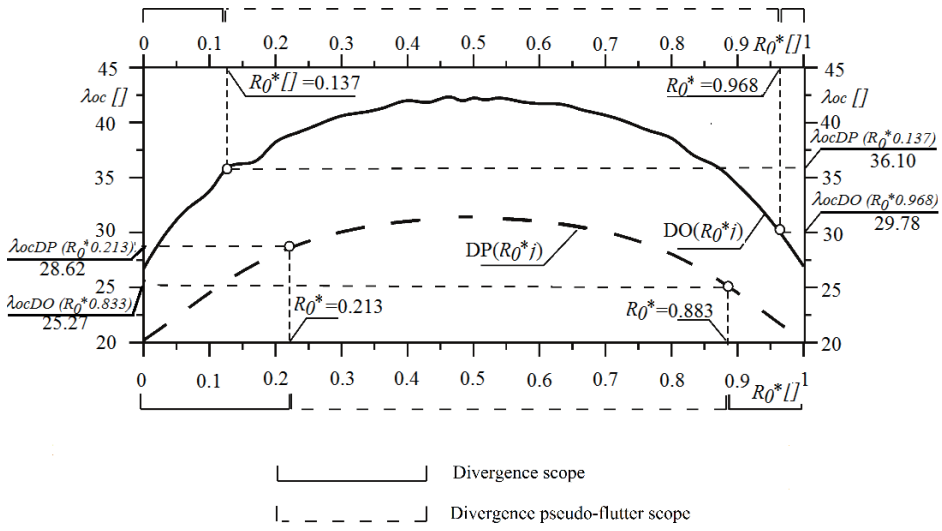

Figure 11 *Divergence and divergence-pseudo-flattery scope of columns DO(R_o^* j), DP(R_o^* j)*

Table 1 *Geometric and physical parameters of the column DO(R_o^* j)*

E [Pa]	ρ [kg/m^3]	L [m]	b [m]	R [m]	l_0 [m]	m [m]
7.5*10^{10}	2790	0.6	0.008	0.059	0.051	0.39

of equations with (n-1) unknowns $C\kappa_i$ (i=1,...,n, κ =1,...,4) was obtained. Based on the result of the system of equations, the remaining integration constants $C\kappa_i$ were determined. The forms of vibrations of the columns, with the natural vibrations frequency parameters $\Omega_o\varsigma$ (ς = 1, 2,…) were described with relations in Equation (34). The scope of changes in the forms of natural vibrations is presented (Figure 10) as a function of external load regarding the selected geometry of the loading and load taking head (R_o^* = 0.5).

In a general case (Mς), the form of vibrations corresponding to ς- of this frequency of natural vibrations (ς = 1, 2,…) has (ς-1) nodes.

Based on numerical calculations, a change in the forms of vibrations ((M1), (M2)) was observed on the curves of the first and second natural vibrations frequency. In the case of the comparative column DO(R_o^* j), this phenomenon was confirmed by experimental studies using the modal analysis.

The obtained nature of changes in eigenvalues (see Figure 7 to 9) and the scope of changes of the forms of natural vibrations along the curve $\lambda_o=f(\Omega_o)$ (see Figure 10), allows to include the optimized and comparative columns, subjected to a specific load, to one of two types of systems: divergent ($(d\Omega_{o1}/d\lambda_o)|\lambda_{o=0}<0$) or divergent - pseudo-flattery ($(d\Omega_{o1}/d\lambda_o)|\lambda_{o=0}>0$). Figure 11 presents the scope of changes in the value of the parameter R_o^* of the head taking the load with the force directed towards the pole, where the optimized column DO(R_o^* j) and the comparative column DP(R_o^* j) are included to one of two above-mentioned types of systems.

8.3 Experimental studies

This section of the paper presents the results of experimental studies and numerical calculations of the optimized system with the selected geometry of the head taking the load with follower force directed towards the positive pole DO(R_o^* j). The physcial and geometric parameters of the analyzed column are given in Table 1.

A rectangular cross-section of the analyzed column of dimensions a and b, was assumed for the calculations and experimental studies. Taking into account the criterion of the constant volume of the system; the width of the cross-section a was assumed (a_i - decision variables of the optimization process) with its fixed thickness b. In the applied modified method of simulated annealing, an additional condition was included in the following form:

$$a \geq b + 0.001\,[\mathrm{m}] \quad i = 1,\ldots,n\,. \tag{49}$$

Geometric inequality constraint in Equation (49) of the optimized column is justified due to the buckling plane of the system assumed in the numerical calculations and experimental systems, described with the minimum moment of inertia with respect to the neutral axis in the bending plane.

An experimental study was carried out at the stand, which was designed and constructed in the Department of Mechanics and Machine Design of the Czestochowa University of Technology. The stand (Figure 12) is composed of a support frame (1) to which the head (2) is attached. The element of the head (2) consists of a screw system by means of which the force loading the analyzed column (5) was generated with the use of a dynamometer (3) and a plate (4). Supports were attached to plates 8(1) and 8(2), which were implementing the required boundary conditions of the column. With four ball bearings (6), used at the pivots of the plate (4), a rectilinear shift was ensured in the guides (7). The guides (7) were attached to plate 8(1). The loading head (9), which was implementing the required boundary conditions at the free end of the analyzed system, was attached to the plate (4). The conditions of rigid bracing of the column is ensured by the element (1), which was attached to plate 8(2) with the housing (11). The head taking the load (12) was attached to the analyzed column with the use of block (13). It is assumed that the components:

- of the loading head (6),
- of the head taking the load to the column (12), (13),

are infinitely rigid. It is justified due to construction purposes. Figure 12 also presents the diagram of the measurement system. The measurement system consists of a modal hammer (15) (Brüel&Kjaer type 8200 + 2646), a laser vibrometer (14) (VH - 1000 - D made by OMETRON), an analyzer (17) (Brüel&Kjaer type 3560C) and a computer (18) with the software PULSE (version 7.0). The modal hammer is connected to the analyzer only when the experimental modal analysis is performed.

As a part of numerical calculations, with a static stability criterion, the shape of the optimized column was determined. Taking into account the rigid elements in Equations (12), (13) of the load taking head (see Figure 12) in the mathematical model of the system, the boundary conditions (11) and (15) at the free end of the column (x_n = l) are modified. Thus, the following is obtained:

$$\begin{cases} W_n(l,t) - (R - l_0)\dfrac{\partial W_n(x_n,t)}{\partial x_n}\Big|^{x_n=l} = 0, \\ \dfrac{\partial^3 W_n(x_n,t)}{\partial x_n^3}\Big|^{x_n=l} - \dfrac{1}{(R-l_0)}\dfrac{\partial^2 W_n(x_n,t)}{\partial x_n^3}\Big|^{x_n=l} - \\ -\dfrac{m}{(EJ_n)}\dfrac{\partial^2 W_n(x_n,t)}{\partial t^2} = 0 \end{cases} \quad (50)$$

where l_0 - total length of rigid elements in Equation (12) and Equation (13) - see Figure 12.

The shape of the optimized column DO(R_o^* 0.0125) (solid lines), obtained based on the solution of the boundary issue, with the use of modified boundary conditions in Equation (50) is shown in Figure 14. The dashed line presents an outline of a relevant comparative column DP(R_o^* 0.0125). In the case of the optimized shape of the system obtained, the critical load increase by 24.3% was achieved. The structural solutions of the research stand presented in Figure 12 are also shown in the picture (Figure 13b). In the pictures (Figures 13a and 13c) the shape of the examined column and the design solution of the load taking head are presented, as well.

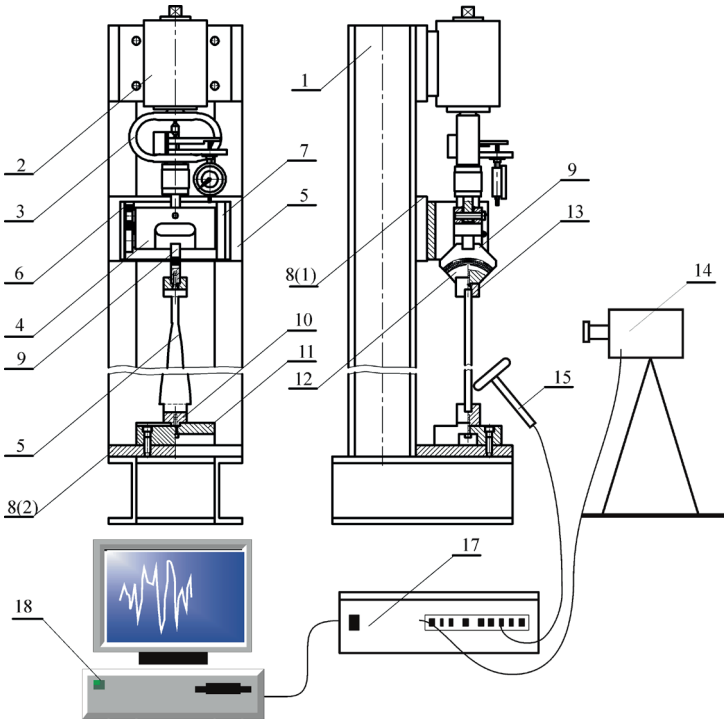

Figure 12 *The stand for testing the natural vibrations of columns located in a vertical position*

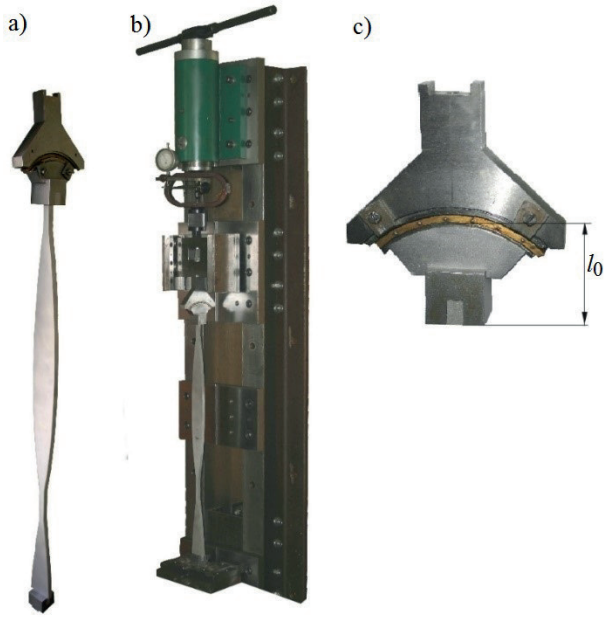

Figure 13 *a) shape of the examined column b) stand for examining vibrations of the slender systems with a mounted column, c) load taking head*

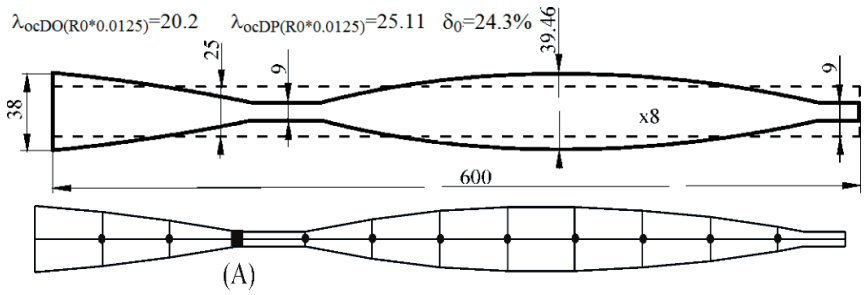

Figure 14 *Shapes of columns: DO(R_o^* 0.0125), DP(R_o^* 0.0125). Model of the optimized column developed for the experimental modal analysis (the system DO(R_o^* 0.0125))*

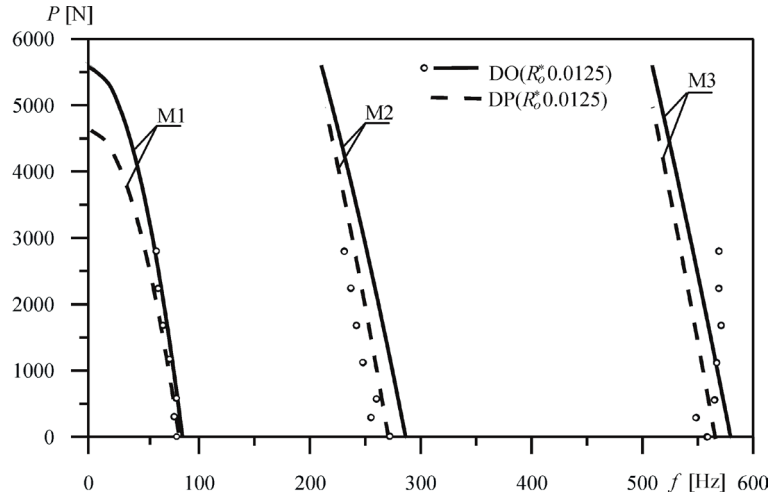

Figure 15 *Curves on the plane load P - natural vibrations frequency f (the system DO(R_o^* 0.0125)*

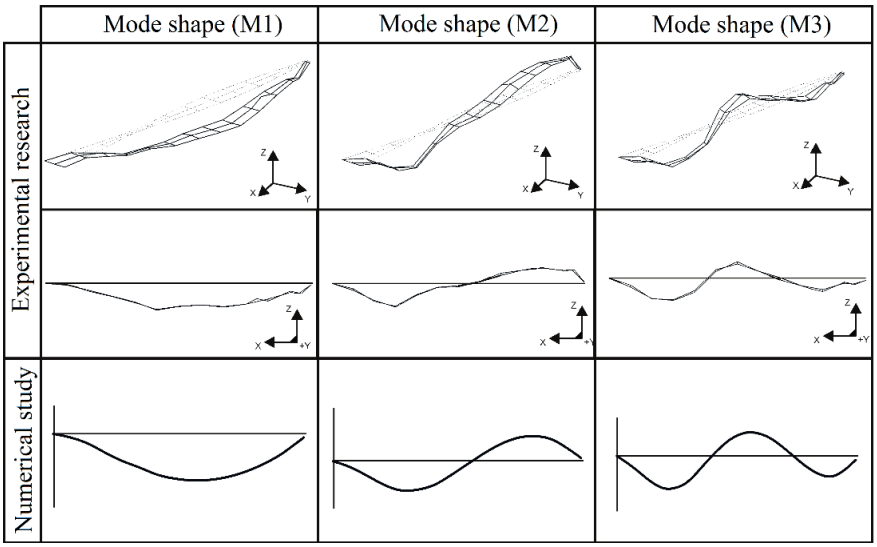

Figure 16 *The forms of vibrations of the column DO(R_o^* 0.0125) obtained based on the numerical calculations and experimental studies*

Taking into account the obtained shape of the optimized column (Figure 14), experimental research was carried out with regard to changes in the frequency of natural vibrations and the form of natural vibrations of the considered system. For this purpose, experimental modal analysis was performed using the professional equipment and software.

Figure 14 presents also a non-deformed form of the examined system. Ten nodes, in which the measurements, were made were distinguished within the research object constructed with the use of PULSE 7.0 software. The forcing is realized by hitting the successive points (•) of the examined column with a modal hammer and simultaneously the velocity of displacement of the node

(A) of the column is measured with the use of a laser vibrometer. The signal from the modal hammer and laser vibrometer is sent to the analyzer and then to the computer using the ME'scopeVES 4.0 software from Vibrat Technology; the values of natural vibrations frequencies and the forms of natural vibrations of the optimized system were obtained. The results of numerical calculations (solid lines - the system DO(R_o^* 0.0125)) and experimental studies (points), regarding the changes in the frequencies of natural vibrations, are presented in Figure 15.

The dashed lines show the course of changes in the eigenvalues of the comparative column DP(R_o^* 0.0125). The scope of changes of the first three frequencies of natural vibrations f, as a function of external load P was given. Comparing the results of numerical calculations and experimental studies of the column DO(R_o^* 0.0125), a good consistency of the results was found. The maximum relative error with the basic natural vibrations frequency, between the experimental results f^e and the frequencies obtained in theory f^t, was 7.24 %.

The forms of the transverse natural vibrations of the column (M1, M2, M3), obtained during the experiments and thanks to numerical calculations, are shown in Figure 16. The relevant results were shown with the external load value P =1640 [N] and the geometric and physical parameters of the system from Table 1.

9 Conclusions

In this work, the issues of stability and natural vibrations of slender elastic systems modelling the bridge span subjected to the follower force directed to the positive pole were analyzed and examined. Based on the principle of minimum potential energy, displacement equations and boundary conditions were determined. Considering the variable flexural stiffness of the systems, the leap equation was derived for the critical load value - the objective function of the optimization problem. The simulated annealing algorithm was used in the considerations. The values of the critical load parameter of columns, optimized for the adopted criterion of constant volume of systems, were obtained. An increase in the critical load of optimized columns of 40.64 % was obtained. It was found that there are such values of the head carrying the load parameters, at which the maximum value of the critical load parameter is obtained. The obtained shapes of optimized columns are characterized by the occurrence of the cross-section narrowing points along the length of the columns. The location of these points depends on the value of the geometrical parameters of the heads carrying the load. Based on the results of numerical calculations, it should be stated that the simulated annealing algorithm is an effective method of searching for the extreme of functions of many variables and can be used to optimize the shape of slender systems. Modifications proposed in the work, the adopted calculation method (modified algorithm of simulated annealing), were aimed at accelerating the process of searching for the optimal solution.

In the field of dynamics of systems (vibration method), based on the Hamilton's principle and total mechanical energy of systems, the corresponding equations for motion equations and boundary conditions were derived within the scope of loss of the rectilinear form of equilibrium. Solving the boundary problem enabled numerical calculations to determine the range of changes in the frequency of vibrations as a function of the load of optimized columns. Diagrams of eigenvalues on the plane were obtained: load parameter λ_o - eigenfrequency parameter Ω_o and eigen vibration forms. It has been shown that the critical load values obtained based on the kinetic stability criterion are the same when applying the static criterion. The correctness of the adopted mathematical model of the system was confirmed by presenting the results of experimental research. Discussing the impact of external load and geometrical parameters of the heads: forcing and taking over the load on the nature of changes in the frequency of natural vibrations, including the corresponding forms of vibrations, the considered systems were classified as divergent or divergent pseudoflatter type systems.

Grants and funding

The authors received no financial support for the research, authorship and/or publication of this article.

Conflicts of interest

The authors declare that they have no known competing financial interests or personal relationships that could have appeared to influence the work reported in this paper.

References

[1] UZNY, S., SOKOL, K. Critical load of a differently mounted columns determined according to the Bernoulli-Euler and Timoshenko theories. *Machine Dynamics Research*. 2015, **39**(2), p. 5-14. ISSN 2080-9948.

[2] TOMSKI, L., UZNY, S. A hydraulic cylinder subjected to Euler's load in aspect of the stability and free vibrations taking into account discrete elastic elements. *Archives of Civil and Mechanical Engineering*

[online]. 2011, **XI** (3), p. 769-785. ISSN 1644-9665. Available from: https://doi.org/10.1016/S1644-9665(12)60115-0

[3] PRZYBYLSKI, J., SOKOL, K. Shape control of an eccentrically loaded column by means of a piezoceramic rod. *Thin - Walled Structures* [online]. 2011, **49**(5), p. 652-659. ISSN 0263-8231, eISSN 1879-3223. Available from: https://doi.org/10.1016/j.tws.2010.09.014

[4] SZMIDLA, J., JURCZYNSKA, A. Stability of geometrically nonlinear pre-stressed column loaded by a force directed towards the positive pole partially lying on winkler elastic foundation. In: International Conference on Numerical Analysis and Applied Mathematics 2014 ICNAAM-2014: proceedings. AIP. 2014. ISBN 978-0-7354-1287-3, ISSN 0094-243X.

[5] COLMENARES, D., ANDERSSON, A., KAROUMI, R. Closed-from solution for mode superposition analysis of continuous beams on flexible supports under moving harmonic loads. *Journal of Sound and Vibration* [online]. 2021, **520**, 116587. ISSN 0022-460X, eISSN 1095-8568. Available from: https://doi.org/10.1016/j.jsv.2021.116587

[6] APSEMETOV, M., MADANBEKOV, N., MUKTAROV, T. Determination of the own forms of vibration of the span of beam bridges on elastic supporting parts. *E3S Web of Conferences* [online]. 2021, **263**, 02018. eISSN 2267-1242. Available from: https://doi.org/10.1051/e3sconf/202126302018

[7] RUILAN, T., XINWEI, Y., ZHANG, Q., XIUYING, G. Vibration reduction in beam bridge under moving loads using nonlinear smooth and discontinuous oscillator. *Advances in Mechanical Engineering* [online]. 2020, **8**(6), p. 1-12. ISSN 1687-8132, eISSN 1687-8140. Available from: https://doi.org/10.1177/168781401665256

[8] WAGG, D., NEILD, S. *Nonlinear vibration with control for flexible and adaptive structures*. *Chapt. 1: Introduction to nonlinear vibration and control, serial solid mechanics and its applications* [online]. Vol. 218. Switzerland: Springer International Publishing, 2015. ISBN 978-90-481-2836-5, p. 1-35. Available from: https://doi.org/10.1007/978-90-481-2837-2

[9] AKOUR, S. N. Parametric study of nonlinear beam vibration resting on linear elastic foundation. *Journal of Mechanical Engineering and Automation* [online]. 2012, **2**(6), p. 114-134. ISSN 2163-2405, eISSN 2163-2413. Available from: https://doi.org/10.5923/j.jmea.20120206.02

[10] GIZEJOWSKI, M. A., SZCZERBA, J., GAJEWSKI, M. D., STACHURA, Z. Buckling resistance assessment of steel I-section beam-columns not susceptible to LT-buckling. *Archives of Civil and Mechanical Engineering* [online]. 2017, **17**, p. 205-221. ISSN 1644-9665. Available from: https://doi.org/10.1016/j.acme.2016.09.003

[11] SZMIDLA, J., JURCZYNSKA, A. Local loss of a rectilinear form of a static equilibrium of geometrically nonlinear system with non-prismatic element under force directed towards the pole. *Acta Physica Polonica A* [online]. 2020, **138**(2), p. 140-143. ISSN 1898-794X. Available from: https://doi.org/10.12693/APhysPolA.138.140

[12] YAGHOOBI, H., TORABI, M. An analytical approach to large amplitude vibration and post-buckling of functionally graded beams rest on non-linear elastic foundation. *Journal of Theoretical and Applied Mechanics*. 2013, **51** (1), p. 39-52. ISSN 1429-2955.

[13] ELMAGUIRI, M. N., HATERBOUCH, M., BOUAYAD, A., OUSSOUADDI, O. Geometrically nonlinear free vibration of functionally graded beams. *Journal of Materials and Environmental Science*. 2015, **6**(12), p. 3620-3633. ISSN 2028-2508.

[14] KUMAR, S., MITRA, A., ROY, H. Geometrically nonlinear free vibration analysis of axially functionally graded taper beams. *An International Journal of Engineering Science and Technology* [online]. 2015, **18**(4), p. 579-593. eISSN 2215-0986. Available from: https://doi.org/10.1016/j.jestch.2015.04.003

[15] SZMIDLA, J., WAWSZCZAK, A. Optimization of the shape of columns implementing selected cases of Euler load using a modified algorithm of simulated annealing a (in Polish). In: 13th Structural Dynamics Symposium DYNKON 2008: proceedings. Vol. 258, Mechanics series74. p. 333-344.

[16] NIKOLIC, A., SALINIC, S. Buckling analysis of non-prismatic columns: a rigid multibody approach. *Engineering Structures* [online]. 2017, **143**, p. 511-521. ISSN 0141-0296, eISSN 1873-7323. Available from: https://doi.org/10.1016/j.engstruct.2017.04.033

[17] SZMIDLA, J., JURCZYNSKA, A. The tapered column shape optimisation in a plane perpendicular to the buckling plane subjected to a load by the follower force directed to the positive pole. *Machine Dynamics Research*. 2015, **39**(2), p. 33-44. ISSN 2080-9948.

[18] ZHOU, G., QIAN, C., CHEN, C. Research on the approximate calculation method of the fundamental frequency and its characteristics a tensioned string bridge. *Processes* [online]. 2022, **10**, 126. eISSN 2227-9717. Available from: https://doi.org/10.3390/pr10010126

[19] GARINEI, A. Vibrations of simple beam-like modelled bridge under harmonic moving loads. *International Journal of Engineering Science* [online]. 2006, **44**(11-12), p. 778-787. ISSN 0020-7225, eISSN 1879-2197. Available from: https://doi.org/10.1016/j.ijengsci.2006.04.013

[20] RASPOPOV, A., ARTYOMOV, V., RUSU, S. The simulation of vibrations of railway beam bridges in the object-oriented environment Delphi. *The Archives of Transport* [online]. 2010, **XXII**(4), p. 463-476. ISSN 0866-9546. Available from: https://doi.org/10.2478/v10174-010-0028-8

[21] ZANGENEH, A., MUSEROS, P., PACOSTE, C., KAROUMI, R. Free vibration of viscoelastically supported beam bridges under moving loads: closed-form equation for maximum resonant response. *Engineering Structures* [online]. 2021, **244**, 112759. ISSN 0141-0296, eISSN 1873-7323. Available from: https://doi.org/10.1016/j.engstruct.2021.112759

[22] KOPIIKA, N., VEGERA, P., VASHKEVYCH, R., BLIKHARSKYY, Z. Stress-strain state of damaged reinforced concrete bended elements at operational load level. *Production Engineering Archives* [online]. eISSN 2353-7779. 2021, **27**(4), p. 242-247.

[23] DOUNGPORN, W., NATHNARONG, K., YONG, H. W. Effect of beam joinery on bridge structural stability. *Advances in Difference Equations* [online]. 2019, **2019**, 225. eISSN 2731-4235. Available from: https://doi.org/10.1186/s13662-019-2158-5

[24] LI, Q. S. Exact solutions for buckling of non-uniform columns under axial concentrated and distributed loading. *European Journal of Mechanics - A/Solids* [online]. 2001, **20**(3), p. 485-500. ISSN 0997-7538, eISSN 1873-7285. Available from: https://doi.org/10.1016/S0997-7538(01)01143-3

[25] LI, Q. S. Stability of non-uniform columns under the combined action of concentrated follower forces and variably distributed loads. *Journal of Constructional Steel Research* [online]. 2008, **64**(3), p. 367-376. ISSN 0143-974X, eISSN 1873-5983. Available from: https://doi.org/10.1016/j.jcsr.2007.07.006

[26] SERNA, M. A., IBANEZ, J. R., LOPEZ, A. Elastic flexural buckling of non-uniform members: closed-form expression and equivalent load approach. *Journal of Constructional Steel Research* [online]. 2011, **67**(7), p. 1078-1085. ISSN 1873-5983, eISSN 0143-974X. Available from: https://doi.org/10.1016/j.jcsr.2011.01.003

This is an open access article distributed under the terms of the Creative Commons Attribution 4.0 International License (CC BY 4.0), which permits use, distribution, and reproduction in any medium, provided the original publication is properly cited. No use, distribution or reproduction is permitted which does not comply with these terms.

DEVELOPING AND STUDYING THE METHOD OF ULTRASONIC PURIFICATION AND UTILIZATION OF INTERNAL COMBUSTION ENGINE EXHAUST GASES

Igor Pak, Adil Kadyrov, Bakhtiyar Askarov, Bahtiyar Suleyev, Akbope Karsakova*

Department of Transport Equipment and Logistics Systems, Abylkas Saginov Karaganda Technical University, Karaganda, Kazakhstan

*E-mail of corresponding author: karsakova84@mail.ru

Igor Pak 0000-0002-6492-1525,
Bakhtiyar Askarov 0009-0007-6956-6976,
Akbope Karsakova 0000-0003-2002-1557
Adil Kadyrov 0000-0001-7071-2300,
Bahtiyar Suleyev 0000-0002-2812-2427,

Resume

A method of purification and utilization of internal combustion engine exhaust gases, due to the ultrasound impact on gases in a special storage tank, has been proposed. Large soot particles of gases due to coagulation are deposited on the bottom of the device and disposed of. The hypothesis of analogy of the gas concentration law and the ratio of soot particles during coagulation has been proven. The soot coagulation coefficient has been determined theoretically and experimentally. An experimental bench has been developed. The technique of assessing coagulation processes by the degree of gas transparency before and after exposure to ultrasound has been developed and used, as well as the technique of calculating equipment and options for designing the devices for ultrasonic purification of exhaust gases.

Article info

Received 20 January 2023
Accepted 19 June 2023
Online 10 July 2023

Keywords:

vehicle
exhaust gas
internal combustion engine
ultrasound
coagulation
ultrasonic purification
soot

Available online: https://doi.org/10.26552/com.C.2023.060

ISSN 1335-4205 (print version)
ISSN 2585-7878 (online version)

1 Introduction

Extreme gas contamination of the air basin, especially in large cities, is one of the urgent environmental problems. Motor transport is one of the main sources of contamination. Exhaust gases are emitted into the atmosphere and pollute it with carbon monoxide, nitrogen oxides, hydrocarbons, sulfur oxides, soot, carcinogens and other toxic components. Traffic blocks, associated with repair operations on the roads, contribute to the increased emission of harmful exhaust gases of internal combustion engines of transport equipment. This leads to increasing the incidence of cardiovascular and pulmonary diseases in the population [1-3].

Among the main methods of cleaning gases from technical pollution existing in industry, the absorption method, thermal afterburning and the thermo-catalytic method that is characterized by high costs, are the most widely used. These methods are effective against harmful components in the gaseous state, but they are ineffective against soot emissions from engine exhaust gases [4-5].

The method is known of cleaning gases of industrial enterprises by coagulation due to ultrasonic impact on the environment aimed at reducing the content of fine soot particles in gases and allowing it to be disposed of. In [6], based on the studies of Dong, Lipkens and Cameron, it was concluded that orthokinetic collisions prevail at low frequencies for intermediate size ratios, while the acoustic trace effect is more significant at higher frequencies for all the particles. Ran et al. [7] developed the ultrasonic scrubber, a device which combines an ultrasonic standing wave field and a water spray to eliminate particles from a gas flow. This device, which is essentially a wet scrubber enhanced by ultrasound, was shown to significantly improve the scavenging of micron-scale particles compared to the use of a water spray alone. The works [8-9] present the results of studies aimed at improving the

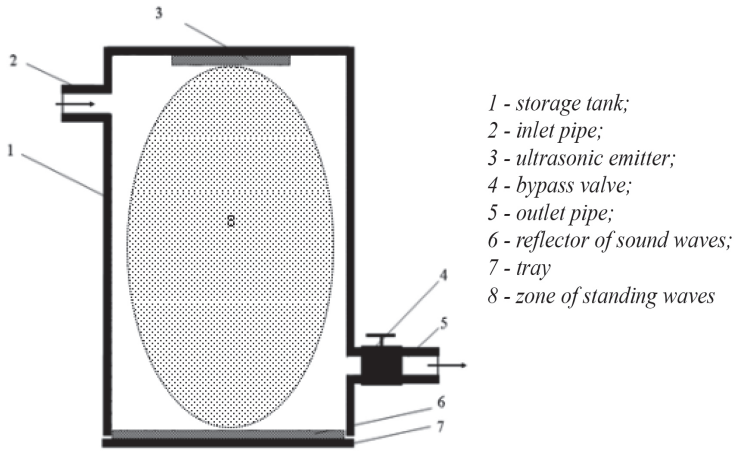

Figure 1 *The device for ultrasound purification and utilization of ICE exhaust gases*

efficiency of gas cleaning equipment based on Venturi pipes using the high-intensity ultrasound. It has been experimentally established that ultrasonic exposure provides an increase in the efficiency of the scrubber for ash particle diameters in the range of 2-90 microns over 96 %, especially in the area of diameters less than 5 microns. The efficiency of capturing ash particles in a scrubber with a size of 2 microns, at a sound pressure level of 150 dB, is about 99 %. This significantly exceeds the degree of gas purification without the use of ultrasonic coagulation (no more than 75 %). In study [10], a modified model for acoustic agglomeration of aerosol particles has been studied.

The hypothesis of the presented study is the assumption of intensifying coagulation of soot particles in the storage tank under the action of ultrasound for their subsequent disposal.

The aim of the study is to establish theoretical and experimental dependences that describe the process of purification and utilization of exhaust gases from an internal combustion engine.

To achieve the aim, the following tasks have been solved:

- a mathematical model of the process of internal combustion engine exhaust gases utilization has been developed and studied;
- an experimental equipment has been developed and it confirmed the results obtained analytically;
- a design has been proposed as well as the method of calculating the system for utilization of internal combustion engine exhaust gases.

The scientific novelty of the study consists in the following:

- the possibility of using ultrasonic mufflers with a capacitive chamber for the disposal of exhaust gases from internal combustion engines of city buses has been confirmed;
- the dependences were been obtained of changing the light transmission and light absorbing ability of the exhaust gas on the time of solid particles settling under the action of ultrasound and without it, as well as the coagulation coefficient dependence on the time of solid particles settling in the storage tank of the device for ultrasonic purification and utilization of internal combustion engines of city buses exhaust gases;
- for the first time, the dependence is obtained of the rate of changing the coagulation coefficient of solid particles on the time of their settling in the storage tank of the device for ultrasonic purification and utilization of internal combustion engine exhaust gases.

Practical usefulness consists in developing a method of calculating a storage device for ultrasonic purification and utilization of exhaust gases.

2 Materials and methods

Using the increased coagulation of soot particles of the exhaust gases due to the action of ultrasound on them, especially in the zone of the formed ultrasonic standing waves has been proposed. At this, the orthokinetic coagulation is supplemented by hydrodynamic coagulation, which leads to acceleration of the collision and adhesion of gas particles [11-12].

The solid particles, enlarged in the course of the coagulation process, mainly soot, settle at the bottom of the device at the intended collection point with its subsequent extraction and disposal.

The following device is proposed for ultrasonic cleaning and disposal of exhaust gases (Figure 1) [3].

The device works as follows. Exhaust gas enters the storage tank through the inlet pipe. From the ultrasonic transducer, located at the top, a direct wave arises that is reflected from the reflector of sound waves located on the container tray. During reflection, the direct and reflected waves move towards each other and, under the certain conditions, a standing wave is formed. When a standing wave occurs, the efficiency of the coagulation process increases due to increasing the amplitude of the resulting wave oscillations [11, 13].

The exhaust gases are made up of different size particles. Depending on their size and oscillation

frequency, the particles are dragged by the sound vibrations to varying degrees, which leads to increasing the frequency of their collisions and intensifying the coagulation processes.

The degree of the particle participation in sound vibrations, in the case of a standing sound wave, is described by the ratio [13]:

$$\frac{U_p}{U_g} = \frac{1}{\left[(4\pi\rho r^2 f/9\eta)^2 + 1\right]^{1/2}}, \quad (1)$$

where U_p, U_g are respectively the amplitudes of the particle and gas oscillations, m;
ρ is the particle density, kg/m^3;
r is the particle radius, m;
f is the gas oscillations frequency under the action of ultrasound, Hz;
η is the dynamic viscosity, Pa·s.

The analysis of Equation (1) has shown that basically the degree of participation of particles in sound vibrations and consequently coagulation, is determined by the value:

$$Z = \frac{\rho r^2 f}{\eta}, \quad (2)$$

where Z is the gas particle drag coefficient [13].

The coagulation process is quantitatively described by the coagulation coefficient k [13]. In work [14], an attempt was made to determine its value and patterns of change by integrating the equation of motion of gas particles. The resulting dependence is very difficult to apply and gives significant discrepancies with practice.

In this work an assumption has been made about the qualitative similarity of the gas concentration model and the coagulation process, that is, by analogy with the kinetic equation [15]:

$$n = n_0 e^{-bt}, \quad (3)$$

where n and n_0 are the number concentrations of the airborne particles, current and at the initial moment, respectively, pcs/m^3; b is the concentration coefficient; t is the time, s, it will be fair that:

$$m = m_0 e^{-kt}, \quad (4)$$

where m and m_0 are respectively the current and the initial gas mass;
k is the coagulation coefficient;
t is the time, s.

The value of the coagulation coefficient is to be experimentally determined.

It is proposed to determine the coagulation coefficient by the degree of gas transparency $\propto_i$ before and after exposure to ultrasound [16].

$$\propto_i = \frac{E_i}{E_{init}}, \quad (5)$$

where E_i is the illumination at present and after the ultrasound impact, lx;
E_{init} is the initial illumination, lx.

To carry out experiments according to the scheme (Figure 2), an experimental setup for ultrasonic cleaning of exhaust gases was developed (Figure 3) [3].

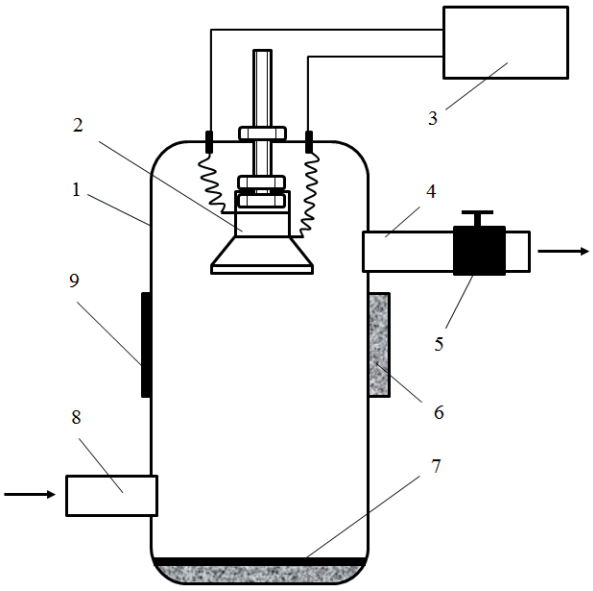

1 - body; 2 - emitter of ultrasonic waves; 3 - generator of ultrasonic vibrations; 4 - outlet pipe; 5 - valve; 6 - light source; 7 - reflector of ultrasonic waves; 8 - inlet pipe; 9 - luxmeter

***Figure 2** A scheme of the experimental setup for ultrasound purification and utilization of exhaust gases*

***Figure 3** Experimental setup for ultrasound purification and utilization of ICE exhaust gases*

Figure 4 *Experimental setup connection*

The material of the case is polyethylene terephthalate. It has good strength characteristics and transparency. A valve is installed on the outlet pipe, which is closed after the setup is filled with exhaust gas. Under the action of ultrasonic waves, generated by the ultrasonic emitter, the processes of coagulation of soot particles are intensified in the exhaust gas, as a result of which the soot particles become larger in size and mass and settle on the surface of the ultrasonic wave reflector.

The purified exhaust gas exits to the atmosphere through the exhaust pipe after opening the valve. To measure the illumination indicators, a light source and a device for measuring illumination have been fixed on the side surfaces opposite to each other.

At the preparatory stage, the assembled device, equipped with an ultrasonic emitter with the radiation frequency of 28 kHz and the power of 60 W, has been connected to the diesel engine of the experimental bench for studying the exhaust gas isolation. The bench has been assembled in the laboratory of the Transport Engineering and Logistics Systems Department of Karaganda Technical University (Figure 4).

A device for measuring illumination and a light source have been fixed on the opposite sides. The entire structure has been placed in a light-tight box to eliminate the effect of changing the ambient light on the results.

Having made the assumption that the average concentration of gas and soot particles is directly proportional to their masses, from Equation (4) was obtained:

$$m_c = m_0 - m_0 e^{-kt} = m_0(1 - e^{-kt}), \tag{6}$$

where m_c is the soot mass, kg;
m_0 is the gas initial mass, kg.

Based on the gas transparency coefficient from Equation (5), the light flux absorption coefficient β_i is equal:

$$\beta_i = 1 - \alpha_i, \tag{7}$$

where α_i is the gas transparency coefficient in the i-th interval of time.

Assuming that n and n_0 the number concentrations of gas particles, respectively current and at the initial moment, are proportional to the degree of absorption of the light flux β, the coagulation coefficient is equal:

$$k_i = -\frac{\ln\dfrac{\beta_i}{\beta_{i-1}}}{t}, \tag{8}$$

where i = 1…10;

t is the time interval between taking the readings, s. t = 60 s.

From Equation (4) the coagulation coefficient is determined as:

$$k = -\frac{\ln\left(1 - \dfrac{m_c}{m_0}\right)}{t}. \tag{9}$$

Based on the hypothesis of a close correlation between coagulation and the degree of gas transparency, Equations (8) and (9) have been equated and the

dependences obtained that are needed to justify the experimental method [11]:

$$-\frac{\ln\left(1-\frac{m_c}{m_0}\right)}{t}=-\frac{\ln\frac{\beta_i}{\beta_{i-1}}}{t}. \quad (10)$$

From here it follows that:

$$m_c=m_0\left(1-\frac{\beta_i}{\beta_{i-1}}\right). \quad (11)$$

Or:

$$m_c=m_0\left(1-\frac{1-\alpha_i}{1-\alpha_{i-1}}\right)=m_0\left(1-\frac{1-\frac{E_i}{E_{init}}}{1-\frac{E_{i-1}}{E_{init}}}\right). \quad (12)$$

Thus, knowing the value of m_0 that can be determined from the volume of the container and the density of the gas, determine the value of m_c, it is necessary to establish experimentally the ratio $\frac{\beta_i}{\beta_{i-1}}$ through the corresponding indicators of illumination. An experimental study has been carried out to confirm the relationship between the degree of transparency and the coagulation coefficient.

3 Results

At the first stage of the experiment, the device was filled with exhaust gas in the engine start mode until the measured illumination decreased from 140 to 60 lx. Then, without turning on the ultrasonic equipment, the illumination was measured with the frequency of 1 minute in the interval of ± 5 seconds from the control point within 10 minutes. At the second stage of the experiment, the device was also filled with exhaust gas until the measured illumination decreased to 60 lx, the ultrasonic equipment was turned on and the illumination was measured at the frequency of 1 minute in the interval of ± 5 seconds, from the control point, within 10 minutes.

Figure 5 shows the reflector of ultrasonic waves after the operation of the experimental setup for ultrasonic purification of exhaust gases.

The results of the two stages of the experiment are presented in Tables 1 and 2.

Comparison of the obtained experimental illumination data to the theoretical ones shows that the nature of changing the theoretical and experimental illumination dependences on time without exposure to ultrasound and with exposure to ultrasound have sufficient convergence of the obtained experimental data with the theoretical ones. Figure 6 shows the theoretical and experimental graphs of the illumination E dependence on time t without the ultrasound action and under the ultrasound action.

At this, the error in the average values of the experimental data in comparison to the theoretical ones makes 16.9 % without exposure to ultrasound and 14.23 % under the ultrasound action.

The experimental data obtained made it possible to use them for determining the indicators of changes in illumination, the degree of transparency, the degree of absorption, the coagulation coefficient and to draw a conclusion about the effectiveness of the ultrasonic coagulation processes.

Table 3 presents the results of calculations of the coagulation coefficient.

As a result of ultrasonic intensification of coagulation

Figure 5 *Ultrasonic wave reflector after operation of the experimental setup*

Table 1 *Illumination values E, lx, without the ultrasound action*

No.	Sampling time, s									
	60	120	180	240	300	360	420	480	540	600
1	62	69	74	77	77	81	81	85	87	83
2	60	73	70	75	80	79	81	84	83	84
3	65	73	75	77	76	78	76	81	84	85
4	68	69	70	77	79	78	81	80	80	84
5	70	72	71	76	73	80	84	82	79	85
6	66	76	75	75	79	78	78	82	88	88
7	64	69	74	74	75	81	77	81	83	85
8	69	67	72	75	75	79	82	82	82	87
9	68	68	74	73	74	78	79	81	88	84
10	64	70	73	74	80	78	79	82	81	82
11	66	69	71	79	75	78	80	86	85	83
$\overline{E}$	65.64	70.45	72.64	75.64	76.64	78.91	79.82	82.36	83.64	84.55

Table 2 *Illumination values E, lx, s under the ultrasound action*

No.	Sampling time, s									
	60	120	180	240	300	360	420	480	540	600
1	81	86	94	100	107	111	115	115	116	119
2	83	93	95	101	104	108	112	115	115	119
3	75	89	99	100	106	106	110	114	117	119
4	79	89	95	103	104	110	112	117	117	118
5	76	92	92	100	103	109	110	116	118	117
6	79	92	92	101	105	106	113	116	120	121
7	78	95	96	98	106	108	113	114	119	117
8	83	84	97	100	108	107	111	113	120	121
9	79	90	96	99	103	107	113	117	118	123
10	81	91	96	102	106	113	113	116	121	124
11	86	88	94	104	105	113	116	118	117	118
$\overline{E}$	80.00	89.91	95.09	100.73	105.18	108.91	112.55	115.55	118.00	119.64

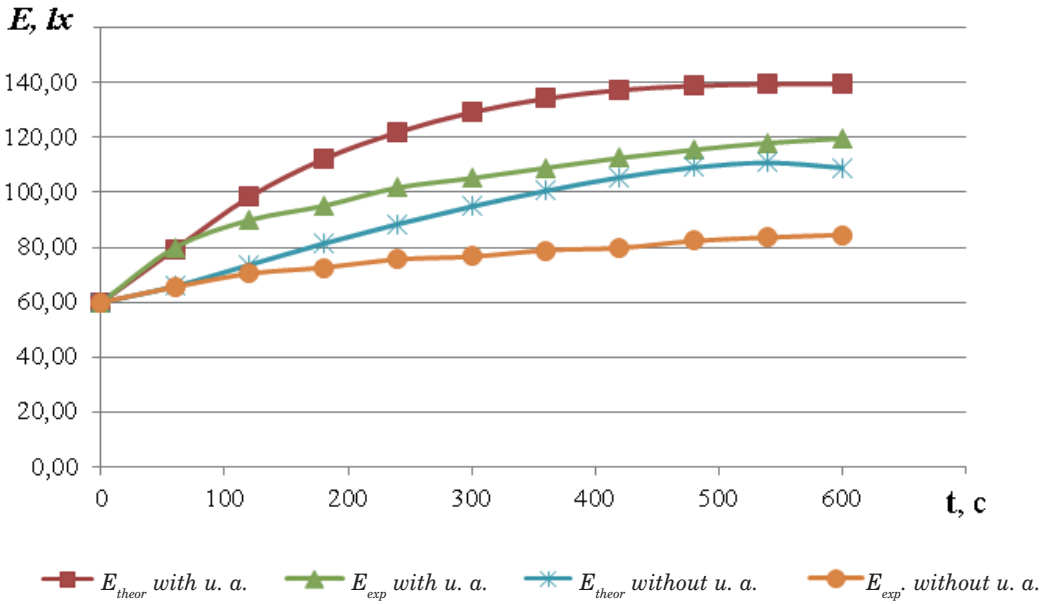

Figure 6 *Theoretical and experimental dependences of illumination E on time t without and with the ultrasound action*

Table 3 *The results of calculating the coagulation coefficient*

Seconds	Illumination indicator, E, lx		Transparence degree, ∝∝		Light flux absorption degree, M		Coagulation coefficient, k	
	Without ultrasound	With ultrasound	Without ultrasound	With ultrasound	Without ultrasound	With ultrasound	Without ultrasound	With ultrasound
0	60.00	60.00	0.429	0.429	0.571	0.571		
60	65.64	80.00	0.469	0.571	0.531	0.429	0.0012	0.0048
120	70.45	89.91	0.503	0.642	0.497	0.358	0.0011	0.0030
180	72.64	95.09	0.519	0.679	0.481	0.321	0.0005	0.0018
240	75.64	100.73	0.540	0.719	0.460	0.281	0.0008	0.0022
300	76.64	105.18	0.547	0.751	0.453	0.249	0.0003	0.0020
360	78.91	108.91	0.564	0.778	0.436	0.222	0.0006	0.0019
420	79.82	112.55	0.570	0.804	0.430	0.196	0.0002	0.0021
480	82.36	115.55	0.588	0.825	0.412	0.175	0.0007	0.0019
540	83.64	118.00	0.597	0.843	0.403	0.157	0.0004	0.0018
600	84.55	119.64	0.604	0.855	0.396	0.145	0.0003	0.0013

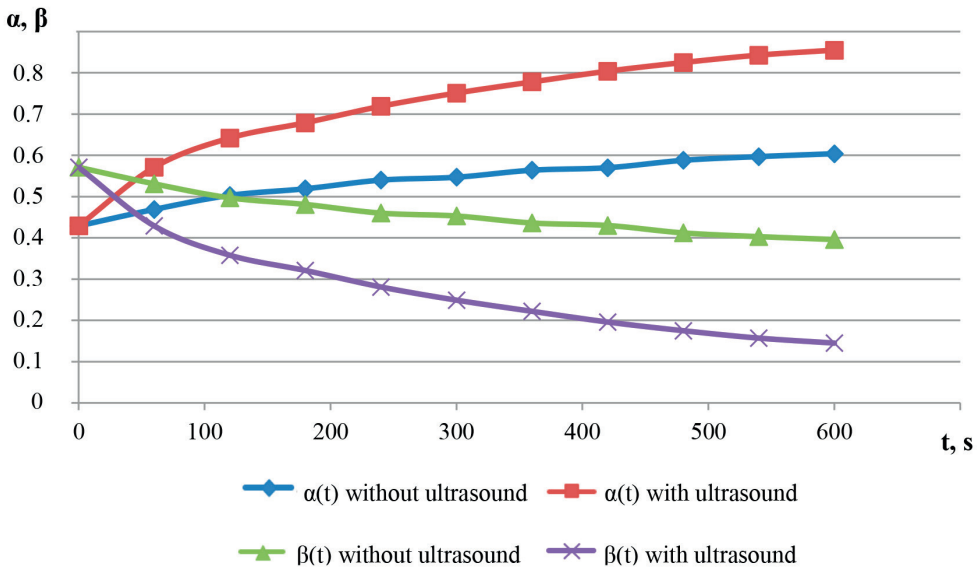

Figure 7 *The transparency degree α and absorption degree β dependence on settling time t*

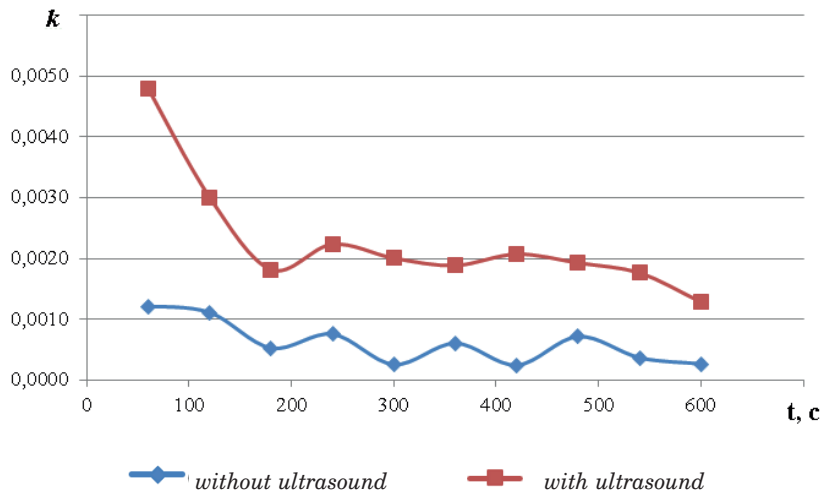

Figure 8 *The coagulation coefficient k dependence on settling time t*

processes, the initial values of the rate of changing the degree of transparency, coagulation coefficient with the ultrasonic exposure are 3 times higher than those without the ultrasonic exposure.

Based on the calculation results, graphs of the degree of transparency and the degree of absorption (Figure 7), the coagulation coefficient (Figure 8) dependence on the settling time have been plotted.

The presented graphic dependencies clearly show a high efficiency of ultrasonic coagulation of exhaust gas particles.

In the work, an approximation was made of the coagulation coefficient values in time t, according to the results of which it has been proposed to use the following cubic regression equation for the coagulation process using ultrasound:

$$k = (-0.0000012t^3 + 0.0012994t^2 - \\ -0.4562322t + 69.30) \cdot 10^{-4}. \quad (13)$$

Figure 9 shows the dependencies k(t) built based on the experimental data and the data calculated using the cubic regression Equation (13).

Since the obtained dependence in Equation (13) has a significant coefficient of determination, differentiation of the function is possible. Then, the rate of changing the coagulation coefficient for processes with ultrasonic action would obey the following dependence:

$$k' = (-0.0000036t^2 + 0.0025988t - \\ -0.4562322) \cdot 10^{-4}. \quad (14)$$

Figure 10 shows the dependence of the coagulation coefficient changing rate on time.

Decreasing the coagulation rate is explained by decreasing the concentration of soot particles in the gas, that is, its purification to a some extent.

The work proposes several constructive options for using the effect of ultrasonic purification and utilization

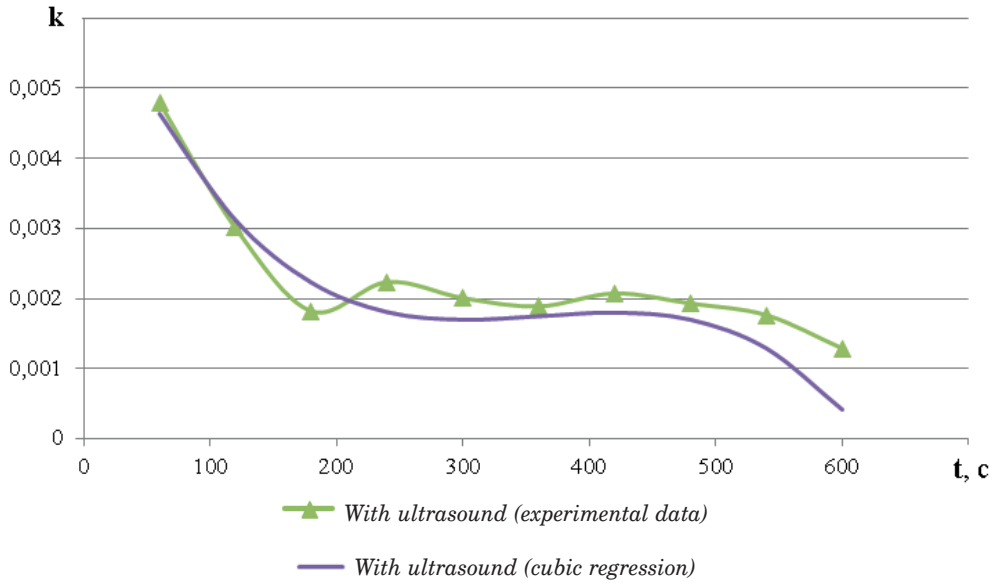

Figure 9 *Changing the coagulation coefficient k with the time t under ultrasound action*

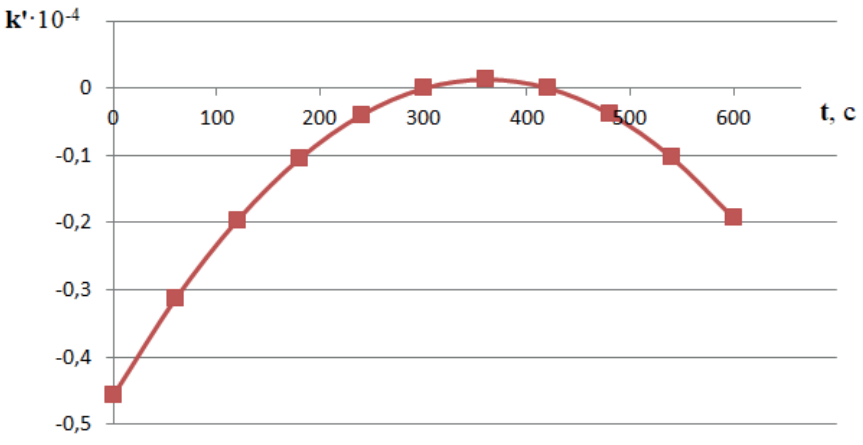

Figure 10 *The coagulation coefficient changing rate k′ dependence on time t*

of internal combustion engine exhaust gases.

Figure 11 shows the scheme of operation of the ultrasonic device for cleaning the exhaust gases of a flow type with the transverse action of ultrasound.

Figure 12 shows the schemes of operation of an ultrasonic device for cleaning the exhaust gases of a flow type with the longitudinal action of ultrasound in two versions: with generation of ultrasonic waves in the direction of the gas flow and against the direction of its movement.

Figure 13 shows a device for ultrasonic cleaning of exhaust gases with exposure to ultrasound at different angles.

One more device for cleaning exhaust gases of a

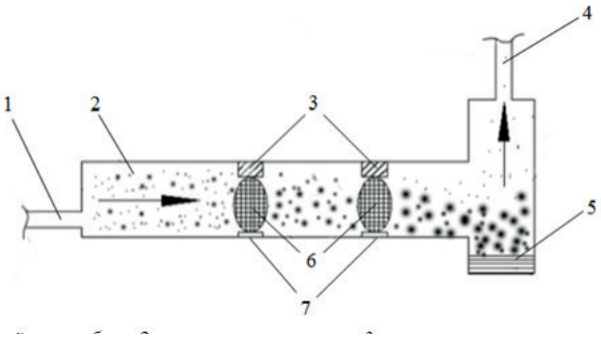

1 - inlet pipe; 2 - muffler body; 3 - emitter of ultrasonic waves; 4 - outlet pipe; 5 - place of collecting and extracting soot particles; 6 - zone of standing waves; 7 - reflector of ultrasonic waves

***Figure 11** The scheme of operation of the ultrasonic muffler the transverse action of ultrasound*

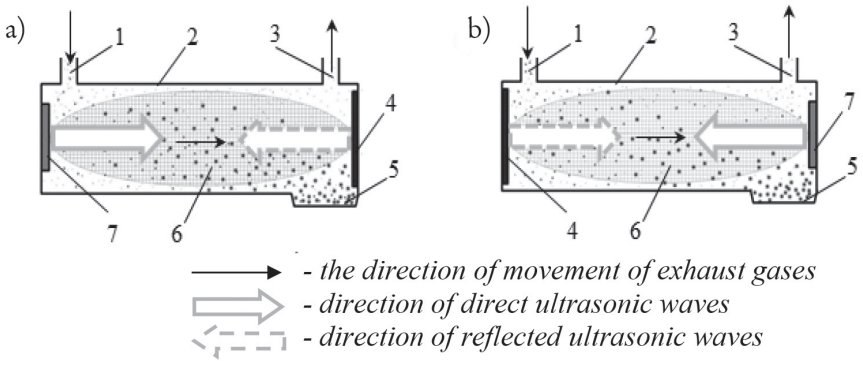

1 - inlet pipe; 2 - muffler body; 3 - outlet pipe; 4 - reflector of ultrasonic waves; 5 - place of collecting and extracting soot particles; 6 - zone of standing waves; 7 - emitter of ultrasonic waves

***Figure 12** Schemes of operation of the ultrasonic muffler with the longitudinal action of ultrasound: a) in the direction of the gas flow; b) against the direction of the gas movement*

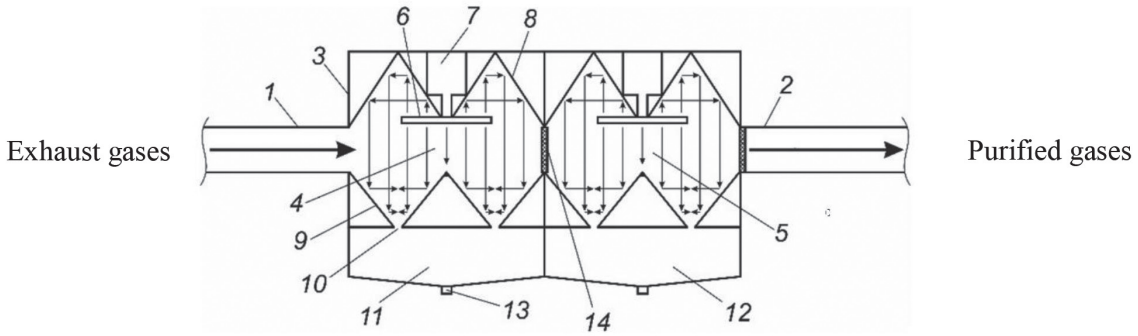

1 - inlet pipe; 2 - outlet pipe; 3 - body; 4 - coagulation chamber; 5 - coagulation chamber; 6 - emitter of ultrasonic vibrations; 7 - transducer of ultrasonic vibrations; 8 - upper reflectors; 9 - lower reflectors; 10 - holes for removal of particles; 11, 12 - storage tanks for collecting particles; 13 - holes with a plug; 14 - filtration grids

***Figure 13** A device for ultrasonic purification of exhaust gases*

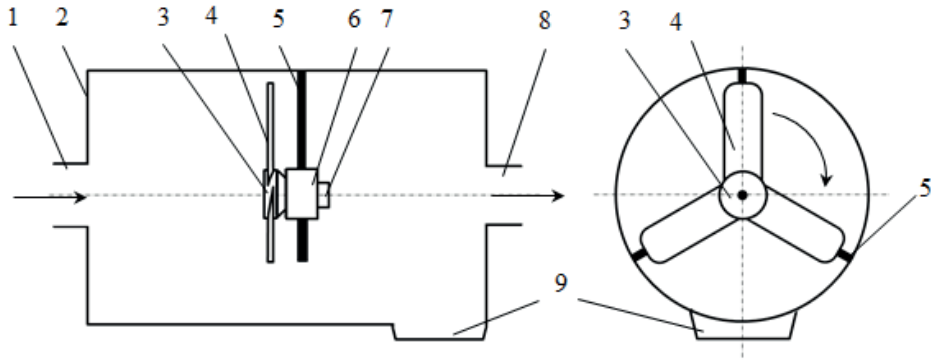

1 - inlet pipe; 2 - body; 3 - ultrasonic emitter; 4 - bladed propeller; 5 - rack; 6 - rotation mechanism; 7 - rotating contact device; 8 - outlet pipe; 9 - place for collecting and extracting soot particles

Figure 14 *A device for purification of exhaust gases with a dynamic system of ultrasonic action*

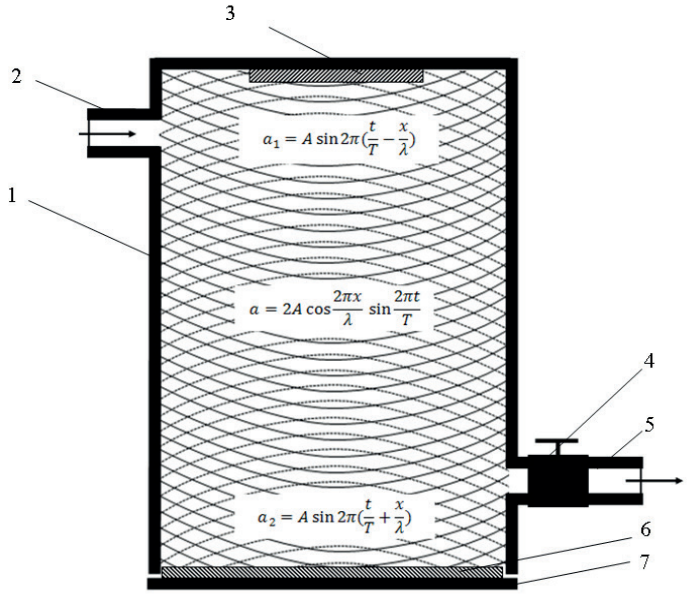

1 - storage tank; 2 - inlet pipe; 3 - ultrasonic generator; 4 - bypass valve; 5 - outlet pipe; 6 - reflector of sound waves; 7 - tray

Figure 15 *The accumulative ultrasonic device for cleaning exhaust gases with the vertical arrangement of ultrasonic equipment*

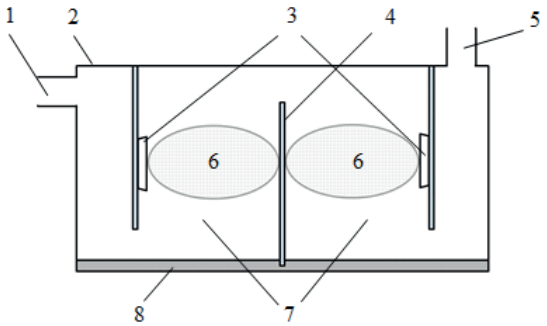

1 - inlet pipe; 2 - body; 3 - ultrasonic emitter; 4 - sound-reflecting partition; 5 - outlet pipe; 6 - zone of standing waves; 7 - coagulation chambers; 8 - tray

Figure 16 *The combined type device for purification of exhaust gases with the horizontal arrangement of ultrasonic equipment*

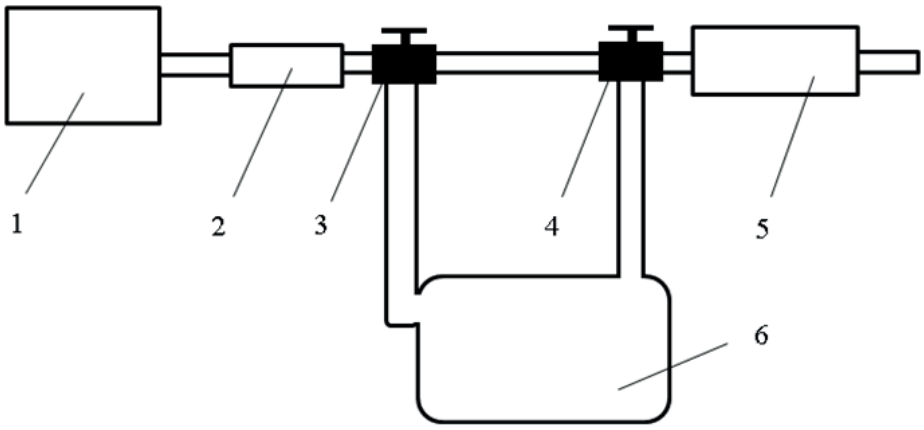

1 - engine; 2 - resonator; 3 - inlet valve; 4 - exhaust valve; 5 - silencer; 6 - ultrasonic cleaning device

Figure 17 *The recommended scheme of mounting the equipment for ultrasonic purification and utilization of exhaust gases*

flow type, with a dynamic system of ultrasonic action, is shown in Figure 14. Here, a bladed propeller serves as an emitter of ultrasonic waves.

The accumulative ultrasonic device for cleaning the exhaust gases, with the vertical arrangement of ultrasonic equipment, is shown in Figure 15.

The device shown in Figure 16, with the horizontal arrangement of ultrasonic equipment, can be used in both flow and storage modes, i.e. it is combined.

All of the above devices make it possible not only to clean exhaust gases but also to utilize the soot particles enlarged and settled as a result of ultrasonic exposure.

Figure 17 shows the recommended scheme of mounting the equipment for ultrasonic purification and utilization of vehicle exhaust gases [3].

4 Example of the calculation technique

The method of calculating the ultrasonic equipment includes:

1) determining the distance between the emitter and the ultrasound reflector for the formation of standing waves, at which the coagulation process occurs most efficiently;
2) checking the compliance with coagulation conditions;
3) calculating the required time of exposure to exhaust gases, for a given degree of purification, to determine the required volume of the storage tank.

1. For formation of the standing waves, it is necessary that the distance between the emitter and the reflector of ultrasonic waves be a multiple of half the wavelength. The ultrasonic wave length is determined by the formula:

$$\lambda = \frac{v}{f}, \tag{15}$$

where v is the sound propagation velocity, v = 300 m/s; f is the oscillation frequency, Hz.

For ultrasonic equipment with the ultrasonic waves radiation frequency of 28 kHz:

$$\lambda = \frac{300}{28000} = 10.7\ mm\,. \tag{16}$$

Thus, the distance between the emitter and the reflector is to be determined by the formula:

$$L = \frac{\lambda}{2} \cdot i\,, \tag{17}$$

where i = 1, 2, 3…

2. For ρ = 1900 kg/m^3; f = 28000 Hz; η = 0.00017 from Equation (2) the drag coefficient Z can be determined, which should have values from 0.54 to 3.51 [13], the range of the particle radii that are most efficiently affected by the ultrasonic equipment:

$$r = \sqrt{\frac{Z\eta}{\rho f}}\,, \tag{18}$$

$$r_0 = \sqrt{\frac{0.54 \cdot 0.00017}{1900 \cdot 28000}} = 1.31 \cdot 10^{-6} m = 1.31 \mu m\,; \tag{19}$$

$$r_0 = \sqrt{\frac{3.51 \cdot 0.00017}{1900 \cdot 28000}} = 3.34 \cdot 10^{-6} m = 3,34 \mu m. \tag{20}$$

In this case, the degree of participation of particles with the size of 1.31 μm and 3.34 μm in the sound vibrations of a standing ultrasonic wave $\frac{U_p}{U_g}$ will be equal to 0.8 and 0.2, respectively.

The results of the calculation indicate that the conditions for occurrence of the ultrasonic coagulation are met and indicate the highly efficient coagulation processes of fine particles of exhaust gases with the radius of 1.31 to 3.34 μm.

3. To determine the volume of the storage tank that is required for the most efficient operation of ultrasonic cleaning and disposal equipment, it is necessary to determine the rational time of ultrasonic exposure to the exhaust gas. The volume of the storage tank is determined by the calculation method described in literature [17].

Here is the entire volume of soot present in the tank, both in suspension and settled on the bottom of the device as a result of coagulation, accepted as a unit and then it is determined what part of the solid particles is settled, using Equation (3) of the calculated concentrations of suspended solid particles of the gas dependence [15]:

$$n = n_0 \exp(-kt) \tag{21}$$

and obtained Equation (14) of the coagulation coefficient changing:

$$k = (-0.0000012t^3 + 0.0012994t^2 - \\ -0.4562322t + 69.3) \cdot 10^{-4} \tag{22}$$

The s value characterizes the share of settled solid particles and will determine the degree of the exhaust gas purification:

$$s = 1 - n \tag{23}$$

$$s = 1 - n_0 \exp(-kt) \tag{24}$$

It is assumed that at the initial time t = 0 all the soot particles are in suspension, i.e. if n = 1, then s = 0.

Table 4 *Calculating the degree of the exhaust gases purification s depending on the time of the ultrasound action*

t	k	n_0	n	s
0	0.00693	1.00	1	0
60	0.004634	1.00	0.76	0.24
120	0.003119	0.76	0.52	0.48
180	0.002228	0.52	0.35	0.65
240	0.001806	0.35	0.23	0.77
300	0.001698	0.23	0.14	0.86
360	0.001747	0.14	0.07	0.93
420	0.001799	0.07	0.03	0.97
480	0.001698	0.03	0.02	0.98
540	0.001288	0.02	0.01	0.99
600	0.000414	0.01	0.01	0.99

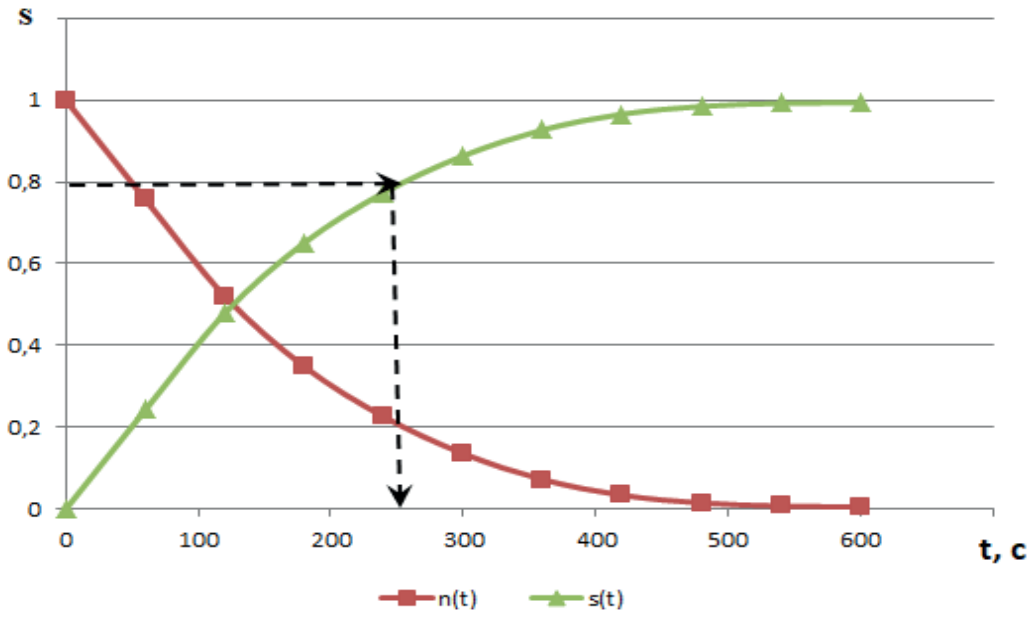

Figure 18 *The graphs of the n(t) and s(t) dependences*

The calculation of the degree of the exhaust gases purification depending on the time of ultrasonic exposure is presented in Table 4.

The graphs of the $n(t)$ and $s(t)$ dependencies are presented in Figure 18.

According to the graph of the exhaust gases degree of purification dependence on time, it is possible to determine the required time of exposure to ultrasound for a given degree of purification. For example, for the 80 % degree of purification, the required time of ultrasonic exposure will be t = 260 s.

5 Conclusions

In the course of studying the operation of devices for ultrasonic purification and utilization of exhaust gases, there has been made the following work and draw the following conclusions:

- analyzing the cleaning methods and composition of the exhaust gases of internal combustion engines substantiates the need for their disposal due to the ultrasonic action;
- the physical essence of the process of exhaust gases coagulation under the action of ultrasound is described, the understanding of which is needed for development of a mathematical model of the process of exhaust gases utilization. A mathematical model of the process of exhaust gases of internal combustion engine utilization, based on the formula of the molecular-kinetic theory of gases, has been developed and studied. The obtained dependence that takes into account the number concentrations of gas and soot particles, which vary depending on the time and the coagulation coefficient, makes it possible to determine the amount of soot settled and to determine the efficiency of cleaning exhaust gases with an ultrasonic device;
- based on the proposed hypothesis of a close relationship between the content of soot particles in suspension and the light transmission capacity of a certain volume of gas, the concept of illumination has been introduced as a parameter for assessing the content of soot particles in suspension;
- an experimental ultrasonic accumulative device has been developed that allows measuring the light transmission of the volume of gas in the device, according to the illumination parameter E and based on the data obtained, determining the change in the concentration of soot particles in suspension, the coagulation coefficient over time without exposure to ultrasound and with exposure to ultrasound;
- experiments have been carried out on the developed experimental equipment and the results obtained have been analytically confirmed. At this, the error in the average values of the experimental data in comparison with the theoretical ones has made 16.9 % without exposure to ultrasound and 14.2 % under the ultrasound action;
- alternate options of using the effect of ultrasonic cleaning of internal combustion engine exhaust gases of transport equipment have been proposed that determine the trends for the further scientific research;
- a method of calculating the capacitive equipment has been developed that makes it possible to determine the main design parameters of ultrasonic cleaning systems for exhaust gases of internal combustion engines and the terms of reference for designing an ultrasonic cleaning system for exhaust gases from internal combustion engines of city buses.

Grants and funding

The authors received no financial support for the research, authorship and/or publication of this article.

Conflicts of interest

The authors declare that they have no known competing financial interests or personal relationships that could have appeared to influence the work reported in this paper.

References

[1] BANDYOPADHYAY, A. Neurological disorders from ambient (urban) air pollution emphasizing UFPM and $PM_{2.5}$. *Current Pollution Reports* [online]. 2016, 2, p. 203-211. eISSN 2198-6592. Available from: https://doi.org/10.1007/s40726-016-0039-z

[2] AKHMALTDINOVA, L., SIROTA, V., BABENKO, D., ZHUMALIYEVA, V., KADYROVA, I., IBRAYEVA, A., AVDIENKO, O. Proinflammatory cytokines and colorectal cancer - the impact of the stage. *Contemporary Oncology / Wspolczesna Onkologia* [online]. 2021, **24**(4), p. 207-210. ISSN 1428-2526, eISSN 1897-4309. Available from: https://doi.org/10.5114/wo.2020.102551

[3] IBATOV, M. K., KADYROV, A. S., PAK, I. A., KADYROVA, I. A., ASKAROV, B. S. Results of experimental studies of the operation of capacitive equipment for ultrasonic cleaning of vehicle exhaust gases. *Coal / Ugol* [online]. 2020, **2**, p. 73-78. ISSN 0041-5790, eISSN 2412-8333. Available from: http://dx.doi.org/10.18796/0041-5790-2020-2-73-78

[4] LUKANIN, V. N., TROFIMENKO, Y. V. *Industrial and transport ecology*. Moscow: Vyssh.shk, 2003. ISBN 5-06-003957-9.
[5] MARKOV, V. A., BASHIROV, R. M., GABITOV, I. I. *Toxicity of exhaust gases of diesel engines*. Moscow: Publishing house of MSTU im. N.E. Bauman, 2002. ISBN 5-7038-1993-8.
[6] DONG, S., LIPKENS, B., CAMERON, T. V. The effects of orthokinetic collision, acoustic wake and gravity on acoustic agglomeration of polydisperse aerosols. *Journal of Aerosol Science* [online]. 2006, **37**(4), p. 540-553. ISSN 0021-8502, eISSN 1879-1964. Available from: https://doi.org/10.1016/j.jaerosci.2005.05.008
[7] RAN, W., SAYLOR, J. R. A mechanistic explanation of the increase in particle scavenging in the ultrasonic scrubber. *Journal of Aerosol Science* [online]. 2015, **87**, p. 88-101. ISSN 0021-8502, eISSN 1879-1964. Available from: https://doi.org/10.1016/j.jaerosci.2015.05.005
[8] KHMELEV, V. N., SHALUNOV, A. V., GOLYKH, R. N., NESTEROV, V. A. The study of regularities of ultrasonic coagulation of two-phase aerosol in gas flow International Conference of Young Specialists on Micro/Nanotechnologies and Electron Devices EDM 2018: proceedings [online]. 2018. ISBN 978-153865021-9, p. 327-332. Available from: https://doi.org/10.1109/EDM.2018.8435083
[9] KHMELEV, V. N., SHALUNOV, A. V., TSYGANOK, S. N., NESTEROV, V. A. Ultrasonic coagulation in venturi scrubbers: features of implementation and effectiveness of application. *Proceedings of Tomsk Polytechnic University. Georesource Engineering* [online]. 2020, **331**(5), p. 128-139. ISSN 2413-1830, eISSN 2500-1019. Available from: http://izvestiya.tpu.ru/archive/article/view/2643/2227
[10] ZU, K., YAO, Y., CAI, M., ZHAO, F., CHENG, D. L. Modeling and experimental study on acoustic agglomeration for dust particle removal. *Journal of Aerosol Science* [online]. 2017, **114**, p. 62-76. ISSN 0021-8502, eISSN 1879-1964. Available from: https://doi.org/10.1016/j.jaerosci.2017.09.001
[11] KHMELEV, V. N., SHALUNOV, A. V., SHALUNOVA, K. V., TSYGANOK, S. N., BARSUKOV, R. V., SLIVIN, A. N. *Ultrasonic coagulation of aerosols*. Biysk: Publishing house of the Altai State Technical University, 2010. ISBN 978-5-9257-0188-1.
[12] GALLEGO-JUAREZ, J. A., GRAFF, K. F. *Power ultrasonics: applications of high-intensity ultrasound*. Cambridge: Woodhead Publishing, 2014. ISBN 978-1782420286.
[13] BERGMAN, L. *Ultrasound and its application in science and technology*. Moscow: Publishing House of Foreign Literature, 1957.
[14] KADYROV, A. S., SARSEMBEKOV, B. K., GANYUKOV, A. A., ZHUNUSBEKOVA, Z. Z., ALIKARIMOV, K. N. Experimental Research of the coagulation process of exhaust gases under the influence of ultrasound. *Communications - Scientific letters of the University of Zilina* [online]. 2021, **23**(4), p. B288-298. ISSN 1335-4205, eISSN 2585-7878. Available from: https://doi.org/10.26552/com.C.2021.4. B288-B298
[15] KARDASHEV, G. A. *Physical methods of intensification of chemical technology processes*. Moscow: Chemistry, 1990. ISBN 5-7245-0674-2.
[16] KADYROV, A., PAK, I., GANYUKOV, A., IMANOV, M., BALABEKOVA, K. Research of operation of equipment for ultrasonic purification of exhaust gases of internal combustion engines. *Journal of Engineering Physics and Thermophysics* [online]. 2021, **94**(6), p. 1407-1414. ISSN 1062-0125, eISSN 1573-871X. Available from: https://doi.org/10.1007/s10891-021-02447-x
[17] IBATOV, M. K., ALIYEV, S. B., BALABAYEV, O. T., ASKAROV, B. S. Main results of experimental studies of open-pit mines diesel locomotive internal combustion engine isolation. *Coal / Ugol*. 2019, **7**, p. 28-30. ISSN 0041-5790, eISSN 2412-8333. Available from: http://dx.doi.org/10.18796/0041-5790-2019-7-28-30

This is an open access article distributed under the terms of the Creative Commons Attribution 4.0 International License (CC BY 4.0), which permits use, distribution, and reproduction in any medium, provided the original publication is properly cited. No use, distribution or reproduction is permitted which does not comply with these terms.

DESIGN OF A BICYCLE'S STRUCTURAL COMPONENTS AND A COMPARISON OF THEIR CHARACTERISTICS IN STEEL, ALUMINUM AND CARBON

Lukáš Pompáš*, František Brumerčík, Ľuboš Kučera, Lukáš Smetanka

Department of Design and Mechanical Elements, Faculty of Mechanical Engineering, University of Zilina, Zilina, Slovak Republic

*E-mail of corresponding author: lukas.pompas@uniza.sk

Lukáš Pompáš 0000-0002-8118-6681,
Ľuboš Kučera 0000-0001-5232-7601,
František Brumerčík 0000-0001-7475-3724,
Lukáš Smetanka 0000-0001-6583-8128

Resume

The design of a bicycle frame in Creo Parametric and the following simulation comparison of three frame materials - steel, aluminium and carbon, using the software from Marc Mentat, are the main subjects of this article. In this article, the authors explain how to model a bicycle frame in three dimensions and contrast it with frames made of the other two materials. The simulation's findings demonstrate how various elements, such as load, affect a steel, aluminium and carbon frame's behaviour in specific circumstances and under identical settings. Engineers may choose the best material and optimize the geometry and topology of the frame, based on the findings of the simulation, to get the best outcomes in terms of the stiffness requirements and rider comfort.

Article info

Received 12 April 2023
Accepted 25 June 2023
Online 7 July 2023

Keywords:

bike frame
materials
simulation
bicycle

Available online: https://doi.org/10.26552/com.C.2023.061

ISSN 1335-4205 (print version)
ISSN 2585-7878 (online version)

1 Main objectives

The modern bike frame design is incredibly inventive and dynamic. For different types of bikes and riders, manufacturers are trying to develop the best and most efficient solutions. The design of the bicycle frame structure and the subsequent simulation to find out the best material to be used for the structure are the main topics of this study, Figure 1 [1-2].

2 Introduction

One of the most important components of a bike's design is the frame. The frame must be rigid and robust enough to support the rider's load and demands of the road while remaining light and comfortable enough to prevent riders' fatigue and enable a pleasurable ride. The frame must also be both aesthetically pleasing and ergonomic, as well [3].

A bicycle's frame is crucial to both its creation and operation. All the other components of the bike, including the forks, seat, wheels, brakes and derailleurs, are held and supported by the frame, [4].

In addition, the frame also determines the geometry and size of the bike, which affect its rideability and rider comfort. Depending on the type of a bike, different materials are used to make frames, such as steel, aluminium, carbon, titanium and more. Each material has its own properties that affect the weight, strength and price of the frames. The right frame can improve the bike's rideability and provide the rider with a comfortable ride. Therefore, it is important to consider the frame and its characteristics when choosing a bike and match it to the rider's needs and intended use, [5].

Bicycle frames can be made of different materials and in different designs, differing in the shape and geometry of the tubes and the way they are connected. The most common frame designs include:

- Classic diamond frame

The classic diamond frame is shaped like a diamond and is the most common frame construction for road, mountain and city bikes. The frame consists of an upper and lower frame beam, a centre frame and a rear frame.

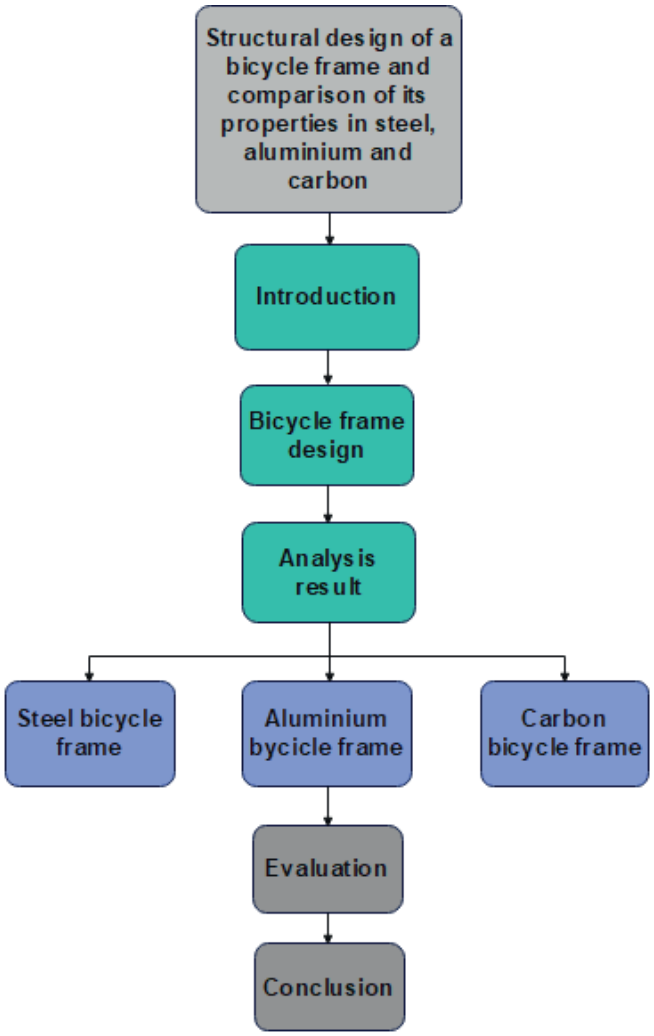

Figure 1 *Algorithm of the article*

This construction allows for an even distribution of the rider's weight and increases stability.

- Transitional frame

To make it simpler to hop on and off the bike, this sort of frame has a diamond shape with a noticeable transition at the front. These frames are frequently found on hybrid or urban bicycles.

- Frame with a sloping top

The top tube of this kind of bike frame slopes and it is rather stiff while riding. Most road bikes use it.

- Time trial period

This kind of frame features a noticeably longer top tube and a narrower angle between the frame and fork since it is intended for time-trial racing, [6-7].

There is currently a lot of focus on use of the new materials, such as super lightweight and extra strong polymers, which have the potential to improve the strength and weight of bicycle frames. In addition, frame manufacturing technology continues to improve, allowing the use of new tube forming and material joining technologies, [8].

The last but not the least, nowadays a lot of attention is also paid to sustainability and the environmental aspect of the production of bicycle frames, which strive to be made from recyclable materials and to minimize the negative impact on the environment, [9].

3 Bicycle frame design

Many conditions must be satisfied to generate a model of the bicycle frame structure. These prerequisites consist of:

1. Material knowledge - Understanding the materials that can be utilized to build a bicycle frame structure is crucial. The most widely utilized materials nowadays are carbon fibre, aluminium and steel.
2. Construction knowledge - Understanding how a bicycle frame is built is necessary when designing a frame. The head, down tube, top tube, seat tube and the rear triangle are just a few of the components that make up the frame. To create a proper model, one must be aware of the shapes and their interactions.

3. Using a CAD application - A suitable CAD program that supports the development of the 3D models is required to generate a model of the bicycle frame structure. The market is filled with CAD software, including Creo Parametric, SolidWorks, Autodesk Inventor and others.
4. Simulation - It is crucial to validate the model of the bicycle frame construction using simulation after it has been built. One can use simulation to make sure that the frame is sturdy and load-resistant enough. The design can be changed if necessary to better meet the specifications.
5. Fabrication - The frame itself needs to be constructed after the design has been confirmed and blueprints have been created. For fabrication, a variety of processes are employed, including welding, pressing and carbon fibre winding.

The successful development of a bicycle frame design model that will be suitably sturdy and load-resistant, depends on the fulfilment of these parameters, as a whole, [10-12].

For creation of the bicycle frame, there are the predetermined conditions for the shape of the individual parts of the bicycle frame:

- The head tube and the vertical tube must have a circular cross-section,
- The top tube shall have a rectangular cross-section,
- The bottom tube must have a square cross-section,
- The rear part of the frame, which consists of the two parts, must have a rectangular cross-section,
- The wall thickness of the parts in question must be 2 millimetres,

A bicycle frame is made up of several components that work together to make its overall structure (see Figure 2). The top tube (2) and bottom tube (3), which are joined on one side by a head tube (1) and on the other by a vertical tube, are the primary components of the bicycle frame (4).

The bicycle frame's primary components are the bottom tube (3) and the top tube (2). Both the upper tube and the lower tube connect the upper and lower portions of the back construction (5), respectively. The top tube often serves as the frame's foundation line and is angled slightly, which changes the geometry of the bicycle. The bottom tube is often stronger and serves as the framework for strengthening the entire frame.

To comply with the requirement that each tube has a wall thickness of 2 mm, the bottom tube of the proposed structure will be the same as the rest of the frame in our design. We next compared the similar frame design for three alternative materials. The portion of the frame that holds the back wheel in place is called the rear structure. Its primary job is to give the bicycle frame stiffness and stability. Although the rear frames are typically built of steel or aluminium, some high-performance versions may incorporate carbon rear structures. The component that joins the downtube is called the downtube. Its main function is to support the frame triangle and ensure the stability of the frame.

3.1 Steel frame

The individual parts of the bicycle steel frame are connected by welding. A welding method called TIG (Tungsten Inert Gas) welding, which is also known as GTAW (Gas Tungsten Arc Welding), is often used to weld the steel frame of a bicycle. The TIG welding is often the preferred welding method for the steel bicycle

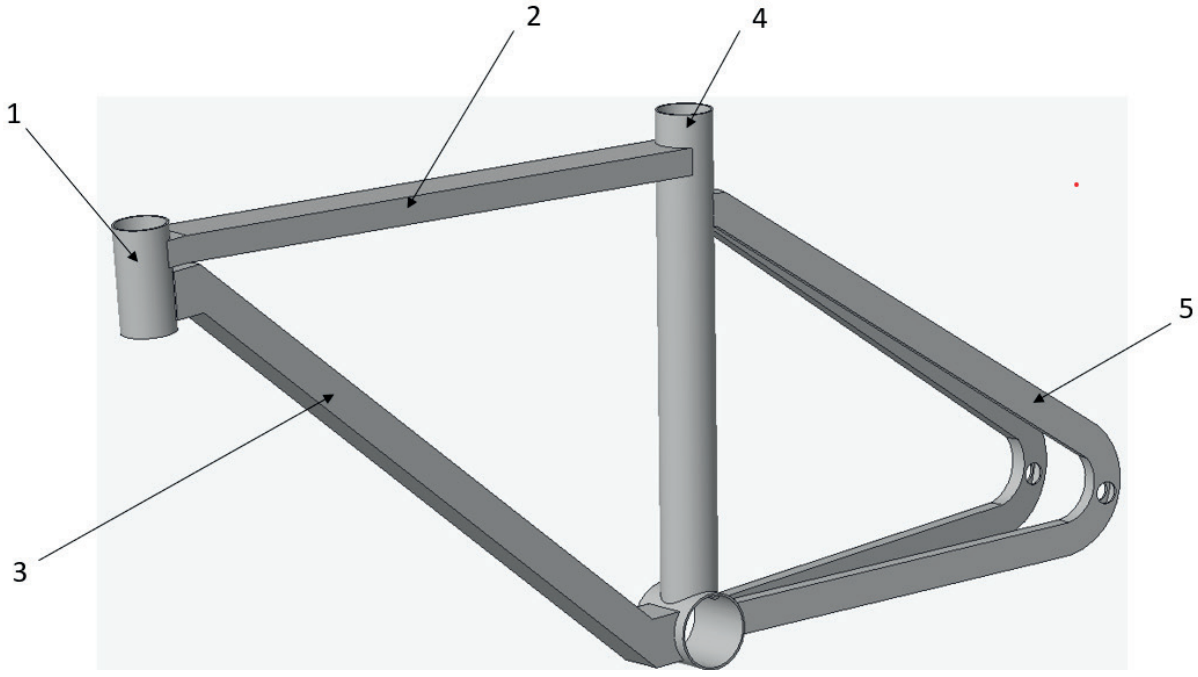

Figure 2 *Bicycle frame design in Creo parametric*

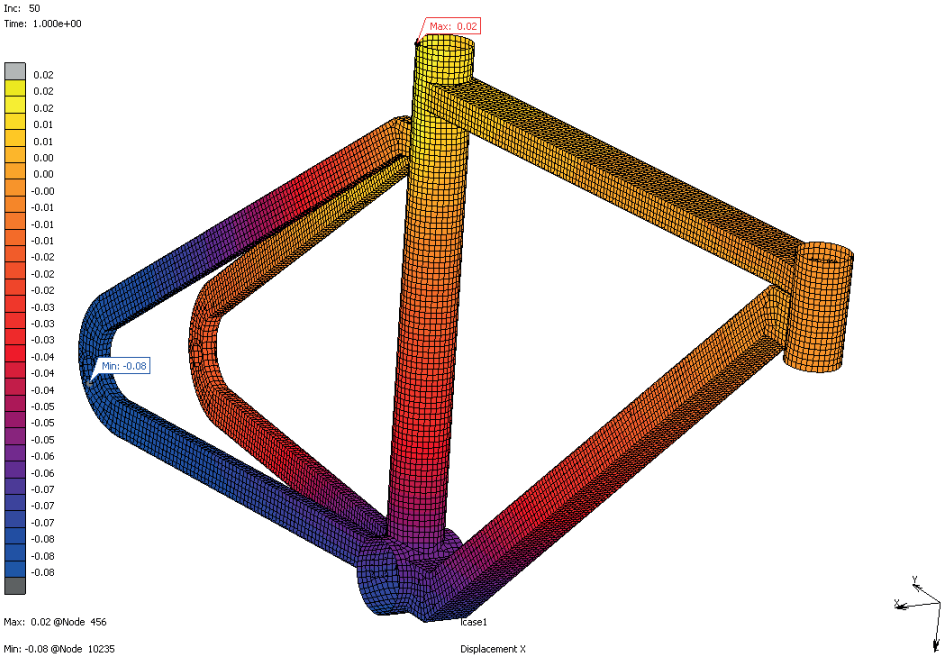

Figure 3 *Results of the displacement of the steel frame of the bicycle in the X-axis*

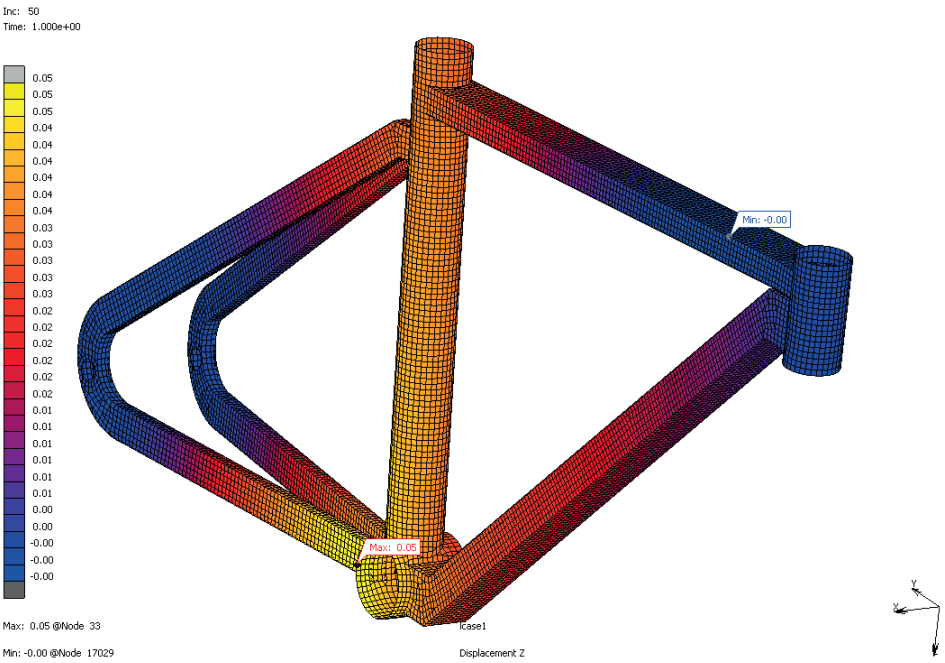

Figure 4 *Results of the displacement of the steel frame of the bicycle in the Z-axis*

frames because it provides higher welding quality and greater accuracy.

The TIG welding uses a special welding rod or wire that is made of a steel-like material. In the welding process, an electric arc heats the welding rod while a shielding gas (often argon) is used to protect the molten metal from reacting with the surrounding air.

The TIG welding allows thin and precise joints to be welded, which is ideal for steel bicycle frames. Steel is a strong and durable material and is therefore a popular material for bicycle frames, especially in the manufacture of the high-quality mountain and road bikes, [13].

3.2 Aluminium frame

Just as welding is used on a steel bicycle frame, welding is also used on an aluminium frame. A welding method called MIG (Metal Inert Gas) welding, which is also known as GMAW (Gas Metal Arc Welding), is often used to weld an aluminium bicycle frame. This welding method is widely used in the production of aluminium bicycle frames.

The MIG welding uses welding wire that contains the welding material and is inserted into the welding rods. This wire is fed with an electric arc, which melts the welding material and fuses it to the aluminium

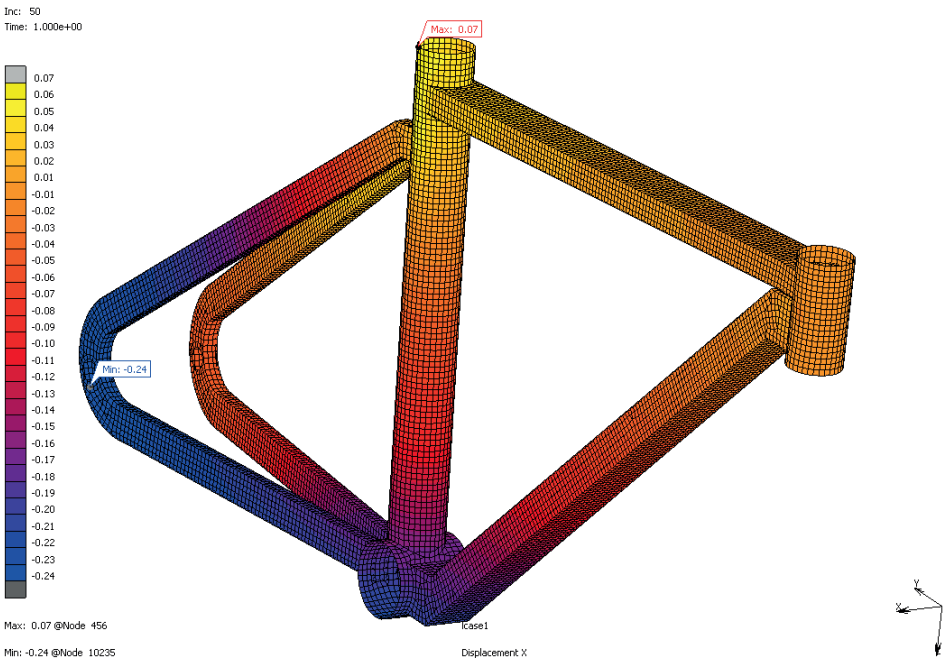

Figure 5 *Results of the displacement of the aluminium frame of the bicycle in the X-axis*

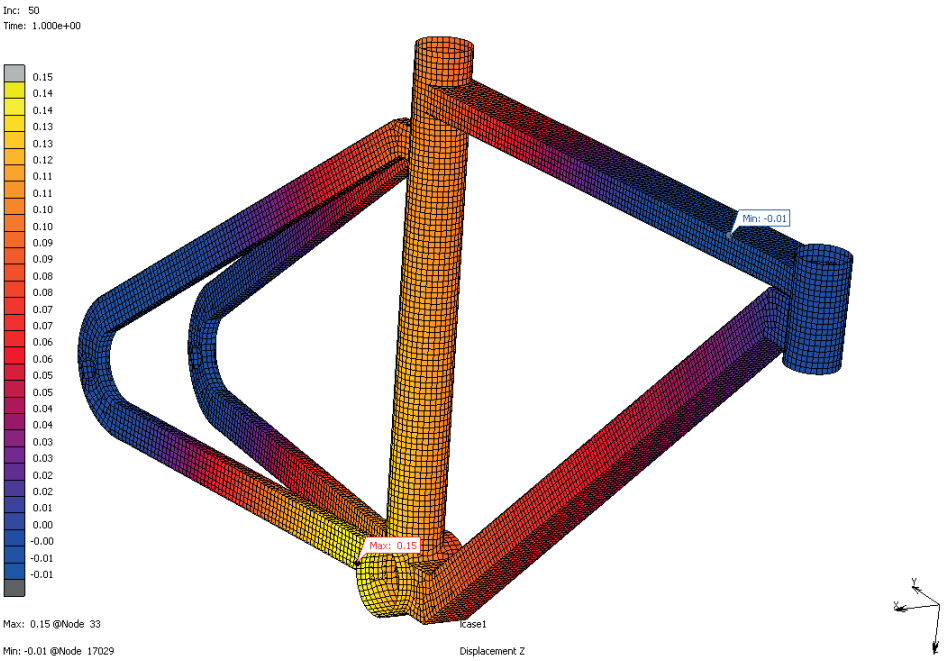

Figure 6 *Results of the displacement of the aluminium frame of the bicycle in the Z-axis*

of the frame. A shielding gas (often argon) is used to protect the molten metal.

Aluminium is a lightweight metal with high thermal conductivity and, therefore, higher currents and special techniques must be used to overcome heat dissipation when welding aluminium frames. The MIG welding is a suitable method for aluminium frames as it provides good joint strength and allows accurate welding.

In addition to the MIG welding, a welding method called TIG welding (GTAW) can also be used in production of the aluminium bicycle frames, which provides even higher welding quality and precision, [14].

3.3 Carbon frame

Manufacturing a carbon bike frame is a process that involves several steps. Here is the usual procedure for making a carbon bicycle frame:

1. Design and modelling: the manufacturing process starts with creation of a frame design in the CAD (Computer-Aided Design) software. Designers create a virtual model of the frame that includes the geometry and details of the design. (Frame design is the same as for steel and aluminium).
2. Mould making: Based on the virtual model, a mould

is created that will be used in the production of the carbon frame. This mould is often made of aluminium or other hard material and plays a key role in creating the shape of the frame.

3. Preparation of carbon plates: the layers of carbon plates are ready for insertion into the mould. These sheets are made of resin impregnated with carbon fibre. The sheets are cut and shaped to fit the mould and to maintain the required properties and lay-up.
4. Impregnation. This process can be carried out in different ways, such as manual impregnation or the use of vacuum and pressure.
5. Inserting into the mould: the impregnated carbon plates are inserted into the mould in the required layered structure. The shape and positioning of the sheets create the desired frame shapes and geometry.
6. Curing and heat treatment: The mould with the embedded carbon sheets is subjected to heat and pressure. The heat helps to cure the resin and form strong bonds between the fibres. The heat treatment can take place in special ovens or autoclaves that provide a controlled environment.
7. Demoulding and finishing: After curing, the frame is dismantled from the mould. This is followed by finishing, which includes removal of excess materials, sanding and any surface finishing, [11].

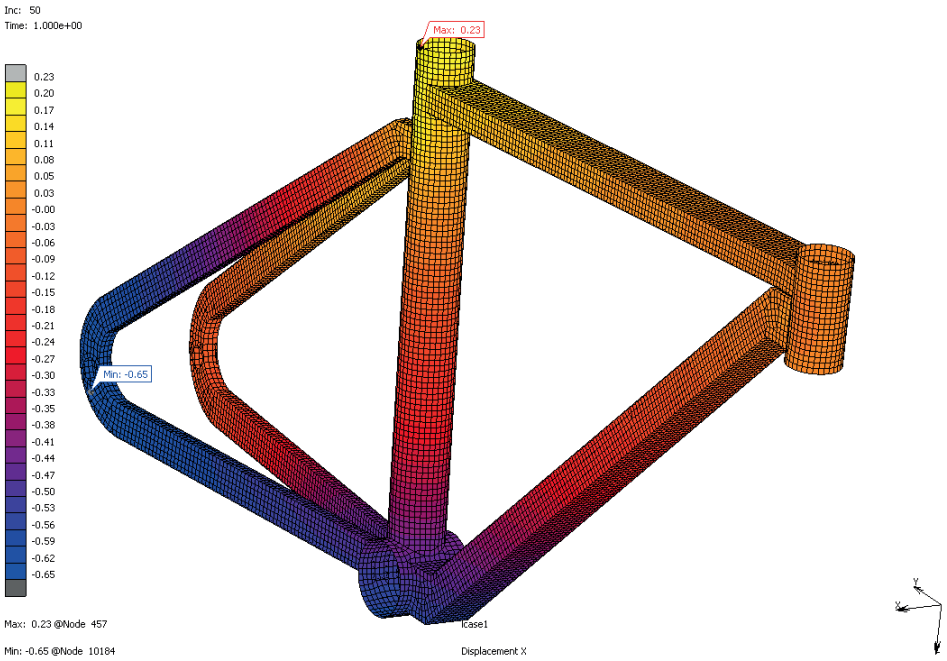

Figure 7 *Results of the displacement of the carbon frame of the bicycle in the X-axis*

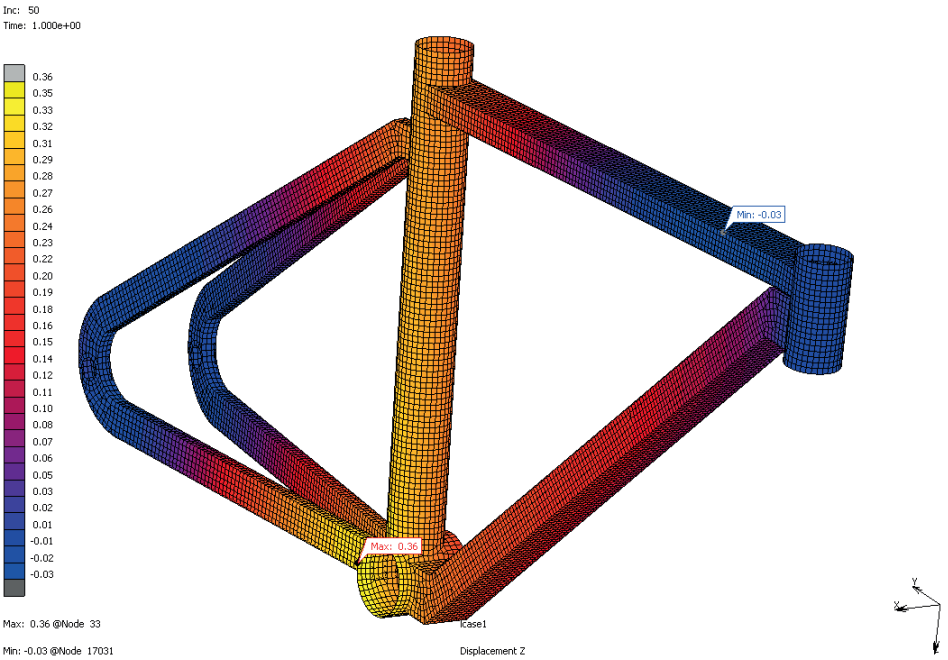

Figure 8 *Results of the displacement of the carbon frame of the bicycle in the Z-axis*

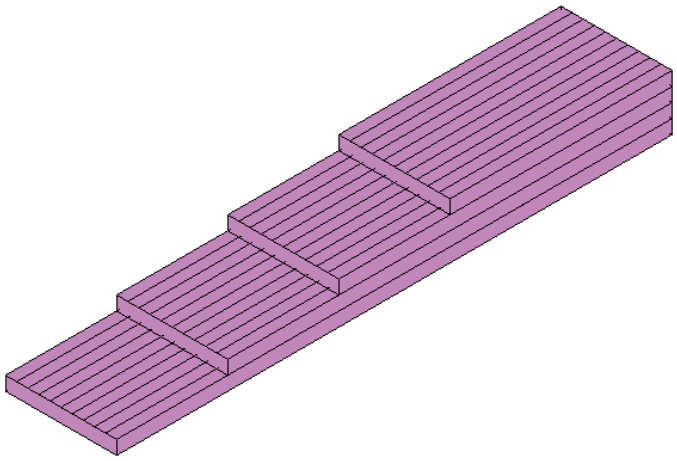

Figure 9 *Arranged layers of carbon fibre*

Table 1 *Displacement values of material frames*

	Steel frame	Aluminium frame	Carbon frame
Displacement X [mm]	0.02	0.07	0.23
Displacement Z [mm]	0.05	0.15	0.36

3.4 Fibre layers

The layers are each 0.5 mm thick. To achieve the 2-mm thickness requirement for the frame tubes, we must fasten four layers of the carbon fibre on top of one another. The illustration shows the layers to be horizontally aligned and at a 0° angle, which is known as overlap.

4 Result of analysis

In Table 1 one can see the values of the displacement results in the X and Z axis direction for each bicycle frame.

From Figures 3-9 one can see the values displacements for all the three-materials frame bicycle that are written in Table 1.

According to testing, the steel frame is more rigid than the aluminium and carbon frames. This indicates that the steel frame is flexible and has less X and Z axis movement. The bike's handling depends on X and Z axis shifts since they have an impact on the bike's stability and handling.

A carbon frame, on the other hand, is less expensive than other frames. A carbon frame will therefore have more X and Z axis shifts, which may compromise its handling and stability. A carbon frame does, however, have some benefits. Compared to a steel frame, it is significantly lighter and more corrosion resistant. This indicates that a carbon frame will last longer and be more durable. At the bottom of tube 4 in Figure 2, a force of 1.5 kN is applied and at an angle of 7° as a foot sweep on the bicycle pedal.

A steel frame bicycle is a particular kind of bicycle with a frame predominantly made of steel tubing. Steel has long been a favourite material for bicycle frames because of its strength, longevity and smooth riding.

The following are some salient features and benefits of bicycles with steel frames.

Steel is a solid material for bicycle frames because of its high strength-to-weight ratio and reputation for strength. Steel frames are appropriate for touring, commuting and off-road cycling because they can resist challenging riding conditions, high loads and challenging terrain, [15].

Undoubtedly, aluminium is the most popular material for bicycle frames. It can be found on a variety of bicycles. Not to mention that it offers a very nice weight/stiffness ratio and a fair price/performance ratio.

Currently, it is primarily utilized on less expensive bikes. Since aluminium is less rigid than steel, it requires thicker walls and greater diameter. Despite having relatively thicker tubes, aluminium frames are nonetheless lighter than the steel frames. Yet, there are disadvantages of using aluminium for bicycle frames. The material does not dampen vibrations as effectively as other materials. Aluminium can also break over time and is significantly less robust owing to material fatigue.

Do not have to worry, it takes many years and some hard driving to fatigue the material and a strong impact to break it, [15].

The majority of more expensive and professional frames are made with this material. Carbon sheets are bonded together to create carbon frames using an adhesive substance like resin. Because of this, carbon fibre frames are utilized in the most serious contests, including:

- Tour de France,
- UCI downhill world cup,
- World enduro series (EWS).

Carbon has the added benefit of making such bikes look considerably nicer. Shapes that are generally impractical with other materials can be made by designers. Because of this, designers can use their imagination to produce not unique designs but the stiffer frames, as well.

On a carbon frame, there are also no welds, leaving all the lines incredibly sleek, [15].

5 Conclusions

The structural design of the bicycle frame, by the established criteria, is developed in this paper. The shape of a bicycle frame is extremely challenging in terms of structural design, which requires attention to several details during the construction or modelling. The frame design is crucial to the rest of the bicycle manufacturing process, as it will determine how the final product will function as a whole. For the bike to be enjoyable and efficient to ride, its design and dimensions should be tailored to riders and their preferences. The last but not the least, the frame should be visually appealing and have an intriguing design to catch the rider's eye. Creo Parametric was used to develop the structure of this bicycle frame according to the best practise described in [16-18].

The design of a bicycle frame can be effectively simulated using the simulation software. A particular bicycle frame served as the basis for simulation. Comparisons were made between the outcomes of a specific construction made of three distinct materials. In more detail, it is a frame with steel, aluminium and carbon fibre reinforcements. We applied the same boundary conditions and force to the bicycle frame for each of these models according to the methods described in [19-21]. We examined these bicycle constructions using simulation software developed by Marc.

Overall, in this paper is shown that the correct choice of material, for a given design and simulation, can lead to a significant improvement in the performance of a bicycle frame and provide the rider with a more comfortable and efficient ride.

Currently, experts are trying to create a carbon frame and get to the parameters of a steel frame using the topological optimization.

Acknowledgements

The research was supported by the Cultural and Educational Grant Agency of the Ministry of Education, Science, Research and Sport of the Slovak Republic under the project No. 045ZU- 4/2021.

Conflicts of interest

The authors declare that they have no known competing financial interests or personal relationships that could have appeared to influence the work reported in this paper.

References

[1] SHELLER, M., URRY, J. The new mobilities paradigm. *Environment and Planning A: Economy and Space* [online]. 2006, **38**(2), p. 207-226. ISSN 0308-518X, eISSN 1472-3409. Available from: https://doi.org/10.1068/a37268

[2] COHEN, B., KIETZMANN, J. Ride on! Mobility Business Models for the Sharing Economy. *Organization and Environment* [online]. 2014, **27**(3), p. 279-296. ISSN 1086-0266, eISSN 1552-7417. Available from: https://doi.org/10.1177/1086026614546199

[3] LI, Q., JI, H., SHEN, Z., YE, G. Data-driven tight frame construction and image denoising. *Applied and Computational Harmonic Analysis* [online]. 2014, **37**(1), p. 89-105. ISSN 1063-5203, eISSN 1096-603X. Available from: https://doi.org/10.1016/j.acha.2013.10.001

[4] HANGGLI, R., KRIESI, H. Frame construction and frame promotion (strategic framing choices). *American Behavioral Scientist* [online]. 2012, **56**(3), p. 260-278. ISSN 0002-7642, eISSN 1552-3381. Available from: https://doi.org/10.1177/0002764211426325

[5] ZAJC, P., BERZELAK, N. Riding styles and characteristics of rides among Slovenian mountain bikers and management challenges. *Journal of Outdoor Recreation and Tourism* [online]. 2016, **15**, p. 10-19. ISSN 2213-0780, eISSN 2213-0799. Available from: https://doi.org/10.1016/j.jort.2016.04.009

[6] VANSTEENWEGEN, P., SOUFFRIAU, W., VAN OUDHEUSDEN, D. The orienteering problem: a survey. *European Journal of Operational Research* [online]. 2011, **209**(1), p. 1-10. ISSN 0377-2217, eISSN 1872-6860. Available from: https://doi.org/10.1016/j.ejor.2010.03.045

[7] PAL, A., ZHANG, Y. Free-floating bike sharing: solving real-life large-scale static rebalancing problems. *Transportation Research Part C-Emerging Technologies* [online]. 2017, **80**, p. 92-116. ISSN 0968-090X, eISSN 1879-2359. Available from: https://doi.org/10.1016/j.trc.2017.03.016

[8] USAMENTIAGA, R., IBARRA-CASTANEDO, C., KLEIN, M., MALDAGUE, X., PEETERS, J., SANCHEZ-BEATO, A. Nondestructive evaluation of carbon fiber bicycle frames using infrared thermography. *Sensors* [online]. 2017, **17**(11), 2679. eISSN 1424-8220. Available from: https://doi.org/10.3390/s17112679

[9] DE VOLDER, M., TAWFICK, S., BAUGHMAN, R. H., HART, A. Carbon nanotubes: present and future commercial applications. *Science* [online]. 2013, **339**(6119), p. 535-539. ISSN 0036-8075, eISSN 1095-9203. Available from: https://doi.org/10.1126/science.1222453

[10] HSIAO, S., CHEN, R., LENG, W. L. Applying riding-posture optimization on bicycle frame design. *Applied Ergonomics* [online]. 2015, **51**, p. 69-79. ISSN 0003-6870, eISSN 1872-9126. Available from: https://doi.org/10.1016/j.apergo.2015.04.010

[11] LIU, T. J.-CH., WU, H.-CH. Fiber direction and stacking sequence design for bicycle frame made of carbon/epoxy composite laminate. *Materials and Design* [online]. 2010, **31**(4), p. 1971-1980. ISSN 0261-3069. Available from: https://doi.org/10.1016/j.matdes.2009.10.036

[12] XIAO, D., LIU, X., DU, W., WANG, J., HE, T. Application of topology optimization to design an electric bicycle main frame. *Structural and Multidisciplinary Optimization* [online]. 2012, **46**(6), p. 913-929. ISSN 1615-147X, eISSN 1615-1488. Available from: https://doi.org/10.1007/s00158-012-0803-7

[13] TOMASZEWSKI, T. Fatigue life analysis of steel bicycle frame according to ISO 4210. *Engineering Failure Analysis* [online]. 2021, **122**, 105195. ISSN 1350-6307, eISSN 1873-1961. Available from: https://doi.org/10.1016/j.engfailanal.2020.105195

[14] CICERO, S., LACALLE, R., CICERO, R., FERNANDEZ, D. M., MENDEZ, D. Analysis of the cracking causes in an aluminium alloy bike frame. *Engineering Failure Analysis* [online]. 2011, **18**(1), p. 36-46. ISSN 1350-6307, eISSN 1873-1961. Available from: https://doi.org/10.1016/j.engfailanal.2010.08.001

[15] AKOO (in Slovak) [online] [accessed 2023-03-30]. Available from: https://akoo.sk/ako-vybrat-material-ramu-na-bicykel/

[16] HRCEK, S., SMETANKA, L., STEININGER, J., PATIN, B. Increase of durability in the area of line contact with curved body geometry. *Mechanism and Machine Theory* [online]. 2022, **176**, 105010. ISSN 0094-114X, eISSN 1873-3999. Available from: https://doi.org/10.1016/j.mechmachtheory.2022.105010

[17] SKYBA, R., HRCEK, S., SMETANKA, L., MAJCHRAK, M. Creation of calculation 3D model of slewing bearing. In: *Current methods of construction design. Lecture notes in mechanical engineering* [online]. MEDVECKY, S., HRCEK, S., KOHAR, R., BRUMERCIK, F., KONSTANTOVA, V. (eds.). Cham: Springer, 2018. ISBN 978-3-030-33145-0, eISBN 978-3-030-33146-7, p. 149-157. Available from: https://doi.org/10.1007/978-3-030-33146-7_18

[18] STEININGER, J., HRCEK, S., SMETANKA, L., SKYBA, R. Optimisation procedure of inner geometry in spherical roller bearings with regard to their durability. *Scientific Journal of Silesian University of Technology-Series Transport* [online]. 2020, **106**, p. 173-181. ISSN 0209-3324, eISSN 2450-1549. Available from: https://doi.org/10.20858/sjsutst.2020.106.15

[19] HRCEK, S., BRUMERCIK, F., SMETANKA, L., LUKAC, M., PATIN, B., GLOWACZ, A. Global sensitivity analysis of chosen harmonic drive parameters affecting its lost motion. *Materials* [online]. 2021, **14**(17), 5057. eISSN 1996-1944. Available from: https://doi.org/10.3390/ma14175057

[20] SKYBA, R., HRCEK, S., SMETANKA, L., MAJCHRAK, M. Strength analysis of slewing bearings. *Transportation Research Procedia* [online]. 2019, **40**, p. 891-897. ISSN 2352-1457, eISSN 2352-1465. Available from: https://doi.org/10.1016/j.trpro.2019.07.125

[21] WEIS, P., KUCERA, L., PECHAC, P., MOCILAN, M. Modal analysis of gearbox housing with applied load. *Procedia Engineering* [online]. 2017, **192**, p. 953-958. ISSN 2352-1457, eISSN 2352-1465. Available from: https://doi.org/10.1016/j.proeng.2017.06.164

This is an open access article distributed under the terms of the Creative Commons Attribution 4.0 International License (CC BY 4.0), which permits use, distribution, and reproduction in any medium, provided the original publication is properly cited. No use, distribution or reproduction is permitted which does not comply with these terms.

NODE RINGING REDUCTION OF SYNCHRONOUS BUCK CONVERTER

Michal Frivaldský[1,*], Marcel Pčola[2], Zdeno Biel[2], Roman Kučera[2], Marek Franko[2], Roman Holček[2]

[1]Faculty of Electrical Engineering and Information Technologies, University of Zilina, Zilina, Slovakia
[2]EVPU a.s., Nova Dubnica, Slovakia

*E-mail of corresponding author: michal.frivaldsky@feit.uniza.sk

Michal Frivaldský 0000-0001-6138-3103, Marek Franko 0000-0003-1829-6455

Resume
This paper discusses the issue related to the switching regulators operated at high switching frequencies, where it is necessary to eliminate the influence of parasitic components of the converter's main circuit. In more detail it deals with the node-ringing phenomena, which is typical for synchronous buck converters. The existence of the parasitic inductances arising from the printed circuit board conductive paths, induce voltages, which are several times higher than nominal input voltage, thus it increases the risk of damage of the power transistors. Therefore, optimization of the circuit is required to reduce the voltage spikes and therefore improve safety margin related to nominal operation. In this paper, node-ringing phenomena is introduced, while the optimization methodologies for its reduction are described and verified by experimental analysis.

Article info
Received 24 May 2023
Accepted 13 June 2023
Online 22 June 2023

Keywords:
power transistor
switching noise
parasitics
snubber

Available online: https://doi.org/10.26552/com.C.2023.054

ISSN 1335-4205 (print version)
ISSN 2585-7878 (online version)

1 Introduction

Current situation in the field of power electronic systems records massive expansion concerning breaking the usual trends. Here we are talking about development of the power semiconductor devices, while significant results are being achieved in terms of performance improvements, as well. The silicon carbide (SiC) is currently leading technology for high-voltage applications, such as electric vehicles, power supplies, motor control circuits and inverters for renewables. This technology offers several advantages over the standard silicon-based power semiconductor devices (IGBT, MOSFETs), which have been used for a long time as the main solution, due to their cost-effectiveness (Figure 1). Due to increasing demands on power density and efficiency of the power systems, the advent of new technological solutions represents a natural process of modernization of all the conventional, as well as specific performance electronic systems [1-3].

Designers of new, more demanding applications such automotive electrical systems and electric vehicles concluded that the new SiC and GaN technologies of power semiconductor structures, with their properties, are more suitable to achieve the desired results [4-5].

Just as modern technologies provide benefits, the use of modern devices also brings certain risk and pitfalls. As was mentioned, power - supply efficiency becomes increasingly important, meeting the high power densities means increasing the switching speed, so the negative trade-offs, like the electromagnetic interference, may occur (Figure 2). Here it is very sensitive issue, which is directly connected to practical design of any power converter, i.e. the printed circuit board (PCB) design represents the design challenge to prevent any unwanted phenomenon. In connection to requirements defined for modern power supplies, the high switching frequencies are required for their operation. One of the negative consequences when dealing with the PCB design and high frequency operation is generation of so-called node-ringing. Parasitic elements of the PCB or device package are responsible for transistor voltage node ringing, which should be optimized to prevent from damage of the component. The effects of these parasites are unexpectedly large and it often happens that a circuit, even if designed without problems, may

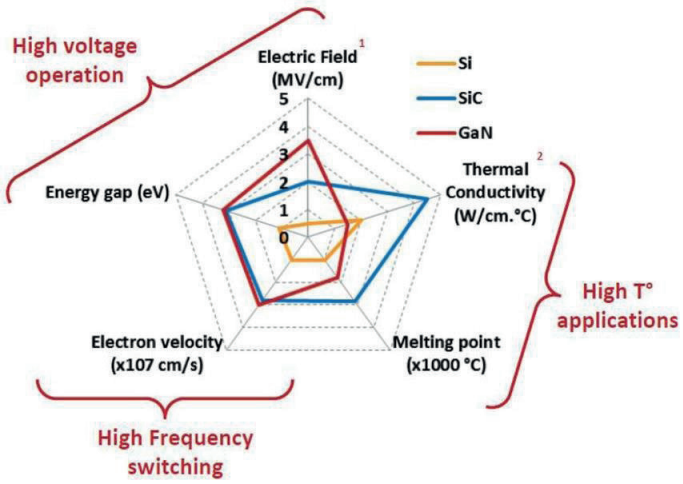

Figure 1 *Comparison of the electrical and operational properties of Si, SiC and GaN technologies of power semiconductor devices*

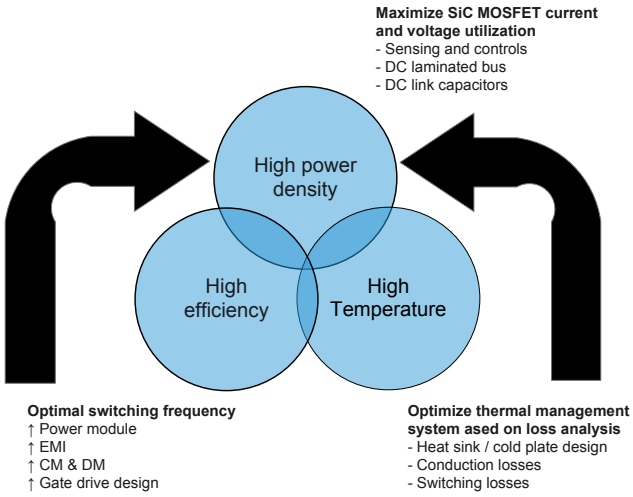

Figure 2 *Diagram representing key demands on the switched mode power supplies*

not operate properly, depending on the layout, due to insufficient attention being paid to these parasitic components [6-7].

In this paper, the focus is given on analysis of the node-ringing origin and its consequence regarding the power loss generation. The study is performed with synchronous buck converter, whose application is redundant power supply system. Initial analysis of the node-ringing is consequently modeled using verified circuit simulation model, while several methods how to the reduce node-ringing phenomenon are being described, as well.

2 Reasons of the node ringing generation

2.1 Main circuit desctiption regarding the node ringing generation

Increasing number of industrial applications, require low output voltage/high current converters. That is related to efficiency maximization, so the buck regulators are of interest when dealing with the power loss minimization. The high output current applications are specific, since the modular converters operated in parallel are utilized to reduce the thermal stress of power components. To be able to provide reliable and safe operation, the minimization of any negative phenomena is a must, while the node-ringing represents a major issue, which must be eliminated for buck regulators operating in a modular system.

Figure 3 shows the principal schematics of synchronous buck converter including the parasitic components of the main circuit. Those are inductances of wirings of PCB and capacitances, which are parasitic components of power transistor itself. The presence and the effect of these parasites is the matter of this research, more precisely the way how to reduce their impact is the main issue. During the converter operation, they are responsible for unwanted oscillations of voltage and current waveforms and the result is overvoltage and overcurrent spikes generation, which negatively affect

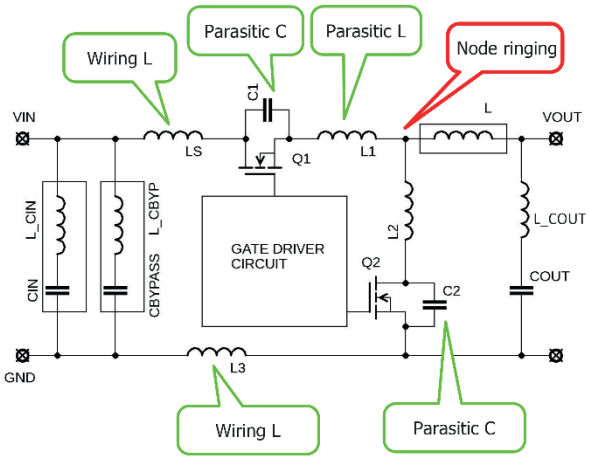

Figure 3 *Principle schematic of synchronous buck converter including the parasitic components*

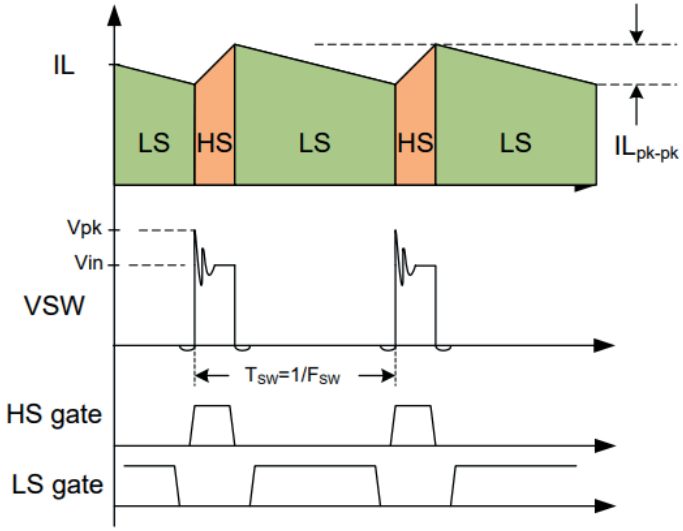

Figure 4 *Time waveforms of synchronous buck converter indicating the node-ringing voltage*

the electromagnetic interference of the power system.

Figure 4 shows time waveforms of converter shown on Figure 3, introducing node-ringing effect, what is seen at the waveform of bottom power switch drain-source voltage.

The principal operation of the synchronous buck converter, operated in continuous conduction mode (CCM), considering nominal conditions, is based on the alternative high-side MOSFET and low-side MOSFET conduction of inductor current during each switching cycle. Cycle initialization is characterized by the green interval when low-side transistor is turned and is carrying the inductor current. After that, the LS MOSFET is turned off and the inductor current is freewheeling through the body diode of the low-side MOSFET. After a short dead time, the HS MOSFET switches on, starting the next conduction interval of inductor current. As the body diode undergoes reverse recovery, the voltage on SW begins to rise and the ringing waveform results from the interaction of parasitic inductances and the switch node capacitance (primarily consisting of the C_{OSS} of the low-side MOSFET) [8]. It must be noticed here that the overvoltage spike caused by node ringing can achieve multiples of the nominal blocking voltage of the transistor, thus possibly leading to its destruction. The amount of this spike directly depends on the value of parasitic inductances of wirings and the reverse recovery of used power semiconductor component [9].

Secondarily, the node-ringing effect affects the operational efficiency of the converter itself, therefore it is worth to deal with the elimination or reduction of the causes that are responsible for the generation of this undesirable phenomenon.

3 Physical prototype of analyzed synchronous buck regulator

Analyzed converter topology is synchronous buck rectifier with interleaved topology. Figure 5 shows the physical prototype of one synchronous buck module,

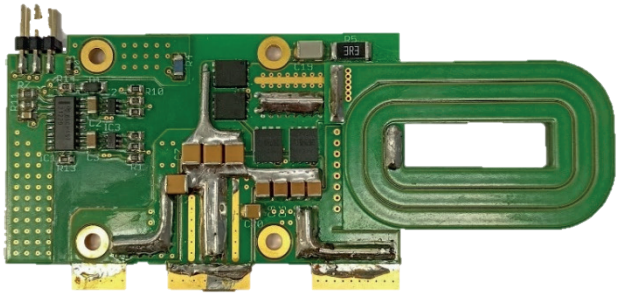

Figure 5 *Module of power converter*

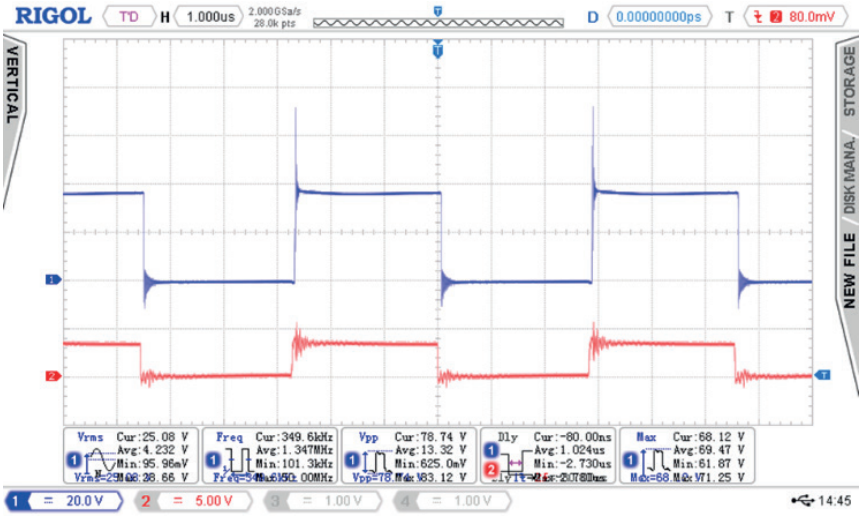

Figure 6 *Drain to source voltage waveform (top) for nominal power of synchronous buck regulator module from Figure 5*

while when it serves for the modular PSU design it contains two. The phase delay between switching of those modules is 180° to reduce the output voltage and current ripple. The modular PSU is designed for supplying the high-power ASIC microchips or high power MCU's where the low voltage and high currents are requested. The modules are constructed on the 6-layer FR4 printed circuit board, where the thickness of internal copper layers is 105 µm and external layers are plated to thickness of 130 µm. The bottom side of PCB is equipped by aluminum heatsink for cooling the power transistors.

Basic parameters for one module:

- Nominal input voltage: 36 V
- Output voltage: 12-22 V
- Maximal output current per module: 35 A
- Maximal output power per module: 600 W
- Maximal eficiency of module: 98.8 %
- Power transistors: 027N10N6 (Infineon)

The complete PSU contains 3 channels (6 power modules) where the maximal output power of one channel is 1200 W and then the maximal output power of whole PSU is 3600 W. As described earlier, the node ringing is one of the problematic issues, which needs to be optimized in buck synchronous regulators. For designed physical sample, measurement of the drain-source voltage of the low-side transistor (Figure 6) indicates, that the optimization should be performed here, as well. The value of the voltage spike, generated on the low-side transistor, is twice the value of the input voltage, i.e. 72 V. In the next part of this paper, two alternatives for optimization are being analyzed, while efficiency of the converter and drain-source voltage peak reduction are the main variables, which are evaluated.

4 Simulation analysis of the node ringing reduction

For the purposes of evaluation, which procedure represents effective solution for the node ringing reduction, it was decided to design the verified simulation model with high level of accuracy [10-12]. For this purpose, the development of the PSpice circuit was performed utilizing highly accurate models of power transistors (ST microelectronics - STL135N8F7AG), which are equipped within physical prototype, as well. The simulation model of the main power circuit is shown in Figure 7. Main circuit contains parasitic components as well, which are responsible for the node ringing generation (stray inductances).

From initial simulation result (Figure 8) it is seen that the voltage spike, generated during the transistor switching, is reaching twice the voltage of the DC supply

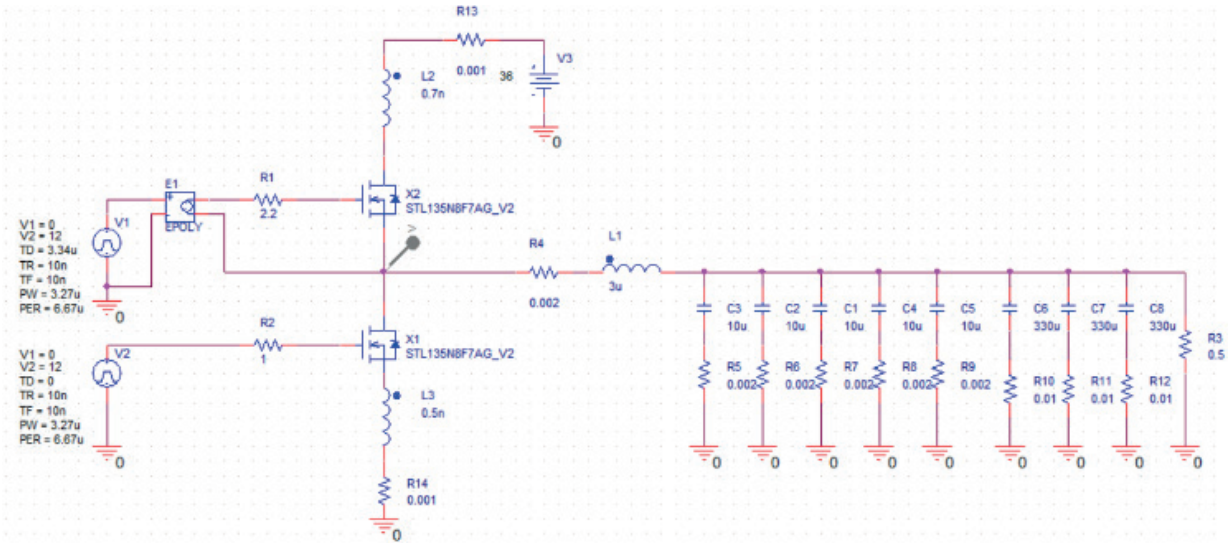

Figure 7 *Simulation model of the considered synchronous buck regulator for the node ringing reduction analysis*

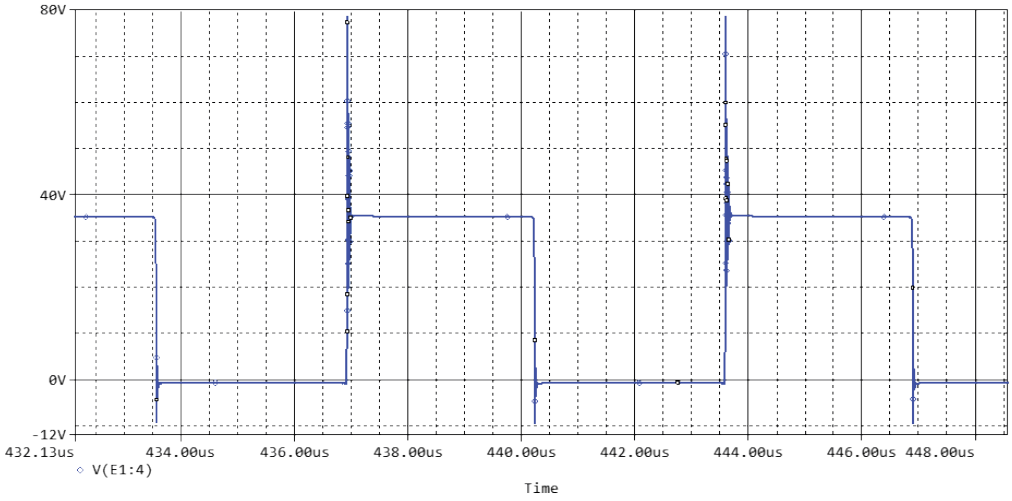

Figure 8 *Simulation result for the drain to source voltage waveform for nominal power of synchronous buck regulator module from Figure 7*

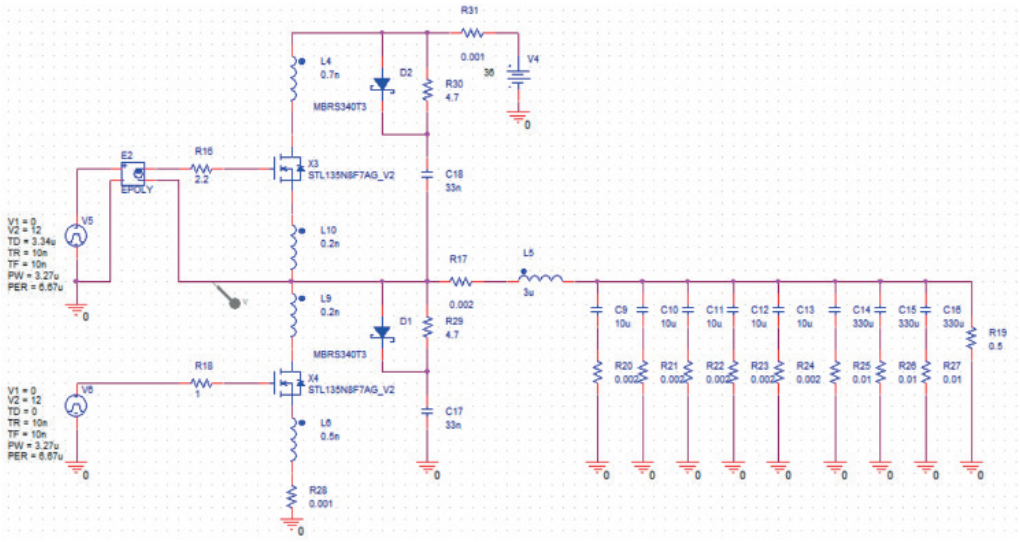

Figure 9 *Simulation model of the considered synchronous buck regulator with snubbers for the node ringing reduction analysis*

voltage. Comparing this result to the measurement (Figure 6), it can be deduced that the result is verified and similar, so the optimization procedure would give the adequate results and information for the optimization needs. We have analyzed two methodologies for the node ringing reduction:

- Slowing the turn-on of the low-side transistor (25 % slow down compared to non-optimized)
- Using the snubber circuits (for studied case: R = 4.7 Ω, C = 33 nF, D = MBRS340T3 Schottky)

According to the first method, reduction of the transistor switching speed may reflect within the increase of the total switching losses of the device, because the transition within the linear region of the volt-amp characteristics is lasting longer. Therefore, the optimal compromise between the reduction of ringing voltage and increase of switching loss must be met. Regarding the second method, it is expected that the power losses of the converter would increase due to fact, that the RCD snubber represents passive snubber circuit dissipating the energy coming from the node-ringing oscillations.

The simulation experiments for the first method have been realized using schematics shown in Figure 8, while for the second method schematics from Figure 9 was used.

As was initially mentioned, two variables are under investigation, i.e. efficiency within the whole power range and drain - source voltage peak caused by the node ringing. Figure 10 shows dependency of the efficiency on output power, while the non-optimized converter is compared to applied methods for the node-ringing reduction. It is seen from the results, that the highest efficiency is achieved for the non-optimized solution. The lowest value of the efficiency within whole power range states for the RCD snubber method, what reflects increased energy dissipation due to RCD snubber functionality, i.e., it dissipates the energy originating from the node ringing overvoltage. If slowing the low-side transistor turn on the process, higher efficiency is obtained, while for 100 % P_{OUT}, the value is 95.24 % what is 1.38 % lower compared to non-optimized solutions and 0.73 % higher compared to the RCD snubber result.

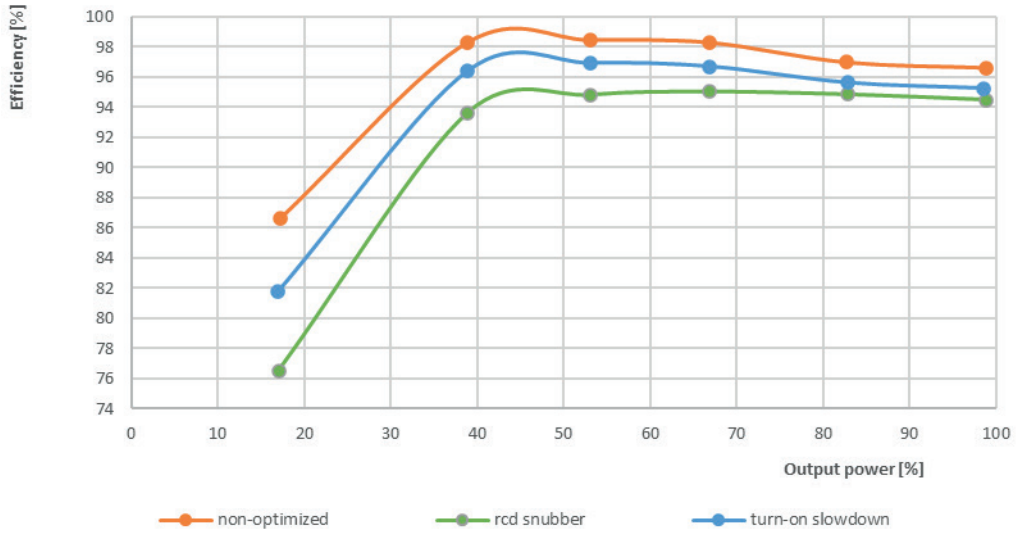

Figure 10 *Efficiency dependency on the output power of the studied converter for the non-optimized sollution and two investigated approaches*

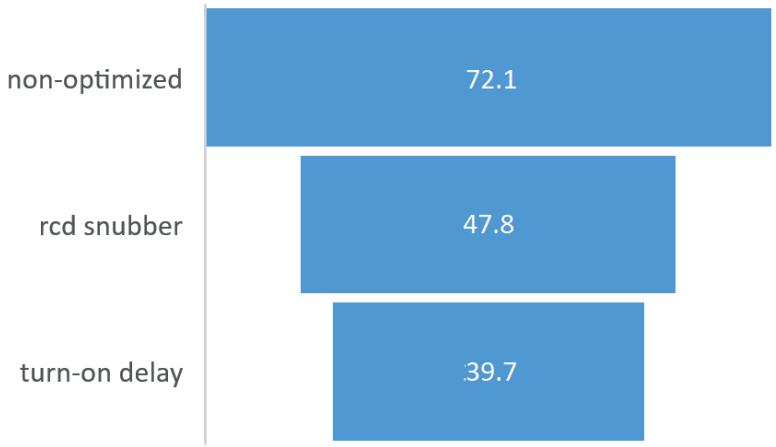

Figure 11 *Voltage spike value for individual study cases*

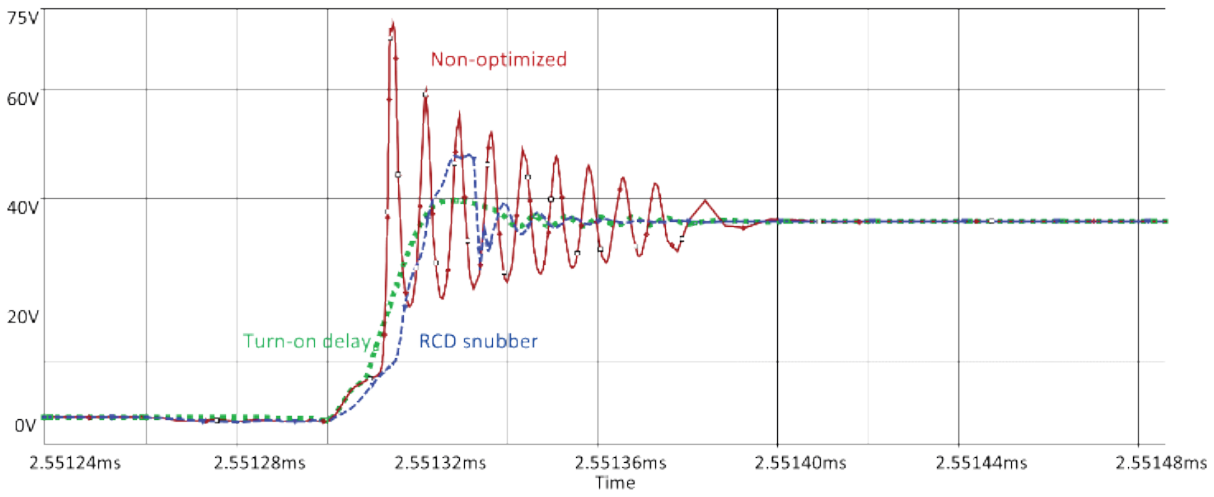

Figure 12 *Time waveform of node-ringing voltage for studied converter and optimization methodologies*

Figure 11 is showing evaluation of the results related to the drain-source peak voltage for the low side transistor of synchronous buck converter. The nominal input voltage is 36 V, while from the results it is seen that the non-optimized solution reached twice the value of input voltage. Considering the RCD snubber, the reduction of the voltage spike by 34 % was achieved, while for the turn-on delay method, reduction reached 45 %. The time waveforms comparison of these results is shown in Figure 12.

5 Conclusion

In this paper, the verification of methodologies for the node-ringing reduction has been the main focus of interests. Initially, discussion, related to the current progress within the power semiconductor technology development, was provided; followed by the description of the synchronous buck converter, the phenomena of node-ringing generation were introduced, as well. It was presented that this issue is dangerous considering the overvoltage damage of the power transistor used within the main circuit. Optimization for reduction is therefore required, while several methodologies are already available. Instead of the printed circuit board layout optimization, there are also other methodologies, which are based on the circuit modification. Here two alternatives have been verified. Once the prototype of the power converter was presented, the node-ringing voltage was measured as well to see the amount of overvoltage generation. The voltage spike reached twice the value of the input voltage of the converter. This result shows, how important it is to prevent from overvoltage damage, when the node-ringing is present. Another issue is electromagnetic emissions (EMI) optimization as well. The evaluation of the optimization methodology influence was provided through the verified circuit simulation model. We investigated the RCD snubber application and methodology, which is characterized by the turn-on slowdown of low-side transistor. The achieved results evaluated the efficiency performance for individual study cases and the amount of voltage spike reduction. From the results is seen that the turn-on slowdown improves voltage spike reduction by 45 % compared to the non-optimized solution. On the other hand, it was negatively reflected in the reduction of efficiency by almost 1.4 % compared to the non-optimized solution. As a conclusion it must be deduced that the node-ringing phenomena is unwanted as it harms the performance of the converter, from the EMI point of view, as from the safe and stable operation.

Acknowledgment

This publication was realized with support of Operational Program Integrated Infrastructure 2014 - 2020 of the project: Innovative Solutions for Propulsion, Power and Safety Components of Transport Vehicles, code ITMS 313011V334, co-financed by the European Regional Development Fund.

Conflicts of interest

The authors declare that they have no known competing financial interests or personal relationships that could have appeared to influence the work reported in this paper.

References

[1] SHAH, F. M., XIAO, H. M., LI, R,. AWAIS, M., ZHOU, G., BITEW, G. T. Comparative performance evaluation of temperature dependent characteristics and power converter using GaN, SiC and Si power devices. In: 2018 IEEE 12th International Conference on Compatibility, Power Electronics and Power Engineering CPE-POWERENG 2018: proceedings [online]. IEEE. 2018. eISSN 2166-9546, p. 1-7. Available from: https://doi.org/10.1109/CPE.2018.8372523

[2] SKAROLEK, P., LETTL, J. Influence of deadtime on Si, SiC and GaN converters. In: 2020 21st International Scientific Conference on Electric Power Engineering EPE: proceedings [online]. IEEE. 2020. eISSN 2376-5631, p. 1-4. Available from: https://doi.org/10.1109/EPE51172.2020.9269208

[3] ZHANG, Y., XIAO, M., MA, Y., CHENG, K. 10 kV GaN power diodes and transistors with performance beyond SiC limit. In: 2022 6th IEEE Electron Devices Technology and Manufacturing Conference EDTM: proceedings [online]. IEEE. 2022. eISBN 978-1-6654-2178-2, p. 113-115. Available from: https://doi.org/10.1109/EDTM53872.2022.9797920

[4] AL-BAYATI, A. M. S., ALHARBI, S. S., ALHARBI, S. S., MATIN, M. A comparative design and performance study of a non-isolated DC-DC buck converter based on Si-MOSFET/Si-Diode, SiC-JFET/SiC-schottky diode and GaN-transistor/SiC-Schottky diode power devices. In: 2017 North American Power Symposium NAPS: proceedings [online], IEEE. 2017. eISBN 978-1-5386-2699-3, p. 1-6. Available from: https://doi.org/10.1109/NAPS.2017.8107192

[5] ALHARBI, S. S., ALHARBI, S. S., AL-BAYATI, A. M. S., MATIN, M. Design and performance evaluation of a DC-DC buck-boost converter with cascode GaN FET, SiC JFET and Si IGBT power devices. In: 2017 North American Power Symposium NAPS: proceedings [online]. IEEE. 2017. eISBN 978-1-5386-2699-3, p. 1-6, Available from: https://doi.org/10.1109/NAPS.2017.8107322

[6] KANTAVARA, S., KUMMANEE, P., SAWACHAN, H., BILSALAM, A. high frequency interleave technique based on high step-up push-pull resonant converter modules. In: 2021 18th International Conference on Electrical Engineering/Electronics, Computer, Telecommunications and Information Technology ECTI-CON: proceedings [online]. IEEE. 2021. eISBN 978-1-6654-0382-5, p. 918-921. Available from: https://doi.org/10.1109/ECTI-CON51831.2021.9454943

[7] LIN, C., SONG, O., WANG, J. A new high efficiency and high power density 48V to 1V converter. In: 2021 IEEE 1st International Power Electronics and Application Symposium PEAS: proceedings [online]. IEEE. 2021. 978-1-6654-1360-2, p. 1-3. Available from: https://doi.org/10.1109/PEAS53589.2021.9628611

[8] AN-4162-switch node ring control in sznchronous buck regulators [online]. 2013. Available from: https://fairchildsemi.com

[9] CHEN, Z., AMARO, I. Optimizing low side gate resistance for damping phase node ringing of synchronous buck converter. In: 2012 IEEE Energy Conversion Congress and Exposition ECCE: proceedings [online]. IEEE. 2012. ISSN 2329-3721, eISSN 2329-3748, p. 1827-1832. Available from: https://doi.org/10.1109/ECCE.2012.6342590

[10] BOTTARO, E., CACCIATO, M., RAFFA, A., RIZZO, S. A., SALERNO, N., VENEZIANO, P. P. Development of a SPICE modelling strategy for power devices in GaN technology. In: 47th Annual Conference of the IEEE Industrial Electronics Society IECON 2021 [online]. IEEE. 2021. eISSN 2577-1647, p. 1-6. Available from: https://doi.org/10.1109/IECON48115.2021.9589710

[11] NARDO, D., SCUTO, A., BUONOMO, S., CHIANTELLO, M., CACCIATO, M., SCARCELLA, G., RIZZO, S. A. GaN HEMT power losses modeling and evaluation in resonant LLC converters. In: 2022 IEEE Applied Power Electronics Conference and Exposition APEC: proceedings [online], IEEE. 2022. eISSN 2470-6647, p. 1637-1644. Available from: https://doi.org/10.1109/APEC43599.2022.9773758

[12] CACCIOTTO, F., SCIORTINO, M., TERMINI, D., CACCIATO, M., RIZZO, S. A., SCELBA, G. Power loss modelling and efficiency optimization of a multi-output Flyback converter. In: 47th Annual Conference of the IEEE Industrial Electronics Society IECON 2021: proceedings [online]. IEEE. 2021. eISSN 2577-1647, p. 1-6. Available from: https://doi.org/10.1109/IECON48115.2021.9589886

This is an open access article distributed under the terms of the Creative Commons Attribution 4.0 International License (CC BY 4.0), which permits use, distribution, and reproduction in any medium, provided the original publication is properly cited. No use, distribution or reproduction is permitted which does not comply with these terms.

EFFICIENCY COMPARISON OF Si IGBT AND SiC MOSFET BASED THREE-PHASE INVERTERS

Zdeno Biel[1,*], Marcel Pčola[1], Jozef Ondrejička[1], Marek Franko[1], Michal Frivaldský[2]

[1]EVPU a.s., Nova Dubnica, Slovakia
[2]Faculty of Electrical Engineering and Information Technologies, University of Zilina, Zilina, Slovakia

*E-mail of corresponding author: biel@evpu.sk

Marek Franko 0000-0003-1829-6455, Michal Frivaldský 0000-0001-6138-3103

Resume
This article deals the implementation of a SiC MOSFETs in a three-phase inverter module, intended for use in auxiliary converters for powering electrical appliances of railway wagons. The basic properties of the SiC semiconductor elements and their differences, compared to IGBT modules, are summarized here. The given block diagram describes the individual blocks of the inverter module and their interconnection. Finally, a measuring setup for measuring the efficiency of inverters is presented. The measured efficiency values of the proposed SiC inverter and the original solution with IGBT modules are compared in the given graphs.

Article info
Received 12 May 2023
Accepted 14 June 2023
Online 27 June 2023

Keywords:
wide band gap
converter
silicon carbide
inverter
efficiency

Available online: https://doi.org/10.26552/com.C.2023.057

ISSN 1335-4205 (print version)
ISSN 2585-7878 (online version)

1 Introduction

In railway applications, voltage source inverters are widely used in various AC power systems. Inverters of the megawatt power are used for powering and controlling the traction motors. In the auxiliary converters, inverters with a power in tens of kW are used to generate an AC network with a fixed or variable frequency for powering auxiliary drives of locomotives or electrical appliances and systems of heating, ventilation and air conditioning (HVAC) of wagons.

Currently, the emphasis in railway transport is on reducing power losses. This results in increasing the efficiency of such devices. Thanks to this, it is possible to achieve a significant savings in the energy consumed during the mass deployment of such modern devices in operation. The effect of this is not only the improvement of economic parameters, but a significant contribution in the field of ecology, as well. The application of new materials and technologies in the field of power electronics also makes it possible to increase the power density of converters. This means that it is possible to reduce the overall dimensions and weight of the devices when using such modern components. One of the key areas of research, related to the field of power converters, is research in the field of semiconductor materials and related technologies. In recent years, attention has been drawn to semiconductor structures with a wide band gap (WBG). These are mainly semiconductor elements (diodes and transistors) based on silicon carbide (SiC) and gallium nitride (GaN). One of the main characteristics of GaN and SiC semiconductors is the high mobility of electrons (therefore, such transistors are often referred to by the abbreviation HEMT - High Electron Mobility Transistor). Thanks to this, it is possible to achieve significantly lower switching losses when using these elements in semiconductor converters, which allows a significant increase in switching frequency compared to converters using conventional silicon (Si) - based semiconductor elements.

According to research work comparing individual losses in WBG semiconductors with Si-based components, the SiC elements, depending on the switching frequency, can achieve 70 % lower losses compared to Si elements and GaN-based elements additional 70 % lower losses compared to SiC elements. At the same temperature on the chip, it is possible to achieve 1.6 times higher output current or 4.6 times higher switching frequency when using the SiC modules compared to Si IGBTs. The reduction of switching losses by applying the GaN-based semiconductor elements makes it possible to achieve a substantial increase in the overall efficiency of the power converter, and thus a subsequent reduction in electricity consumption. The

possibility of applying a significantly higher switching frequency in the converter allows the use of magnetic components (high-frequency transformers and chokes) with smaller dimensions and weight. This fact, together with reduced requirements for cooling SiC-based semiconductor elements due to lower switching losses, leads to a reduction in the dimensions and weight of such power converters [1-2]. The report [3] provides an estimate of the energy savings' potential in various application areas when using WBG elements; it shows the expected technological readiness of various devices and outlines preliminary ways of possible regulations that would speed up the market entry of applications based on WBG elements.

2 Implementation of an SiC MOSFETs into a three-phase inverter module.

A three-phase inverter module with a maximal output power of 52 kW was chosen for implementation of the SiC MOSFETs. The expected use of this inverter module is in auxiliary converters of railway wagons. The inverter ensures the conversion of the 680V DC bus voltage into the output three-phase voltage for powering the appliances and the HVAC system of the wagon.

The SiC MOSFETs are manufactured in a wide range of rated currents, with the most common voltage levels being 1200 V and 1700 V. In some cases, manufacturers of SiC elements strive for case compatibility with Si IGBTs to allow a direct replacement. For higher operating frequencies, cases with eliminated parasitic inductances are preferable due to the limitation of switching overvoltage.

Due to minimal structural modifications, the SiC MOSFETs in 62 mm cases, dimensionally compatible with the original IGBT modules FF200R12KT4, were used in the inverter. The SiC modules CAS300M12BM2 from the manufacturer Wolfspeed were chosen, which contain the two SiC MOSFETs in a half-bridge topology. The basic parameters of this module are: V_{DS} = 1.2 kV, $R_{DS(on)}$ = 5 mΩ. $I_{D90°C}$ = 285 A. Three such modules were used in the power circuit of the inverter. Each half-bridge is connected by a low-inductive busbar to the DC bus capacitors. To further reduce the resulting parasitic inductance, a local capacitive snubber was used on each SiC half-bridge. Schematic diagram of the inverter power circuit is shown in Figure 1.

When designing the converters based on SiC transistors, it is necessary to take into account the following differences compared to the IGBT elements:

- The gate voltage of SiC is usually higher, (18 V to 20 V).
- The negative voltage for turning off the SiC must not be too large (it is typically 0 to -5 V), because it causes the degradation in long-term operation.
- The threshold voltage V_{gs} is usually lower in SiC (2.2-5.6 V). This increases the demands on the design (resistance to disturbances and influence of the du/dt of the collector voltage on the excitation).
- SiC behaves like a resistor, when increasing the current through SiC, the voltage drop on it increases linearly, unlike the IGBT.
- SiC has a very low short-circuit resistance and withstands high current only for a very short time, unlike the IGBT element, which usually withstands a short circuit for 10µs. However, turning it off too quickly will cause an overvoltage to enter the element. Therefore, it is desirable to minimize the parasitic inductance of the SiC components as well as the capacitors connected to the supply terminals of the element.
- The SiC MOSFETs achieves high du/dt slopes, which cause higher interference and the corresponding driver must have sufficient resistance, typically 100 kV/µs is required as a minimum.

For these reasons, it is necessary to pay great attention to design of the power circuits and SiC MOSFETs gate drivers [4].

To ensure a pure sinusoidal voltage with low harmonic distortion, a sinusoidal LC filter is connected to the output of the inverter. The phase currents of the inverter are measured by hall sensors. A sensor with galvanic separation is used to measure the DC bus

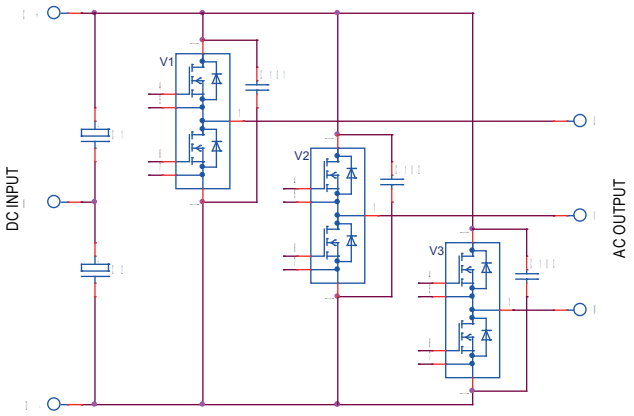

Figure 1 *Schematic diagram of the SiC inverter power circuit*

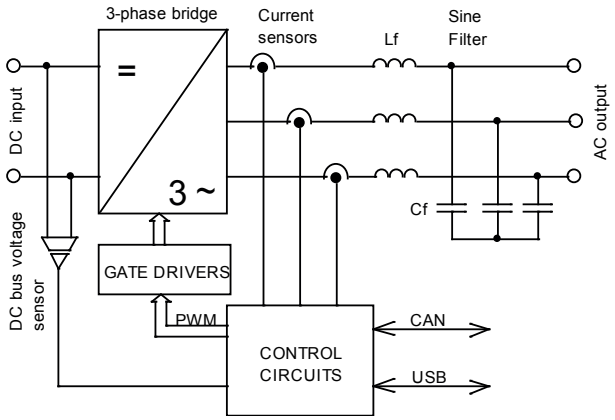

Figure 2 *Block diagram of the inverter*

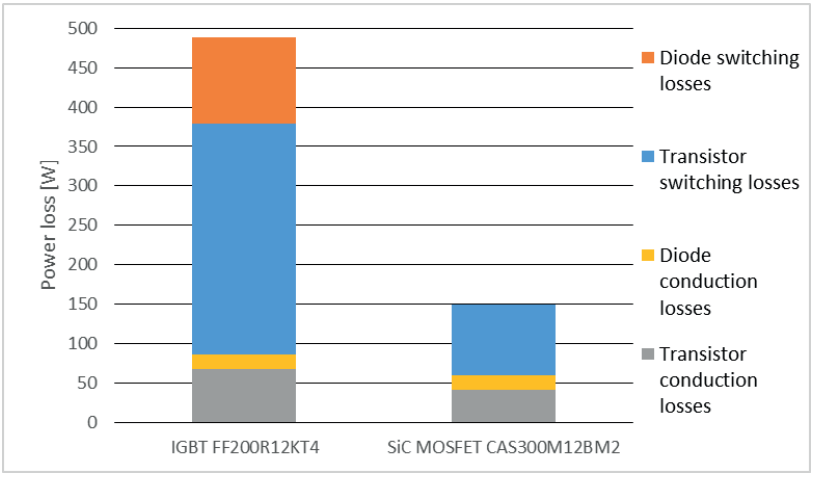

Figure 3 *Distribution of IGBT and SiC MOSFET module power losses when the inverter is loaded with a power of 52 kVA and a switching frequency is 15kHz*

voltage. Analog signals from the sensors are processed by the control circuit, which, based on the implemented control software in the digital signal processor, generates the PWM (pulsed width modulation) control signals for the gate drivers. The control circuit includes overcurrent and overvoltage protection, ensures communication with the superior system via the CAN bus, enables advanced diagnostics and parameter setting via USB.

The gate drivers ensure the generation of gate voltages suitable for SiC MOSFETs based on the PWM signals from the control circuit. In addition, they provide the short-circuit protection by immediately closing the transistors, when a short circuit occurs. The block diagram of the inverter including the sine filter is shown in Figure 2.

3 Analysis of power losses of IGBT and SiC MOSFET modules

Losses in power semiconductor components are divided into conduction losses P_{cond} and switching losses P_{sw}.

Conduction losses arise as a result of the voltage drop on the equivalent resistance of the transistor and u_{CE0} when the current flows in the switched on state. The average value of the conduction losses of the IGBT transistor can be expressed from the equivalent circuit as follows:

$$P_{cond\,IGBT} = u_{CEO} I_{CAV} + r_C I^2_{Crms}\,, \tag{1}$$

where u_{CE0} is on state zero current collector-emitter voltage and r_C is the collector emitter on-state resistance. I_{CAV} and I_{Crms} are the average and RMS values of transistor collector current, respectively.

The conduction losses of the anti-parallel freewheeling diode can be expressed similarly.

$$P_{cond\,D} = u_{D0} I_{DAV} + r_D I^2_{Drms}\,. \tag{2}$$

The conduction losses of the SiC MOSFET transistor can be easily calculated as the on-state resistance R_{Dson} losses when the current I_{DSrms} flows.

$$P_{cond\,MOSFET} = R_{DSon} I^2_{DSrms}\,. \tag{3}$$

The switching losses of the transistor and the diode can be expressed using the switching energy curves $E_{on} = f(I_C)$, $E_{off} = f(I_C)$, $E_{rec} = f(I_F)$, from the datasets of

power semiconductor modules.

$$P_{SW\,T} = (E_{on\,T} + E_{off\,T}) \cdot f_{SW}\,, \tag{4}$$

$$P_{SW\,D} = E_{rec} \cdot f_{SW}\,. \tag{5}$$

The reverse recovery energy E_{rec} of the SiC MOSFET body diode is very small, so it can be neglected.

Based on the above equations and data from the datasheets, the loss components for the IGBT module FF200R12KT4 and SiC MOSFET CAS300M12BM2 were calculated. Losses were calculated for a three-phase bridge at a nominal load of 52kVA at a power factor of 0.8 and for a switching frequency of 15 kHz. This is the maximum theoretical value of the switching frequency for the IGBT module to avoid the thermal overload of the chip at the given heat sink temperature resistance of 0.04 K/W. Individual loss components for IGBT and SiC MOSFET are graphically compared in Figure 3. Power loss values are shown for one half-bridge module. It can be seen from the graph that the total losses of the SiC module are one third compared to the IGBT module [5-8].

4 Efficiency measurement

To compare the achieved efficiencies of the new inverter to the SiC MOSFETs and the old IGBT inverter, a series of measurements was performed. The block diagram of the experimental setup is in Figure 4. The inverter module was placed in a test stand ensuring forced cooling and powered by a nominal voltage of 680V from a DC power supply. A sine filter, consisting of 0.325mH chokes and 40uF filter capacitors connected to Y, was included at the output of the inverter. The output voltage of the inverter was 3 x 400 V AC 50 Hz. Input DC and output filtered AC voltages and currents were measured by a YOKOGAWA WT3000 power analyzer. The resulting efficiency is calculated from the measured values directly by this analyzer. The output of the inverter was loaded by RL load with a power of 52 kVA.

The requirements for the quality of the output voltage (low content of harmonics and low distortion of the sine voltage) are reflected in the fact that in most projects a sine filter must be used at the output of the inverter. Therefore, this configuration was used during the measurement, as well. The efficiency of the inverter itself and the efficiency of the inverter including the sine filter were measured. The measured values of the efficiency of the IGBT inverter as a function of the switching frequency, for the inverter excluding and including the sine filter, are shown on the left of Figure 5. To verify the suitability of the designed cooling system, the most important is the measurement of losses and efficiency at a maximum load of 52 kVA. At the same time as measuring the efficiency, the temperatures of the heatsink and other key components of the inverter were monitored. To compare the efficiency of the SiC and IGBT inverters, the efficiency of the SiC inverter was measured at the same 52 kVA load. The measured efficiency values of the SiC inverter are shown on the right graph of Figure 5.

The low switching losses of SiC MOSFETs allow higher switching frequencies to be achieved. Therefore, the efficiency measurement was performed for a much wider switching frequency range, up to 60 kHz.

Efficiency at low frequency is decreased due increased losses in magnetic core of sinus filter choke. Higher sine choke losses and increased current ripple of phase current increase the RMS value of phase current and, as a consequence, losses of inverter are higher. Efficiency increases monotonically up to a certain value of the switching frequency (around 13-15 kHz in case of SiC inverter). Thanks to the inductance of the sine filter and the inductance of the load, the ripple of the current and thus its RMS value decrease as the switching frequency increases. A decrease in the RMS value of the current causes a decrease in SiC element losses and

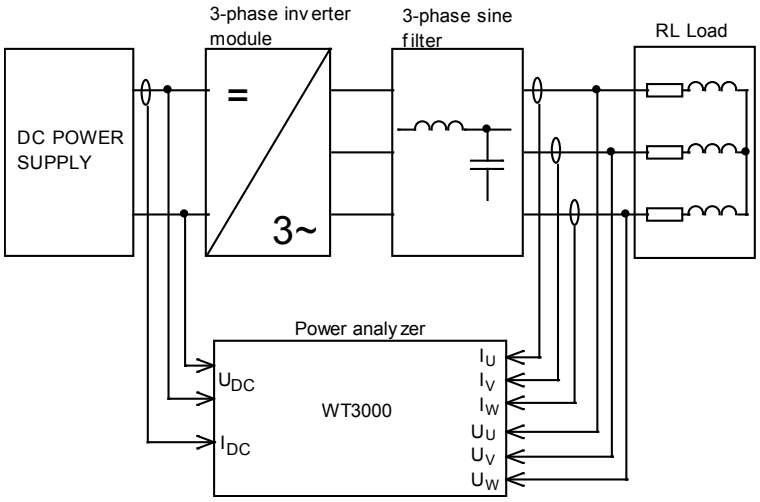

Figure 4 *Block diagram of the measuring setup*

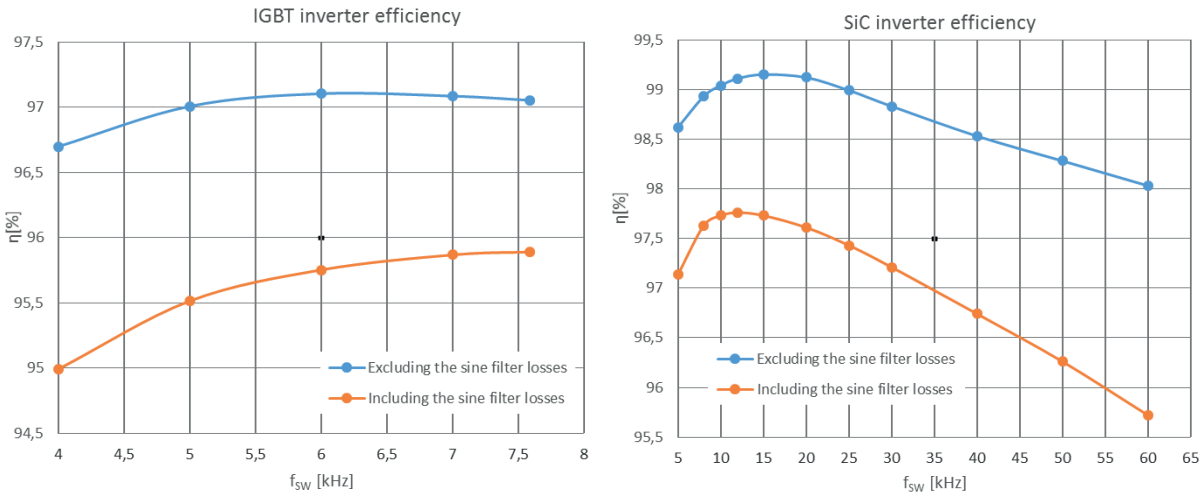

Figure 5 *The efficiency of the IGBT inverter (left) and SiC (right) as a function of the switching frequency*

thus an increase in the efficiency of the inverter itself. As the current ripple decreases, the losses of the sine filter also decrease. When the switching frequency was further increased, the efficiency began to decrease due to the increasing switching losses of the SiC MOSFETs, which became dominant. The highest efficiency of the SiC inverter itself, 99.15 %, was observed at a switching frequency of 15 kHz. The highest efficiency of the SiC inverter including the sine filter was 97.76 % at an applied switching frequency of 12 kHz. A comparison of SiC and IGBT inverter efficiency best illustrates the benefit of SiC semiconductor elements. If the highest measured efficiencies of the SiC and IGBT versions of the inverter are compared, then in the case of the inverter itself there was an improvement in efficiency by 2.047 % in favor of the SiC elements. In a comprehensive comparison of the efficiency of inverters including sine filters, it can be seen that there was an improvement in efficiency by 1.87 %.

5 Conclusion

The performed measurements confirm the contribution of the SiC semiconductor elements. At the inverter output power of 52 kVA, using the SiC elements would save approximately 1 kW of power losses. This benefit can be practically used in the design of power converters. During the design, it is possible to choose how high the switching frequency will be set and what will be prioritized during the design. Setting the frequency at which:

- the maximum power conversion efficiency is achieved
- the same efficiency as the original IGBT solution is achieved and thus the magnetic circuits are maximally reduced
- a compromise is reached between improving the efficiency and reducing the magnetic circuits.

Acknowledgements

This publication was realized with support of Operational Program Integrated Infrastructure 2014 - 2020 of the project: Innovative Solutions for Propulsion, Power and Safety Components of Transport Vehicles, code ITMS 313011V334, co-financed by the European Regional Development Fund.

Conflicts of interest

The authors declare that they have no known competing financial interests or personal relationships that could have appeared to influence the work reported in this paper.

References

[1] GURPINAR, E., CASTELLAZZI, A. Single-phase t-type inverter performance benchmark using Si IGBTs, SiC MOSFETs, and GaN HEMTs. *IEEE Transactions on Power Electronics* [online]. 2016, **31**(10), p. 7148-7160. ISSN 0885-8993, eISSN 1941-0107. Available from: https://doi.org/10.1109/TPEL.2015.2506400

[2] SU, G. Comparison of Si, SiC, and GaN based isolation converters for onboard charger applications. In: 2018 IEEE Energy Conversion Congress and Exposition ECCE: proceedings [online]. IEEE. 2018. eISBN 978-1-4799-7312-5, p. 1233-1239. Available from: https://doi.org/10.1109/ECCE.2018.8558063

[3] MAKOSCHITZ, M., KRISCHAN, K., BERGMANN, P., DIAZ, A., BRUENIGER, R. Wide band gap technology: efficiency potential and application readiness map. 4E Power Electronic Conversion Technology Annex (PECTA). IEA, 2020.

[4] PULVIRENTI, M., SALVO, L., SCIACCA, A. G., SCELBA, G., CACCIATO, M. Modeling of SiC-MOSFET converter leg including parasitics of printed circuit board layout and device packaging. In: 2020 22nd European Conference on Power Electronics and Applications EPE'20 ECCE Europe: proceedings [online]. IEEE. 2020. eISBN 978-9-0758-1536-8, p. P.1-P.10. Available from: https://doi.org/10.23919/EPE20ECCEEurope43536.2020.9215618

[5] HAN, D., NOPPAKUNKAJORN, J., SARLIOGLU, B. Analysis of a SiC three-phase voltage source inverter under various current and power factor operations. In: 39th Annual Conference of the IEEE Industrial Electronics Society IECON 2013 [online]. IEEE. 2013. eISBN 978-1-4799-0224-8, p. 447-452. Available from: https://doi.org/10.1109/IECON.2013.6699177

[6] TURZYNSKI, M., KULESZA, W. J. A simplified behavioral MOSFET model based on parameters extraction for circuit simulations. *IEEE Transactions on Power Electronics* [online]. 2016, **31**(4), p. 3096-3105. ISSN 0885-8993, eISSN 1941-0107. Available from: https://doi.org/10.1109/TPEL.2015.2445375

[7] WU, R., WEN, J., WU, J., CHEN, Z., PENG, C., WANG, Y. Analysis of power losses in voltage source converter with new generation IGBTs. In: 2012 IEEE International Conference on Computer Science and Automation Engineering CSAE: proceedings [online]. IEEE. 2012. ISBN 978-1-4673-0088-9, eISBN 978-1-4673-0089-6, p. 674-678. Available from: https://doi.org/10.1109/CSAE.2012.6272683

[8] ZHANG, L., YUAN, X., WU, X., SHI, C., ZHANG, J., ZHANG, Y. Performance evaluation of high-power SiC MOSFET modules in comparison to Si IGBT modules. *IEEE Transactions on Power Electronics* [online]. 2019, **34**(2), p. 1181-1196. ISSN 0885-8993, eISSN 1941-0107. Available from: https://doi.org/10.1109/TPEL.2018.2834345

This is an open access article distributed under the terms of the Creative Commons Attribution 4.0 International License (CC BY 4.0), which permits use, distribution, and reproduction in any medium, provided the original publication is properly cited. No use, distribution or reproduction is permitted which does not comply with these terms.

STRENGTH CHARACTERISTICS OF FE-SMA REINFORCEMENT IN RC BEAM WITH EXPERIMENTATION AND FINITE ELEMENT MODELING

Priyanka Jadhav[1], Archana Gite[2], Rajan L. Wankhade[3,*]

[1]Department of Civil Engineering, Terna Engineering College Nerul, Navi Mumbai, Maharashtra, India
[2]Department of Civil Engineering, Saraswati College of Engineering, Maharashtra, India
[3]Department of Civil Engineering, Netaji Subhas University of Technology, New Delhi, India

*E-mail of corresponding author: rajan.wankhade@nsut.ac.in

Priyanka Jadhav 0000-0001-9988-9353, Rajan L. Wankhade 0000-0002-6141-8924

Resume

The work presented here aims at investigating the feasibility of iron-based Fe-SMA (shape memory alloy) reinforcement as an alternative to conventional steel reinforcement. The conventional steel reinforcement shows large plastic strain, low resistance to corrosion, low resistance to fatigue and also inadequate recentering capability. As a result, advanced materials available in the form of superelastic (SE) shape memory alloy (SMA) are fabricated to form structural reinforcements. This FE-SMA mitigates the problem of long-lasting deflection by using its reversible stress-strain capability. This iron-based Fe-SMA may be stimulated between the temperatures of 90 to 150°C, with which it is possible to strengthen the reinforced concrete (RC) beams without any crucial damage. The stress-strain behavior in tension, corrosion resistivity, pull-out tests of Fe-SMA reinforcement and flexural strength of RC beam were evaluated experimentally. The FE-SMA exhibits recovery stresses of 250-300 MPa subjected to a temperature of 160°C. A comparison of load-carrying capacity of iron-based Fe-SMA reinforcement is also shown.

Article info

Received 9 December 2022
Accepted 28 February 2023
Online 12 April 2023

Keywords:

Fe-SMA
RC beam
flexural strength
stress-strain relationship

Available online: https://doi.org/10.26552/com.C.2023.043

ISSN 1335-4205 (print version)
ISSN 2585-7878 (online version)

1 Introduction

In recent years; researchers are focusing to employ the smart materials technology in composite structures. SMA characteristics and behavior of Fe-30Mn-1Si alloy as a single crystal were put forth by Sato et al. [1]. Reinforced cement concrete is one of the areas where SMA materials can be used. In reinforced concrete structures, we use conventional steel as reinforcement, which has its own deficiency in terms of structural response. This deficiency can be overcome by Shape Memory Alloy (SMA) bars. The SMA is an alloy, which has a property to regains its unique shape and size upon the removal of stress or by application of a temperature field [2]. The four basic types of SMA are: (a) copper-zinc (b) aluminum-nickel (c) copper-aluminum-nickel and (d) nickel-titanium (NiTi) alloys. These may also be fabricated by casting zinc, iron, copper and gold.

There exist two main groups of iron-based SMA's. The first group of it comprise Fe-Pt, Fe-Pd and Fe-Ni-Co, exhibiting the same features as Ni-Ti, thermoelastic martensitic transformations with a precise thermo hysteresis. The second group comprises alloys of Fe-Ni-C and Fe-Mn-Si, showing extensive thermal hysteresis in transformation.

Effectiveness of equiatomic and near-equiatomic titanium-nickel alloys and compositions showing shape memory and superelastic behavior are described by Duerig and Pelton [3]. SMA reinforcements and composites are mostly employed as self-restoration of structural members in various applications [4-9]. Janke et al. [10] emphasized the behavior of SMAs in terms of super elasticity, martensite damping and variable stiffness to be used as highly non-linear material. Song et al. [11] explored a review of use of the SMA for active-passive and semi-active controls of reinforced cement concrete RCC structures. Alam et al. [12] predicted analytically the seismic response of superelastic SMA

in RCC structural components. It became necessary to model the SMA reinforcements properly to evaluate the structural response in tension and compression [13-16]. Hence, the passive smart self-repairing concrete beams by incorporating SMA wires and fibers are also found to be fabricated [17]. Mathematical models are developed to examine accurate strain-temperature behavior of SMA actuators [18]. Both experimental investigation and finite element modeling is an effective approach to examine the SMA rebar characteristics [19-20]. Nehdi et al. [21] focused on casting corrosion-resistant RCC beam-column with required energy dissipation (seismic) through SMA FRP fiber reinforced polymer hybrid beam-column joint and FRP ties. Experimental results showed that over strength factor of the SMA-RC frame was analogous to that of the steel RC frame with a difference of 8 %. SMA frame has ductility at least 16 % less compared to that of steel RC frames whereas for steel-SMA frames it ranges from 8 to 18 % less from that of steel RC frames. Properties and application of iron based SMA alloys are given in literature [22].

Speicher et al. [23] investigated the response of beam-to-column connection frame in NiTi-SMA. These SMA alloys are also effective in controlling the response of structure in seismic excitations [24]. Paul and Saha [25] found out the load-carrying capacity of RC bridge longitudinal girder having the T-beam by providing SMA bars in place of conventional steel reinforcement. Abdulridha et al. [26] examined the influence of various loads on the NiTi SMA reinforced beam in comparison to conventional steel reinforcement. Experimental examination on performance of the RC structural members, having hybrid SMA and FRP bars as reinforcement, subjected to seismic loading, is found to be useful [27-28]. Choi et al. [29] examined the influence of using the welded SMA rings on a column to reduce development of micro cracks. Results show that composite reinforcement bars, fabricated from SMA alloys, are more effective in controlling the seismic behavior of structures [30]. A similar type of work has also been put forth by employing pizolaminated beams and plates for structural control [31-34]. Mechanical properties are studied to investigate the load recovery in the SMA hybrid components [35-36]. Cladera et al. [37] stated a state of the art for characteristics and employed the iron-based SMA to study properties including recovery stress, weldability, resistance to corrosion and workability of iron-based SMA.

Czaderski et al. [38] opened up the feasibility of iron-based SMA strips for strengthening the prestressed concrete structures. Sepulveda et al. [39] experimentally verified a prototype of a partially restrained connection using the copper-based SMA. Malagisi et al. [40] modeled smart concrete beams with actuating SMA. In the pre-stressed concrete SMA reinforcements have more advantages due to their stress recovery property [41]. Some smart composites manufactured with pizolaminated structures are also effective in controlling structural response [42]. Bendine and Wankhade [43] employed finite element modeling to study characteristics of actuated piezolaminated smart beams. Hence, dynamic excitations of actuated beams and plates can also be controlled by use of such smart materials [44]. Fatigue properties of Fe-28Mn-6Si-5Cr-0.5Nbc alloy are examined for its utility in structural applications [45]. Furthermore, the genetic algorithm is developed to find optimal locations of active materials in the composites [46-47]. Actuation and sensing behavior of smart composites have been demonstrated to study control response of beams and plates [48-49].

Based on the above scenario, we performed experimental work to investigate the performance analysis of conventional steel and Fe-SMA rebar, stress-strain behavior in tension, corrosion resistivity and pull-out responses of the Fe-SMA reinforcement in comparison to the conventional reinforcement. An experimental research work is proposed utilizing the Fe-SMA as reinforcement in reinforced concrete (RC) beam to compare the flexural strength with conventional steel reinforcement in RC beam and results are validated using ANSYS 16. Coarse and fine aggregates in RC beam are used conforming to IS 383: 1970 standard specification [50]. Further for test on reinforcement bars IS 11309: 1985 standard is followed to conduct pull-out test [51]. A comparison of load-carrying capacity of Fe-SMA reinforcement using ANSYS 16 is carried out to obtain more durable reinforcement having longer lifetime than that of conventional reinforcement. The comparative study between the costs of various types of reinforcing bars used for construction purposes is carried to obtain cheaper alloys as an alternative to expensive NiTi alloys.

2 Phenomenon of iron-based shape memory alloy (Fe-SMA)

Basically, the SMAs exhibit the complaisant tendency of memorizing their shape after being deflected, either quickly upon stress removal or under thermal effect.

The SMAs comprise more than one crystal structure like other alloys and to be termed as polymorphism. Temperature and external loading both govern the preponderating nature of crystal structure in such polycrystalline metals and alloys.

The tendency of SMAs to be active and stronger in the austenite phase and in the martensite phase, i.e. at lower temperatures it is feeble, can be employed effectively in RC members. The transition temperature of SMAs varies from, about -50 °C to 166 °C, depending upon their compositions. It shows a simplified two-dimensional representation of the material's crystalline arrangement.

Phase transformation in SMA occurs at four characteristic temperatures as (1) the austenite

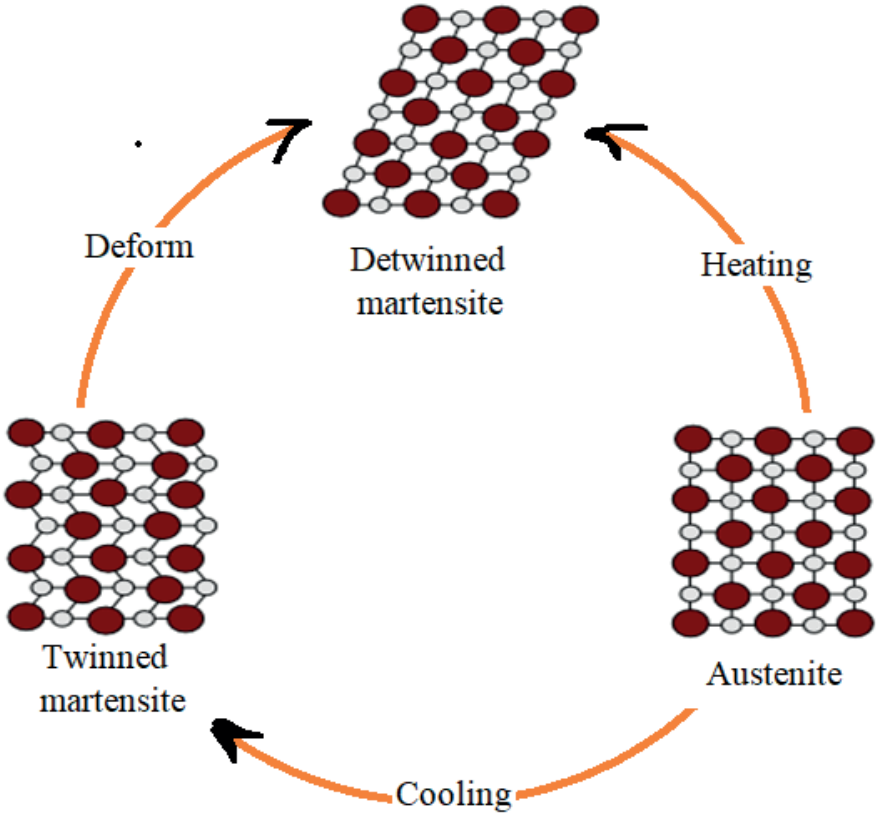

Figure 1 *Different phases of shape memory alloys*

start temperature As, where the material starts to transform from twinned martensite to austenite, (2) austenite finish temperature Af, where the material is completely transformed to austenite, (3) martensite start temperature Ms, where austenite begins to transform into twinned martensite, (4) martensite finish temperature Mf, where the transformation to martensite is completed. Figure 1 depicts these transformation phases as temperatures increase with applied stress.

2.1 The martensitic transformation

Shape Memory Effect (SME)

The shape memory effect is the capability of SMA material to achieve its pre-deformed shape after being deformed by means of a thermal effect. Below the Mf temperature, the SMA remains in the twinned martensite phase. After the application of loading above the critical level, the material transforms to a detwinned martensite phase to maintain this phase even after the stress removal. Above the Af temperature, if the SMA material is heated, it re-achieves its original shape/size. Hence, warming the material above Af results in the gaining of the austenite phase and thus a complete shape recovery. By the consequent cooling, the SMA transforms to the initial twinned martensite phase without any enduring deformation.

The super elastic effect (SE) may be termed as the restoration of large strain by virtue of the stress-induced martensitic phase transformations under definite temperature. The SMA remains in its austenite phase at a temperature above Af. After the application of higher stress to the material in the austenite phase, the SMA mold into the detwinned martensite. A partial shape recovery can be seen if the temperature remains in between Af and As. In addition, the martensitic transformations may not be brought about by applied stress if the temperature was above the critical temperature (Md), as the material may get stabilized in the austenite phase only.

2.2 Advantages of Fe-SMA over conventional reinforcement

The Fe-SMA exhibits an immense temperature transformation hysteresis with a higher elastic stiffness. In addition, as compared to the conventional steel reinforcement their corrosion resistance and weld ability are superior.. The shape memory alloys are benefited from the potency of recentering and recovering more than 80 % of the induced strains; high modulus of elasticity; similar behavior in tension and compression. It is again used for making machined components such as bolts; high resistance against corrosion and with high resistance against fatigue as compared to

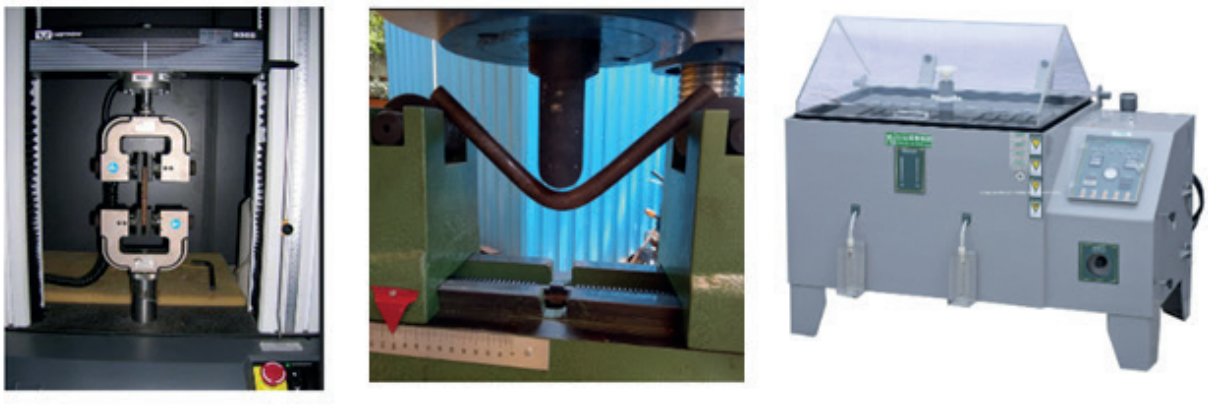

(a) (b) (c)

Figure 2 *(a) Tensile test; (b) Bend test; (c) Salt spray test*

conventional reinforcement. After considering all the options, shape memory alloys can be considered as an alternative reinforcement over the conventional one, by finding optimum benefits, while neglecting the maximum possible deficiencies of the same.

The primary aim of the present study is to investigate the performance of fabricated Fe-SMA reinforcing bars over conventional reinforcing bars along with comparison of the RC beams with and without Fe-SMA reinforcement, both experimentally and analytically using ANSYS. Based on the presented literature review, the following objectives have been drawn:

3 Experimental study

The experimental study is designed to facilitate the investigation on the feasibility of Fe-SMA reinforcing bars in RC structures in terms of tensile strength, corrosion resistivity, load-carrying capacity and pull-out resistance. Fe-SMA reinforcing bars were fabricated with optimum gradation [Iron (Fe)-72 %, Manganese (Mn)-6.57 %, Silicon (Si)-0.21 %, Chromium (Cr)-15.82 %, Nickel (Ni)-4.08 %)] of 10mm diameter, on which chemical test was carried out as per IS 9879:1998 to achieve desired optimum gradation [52]. IS 9103: 1999 standard is also used for concrete admixtures-specifications [53]. Tensile test, bend test and corrosion test were carried out on mild steel, TOR steel and Fe-SMA reinforcing bars and shown in further sections. Flexural test under the three-point bending test condition was performed on RC beams with conventional reinforcement, Fe-SMA reinforcement and combination of conventional and Fe-SMA reinforcement. Pull-out test on concrete with mild steel, TOR steel and Fe-SMA reinforcing bars was performed to achieve greater bond strength.

3.1 Test on reinforcing bars

The Fe-SMA reinforcement was fabricated from Iron, Manganese, Silicon, Chromium and Nickel as stated. This gradation helps to verify the strength of bars under different tests. Hence, the tensile test, bend test and salt spray test were performed on TOR steel, mild steel and Fe-SMA reinforcing bars respectively as shown in Figures 2(a)-2(c), respectively.

3.2 Test on RC beams and cubes

A Material and mixes

Concrete

The concrete is formed with different ingredients and materials. The admixture used was MasterRheobuild-1124 superplasticizer, 2 % by mass of cementitious material as per IS 9103:1999 standard [53]. The specific gravity of the admixture was found to be 1.145. Reinforcements used for beam specifications were based on IS 1786: 2008 standard specifications required for concrete [54]. The mix proportion used was 1:2:2.87 with a water-cement ratio used was 0.35 as per IS 10262:2009 standard [55]. ASTM B117: 2011 standard guidelines are employed for different test conditions and method [56]. The raw material, consisting of Ordinary Portland cement of 53 grade, conforming to Indian Standard IS 12269:2013, was used throughout the experimental program [57]. The minimum fineness was 225m^2/kg. The standard consistency was 30.5 %, whereas the initial and final setting times were 30 min and 600 min, respectively. The specific gravity of cement was 3.14 and its compressive strength after 28 days was 53 MPa. The coarse aggregate-I (CA-I) and coarse aggregate-II (CA-II) of maximum size 10 mm and 20 mm, respectively, were used.. The bulk density of CA-I and CA-II was 1.5gm/cm^3 and 1.589 gm/cm^3, respectively. The specific gravity of CA-I and CA-II was found to be 2.8 and 2.82, respectively. The crushed sand and natural sand conforming to zone-II is used with bulk density of 1.712 gm/cm^3. The specific gravity of crushed sand was found to be 2.76. The cement content was 384 kg/m^3..

Table 1 *Final Batch weight in kg/m³ of concrete and material and mechanical property of Fe-SMA*

Cement (kg/m³)	PFA (kg/m³)	CA-II (kg/m³)	CA-I (kg/m³)	CFA (kg/m³)	Water (kg/m³)	Admixture (kg/m³)	Total (kg/m³)
384	96	613	408	755	220	6.24	2482

Reinforcement	Material and mechanical property	Range
Fe-SMA	Elastic Modulus (GPa)	75-165
	Yield Stress (MPa)	400-550
	Failure Strain (%)	40
	Optimum Prestrain (%)	2-4
	Activation Temperature (⁰C)	160-500
	Recovery Stress (MPa)	130-580

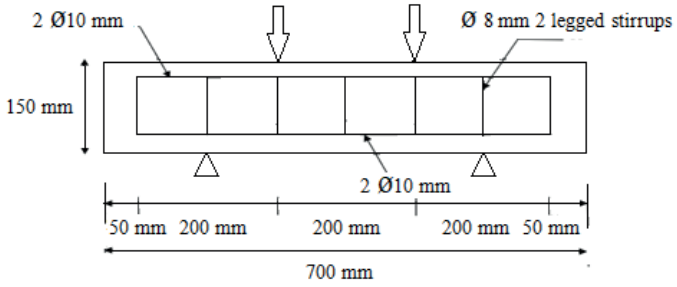

(a)

(b)

Figure 3 *Flexural test (a) Loading and reinforcement details (b) setup*

Reinforcement

A bilinear stress-strain curve has been used for the steel behavior. The values of elastic modulus and Poisson's ratio of steel are 200 GPa and 0.3, respectively. The steel is assumed to have a yield strength of 500 MPa. The Fe-SMA reinforcement with optimum gradation is used. Table 1 shows the mix design used in this study.

B Experimental setup for the three-point bending test

The RC beams were cast with the dimension of 150mm x150mm x700mm. Results from the three-point bending test are obtained for three combinations.

a) Conventional reinforcement of 2Ø10 mm at the top and 2Ø 10 mm at the bottom,
b) Fe-SMA reinforcement 2Ø 10 mm at the top and 2Ø 10 mm at the bottom,
c) Combination of conventional reinforcement Ø10 mm at the top, Ø10 mm at the bottom and Fe-SMA reinforcement Ø10 mm at the top with Ø10 mm at the bottom.

The thickness of the layer cover was 25 mm. The axial distance of the stirrup was 100 mm. The load applied was up to 100 kN, as per IS 516:2021 standard [58], flexural test using a three-point bending test setup was carried out as shown in Figure 3.

The test specimen for pull-out test was basically

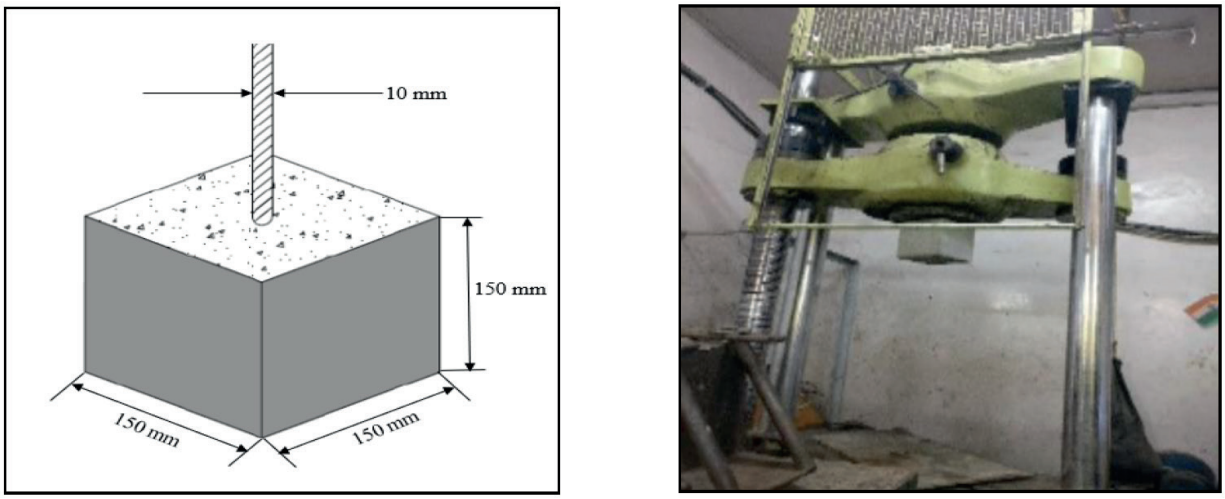

Figure 4 *Pull-out test (a) Specimen details (b) setup*

Table 2 *Material types and element types of the finite element model*

Material types	ANSYS elements
Concrete	Solid 65
Steel support	Solid 45
Steel reinforcement (main r/f and stirrups)	Link 8
Fe-SMA reinforcing bars	Link1

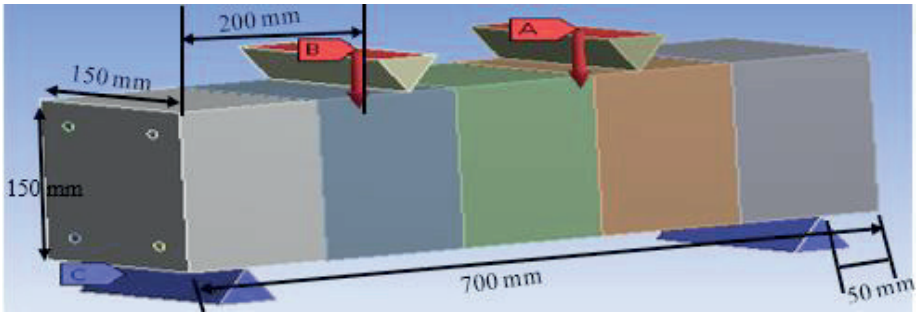

Figure 5 *FE model in ANSYS for RC beam reinforced with a combination of conventional reinforcement and Fe-SMA reinforcing bars under the four-point bending test condition*

a concrete cube of 150 mm x 150 mm x 150 mm dimension with a bar embedded coaxially. The upper end of the bar under test was projected up to the length of 500 mm. Double nuts were fitted in it above the 400 mm high spring-return central-hold jack, as shown in Figure 4. Therefore, the ultimate pullout force is directly proportional to the compressive strength.

4 Analytical study

4.1 Finite element modeling

The static analysis is performed on a concrete beam modeled with dimensions 150 mm x 150 mm x 700 mm. The beam is reinforced with conventional reinforcement as well as with Fe-SMA reinforcement for undergoing flexural test under the four-point bending test conditions. To reduce the time for analysis, half RC beam was modeled. Thus, Figure 5 shows arrangement of reinforcement in the beam. Results from the four-point bending test are obtained for three combinations same used in the experimental program, (a) conventional reinforcement of 2Ø10 mm at the top and 2Ø 10 mm at the bottom, (b) Fe-SMA reinforcement 2Ø 10mm at the top and 2Ø 10 mm at the bottom and (c) combination of conventional reinforcement Ø10 mm at the top, Ø10 mm at the bottom and Fe-SMA reinforcement Ø10 mm at the top with Ø10 mm at the bottom. Table 2 summaries the material types and element types of the model in ANSYS 16.

4.2 Mesh, loading and support condition

The RC beam, with and without Fe-SMA reinforcement, model with a particular mesh sizing is calculated in such a way that the better results are

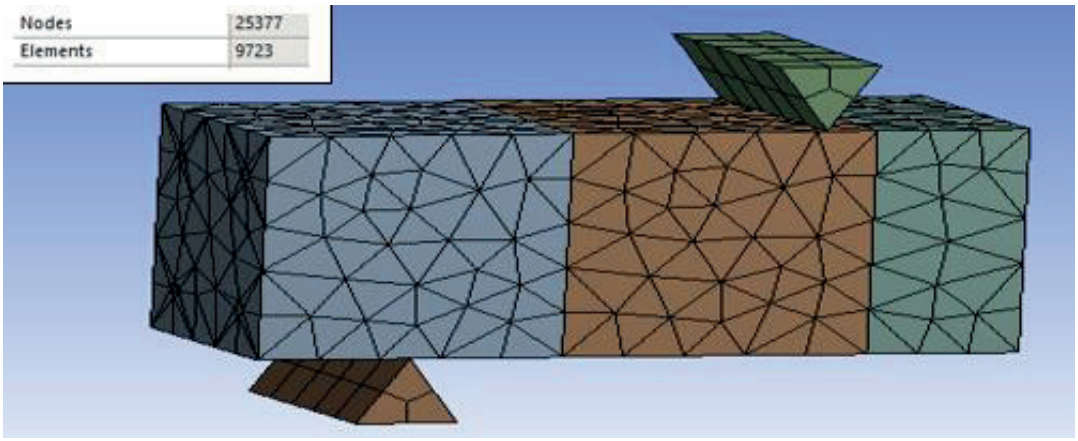

Figure 6 *Mesh for static analysis under the four-point bending test of RC beam reinforced with and without Fe-SMA reinforcement*

obtained from the elements. The inherent assumption is that there is full displacement compatibility between the reinforcement and the concrete and that no bond slippage occurs. Figure 6 represents the model of the beam under consideration with its meshing in ANSYS. Proper mesh and elements are demonstrated for convergence criteria. At first, the beam is modeled with normal reinforcement and solved to get the results. In the next step, the same beam is modeled with Fe-SMA reinforcement for comparison. Only half of the beam is shown here with the FE mesh in the enlarged view. Displacement boundary conditions are needed to constrain the model to get a unique solution. The support was modeled as roller support at one end and the other end as a hinged support. Loading is applied as per the four-point bending test for flexure.

5 Results and discussion

This paper focuses on feasibility of the Fe-SMA reinforcing bars as an alternative to conventional reinforcement in structural engineering. Fabricated Fe-SMA reinforcing bars were used for experimentation. Tensile test, bend test and corrosion test were carried out on mild steel, TOR steel and Fe-SMA reinforcing bars to achieve mechanical and corrosion properties. The pull-out test on concrete with mild steel, TOR steel and Fe-SMA reinforcing bars was also performed to check the bond strength. Flexural test under three-point bending test condition was performed on RC beams with conventional reinforcement, Fe-SMA reinforcement and a combination of conventional reinforcement both experimentally and then analytically in ANSYS 16. The results are compared for conventional and Fe-SMA reinforcement with respect to the flexural strength of the beam. To interpret a comparison between the conventional reinforcement and Fe-SMA reinforcement, with respect to the stress, deformation and fatigue properties of reinforcing bars were evaluated, as well. Based on this scenario, results are presented.

5.1 Chemical test on Fe-SMA reinforcing bars

The chemical test is carried out on Fe-SMA reinforcing bars and results are provided further. The main elements of Fe-SMA bars are iron, manganese, silicon, chromium and nickel. The addition of manganese at 6.57% and silicon with 0.21% allows the shape memory effect to occur. The addition of chromium with 15.82% and nickel with 4.08% improves its corrosion resistance and improves effectiveness in restraining.

5.2 Tensile test on reinforcing bars

A tensile test is carried on mild steel, TOR steel and Fe-SMA reinforcing bars as per ASTM A370 [59]. Table 3 shows results related to the tensile test on reinforcing bars. Stress-strain graphs for mild steel, TOR steel and Fe-SMA reinforcing bars, Figures 7 (a), (b) and (c), reveal many properties like 0.2% proof stress and ultimate tensile strength, including data to establish the modulus of elasticity of mild steel, TOR steel and Fe-SMA, respectively. Figure 7 (c) shows flag shaped curve, which indicates at the loading stage, SMA takes a large level of strain as the stress remains fairly constant and then at unloading the SMA recovers strain at a lower stress stage. Figures 8 (a), (b) and (c) show the cup and cone fracture of TOR steel, mild steel and Fe-SMA reinforcing bars after the tensile test, respectively. Table 3 shows 0.2% proof stress for mild steel, TOR steel and Fe-SMA are 681 MPa, 504 MPa, 868 MPa, respectively. This indicates that there is a 22% and 42% precedent beginning of nonlinear deformation of Fe-SMA as compared to mild steel and TOR steel, respectively.

The ultimate tensile strength of steel, mild steel and Fe-SMA are 743 MPa, 621 MPa and 1037 MPa, respectively. This indicates that Fe-SMA has 40% and 29% maximum capacity to withstand while being stretched or pulled before breaking as compared to mild steel and TOR steel respectively. The modulus of

Table 3 *Tensile test on reinforcing bars*

Specimen	Dia. (mm)	Maximum Load (kN)	0.2% proof stress (MPa)	U.T.S (MPa)	Modulus (GPa)
TOR steel	10	45.81	504	621	187
Mild steel	10	58.09	681	743	200
Fe-SMA	10	81.09	868	1037	208

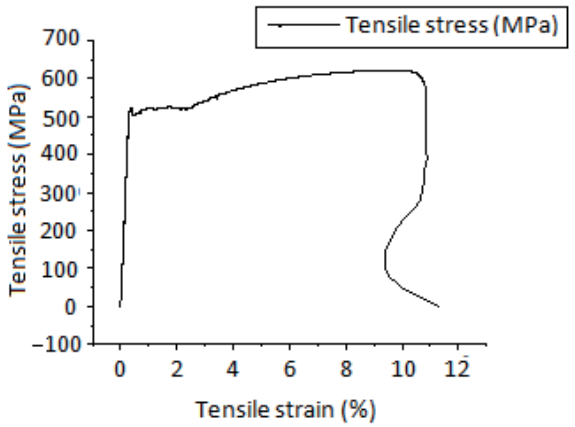

(a)

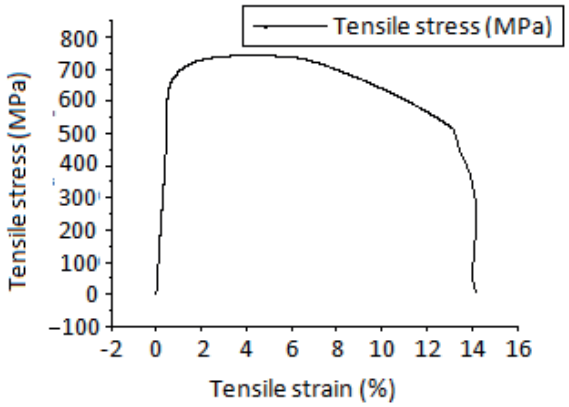

(b)

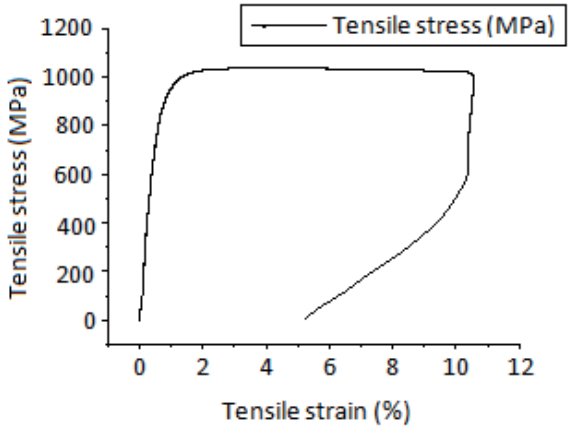

(c)

Figure 7 *Stress-Strain curves for (a) mild steel (b) TOR steel (c) FE-SMA*

Figure 8 *Specimen after the tensile test (a)mild steel (b) TOR steel (b) Fe-SMA*

Table 4 *Bend test of reinforcing bars*

Specimen	Diameter (mm)	Bend	Remark
Mild steel	10	4D	Satisfactory
TOR steel	10	4D	Satisfactory
Fe-SMA	10	4D	Satisfactory

Table 5 *Corrosion test of reinforcing bars*

Specimen	Dia. (mm)	Period (h)	Observation
Mild steel	10	24	Red pitting observed
TOR steel	10	24	Red pitting observed
Fe-SMA	10	24	Slightly red pitting at cutting edge

Table 6 *Pull-out test*

Case	Material	Diameter of bar (mm)	Maximum Load (kN)	Bond strength (N/mm^2)
1	RC cube with mild steel	10	22.6	0.72
2	RC cube with TOR steel	10	22.8	0.73
3	RC cube with Fe-SMA	10	15.1	0.48

elasticity for mild steel, TOR steel and Fe-SMA are 200 GPa, 187 GPa and 208 GPa respectively. This indicates that Fe-SMA is for 4% and 10% stiffer material, as compared to mild steel and TOR steel, respectively.

5.3 Bend test on reinforcing bars

The bend test was a simple and inexpensive qualitative test that can be used to evaluate both the ductility and soundness of a material. The bend test is carried out on mild steel, TOR steel and Fe-SMA reinforcing bars to suggest the suitability for concrete structures. Figure 9 shows the results of the bend test on mild steel, TOR steel and Fe-SMA, respectively. The results of this test show satisfactory remarks, which indicates that none of the material failed under pressure as no fracture occurred on mild steel, TOR steel and Fe-SMA. It is observed that during the test there no crack has developed in TOR steel, mild steel nor the Fe-SMA reinforcement, after undergoing a 180° bend. Hence, those reinforcement bars can be effectively used with concrete as a ductile material further loaded with bending forces. However, when those reinforcements are used in concrete, cracks, which are measurable, get developed in concrete, while with use of the Fe-SMA, these cracks in concrete get diminished and recovered due to the self-healing properties. Table 4 shows the bend test results and their remarks.

5.4 Corrosion test on reinforcing bars

Corrosion test was carried out on mild steel, TOR steel and Fe-SMA reinforcing bars and the results were compared. Table 6 shows the results of the corrosion test mild steel, TOR steel and Fe-SMA respectively. Figure 10 shows specimens before and after the test. Table 5 shows that in the salt solution of 5% (in weight) of NaCl, (more than seawater, which is only 1.8% to max 3%) maintained at 35 ºC with pH ranges from 6.5 to 7.2 for 24 h, red pitting was observed on the mild and TOR steel, whereas for the Fe-SMA reinforcing bars slightly red pitting was observed at the cutting edge. These results indicate that the Fe-SMA reinforcing bars are more corrosive resistant than the mild and TOR steels.

5.5 Pull-out test

The pull-out test is carried out on reinforcing concrete embedded with mild steel, TOR steel and Fe-SMA reinforcing bars to verify the maximum load and bond strength. Figure 11 shows specimens after the pull-out test. Table 6 shows the maximum load of 22.6 kN, 22.8 kN and 15.1 kN acted on a cube reinforced with mild steel, TOR steel and Fe-SMA reinforcing bars respectively. Similarly, bond strengths were observed as 0.72 N/mm^2, 0.73 N/mm^2, 0.48 N/mm^2, for cubes reinforced with mild steel, TOR steel and Fe-SMA reinforcing bars, respectively. This indicates that the maximum load and bond strength of a cube embedded with Fe-SMA reinforcing bars is 34% smaller than mild and TOR steel. Thus, the bond strength is proportional to the contact surface of the steel to the concrete. A deformed reinforcing bar adheres better than a plain one because it has a greater bearing surface. The rougher the surface of the steel, the better it adheres to concrete. Thus, steel with a light, firm layer of rust is

(a) *(b)* *(c)*

Figure 9 *Specimens after bend test (a) mild steel (b) TOR steel (c) Fe-SMA*

(a) *(b)* *(c)*

Figure 10 *Reinforcing bars sample before and after corrosion test (a) mild steel (b) TOR steel (c) Fe-SMA*

Table 7 *Comparison of Flexural Strengths for RC beams reinforced with Conventional and FE-SMA*

Case	Reinforced concrete beam	Beam size (mm)	Maximum Load (kN)	Flexural strength (MPa)	
				Experimental results	Analytical results
1	Conventional reinforcement #2-10 mm Ø (top) #2-10 mm Ø (bottom)	150 x 150 x 700	71.48	12.65	12.43
2	Fe-SMA reinforcement #2-10 mm Ø (top) #2-10 mm Ø (bottom)	150 x 150 x 700	88.81	16.08	15.89
3	Conventional reinforcement #1-10 mm Ø (top) #1-10 mm Ø (bottom) Fe-SMA reinforcement #1-10 mm Ø (top) #1-10 mm Ø (bottom)	150 x 150 x 700	73.28	13.04	12.94

superior to clean steel; however, steel with loose or scaly rust is inferior.

5.6 Flexural test on the RC beams

Flexural test under the four-point bending test condition is carried out on RC beams experimentally to compare the flexural strength of RC beams with and without Fe-SMA reinforcement and the same results are validated using ANSYS 16. Table 7 shows the experimental and analytical results of RC beams with and without Fe-SMA reinforcement. Figures 12 (a), (b) and (c) show the flexural strength acting on RC beam with and without Fe-SMA reinforcement obtained from analytical results using ANSYS.

Table 7 shows that experimental results for the flexural strength of RC beams, with and without Fe-SMA reinforcement, are in good agreement with the analytical results for the flexural strength of RC beams with and without Fe-SMA reinforcement. The flexural strength of the RC beam reinforced with Fe-SMA and a combination of Fe-SMA and conventional reinforcement is observed to be 16.08 MPa and 13.04 MPa is 22 % greater than the RC beam reinforced with conventional reinforcement. There is a marginal increase of 3 % in the flexural strength of the combination of conventional reinforcement and Fe-SMA. This proves that Fe-SMA can withstand in severe conditions for longer period, as compared to conventional reinforcement.

5.7 Total deformation of RC beam

Total deformation is carried out on RC beams with and without Fe-SMA reinforcement, both experimentally and analytically. Figure 13 (a) shows the crack closure of the RC beam with Fe-SMA reinforcement at the maximum deflection is 0.53 mm and after the unloading it is 0.13 mm. Even if there was a marginal increase in total deformation of the RC beam with Fe-SMA reinforcement, it shows strain recovery of 75 %. This results in crack vanishing in the RC beam with Fe-SMA reinforcement, as shown in Figure 13 (b). Figures 14 (a), (b) and (c) represent the total deformation on the RC beams with and without the Fe-SMA reinforcement. Analytical results show that the total deformation of Fe-SMA reinforcement is 0.04897 mm, which is marginally higher than that of the conventional reinforcement and a combination of conventional and Fe-SMA reinforcements, which is observed to be 0.03879.

5.8 Load-strain response and recovery stress

Further, for measuring the recovery strain of the

(a) (b) (c)

Figure 11 *Pull-out test (a) mild steel (b) TOR steel (c) Fe-SMA*

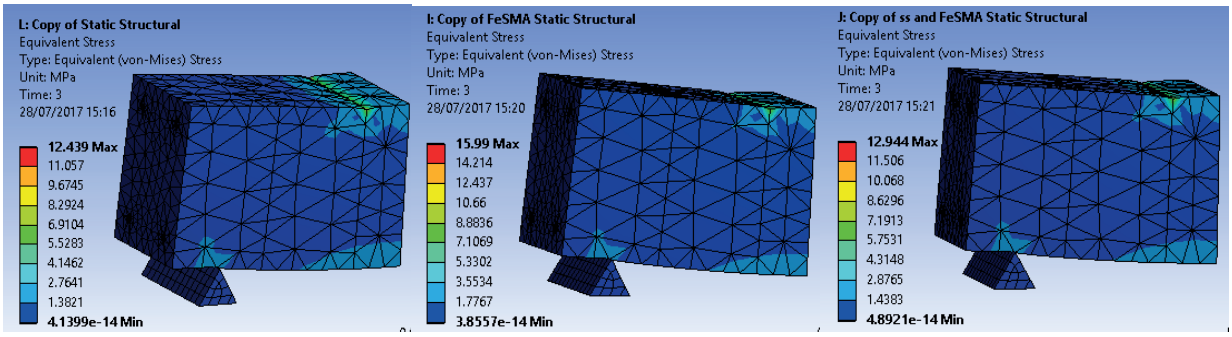

(a) (b) (c)

Figure 12 *Flexural strength on RC beam (a) conventional reinforcement (b) Fe-SMA reinforcing bars (c) combination of conventional reinforcement and Fe-SMA reinforcement*

(a) (b)

Figure 13 *Crack behavior of RC beam with Fe-SMA reinforcement (a) at maximum deflection (b) recentering of RC beam with Fe-SMA reinforcement after unloading*

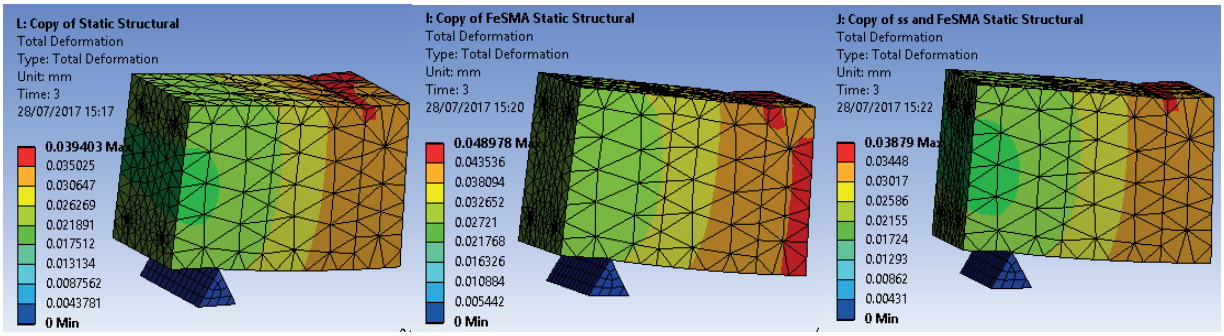

(a) (b) (c)

Figure 14 *Total Deformation on RC beams (a) conventional reinforcement (b) Fe-SMA reinforcing bars (c) combination of conventional reinforcement and Fe-SMA reinforcement*

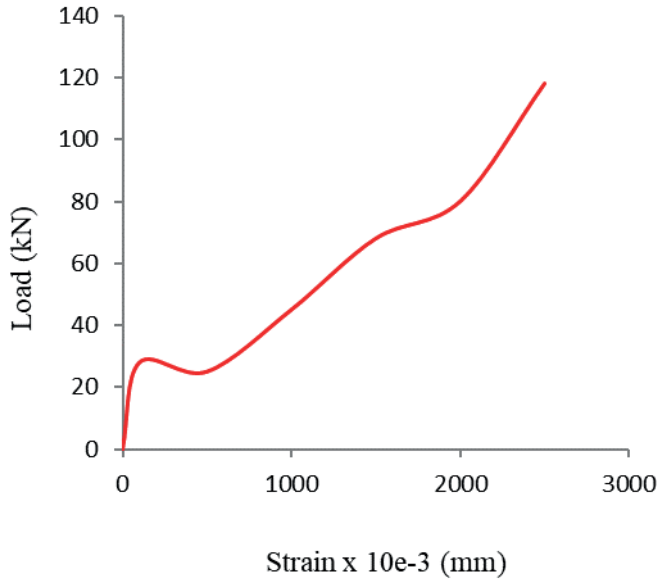

Figure 15 *Load-strain response of the Fe-SMA reinforcement*

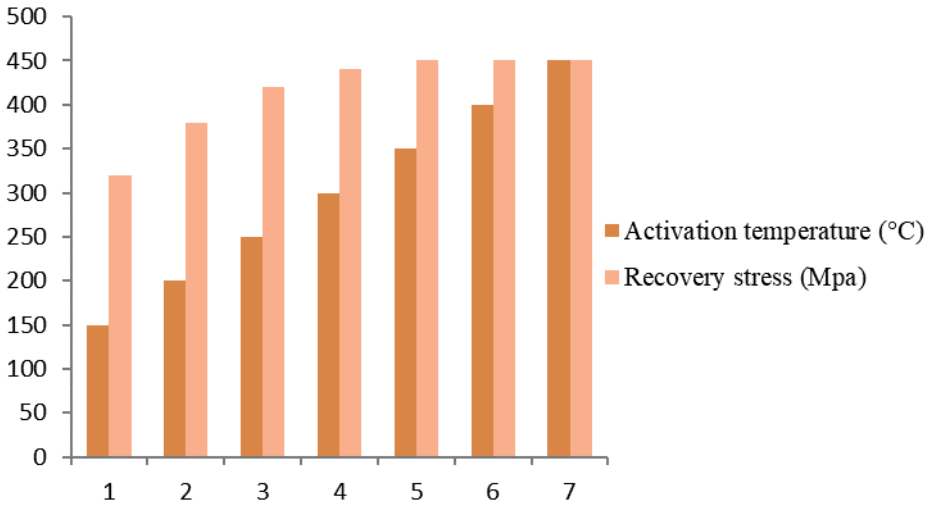

Figure 16 *Recovery stress with respect to an activation temperature*

reinforcement, the strain gauges were attached to Fe-SMA reinforcing bars at the mid-span. Those bars are longitudinal reinforcing bars provided into the concrete beam. Hence, Figure 15 shows the load versus strain response of the Fe-SMA reinforcement. Again, it can be stated that the Fe-SMA reinforcing bar has a lower modulus of elasticity as compared to the conventional reinforcement. When the flexural cracks occur, high strains are developed at the mid-span of the beam. The yield point of both the Fe-SMA and conventional reinforcement differs.

Now, it is obvious that at the higher activation temperatures recovery stress shows larger values. After heating the Fe-SMA at temperatures in the range of 150 - 450 °C, the recovery stress increased from 320 MPa to 450 MPa, as indicated in Figure 16. We generally do not require higher activation temperatures for concrete structures to maintain proper bonds between the concrete and Fe-SMA. This property of recovery stress is of a great interest for such adaptive Fe-SMA reinforcements in terms of diminishing the crack propagation in concrete members. We used this phenomenon of SM alloy reinforcements for actively monitoring the self-recovery of the beam. After increasing the cycle-fatigue load these activated Fe-SMAs revealed an insignificant decrease in stiffness. Perhaps, a decrease in recovery stress occurs with an increase in cyclic loads. The reversible phase transformation-induced deformations are observed at this stage..

6 Conclusions

In the present research, the feasibility of the Fe-SMA reinforcing bars, to be used as an alternative to conventional reinforcement in structural engineering, was considered. Tensile test, bend test and corrosion test were carried out on TOR steel, mild steel and Fe-SMA reinforcing bars and test results were compared. The pull-out test on concrete with TOR steel, mild steel and Fe-SMA reinforcing bars was performedto check the bond strength. The Flexural test, under the four-point bending test conditions, was performed on RC beams with conventional reinforcement, Fe-SMA reinforcement and a combination of conventional reinforcement, both experimentally and analytically in ANSYS 16, to evaluate the comparison between the conventional and Fe-SMA reinforcement, with respect to its flexural strength and too interpret the comparison between the conventional and Fe-SMA reinforcement, with respect to the stress, deformation developed in beams and fatigue properties of reinforcing. The conclusions from the above study have been drawn as follows:

Chemical test results reveal that corrosion resistance of the Fe-SMA reinforcing bars was enhanced due to the addition of silicon along with manganese and chromium in iron. The tensile strength of Fe-SMA reinforcing bars is greater than those of both mild and TOR steels, which shows that the Fe-SMA reinforcing bars would sustain severe loads for a longer time than the conventional reinforcing bars. There is no crack observed on TOR steel, mild steel and Fe-SMA reinforcing bars after a 180° bend which reveals that they are satisfactory to be used as reinforcements. The corrosion test results reveal that the Fe-SMA reinforcing bar is more corrosion resistant than the conventional reinforcement, as there was slightly red pitting observed at the cutting edge. The bond strength of Fe-SMA reinforcing bar is smaller than that of the TOR steel and mild steel. Therefore, the deformed Fe-SMA reinforcing bars should be used instead of plain Fe-SMA reinforcing bars, to achieve better bond strength. Flexural strength result reveals that the RC beam reinforced with Fe-SMA reinforcing bars can withstand in severe conditions and has a greater load-carrying capacity than the conventional reinforcing bars. There is a good agreement between the experimental and analytical results. Total deformation

of an RC beam with Fe-SMA reinforcement full replacement is marginally higher than the conventional RC beam, however, it has the capability of recentering, crack vanishing and recovering due to the chemical composition of the Fe-SMA reinforcing bars. The service life of the Fe-SMA reinforcement is far longer than that of the conventional reinforcement. It is demonstrated that the conventional reinforcement in RC beam can be replaced by 50 % or 100 % by super elastic iron-based shape memory alloy, very effectively in terms of strength and life of the material. The Fe-SMA is a cost-effective alternative to NiTi-based alloys.

Grants and funding

The authors received no financial support for the research, authorship and/or publication of this article.

Conflicts of interest

The authors declare that they have no known competing financial interests or personal relationships that could have appeared to influence the work reported in this paper.

References

[1] SATO, A., CHISHIMA, E., SOMA, K., MORI, T. Shape memory effect in y transformation in Fe-30Mn-1Si alloy single crystals. *Acta Metallurgica* [online]. 1982, **30**(6), p. 1177-1183. ISSN 0001-6160. Available from: https://doi.org/10.1016/0001-6160(82)90011-6

[2] OTSUKA, H. Fe-Mn-Si based shape memory alloys. *MRS Online Proceedings Library* [online]. 1991, **246**(1), p. 309-320. eISSN 1946-4274. Available from: https://doi.org/10.1557/PROC-246-309

[3] DUERIG, T. W., PELTON, A. R. Ti-Ni shape memory alloys. In: *Materials properties handbook: titanium alloys*. WELSCH, G., BOYER, R., COLLINGS, E. W. (eds.). American Society for Metals, 1994. ISBN 0-87170-481-1, p. 1035-1048.

[4] CROCI, G., BONCI, A., VISKOVIC, A. Use of shape memory alloy devices in the basilica of St Francis of Assisi. In: Final Workshop of ISTECH Project - Shape Memory Alloy Devices for Seismic Protection of Cultural Heritage Structures: proceedings. 2000. p. 110-113.

[5] INDIRLI, M., CASTELLANO, M. G., CLEMENTE, P., MARTELLI, A. Demo-application of shape memory alloy devices: the rehabilitation of the S. Giorgio Church Bell-Tower. In: SPIE's 8th Annual International Symposium on Smart Structures and Materials: proceedings [online]. Vol. 4330. 2001. p. 262-272. Available from: https://doi.org/10.1117/12.434126

[6] MAZZOLANI, F. M., MANDARA, A. Modern trends in the use of special metals for the improvement of historical and monumental structures. *Engineering Structures* [online]. 2002, **24**(7), p. 843-856. ISSN 0141-0296, eISSN 1873-7323. Available from: https://doi.org/10.1016/S0141-0296(02)00023-8

[7] SONG, G., MO, Y. L., Increasing concrete structural survivability using smart materials. A proposal submitted to Grants to Enhance and Advance Research (GEAR). Houston: University of Houston, 2003.

[8] FUKUTA, T., IIBA, M., KITAGAWA, Y., SAKAI, Y. Experimental study on stress-strain property of shape memory alloy and its application to self-restoration of structural members. In: 13th World Conference on Earthquake Engineering: proceedings. 2004. Paper No. 610.

[9] LI, H., LIU, M., OU, J. Vibration mitigation of a stay cable with one shape memory alloy damper. *Structural Control and Health Monitoring* [online]. 2004, **11**(1), p. 1-36. eISSN 1545-2263. Available from: https://doi.org/10.1002/stc.29

[10] JANKE, L., CZADERSKI, C., MOTAVALLI, M., RUTH, J. Applications of shape memory alloys in civil engineering structures - overview, limits and new ideas. *Materials and Structures* [online]. 2005, **38**, p. 578-592. ISSN 1359-5997, eISSN 1871-6873. Available from: https://doi.org/10.1007/BF02479550

[11] SONG, G., MA, N., LI, H.-N. Applications of shape memory alloys in civil structures. *Engineering Structures* [online]. 2006, **28**(9), p. 1266-1274. ISSN 0141-0296, eISSN 1873-7323. Available from: https://doi.org/10.1016/j.engstruct.2005.12.010

[12] ALAM, M. S., YOUSSEF, M. A., NEHDI, M. Analytical prediction of the seismic behaviour of super elastic shape memory alloy reinforced concrete elements. *Engineering Structures* [online]. 2008, **30**(12), p. 3399-3411. ISSN 0141-0296, eISSN 1873-7323. Available from: https://doi.org/10.1016/j.engstruct.2008.05.025

[13] EL-BORGI, S., NEIFAR, M., BEN JABEUR, M., CHERIF, D., SMAOUI, H. Use of copper shape memory alloys in retrofitting historical monuments. *Smart Structures and Systems* [online]. 2008, **4**(2), p. 247-259. ISSN 1738-1584, eISSN 1738-1991. Available from: https://doi.org/10.12989/sss.2008.4.2.247

[14] INDIRLI, M., CASTELLANO, M. Shape memory alloy devices for the structural improvement of masonry heritage structures. *International Journal of Architectural Heritage* [online]. 2008, **2**(2), p. 93-119. ISSN 1558-3058, eISSN 1558-3066. Available from: https://doi.org/10.1080/15583050701636258

[15] KUMAR, P. K., LAGOUDAS, D. C. Introduction to shape memory alloys. In: *Shape memory alloys modeling and engineering applications* [online]. LAGOUDAS, D. C. (ed.). New York, NY: Springer, 2008. ISBN 978-0-387-47684-1, eISBN 978-0-387-47685-8, p. 1-51. Available from: https://doi.org/10.1007/978-0-387-47685-8

[16] MARUYAMA, T., KURITA, T., KOZAKI, S., ANDOU, K., FARJAMI, S., KUBO, H. Innovation in producing crane rail fishplate using Fe-Mn-Si-Cr based shape memory alloy. *Materials Science and Technology* [online]. 2008, **24**(8), p. 908-912. ISSN 0267-0836, eISSN 1743-2847. Available from: https://doi.org/10.1179/174328408X302585

[17] KUANG. Y.-CH., OU, J.-P. Passive smart self-repairing concrete beams by using shape memory alloy wires and fibers containing adhesives. *Journal of Central South University of Technology* [online]. 2008, **15**, p. 411-417. ISSN 2095-2899, eISSN 2227-5223. Available from: https://doi.org/10.1007/s11771-008-0077-9

[18] NASCIMENTO, M. M. S. F., DE ARAUJO, C. J., DE ALMEIDA, L. A. L., DA ROCHA NETO, J. S., LIMA, A. M. N. A mathematical model for the strain -temperature hysteresis of shape memory alloy actuators. *Materials and Design* [online]. 2009, **30**(3), p. 551-556. ISSN 0261-3069. Available from: https://doi.org/10.1016/j.matdes.2008.05.062

[19] ALSALEH, R., CASCIATI, F., EL-ATTAR, A. AND EI-HABBAL, I. M., Experimental investigation toward an SMA retrofitting application. In: 5th European Workshop on Structural Health Monitoring: proceedings. 2010. ISBN 978-1605950242, p. 1116-1123.

[20] KHALOO, A. R., ESHGHI, I., PIRAN, P. Study of behavior of reinforced concrete beams with smart rebar using finite element modeling. *International Journal of Civil Engineering* [online]. 2010, **8**(3), p. 221-231. ISSN 1735-0522. Available from: http://ijce.iust.ac.ir/article-1-166-en.html

[21] NEHDI, M., SHAHRIA ALAM, M., YOUSSEF, M. A. Development of corrosion-free concrete beam column joint with adequate seismic energy dissipation. *Engineering Structures* [online]. 2010, **32**, p. 2518-2528. ISSN 0141-0296, eISSN 1873-7323. Available from: https://doi.org/10.1016/j.engstruct.2010.04.020

[22] MARUYAMA, T., KUBO, H., OHKATA, I., TSUCHIYA, K., MIYAZAKI, S. *Ferrous (Fe-based) shape memory alloys (SMAs): properties, processing and applications*. Cambridge: Woodhead Publishing Limited, 2011. p. 141-159.

[23] SPEICHER, M. S., DESROCHES, R., LEON, R. T. Experimental results of a NiTi shape memory alloy (SMA)-based recentering beam-column connection. *Engineering Structures* [online]. 2011, **33**(9), p. 2448-2457. ISSN 0141-0296, eISSN 1873-7323. Available from: https://doi.org/10.1016/j.engstruct.2011.04.018

[24] OZBULUT, O. E., HURLEBAUS, S., DESROCHES, R. Seismic response control using shape memory alloys: a review. *Journal of Intelligent Material Systems and Structures* [online]. 2011, **22**(14), p. 1531-1549. ISSN 1045-389X, eISSN 1530-8138. Available from: https://doi.org/10.1177/1045389X11411

[25] PAUL, N. K., SAHA, S. Improvement of load-carrying capacity of a RCC t-beam bridge longitudinal girder by replacing steel bars with SMA Bars. *International Journal of Civil and Environmental Engineering*. 2017, **11**(7), p. 1008-1012. ISSN 2227-2763, eISSN 2077-1258.

[26] ABDULRIDHA, A., PALERMO, D., FOO, S., VECCHIO, F. J. Behavior and modeling of superelastic shape memory alloy reinforced concrete beams. *Engineering Structures* [online]. 2012, **49**, p. 893-904. ISSN 0141-0296, eISSN 1873-7323. Available from: https://doi.org/10.1016/j.engstruct.2012.12.041

[27] SHAHRIA ALAM, M., MONI, M., TESFAMARIAM, S. Seismic over strength and ductility of concrete buildings reinforced with superelastic shape memory alloy rebar. *Engineering Structures* [online]. 2012, **34**, p. 8-20. ISSN 0141-0296, eISSN 1873-7323. Available from: https://doi.org/10.1016/j.engstruct.2011.08.030

[28] MUNTASIR BILLAH, A. H. M., SHAHRIA ALAM, M. Seismic performance of concrete columns reinforced with hybrid shape memory alloy (SMA) and fiber Reinforced polymer (FRP) bars. *Construction and Building Materials* [online]. 2012, **28**(1), p. 730-742. ISSN 0950-0618, eISSN 1879-0526. Available from: https://doi.org/10.1016/j.conbuildmat.2011.10.020

[29] CHOI, E., PARK, S.-H., CHO, B.-S., HUI, D. Lateral reinforcement of welded SMA rings for reinforced concrete columns. *Journal of Alloys and Compounds* [online]. 2013, **577**(S1), p. S756-S759. ISSN 0925-8388, eISSN 1873-4669. Available from: https://doi.org/10.1016/j.jallcom.2012.02.135

[30] ZAFAR, A., ANDRAWES, B. Seismic behavior of shape memory composite bars in RC moment frames. In: 15th World Conference on Earthquake Engineering: proceedings. 2012.

[31] BAJORIA, K. M., WANKHADE, R. L. Free vibration of simply supported piezolaminated composite plates using finite element method. *Advanced Materials Research* [online]. 2012, **587**, p 52-56. ISSN 1662-8985. Available from: https://doi.org/10.4028/www.scientific.net/AMR.587.52

[32] WANKHADE, R. L., BAJORIA, K. M. Stability of simply supported smart piezolaminated composite plates using finite element method. In: International Conference on Advances in Aeronautical and Mechanical Engineering - AME 2012: proceedings. Vol. 1. 2012. ISBN 978-981-07-2683-6, p. 14-19.

[33] WANKHADE, R. L., BAJORIA, K. M. Free vibration and stability analysis of piezolaminated plates using finite element method. *Smart Materials and Structures* [online]. 2013, **22**(12), 125040. ISSN 0964-1726, eISSN 1361-665X. Available from: https://doi.org/10.1088/0964-1726/22/12/125040

[34] WANKHADE, R. L., BAJORIA, K. M. Buckling analysis of piezolaminated plates using higher order shear deformation theory. *International Journal of Composite Materials* [online]. 2013, **3**(4), p. 92-99. ISSN 2166-479X, eISSN 2166-4919. Available from: https://doi.org/10.5923/j.cmaterials.20130304.02

[35] JALAEEFAR, A., ASGARIAN, B. Experimental investigation of mechanical properties of nitinol, structural steel and their hybrid component. *Journal of Materials in Civil Engineering* [online]. 2013, **25**(10), p. 1498-1505. ISSN 0899-1561, eISSN 1943-5533. Available from: https://doi.org/10.1061/(ASCE)MT.1943-5533.0000701

[36] NAZIM, O.-B., BOUZID, A.-H., BRAILOVSKI, V. On the use of shape memory alloy studs to recover load loss in bolted joints. *Journal Pressure Vessel Technology* [online]. 2013, **135**(2), PVT-11-1178. ISSN 0094-9930, eISSN 1528-8978. Available from: https://doi.org/10.1115/1.4023416

[37] CLADERA, A., WEBER, B., LEINENBACH, C., CZADERSKI, C., SHAHVERDI, M., MOTAVALLI, M. Iron-based shape memory alloys for civil engineering structures: an overview. *Construction and Building Materials* [online]. 2014, **63**, p. 281-293. ISSN 0950-0618, eISSN 1879-0526. Available from: https://doi.org/10.1016/j.conbuildmat.2014.04.032

[38] CZADERSKI, C., SHAHVERDI, M., BRONNIMANN, R., LEINENBACH, C., MOTAVALLI, M. Feasibility of iron-based shape memory alloy strips for prestressed strengthening of concrete structures. *Construction and Building Materials* [online]. 2014, **56**, p. 94-105. ISSN 0950-0618, eISSN 1879-0526. Available from: https://doi.org/10.1016/j.conbuildmat.2014.01.069

[39] SEPULVEDA, J., BOROSCHEK, R., HERRERA, R., MORONI, O., SARRAZIN, M. Steel beam -column connection using copper-based shape memory alloy dampers. *Journal of Constructional Steel Research* [online]. 2008, **64**(4), p. 429-435. ISSN 0143-974X, eISSN 1873-5983. Available from: https://doi.org/10.1016/j.jcsr.2007.09.002

[40] MALAGISI, S., MARFIA, S., SACCO, E., TOTI, J. Modeling of smart concrete beams with shape memory alloy actuators. *Engineering Structures* [online]. 2014, **75**, p. 63-72. ISSN 0141-0296, eISSN 1873-7323. Available from: https://doi.org/10.1016/j.engstruct.2014.05.035

[41] CZADERSKI, CH., SHAHVERDI, M., MOTAVALLI, M., WEBER, B. Iron-based shape memory alloys (Fe-SMA) - a new material for prestressing concrete structure. In: 3rd Conference on Smart Monitoring, Assessment and Rehabilitation of Structures SMAR 2015: proceedings. 2015.

[42] BAJORIA, K. M., WANKHADE, R. L. Vibration of cantilever piezolaminated beam with extension and shear mode piezo actuators. In: SPIE Smart Structures and Materials + Nondestructive Evaluation and Health Monitoring: proceedings. Vol. 9431. 2015. 943122. Available from: https://doi.org/10.1117/12.2084271

[43] WANKHADE, R. L., BENDINE, K. Vibration control of FGM piezoelectric plate based on LQR genetic search. *Open Journal of Civil Engineering* [online]. 2016, **6**(1), p. 1-7. ISSN 2164-3164, eISSN 2164-3172. Available from: https://doi.org/10.4236/ojce.2016.61001

[44] WANKHADE, R. L., BAJORIA, K. M. Shape control and vibration analysis of piezolaminated plates subjected to electro-mechanical loading. *Open Journal of Civil Engineering* [online]. 2016, **6**(3), p. 335-345. ISSN 2164-3164, eISSN 2164-3172. Available from: https://doi.org/10.4236/ojce.2016.63028

[45] NAGASHIMA, N., SAWAGUCHI, T., OGAWA, K. Fatigue properties of Fe-28Mn-6Si-5Cr-0.5Nbc alloy. *Procedia Structural Integrity* [online]. 2016, **2**, p. 1435-1442. eISSN 2452-3216. Available from: https://doi.org/10.1016/j.prostr.2016.06.182

[46] WANKHADE, R. L., BAJORIA, K. M. Numerical optimization of piezolaminated beams under static and dynamic excitations. *Journal of Science: Advanced Materials and Devices* [online]. 2017, **2**(2), p. 255-262. ISSN 2468-2284, eISSN 2468-2179. Available from: https://doi.org/10.1016/j.jsamd.2017.03.002

[47] BENDINE, K., WANKHADE, R. L. Optimal shape control of piezolaminated beams with different boundary condition and loading using genetic algorithm. *International Journal of Advanced Structural Engineering* [online]. 2017, **9**(4), p. 375-384. ISSN 2008-3556, eISSN 2008-6695. Available from: https://doi.org/10.1007/s40091-017-0173-x

[48] WANKHADE, R. L., BAJORIA, K. M. Vibration analysis of piezolaminated plates for sensing and actuating applications under dynamic excitation. *International Journal of Structural Stability and Dynamics* [online]. 2019, **19**(10), 1950121. ISSN 0219-4554, eISSN 1793-6764. Available from: https://doi.org/10.1142/S0219455419501219

[49] WANKHADE, R. L., BAJORIA, K. M. Vibration attenuation and dynamic control of piezolaminated plates with coupled electromechanical actuation. *Archive of Applied Mechanics* [online]. 2021, **91**, p. 411-426. ISSN 0939-1533, eISSN 1432-0681. Available from: https://doi.org/10.1007/s00419-020-01780-6

[50] IS 383: 1970. Specification for coarse and fine aggregates from natural sources for concrete.

[51] IS 11309: 1985. Method of conducting pull-out test on anchor bars and rock bolts.

[52] IS 9879: 1998. Method for emission spectrometric analysis of austenitic and ferritic stainless steels point to plane technique.

[53] IS 9103: 1999. Concrete admixtures-specifications.

[54] IS 1786: 2008. Indian standard code for high strength deformed steel bars and wires for concrete reinforcement.

[55] IS 10262: 2009. Concrete mix proportioning-guidelines.

[56] ASTM B117: 2011. Test conditions, method and application.
[57] IS 12269: 2013. Ordinary portland cement. 53 grade-specifications.
[58] IS 516 (Part-1 Sec-I): 2021. Compressive, flexural and split tensile strength.
[59] ASTM A370: 2021. Standard test methods and definitions for mechanical testing of steel products.

This is an open access article distributed under the terms of the Creative Commons Attribution 4.0 International License (CC BY 4.0), which permits use, distribution, and reproduction in any medium, provided the original publication is properly cited. No use, distribution or reproduction is permitted which does not comply with these terms.

MECHANICAL PROPERTIES INVESTIGATION AND OPTIMIZATION OF AMBIENTLY CURED ALKALI-ACTIVATED CONCRETE

Kothoju Saibaba*, B. Kondraivendhan

Department of Civil Engineering, SVNIT, Surat, Gujarat, India

*E-mail of corresponding author: d16am012@amd.svnit.ac.in

Kothoju Saibaba 0000-0001-7115-2800, B. Kondraivendhan 0000-0002-1589-919X

Resume

The mechanical, microstructural and statical interpretation of the Alkali Activated Concrete (AAC), prepared using fly ash with crushed granulated corex slag as the binder ingredient, are examined in this work. Here, cast in-situ alkali-activated concrete strengths and substitute slag concentrations of 0-50 % by fly-ash weight were undertaken to determine a workable manufacturing process and were all considered for up to 28 days. Moreover, in microstructural research, C-A-S-H gel is produced by adding Ground Granulated Corex Slag (GGCS) to the binder-generated structural changes in the in-situ alkali-activated concrete. As a result, this research obtained perfect mixture fractions by synthesizing 25 % GGCS with 0.4 % of the liquid-to-binder ratio, in addition, a unified desirability of 80 % was attained.

Article info

Received 15 December 2022
Accepted 10 March 2023
Online 19 April 2023

Keywords:

fly-ash
ground granulated corex slag (GGCS)
alkali-activated slag-concrete (AASC)
response surface
mechanical properties
microstructural analysis

Available online: https://doi.org/10.26552/com.C.2023.044

ISSN 1335-4205 (print version)
ISSN 2585-7878 (online version)

1 Introduction

Concrete use is expanding quickly due to the rising industrialization and housing need. The majority of infrastructure is presently built with concrete. Ordinary Portland Cement (OPC) is a vital element when making conventional concrete. The only additional material used more frequently than concrete on Earth is water [1]. One of the workable solutions for lowering the CO2 emissions has been suggested as creation of the low-carbon replacement binders [2]. An OPC binder can be replaced with geopolymer, a green substance that is ecologically friendly and devoid of cement. In an alkaline environment, the silica-alumina pebbles undergo a rapid chemical reaction that results in a 3D polymer sequence with a ring structure containing Si-O-Al-O links [3].

On the other hand, the OPC is not necessary when using alkali-activated concrete. The binder was produced when an aluminosilicate material was subjected to strong alkaline solutions. It is clear that throughout the manufacturing of OPC, enormous volumes of CO2 were released into the atmosphere in addition to depleting natural resources. It is necessary to use a green substitute material to counteract these impacts. Making environmentally friendly concrete requires using alternative resources [4]. Geopolymer concrete is made by mixing aggregates and residual material with cementing gel geopolymer [5]. Alkali-activated binders generate up to 80 % less CO2 than the Portland cement. [6].

Despite having existed since the nineteenth century [7] and possessing several advantageous qualities, the geopolymer system is not as frequently utilized in producing concrete as OPC. Cons of the two-part geopolymer binders have limited their usage in concrete production [8]. Though the technical features of the concrete made with this binder are improved, it may provide extra environmental advantages, as well [9]. It was found that increased ratio of calcium fly ash in concrete provides a compressive strength of 65 MPa without the use of high-temperature curing [10]. The activator, on the other hand, was still fluid, [11]. Creation of an one-part geopolymer mix has been attempted. Their research focused on creating one-part binders suitable from an economic and environmental standpoint, [12].

Burning coal in thermal power plant boilers produces a waste product known as fly ash. Fly ash is mainly

composed of alumina with silica, with small amounts of iron oxide, lime and magnesia added for balance. Massive volumes of fly ash are produced due to fast industrialization, as it accumulates over time and poses a risk to the environment. Alumina and silica-carrying components are required for geopolymer reactions and fly ash has attracted the attention of researchers as a relevant resource for geopolymer product development [13]. Fly ash is utilized to create geopolymers to reduce the fly ash's steadily growing environmental effect and protect naturally occurring aluminosilicate minerals [14]. It also offers the advantages of being workable, accessible, mechanically sound and improving end product durability [15]. Fly ash and alkali mix during polymerization create a cementitious substance comprised of alumina-silicate-hydrate (A-S- H) gel [16]. Poor fly ash reactivity has shown to be challenging since it results in a sluggish setting and strength properties. Before the final cemented structure is formed, fly ash is typically only partially broken down [17-18]. Granulated Blast Furnace Slag (GBFS), for example, has been utilized to improve the reactivity of geopolymer precursors, according to [19]. The main constituents of GBFS, which is granular and glassy, include oxides like SiO2, CaO, Al2O3 and MgO. It is created by rapidly cooling molten blast furnace (BF) slag, a by-product of iron manufacturing, often by submersion in water, followed by crushing to improve reactivity. The process causes the Ca in the slag to hydrate, forming C-S-H gel, a cementitious phase that enhances the setting and strength features [20].

Ordinary Portland cement concrete (OPCC) and alkali-activated slag concrete (AASC) have benefits, including improved durability, high strength and minimal environmental effect. Hydrated sodium silicate gel, with crystalline hydrated calcium silicate gel (C-A-S-H or C-S-H), are the primary reaction products of AASC (N-A-S- H). Due to its low CaO/SiO2 ratio and other microstructural changes, the C-S-H gel in AASC varies from that seen in Portland cement concrete [21]. Studies [22-23] have shown that the kind and nature of the starting material Ground Granulated Blast Furnace Slag (GGBFS), the quantity and composition of the alkaline activator solution, as well as the curing conditions, have a significant impact on the mechanical and toughness properties of AASC. Consequently, it is crucial to fully understand a novel type of concrete's mechanical performance and toughness characteristics before using it in a building. To serve as a reliable foundation material for AASC, GGBFS also needs sufficient amounts of calcium and silica with alumina species. When alkali hydroxide or alkali silicate are used as activators separately, rather than both, the strength is lower [24]. Multiple investigations have been conducted on the mechanical strength and robustness characteristics of AASC. It is not easy to find information on how to blend materials for AASC with the appropriate compressive strength [25]. By choosing the right proportions of concrete components from the literature [26-27], it is possible to create alkali-activated concretes with the requisite strength. Based on its compressive strength, concrete's flexural and split tensile strengths may be estimated using the codified equations [28].

To examine the effects, connections and interconnections among dependent variables (responses) and independent elements, the Response Surface Methodology (RSM) links the output outcome to independent variables [29]. The response surface approach has been used to build models and enhance mixes in various academic fields. Several sectors started using statistical design approaches in the 1930s due to Box and Wilson's creation of the response surface procedure in 1951 [9]. The response surface approach is commonly applied in producing conventional OPC and geopolymers to imitate and enhance experimental findings [30].

Davidovits [12], initially utilized RSM to predict the compressive strength of a mixed paper concrete in terms of optimizing the model. The research was backed by several scientists [31] [32-33]. In their recent work [34], hybrid design systems for roller-compacted concrete were created using the RSM approach. They improved the performance of roller-compacted rubber concrete (RCR) mixes and reduced water absorption. By predicting their mechanical and post-cracking behaviour, [35] built and refined engineered geopolymer composites and effectively increased the compressive strength and ductility of the necessary cementitious composites.

In recent research, anhydrous GCS raw materials were converted into one-part alkali-activated binders. However, few researchers have used the RSM approach to develop and predict the behaviour of one-part geopolymer binders manufactured from anhydrous corex slag and supplemented with low calcium fly ash [36]. In the current study, alkali-activated concrete was made and allowed to cure at room temperature and in an oven. It could also be cast in place. The strength and microstructures of cast in-situ alkali-activated concrete were investigated at various Ground Copper Slag (GCS) levels while utilizing the conventional sodium silicate and sodium hydroxide combination. In one section, RSM was used to conduct optimization research on fly ash and GCS parameters to produce the most resilient alkali-activated concrete.

2 Materials and methods

2.1 Materials

2.1.1 Flyash

Fly ash was the main source of aluminosilicates employed in this experiment's geopolymer binder (ASTM Class F). Ninety-five percent of the fly ash used in this

investigation, which had a relative density of 2.2 as well as a mesh size of 45 microns, went through the sieve. Table 1 shows the chemical composition as established by chemical characterization.

2.1.2 Ground granulated Corex slag

This study utilized ground granulated Corex slag as a supplementary binder (GGCS). It is a by-product of the iron industry, which primarily consists of minerals with the chemical composition of calcium aluminosilicate. Owing to its strong reactivity with particular surface area, it was believed that using the GGCS as a fly ash replacement in one-part alkali-activated substances would improve their tensile qualities. Table 1 displays the chemical makeup of the GGCS oxide utilized in this study, with GGCS slag replacing fly ash at weight percentages of 0%, 10%, 20%, 30%, 40% and 50%, respectively.

2.1.3 Alkaline solution

Sodium Hydroxide (NaOH) with sodium silicate (Na_2SiO_3) solutions were mixed to produce the activator solution. The 97-98% pure NaOH pellets and tap water were combined to create a sodium hydroxide solution with the right concentration. A local commercial supplier provided sodium silicate solution in the ready-made form.

Composition of Sodium silicate: Color: colourless/ White liquid physical state; Density: 1.44 : 1.56 g/cm3, Mass percentage: 44:48 of total solids, respectively. The densities of sodium hydroxide and complete alkaline solutions were 1.15 and 1.5 g/cm3, respectively. This investigation used a single alkaline solution with a constant NaOH concentration of 8M.

2.1.4 Aggregates

The coarse aggregate is crushed rock granite, whereas the fine aggregate is local sand, Table 2. For fine and coarse aggregates, the specific gravity and bulk modulus, with void ratio, are 2.52, 1.54 g/cm3, 0.632 and 2.47, 1.678 g/cm3, 0.456. A constant weight ratio of 0.7 was used for coarse aggregate to total aggregate.

Figures 1 and 2 show the fly ash XRD pattern and the Corex slag XRD pattern for the method, respectively, with intensity on the Y-axis and 2θ on the X-axis.

The chemical analysis of GGCS powder and fly ash was carried out using an Inductively coupled plasma optical emission spectrometer Loss on ignition (LOI) was measured by calculating the weight loss upon heating. Instrument used in the present study is Bruker AVANCE III 700 MHz NMR spectrometer equipped with a 5 mm triple resonance cryoprobe with Z-gradient. The phase assemblages of AAMs were generated using the simulated precursors with 80 wt % SiO2 + CaO + Al2O3 as the primary contents, which play the most crucial role during the alkali-activation of aluminosilicate materials.

Table 3 shows the mixed proportions of AASC concrete. Here, L/B denotes the liquid-to-binder ratio, M denotes moles and FA and CA are Fine and Coarse Aggregate. This table gives a detailed explanation of mix designation, Fly ash, corex slag, NaOH and other parameters with their proportions.

2.1.5 Mixing, sample preparation and curing

To create the necessary molarity of sodium hydroxide solution, sodium hydroxide pellets are diluted with water. For example, 255 g of sodium hydroxide pellets are dissolving in water to create 1 kilogram of an 8 M sodium hydroxide solution. The concentration of the sodium hydroxide solution affects the mass of

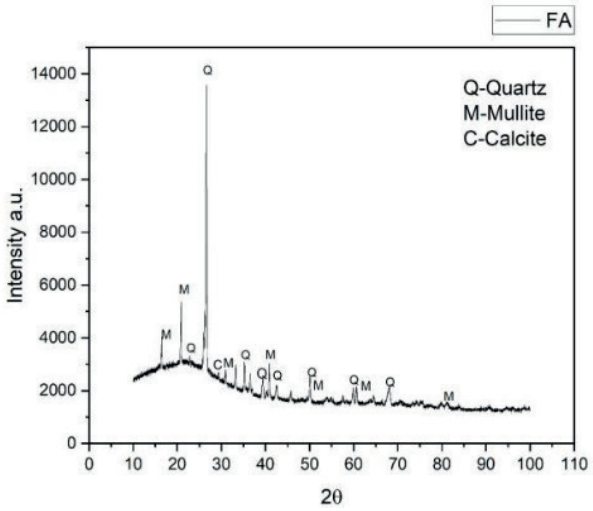

Figure 1 *Fly ash XRD Pattern*

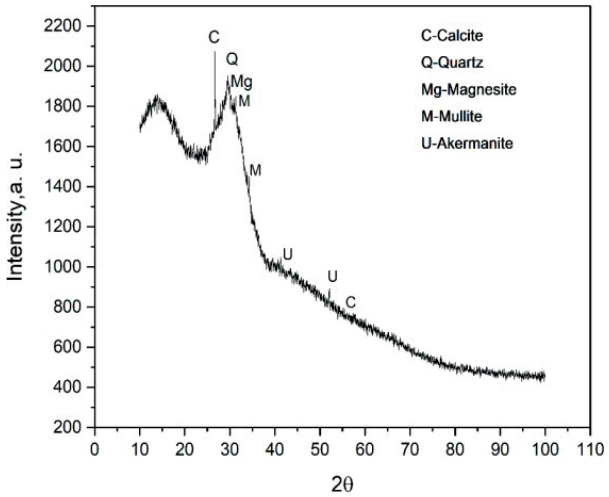

Figure 2 *Corex slag XRD Pattern*

Table 1 *Fly ash and GGCS Oxide Compositions*

Oxide	Fly ash (Wt. %)	GGCS (Wt. %)
Calcium oxide, CaO	3.62	35.79
Silicon oxide, SiO_2	56.38	34.58
Aluminium oxide, Al_2O_3	23.30	17.28
Iron oxide, Fe_2O_3	15.92	0.92
Magnesium oxide, MgO	0.34	8.05
Potassium oxide, K_2O	-	-
Loss of ignition, LOI	0.79	0.97

Table 2 *Basic Properties Coarse and Fine Aggregates*

Basic Property	Fine Aggregate	Coarse Aggregate
Specific Gravity	2.54	2.78
Water absorption	2%	0.6%
Fineness modulus	2.62	7.28
Bulk density	1.39	1.48

Table 3 *Mix Proportions of AASC concrete*

Mix designation	Fly ash (kg/m^3)	Corex slag (kg/m^3)	L/B ratio	NaOH (kg/m^3)	Na_2SiO_3 (kg/m^3)	M	FA (kg/m^3)	CA (kg/m^3)	SiO_2/Al_2O_3
A1F100S0	444.45	0	0.35	44.45	111.1	8	540	1260	2.42
A1F90S10	400.00	44.44	0.35	44.45	111.1	8	540	1260	2.38
A1F80S20	355.56	88.89	0.35	44.45	111.1	8	540	1260	2.35
A1F70S30	311.11	133.33	0.35	44.45	111.1	8	540	1260	2.30
A1F60S40	266.69	177.76	0.35	44.45	111.1	8	540	1260	2.30
A1F50S50	222.22	222.22	0.35	44.45	111.1	8	540	1260	2.25
A2F100S0	428.50	0	0.40	49	122.5	8	540	1260	2.42
A2F90S10	385.65	42.85	0.40	49	122.5	8	540	1260	2.38
A2F80S20	342.8	85.70	0.40	49	122.5	8	540	1260	2.35
A2F70S30	299.95	128.55	0.40	49	122.5	8	540	1260	2.30
A2F60S40	257.10	171.40	0.40	49	122.5	8	540	1260	2.30
A2F50S50	214.25	214.25	0.40	49	122.5	8	540	1260	2.25
A3F100S0	413.80	0	0.45	53	133	8	540	1260	2.42
A3F90S10	372.42	41.38	0.45	53	133	8	540	1260	2.38
A3F80S20	331.04	82.76	0.45	53	133	8	540	1260	2.35
A3F70S30	289.66	124.14	0.45	53	133	8	540	1260	2.30
A3F60S40	248.28	165.52	0.45	53	133	8	540	1260	2.30
A3F50S50	206.90	206.90	0.45	53	133	8	540	1260	2.25

sodium hydroxide pellets in the liquid. An amount of 39 g of sodium hydroxide pellets is needed to make a 1M sodium hydroxide solution kilogram. After that, the sodium hydroxide and sodium silicate solutions are blended. The moisture content of the sodium silicate solution is disregarded, while creating sodium hydroxide solution or calculating sodium hydroxide concentration. One day prior to casting, the sodium silicate with sodium hydroxide solutions are adequately combined to achieve ideal solution mixing.

NaOH and Na_2SiO_3 solutions were thoroughly combined in this study's alkaline solution, Na_2SiO_3, then heated to 25 ± 2 °C 24 hours before usage. The activators' dosages are listed as a percentage of the binder, varying NaOH to (0.35, 0.40 and 0.45). A drum mixer with a saturated dry surface condition thoroughly mixed coarse and fine materials with a binder during dry Mixing. The alkaline liquid was adequately mixed and diluted with water. The two components were then blended for 5 minutes at a temperature of 27 ± 2 °C after combining the dry mixture and liquid combination. Preparing the alkaline solution 24 hours in advance was the major challenge with the Mixing procedure. This issue limits the use of fly ash-based geo-polymer

concrete and makes precast concretes a better fit. The issue of temperature increase during the production of alkaline solutions is another.

After mixing, the cement was poured into concrete molds measuring 150 mm x 150 mm x 150 mm, vibrating for 45 seconds and then allowed to dry for 24 hours. Twenty-four hours after the casting, the samples were de-molded and dried in ambient and oven settings. Until the testing age was attained, specimens were ambiently cured at room temperature (25 °C and 75% relative humidity) (28 and 56 Days). However, for oven curing, the de-molded samples were held in the oven at a temperature of (60 °C for 24 hours) but then left at room temperature until the age of testing. For outdoor cured specimens, humidity and temperature management are not necessary. At 28 and 56 days old, AAC samples underwent compressive strength testing.

2.2 Methods

The resultant mix proportions, indicated in Table 2, were created to create a total of 12 concrete mixes so that the parameters chosen for this investigation covered all of the mix design's limitations. Because of that, the study's changeable parameters include the ratio of alkaline solution to binder, curing and GGCS.

2.2.1 Mechanical strength tests

To examine the mechanical features of AAC, three cubes (150 x 150 x 150 mm) and three cylinders (100 mm diameter x 200 mm height), with three prisms (500 x 100 x 100 mm), were cast for each mix then evaluated for compressive, split tensile and flexural strength after 28 and 56 days of curing. Compressive including flexural strength testing was conducted by IS 516:1959 [8] (or ASTM C78), whilst split tensile tests were carried out by IS 5816: 1999 [9], (or ASTM C496). The AAC's flexure strength is evaluated using the three-point loading test.

2.2.2 Creation of statistical models utilizing the response surface approach

This research examined the combined impact of flyash and GGCS on behavior of the cast-in-situ alkali-activated concrete to establish a connection between input factors and output responses. The most potent combinations are discovered through the numerical optimization, which also decreases water absorption. The response surface analysis used a unique sequence of predictors to demonstrate statistical correlations among results with independent variables. Given that it can be employed when there are two independent variables, the central composite model was the most extensively applied with a reliable model [31, 37-41]. Design expert software was used for the experimental design. The cast in-situ alkali-activated concrete mix design formulas were randomly chosen for the two independent variables using a face-centered central composite design (FCCD). Flyash percentages ranging from 0 to 100% and GGCS percentages ranging from 10 to 50% by weight of the flyash were the design parameters examined. The results of this experiment included increases in compression strength, split tensile strength, flexural strength and overall weight decrease. For each response, the computer-generated five randomly duplicated combinations totaling thirty. The software uses the five duplications to compare the experiment's accuracy to any possible defects.

2.2.3 Field emission scanning electron microscopy

On a field emission scanning electron microscope equipped with EDAX (ULTRA plus, Carl Zeiss), the interfacial transition zone of concrete examples (20 mm in length, 20 mm in width and 25 mm in height) was investigated. Before testing, the samples' surfaces were coated with Au/Pd to make them conductive. Unreacted nanoparticles and cracks, including bonding among the aggregate and then paste, were all studied in the microstructures. Variations in elemental composition were mapped using EDAX from one location to the next.

3 Results and discussion

3.1 Compressive strength

The AAC compressive strength is determined by various parameters, including the binder content, alkaline content and aggregate used in the mix. Several trial mixes were created and tested. Two mixes were chosen based on the outcomes of the experiments. Figures 3-5 display the compressive strength of AAC at various ages (28 and 56 days) and the liquid-to-binder ratio (0.35, 0.40 and 0.45). With an increase in GGCS concentration in the mix, the compressive strength of both ambient and oven-cured AAC was increased. The presence of calcium was crucial in achieving AAC strength, which was further improved by producing C-A-S-H gels. After 28 days, ambient and oven-cured F70S30 samples have compressive strengths of 50.55 MPa and 53.77 MPa, correspondingly.

3.2 XRD analysis

The XRD is an important method used for cement concrete samples' quantitative and qualitative analysis. Here, pan analytical equipment is utilized. By using the XRD test results, a graph between the angle at which the wave was diffracted and intensity of X-Ray was

determined. The XRD test was conducted on samples on the 28-th day. Figures 15-18 show XRD for AAC samples cured at ambient and oven conditions for 28 days for the mix F70S30. The diffractometer having a wavelength $\chi = 1.54\text{Å}$ at the scan step time [s] = 72.97. Scan Axis is $20 - \omega$, start position, end position, step size, scan step time for 2θ is 10.0126, 99.9856, 0.0130, 72.9710 and scan type is continuous.

Some dissolvable minerals, such as quartz and mullite, have survived in all products, as evidenced by face-cantered XRD patterns. The peak (between 26° and 30°) in the fly ash and GGCS-based AAC XRD patterns indicates that the geopolymer material has semi-crystalline and amorphous structures. The peak (between 26° and 30°) in the reaction products with relatively lower intensities indicates that the alkali-activated material has an almost completely amorphous structure.?? It was discovered that the alkali activators in both regimes have a diffuse hump between 26° and 30°. When partial replacement of fly ash with GGCS (20% and 30%) in ambient conditions was compared to the patterns of both grades, no significant change in AAC was detected.

3.3 Effect of curing on compressive strength

This study examined the AAC's compressive strength in relation to the impacts of ambient plus oven curing. Oven-cured samples get a greater compressive strength than ambient-cured samples. The strength gain is more significant since the polymerization procedure is frequently accelerated at a temperature greater than ambient. When it comes to casting in place, it is critical to cure at room temperature. High strength gains for F70S30, when exposed to ambient curing, is around 50.55 MPa, whereas the strength gains for F70S30, when exposed to oven curing, is around 53.35 MPa for 8M. With the addition of GGCS, ambient curing yielded satisfactory results without needing oven curing. As a result, oven curing can be avoided if AAC is manufactured with GGCS instead of fly ash. There was a quick rise in compressive strength up to 7 days after increasing the GGCS concentration in the mix and changing the liquid-to-binder ratio and the strength continued to improve up to 28 days. A blend with a 30% GGCS content in the overall binder composition provides more strength than a mix with a 50% GGCS content. The addition of calcium causes the strength of fly ash and GGCS-based AAC to increase. Including soluble calcium increases compressive strength, which speeds up the hardening process.

3.4 Effect of age on the strength of concrete

The connection between 7-day strength with 28-day strength is crucial for AAC. The study is also being done to determine how strong AAC is after 28 and 56 days. The liquid-to-binder concentration, alkaline activator solution molarity and curing regime have the most considerable effects on the compressive strength of AAC. After 28 days of healing, oven-cured samples have an advanced compressive strength with respect to the ambient-cured ones. The strength of the oven-cured sample is roughly two times that of the ambient-cured specimen after 28 and 56 days of curing.

The early strength was quite active after seven days, while the later strength gain was reduced. The initial curing temperature influences the polymerization process. The amount of heating is crucial in increasing the strength of AAC, regardless of the concrete composition. Strength improvements happen more quickly at an early age than they do later. It was seen with both types of curing. However, oven-cured AAC exhibits a better growth in strength than the ambient curing. The early rate of strength progress within 28 days is substantial, but the strength gain was not as noticeable later as it is in typical concrete. The 28-day compressive strength to 56-day compressive strength ratio illustrates this. This ratio varied for samples that were ambiently cured from 1.04 to 1.35. In an oven-cured sample, the compressive strength ratio at 28 days to the compressive strength at 56 days ranged from 1.06 to 1.32. It unequivocally demonstrates that, compared to regular concrete, which has a ratio of 1.50, acquiring compressive strength beyond 28 days is extremely slow.

Additionally, a 2-dimensional plot was used to graphically illustrate the contour plot of the developed model, as seen in Figure 6. All the contour lines represented the optimal interaction between the GGCS and the curing regime. The independent variables in the model demonstrate complete synergy with one another. In the contour plot, the yellowish and greenish regions denote a fantastic combination that results in the best strength values. According to the three-dimensional surface diagram in Figure 6 the ambient cured, alkali-activated mixes' compressive strength was raised and the setting time was shortened by adding GGCS to the mixtures. The presence of GGCS in the binder has a massive impact on the setting time of the pastes, causing them to harden more quickly since the model includes significant quantities of calcium oxide.

3.5 Split tensile strength

Figures 7-10 display the ambient, as well as the oven-cured specimens at the ages of 28 and 56 days. For Mix F90S10 - F50S50, the split tensile strength of AAC after 28 days was in the range of 2.25-4.80 MPa for ambient and oven curing, individually. It demonstrates that simple curing of the AAC specimens outside at average temperature is sufficient to achieve split tensile strength. It is owing to the geopolymer gel's tight connection with the aggregate particle.The split tensile

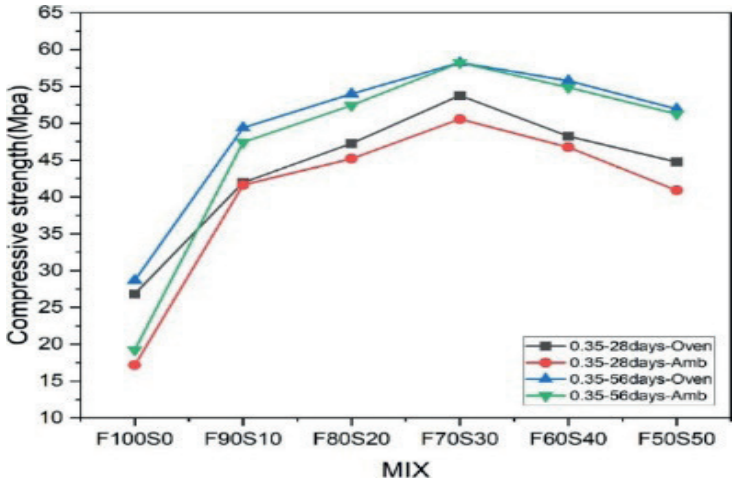

Figure 3 *Compressive strength results of L/B = 0.35*

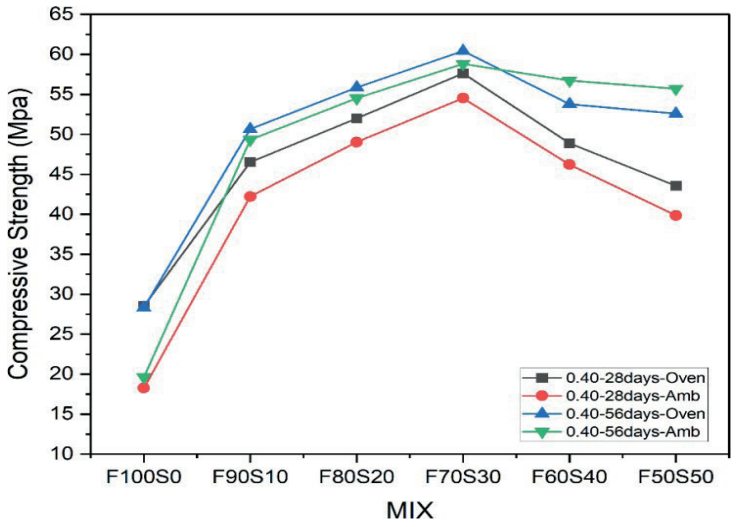

Figure 4 *Compressive strength results of L/B = 0.40*

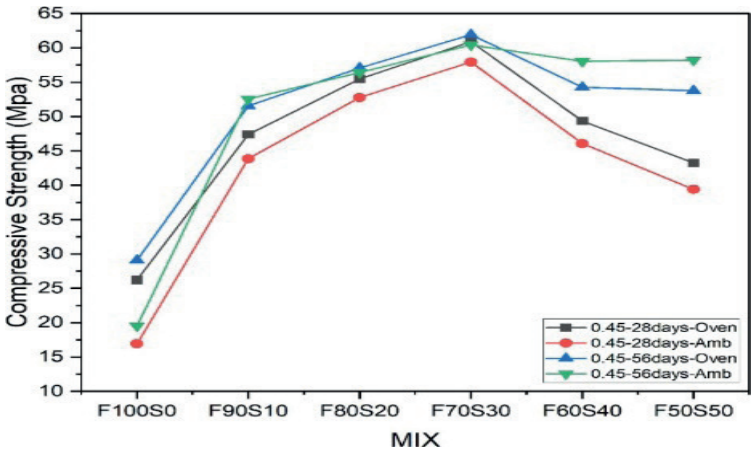

Figure 5 *Compressive strength results of L/B = 0.45*

strength of AAC samples treated under atmospheric temperatures rose to a satisfactory level with the calculation of GGCS for fly ash to the combination [22]. The material's tensile strength grew as the GGCS content did. Speculate that the rise in AAC strength is due to the continual creation of N-A-S-H and C-A-S-H gels. An empirical equation was established for ambient and oven curing using the experimentally obtained compressive and splitting tensile strength values of fly ash and GGCS-based concrete, as shown in Equations (1) and (2), respectively. The connection between the compressive and tensile strengths in conventional concrete is 0.7 * f_{ck}, but this value is lower when compared to traditional concrete.

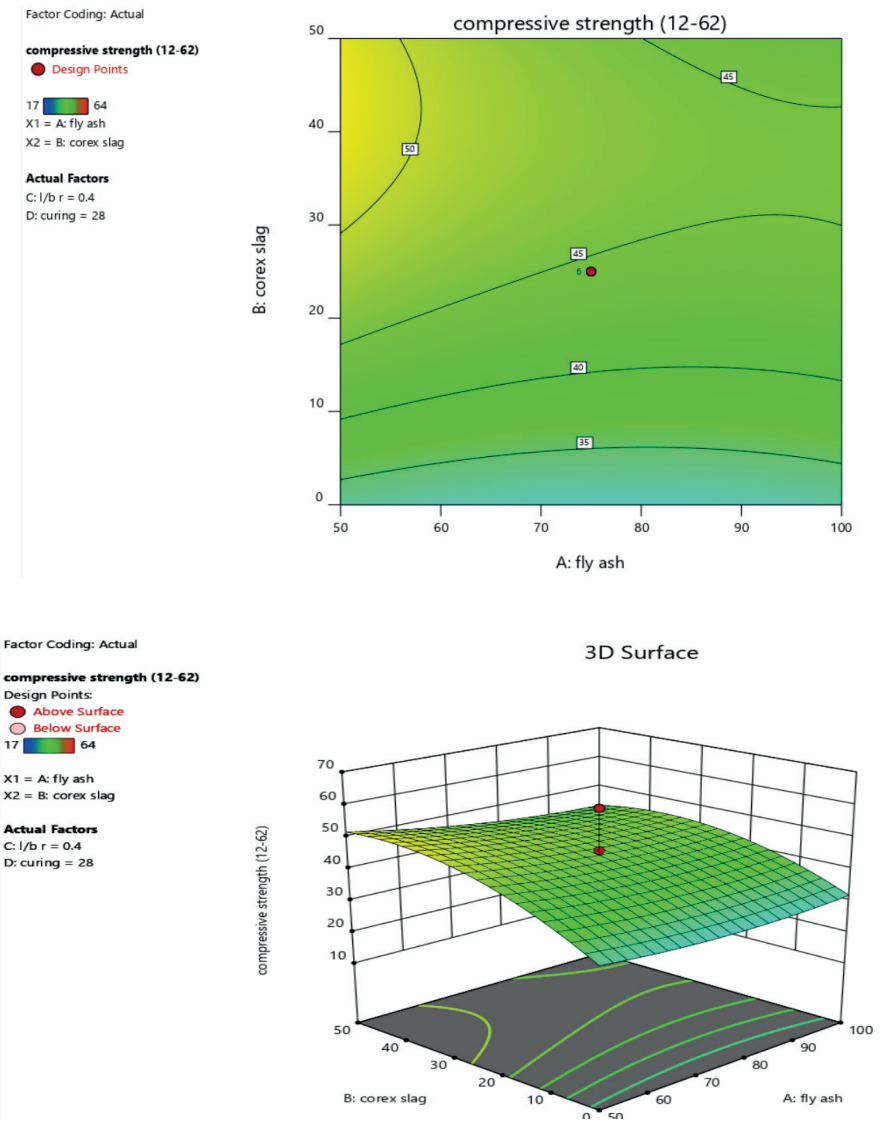

Figure 6 *2-D and 3-D response surface diagram for compressive strength*

$$Fsplit = 0.338 * \sqrt{fck} - ambient\ curing \quad (1)$$

$$Fsplit = 0.4178 * \sqrt{fck} - Oven\ curing \quad (2)$$

The splitting tensile strength is fsplit, while the Characteristic strength is fck.

3.6 Flexural strength

The flexural strength of the oven-cured specimens is superior to ambient-cured samples because of the quick polymerization process, as demonstrated in Figures 11 to 13. The flexural strength of ambient-cured AAC was 4.1 MPa, while that of oven-cured samples was 4.5 MPa. The flexural strength of AAC is increased as the GGCS content is improved. The GGCS component is essential for creating the C-A-S-H gel in the mix, increasing AAC strength. The contribution of strength is due to this gel formation. Equations (3) and (4) show the relationship between the compressive and flexural strengths

$$Fsplit = 0.412 * \sqrt{fck} - ambient\ curing \quad (3)$$

$$Fsplit = 0.437 * \sqrt{fck} - Oven\ curing\ . \quad (4)$$

The two-dimensional contour plots, presented in Figures 10 and 14, provide for precise observation of the change in splitting tensile with flexural strength across the mixes in the three-dimensional surface diagram (a). A yellowish area in Figures 10 and 14 represented the required variable combination. It demonstrates an excellent working relationship between the fly-ash and GGCS. The impact of the two factors (GGCS and other materials) on the split tensile strength with flexural strength after 28 days of ambient healing is depicted in a 3D dimensional diagram in Figures 10 and 14.

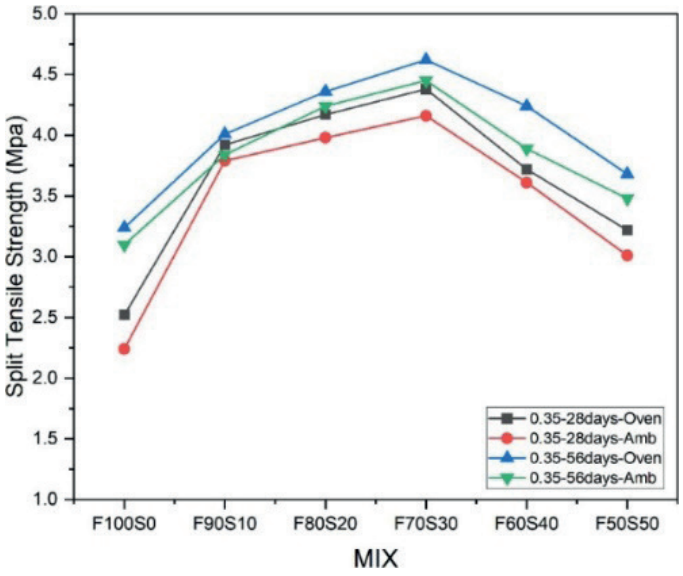

Figure 7 *Split tensile strength 0.35 liquid to binder ratio*

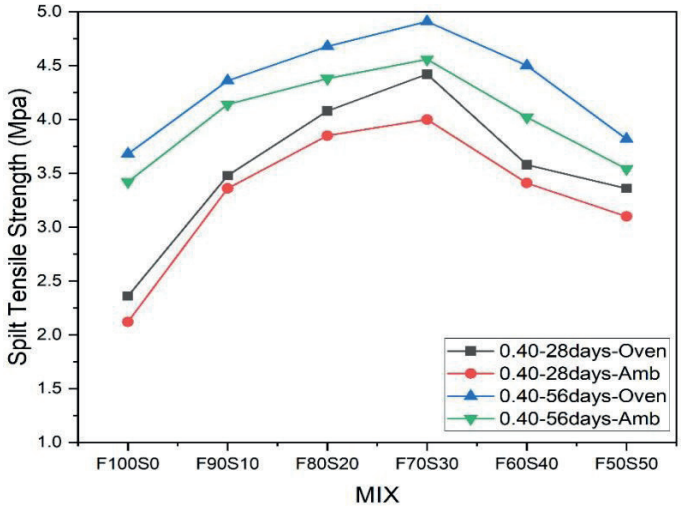

Figure 8 *Split tensile strength 0.40 liquid to binder ratio*

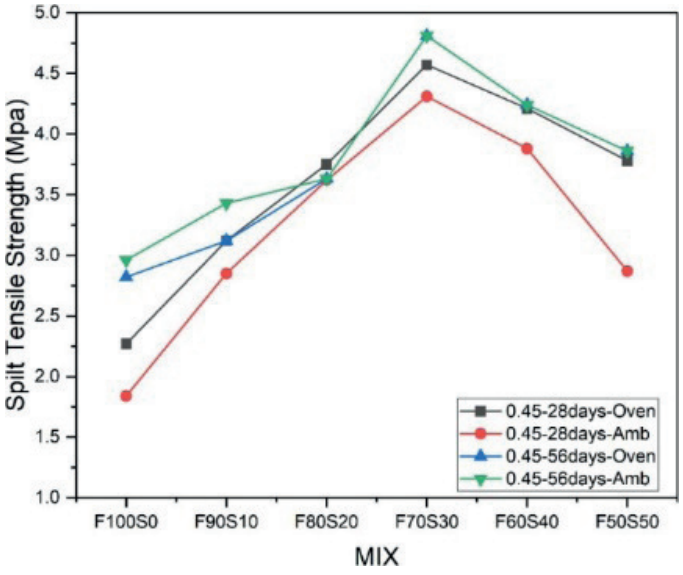

Figure 9 *Split tensile strength 0.45 liquid to binder ratio*

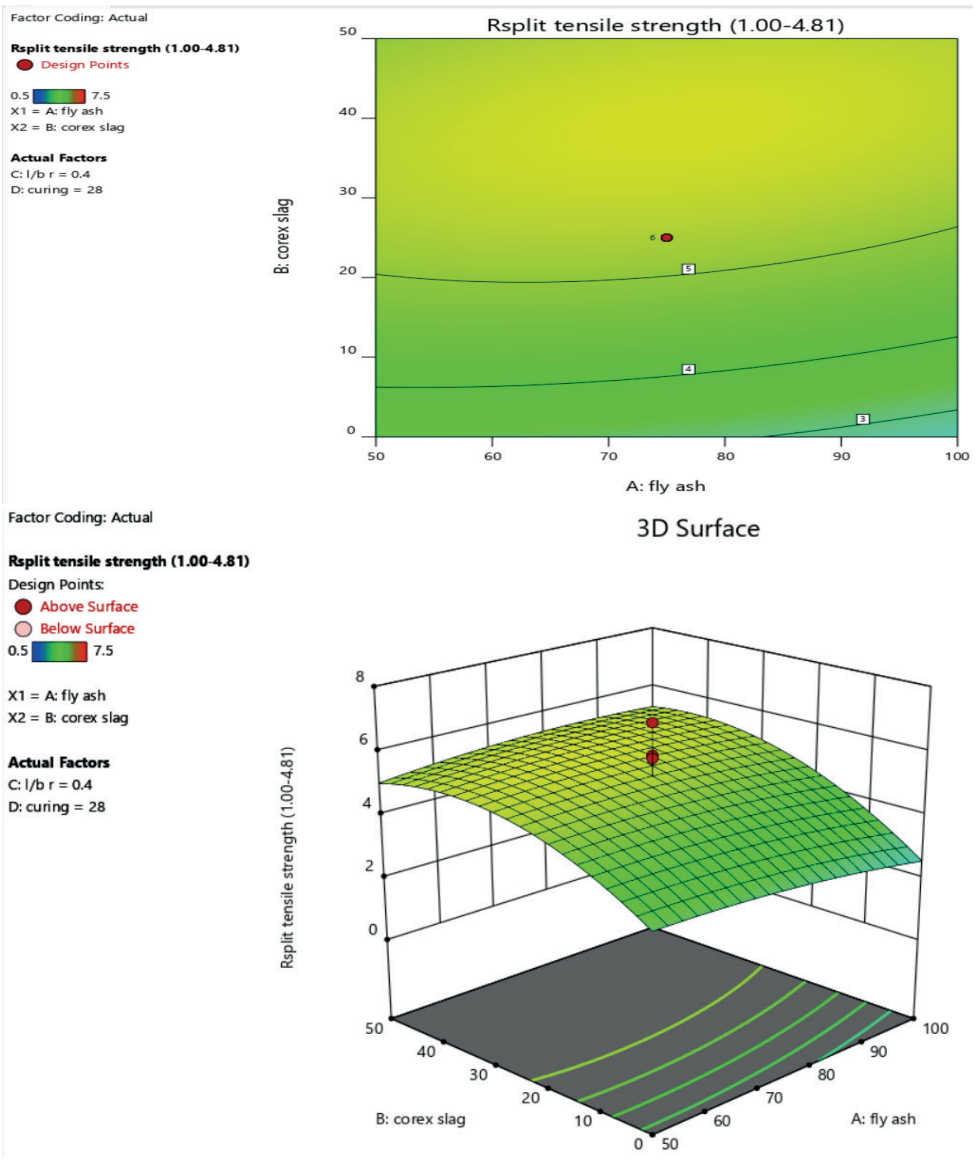

Figure 10 *2-D and 3-D Response surface diagram for split tensile strength*

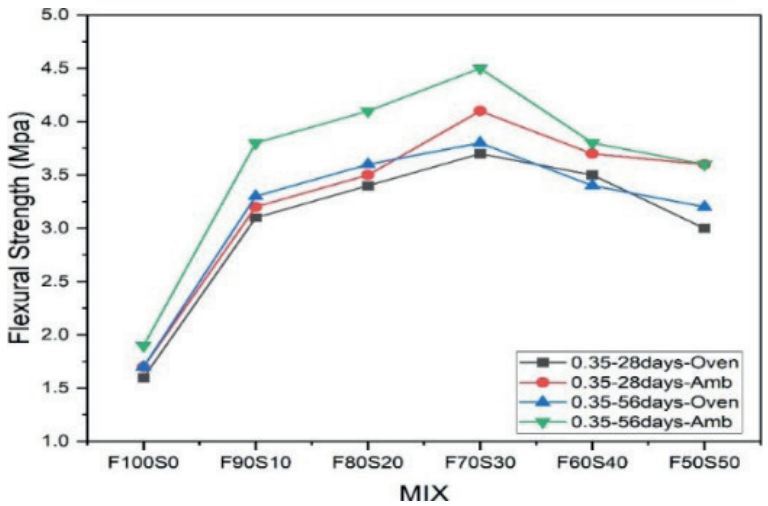

Figure 11 *Flexural strength results of L/B = 0.35*

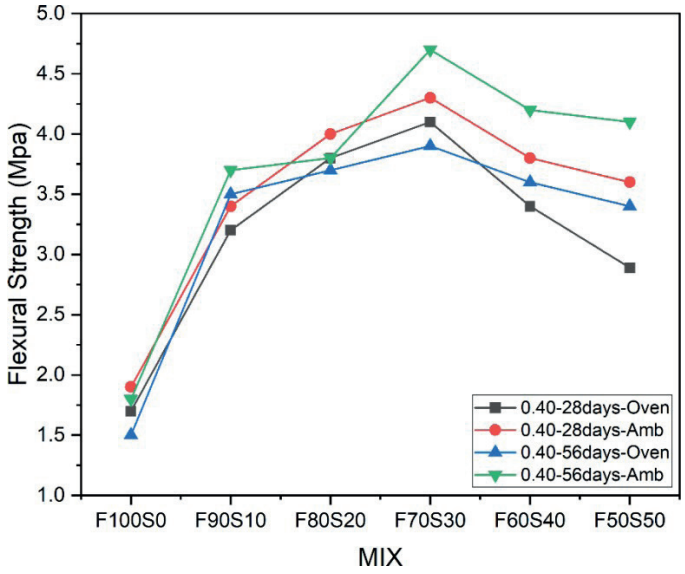

Figure 12 *Flexural strength results of L/B = 0.40*

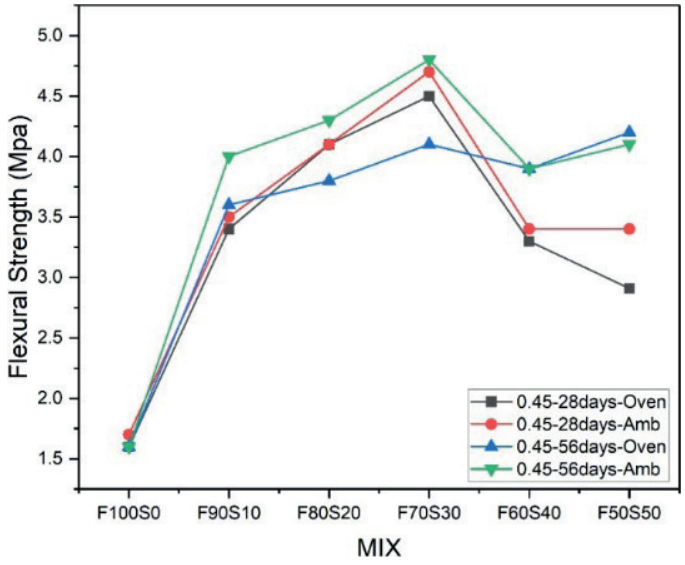

Figure 13 *Flexural strength results of L/B = 0.45*

3.7 SEM analysis

Using backscattered electron imaging, the AAC samples were analyzed. The fracture surfaces of materials, made using sodium silicate with sodium hydroxide solutions and cured in ambient as well as in an oven, respectively, are shown in Figures 19-22. The materials are heterogeneous and contain a significant amount of unreacted fly ash, as shown by the micrographs. A notable change in how the matrix-forming phases looked was seen for various curing regimes. The fly ash spheres were embedded in a glass-like matrix in the sample of ambiently cured silicate, while in the sample of oven-cured silicate, a composite matrix, made up of some glass-like and other more crystalline areas, had formed. Using micrographs of the fly ash activated in [4] to compare these pictures demonstrates that in this study, prolonged room-temperature procuring caused many fly ash dissolution and a continuous matrix phase to develop. It helped the AAC materials to become more homogeneous, which was advantageous.

3.8 Interpretation of the test results using statistics

Each of the existing models has undergone statistical analysis and validation. To determine the relevance of experimental factors, the analysis was done at a level of 5%. Flexural strength, splitting tensile strength and compressive strength were the dependent variables in this experiment. In addition, the independent parameters Flyash, GGCS, liquid-to-binder ratio and curing regime were used. The resulting p-values in Tables 4-6 demonstrate that each factor was significant at a 95% level and was regarded as a critical factor in the test's outcome.

The regression coefficient (R2) value was utilized

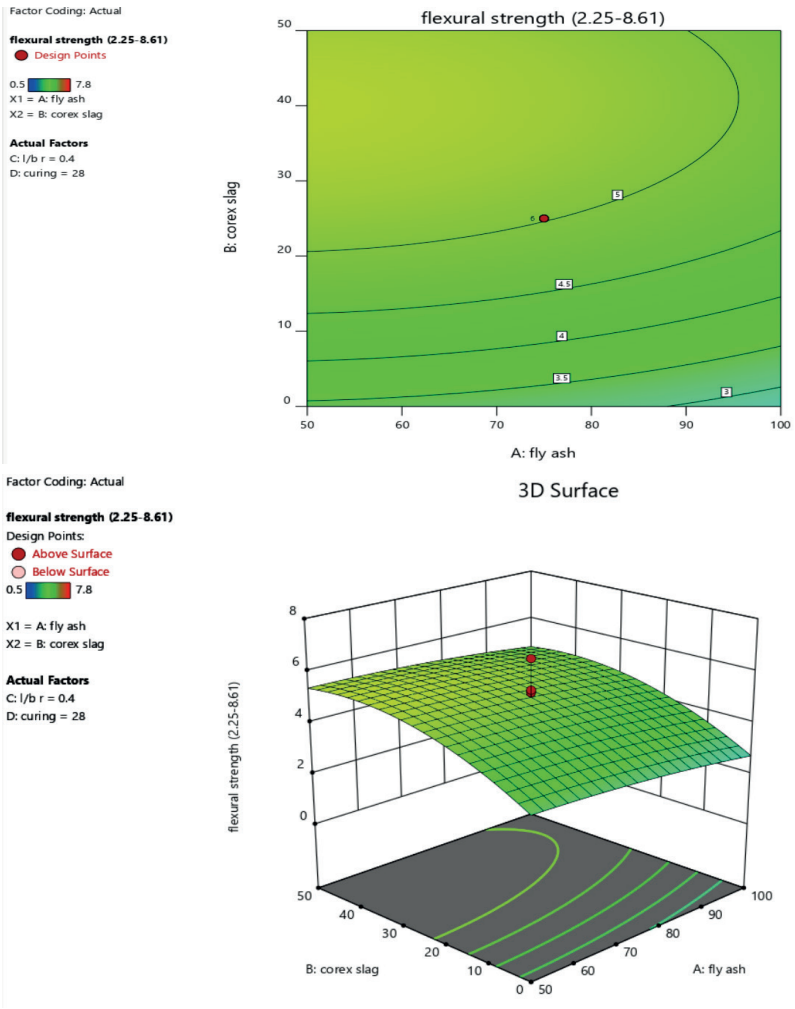

Figure 14 *2-D and 3-D response surface diagram for flexural strength*

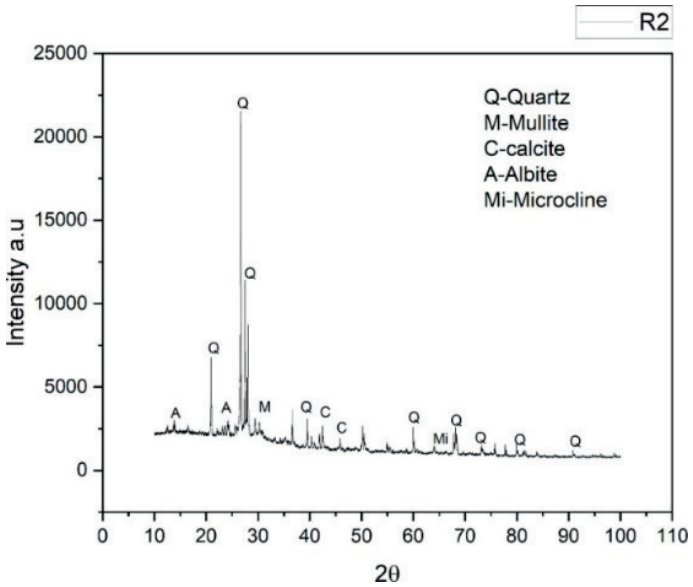

Figure 15 *XRD Mix F70S30 0.35 L/B Ambient*

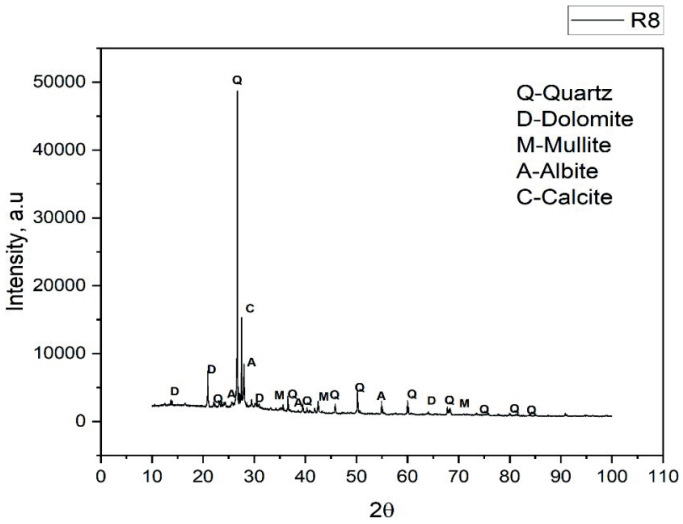

Figure 16 *XRD Mix F70S30 0.45 L/B Ambient*

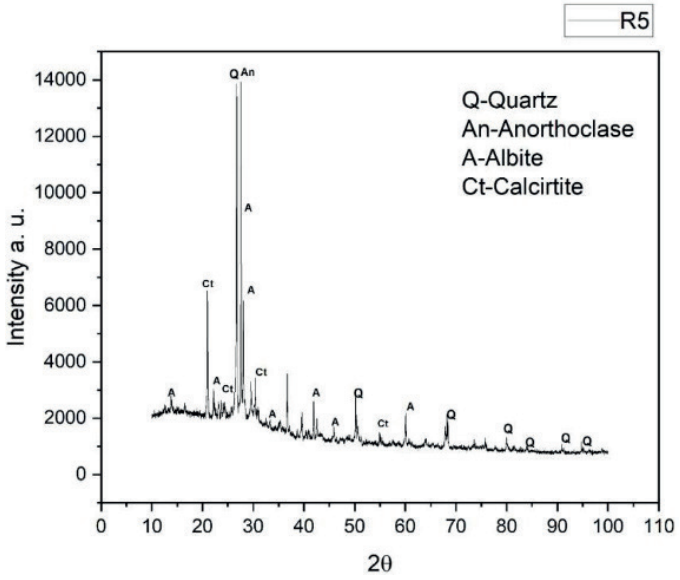

Figure 17 *XRD Mix F70S30 0.35 L/B Oven*

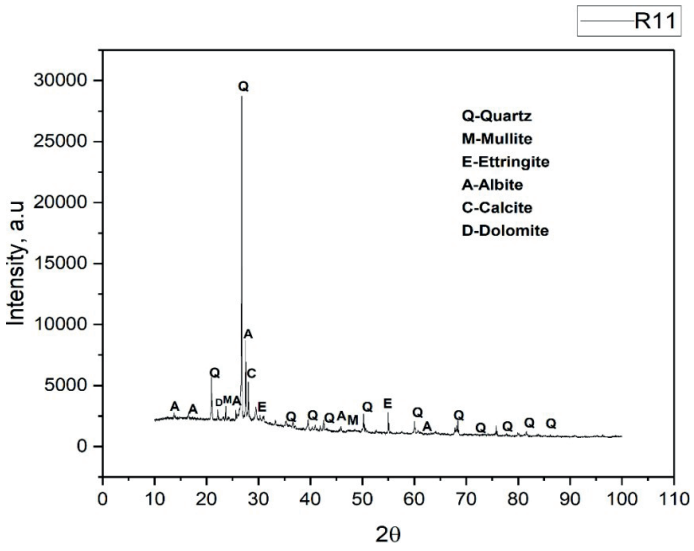

Figure 18 *XRD Mix F70S30 0.45 L/B Oven*

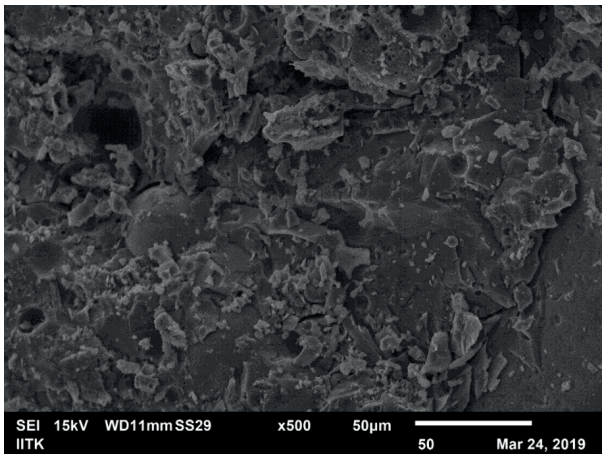

Figure 19 *SEM Mix F70S30 0.35 L/B Oven*

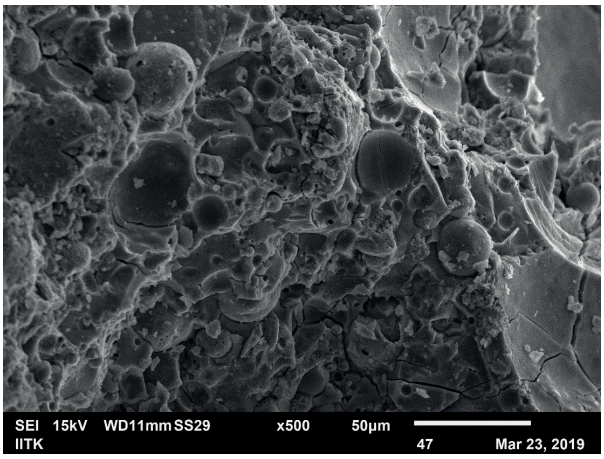

Figure 21 *SEM Mix F70S30 0.45 L/B Oven*

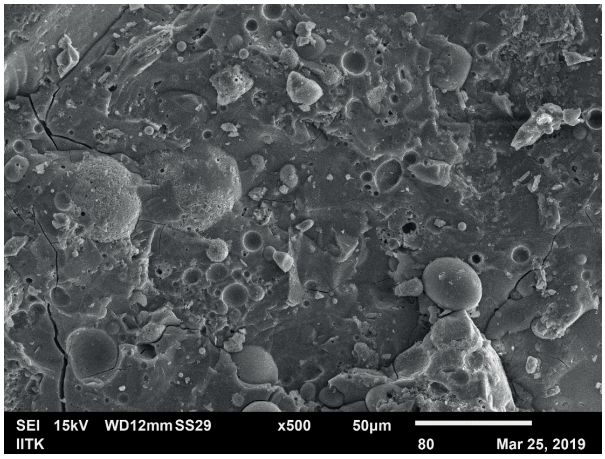

Figure 20 *SEM Mix F70S30 0.35 L/B AMB*

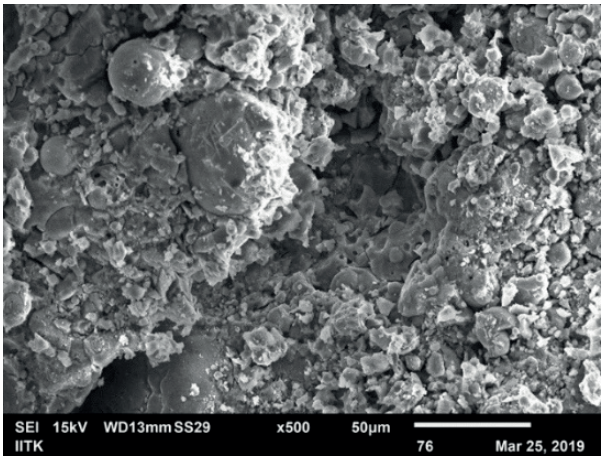

Figure 22 *SEM Mix F70S30 0.45 L/B AMB*

to evaluate the model's quality as can be shown in Tables 4-6, the models for compressive strength and split tensile strength. Flexural strength has high R2 values of 0.9947, 0.9925 and 0.9949, respectively, indicating excellent agreement between the projected and experimental data.

It is also important to note that there is less than 0.1 difference between the anticipated and adjusted R2 values, indicating agreement. As shown in Table 7, all of the models had enough precision values greater than 4, suggesting that they might be utilized to explore the solution space. The lack of fit can also be used to judge a model's quality; a lower value for the lack of fit implies a model that is worthier. Interestingly, all models' lack of fit P- values were significant, as shown in Tables 4-6, indicating high fitness for all the model answers.

To evaluate the data distribution and ensure that it is suitable, a standard probability plot is a form of a graph that is utilized [35, 42]. Figure 23 illustrates the normal distribution of the data for all residual responses by the virtually straight-line-like distribution of the points for all dependent variables. The competency and suitability of the modelling techniques were graphically evaluated by plotting the projected vs actual outcomes. The projected vs. actual results plot in Figure 23 show how the anticipated response model predicted the outcomes. The seamless fit of the data points to a straight line demonstrates a good correspondence between experimental findings and predictions made by the models in use. Since the cast in-situ alkali-activated concrete has various strengths, the existing response models were relevant and adequate in determining those strengths. However, an ANOVA approach may be used to predict the compressive strength of the cast-in-situ concrete, as demonstrated in Equation (1). Each response model was quadratic. Through the variance analysis, relationships and influences between variables and responses were established. These relationships are shown in Equation (8).

$$\begin{aligned} &\textit{Compressive strength} = 34.00 + 2.67A - \\ &- 0.6667B + 0.1667C + 12.82D + 0.25AB - \\ &- 0.125AC + 0.75AD + 0.125BC + 0.5BD - \\ &- 0.375CD + 0.1458A2 - 0.3542B2 + 0.0208C2 + \\ &+ 0.6458D2 \end{aligned} \tag{5}$$

$$\begin{aligned} &\textit{Split tensil strength} = 2.74 + 0.14A + 0.015B + \\ &+ 0.0841C + 1.17D + 0.1888AB - 0.1201AC + \\ &+ 0.0049AD + 0.1649BC - 0.151BD + 0.1013CD + \\ &+ 0.0121A2 + 0.0746B2 + 0.0346C2 - 0.0367D2 \end{aligned} \tag{6}$$

$$\begin{aligned} Flexural\ strenght &= 4.65 + 0.2362A + 0.2054B - \\ &- 0.1954C + 1.69D + 0.0056AB + 0.0731AC - \\ &- 0.1381AD - 0.0319BC - 0.0031BD + 0.0994CD + \\ &+ 0.0047A2 - 0.0266B2 - 0.0128C2 + 0.1984D2. \end{aligned} \quad (7)$$

3.9 Optimization and validation study

To improve the strengths of the proposed concrete mixes, quantitative multi-objective optimization was utilized to establish the proper GGCS and liquid-to-binder ratio. Establishing desirable values for independent variables is the aim of optimization research to reach the optimization objectives. The RSM approach, which identifies the desired result's relevance purpose, was used to boost the replies that were affected by the numerous elements [32, 41]. The outcomes of numerical optimization solutions, based on the optimization objective, are shown in Table 8. The design expert program produced the ideal mixture fractions by combining 25 % of GGCS with 0.4 % of the

Table 4 *Compressive strength*

Factor	SS	DF	M.S	F-Value	P-Value	Remark
Model	4168.80	14	297.77	201.50	< 0.0001	Significant
A-Flyash	170.67	1	170.67	115.49	< 0.0001	
B-GGCS	10.67	1	10.67	7.22	0.0169	
C-L/B	0.6667	1	0.6667	0.4511	0.5120	
D-Curing	3952.67	1	3952.67	2674.74	< 0.0001	
AB	1.0000	1	1.0000	0.6767	0.4236	
AC	0.2500	1	0.2500	0.1692	0.6867	
AD	9.00	1	9.00	6.09	0.0261	
BC	0.2500	1	0.2500	0.1692	0.6867	
BD	4.00	1	4.00	2.71	0.1207	
CD	2.25	1	2.25	1.52	0.2362	
A2	0.5833	1	0.5833	0.3947	0.5393	
B2	3.44	1	3.44	2.33	0.1479	
C2	0.0119	1	0.0119	0.0081	0.9297	
D2	11.44	1	11.44	7.74	0.0139	
Residual	22.17	15	1.48			
Lack of Fit	20.17	10	2.02	5.04	0.0441	Significant

Table 5 *Split tensile strength*

Factor	SS	DF	M.S	F-Value	P-Value	Remark
Model	34.82	14	2.49	138.09	< 0.0001	significant
A-fly ash	0.4279	1	0.4279	23.76	0.0002	
B-corex slag	0.0049	1	0.0049	0.2741	0.6088	
C-l/b r	0.1544	1	0.1544	8.57	0.0110	
D-curing	29.69	1	29.69	1648.57	< 0.0001	
AB	0.4960	1	0.4960	27.54	0.0001	
AC	0.2006	1	0.2006	11.13	0.0049	
AD	0.0003	1	0.0003	0.0188	0.8928	
BC	0.3785	1	0.3785	21.01	0.0004	
BD	0.3133	1	0.3133	17.39	0.0009	
CD	0.1428	1	0.1428	7.93	0.0137	
A^2	0.0040	1	0.0040	0.2211	0.6454	
B^2	0.1515	1	0.1515	8.41	0.0116	
C^2	0.0326	1	0.0326	1.81	0.2000	
D^2	0.0366	1	0.0366	2.03	0.1760	
Residual	0.2522	14	0.0180			
Lack of Fit	0.2429	9	0.0270	14.54	0.0044	significant

Table 6 *Flexural Strength*

Factor	SS	DF	M.S	F-Value	P-Value	Remark
Model	73.96	14	5.28	207.06	< 0.0001	Significant
A-fly ash	1.34	1	1.34	52.51	< 0.0001	
B-corex slag	1.01	1	1.01	39.70	< 0.0001	
C-l/b r	0.9165	1	0.9165	35.92	< 0.0001	
D-curing	68.92	1	68.92	2701.46	< 0.0001	
AB	0.0005	1	0.0005	0.0198	0.8898	
AC	0.0856	1	0.0856	3.35	0.0870	
AD	0.3053	1	0.3053	11.97	0.0035	
BC	0.0163	1	0.0163	0.6372	0.4372	
BD	0.0002	1	0.0002	0.0061	0.9387	
CD	0.1580	1	0.1580	6.19	0.0251	
A^2	0.0006	1	0.0006	0.0236	0.8799	
B^2	0.0194	1	0.0194	0.7586	0.3975	
C^2	0.0045	1	0.0045	0.1765	0.6804	
D^2	1.08	1	1.08	42.34	< 0.0001	
Residual	0.3827	15	0.0255			
Lack of Fit	0.3577	10	0.0358	7.15	0.0212	significant

Table 7 *Qualities that make a response model valid*

Response	Compressive strength (MPa)	Split tensile strength (MPa)	Flexural strength (MPa)
Standard deviation	1.22	0.1342	0.1597
Mean	34.37	2.83	4.78
Coefficient of variation (CV %)	3.54	4.74	3.34
R^2	0.9947	0.9928	0.9949
Predicted R^2	0.9716	0.9538	0.9718
Adjusted R^2	0.9898	0.9856	0.9900
Adequate precision	59.71	48.34	60.016

Table 8 *Optimization benchmark*

Factor and Responses	Target	Minimum value	Maximum Value
Flyash	In range	50	100
GGCS	In range	0	50
L/B ratio	In range	0.35	0.45
Curing	Type	28	60
Compressive Strength	Maximize	12	62
Split tensile strength	Maximize	1	4.81
Flexural Strength	Maximize	2.25	8.61

liquid-to-binder ratio. Improved responses with an 80% united desirability were attained. the second series of experiments were conducted utilizing the ideal mixture proportions with two other distinct mixes to assess the optimized combination percentage within the design mixes, the applicability of the results obtained and the overall response modelling. Table 9 provides an overview of the optimization criteria. Using Equation (4), the difference between experimental and anticipated values was assessed and reported as a percentage, as seen in Table 9.

The optimization benchmark for the proposed methodology is displayed in Table 8. Table 8 displays the factors and responses for various attributes: the target, minimum and maximum value.

The average probability curve of the developed models is displayed in Figure 23. The normal percentage probability is shown on the Y-axis, while the X-axis

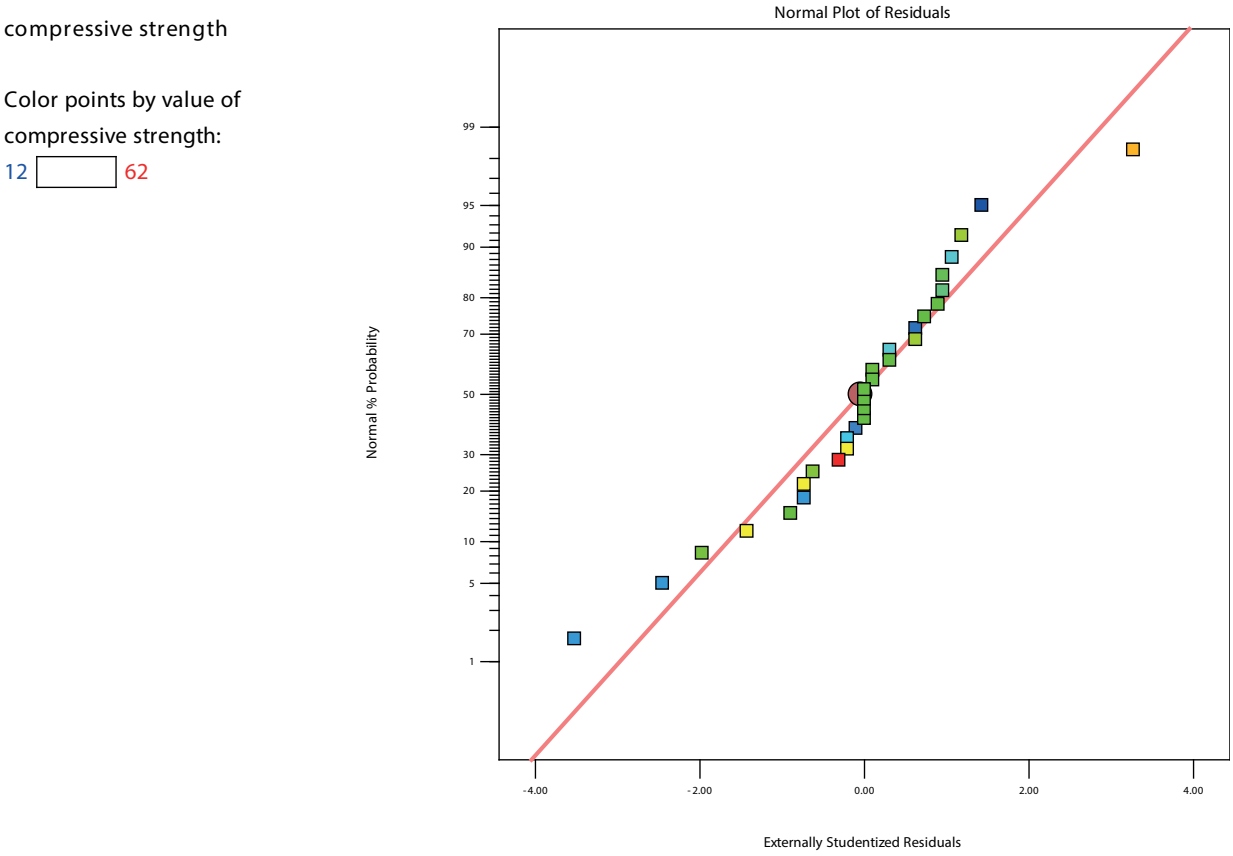

Figure 23 *Normal probability plot of the developed models*

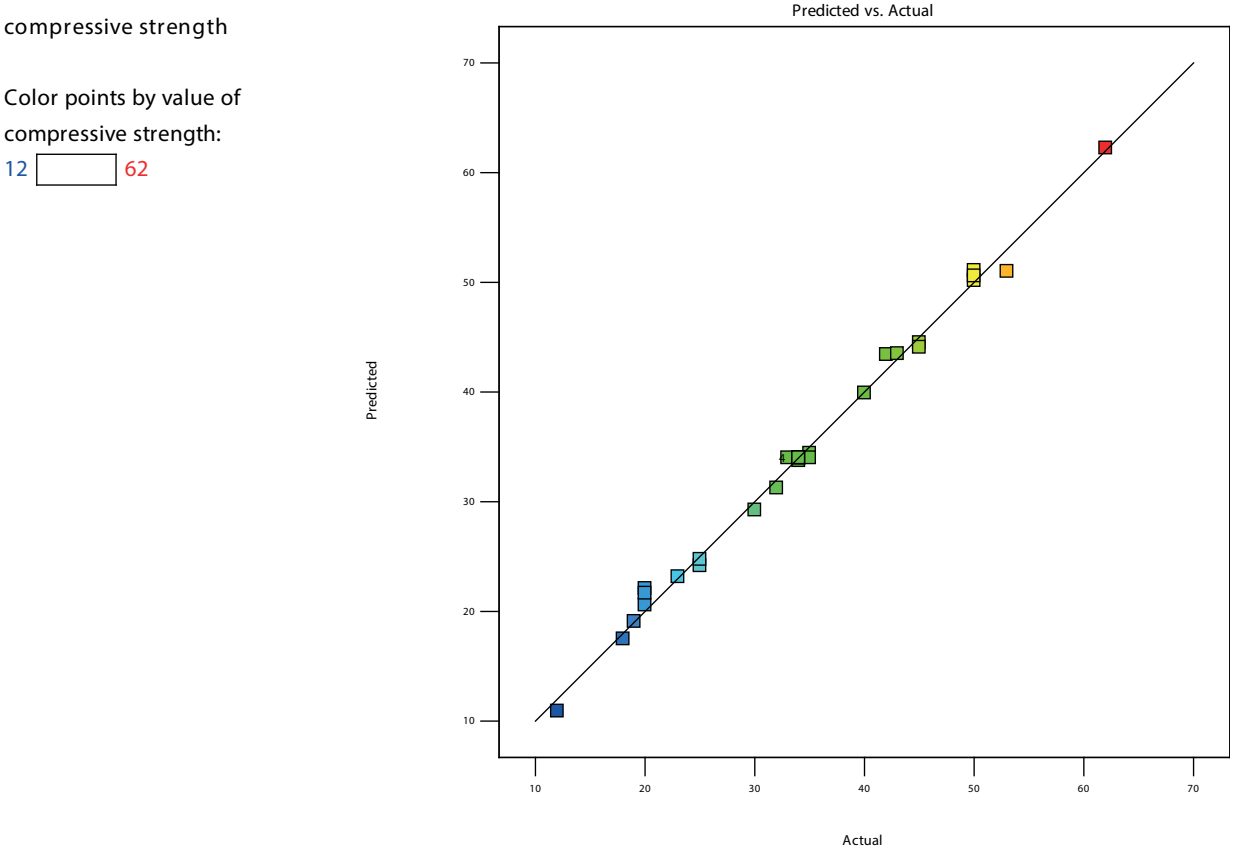

Figure 24 *Predicted vs actual plot of the developed models*

Table 9 *Model verification*

Responses	Liquid Binder ratio	GGCS	Predicted Outcomes	Experimental outcome	Error(%)
Compressive strength	0.35	50	49.15	51.95	5.39
	0.40	30	58.26	60.44	3.61
	0.45	10	50.18	52.56	4.53
Split tensile strength	0.35	50	3.51	3.68	4.62
	0.40	30	4.76	4.91	3.05
	0.45	10	2.78	2.96	6.08
Flexural strength	0.35	50	3.38	3.6	6.11
	0.40	30	4.43	4.7	5.74
	0.45	10	3.85	4	3.75

displays the externally studentized residuals.

The derived models' projected vs the actual plot is displayed in Figure 24. The actual values are shown on the X-axis and the predicted values for our proposed approach are shown on the Y-axis.

$$Error(\%) = \frac{Experimental\ value - predicted\ value}{Experimental\ value} * 100\%. \quad (8)$$

4 Conclusions

This work has intended to characterize and improve the cast-in-situ alkali-activated concrete using the response surface approach. The scientific results of this investigation allow for the following deductions:

Since the strength gains of 24.5% and 18.6% were attained at 28 and 56 days, respectively, the strength gain of the cast-in-situ alkali-activated concrete was identical to that of the regular Portland cement. Strength growth is significantly increased when the GGCS replaces fly ash to a greater extent. However, as shown by the microstructural investigation, adding GGCS to the binder induces structural aluminosilicate changes in the in-situ alkali-activated concrete that has been created. The alterations were connected to the source materials' reactive alumina and silica polymerization.

The quadratic nature of all the response models suggests a strong correlation between the factors and the replies.

The RSM optimization study's findings reveal that adding 25% GGCS and a 0.40 liquid-to-binder ratio to the total weight of the critical materials led to the optimum strengths.

The experimental data and the predictions showed a strong correlation. The results of the validation were quite similar to the measured data.

Grants and funding

The author received no financial support for the research, authorship and/or publication of this article.

Conflicts of interest

The author declare that they have no known competing financial interests or personal relationships that could have appeared to influence the work reported in this paper.

References

[1] HARDJITO, D., RANGAN, B. V. Development and properties of low-calcium fly ash-based geopolymer concrete. Research Report GC 1. Perth, Australia: Faculty of Engineering, Curtin University of Technology, 2005.

[2] FLATT, R. J., ROUSSEL, N., CHEESEMAN, C. R. Concrete: an eco-material that needs to be improved. *Journal of the European Ceramic Society* [online]. 2012, **32**(11), p. 2787-2798. ISSN 0955-2219. Available from: https://doi.org/10.1016/j.jeurceramsoc.2011.11.012

[3] COLLINS, F., SANJAYAN, J. G. Cracking tendency of development and properties alkali-activated slag concrete subjected to restrained shrinkage. *Cement and Concrete Research* [online]. 2000, **30**(5), p. 791-798. ISSN 0008-8846, eISSN 1873-3948. Available from: https://doi.org/10.1016/S0008-8846(00)00243-X

[4] VORA, P. R., DAVE, U. V. Parametric studies on compressive strength of geopolymer concrete. *Procedia Engineering* [online]. 2013, **51**, p. 210-219. ISSN 1877-7058. Available from: https://doi.org/10.1016/j.proeng.2013.01.030

[5] WALLAH, S., RANGAN, B. V. Low-calcium fly ash-based geopolymer concrete: long-term properties. Research Report GC 2. Perth, Australia: Faculty of Engineering, Curtin University of Technology, 2006.

[6] PACHECO-TORGAL, F., CASTRO-GOMES, J., JALALI, S. Alkali-activated binders: a review: Part 1. Historical background, terminology, reaction mechanisms and hydration products. *Construction and Building Materials* [online]. 2008, **22**(7), p. 1305-1314. ISSN 0950-0618, eISSN 1879-0526. Available from: https://doi.org/10.1016/j.conbuildmat.2007.10.015

[7] WHITING, J. Manufacture of cement. US Patent No. 544,706. 1895.

[8] DAVIDOVITS, J. Geopolymers: inorganic polymeric new materials. *Journal of Thermal Analysis and Calorimetry* [online]. 1991, **37**(8), p. 1633-1656. ISSN 1388-6150, eISSN 1588-2926. Available from: https://doi.org/10.1007/BF01912193

[9] NEUPANE, K. Fly ash and GGBFS based powder-activated geopolymer binders: a viable sustainable alternative of portland cement in concrete industry. *Mechanics of Materials* [online]. 2016, **103**, p. 110-122. ISSN 0167-6636, eISSN 1872-7743. Available from: https://doi.org/10.1016/j.mechmat.2016.09.012

[10] HARUNA, S., MOHAMMED, B. S., SHAHIR-LIEW, M., ALALOUL, W. S., HARUNA, A. Effect of water-binder ratio and NaOH molarity on the properties of high calcium fly ash geopolymer mortars at outdoor curing. *International Journal of Civil Engineering and Technology (IJCIET)*. 2018, **9**(10), p. 1339-1352. ISSN 0976-6308, eISSN 0976-6316.

[11] HAJIMOHAMMADI, A., VAN DEVENTER, J. S. Characterization of one-part geopolymer binders made from fly ash. *Waste and Biomass Valorization* [online]. 2017, **8**(1), p. 225-233. ISSN 1877-2641, eISSN 1877265X. Available from: https://doi.org/10.1007/s12649-016-9582-5

[12] DAVIDOVITS, J. The manufacture of geopolymer cements. In: *Geopolymer chemistry and applications*. DAVIDOVITS, J. 4. ed. Saint-Quentin, France: Geopolymer Institute, 2015. ISBN 978-2951482098, p. 499-521.

[13] VAN DEVENTER, J. S. J., PROVIS, J. L., DUXSON, P. Technical and commercial progress in the adoption of geopolymer cement. *Minerals Engineering* [online]. 2012, **29**, p. 89-104. ISSN 0892-6875, eISSN 1872-9444. Available from: https://doi.org/10.1016/j.mineng.2011.09.009

[14] SARKER, P. K., HAQUE, R., RAMGOLAM, K. V. Fracture behaviour of heat cured fly ash based geopolymer concrete. *Materials and Design* [online]. 2013, **44**, p. 580-586. ISSN 0264-1275. Available from: https://doi.org/10.1016/j.matdes.2012.08.005

[15] MOHAMMED, B. S., ACHARA, B. E., NURUDDIN, M. F., YAW, M., ZULKEFLI, M. Z. Properties of nano-silica-modified self-compacting engineered cementitious composites. *Journal of Cleaner Production* [online]. 2017, **162**, p. 1225-1238. ISSN 0959-6526, eISSN 1879-1786. Available from: https://doi.org/10.1016/j.jclepro.2017.06.137

[16] MOHAMMED, B. S., FANG, O. C., HOSSAIN, K. M. A., LACHEMI, M. Mix proportioning of concrete containing paper mill residuals using response surface methodology. *Construction and Building Materials* [online]. 2012, **35**, p. 63-68. ISSN 0950-0618, eISSN 1879-0526. Available from: https://doi.org/10.1016/j.conbuildmat.2012.02.050

[17] YAO, Z. T., XIA, M. S., SARKER, P. K., CHEN, T. Z. A review of the alumina recovery from coal fly ash, with a focus in China. *Fuel* [online]. 2014, **120**, p. 74-85. ISSN 0016-2361, eISSN 1873-7153. Available from: https://doi.org/10.1016/j.fuel.2013.12.003

[18] CHATTERJEE, A. K. Technological initiatives and status of fly ash in India. In: *Fly ash: sources applications and potential environmental impacts*. SARKER, P. K. (Ed.). USA: Nova, 2014. ISBN 978-1-62948-044-2, p. 315-359.

[19] NEMATOLLAHI, B., SANJAYAN, J., SHAIKH, F. U. A. Synthesis of heat and ambient cured one-part geopolymer mixes with different grades of sodium silicate. *Ceramics International* [online]. 2015, **41**(4), p. 5696-5704. ISSN 0272-8842, eISSN 1873-3956. Available from: https://doi.org/10.1016/j.ceramint.2014.12.154

[20] SARKER, P. K. Analysis of geopolymer concrete columns. *Materials and Structures* [online]. 2009, **42**(6), p. 715-724. ISSN 1359-5997, eISSN 1871-6873. Available from: https://doi.org/10.1617/s11527-008-9415-5

[21] MERMERDAS, K., ALGIN, Z., OLEIWI, S. M., NASSANI, D. E. Optimization of lightweight GGBFS and FA geopolymer mortars by response surface method. *Construction and Building Materials* [online]. 2017, **139**, p. 159-171. ISSN 0950-0618, eISSN 1879-0526. Available from: https://doi.org/10.1016/j.conbuildmat.2017.02.050

[22] CHINDAPRASIRT, P., DE SILVA, P., SAGOE-CRENTSIL, K., HANJITSUWAN, S. Effect of SiO2 and Al2O3 on the setting and hardening of high calcium fly ash-based geopolymer systems. *Journal of Materials Science* [online]. 2012, **47**(12), p. 4876-4883. ISSN 0022-2461, eISSN 1573-4803. Available from: https://doi.org/10.1007/s10853-012-6353-y

[23] BERNAL, S., DE GUTIERREZ, R., DELVASTO, S., RODRIGUEZ, E. Performance of an alkali-activated slag concrete reinforced with steel fibers. *Construction and Building Materials* [online]. 2010, **24**(2), p. 208-214. ISSN 0950-0618, eISSN 1879-0526. Available from: https://doi.org/10.1016/j.conbuildmat.2007.10.027

[24] PHOO-NGERNKHAM, T., MAEGAWA, A., MISHIMA, N., HATANAKA, S., CHINDAPRASIRT, P. Effects of sodium hydroxide and sodium silicate solutions on compressive and shear bond strengths of FA-GBFS geopolymer. *Construction and Building Materials* [online]. 2015, **91**, p. 1-8. ISSN 0950-0618, eISSN 1879-0526. Available from: https://doi.org/10.1016/j.conbuildmat.2015.05.001

[25] OUELLET-PLAMONDON, C., HABERT, G. Life cycle assessment (LCA) of alkali-activated cements and concretes. In: *Handbook of alkali-activated cements, mortars and concretes* [online]. PACHECO-TORGAL, F., LABRINCHA, J., LEONELLI, C., PALOMO, A., CHINDAPRASIT, P. (Eds.). Woodhead Publishing Elsevier, 2015. ISBN 978-1-78242-276-1, p. 663-686. Available from: https://doi.org/10.1016/C2013-0-16511-7

[26] RAO, G. M., RAO, T. D., SESHU, R. D., VENKATESH, A. Mix proportioning of geopolymer concrete. *Cement Wapno Beton* [online]. 2016, **21**(4), 274. ISSN 1425-8129.

[27] THUNUGUNTLA, C. S., GUNNESWARA RAO, T. D. Mix design procedure for alkali-activated slag concrete using particle packing theory. *Journal of Materials in Civil Engineering* [online]. 2018, **30**(6), 04018113. ISSN 0899-1561, eISSN 1943-5533. Available from: https://doi.org/10.1061/(ASCE)MT.1943-5533.0002296

[28] PROVIS, J. L. Alkali-activated materials. *Cement and Concrete Research* [online]. 2018, **114**, p. 40-48. ISSN 0008-8846, eISSN 1873-3948. Available from: https://doi.org/10.1016/j.cemconres.2017.02.009

[29] MOHAMMED, B. S., KHED, V. C., NURUDDIN, M. F. Rubber crete mixture optimization using response surface methodology. *Journal of Cleaner Production* [online]. 2018, **171**, p. 1605-1621. ISSN 0959-6526, eISSN 1879-1786. Available from: https://doi.org/10.1016/j.jclepro.2017.10.102

[30] SARKER, P. K. Bond strength of reinforcing steel embedded in fly ash-based geopolymer concrete. *Materials and Structures* [online]. 2011, **44**(5), p. 1021-1030. ISSN 1359-5997, eISSN 1871-6873. Available from: https://doi.org/10.1617/s11527-010-9683-8

[31] MONTGOMERY, D. C. *Design and analysis of experiments*. John Wiley and Sons, 2019. ISBN 978-1-119-49244-3.

[32] MTARFI, N. H., RAIS, Z., TALEB, M., KADA, K. M. Effect of fly ash and grading agent on the properties of mortar using response surface methodology. *Journal of Building Engineering* [online]. 2017, **9**, p. 109-116. eISSN 2352-7102. Available from: https://doi.org/10.1016/j.jobe.2016.12.004

[33] MOHAMMED, B. S., LIEW, M. S., ALALOUL, W. S., AL-FAKIH, A., IBRAHIM, W., ADAMU, M. Development of rubberized geopolymer interlocking bricks. *Case Studies in Construction Materials* [online]. 2018, **8**, p. 401-408. eISSN 2214-5095. Available from: https://doi.org/10.1016/j.cscm.2018.03.007

[34] MOHAMMED, B. S., ADAMU, M. Mechanical performance of roller compacted concrete pavement containing crumb rubber and nano silica. *Construction and Building Materials* [online]. 2018, **159**, p. 234-251. ISSN 0950-0618, eISSN 1879-0526. Available from: https://doi.org/10.1016/j.conbuildmat.2017.10.098

[35] ZAHID, M., SHAFIQ, N., ISA, M. H., GIL, L. Statistical modeling and mix design optimization of fly ash based engineered geopolymer composite using response surface methodology. *Journal of Cleaner Production* [online]. 2018, **194**, p. 483-498. ISSN 0959-6526, eISSN 1879-1786. Available from: https://doi.org/10.1016/j.jclepro.2018.05.158

[36] SIYAL, A. A., AZIZLI, K. A., MAN, Z., ISMAIL, L., KHAN, M. I. Geopolymerization kinetics of fly ash based geopolymers using JMAK model. *Ceramics International* [online]. 2016, **42**(14), p. 15575-15584. ISSN 0272-8842, eISSN 1873-3956. Available from: https://doi.org/10.1016/j.ceramint.2016.07.006

[37] BALA, N., NAPIAH, M., KAMARUDDIN, I. Nanosilica composite asphalt mixtures performance-based design and optimization using response surface methodology. *International Journal of Pavement Engineering* [online]. 2020, **21**(1), p. 29-40. Available from: https://doi.org/10.1080/10298436.2018.1435881

[38] BALA, N., KAMARUDDIN, I., NAPIAH, M., SUTANTO, M. H. Polymer nanocomposite-modified asphalt: characterization and optimization using response surface methodology. *Arabian Journal for Science and Engineering* [online]. 2019, **44**(5), p. 4233-4243. ISSN 2193-567X, eISSN 2191-4281. Available from: https://doi.org/10.1007/s13369-018-3377-x

[39] MOHAMMED, B. S., KHED, V. C., LIEW, M. S. Optimization of hybrid fibres in engineered cementitious composites. *Construction and Building Materials* [online]. 2018, **190**, p. 24-37. ISSN 0950-0618, eISSN 1879-0526. Available from: https://doi.org/10.1016/j.conbuildmat.2018.08.188

[40] MOHAMMED, B. S., ADAMU, M. Evaluating the static and dynamic modulus of elasticity of roller compacted rubber crete using response surface methodology. *International Journal of GEOMATE* [online]. 2018, **14**(41), p. 186-192. Available from: https://doi.org/10.21660/2018.41.42833

[41] ANDERSON, M. J., WHITCOMB, P. J. *RSM simplified: optimizing processes using response surface methods for design of experiments* [online]. 2. ed. New York: Productivity Press, 2016. ISBN 9781315382326. Available from: https://doi.org/10.1201/9781315382326

[42] MOHAMMED, B. S., LIEW, M. S., ALALOUL, W. S., AL-FAKIH, A., IBRAHIM, W., ADAMU, M. Development of rubberized geopolymer interlocking bricks. *Case Studies in Construction Materials* [online]. 2018, **8**, p. 401-408. Available from: https://doi.org/10.1016/j.cscm.2018.03.007

This is an open access article distributed under the terms of the Creative Commons Attribution 4.0 International License (CC BY 4.0), which permits use, distribution, and reproduction in any medium, provided the original publication is properly cited. No use, distribution or reproduction is permitted which does not comply with these terms.

HIGHLY SECURE AND ACCURATE DEEP SLICING IN 5G WIRELESS NETWORKS FOR EFFICIENT RESOURCE UTILIZATION

Ambidi Naveena

Electronics and Telematics Engineering Department, G. Narayanamma Institute of Technology and Science (for women), Shaikpet, Hyderabad, Telangana, India

E-mail of corresponding author: naveenaambidi@gmail.com

Ambidi Naveena 0000-0002-0691-9494

Resume

Both the current cellular network and the planned 5G mobile network need to meet high dependability standards, very low latency requirements, larger capacity, better security and fast user communication. In order to support multiple independent tenants on the same physical infrastructure, mobile carriers are working towards end-to-end network resource allocation in 5G networks. Future communication networks will require data-driven decision making due to the increase in traffic and the accelerated performance of 5G networks. With the use of in-network deep learning and prediction, a "deep slice" model was built in this study to control network load efficiency and network availability. Even in the event of a network outage, the suggested model is capable of making wise selections and choosing the best network slice.

Article info

Received 16 August 2022
Accepted 1 February 2023
Online 24 April 2023

Keywords:

cellular communications
CNN
prediction
network slicing
deep slicing

Available online: https://doi.org/10.26552/com.C.2023.042

ISSN 1335-4205 (print version)
ISSN 2585-7878 (online version)

1 Introduction

The International Telecommunication Union (ITU) published a paper in February 2017 that outlined important requirements, including baseline standards for the technical performance for IMT-2020 for 5G mobile communication technology. The minimum bandwidth need for next-generation services is 1 GHz, the maximum data transfer rate is 20 Gbps and the smallest latency time is 1 ms. These are the basic needs for a variety of 5G services as well as the technological requirements to achieve the three main goals of 5G: ultra-fast, super-connection and ultra-low latency. Compared to 4G mobile communication, 5G mobile communication is more innovatively improved in terms of speed, employing protocol and network setups [1].

Twenty times quicker than current long-term evolution (LTE), the 5G wireless network is designed as a soft defined network (SDN), while the 5G core network has been switched from a centralized to a decentralized kind to reduce traffic transmission latency. Development of ubiquitous, digital services with anytime, everywhere connection will rely heavily on 5G networks. A wide range of applications, from ubiquitous internet access to driverless cars, will be made possible by them. The present COVID-19 pandemic age appears to have confirmed the value and significance of communication networks and related services [2].

With the advent of Beyond 5G systems, which offer cutting-edge services like holographic communications, Virtual Reality (VR), this function is anticipated to become even more important for implementation of a future digital society. An “IoT communication environment” may be realized by offering a quicker “mobile communication environment,” when the capacity and speed of data transmission and reception across the wired and wireless networks is equal. Such an ecosystem can deliver realistic media content in 4K, VR and 8K, while also ensuring low power consumption in Internet of Things devices and service reliability even in settings with many connected devices, thanks to cutting-edge technology like AR, VR, drones and smartphones [3].

The ITU-R divided the three main 5G mobile network services into three categories: ultrahigh speed and big capacity (Enhanced Mobile Broadband (eMBB),

Ultra-Reliable Low Latency Communications (uRLLC) and Massive Machine-Type Communications (mMTC)), depending on the needs of each service in terms of bandwidth, speed and latency. The technology aspires to deliver up to 20 times the speed, 10 times the number of connections to IoT devices and 10 times the number of low-latency services, compared to 4G mobile communication technology. In addition to undertaking an examination of LTE security threats, the European Union Agency for Cyber security (ENISA) divided 5G network threat types into seven categories. It then used the CIA criteria to examine them as a threat landscape. Through the use of the 5G threat surface, 5G America in the USA classified the possible security risks [4].

The biggest challenge for 5G is the sheer volume of networked devices, including vital infrastructure that must be utilized in a brand-new IoT paradigm with unequal resources. To achieve the desired functionality, challenges must be overcome, including protection against DoS attacks on end-user devices, protection against DoS attacks on radio interfaces, devices and networks, distributed control systems that require coordination to prevent Signal storms and protection against DoS attacks on infrastructure. Additionally, similar issues are highlighted by Next Generation Mobile Networks (NGMN) [5].

The remaining portions of this article are structured as follows: The existing work is presented in Section 2. Section 3 present the proposed deep slicing in 5G wireless networks. The result analysis is presented in the section 4. Section 5 concludes the work.

2 Literature survey

Park et al. proposed the potential security risks that could exist in the 5G NSA network, they were examined, validated on the live network and recommendations for security improvements were made. In addition, authors examined the necessity for the new security strategies rather than conventional security methods and associated research and demonstrated the persistent weaknesses in the current mobile network system. 5G mobile communication network backgrounds and historical data collected to match with current situation to detect the threats in real-world mobile networks in service. Before releasing the new services, it is vital to assess the potential security risks they may pose as well as appropriate mitigation strategies. [6].

Ortiz et al. developed INSPIRE-5Gplus1 project, which is creating a smart, reliable and responsible 5G security platform. This platform utilizes cutting-edge methods for closed-loop and end-to-end security management in 5G and Beyond 5G networks, including Distributed Ledger Technologies (DLT), Machine Learning (ML), Artificial Intelligence (AI), Trusted Execution Environment (TEE) and Network Softwarization. Security management with Security Service Level Agreements (SSLAs) and liability management are the key aspects of INSPIRE-5Gplus1 platform. [7].

Suomalainen et al. proposed the most significant issue that arises from the direct use of ML ideas in the 5G network infrastructure, which is weakened network security. In addition to providing potential vulnerabilities and attack pathways against the availability and integrity of 5G services, ML enables user surveillance and privacy violation assaults that were previously unattainable with conventional adversarial tactics. This work's primary goal was to promote further study into the secure application of ML methods in 5G and other future wireless networks [8].

Waziri et al. proposed an enhanced reference monitor algorithm for the Software Defined Networking (SDN) controller for 5G security. Over 50 billion connections are anticipated, which the present 4G network cannot support. While ubiquitous mobile broadband is the primary goal of 4G networks, 5G technological characteristics will need to significantly improve. Software's adaptability is essential for fulfilling unanticipated future service requirements. In this context, Software Defined Networking (SDN) has lately gained traction in the networking sector, albeit a precise standard on how to assess security risks on SDN for 5G has not yet been implemented. To implement the access control policy, this paper suggests using the 5-ENSURE architecture to integrate Reference Monitor (RM) with SDN controllers. The Study will also isolate and handle malicious packets in a distributed manner among nodes rather than only permitting or denying access based on access policy [9].

More than 50 billion connections are anticipated as a result, more than 4G can manage at this time. While ubiquitous mobile broadband is the primary focus of 4G networks, 5G technology requirements must significantly outpace those. To accommodate the unanticipated future service need, software flexibility is essential. In this context, Software Defined Networking (SDN) has just recently gained traction in the networking sector and a clear standard has not yet been set on how to assess the security risks on SDN for 5G. This study suggests using the 5-ENSURE architecture and combining Reference Monitor (RM) with SDN controllers to apply access control policies. [10].

Sciancalepore et al. proposed the development of three crucial network slicing building elements that are in charge of (i) traffic analysis and prediction per network slice, (ii) admission control choices for network slice requests and (iii) adaptive load forecast correction based on measured deviations. These findings demonstrate a trade-off between cautious forecasting setups and more aggressive ones, as well as extremely significant potential advantages in terms of system usage [11].

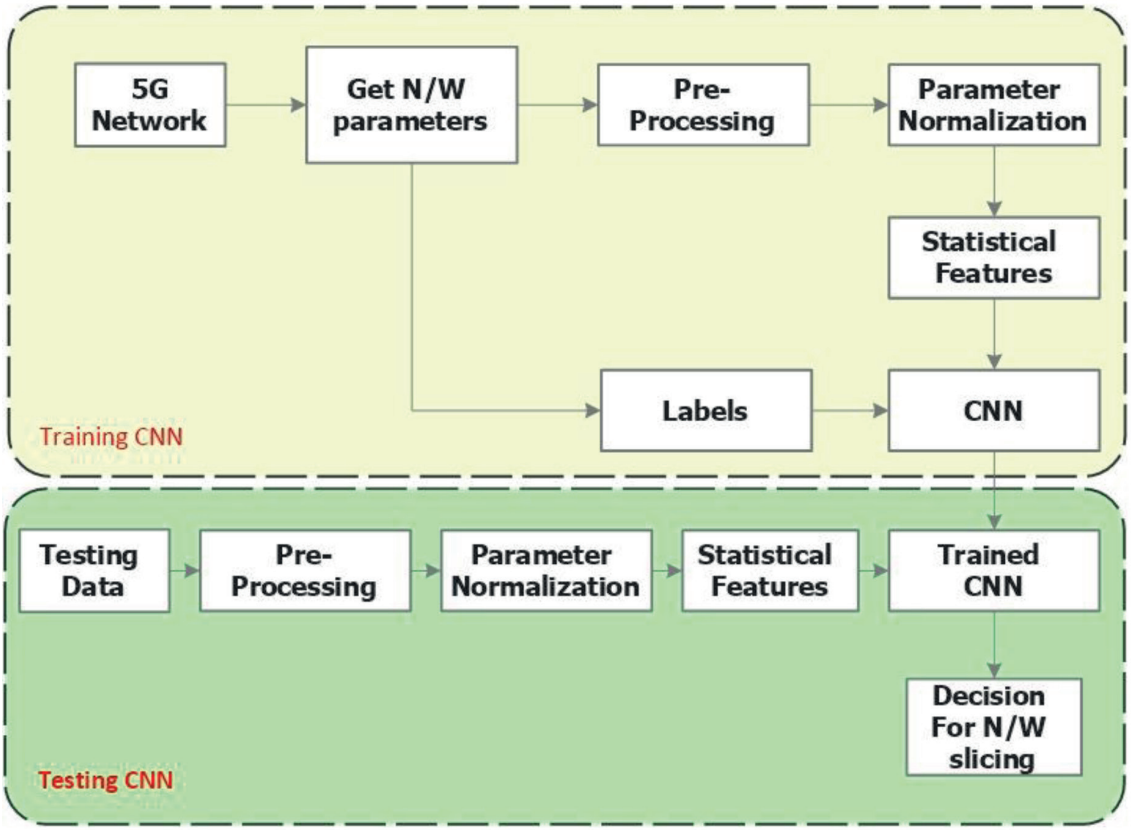

Figure 1 *Block diagram of the proposed method*

Feng et al. proposed a wireless network virtualization paradigm including the data plane, cognitive plane and control plane as its three components. To support the suggested concept, a unique control signaling method has been developed, as well. A hierarchical control method, based on the cell-clustering, has been employed with dynamically optimized resource consumption from the standpoint of network virtualization. To show how the schemes operate under the suggested paradigm to enhance resource efficiency and the user experience, two cases of application have been examined [12].

The main objectives of the proposed methods are

- Create a productive technique to improve the system's overall effectiveness in terms of system throughput and energy efficiency.
- The interference in 5G networks and IoT systems is reduced or eliminated.

3 Proposed method

The risks and security issues the 5G ecosystem faces are largely the same as those that 4G/LTE users are now dealing with. To achieve the service level agreements for a variety of applications and services, 5G networks will also have unique requirements on throughput, latency and security, especially with a diversified ecosystem for the IoT devices [13]. Utilize the 5G network to obtain network parameter, employing the FoG computing for preprocessing. After a parameter has been normalized, apply statistical characteristics. Apply CNN network for categorization at the end.

3.1 Block diagram

Efficient resource utilization in 5G networks can improve the quality of the service in terms of connectivity, speed and quality etc. Frequency slicing can improve the resources' utilization in networks. The proposed block diagram for resources' utilization using slicing with CNN is shown in Figure 1. Initially, the network parameters are extracted to perform the resource utilization process. All the collected parameters are normalized using min max level to perform highly accurate feature extraction process. Statistical features are extracted to feed the CNN for training and classification further.

3.2 Preprocessing

3.2.1 Fog computing

Fog nodes in 5G are situated at the radio access network's edge (RANs). Researchers from Cisco characterized fog computing as "a platform that provides compute, communication and data storage capabilities between end devices and standard cloud computing

platforms." Although many issues have been solved by integrating cloud computing and end devices, the concentration of resources in cloud computing creates a significant disconnect between the IoT devices and the cloud [13-14]. The resulting massive communication latency and computing overhead will surely rise.

3.3 Parameter normalization

Data must be standardized in order to get the best results while learning the deep learning network parameters. The subsequent equation is applied to each feature in this work's data normalization, using the min-Max method [15]. The general equation, used to perform the normalization process is given as:

$$normalization = \frac{y - y_{\min}}{y_{\max} - y_{\min}}, \quad (1)$$

where y defines the data to be normalized, $y_{\min}$ is the value of minimum, $y_{\max}$ is the value of maximum.

3.4 Statistical features

Network characteristics gathered include the protocol's packet size, the number of packets per flow, different payload patterns, the size of the payload and the protocol's request time distribution [16]. Initial raw packet captures are transformed to network flows for simpler analysis in order to identify the characteristics from these profiles. The first packet defines the forward (source to destination) and backward (destination to source) directions for bidirectional flows created with CICFlowMeter. Therefore, they are estimated independently both for forward and backward directions, using the 83 statistical data acquired from the flows, such as time, number of packets, number of bytes and packet length.

3.4.1 Arithmetic features

Standard Deviation: The standard deviation in statistics is a metric for the variation of the distribution of a collection of data. The formula for the sample standard deviation is:

$$\sigma = \sqrt{\frac{1}{N-1}\sum_{i=1}^{N}(x_i - \bar{x})^2}, \quad (2)$$

where x_n are the observed values, $\bar{x}$ is the mean value, N is the number of observations.

Mean: By adding up all of the numerical values of the observations and dividing the result by the total number of observations, the mean of a set of observed data can be calculated. It is given in Equation (3).

$$\bar{x} = \frac{1}{n}\left(\sum_{i=1}^{n} x_i\right) = \frac{x_1 + x_2 + \cdots + x_n}{n}. \quad (3)$$

Kurtosis: Kurtosis is a statistical metric used to assess how "tailed" a real-valued random variable's probability distribution, given by:

$$\text{Kurtosis}[X] = E\left[\left(\frac{X-\mu}{\sigma}\right)^4\right] = \frac{E[(X-\mu)^4]}{(E[(X-\mu)^2])^2} = \frac{\mu_4}{\sigma^4}, \quad (4)$$

where μ_4 is the fourth central moment and σ is the standard deviation. K denotes the kurtosis.

Skewness: In probability theory and statistics, skewness is a measure of the asymmetry of the probability distribution of a real-valued random variable in regard to its mean.

The skewness of a random variable X is the third standardized moment $\tilde{\mu}_3$ defined as:

$$\tilde{\mu}_3 = E\left[\left(\frac{X-\mu}{\sigma}\right)^3\right] = \frac{\mu_3}{\sigma^3} = \frac{E[(X-\mu)^3]}{(E[(X-\mu)^2])3/2} = \frac{k_3}{k_2^{3/2}}, \quad (5)$$

where μ represents the mean, σ represents the standard deviation, E represents the expectation operator, μ_3 is the third central moment and κ_t is the t-th cumulants.

3.5 CNN

Three factors make the CNN's structure: dataset quantity, quality and type. The many receptive layers can process elements of the input layer. These networks may be set up such that an output picture with a high resolution may be produced by creating an overlap of the input region. Convolutional neural networks (CNNs) are used for feature detection. Following feature extraction, a classifier is created using all the fully linked layers. Convolutional layers and pooling layers couple less frequently since a fully linked CNN is not required. It is regarded as CNN's beating centre [17]. Convolution is used when the two mathematical functions are combined, with the outcome also being a function. By moving the filter, convolution is carried out over the input. The result of matrix multiplication for each place is added to the feature map, as a total [18]. The input picture for this layer is s*s*p, where s is the image's height and width and p is a channel with many filters, each of which is t*t*q in size. The picture dimension is lower than t and q can be the same as channel s [19].

Pooling Layer: between the CNN and the convolution layer, there is an inclusion of a pooling layer. The major objective of this layer is to reduce the dimensionality to get minimal computation and fewer parameters. Max pooling is the most significant pooling. It is employed to select the highest value available in each window [20-23].

Fully Connected Layer: The Fully Connected

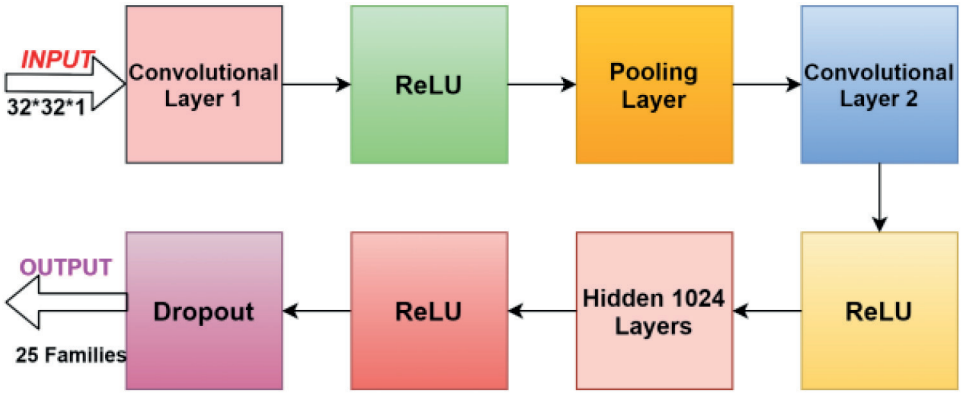

Figure 2 *Architecture of CNN*

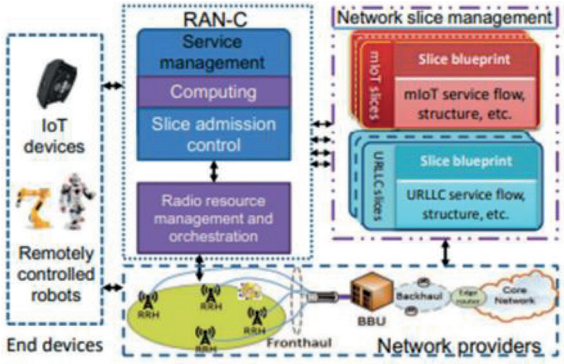

Figure 3 *Systematic diagram of RAN Slicing*

Layer, which classifies input pictures as a last layer after convolutional and pooling, is used. Having neurons that are linked to the preceding layer performs activation activities in a layer that is completely connected. It will also offer information security to identify and categorize bad code in addition to malware detection. Figure 2 depicts the structure of CNN.

3.6 RAN slicing

Slicing the radio access network (RAN) is a key idea for effectively distributing the current network infrastructure across several vertical applications. Running numerous logical or virtual networks as distinct business activities on a single RAN is characterized as RAN slicing. Every network slice is a separate logical network that has been designed to meet the quality-of-service (QoS) requirements of a certain application. Additionally, various sophisticated radio access technologies (RATs), including massive MIMO, coordinated multi-point (CoMP) transmission and full-duplex need to be investigated in order to meet the hard connectivity requirements. One of the most important RATs that satisfies the rigid reliability criterion for tactile applications is coMP transmission, which generates spatial variety with redundant communication channels. The division of a RAN using the CoMP transmission mechanism (referred to as a CoMP-enabled RAN) into many virtual networks is the definition of the idea of CoMP-enabled RAN slicing. The systematic diagram of RAN Slicing is shown in Figure 3.

4 Results and discussions

4.1 Dataset

uses the deep learning to achieve effective and dependable network slicing in 5G networks. It contains the day and time of each linking, which may also assist the network forecast of the amount of connections at any particular moment in the future and it would be knowledgeable of which networking slices will be obligatory or demanded by those links, based on information gathered from the previous data.

4.2 False positive rate

The percentage of negative test results that regardless result in positive test results is known as the false positive rate; it is the conditional probability of a positive test result given the absence of a specific event. The significance level is matched by the false positive rate. One less than the false positive rate is the test's specificity.

4.3 Positive predictive value

The positive and negative predictive values are the proportions of occurrences in statistical and screening procedures that are really positive and genuinely negative findings (PPV and NPV, respectively). The effectiveness of a diagnostic test or other statistical metric is described by the PPV and NPV. The correctness of such a statistic can be inferred from a high result. As opposed to true positive and true negative rates, which are inherent to the test, the PPV and NPV also depend on the prevalence of the test. The equations for PPV and NPV are given in Equations (6) and (7), respectively.

$$PPV = \frac{No.of\ TP}{No.of\ TP + No.FP}, \tag{6}$$

$$NPV = \frac{No.of\ TN}{No.of\ TN + No.FN}. \tag{7}$$

Throughput: It is a gauge of how quickly a node can send data across a network. Throughput, then, is the typical rate of successfully delivering messages through a communication connection.

Packet Delivery Ratio: the proportion of packets successfully received by the destination node to those successfully sent by the source node. The packet delivery ratio is given as:

$$Packet\ Delivery\ Ratio = \frac{Total\ number\ of\ packets\ received}{Total\ number\ of\ packets\ send}. \tag{8}$$

Highlights of the DeepSlice simulation model's

Table 1 *Highlights of DeepSlice's simulation model's features*

Input type	Packet Loss Rate	Packet Delay Budget (ms)	Normalized Duration (s)
Smart phone	10^{-2}	60	257
IoT devices	10^{-2}	50	54
Smart transportation	10^{-6}	10	52
AR / VR / Gaming	10^{-3}	50	534
Smart City / Home	10^{-2}	10	100
Unknown Device Type	10^{-6}	10	60

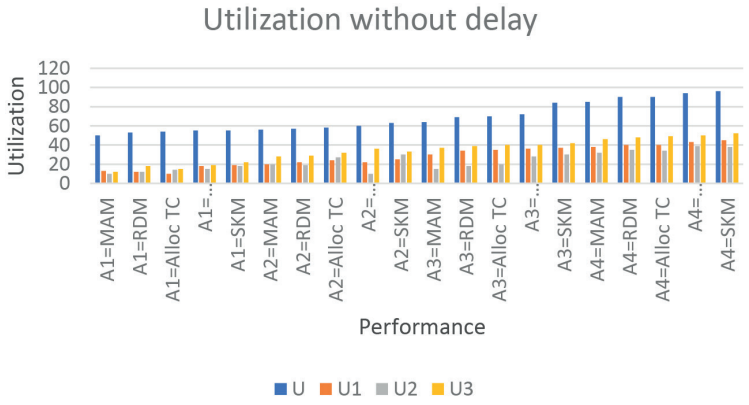

Figure 4 *Performance of utilization without delay*

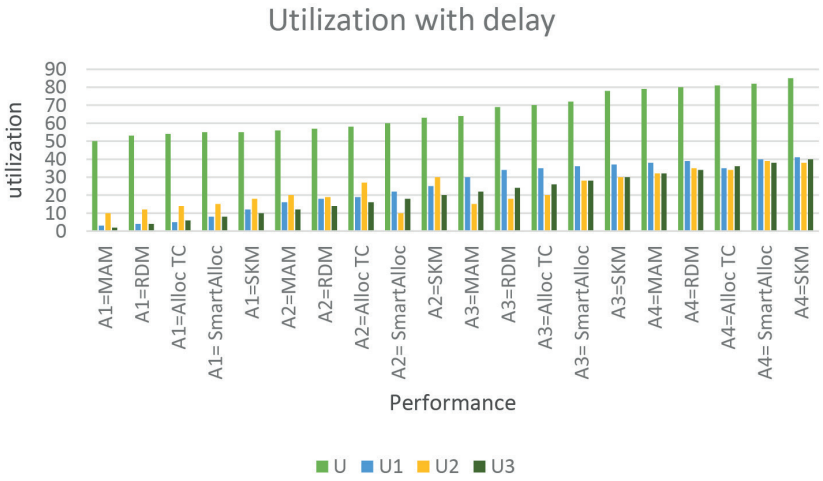

Figure 5 *Performance of utilization with delay*

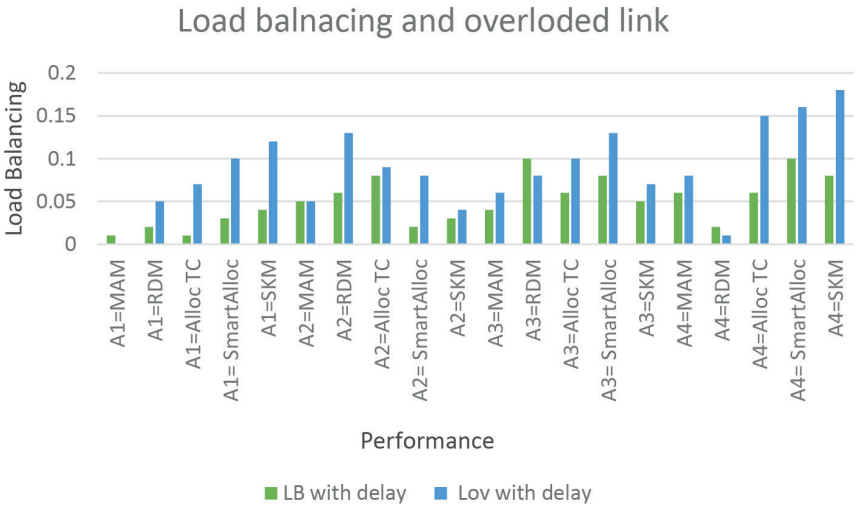

Figure 6 *Performance of load balancing with delay*

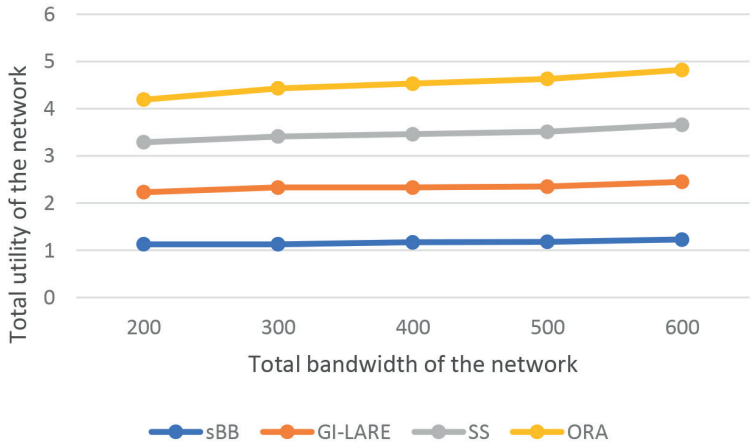

Figure 7 *Impact of the total bandwidth on the total utility of the network at 10 ms delay bound*

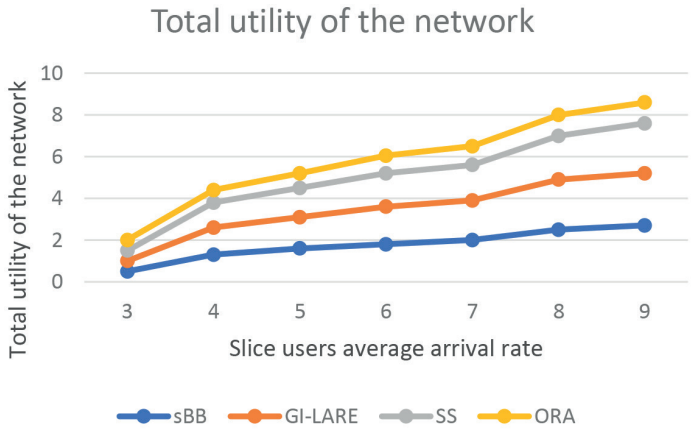

Figure 8 *Effect of the slice user density on the total utility of the network*

characteristics are listed in Table 1. As expected, each of these inbound requests is routed to one or more of the network slices. The first responders in an emergency may use smartphones to make phone calls, access the internet and send the text messages, all at once.

Figure 4 shows the performance of utilization without delay. Figure 5 depicts the performance of utilization with delay. Figure 6 displays the performance of load balancing with delay. Figure 7 depicts the effect of network utility on total bandwidth at a 10 ms delay bound. The impact of slice user density on the overall network utility is seen in Figure 8.

5 Conclusions

To support the connecting of IoT devices, the 5G network adopted a software-defined architecture, bringing technological advantages. In this work, the 5G parameters from the 5G network were obtained and preprocessed using the Fog computing methodologies. Then the preprocessing parameter are normalized. Then, the feature is extracted using the statistical features, like standard deviation, mean, kurtosis, skewness from the normalized parameter. Finally, the CNN is trained by using extracted arithmetic features to perform highly accurate packet slicing process. While the 5G Security is a step forward, the vulnerabilities associated with interconnecting with the older networks against a considerably higher volume of data and applications continue to increase. When compared to other previous works, the CNN-based RAN slicing approach used in this work delivers the high efficiency and secure data of the 5G network.

Grants and funding

The author received no financial support for the research, authorship and/or publication of this article.

Conflicts of interest

The author declare that they have no known competing financial interests or personal relationships that could have appeared to influence the work reported in this paper.

References

[1] BHARDWAJ, A. 5G for military communications. *Procedia Computer Science* [online]. 2020, **171**, p. 2665-2674. eISSN 1877-0509. Available from: https://doi.org/10.1016/j.procs.2020.04.289

[2] YESMIN, T., AGASTI, S., CHAKRABARTI, K. 5G security and privacy issues: a perspective view. In: *ICT with intelligent applications. Smart innovation, systems and technologies* [online]. SENJYU, T., MAHALLE, P.N., PERUMAL, T., JOSHI, A. (Eds.). Vol. 248. Singapore: Springer, 2022. ISBN 978-981-16-4176-3, eISBN 978-981-16-4177-0, p. 89-98. Available from: https://doi.org/10.1007/978-981-16-4177-0_12

[3] DANGI, R., JADHAV, A., CHOUDHARY, G., DRAGONI, N., MISHRA, M. K., LALWANI, P. ML-Based 5G network slicing security: a comprehensive survey. *Future Internet* [online]. 2022, **14**(4), 116. eISSN 1999-5903. Available from: https://doi.org/10.3390/fi14040116

[4] SHI, W., XU, W., YOU, X., ZHAO, CH., WEI, K. Intelligent reflection enabling technologies for integrated and green internet-of-everything beyond 5G: communication, sensing and security. *IEEE Wireless Communications* [online]. 2022, Early Access, p. 1-8. ISSN 1536-1284, eISSN 1558-0687. Available from: https://doi.org/10.1109/MWC.018.2100717

[5] KIM, H. 5G core network security issues and attack classification from network protocol perspective. *Journal of Internet Services and Information Security (JISIS)* [online]. 2020, **10**(2), p. 1-15. ISSN 2182-2069, eISSN 2182-2077. Available from: https://doi.org/10.22667/JISIS.2020.05.31.001

[6] PARK, S., KIM, D., PARK, Y., CHO, H., KIM, D., KWON, S. 5G security threat assessment in real networks. *Sensors* [online]. 2021, **21**(16), 5524. eISSN 1424-8220. Available from: https://doi.org/10.3390/s21165524

[7] ORTIZ, J., SANCHEZ-IBORRA, R., BERNABE, J. B., SKARMETA, A., BENZAID, CH., TALEB, T., ALEMANY, P., MUNOZ, R., VILALTA, R., GABER, CH., WARY, J.-P., AYED, D., BISSON, P., CHRISTOPOULOU, M., XILOURIS, G., MONTES DE OCA, E., GUR, G., SANTINELLI, G., LEFEBVRE, V., PASTOR, A., LOPEZ, D. INSPIRE-5Gplus: intelligent security and pervasive trust for 5G and beyond networks. In: 15th International Conference on Availability, Reliability and Security: proceedings [online]. 2020. ISBN 978-1-4503-8833-7, p. 1-10. Available from: https://doi.org/10.1145/3407023.3409219

[8] SUOMALAINEN, J., JUHOLA, A., SHAHABUDDIN, S., MAMMELA, A., AHMAD, I. Machine learning threatens 5G security. *IEEE Access* [online]. 2020, **8**, p. 190822-190842. eISSN 2169-3536. Available from: https://doi.org/10.1109/ACCESS.2020.3031966

[9] WAZIRI, J. U., OMOKHUALE, E. Development of enhance reference monitor algorithm for software defined networking (SDN) controller for 5G security. *International Journal of Multidisciplinary Research and Growth Evaluation* [online]. 2022, **3**(3), p. 226-241. eISSN 2582-7138. Available from: https://doi.org/10.54660/anfo.2022.3.3.15

[10] PRADHAN, D., SAHU, P. K., GOJE, N. S., GHONGE, M. M., TUN, H. M., RAJESWARI, R., PRAMANIK, S. Security, privacy, risk and safety toward 5G green network (5G-GN). In: *Cyber security and network security* [online]. PRAMANIK, S., SAMANTA, D., VINAY, M., GUHA, A. (Eds.). Scrivener Publishing LLC, 2022. ISBN 9781119812494, eISBN 9781119812555, p. 193-216. Available from: https://doi.org/10.1002/9781119812555.ch9

[11] SCIANCALEPORE, V., SAMDANIS, K., COSTA-PEREZ, X., BEGA, D., GRAMAGLIA, M., BANCHS, A. Mobile traffic forecasting for maximizing 5G network slicing resource utilization. In: IEEE Conference on Computer Communications INFOCOM 2017: proceedings [online]. IEEE. 2017. ISBN 978-1-5090-5337-7, eISBN 978-1-5090-5336-0, p. 1-9. Available from: https://doi.org/10.1109/INFOCOM.2017.8057230

[12] FENG, Z., QIU, CH., FENG, Z., WEI, Z., LI, W., ZHANG, P. An effective approach to 5G: wireless network virtualization. *IEEE Communications Magazine* [online]. 2015, **53**(12), p. 53-59. ISSN 0163-6804, eISSN 1558-1896. Available from: https://doi.org/10.1109/MCOM.2015.7355585

[13] EL-MEKKAWI, A., HESSELBACH, X., PINEY, J. R. Evaluating the impact of delay constraints in network services for intelligent network slicing based on SKM model. *Journal of Communications and Networks* [online]. 2021, **23**(4), p. 281-298. ISSN 1229-2370, eISSN 1976-5541. Available from: https://doi.org/10.23919/JCN.2021.000024

[14] OLADEJO, S. O., FALOWO, O. E. Latency-aware dynamic resource allocation scheme for multi-tier 5G network: a network slicing-multitenancy scenario. *IEEE Access* [online]. 2020, **8**, p. 74834-74852. eISSN 2169-3536. Available from: https://doi.org/10.1109/ACCESS.2020.2988710

[15] SHAHRIAR, N., TAEB, S., CHOWDHURY, S. R., ZULFIQAR, M., TORNATORE, M., BOUTABA, R., MITRA, J., HEMMATI, M. Reliable slicing of 5G transport networks with bandwidth squeezing and multi-path provisioning. *IEEE Transactions on Network and Service Management* [online]. 2020, **17**(3), p. 1418-1431. eISSN 1932-4537. Available from: https://doi.org/10.1109/TNSM.2020.2992442

[16] RAMRAO, J. V., JAIN, A. Dynamic 5G network slicing. *International Journal of Advanced Trends in Computer Science and Engineering* [online]. 2021, **10**(2). ISSN 2278-3091. Available from: https://doi.org/10.30534/ijatcse/2021/741022021

[17] ZHANG, Z., WANG, Q. Application status and prospects of 5G technology in distribution automation systems. *Wireless Communications and Mobile Computing* [online]. 2021, **2021**, 5553159. ISSN 1530-8669, eISSN 1530-8677. Available from: https://doi.org/10.1155/2021/5553159

[18] XIAO, Y., ZHANG, J., JI, Y. Resource-efficient slicing with topology-level protection in optical access/aggregation networks for 5G and beyond. In: 2021 Optical Fiber Communications Conference and Exhibition OFC: proceedings [online]. IEEE. 2021. ISBN 978-1-943580-86-6, p. 1-3. Available from: https://doi.org/10.1364/OFC.2021.W1F.4

[19] AMATO, E., TONINI, F., RAFFAELLI, C., MONTI, P. A resource sharing method for reliable slice as a service provisioning in 5G metro networks. In: 2021 International Conference on Optical Network Design and Modeling ONDM: proceedings. 2021. ISBN 978-3-9031-7633-1, p. 1-3.

[20] WANG, X., LU, X., FU, M., LIU, J., YANG, H. Optimization for survivable 5G network slice provisioning with augmented infrastructure. In: 2021 9th International Conference on Communications and Broadband Networking: proceedings [online]. 2021. ISBN 978-1-4503-8917-4, p. 192-196. Available from: https://doi.org/10.1145/3456415.3456446

[21] HOSSAIN, A., ANSARI, N. 5G multi-band numerology-based TDD RAN slicing for throughput and latency sensitive services. *IEEE Transactions on Mobile Computing* [online]. 2021, Early Access. ISSN 1536-1233, eISSN 1558-0660. Available from: https://doi.org/10.1109/TMC.2021.3106323

[22] ZHOU, H., ELSAYED, M., EROL-KANTARCI, M. RAN resource slicing in 5G using multi-agent correlated q-learning. In: 2021 IEEE 32nd Annual International Symposium on Personal, Indoor and Mobile Radio Communications PIMRC: proceedings [online]. IEEE. 2021. ISBN 978-1-7281-7587-4, eISBN 978-1-7281-7586-7, ISSN 2166-9570, eISSN 2166-9589, p. 1179-1184. Available from: https://doi.org/10.1109/PIMRC50174.2021.9569358

[23] KAYTAZ, U., SIVRIKAYA, F., ALBAYRAK, S. Hierarchical deep reinforcement learning based dynamic RAN slicing for 5G V2X. In: 2021 IEEE Global Communications Conference GLOBECOM: proceedings [online]. IEEE. 2021. ISBN 978-1-7281-8105-9, eISBN 978-1-7281-8104-2, p. 1-6. Available from: https://doi.org/10.1109/GLOBECOM46510.2021.9685588

UNIVERSITY
OF ŽILINA

1953 70 2023

In its over 70 years of successful existence, the University of Žilina (UNIZA) has become one of the top universities in Slovakia.

The mission of UNIZA is to develop education on the basis of science, research and art activities within national and democratic traditions, to develop harmonic personality, knowledge, the good and creativity of a man and to contribute to the advancement of education, science, and culture for the welfare of the whole society.

Professional profile of UNIZA is unique and includes transport (road, railway, water, air), transport and postal services, communications, civil engineering construction, electrical engineering, telecommunications, informatics, information and communication technologies, management and marketing, mechanical engineering, materials and technologies, robotics, machinery design, energies, civil engineering, crisis and security management, civil security, fire protection, forensic engineering, applied mathematics, teacher training, library and information sciences, social pedagogy and high mountain biology. Results of science and research activities of the University have an important influence not only on the educational activities but also on the development of international cooperation or interconnection with practice.

UNIVERSITY PARTS
7 faculties
9 research and educational institutes and centres
3 specialized professional and training workplaces
3 information workplaces
1 economic and administrative department
4 dedicated facilities

EDUCATION
7 faculties:
8 000 students
more than 88 000 graduates
172 study programmes

SCIENCE AND RESEARCH
699 creative workers
785 000 hours, annual research capacity
190 domestic scientific projects
45 foreign projects
30 scientific and technical journals
50 scientific and professional events per year

INTERNATIONAL COOPERATION
The University of Žilina in Žilina has almost 50 valid university-wide bilateral agreements, and cooperates with foreign universities in the EU, Asia, America and Africa. It cooperates on foreign non-research projects and has concluded more than 300 agreements in the ERASMUS + programme.

UNIVERSITY OF ŽILINA
Science & Research Department

Univerzitná 8215/1,
010 26 Žilina,
Slovakia

Ing. Janka Macurová
tel.: +421 41 513 5143
e-mail: janka.macurova@uniza.sk

This is an open access article distributed under the terms of the Creative Commons Attribution 4.0 International License (CC BY 4.0), which permits use, distribution, and reproduction in any medium, provided the original publication is properly cited. No use, distribution or reproduction is permitted which does not comply with these terms.

IMPACT OF ROUGHNESS AND FRICTION PROPERTIES OF ROAD SURFACE OF URBAN STREETS ON THE TRAFFIC SAFETY

Amir Beketov*, Shakhnoza Khalimova

Department of Urban Roads and Streets, Tashkent State Transport University, Tashkent, Uzbekistan

*E-mail of corresponding author: beketovamir@tstu.uz

Amir Beketov 0000-0003-2075-454X, Shakhnoza Khalimova 0000-0002-4753-390X

Resume

Results of the study of the roughness and friction properties of the road surface of urban streets influence on the traffic safety are presented in this article. As a result of this study, an empirical dependence was obtained, reflecting the relationship between the traffic speed and a load factor under different traffic conditions; the relationship between the flow density and street capacity was also determined. The maximum permissible value of the friction coefficient for experimental streets is 0.4, and 50 % of the object of study meets the requirements of operation; 50 % does not. From the proposed graph of the relative dependence of pavement roughness and safety factor, it follows that the most dangerous are the streets, the pavement roughness of which is in unsatisfactory condition. To effectively solve the problem of destruction of the road surfaces, it is first of all necessary to eliminate the cause of the damage that occurs, not just its consequences.

Article info

Received 4 January 2023
Accepted 15 May 2023
Online 31 May 2023

Keywords:

pavement roughness
road surface conditions
traffic flow
traffic safety
traffic speed
urban streets

Available online: https://doi.org/10.26552/com.C.2023.051

ISSN 1335-4205 (print version)
ISSN 2585-7878 (online version)

1 Introduction

At present, on urban streets, the intensity of vehicle traffic is increasing, while the transport and operational performance of roads are at a low level, which creates unfavorable traffic conditions and undoubtedly affects the traffic safety.

The roughness of the road surface is one of the main indicators characterizing the convenience of driving on the road and having a decisive influence on the speed of vehicles and the transport function of the road as a whole. This is a vibrational effect that is detrimental to both the car and the driver [1]. In addition, the working conditions of the driver become more difficult due to the fact that he has to constantly monitor the condition of the road, the presence of potholes and cracks on the road, slow down and increase speed and adapt to the state of transport, which often changes the trajectory of movement. Such situations force the driver to focus on maneuvers and not on other components that are important in terms of, and traffic safety. Under such conditions, an increase in number of accidents is inevitable [2].

The scope and volume of research devoted to the topic vary over a very wide range. The largest number of research works have been carried out in the field of influence of the roughness and friction properties of the road surface, as well as the road conditions, on the traffic safety. In other areas, the amount of research work is negligible.

The aim of this research was to study the impact of the roughness and friction properties of the road surface of urban streets on the traffic safety. To achieve this goal, it is necessary to solve the following research tasks: analysis of the studies performed on the topic; analysis of the current state of transport and operational indicators of the road surface for the traffic safety of urban main streets; study of the impact of road surface roughness on the traffic safety; study of the impact of friction properties of the road surface on the traffic safety. The object of research is the central streets of the cities of Tashkent (Buyuk Ipak Yuli St., Fargona Yuli St. and Izzat St.) and Chirchik (Alisher Navoi Ave., Amir Temur Ave. and Soglom Avlod St.). The subject of the study is the road surface of urban streets.

2 Literature review

The highway safety is a major priority for the public and for transportation agencies [3]. The studies of Lee, Abdel-Aty, and Nyame-Baafi [4] developed four different safety performance functions to evaluate the impact of road roughness, as measured by the International Roughness Index (IRI), on crashes using interstate highway data from five US states representing different geographic and weather regions: Arizona, Colorado. , Florida, Maryland and Michigan. The modeling results identify many significant variables, including the traffic volume and proportion of trucks, through lane count, shoulder type, median width, high-occupancy vehicle (HOV) lane operation and HOV lane count, speed limit, area type and IRI-related factors. The results indicate that increased IRI contributes to large numbers of total crashes.

The condition assessment of pavement has a predominant role in delivering safety and comfort to users. Roughness is considered the most important characteristics as it affects the road safety and vehicle operating costs. Authorities spend a significant quantity of resources on using conventional methods for measuring roughness. Many studies are performed to estimate roughness by deploying smartphone sensors. However, no consideration is given to influence of the speed of the host vehicle in roughness evaluation using smartphones. Results of the smartphone-based pavement roughness estimation experiment showed a high correlation value of 0.73 and proved the accuracy of the method [5].

The influence of the road surfaces' roughness on the conditions for the movement of mixed flows was studied by Azizov [6]. According to the results of the author's research, the assessment of the roughness of the pavement, along the track of the car and along the edge of the carriageway shows that in all the cases the roughness of the pavement is worse at the edge of the carriageway than in the middle part; vibrations of tractor trailers increase with deterioration of the pavement (Figure 1).

The work of Eshkabilov and Yunusov [7] presents experimental studies based on the road profile measurements using accelerometers and the international roughness index (IRI) assessment tools and practical recommendations regarding the processing of measured acceleration data, from the point of view of a digital filter plan and the transformation of vertical data accelerations into displacement data. The capabilities of various applications used to measure the roughness of the road surface using smartphones, as well as the possibilities, advantages and disadvantages of creating a road database in the conditions of Uzbekistan, were studied in the work of Urokov and Soataliev [8].

The issues of assessing the conditions for the occurrence of a dangerous traffic situation due to a decrease in the traffic safety on uneven road surfaces were considered by Filippov, Smirnova, and Kiyashko [9]. It is proposed to introduce a partial accident rate that takes into account the roughness of the coatings into the methodology of the accident rate.

The factors that determine the force of friction (adhesion) in the contact of automobile tires with the pavement of the roadway are considered in the works of Nemchinov [10]. The role of the surface roughness of road surfaces in formation of the friction force is noted. An assessment is given to devices for assessing the adhesion qualities of the road surfaces.

Changes in the value of the adhesion coefficient under the influence of various factors are considered in the works of Evtyukov and Evtyukov [11]. The dependence of the adhesion coefficient on the state of the type of road surface and on the speed of the car for surfaces with different roughness is presented in detail. The indicators of reliability of the contact of a car tire with the road surface are presented, as well.

Specifically, Uzbekistan researchers had been working on evaluation of the impact of uneven road surfaces on traffic safety and development of the network of urban roads and streets by using experience of researchers from other countries in urban street management systems [12-13]. The Canadian scientists

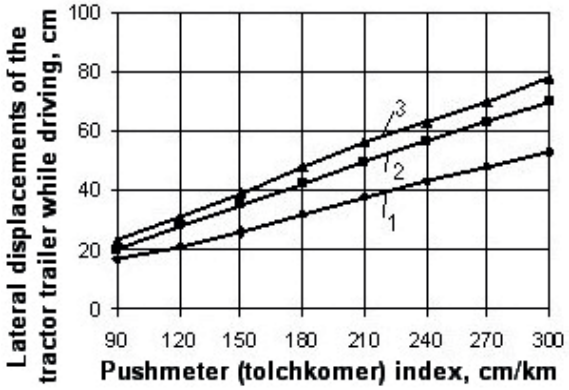

Figure 1 *Lateral vibrations of the tractor train depending on the condition of the coating: 1 - tractor trains consisting of 1 trailer; 2 - tractor trains consisting of 3 trailers; 3 - tractor trains consisting of 5 trailers*

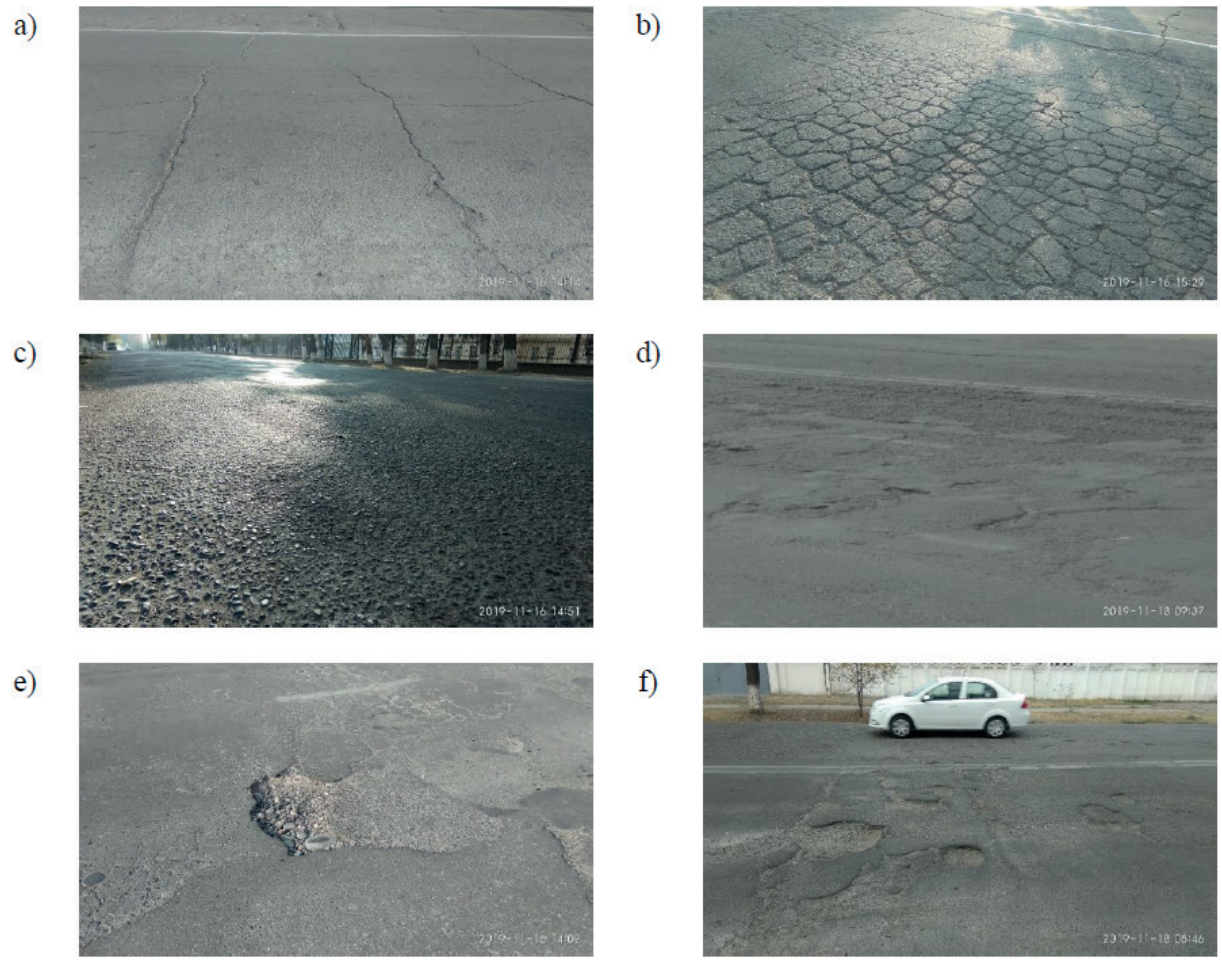

Figure 2 *Various defects on the pavement of the object of study: a) transverse cracks on PK 6+00 Amir Temur Ave., Chirchik; b) a grid of cracks at PK 8+50 Soglom Avlod St., Chirchik; c) peeling at PK 46+50 Amir Temur Ave., Chirchik; d) chipping at PK 59+00 Fargona Yuli St., Tashkent; e) potholes at PK 3+25 Amir Temur Ave., Chirchik; f) pitting at PK 3+25 Izzat St., Tashkent*

[14-19] have had valuable results on their explorations that are associated with analysis of influences on as-built pavement roughness in asphalt overlays at long-term pavement performance test sites, as well as determining the road surface and weather conditions that have a significant impact on the traffic stream characteristics. On the other hand, effects of vehicular speed on assessment of the pavement road roughness have been studied by other researchers [20-24]. As a result, the topic continues to be authentic by influencing its effect on other case studies.

Based on the review of previous studies, it was determined that the scope and volume of research works devoted to the "study of the impact of roughness and friction properties of road surfaces of urban streets on traffic safety" vary widely.

3 Methodology

The road surface is the uppermost part of the pavement, which is directly affected by the wheels of cars and weather and climatic factors. Destruction can be caused by: low quality of work; insufficient or incorrect consideration of hydrogeological conditions; and the use of low-quality materials. Of great importance in ensuring the stability of road pavement is the timely repair of destroyed sections of the road surface. The appearance of residual (irreversible) deformations that are not eliminated in a timely manner leads to significant damage, both under the influence of vehicle traffic and under the influence of weather and climatic factors. The loss of pavement roughness is caused by the continuous impact of car wheels and natural and climatic factors. The loss of roughness is greatly influenced by errors made in the design, construction and maintenance of pavements [25].

Currently, on the streets of the cities of Uzbekistan, the intensity of vehicle traffic is increasing and the transport and operational indicators of roads are at a low level. This creates unfavorable conditions for the movement of vehicles and undoubtedly affects the traffic safety. Additionally, a huge variety of road defects can cause serious accidents. Basically, such defects include pitting, rutting, breaks, potholes, waves, chipping, peeling, a network of cracks, transverse cracks, etc.

Table 1 *Unified form of statements of defects of the object of study*

Object of study	Road surface defects									
	Transverse cracks (m^2)	Grid of cracks (m^2)	Peeling (m^2)	Chipping (m^2)	Waves (m^2)	Potholes (m^2)	Pitting (m^2)	Total pavement area with defects (m^2)	Total pavement area (m^2)	Percentage of defect area (%)
Buyuk Ipak Yuli St., Tashkent	43	8149	1821	2848	820	498	50	14229	102900	13.8
Fargona Yuli St., Tashkent	63	7103	12760	5916	498	648	1400	28388	142800	19.9
Izzat St., Tashkent	28	1480	1858	875	0	883	1750	6874	24500	28
Alisher Navoi Ave., Chirchik	134	1310	3721	0	0	0	0	5165	117600	4.4
Amir Temur Ave., Chirchik	51	7305	2535	820	500	700	150	12061	62300	19.4
Soglom Avlod St., Chirchik	26	3070	940	3720	0	590	0	8346	32200	25.9

Asphalt and concrete pavements are very convenient for vehicle traffic. Despite its good technological and operational properties, such a coating is sensitive to changes in temperature and humidity: the binder material contained in the coating becomes obsolete over time and the strength and deformation properties change [26].

To analyze the current state of the object of study, which identified the streets of the cities of Tashkent (Buyuk Ipak Yuli St., Fargona Yuli St. and Izzat St.) and Chirchik (Alisher Navoi Ave., Amir Temur Ave. and Soglom Avlod St.), visual inspections and measurement work were carried out, and photographs of various pavement defects were taken (Figure 2):

A visual assessment of the condition of the road surface allows obtaining data on its condition, identifying places that are subject to assessment of the strength of the pavement and determining the amount of damage necessary for planning repairs and maintenance [27].

The destruction of asphalt concrete pavements occurs as a result of the complex impact of such factors as: miscalculations in the design of a highway, the use of outdated technologies and low-quality materials in the construction of a road, violations of technologies and rules for the road construction, adverse weather conditions and an increase in traffic loads.

In the process of data collection, lists of defects of the object of study were compiled and experimental sites were identified for conducting the planned experiments of the study. Below is a unified form of statements of defects of the object of study (Table 1):

From Table 1, it can be seen that on almost all the streets of the object of study, there are many different defects in the pavement, including potholes and pitting and their distribution occupies a considerable area. So, the most common type of defect, in terms of the area of the road surface, is a network of cracks, which was formed during the further development of individual cracks over time. In addition, the further development of the network of cracks can lead to more serious types of defects, such as potholes, chipping, breaks, peeling, pitting, etc. This condition of the road surface affects the modes of movement of vehicles, their speed and trajectory and may even cause accidents.

4 Results and discussion

4.1 Study of the impact of roughness of the road surface of urban streets on the traffic safety

The roughness of the road surface is one of the main indicators characterizing the convenience of driving on a highway and having a decisive influence on the speed and safety of traffic [25]. During the maintenance of roads, the roughness of the road surface deteriorates due to its damage and deformation under the influence of traffic loads and weather conditions.

The effect of pavement roughness on the transport and operational qualities of roads has been studied to a much greater extent than its effect on the traffic safety. Uneven road surfaces can cause the driver to lose control of the vehicle. At the same time, accidents, such as a collision of cars in a traffic stream, occur, as a rule, when braking in front of a car due to its entry into an uneven area. The same accidents occur when

Table 2 *Evaluation of pavement roughness in experimental streets*

Street name	Number of gaps under the rail (%)				Roughness condition
	less than 3 mm	3-5 mm	more than 5 mm	the biggest	
Alisher Navoi Ave., Chirchik (PK 29+00 - PK 34+00)	96	3	1	6 mm	Excellent
Buyuk Ipak Yuli St., Tashkent (PK 3+00 - PK 8+00)	91	7	2	7 mm	Good
Soglom Avlod St., Chirchik (PK 5+00 - PK 10+00)	82	13	5	9 mm	Satisfactory
Amir Temur Ave., Chirchik (PK 45+00 - PK 50+00)	81	14	5	10 mm	Satisfactory
Fargona Yuli St., Tashkent (PK 54+00 - PK 59+00)	39	47	14	12 mm	Unsatisfactory
Izzat St., Tashkent (PK 15+00 - PK 20+00)	41	44	15	13 mm	Unsatisfactory

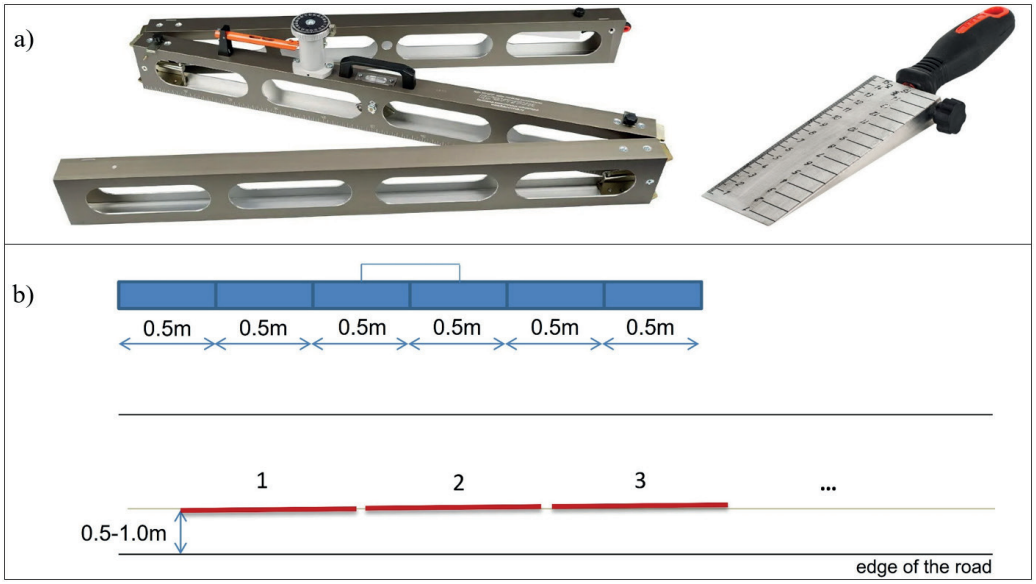

Figure 3 *Technical specifications of the instrument in pavement roughness measurements: a) a three-meter rail and a wedge gauge; b) measurement site*

a car enters the oncoming lane to avoid bumps in its own lane. The condition of the pavement of the carriageway of roads in terms of longitudinal roughness is assessed by comparing the actual roughness indicators with the minimum allowable ones. The road surface satisfies the required operating conditions for roughness if the value of the actual roughness index is less than the minimum allowable value or equal to this value [28].

To study the effect of the road surface roughness on the traffic safety, the surface roughness was measured on all the experimental sections of streets with a three-meter rail (Table 2) and its condition was assessed according to the regulatory requirements of IKN 05-2011 and MSHN 25-2005 [27, 29]. Technical specifications of the instrument in pavement roughness measurements are shown in Figure 3.

It is known that the main indicator that determines the target function of roads and urban streets is the speed of movement. This indicator is influenced by many factors, some of which are: the intensity and composition of the traffic flow; the width of the carriageway and the number of lanes in each direction; the flux density; the density of the road network; the level of traffic organization; visibility conditions, etc.

Development of engineering measures for organization of traffic is possible only if there is information characterizing the traffic flows in which the movement occurs. Based on the traffic research and the practice of its organization, numerous meters have been developed that characterize the movement of the traffic flow. The primary indicators include the total intensity and composition of the traffic flow over a relatively long period of time.

The intensity of traffic and the composition of the traffic flow of the object of study are shown in Figures 4-5.

Based on observations of the composition of the traffic flow on the experimental streets, a tendency for a high proportion of cars has been established. Figure 5 shows the composition of the traffic flow in the form of a cyclogram, reflecting the ratio of cars by type to the total number.

Roughness has a great influence on the traffic speed. The influence of roughness on the maximum

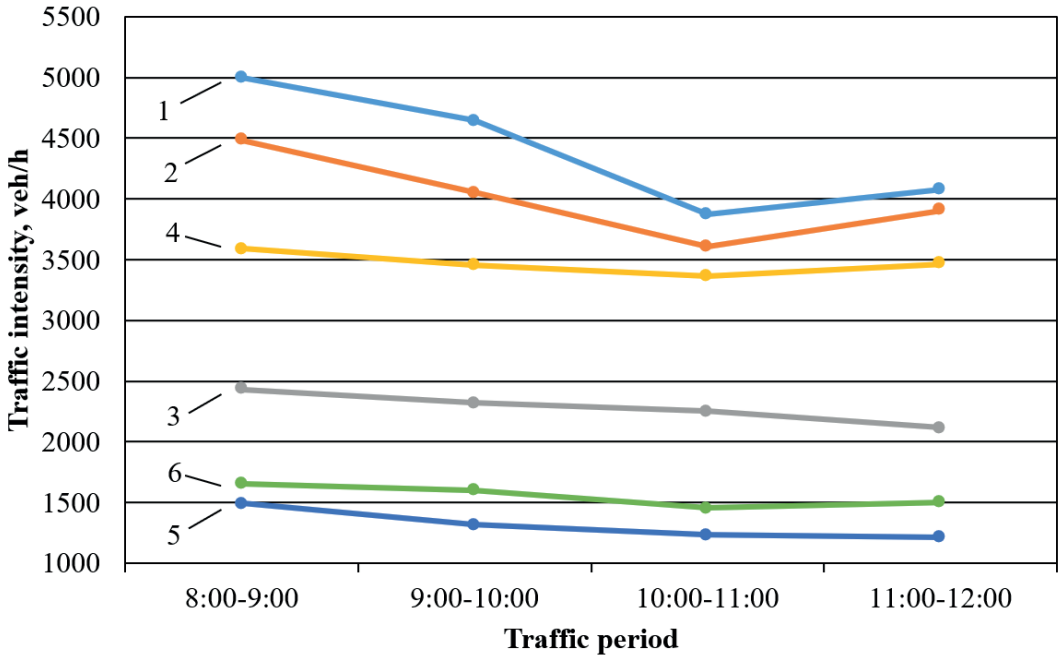

Figure 4 *Traffic intensity at the object of study: 1 - Buyuk Ipak Yuli St. (Tashkent); 2 - Fargona Yuli St. (Tashkent); 3 - Izzat St. (Tashkent); 4 - Alisher Navoi Ave. (Chirchik); 5 - Amir Temur Ave. (Chirchik); 6 - Soglom Avlod St. (Chirchik)*

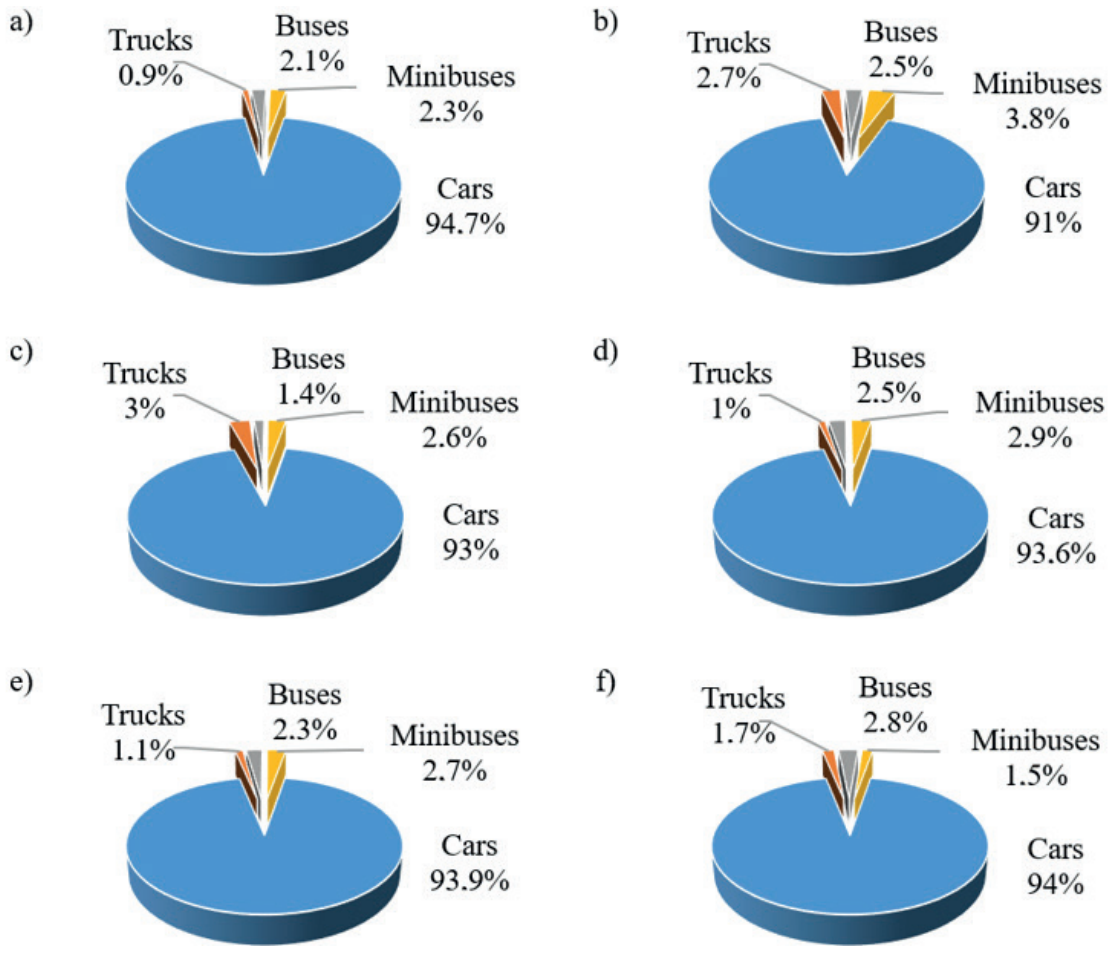

Figure 5 *The composition of the traffic flow at the object of study: a) Buyuk Ipak Yuli St. (Tashkent); b) Fargona Yuli St. (Tashkent); c) Izzat St. (Tashkent); d) Alisher Navoi Ave. (Chirchik); e) Amir Temur Ave. (Chirchik); f) Soglom Avlod St. (Chirchik)*

speed is determined in the case of measuring roughness, by setting the PKRS (Device to Control Roughness and Adhesion) according to the formula of Vasilyev [30]:

$$V_{\max} = 7500/\sqrt{S_c} + 0.15\,S_c, km/h\,, \quad (1)$$

where: S_c - pavement roughness, cm/km.

When measuring the roughness with the pushmeter (tolchkomer), the maximum speed is determined by the formula of Sidenko [30]:

$$V_{\max} = 850/\sqrt{S_c}, km/h\,, \quad (2)$$

where: S_c - pavement roughness, cm/km.

According to Silyanov and Domke [25], as the roughness deteriorates, the speed of cars of all types decreases (Figure 6).

The measured and evaluated state of roughness on the experimental streets indirectly affects the speed of movement and, therefore, the speed of movement along these streets, which have the same design speed, was also measured. The street section was chosen to measure the speed of cars with a stopwatch; the measurement distance was 50 m and the number of vehicles was 120. The first step in the processing of observational data is the compilation of a summary. To compile a summary, all velocities obtained as a result of observations are combined into numbers. The results of experimental measurements and estimates are given in Table 3.

When developing mathematical statistics, modal and cumulative speed curves along the experimental streets were constructed using field measurements of speed (Figure 7).

With help of the cumulative curve, the values of

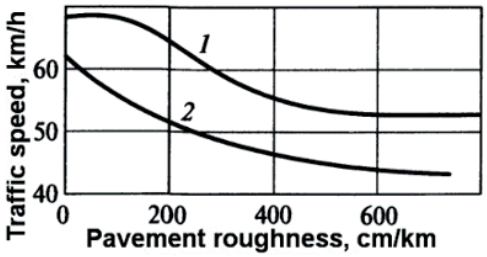

Figure 6 *Impact of pavement roughness on speed according to Silyanov and Domke: 1 - cars; 2 - trucks [25]*

Table 3 *Example of digits and summary of vehicle speeds*

Pavement roughness condition	Speed value 15, 50, 85, 95 % security				
	V_m	V_{15}	V_{50}	V_{85}	V_{95}
Excellent	67	51	57	68	70
Good	61	47	60	67	69
Satisfactorily	55	41	51	57	59
Unsatisfactorily	35	30	35	39	45

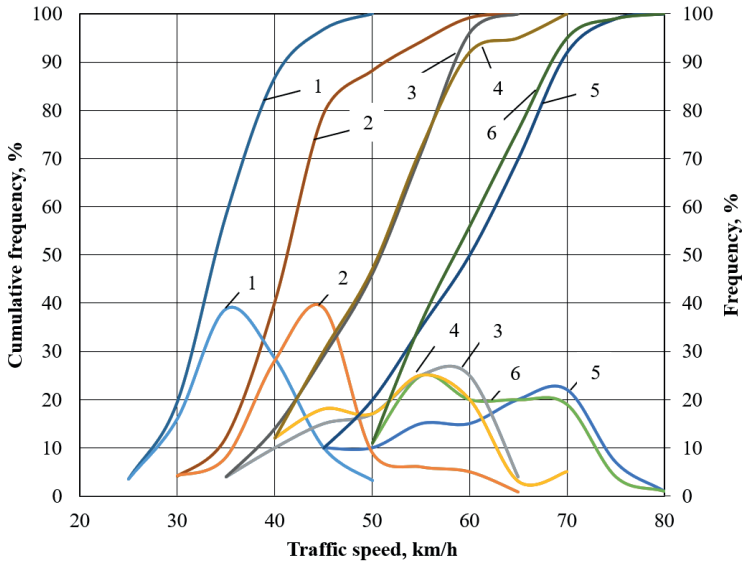

Figure 7 *Modal and cumulative speed curves: 1 - Izzat St., Tashkent; 2 - Fargona Yuli St., Tashkent; 3 - Amir Temur Ave., Chirchik; 4 - Soglom Avlod St., Chirchik; 5 - Buyuk Ipak Yuli St., Tashkent; 6 - Alisher Navoi Ave., Chirchik*

the speeds corresponding to 15, 50, 85 and 95% of the security are determined. The speed values of 15% security show the speed of cars that are overtaken by the remaining 85% of cars. These 15% of cars are usually the source of accidents. Therefore, with artificial regulation of traffic, it is advisable to take this speed as the minimum allowable. The values of modal speed (V_m) occur often in the sample of spot speed in the given data [31].

Traffic hazards were assessed using a safety factor and the results were statistically analyzed. Safety coefficients are the ratios of the maximum speed of movement on the site to the maximum speed of entry of cars into this section:

$$F_S = V_S / V_{en}, \quad (3)$$

where: V_s - the maximum speed of movement on the site, km/h;

V_{en} - the maximum speed of entry into this section, km/h.

The safety factor method takes into account the movement of a single vehicle, which is a good measure for safety and typical for traffic conditions on roads with low intensity or hours of slowdown in traffic on busier roads. This does not prevent its use for all the types of roads since overtaking is practically excluded at high traffic intensity and the calculation for a single car is directed towards a safety margin.

Sections with safety factors less than 0.8 are unacceptable in new road projects. In reconstruction and overhaul projects, safety factors are taken into account according to MSHN 25-2005 [29].

To assess the safety factors, sections were allocated at a distance of 100 meters from all experimental streets and the maximum speed of an individual car on these streets was determined using a stopwatch. It was found that the street safety factor changes with the speed and roughness of the pavement (Table 4).

Table 4 shows that when vehicles pass from the excellent condition to the unsatisfied condition, the safety index is $F_s < 1$, which means that the condition of the pavement is uneven. If the safety index is $F_s = 1$, it means that the condition of the pavement is uniform in this section. It would seem that by forcing drivers to slow down, uneven pavements should reduce the number of accidents. However, the analysis of the road traffic accidents often shows that they often focus on areas whose geometric characteristics and longitudinal profile are quite favorable, where after areas with even coverage there are areas with uneven coverage.

4.2 Study of the impact of the friction properties of the road surface of urban streets on traffic safety

The friction properties of the road surface are one of the important transport and operational indicators of highways and urban streets. It shows the reliability of the contact of a car tire with the road surface and, in many cases, affects the traffic safety. The poor condition of the friction properties significantly worsens driving conditions, causing vibrations that are harmful to the driver and vehicles and significantly complicating the working conditions of drivers. With significant fluctuations, the tire can also be detached from the pavement surface, resulting in a complete loss of controllability and stability, which at high speed can lead to a dangerous traffic situation and an accident. The condition of road surfaces in terms of friction is assessed by comparing the actual value of the coefficient of longitudinal adhesion with its minimum allowable

Table 4 *Changes in safety factor depending on roughness condition*

Roughness condition	Safety factor values, F_S			
excellent	1			
good	0.9	1		
satisfactorily	0.75	0.8	1	
unsatisfactorily	0.55	0.6	0.75	1

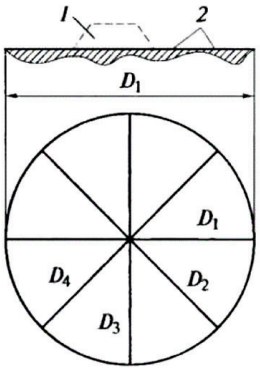

Figure 8 *"Sand spot" method: 1 - a hill of sand before leveling; 2 - sand after leveling*

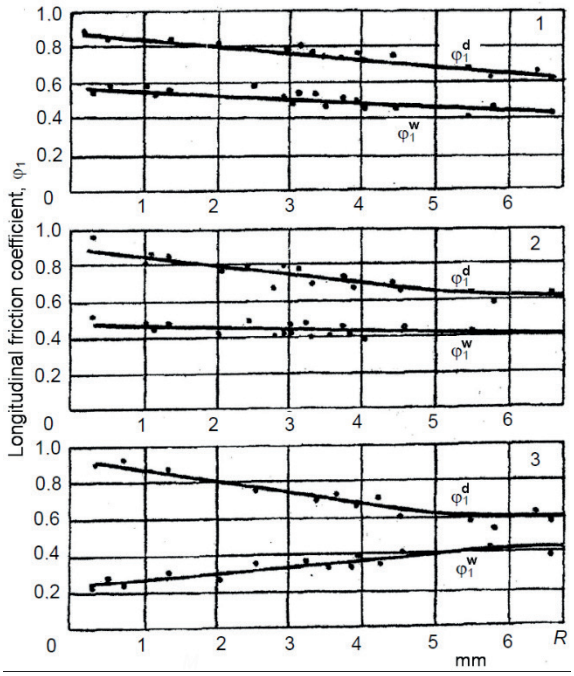

Figure 9 *Dependence of the adhesion coefficient on the macroroughness of the road surface. Tire 6.45-13 R with a new tread pattern. φ_d, φ_w - coefficient of longitudinal adhesion, on a dry and wet rough wear layer, respectively. Traffic speed, km/h: 1 - 40 km/h; 2 - 60 km/h; 3 - 80 km/h [33]*

value. The road surface meets the requirements for operation if the actual value of the friction coefficient is greater than or equal to the minimum allowable value. The minimum allowable friction coefficient is 0.3 when measured with a tire without a tread pattern and 0.4 when measured with a tire with a tread pattern [32].

The "sand spot" method is a set of equipment that includes a measuring container of a volume of at least 20 cm^3, a flat disk (stamp) of a diameter of 10 cm for distributing sand, a measuring ruler of a length of at least 30 cm and a sweeping brush. Measurements require clean, fine (particle size no more than 0.2-0.3 mm) natural sand in an air-dry state, gypsum or quick-hardening cement and water. When taking measurements, a certain volume of sand (20-50 cm^3) is poured onto the surface of the coating and, using a stamp, it is evenly distributed flush with the surface of the friction properties protrusions, giving the sand spot the shape of a circle, rectangle, or square (Figure 8) [28].

Then the diameter of the circle is measured in four mutually perpendicular directions (D_1 - D_2) and the arithmetic mean diameter is calculated, by which the average depth of the friction property depressions is determined:

$$\Delta_{av} = 4V_n/\pi D^2, \quad (4)$$

where: V_n - sand volume, cm^3;
D - average circle diameter, cm.

If it is necessary to determine the height of the protrusions, the surface occupied by sand is contoured, the sand is removed from the depressions of macroroughness with a brush and the cleaned surface of the coating is lubricated with technical glycerin. Then, an impression is taken from the coating: a liquid dough is made from gypsum, quick-hardening cement, or other similar material and is distributed over the surface under study with a layer of 1.0-1.5 cm. After 5-7 minutes, the impression is separated from the coatings and held for 10-15 minutes until it hardened. After that, the volume of friction property depressions is determined (numerically equal to the volume of friction property protrusions) using the "sand spot" method and the average height of the protrusions is calculated [28].

As a result of Nemchinov's proposal of the dependence of the friction (adhesion) coefficient on the contact of automobile tires with the pavement of the roadway, it was found that on the wet pavements at low speeds, with an increase in friction properties, the adhesion coefficient decreases and with an increase in speed, it first stabilizes and then even increases with an increase in the average height of the protrusions up to 5.5 mm (Figure 9) [33].

To study the effect of road surface friction properties on traffic safety, the pavement friction properties were measured at every 1000 m of all the experimental streets using the "sand spot" method and their condition was evaluated using the method proposed by Nemchinov and according to the regulatory requirements of IKN 05-2011 and MSHN 25-2005 [27, 29]. The condition of the road surfaces in terms of friction is assessed by comparing the actual value of the coefficient of longitudinal adhesion with its minimum allowable value (Table 5).

Table 5 *Evaluation of pavement friction properties of experimental streets*

Street name	Measurement site	Δ_{av}, cm	φ_w	The state of friction properties according to the requirements of operation
Buyuk Ipak Yuli St., Tashkent	PK 10+00	0.4	0.5	satisfies
	PK 20+00	0.65	0.42	satisfies
	PK 30+00	0.88	0.26	does not satisfy
	PK 40+00	0.9	0.25	does not satisfy
	PK 50+00	0.74	0.35	does not satisfy
	PK 60+00	0.44	0.48	satisfies
Fargona Yuli St., Tashkent	PK 10+00	0.52	0.45	satisfies
	PK 20+00	0.86	0.34	does not satisfy
	PK 30+00	0.5	0.45	satisfies
	PK 40+00	0.77	0.35	does not satisfy
	PK 50+00	0.89	0.25	does not satisfy
	PK 60+00	0.74	0.35	does not satisfy
Izzat St., Tashkent	PK 10+00	0.63	0.42	satisfies
	PK 20+00	0.82	0.32	does not satisfy
Alisher Navoi Ave., Chirchik	PK 10+00	0.52	0.45	satisfies
	PK 20+00	0.55	0.44	satisfies
	PK 30+00	0.7	0.38	does not satisfy
	PK 40+00	0.65	0.42	satisfies
	PK 50+00	0.89	0.25	does not satisfy
	PK 60+00	0.36	0.5	satisfies
	PK 70+00	0.5	0.45	satisfies
Amir Temur Ave., Chirchik	PK 10+00	0.82	0.32	does not satisfy
	PK 20+00	0.88	0.26	does not satisfy
	PK 30+00	0.75	0.35	does not satisfy
	PK 40+00	0.75	0.35	does not satisfy
	PK 50+00	0.33	0.5	satisfies
Soglom Avlod St., Chirchik	PK 10+00	0.7	0.38	does not satisfy
	PK 20+00	0.8	0.3	does not satisfy

The road surface meets the requirements for operation if the actual value of the friction coefficient is greater than or equal to the minimum allowable value. The maximum permissible value of the friction coefficient is 0.3 when measured by a tire without a tread pattern and 0.4 when measured by a tire with a tread pattern [27].

The measured and estimated friction properties of the experimental streets indirectly affect the speed of movement and therefore, the speed of movement along these streets was also measured. This indicator is also influenced by the level of traffic congestion on the road. When processing the data, a graph was constructed of dependence of the speed of the traffic flow on the value of the load factor (Figure 10), from which it follows that in the interval $0 \leq z \leq 0.2$, the traffic flow moves at a speed of 55 to 70 km/h; in the interval $0.2 \leq z \leq 0.45$ - from 35 to 55 km/h,; in the interval $0.45 \leq z \leq 0.7$ - from 20 to 45 km/h,; and in the interval $0.7 \leq z \leq 1$ traffic speed is less than 20 km/h.

According to results of the study of the traffic flow conditions on the experimental streets, the relationship between the flow density and street capacity was determined (Figure 11).

From any of the graphs shown in Figure 11, it can be clearly seen how the throughput of the street changes depending on the flow density and that with an increase in the flow density, the throughput of the street decreases. Additionally, on some streets (Izzat St., Tashkent; Soglom Avlod St., Chirchik), the indicators are low due to the fact that the geometric parameters and road conditions are in an inappropriate condition.

5 Conclusions

Based on the review of previous studies, it was determined that the scope and volume of research works devoted to the «study of the impact of roughness and friction properties of road surfaces of urban streets on traffic safety» vary widely. It was determined that on almost all the streets of the object of study there are many

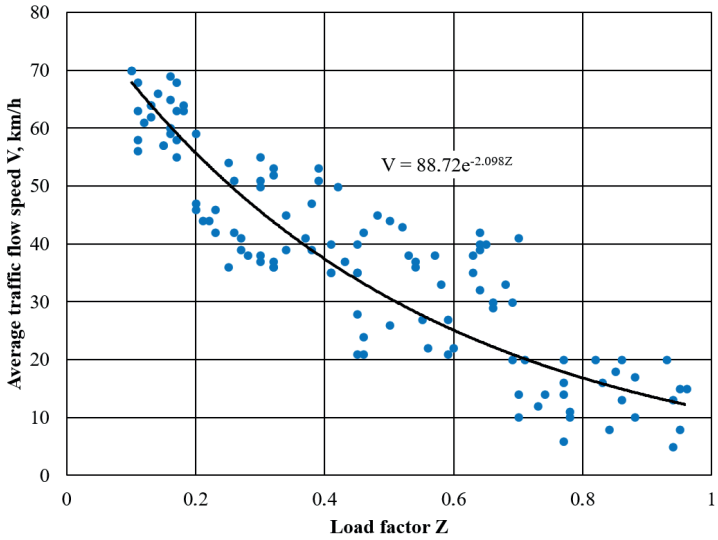

Figure 10 *A graph of the relationship between the traffic speed and a load factor under different traffic conditions*

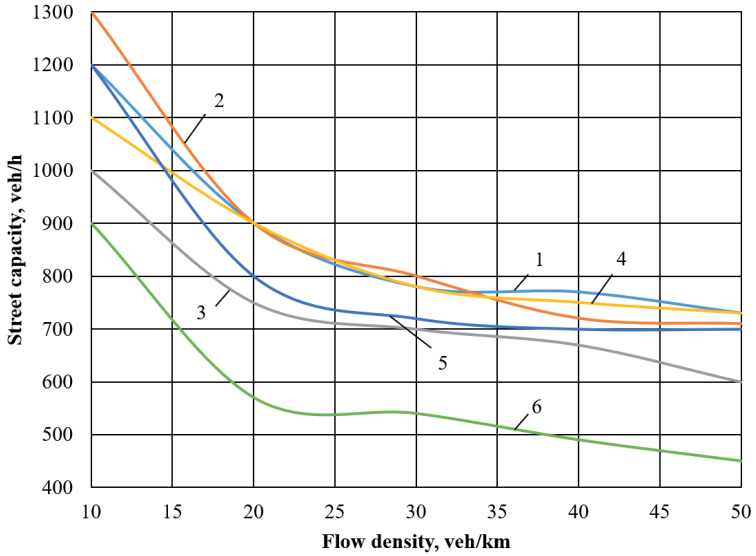

Figure 11 *A graph of the relationship between the flow density and a street capacity: 1 - Buyuk Ipak Yuli St. (Tashkent); 2 - Fargona Yuli St. (Tashkent); 3 - Izzat St. (Tashkent); 4 - Alisher Navoi Ave. (Chirchik); 5 - Amir Temur Ave. (Chirchik); 6 - Soglom Avlod St. (Chirchik)*

different defects in the pavement, including potholes and pitting and their distribution occupies a considerable area.

To study the influence of the roughness and friction properties of the road surface on the traffic safety, the relative dependence of pavement roughness and safety factor was proposed; an empirical dependence was obtained, reflecting the relationship between the traffic speed and a load factor, under different traffic conditions; and the relationship between the flow density and a street capacity was determined. The maximum permissible value of the friction coefficient for experimental streets is 0.4 and 50% of the object of study meets the requirements of operation; 50% does not. From the proposed graph of the relative dependence of the pavement roughness and a safety factor, it follows that the most dangerous (F_s < 0.6) are the Fargona Yuli and Izzat streets of the city of Tashkent, the pavement roughness of which is in unsatisfactory condition. The measured and estimated friction properties of the experimental streets indirectly affect the speed of movement and, therefore, the speed of movement along these streets was also measured. This indicator is also influenced by the level of traffic congestion on the road. From the proposed graph of the relationship between the flow density and a street capacity, it can be seen that as the flow density increases, the street capacity decreases.

Grants and funding

The authors received no financial support for the research, authorship and/or publication of this article.

Conflicts of interest

The authors declare that they have no known competing financial interests or personal relationships that could have appeared to influence the work reported in this paper.

References

[1] MUCKA, P. Vibration dose value in passenger car and road roughness. *Journal of Transportation Engineering, Part B: Pavements* [online]. 2020, **146**(4), 04020064. eISSN 2573-5438. Available from: https://doi.org/10.1061/JPEODX.0000200

[2] MUCKA, P., STEIN, G. J., TOBOLKA, P. Passsenger ride comfort and international roughness index specifications in the Slovak Republic. *Communications - Scientific Letters of the University of Zilina* [online]. 2019, **21**(1), p. 14-21. ISSN 1335-4205, eISSN 2585-7878. Available from: https://doi.org/10.26552/com.C.2019.1.14-21

[3] LEE, J., ABDEL-ATY, M., NYAME-BAAFI, E. Investigating the effects of pavement roughness on freeway safety using data from five states. *Transportation Research Record: Journal of the Transportation Research Board* [online]. 2020, **2674**(2), p. 127-134. ISSN 0361-1981, eISSN 2169-4052. Available from: https://doi.org/10.1177/036119812090583

[4] POPOOLA, M. O., APAMPA, O. A., ADEKITAN, O. Impact of pavement roughness on traffic safety under heterogeneous traffic conditions. *Nigerian Journal of Technological Development* [online]. 2020, **17**(1), p. 13-19. ISSN 0189-9546, eISSN 2437-2110. Available from: https://doi.org/10.4314/njtd.v17i1.2

[5] JANANI, L., DOLEY, R., SUNITHA, V., MATHEW, S. Precision enhancement of smartphone sensor-based pavement roughness estimation by standardizing host vehicle speed. *Canadian Journal of Civil Engineering* [online]. 2022, **49**(5), p. 716-730. ISSN 0315-1468, eISSN 1208-6029. Available from: https://doi.org/10.1139/cjce-2021-018

[6] AZIZOV, K. K. Fundamentals of traffic safety of mixed automobile and tractor flows / Osnovy bezopasnosti dvijeniya smeshannyx avtomobilno-traktornyx potokov (in Russian). Tashkent: Fan AN RUz, 2008. ISBN 978-9943-09-552-6

[7] ESHKABILOV, S., YUNUSOV, A. Measuring and assessing road profile by employing accelerometers and IRI assessment tools. *American Journal of Traffic and Transportation Engineering* [online]. 2018, **3**(2), p. 24-10. eISSN 2578-8604. Available from: https://doi.org/10.11648/j.ajtte.20180302.122

[8] UROKOV, A., SOATALIEV, R. Analysis of modern and resource-saving technologies used in assessing the transport performance of highways. *Scientific Journal of Vehicles and Roads* [online]. 2021, **1**(3), p. 6-11. Available from: https://transportjournals.uz/index.php/vihles/article/view/42

[9] FILIPPOV, V. V., SMIRNOVA, N. V., KIYASHKO, D. I. Evaluation of the impact of uneven road surfaces on traffic safety / Otsenka vliyaniya nerovnostey dorojnyx pokrytiy na bezopasnost dvijeniya (in Russian). *Bulletin of Kharkiv National Automobile and Road University*. 2009, **47**, p. 63-65.

[10] NEMCHINOV, M. V. Ensuring and evaluating the friction qualities of road surfaces / Obespechenie i otsenka ssepnyx kachestv dorojnyx pokrytiy (in Russian). *Science and Technology in the Road Industry*. 2004, **4**, p. 12-14. ISSN 1993-8543.

[11] YEVTYUKOV, S. A., YEVTYUKOV, S. S. Parameters influencing the friction qualities of road surfaces / Parametry, vliyayushie na ssepnye kachestva pokrytiy avtodorog (in Russian). *Vestnik Tuvinskogo Gosudarstvennogo Universiteta, Texnicheskie i Fiziko-Matematicheskie Nauki*. 2013, **3**, p. 75-82. eISSN 2310-7081.

[12] BEKETOV, A. K., SAYDAMETOVA, F. J., ERGASHOVA, M. Z., KHALIMOVA, S. R. Foreign experience in urban streets management system. *Academic Research in Educational Sciences*. 2022, **3**(1), p. 891-896. eISSN 2181-1385.

[13] SAYDAMETOVA, F., BEKETOV, A., KHALIMOVA, S., YUNUSOV, A. The development of the network of urban roads and streets (on the example of the city of Urgench). *Acta of Turin Polytechnic University in Tashkent* [online]. 2022, **12**(1), p. 55-61. eISSN 2181-1512. Available from: https://acta.polito.uz/index.php/journal/article/view/124

[14] KARAN, M. A., HAAS, R., KHER, R. Effects of pavement roughness on vehicle speeds. *Transportation Research Record: Journal of the Transportation Research Board* [online]. 1976, **602**, p. 122-127. ISSN 0361-1981, eISSN 2169-4052. Available from: http://onlinepubs.trb.org/Onlinepubs/trr/1976/602/602-023.pdf

[15] RAYMOND, C. M., TIGHE, S. L., HAAS, R., ROTHENBURG, L. Analysis of influences on as-built pavement roughness in asphalt overlays. *International Journal of Pavement Engineering* [online]. 2003, **4**(4), p. 181-192. ISSN 1029-8436, eISSN 1477-268X. Available from: https://doi.org/10.1080/10298430310001653077

[16] SMITH, J. T., TIGHE, S. L. Assessment of overlay roughness in long-term pavement performance test sites: Canadian case study. *Transportation Research Record: Journal of the Transportation Research Board* [online]. 2004, **1869**(1), p. 126-135. ISSN 0361-1981, eISSN 2169-4052. Available from: https://doi.org/10.3141/1869-15

[17] KWON, T. J., FU, L., JIANG, C. Effect of winter weather and road surface conditions on macroscopic traffic parameters. *Transportation Research Record: Journal of the Transportation Research Board* [online]. 2013, **2329**(1), p. 54-62. ISSN 0361-1981, eISSN 2169-4052. Available from: https://doi.org/10.3141/2329-07

[18] OMER, R., FU, L. Road surface condition classification method and system. U.S. Patent Application No. 14/403,505.

[19] GOLSHAN KHAVAS, R., HELLINGA, B. Determining road surface and weather conditions which have a significant impact on traffic stream characteristics. In: Transportation Research Board 95th Annual Meeting: proceedings. 2016.

[20] ALESSANDRONI, G., CARINI, A., LATTANZI, E., FRESCHI, V., BOGLIOLO, A. A Study on the influence of speed on road roughness sensing: the smart road sense case. *Sensors* [online]. 2017, **17**, p. 305. eISSN 1424-8220. Available from: https://doi.org/10.3390/s17020305

[21] LOPRENCIPE, G., ZOCCALI, P., CANTISANI, G. Effects of vehicular speed on the assessment of pavement road roughness. *Applied Sciences* [online]. 2019, **9**(9), 1783. eISSN 2076-3417. Available from: https://doi.org/10.3390/app9091783

[22] PADILLA, J. A., VICTORIA JR, A. N., DELA CRUZ, O. G., DESPABELADERA, C. T., CREENCIA, C. J. N. Evaluation of international roughness index by speed-related quality criteria in the Philippines. In: Annual International Conference on Architecture and Civil Engineering: proceedings [online]. 2019. Available from: https://doi.org/10.5176/2301-394X_ACE19.523

[23] NGUYEN, X. H., NGUYEN, T. Q., TRAN, P. H. The effect of road surface roughness to recommended speed of vehicles. *IOP Conference Series: Materials Science and Engineering* [online]. 2020, **886**(1), 012014. ISSN 1757-8981, eISSN 1757-899X. Available from: https://doi.org/10.1088/1757-899X/886/1/012014

[24] MISAGHI, S., TIRADO, C., NAZARIAN, S., CARRASCO, C. Impact of pavement roughness and suspension systems on vehicle dynamic loads on flexible pavements. *Transportation Engineering* [online]. 2021, **3**, 100045. eISSN 2666-691X. Available from: https://doi.org/10.1016/j.treng.2021.100045

[25] SILYANOV, V. V., DOMKE, E. R. Transport and operational qualities of automobile roads and urban streets / Transportno-ekspluatatsionnye kachestva avtomobilnyx dorog i gorodskix ulis (in Russian). 2. ed. Moscow: Akademiya, 2008. ISBN 4864-2

[26] AMIROV, T. Z., ZAFAROV, O. Z., YUSUPOV, Z. M. Cracks in asphalt concrete pavements: causes and negative consequences / Treshiny na asfaltobetonnyx pokrytiyax: prichiny obrazovaniya i otritsatelnye posledstviya (in Russian). *Young scientist*. 2016, **6**(110), p. 74-75. ISSN 2072-0297.

[27] IKN 05-2011. Rules for diagnosing and assessing the condition of automobile roads / Pravila diagnostiki i otsenki sostoyaniya, avtomobilnyx dorog (in Russian). Tashkent: State Joint Stock Company for the Construction and Maintenance of Automobile Roads (SJSC Uzavtoyul), 2011.

[28] VASILEV, A. P. Maintenance of automobile roads / Ekspluatatsiya avtomobilnyx dorog (in Russian). Moscow: Academy, 2010. ISBN 978-5-7695-9763-3, 978-5-7695-9765-7.

[29] MSHN 25-2005. Instructions for ensuring traffic safety on automobile roads / Ukazaniya po obespecheniyu bezopasnosti dvijeniya na avtomobilnyx dorogax (in Russian). Tashkent: State Joint Stock Company for the Construction and Maintenance of Automobile Roads (SJSC Uzavtoyul), 2005.

[30] VASILYEV A. P., SIDENKO V. M. Maintenance of automobile roads and organization of traffic / Ekspluatasiya avtomobilnix dorog i organizasiya dorojnogo dvijeniya (in Russian). Moscow: Transport, 1990. ISBN 5-277-00877-2

[31] AZIZOV, K. K., URAKOV, A. K. Road safety / Bezopasnost dorojnogo dvijeniya (in Russian). Tashkent: LLC VneshInvestProm, 2019. ISBN 978-9943-4444-2-3

[32] AZIZOV, K. K., POSPELOV, P. I., URAKOV, A. K. Road conditions and traffic safety / Dorojnye usloviya i bezopasnost dvijeniya (in Russian). Tashkent: LLC VneshInvestProm, 2019. ISBN 978-9943-4885-1-2

[33] NEMCHINOV, M. V. Design and construction technologies of rough wear layers on road surfaces / Proektirovanie i texnologii stroitelstva sheroxovatyx sloyov iznosa na pokrytiyax avtomobilnyx dorog (in Russian). Moscow: MADI, 2019.

This is an open access article distributed under the terms of the Creative Commons Attribution 4.0 International License (CC BY 4.0), which permits use, distribution, and reproduction in any medium, provided the original publication is properly cited. No use, distribution or reproduction is permitted which does not comply with these terms.

THE DANGEROUS FACTORS IDENTIFICATION FEATURES OF OCCUPATIONAL HAZARDS IN THE TRANSPORTATION CARGO PROCESS

Vitaliy Tsopa[1], Serhiy Cheberyachko[2], Yana Litvinova[2], Mariia Vesela[2], Oleg Deryugin[2,*], Ivan Bas[2]

[1]International Institute of Management, Kyiv, Ukraine
[2]Dnipro University of Technology, Dnipro, Ukraine

*E-mail of corresponding author: oleg.kot@meta.ua

Vitaliy Tsopa 0000-0002-4811-3712,
Yana Litvinova 0000-0003-2806-4076,
Oleg Deryugin 0000-0002-2456-7664
Serhiy Cheberyachko 0000-0003-3281-7157,
Mariia Vesela 0000-0001-9318-9110,

Resume
The article highlights the problem of occupational safety of a technological truck driver by improving the process of determining the level of occupational risk by studying the relationships between various external and internal hazards. A special algorithm is proposed, the main difference of which from the known ones is the procedure for analyzing and determining the causes of dangerous factors, for which it is proposed to use the "Decision-Making Trial and Evaluation" method (further - fuzzy Dematel). A cause-and-effect relationship has been established between dangerous factors that affect the work of a truck driver while driving a vehicle.

Article info
Received 3 April 2023
Accepted 20 June 2023
Online 28 June 2023

Keywords:
a driver
professional risk
fuzzy Dematel method
management decisions

Available online: https://doi.org/10.26552/com.C.2023.058

ISSN 1335-4205 (print version)
ISSN 2585-7878 (online version)

1 Introduction

With the industrialization spread in the world, the responsibility of employers for occupational safety has increased. This has led to necessity to introduce various legal acts both at the international [1] and national levels regarding occupational health and safety at work. In particular, the convention of the International Labor Organization (ILO) and the European Union (EU) 89/391/EEC "Framework directive on health and safety at work" has been adopted at the international level, and at the national level - the corresponding legislation on labor protection and [2-5], which contains requirements for both employers and employees, the basis of which is the occupational risk assessment (hereinafter -OR). It is considered that its introduction allows to significantly increase the level of labor safety, due to elimination of industrial hazards that affect employees during the professional activities' performance. The appropriate, high-quality assessment of occupational health and safety is a very important stage of the occupational safety and health management system.

The evaluation procedure of the assessing occupational risks, according to ISO 31000:2018, ISO 39001:2012, ISO 45001:2018 and others, consists of several main steps: identification of hazards and dangerous factors (hereinafter - DF), determination of the damage level and occurrence probability of a dangerous event, establishment of causal consequential links between danger, DF and dangerous event, on the one hand and dangerous event and consequences, on the other. Next, the value of OR is directly assessed, which is the basis for justifying the protective and preventive measures. The last step is to check the OR assessment. Despite the fact that all the steps are quite important, and a mistake made at any stage can nullify the entire procedure, it is considered that the most difficult and responsible step is the first one: the identification of hazards and DF. Ignoring any hazard or DF can lead to catastrophic consequences that no one has expected. Therefore, in each specific case, there is a necessity to process fairly significant volumes of information: processing the letters of incapacity for work, accident materials investigation, results of sanitary and hygienic, ergonomic analyzes of the workplace, maps of working conditions, results of monitoring the performance of production operations, questionnaires, employees surveys to find out, not only the presence of the dangers themselves, but the causes

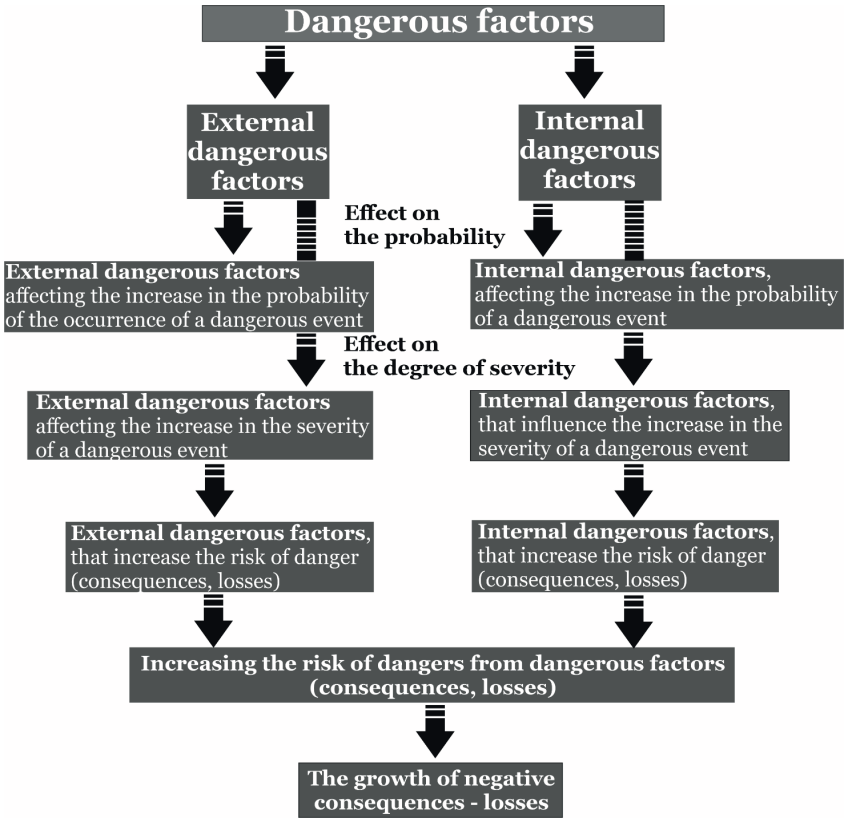

Figure 1 *Dangerous Factors' threat*

- DFs, as well, which lead to and have an impact on the increase in the occurrence probability and severity of incidents, emergency situations, traffic accidents (hereinafter - TA), accidents or emergency situations (Figure 1).

Also, it can be noted that this process is strongly influenced by the professional expert subjective opinion. A cohort of various cognitive biases (too much information, planning errors, optimism bias, fundamental attribution error, and others) quite often leads to incorrect evaluation decisions, calculations of the OR value [6-7] - neglect of obvious facts. At the same time, the processing of the entire set of the DFs would lead to a significant increase in the maps size for the OR assessment, the complexity of their understanding and reading, and most importantly, the selection of the most significant factors of incidents. Therefore, research aimed at improving this procedure, namely reducing the influence of the judgments subjectivity when calculating OR, is a rather urgent task [8].

2 Analysis of relevant literature

Several different approaches are proposed for evaluating the OR in transportation processes: qualitative, semi-qualitative (when the occurrence probability of a dangerous event and the severity of the consequences are set by experts based on their own experience) and quantitative. Experts indicate that the latter is the most appropriate, as it allows to assess reliably the level of the OR. However, a significant amount of statistical data is needed to determine the probability of the dangerous event occurrence. The issue raised in the case of road freight transportation (further - RFT) of hazardous substances that pose a significant threat to humans and the environment becomes especially relevant [9]. The author suggests that during the OR assessment, it is necessary to take into account the influence of the physical and chemical properties of the cargo being transported. However, the author, having disclosed in detail the consequences of such accidents and at the same time substantiating the need to take into account the type of cargo for the evaluation of the OR, does not indicate a specific procedure that would allow establishing the value of the OR. In the study [10], it is also suggested to pay attention to the type of cargo, the quality of the driver training and the influence of the environment, using the usual matrix system of the occupational risks evaluation. Moreover, they do not pay attention to the cumulative effect of the mentioned dangerous factors (PMs), but evaluate their impact separately from each other, which can lead to a significant error in the calculations of OR. In addition, no less important for reducing the level of professional risks is the construction of rational traffic routes, thanks to which a reduction in the distraction of the driver's attention during transportation is achieved [11]. In another publication [12], the authors cited the results of the influence of a large number of participants in the

transportation process and their possible incompetent actions, which lead to an increase in random factors and the resulting OR. To identify the transportation risks, the authors suggest using the SWOT analysis, which does not allow for the ranking of OR, but only indicates the presence of a number of strengths and weaknesses with the identification of threats that affect the RFT. The interesting solution for the occupational risks assessment was proposed by the authors in [13], to identify the OR that appears in the transport chain. At the same time, for each step, it was proposed to determine, instead of the severity of the consequences, the quality of the cargo transportation process. The result is the amount of OR when performing the RFT of the corresponding type of cargo. At the same time, having proposed a good idea, the authors subsequently followed the path of semi-quantitative analysis, which requires appropriate preparation for conducting such an analysis. Another unusual approach to the assessment of transport risks was shared by the authors in [14], where it is proposed to carry out a OR assessment by the Functional Resonance Analysis Method (FRAM method), which allows to consider the influence on the final result of four factors, which are set by the functions of time, control, availability of preconditions and a sufficient number of resources. On the one hand, this approach allows for more thorough determination of the occupational risks of failure to perform the transport work, and on the other hand, it forces a qualitative assessment of the function variability, which can introduce additional errors into the transport process risk assessment.

The conducted analysis indicates the need to develop or improve the process of DFs identification, which increase the probability of a dangerous event to reduce the procedure subjectivity for the management of OR in road freight transportation.

The purpose of this study was to improve identifying the to improve the process of identifying the dangerous factors that increase the probability of a dangerous event occurrence and the severity of its consequences to reduce the subjectivity of judgments during the managing professional risks procedure ine implementation of the road freight transportation.

3 Materials and methods

For the above mentioned procedure it was planned to use the fuzzy Dematel method, which is based on paired comparison and decision-making tools based on the Graph theory [15-16], which would allow the causal relationships transformation in structural-visual models and together with verification of experts' assessments of emissions according to the Grubbs criterion to identify and understand the most relevant interdependencies between various DFs that cause human harm.

The fuzzy Dematel method is superior to other multi-criteria management decision-making methods, such as "Interpretive structural modeling" (ISM) and "Analytic Hierarchy Process" (AHP) methods, as it allows to assess the overall degree of influence of various factors or problems effectively, to identify the cause-and-effect groups and establish causal relationships [15-17]. The use of fuzziness in the fuzzy Dematel method allows to use imprecise information that is typical for ordinary human judgments. It includes four main stages [18-20].

Formation of data for analysis. To identify areas where the process improvement is possible, data relevant to the problem under consideration must be collected so that various quantitative and qualitative operations can be applied to refine the details.

Identification of received data. The information collected at the stage A is important for identifying the potential problems (PP) that prevent the normal operation of the technological (transportation) process under consideration. Based on the nature of the received information, the quantitative and qualitative data analysis is carried out. It is also possible to convert the qualitative (logistic statements) data into quantitative data and vice versa.

Analysis of relationships. The number of problems highlighted in this step can vary from a few units to very large values. It is believed that none of the problems exists by itself, without the connection to the others. In other words, each problem can drive others or depend on other problems. Therefore, it is important to analyze the interrelationships between problems.

Interpretation of the obtained results. At this stage, the results of the analysis carried out at the relationships analysis stage are interpreted.

The above four stages can be divided into several consecutive steps of the research (Figure 2), which will allow to obtain the appropriate result from the analysis of the impact of certain DFs on the efficiency of the technological (transportation) process.

At the first step, a group of experts-specialists in the relevant field is formed, who have theoretical and practical experience in the relevant field of activity to identify the DFs related to the professional activity of the driver and their consequences. Five experts were selected to carry out this procedure (Table 1).

At the second step, evaluation criteria are determined and the fuzzy linguistic scale is developed for expert evaluation. At this stage, various criteria and degrees of each problem's relative importance are determined, and presented in the linguistic classification terms: very high impact, high impact, low impact, very low impact and no impact. Answers of experts were transformed into the fuzzy numbers using a fuzzy scale (Table 2). Triangular fuzzy numbers were used; the triangular fuzzy number $\tilde{z}$ is defined as follows: $\tilde{z} = (l, m, u)$, where l, m and u are real numbers and $l \leq m \leq u$.

I Stage - Data formation for analysis

Step 1. Formation of a group of experts-specialists in the relevant field who have theoretical and practical experience in the relevant field of activity in order to identify dangerous factors related to the professional activity of the employee and their consequences.

Step 2. Determination of evaluation criteria and development of a fuzzy linguistic scale for expert evaluation.

II Stage - Identification of the received data

Step 3. Construction of the fuzzy normalized matrix of direct connection $\widetilde{Z}_k$ based on the results of expert judgments of the problem under consideration.

Step 4. Analysis of the initial normalized fuzzy direct matrix and transformation of the scale of evaluation criteria into a scale of comparable values into triangular numbers of the developed evaluation criteria.

III Stage - Analysis of relationships

Step 5. Construction and calculation of the direct matrix of connections T of the normal relation.

Step 6. The values of the expressions $R_i + C_j$ and $R_i - C_j$ are defuzzified (transformation of a fuzzy set into a distinct number by the degree of membership) using the method of using the technique of defuzzification of the center of the value area (CVA).

IV Stage - Interpretation of the obtained results

Step 7. Construction of a causal diagram. Analysis of the obtained results.

Figure 2 *Algorithm of the fuzzy DEMATEL method*

Table 1 *Data from experts participating in research*

Information	Amount
Number of experts	5
Work experience in transport logistics positions	from 10 to 14 years
Education of experts	majored in transport technologies
Work experience	more 10 years
Availability of an auditor's certificate for the company's quality and safety management systems	Yes
Advanced training in risk assessment according to requirements ISO 45001	Yes

Table 2 *Word phrases and corresponding fuzzy numbers [21]*

Final equivalent	Description	A vague equivalent		
Very high impact	VH	0.75	1	1
High impact	H	0.5	0.75	1
Low impact	L	0.25	0.5	0.75
Very low impact	VL	0	0.25	0.5
No influence	NO	0	0	0.25

The membership function $\mu_{\tilde{z}}$ is defined as follows:

$$\mu_{\tilde{z}} = \begin{cases} \dfrac{x-l}{m-l} \; at \; l \le x \le m \\ \dfrac{u-x}{u-m} \; at \; m \le x \le u \\ 0 \; in \; all \; other \; cases \end{cases}. \tag{1}$$

The third step involves the construction of a fuzzy normalized matrix of direct communication based on the results of expert judgments of the problem under consideration. Fuzzy matrices $\tilde{z}_1, \tilde{z}_2, \tilde{z}_3, \ldots, \tilde{z}_p$ are formed. Triangular fuzzy numbers were generated according to the judgments of the experts who participated in the peer review. The initial direct matrix is the fuzzy matrix $\tilde{z}_k$:

$$\tilde{z}^k = \begin{bmatrix} 0 & \tilde{z}_{12}^{(k)} & \ldots & \tilde{z}_{n1}^{(k)} \\ \tilde{z}_{21}^{(k)} & 0 & \ldots & \tilde{z}_{n1}^{(k)} \\ \ldots & \ldots & \ldots & \ldots \\ \ldots & \ldots & \ldots & \ldots \\ \tilde{z}_{n1}^{(k)} & \ldots & \ldots & 0 \end{bmatrix}, \tag{2}$$

where $\mu_{\tilde{z}} = 1,2,3,\ldots,p; \tilde{z}_{ij}^{(k)} = \left(l_{ij}^{(k)}, m_{ij}^{(k)}, u_{ij}^{(k)}\right)$.

Without loss of generality $\tilde{z}_u^{(k)} = (i = 1,2\ldots n)$ was treated as a triangular fuzzy number $\tilde{z} = (0,0,0)$, when it is required.

In the fourth step, the normalized fuzzy matrix of direct connections is analyzed. Suppose that:

$$r_k = \max_{i=1}^{n}\left(\sum_{j=1}^{n} u_{ij}^{k}\right). \quad (3)$$

A linear transformation was used to transform the criteria scale into a scale of comparable values, and a normalized fuzzy matrix of direct relationships, obtained as a result of expert evaluation, has the following form given in Equation (4):

$$\tilde{x}^k = \begin{bmatrix} \tilde{x}_{11}^{(k)} & \tilde{x}_{12}^{(k)} & \ldots & \tilde{x}_{1n}^{(k)} \\ \tilde{x}_{21}^{(k)} & \tilde{x}_{22}^{(k)} & \ldots & \tilde{x}_{2n}^{(k)} \\ \ldots & \ldots & \ldots & \ldots \\ \ldots & \ldots & \ldots & \ldots \\ \tilde{x}_{n1}^{(k)} & \tilde{x}_{n2}^{(k)} & \ldots & \tilde{x}_{nn}^{(k)} \end{bmatrix}, \quad (4)$$

where k = 1, 2, 3, ..., p.

$$\tilde{x}_{ij}^{(k)} = \frac{\tilde{z}_{ij}^{(k)}}{r^k} = \left(\frac{l_{ij}^{(k)}}{r^k}, \frac{m_{ij}^{(k)}}{r^k}, \frac{u_{ij}^{(k)}}{r^k}\right). \quad (5)$$

Similar to the conventional Dematel method, we assume that there is at least one value of i such that

$$\sum_{j=1}^{n} u_{ij}^{k} < \sum_{j=1}^{n} r^k.$$

$\tilde{X}$ denotes the average value of the judgments of all the experts who participated in the evaluation of the technological process:

$$\tilde{X} = \frac{\tilde{x}^1 + \tilde{x}^2 + \ldots + \tilde{x}^p}{p}. \quad (6)$$

$$\tilde{X} = \begin{bmatrix} \tilde{X}_{11} & \tilde{X}_{12} & \tilde{X}_{1n} \\ \tilde{X}_{21} & \tilde{X}_{22} & \tilde{X}_{2n} \\ & & \\ \tilde{X}_{n1} & \tilde{X}_{n2} & \tilde{X}_{nn} \end{bmatrix} \quad (7)$$

where $\tilde{X}_{ij} = \dfrac{\sum_{k=1}^{p} \tilde{x}_{ij}^{(k)}}{p}$.

The fifth step is to calculate the overall fuzzy matrix of connections $\tilde{T}$. It is known that $\lim_{W\to\infty} X^W = \Theta$, where Θ is the zero matrix. In addition, it is known that $\lim_{W\to\infty}(1 + \tilde{X} + \tilde{X}^2 + \ldots + \tilde{X}^W) = X \cdot (1 - \tilde{X})^{-1}$. Both of these relations are proved in [22-23]. The last matrix is a general fuzzy matrix of connections $\tilde{T}$.

The sixth step consists in calculating the general matrix of connections $\tilde{T}$. Significance and relative position vectors are calculated, as well.

In the seventh step, all the fuzzy numbers are converted to exact values. For this, the following variant of the CFCS method is used. Suppose there are triangular fuzzy numbers $\tilde{N}_k = (l_k, m_k, u_k)$; $k = 1, 2, \ldots, n$. Provided that $L = \max(l_k)$; $R = \max(u_k)$; $\Delta = R - L$. That is, the usual value is calculated according to the following formula:

$$\tilde{N}_k^{def} = L + \Delta \times \left(\frac{(m_k - L)(\Delta + u_k - m_k)^2 \times}{\times (R - l_k) + (u_k - L)^2(\Delta + m_k - l_k)^2} \times \right. \\ \left. \times \frac{}{(\Delta + m_k - l_k)^2(\Delta + u_k - m_k)^2(R - l_k) + } \right. \\ \left. + (u_k - L)(\Delta + m_k - l_k)^2(\Delta + u_k - m_k)\right). \quad (8)$$

Based on the results of the calculation carried out in step 7, a cause-and-effect diagram was built. Its feature is determination of the causal and consequential dangerous factors. As a result, $r + c$ indicates the importance of criterion i in the system and $r - c$ shows the effect of criterion i in the system. If $r - c$ is positive, the effect of criterion i belongs to the group of reasons, and if $r - c$ is negative, the effect of the criterion belongs to the group of "dependents", which allows establishing the most important (causal) ones, according to which the risks are determined when performing the road freight transportation.

4 Research results

To assess the risks in implementation of the RFT, one can use the "Bowtie" model [24], which is the most widespread, as it allows to clearly establish, by visualizing, the cause-and-effect relationships. Moreover, with its help, it is quite simple to show the effect of DFs, which increase the probability of the dangerous event occurrence (Figure 3). The latter, in accordance with the requirements of the international standards of the ISO 9000, ISO 14000, ISO 39000, ISO 45000 series, include all the external and internal threats, challenges, inconsistencies that are identified during audits, analyzes by management, investigation of incidents, accidents during implementation RFT [11-12].

Thus, the analysis of various literary sources [25-27], as well as familiarity with the main causes of traffic accidents, made it possible to establish the main dangers (Table 3) that lead to traffic accidents and represent any source with the possibility of causing injury and deterioration of driver health.

Considering that the dangerous event occurrence is significantly influenced by various factors that increase its occurrence and the severity of its consequences, there is a necessity to build an appropriate register that would take into account at least several different groups of factors: human, organizational, social, technical, climatic, ergonomic ones. In each of the groups listed in Tables 4 and 5, specific dangerous factors that belong to one or another organization are considered. They are formed from working conditions, economic situation, technology and other components of organizational culture, which includes common/individual language/knowledge, acceptable technical solutions, common values, views, explicit/implicit symbols, shared experience, social customs and social norms, "maps meanings" that make social life understandable for employees of a separate company.

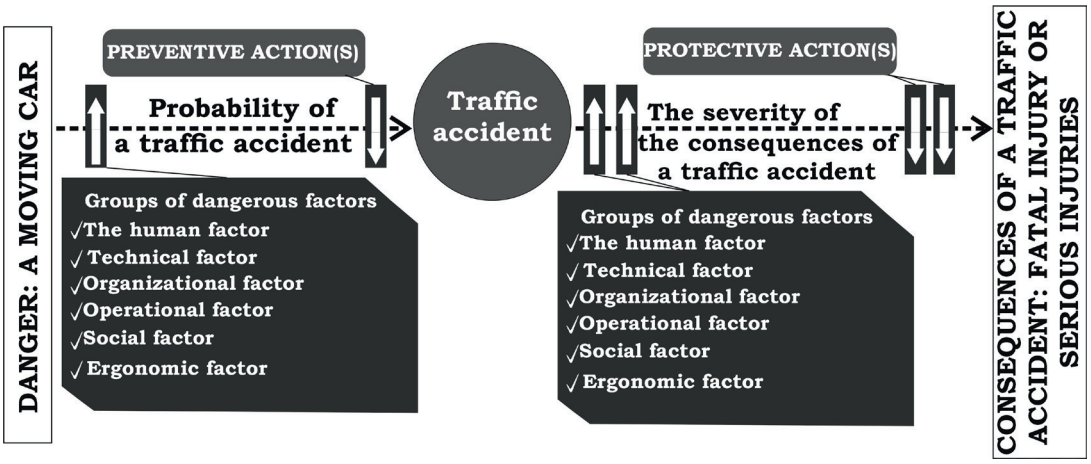

Figure 3 *The OR management model in the presence of DF in the external and internal environment of an organization*

Table 3 *Register of dangers affecting the motor vehicle driver*

Threat	Dangerous event	General DF		Consequences of a dangerous event
		Affecting the probability of the occurrence of a dangerous event	Affecting the degree of severity of the consequences of the occurrence of a dangerous event	
A moving car	Traffic accident	Organizational factors; the condition of the driver; technical condition of the car; climatic factor, social factor	The condition of the driver, the technical condition of the car, the condition of the water, operational and organizational factors	Serious injuries: broken bones, ruptured internal organs, skull fracture and brain contusion, etc.
Running car engine	Fire	Technical condition of the car, operational	Technical condition of the car, condition of the driver, operational, organizational factor	Serious injuries: burns and others
A working car engine in which fuel vapors have accumulated	Explosion	Technical condition of the car	Technical condition of the car, water condition, operational, organizational factor	Severe injuries: broken bones, ruptured internal organs, skull fracture and brain contusion, burns, etc.

As it has been already mentioned, a necessary condition for a successful occupational risks assessment is identification of all the potential hazards and their DFs, which is the basis of the first step in the OR assessment - hazard identification. The main complexity of the mentioned process includes the processing of a significant amount of information, that is, determination of the influence of one or another factor based on the establishment of cause-and-effect relationships, which would be carried out using the DEMATEL method, the algorithm of actions according to which is described above. A group of experts (Table 1) separately from each other, conducted pairwise comparisons of the determined dangerous factors (Table 4 and 5) and filled in the corresponding matrix-diagram (Figure 4) with pre-established criteria (Table 2). Unfortunately, this process is significantly influenced by the subjective judgments of experts, which are reinforced by possible cognitive distortions. Therefore, there is a necessity to apply various mathematical approaches to process the results received from experts and check their estimates for emissions, the Grubbs' criterion is used:

$$G_{\max} = \frac{X_n - \bar{X}}{S}, \tag{9}$$

where X_n is the proposed expert assessments, $\bar{X}$ is the sample mean and S is the mean square deviation.

Where it is necessary to calculate the mathematical expectation or the average value of the obtained results:

$$\bar{X} = \frac{1}{n}\sum_{i=1}^{n} X_i . \tag{10}$$

It is also necessary to calculate the mean square deviation:

$$s = \sqrt{\frac{1}{n-1}\sum_{i=1}^{n}(X_i - \bar{X})^2} . \tag{11}$$

With help of the following formulas, one checks for outliers the maximum and minimum results of expert assessments, provided that the indicator exceeds the critical value:

$$\begin{cases} G_{\max} \geq G_{n,1-\alpha} \\ G_{\min} \geq G_{1,1-\alpha} \end{cases}, \tag{12}$$

Table 4 *An example of a low-risk register - a moving truck (when carrying out an RFT) - part 1*

A group of dangerous factors	Designation of the factor	Dangerous factor (DF)
Human	A_1	Distractions while driving - texting or talking on a cell phone
	A_2	Lack of system understanding skills and safe decision-making skills
	A_3	Aggressive behavior while driving a truck
	A_4	Negative physical state of health and psycho-physiological state of the driver
	A_5	Lack of regular and periodic training to improve professional skills
Technical	A_6	Non-compliance of the truck with the physical and chemical properties of the transported cargo
	A_7	Inconsistency of the carrying capacity of a vehicle with the amount of cargo being transported
	A_8	Operation of a technically defective truck and equipment
	A_9	Low-quality spare parts and untimely installation and replacement of units and assemblies according to the terms of maintenance and repair.
	A_{10}	Operation of the equipment after the warranty period of operation
	A_{11}	Untimely replacement of hydraulic fittings during maintenance
	A_{12}	Negligence in observing the technical condition of the truck's passive safety systems (airbags, safety belts, impact-absorbing bumpers, etc.).
	A_{13}	Lack of appropriate equipment of the truck to perform the RFT
	A_{14}	Lack of high-quality supervision and technical inspection of the technical condition of the truck

Table 5 *An example of a low-risk register - a moving truck (when carrying out an RFT) - part 2*

A group of dangerous factors	Designation of the factor	Dangerous factor (DF)
Organizational	A_{15}	Lack of emergency equipment (fire extinguisher, etc.), first aid kits
	A_{16}	Exceeding the standard working time of a truck driver (driver fatigue)
	A_{17}	Overloading of a truck when carrying out the RFT
	A_{18}	The cabin is dirty, there are foreign objects in the driver's seat
	A_{19}	Lack of regular diagnostics and appropriate maintenance
Operating	A_{20}	Inconsistency of tire pressure with the road conditions
	A_{21}	Unadjusted electronic driver assistance systems when driving a truck
	A_{22}	Lack of proper pre-race medical control of the driver's health
	A_{23}	Fog, rain, snow/night time - poor visibility of the road by the driver
Social	A_{24}	Lack of financial support in a difficult situation
	A_{25}	Low wages
	A_{26}	Absence of monetary supplements for the difficulty of performing professional functions
	A_{27}	Overtime work schedule
Ergonomic	A_{28}	Lack of ease of steering wheel adjustment
	A_{29}	Lack of sufficient and convenient visibility at the workplace
	A_{30}	Lack of adequate air conditioning/heating system

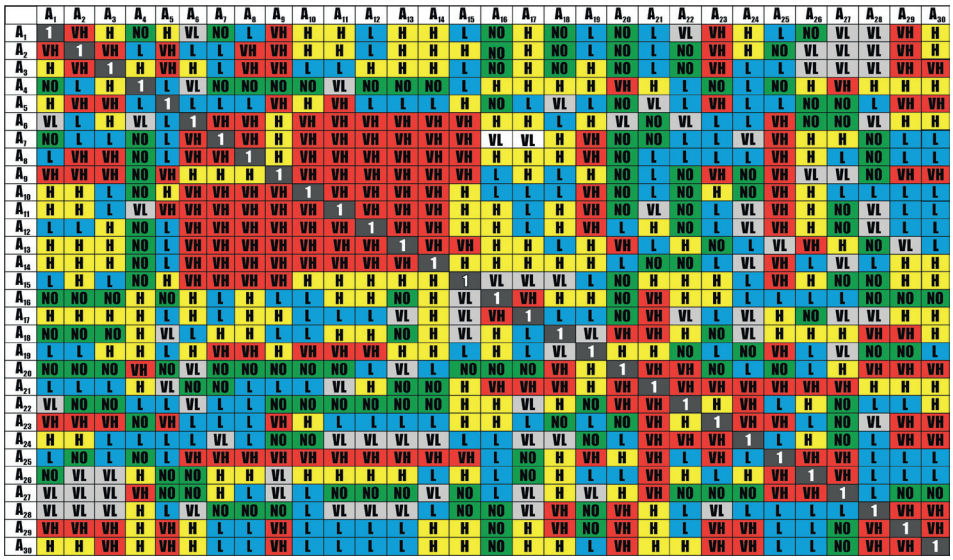

Figure 4 *An example of the matrix of pairwise comparisons, which is filled out by experts*

where α is the level of significance, which is determined in accordance with the requirements [28].

In the case of non-fulfillment of the specified inequality, the results of evaluations will be considered as emissions that must be excluded. In addition, the experts who gave such an assessment are clarified to identify the reasons for e validity of their choices of points during the examination. Critical values of statistics are chosen based on the distribution law of a random variable. Those values can be found for a normal distribution according to the requirements of [28]. In the case of suspicion of two outliers, Grubbs' two-outlier statistic is used to evaluate the population of results.

The dimensions of the matrix-diagram are determined by the number of the DFs that affect the activity of drivers when performing the road freight transportation. In this case, an appropriate number (thirty) of DFs was proposed during the implementation of the RFT, although this list is far from complete. Each expert analyzes the causal relationship between a pair of DFs. At the same time, the connection can be absent, weak or strong, which is encoded by the corresponding symbols. The subjectivity of experts' judgments at this stage is reduced during the averaging of their results after steps 4, 5, when the general matrix of connections of the determined DFs is built. In this case, the judgment of experts is, as a rule, based on the OR control approach. In addition, to reduce the influence of subjectivity of judgments during the transformations of the values of the relationship between DFs established by experts, a threshold indicator (μ) at the level of 0.5 was introduced, which makes it possible to filter out rather insignificant connections in which the experts were not sure [25]. It is worth noting that to reduce the subjectivity of experts' judgments, when calculating the degree of importance and impact of the OR, the standard deviation σ was considered to determine the threshold indicator (μ), which was determined from the matrix of the overall impact. The threshold value is set by calculating the sum of the mean and standard deviation ($\mu + \sigma$). At the same time, it is considered that all the DFs from each group will lead to a dangerous event and, in general, cause harm to human life or disruption of the performance of the transport task during the implementation of the road freight transportation. In addition, when compiling a matrix-diagram, experts are invited to take into account the possibility of controlling the value of each factor. Next, processing of the results of the conversion is carried out, which allows obtaining the prioritization of DFs (Table 6 and 7) and conducting a detailed analysis to determine their impact on a dangerous event. So, in the given example, the largest indicator ($r + c$) is recorded in the DF numbered A_2, A_3, A_4, A_{11}, A_{12}, A_{14}, A_{15}, A_{16}, A_{15}, A_{17}, A_{18}, A_{20}, A_{21}, A_{22}, A_{23}, A_{25}, A_{26}, A_{27}, A_{28}, A_{29}, A_{30} (Figure 5), while taking into account only those dangerous factors in which the difference (r - c) had positive values.

Based on [26], the determined causal factors can be divided into decisive, that is, those that affect the probability of the dangerous event occurrence and secondary - those that have a less strong influence $\tilde{N}_k = (l_k, m_k, u_k); k = 1,2,\ldots,n$. For this, used the condition that the level of influence, which is calculated as r - c, should be bigger than the average number of S_{cp}. matrices of general influence. The basis of this transformation is the combination of r and c criteria into a single matrix by transforming the "positive" indicator of the value of each factor into a "positive" one. Additionally, an alternative approach for determining the significant dangerous factors is presented. Thus, the causal dangerous factors are determined by fulfilling the condition $r_i/c_i > 1$ or $r_i - c_i > 0$. The next step is to establish the significance of the causal dangerous factor. For this purpose, it is proposed to determine the range for the indicator of the level

Table 6 *Prioritization of DFs based on degree of importance (r + c) and level of influence (r - c) - part 1*

DF	Calculated data		Degree of importance	Level of influence	Determination of the type of DF	Determining the significance of the impact of the causative DF	Definition of the DF used in risk calculations (if causal and significant)
	r	*c*	*r + c*	*r - c*			
A_1	28.44	28.73	57.17	-0.29	consequential	not considered	not used
A_2	32.53	28.28	60.11	3.65	causal	essential*	used
A_3	31.36	28.24	59.10	3.12	causal	essential	used
A_4	26.69	29.24	55.93	-2,55	consequential	not considered	used
A_5	28.02	28.39	56.41	-0.37	consequential	not considered	used
A_6	28.02	29.79	57.81	-1.77	consequential	not considered	used
A_7	29.26	28.10	57.36	1.16	causal	not essential*	used
A_8	27.71	29.21	56.92	-1.50	consequential	not considered	used
A_9	28.93	28.12	57.05	0.81	causal	not essential	used
A_{10}	27.72	28.53	56.25	-0.81	consequential	not considered	used
A_{11}	25.74	28.70	54.44	-2.96	consequential	not considered	used
A_{12}	30.55	28.48	59.03	2.07	causal	essential	used
A_{13}	27.77	28.93	56.70	-1.16	consequential	not considered	used
A_{14}	32.26	28.61	60.87	3.65	causal	essential	used

Table 7 *Prioritization of DFs based on degree of importance (r +c) and level of influence (r - c) - part 2*

DF	Calculated data		Degree of importance	Level of influence	Determination of the type of DF	Determining the significance of the impact of the causative DF	Definition of the DF used in risk calculations (if causal and significant)
	r	*c*	*r + c*	*r - c*			
A_{15}	31.14	29.31	60.45	1.83	causal	essential*	used
A_{16}	30.58	29.16	59.74	1.42	causal	essential	used
A_{17}	31.13	28.82	59.95	2.31	causal	essential	used
A_{18}	31.23	28.40	59.63	2.83	causal	essential	used
A_{19}	26.53	27.55	54.08	-1.02	consequential	not considered	not used
A_{20}	28.60	27.94	56.54	0.66	causal	not essential*	not used
A_{21}	27.08	27.82	54.90	-0.74	consequential	not considered	not used
A_{22}	31.49	29.33	60.82	2.16	causal	essential	used
A_{23}	30.61	29.20	59.81	1.41	causal	essential	used
A_{24}	28.72	29.14	57.86	-0.42	consequential	not considered	not used
A_{25}	26.00	27.86	53.86	-1.86	consequential	not considered	not used
A_{26}	25.85	28.05	53.90	-2.20	consequential	not considered	not used
A_{27}	30.09	28.51	58.60	1.58	causal	essential	used
A_{28}	27.77	27.63	55.40	0.14	causal	not essential	not used
A_{29}	26.18	27.87	54.05	-1.69	consequential	not considered	not used
A_{30}	26.91	28.39	55.30	-1.48	consequential	not considered	not used

Note* causative case at $r - c > 0$ *or* $r/c > 1$; * causative case at $r - c \leq 0$ *or* $r/c \leq 1$; *essential $S_{cp} > 1.2$ *or* $\max(r - c) \geq (r - c) > 0.2\max(r - c)$; *not essential $S_{cp} \leq 1.2$ *or* $0.2\max(r - c) > (r - c) > 0$.

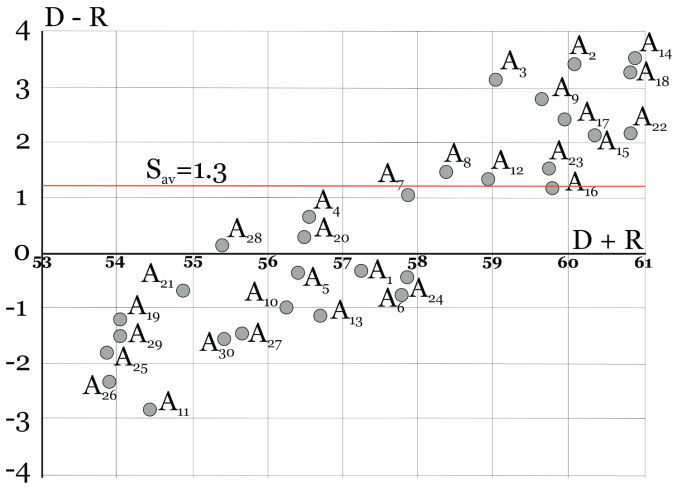

Figure 5 *The connection map example between the measurements of DF (S_{av} average number of the matrix of general influence is 1.3)*

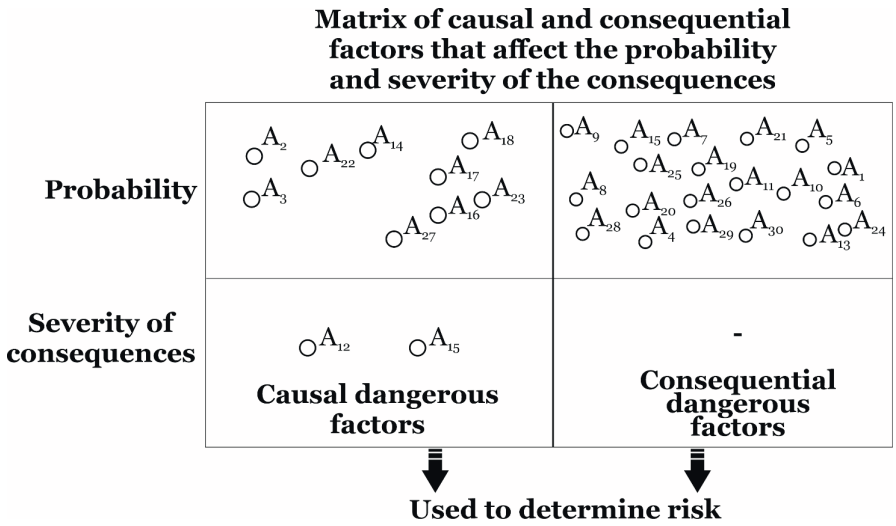

Figure 6 *Division of consequential DFs into influential ones in terms of probability and severity of consequences according to criteria*

of influence (r_i - c_i) from the principle "As low as reasonably practicable" (ALARP), that is, the residual level of risk should be reduced as much as it is practically possible. In this case, the following condition is provided: $\max(r-c) \geq (r_i - c_i) > 0.2\max(r-c)$, i.e., the level of influence is limited up to 80 % of all the cases. As a result of the calculations, only 11 dangerous factors A_2, A_3, A_{12}, A_{14}, A_{15}, A_{16}, A_{17}, A_{18}, A_{22}, A_{23}, A_{27} would satisfy the given condition.

The obtained results would be divided into four zones in accordance with the recommendations [29] (Figure 6). The first zone includes the causal factors that affect the probability of the dangerous event occurrence, the calculation of which satisfied the above-mentioned condition - A_2, A_3, A_{12}, A_{14}, A_{15}, A_{16}, A_{17}, A_{18}, A_{22}, A_{23}, A_{27}.

The second level includes consequential factors that have an impact on probability of a dangerous event occurrence, as well. The third level allows to establish the causal factors that affect the severity of the consequences, which include A_{12}, A_{15}. In the fourth zone, there are also the consequential factors that affect the severity of the consequences, but they were not identified in this study.

In this study, it is assumed that for the further analysis of the occurrence assessment of a dangerous event, we select only dangerous factors that are the causes and form the corresponding impact on the dangerous event and the severity of consequences. Constructed prioritization of the dangerous factors, compatible with their ranking, makes it possible to obtain a map of connections from which it is clearly visible how the faults are related to each other and which of them are causal and which are consequential. If the first (causal) faults are eliminated, the second ones will disappear or at least weaken the influence, as well, however, experts still need to further analyze the results to identify possible inaccuracies.

The last step of the procedure is to clarify the cause-and-effect relationships between the hazard and the dangerous event and the consequences severity,

Table 8 *The form for determining the cause-and-effect relationship between a hazard, a dangerous event, DF and the consequences of an RFT*

Danger	DFs that affect the increase in the probability of a dangerous event occurring	Dangerous event	DFs that affect the increase in severity from the occurrence of a dangerous event	Consequences
Moving truck	A_2. Lack of system understanding skills and safe decision-making skills by a driver on the road A_3. Aggressive behavior while driving a truck A_{14}. Lack of high-quality supervision and technical inspection of the technical condition of the truck A_{16}. Exceeding the standard working time of a truck driver (driver fatigue) A_{17}. Overloading of a truck when carrying out RFT A_{18}. The cabin is dirty, there are foreign objects in a driver's seat A_{22}. Lack of proper pre-race medical control of driver's health A_{23}. Fog, rain, snow/nighttime - poor visibility A_{27}. Overtime work schedule	Traffic accident	A_{12}. Negligence in observing the technical condition of the truck's passive safety systems (airbags, safety belts, impact-absorbing bumpers, etc.). A_{15}. Lack of emergency equipment (fire extinguisher, etc.), first aid kits	Driver injuries (disability, death)

taking into account the established significant DFs. In particular, one can fill out the appropriate form (Table 8), which allows to further evaluate the OR when implementing the road freight transportation.

5 Discussion

The DFs' identification process involves the cause and sources of risk determination, as well as events and situations that may have general results regarding the objectives and nature of the OR. Taken together, this is the foundation for justification of the effective preventive and protective measures. From this example, six main DFs have been identified, which have the greatest impact on both the probability of an incident occurring, as well as six DFs that affect the severity of the consequences, which allows for a more thorough study of these factors' influence on the magnitude of the risk in the future. The specified DFs were determined based on determination of the cause-and-effect relationships, by evaluating pairwise comparisons to establish the most influential DFs on the occurrence probability of a dangerous event by degree of importance, and for the severity of consequences - by the level of influence, which are determined by transforming a vague set into a clear number by the affiliation degree, which occurs during the relevant calculations using the Dematel method. This conclusion is supported by the existing classic studies conducted using the fuzzy Dematel method [30-31], which can be classified into three types: the first type is relationships identification between factors or criteria; the second type is determination of the key factors based on cause-and-effect relationships and degrees of interrelationship between them; the third type is the weighting criteria determination by analyzing the relationships and levels of criteria influence. The last two types make it possible to transform the relationships between the factors into an understandable structural model of the system and divide them into a group of causes and a group of consequences [32]. For this, a threshold value, such as the mean of the total effect matrix, is set to filter out minor effects. Thanks to a detailed review of the Dematel methodology, there is an opportunity to reduce the influence of subjective judgments of experts through the uncertainty assessment in the decision-making process using the fuzzy sets to capture the relationships of mutual influence between quality attributes [33].

When determining the significant DFs, one should also pay attention to development of a dangerous event, evaluate the effectiveness of all the existing control measures, for example, design specifications, timeliness of providing medical assistance, and propose those that would significantly reduce the level of OR. This will make it possible to adjust the threshold indicator to avoid errors and reduce the subjectivity influence. It should be noted that most of the relevant DFs are interdependent, which also needs to be taken into account when establishing causal and consequential DFs. The higher the relationship weight is set, the better the score will be compared to others.

For example, certain limitations must be considered when interpreting the obtained results. First, the

magnitude of established causal relationships cannot be established between variables. Yes, it cannot be ruled out that the frequent aggressive driving of the A_3 can be reduced with appropriate controls or better professional training. Secondly, the threshold indicator is set without distinguishing groups of factors, although it can be considered that the human factor has the greatest influence on the road accident occurrence [34-35]. In other words, in this study, DFs were assessed as a broad construct, and future studies could further focus on specific threats based on their occupational context.

6 Conclusions

To carry out the process of hazards and DFs identification, it is proposed to provide an appropriate ranking of the latter to identify the most important (causal) ones, according to which the OR is determined during the implementation of the road freight transportation.

A register of the DFs has been developed, which include six typical groups: human, organizational, technical, operational, social, ergonomic, which increase the probability of a dangerous event occurring during the implementation of RFT.

Based on the cause-and-effect relationships, using the fuzzy Dematel method, using the Grubbs criterion, the most influential variables that affect the probability of a dangerous event and the severity of consequences are determined to assess the risk of a road accident.

It is suggested that the most influential dangerous factors are determined by comparing the indicator of the influence level of DFs (c) to the average number of the matrix of total impact (S_{cp}), when the condition ($c_i \geq S_{cp}$) is fulfilled, and if the condition that $r_i / c_i > 1$ or $r_i - c_i > 0$ is fulfilled, followed by determination of the DF significance by limiting the exposure level indicator to a certain range, which is calculated based on the "As low as reasonably practicable" (ALARP) principle, i.e. the residual risk level should be reduced as much as it is practically possible.

It is proposed to reduce the subjectivity of experts' judgments, regarding the influence of DFs on probability of a dangerous event occurrence, when calculating their degree of importance and impact using the fuzzy Dematel method to adjust the threshold indicator that excludes weak relationships during a pairwise comparison of DFs, by taking into account the standard deviation, which was determined from the general influence matrix, using the Grubbs test.

An improved bow tie model, which visualizes the cause-and-effect relationship between danger and a dangerous event in the implementation of freight road transportation, which provides for the risk assessment to take into account dangerous factors that increase the probability of an incident and the severity of the consequences of its occurrence.

Grants and funding

The authors received no financial support for the research, authorship and/or publication of this article.

Conflicts of interest

The authors declare that they have no known competing financial interests or personal relationships that could have appeared to influence the work reported in this paper.

References

[1] Conventions and recommendations - International Labour Organization (ILO) [online] [accessed 2023-02-15]. Available from: https://www.ilo.org/global/standards/introduction-to-international-labour-standards/conventions-and-recommendations/lang--en/index.htm

[2] On labor protection - Law of Ukraine [online] [accessed 2023-02-15]. Available from: https://zakon.rada.gov.ua/laws/show/2694-12/ed20110625#Text

[3] Order on the approval of the standard regulation on the procedure for conducting training and testing knowledge on occupational health and safety issues and the list of high-risk jobs [online] [accessed 2023-02-15]. Available from: https://zakon.rada.gov.ua/laws/show/z0231-05?lang=en#Text

[4] Resolution on approval of the procedure for investigating and recording accidents, occupational diseases and accidents at work [online] [accessed 2023-02-15]. Available from: https://zakon.rada.gov.ua/laws/show/en/337-2019-%D0%BF?lang=en#Text

[5] On the main principles of state supervision (oversight) in the area of commercial activity - Law of Ukraine [online]. [accessed 2023-02-15]. Available from: https://zakon.rada.gov.ua/laws/show/877-16?lang=en#Text

[6] STEPHENS, A., OHTSUKA, K. Cognitive biases in aggressive drivers: does illusion of control drive us off the road? *Personality and Individual Differences* [online]. 2014, **68**, p. 124-129 [accessed 2023-02-15]. ISSN 0191-8869. Available from: https://doi.org/10.1016/j.paid.2014.04.016

[7] TSOPA, V., CHEBERIACHKO, S., YAVORSKA, O., DERYUGIN, O., ALEKSIEIEV, A. Improvement of the safe work system. *Naukovyi Visnyk Natsionalnoho Hirnychoho Universytetu* [online]. 2022, **6**, p. 104-111 [accessed 2023-02-15]. ISSN 2071-2227, e-ISSN 2223-2362. Available from: https://doi.org/10.33271/nvngu/2022-6/104

[8] MAIREAN, C., HAVARNEANU, G., BARIC, D., HAVARNEANU, C. Cognitive biases, risk perception, and risky driving behaviour. *Sustainability* [online]. 2022, **14**(1), 77 [accessed 2023-02-15]. ISSN 2071-1050. Available from: https://doi.org/10.3390/su14010077

[9] STOLECKA, K. Hazards of the road transportation of hazardous materials. *System Safety: Human - Technical Facility - Environment* [online]. 2020, **2**(1), 237-246 [accessed 2023-02-15]. ISSN 2657-5450. Available from: https://doi.org/10.2478/czoto-2020-0029

[10] LI, H., WANG, Y. Research on the road transport risk of domestic hazardous chemicals. In: 3rd Annual International Conference on Management Science and Engineering MSE 2017: proceedings. Vol. 50. Advances in Economics, Business and Management Research. 2017. ISSN 2352-5428, p. 164-171. Available from: https://doi.org/10.2991/mse-17.2017.42

[11] LITVINOVA, Y. Finding ways of building sustainable trails cargo transportation using optimization methods and computational tools. In: 25th International Scientific Conference Transport Means 2021: proceedings. 2021. ISSN 1822-296X, eISSN 2351-7034, p. 514-519.

[12] DOROSH, A., DEMCHENKO, Y., MARKUL, R., BERDYCHEVSKA, T. Analysis of risks of international road cargo transportation. *Transport Systems and Transportation Technologies* [online]. 2020, **20**, p. 12-19 [accessed 2023-03-10]. ISSN 2222-419X. Available from: https://doi.org/10.15802/tstt2020/217388

[13] STAZNIK, A., BABIC, D., BAJOR, I. Identification and analysis of risks in transport chains. *Journal of Applied Engineering Science* [online]. 2017, **15**(1), p. 61-70 [accessed 2023-03-10]. ISSN 1451-4117. Available from: http://dx.doi.org/10.5937/jaes15-12179

[14] BAZALUK, O., KORIASHKINA, L., CHEBERYACHKO, S., DERYUGIN, O., ODNOVOL, M., LOZYNSKYI, V., NESTEROVA, O. Methodology for assessing the risk of incidents during passenger road transportation using the functional resonance analysis method. *Heliyon* [online]. 2022, **8**(75), e11814 [accessed 2023-03-10]. ISSN 2405-8440. Available from: http://dx.doi.org/10.1016/j.heliyon.2022.e11814

[15] MARTO, A., HAJIHASSANI, M., JAHED ARMAGHANI, D., TONNIZAM MOHAMAD, E., MAKHTAR, A. A novel approach for blast-induced flyrock prediction based on imperialist competitive algorithm and artificial neural network. *The Scientific World Journal* [online]. 2014, **2014**, 643715 [accessed 2023-03-10]. ISSN 2356-6140, eISSN 1537-744X. Available from: https://doi.org/10.1155/2014/643715

[16] TRIVEDI, R., SINGH, T., RAINA, A. Prediction of blast-induced flyrock in Indian limestone mines using neural networks. *Journal of Rock Mechanics and Geotechnical Engineering* [online]. 2014, **6**(5), p. 447-454 [accessed 2023-03-10]. ISSN 1674-7755. Available from: https://doi.org/10.1016/j.jrmge.2014.07.003

[17] CHAUHAN, A., SINGH, A., JHARKHARIA, S. An interpretive structural modeling (ISM) and decision-making trail and evaluation laboratory (DEMATEL) method approach for the analysis of barriers of waste recycling in India. *Journal of the Air and Waste Management Association* [online]. 2018, **68**(2), p. 100-110 [accessed 2023-03-10]. ISSN 1096-2247. Available from: https://doi.org/10.1080/10962247.2016.1249441

[18] PANDEY, M., LITORIYA, R., PANDEY, P. Application of fuzzy DEMATEL approach in analyzing mobile application issues. *Programming and Computer Software* [online]. 2019, **45**(5), p. 268-287 [accessed 2023-03-10]. ISSN 0361-7688, eISSN 1608-3261. Available from: https://doi.org/10.1134/S0361768819050050

[19] SEKER, S., ZAVADSKAS, E. Application of fuzzy DEMATEL method for analyzing occupational risks on construction sites. *Sustainability* [online]. 2017, **9**(11), 2083 [accessed 2023-03-10]. ISSN 2071-1050. Available from: https://doi.org/10.3390/su9112083

[20] SADEHNEZHAD, F., ZARANEJAD, M., GHEITANI, A. Using combinational method DEMATEL and ANP with fuzzy approach to evaluate business intelligence performance. *European Online Journal of Natural and Social Sciences* [online]. 2013, **2**(3), p. 1374-1386 [accessed 2023-03-10]. ISSN 1805-3602. Available from: https://european-science.com/eojnss/article/view/757

[21] TSOPA, V., CHEBERIACHKO, S., YAVORSKA, O., DERYUGIN, O., BAS, I. Increasing the safety of the transport process by minimizing the professional risk of a dump truck driver. *Mining of Mineral Deposits* [online]. 2022, **16**(3), p. 101-108 [accessed 2023-03-10]. ISSN 2415-3443, eISSN 2415-3435. Available from: https://doi.org/10.33271/mining16.03.101

[22] LIN, C., WU, W. A causal analytical method for group decision-making: under fuzzy environment. *Expert Systems with Applications* [online]. 2007, **34**(1), p. 205-213 [accessed 2023-03-10]. ISSN 0957-4174. Available from: https://doi.org/10.1016/j.eswa.2006.08.012

[23] CHEBERIACHKO, S., YAVORSKA, O., DERYUGIN, O., LANTUKH, D., BAS, I., KRUZHILKO, O., MELNYK, V. Improving safety of passenger road transportation. Transactions on transport sciences [online]. 2023, **14**(2), p. 1-10 [accessed 2023-02-08]. eISSN 1802-9876. Available from: https://doi.org/10.5507/tots.2023.003

[24] NECHAYEVA, I., DONCHIK, D. Use of BOWTIE tie technology in risk assessment practice. *Economy and Society* [online]. 2021, **33**, 51 [accessed 2023-03-17]. eISSN 2524-0072. Available from: https://doi.org/10.32782/2524-0072/2021-33-51

[25] SU, C.-M., HORNG, D.-J., TSENG, M.-L., CHIU, A.S.F., WU, K.-J., CHEN, H.-P. Improving sustainable supply chain management using a novel hierarchical grey-DEMATEL approach. *Journal of Cleaner Production* [online]. 2015, **134**, p. 469-481 [accessed 2023-03-17]. eISSN 2524-0072. Available from: http://dx.doi.org/10.1016/j.jclepro.2015.05.080

[26] WU, W.-W., LAN, L. W., LEE, Y.-T. Exploring decisive factors affecting an organization's SaaS adoption: a case study. *International Journal of Information Management* [online]. 2011, **31**(6), p. 556-563 [accessed 2023-03-17]. ISSN 0268-4012. Available from: http://dx.doi.org/10.1016/j.ijinfomgt.2011.02.007

[27] TSENG, M.-L. A causal and effect decision making model of service quality expectation using grey-fuzzy DEMATEL approach. *Expert Systems with Applications* [online]. 2009, **36**(4), p. 7738-7748 [accessed 2023-03-17]. ISSN 0957-4174. Available from: https://doi.org/10.1016/j.eswa.2008.09.011

[28] DSTU GOST ISO 5725-2:2005 (GOST ISO 5725-2-2003, IDT). Accuracy (correctness and precision) of measurement methods and results. Part 2. The main method of determining the repeatability and reproducibility of the standard measurement method [online] [accessed 2023-03-17]. Available from: http://online.budstandart.com/ua/catalog/doc-page?id_doc=84968

[29] WU, W.-W., LEE, Y.-T. Developing global managers' competencies using the fuzzy DEMATEL method. *Expert Systems with Applications* [online]. 2007, **32**(2), p. 499-507 [accessed 2023-03-17]. ISSN 0957-4174. Available from: https://doi.org/10.1016/j.eswa.2005.12.005

[30] LIANG, H., REN, J., GAO, Z., GAO, S., LUO, X., DONG, L., SCIPIONI, A. Identification of critical success factors for sustainable development of biofuel industry in China based on grey decision-making trial and evaluation laboratory (DEMATEL). *Journal of Cleaner Production* [online]. 2016, **131**, p. 500-508 [accessed 2023-03-17]. ISSN 0959-6526, eISSN 1879-1786. Available from: https://doi.org/10.1016/j.jclepro.2016.04.151

[31] ABDULLAH, L., ZULKIFLI, N. Integration of fuzzy AHP and interval type-2 fuzzy DEMATEL: an application to human resource management. *Expert Systems with Applications* [online]. 2015, **42**(9), p. 4397-4409 [accessed 2023-03-17]. ISSN 0957-4174. Available from: https://doi.org/10.1016/j.eswa.2015.01.021

[32] HUANG C.-Y., SHYU J. Z., TZENG G.-H. Reconfiguring the innovation policy portfolios for Taiwan's SIP mall industry. *Technovation* [online]. 2007, **27**(12), p. 744-765 [accessed 2023-03-17]. ISSN 0166-4972. Available from: https://doi.org/10.1016/j.technovation.2007.04.002

[33] AZADEH, A., ZARRIN, M., ABDOLLAHI, M., NOURY, S., FARAHMAND, S. Leanness assessment and optimization by fuzzy cognitive map and multivariate analysis. *Expert Systems with Applications* [online]. 2015, **42**(15-16), p. 6050-6064 [accessed 2023-03-17]. ISSN 0957-4174. Available from: https://doi.org/10.1016/j.eswa.2015.04.007

[34] MAIREAN, C., DIACONU-GHERASIM, L. Time perspective, risk perception on the road, and risky driving behavior. *Current Psychology* [online]. 2023, **42**, p. 5611-5620 [accessed 2023-03-17]. ISSN 1936-4733, eISSN 1046-1310. Available from: https://doi.org/10.1007/S12144-021-01921-2

[35] O'BRIEN, F., GORMLEY, M. Risk-perception and dangerous driving among adolescents: outcome- and behavior-focused questions yield opposite results. *Journal of Adolescence* [online]. 2016, **52**, p. 89-94 [accessed 2023-03-17]. ISSN 1095-9254. Available from: https://doi.org/10.1016/j.adolescence.2016.07.010

Dear colleague,

We would like to send you a copy of the journal Communications - Scientific Letters of the University of Zilina.

Journal Communications - Scientific Letters of the University of Zilina are a well-established open-access scientific journal aimed primarily at the topics connected with the field of transport. The main transport-related areas covered include Civil engineering, Electrical engineering, Management and informatics, Mechanical engineering, Operation and economics, Safety and security, Travel and tourism studies. The full list of main topics and subtopics is available at: *https://komunikacie.uniza.sk/artkey/inf-990000-0500_Topical-areas.php*

Journal Communications - Scientific Letters of the University of Zilina is currently indexed and accepted by CEEOL, Crossref (DOI), DOAJ, EBSCO Host, Electronic Journals Library (EZB), ERIH Plus, Google Scholar, Index Copernicus International Journals Master list, iThenticate, JournalGuide, Jouroscope, Norwegian Register for Scientific Journals Series and Publishers, ROAD, ScienceGate, SCImago Journal & Country Rank, SciRev, SCOPUS, WorldCat (OCLC).

Journal Communications - Scientific Letters of the University of Zilina is preserved in CLOCKSS and Portico to guarantee long-term digital preservation and is archived in the national deposit digitalne pramene.

Authors can share their experiences with publishing in our journal on SciRev.

Journal Communications - Scientific Letters of the University of Zilina is under evaluation for inclusion to Web of Science database.

I would like to invite authors to submit their papers for consideration. We have an open-access policy and there are **no publication, processing or other fees** charged for published papers. Our journal operates a standard single-anonymised review procedure, the successful completion of which is a prerequisite for paper publication.

The journal is issued four times a year (in January, in April, in July and in October).

I would also like to offer you the opportunity of using already published articles from past issues as source of information for your research and publication activities. All papers are available at our webpage: http://komunikacie.uniza.sk, where you can browse through the individual volumes. Our journal offers access to its contents in the open access system on the principles of the license **Creative Commons (CC BY 4.0)**.

For any questions regarding the journal Communications - Scientific Letters of the University of Zilina please contact us at: *komunikacie@uniza.sk*

We look forward to future cooperation.

Sincerely

Branislav Hadzima
editor-in-chief

KOMUNIKÁCIE
COMMUNICATIONS

VEDECKÉ LISTY ŽILINSKEJ UNIVERZITY
SCIENTIFIC LETTERS OF THE UNIVERSITY OF ZILINA

VOLUME 25 Number 3

July 2023

Editor-in-Chief:
Branislav HADZIMA - SK

Associate Editor:
Jakub SOVIAR - SK

Executive Editor:
Sylvia DUNDEKOVA - SK

Language Editor:
Ruzica NIKOLIC - SK
Marica MAZUREKOVA - SK

Graphical Editor:
Juraj ZBYNOVEC - SK

Honorary Members:
Otakar BOKUVKA - SK
Jan COREJ - SK (in memoriam)
Milan DADO - SK
Pavel POLEDNAK - CZ

Scientific Editorial Board:
Greg BAKER - NZ
Abdelhamid BOUCHAIR - FR
Pavel BRANDSTETTER - CZ
Mario CACCIATO - IT
Jan CELKO - SK
Andrew COLLINS - GB
Samo DROBNE - SI
Erdogan H. EKIZ - MA
Michal FRIVALDSKY - SK
Juraj GERLICI - SK
Vladimir N. GLAZKOV - RU
Ivan GLESK - GB
Mario GUAGLIANO - IT
Mohamed HAMDAOUI - FR
Andrzej CHUDZIKIEWICZ - PL
Jaroslav JANACEK - SK
Zdenek KALA - CZ
Antonin KAZDA - SK
Michal KOHANI - SK
Tomasz N. KOLTUNOWICZ - PL
Jozef KOMACKA - SK
Matyas KONIORCZYK - HU
Gang LIU - CN
Tomas LOVECEK - SK
Frank MARKERT - DK
Jaroslav MAZUREK - SK
Marica MAZUREKOVA - SK
Vladimir MOZER - CZ
Jorge Carvalho PAIS - PT
Peter POCTA - SK
Maria Angeles Martin PRATS - ES
Pavol RAFAJDUS - SK
Che-Jen SU - TW
Giacomo SCELBA - IT
Janka SESTAKOVA - SK
Eva SVENTEKOVA - SK
Eva TILLOVA - SK
Anna TOMOVA - SK
Audrius VAITKUS - LT
Yue XIAO - CN
Franco Bernelli ZAZZERA - IT

Executive Editorial Board:
Michal BALLAY - SK
Martin BOROS - SK
Marek BRUNA - SK
Kristian CULIK - SK
Jan DIZO - SK
Lukas FALAT - SK
Filip GAGO - SK
Lubica GAJANOVA - SK
Stefan HARDON - SK
Martin HOLUBCIK - SK
Maros JANOVEC - SK
Daniel KAJANEK - SK
Matus KOZEL - SK
Lenka KUCHARIKOVA - SK
Matus MATERNA - SK
Daniela MICHALKOVA - SK
Eva NEDELIAKOVA – SK
Filip PASTOREK - SK
Pavol PECHO - SK
Jozef PROKOP - SK
Marek PRUDOVIC - SK
Michal SAJGALIK - SK
Anna SIEKELOVA - SK
Simona SKRIVANEK KUBIKOVA - SK
Michal TITKO - SK
Vladislav ZITRICKY - SK

Each paper was reviewed by at least two reviewers.
Individual issues of the journal can be found on: http://komunikacie.uniza.sk
The full author quidelines are available at: https://komunikacie.uniza.sk/artkey/inf-990000-0400_Author-guidelines.php
Published quarterly by University of Žilina in EDIS - Publishing House of the University of Žilina.

Communications is currently indexed, abstracted and accepted by CEEOL, CLOCKSS, Crossref (DOI), digitálne pramene, DOAJ, EBSCO Host, Electronic Journals Library (EZB), ERIH Plus, Google Scholar, Index Copernicus International Journals Master list, iThenticate, JournalGuide, Jouroscope, Norwegian Register for Scientific Journals Series and Publishers, Portico, ROAD, ScienceGate, SCImago Journal & Country Rank, SciRev, SCOPUS, WorldCat (OCLC).
Journal Komunikácie - vedecké listy Žilinskej univerzity v Žiline / Communications - Scientific Letters of the University of Žilina is under evaluation for inclusion to Web of Science database.

Contact:
Komunikácie - vedecké listy Žilinskej univerzity v Žiline
Communications - Scientific Letters of the University of Žilina
University of Žilina
Univerzitná 8215/1
010 26 Žilina
Slovakia

E-mail: komunikacie@uniza.sk
Web: https://komunikacie.uniza.sk

ISSN (print version): 1335-4205
ISSN (online version): 2585-7878

Registered No. (print version): EV 3672/09
Registered No. (online version): EV 3/22/EPP
Publisher, owner and distribution:
University of Žilina, Univerzitná 8215/1,
010 26 Žilina, Slovakia

Company identification number IČO: 00 397 563
Frequency of publishing: four times a year
Circulation: 80 printed copies per issue
Print edition price: free of charge

Publishing has been approved by:
Ministry of Culture, Slovak Republic
© University of Žilina, Žilina, Slovakia

This is an open access article distributed under the terms of the Creative Commons Attribution 4.0 International License (CC BY 4.0), which permits use, distribution, and reproduction in any medium, provided the original publication is properly cited. No use, distribution or reproduction is permitted which does not comply with these terms.

UNIVERSITY
OF ŽILINA

1953 70 2023

In its over 70 years of successful existence, the University of Žilina (UNIZA) has become one of the top universities in Slovakia.

Scientific conferences

organized by University of Žilina

World Multidisciplinary Earth Sciences Symposium 2023 – WMESS
Date and venue: 28. 8. – 1. 9. 2023, Prague (CZ)
Contact: marian.drusa@fstav.uniza.sk

World Multidisciplinary Civil Engineering-Architecture-Urban Planning Symposium 2023 - WMCAUS
Date and venue: 4. – 8. 9. 2023, Prague (CZ)
Contact: marian.drusa@fstav.uniza.sk

Current Problems of Physics Education and Possible Solutions
Date and venue: 13. – 14. 9. 2023, Zuberec (SK)
Contact: peter.hockicko@uniza.sk

39th DANUBIA – ADRIA Symposium on Advances in Experimental Mechanics 2023
Date and venue: 26. – 29. 9. 2023, Siofok, Balaton (HU)
Contact: frantisek.novy@fstroj.uniza.sk
Web: https://das.tuwien.ac.at

Horizons of Railway Transport 2023
Date and venue: 2. – 3. 10. 2023, Hotel Permon, Podbanské (SK)
Contact: gasparik@uniza.sk

Horizons of Railway Transport 2023
Date and venue: 27. – 28. 9. 2023, Hotel Permon, Podbanské (SK)
Contact: gasparik@uniza.sk

Globalization and its socio-economic consequences 2023
Date and venue: October 2023, hotel Afrodita, Rajecké Teplice (SK)
Contact: tomas.kliestik@fpedas.uniza.sk
Web: https://ke.uniza.sk/en/conference

International Scientific Conference POSTPOINT 2023
Date and venue: October 2023, Žilina (SK)
Contact: martina.kovacikova@uniza.sk

UNIVERSITY OF ŽILINA
Science & Research Department

Univerzitná 8215/1,
010 26 Žilina,
Slovakia

Ing. Janka Macurová
tel.: +421 41 513 5143
e-mail: janka.macurova@uniza.sk